PHYSICS AND CHEMISTRY OF FISSION 1973

VOL. II

Proceedings of a Symposium
Rochester
New York
13-17 August
1973

INTERNATIONAL ATOMIC ENERGY AGENCY, VIENNA, 1974

PHYSICS AND CHEMISTRY OF FISSION 1973

VOL. II

The following States are Members of the International Atomic Energy Agency:

AFGHANISTAN
ALBANIA
ALGERIA
ARGENTINA
AUSTRALIA
AUSTRIA
BANGLADESH
BELGIUM
BOLIVIA
BRAZIL
BULGARIA
BURMA
BYELORUSSIAN SOVIET SOCIALIST REPUBLIC
CAMEROON
CANADA
CHILE
COLOMBIA
COSTA RICA
CUBA
CYPRUS
CZECHOSLOVAK SOCIALIST REPUBLIC
DENMARK
DOMINICAN REPUBLIC
ECUADOR
EGYPT, ARAB REPUBLIC OF
EL SALVADOR
ETHIOPIA
FINLAND
FRANCE
GABON
GERMAN DEMOCRATIC REPUBLIC
GERMANY, FEDERAL REPUBLIC OF
GHANA
GREECE
GUATEMALA
HAITI
HOLY SEE
HUNGARY
ICELAND
INDIA
INDONESIA
IRAN
IRAQ
IRELAND
ISRAEL
ITALY
IVORY COAST
JAMAICA
JAPAN
JORDAN
KENYA
KHMER REPUBLIC
KOREA, REPUBLIC OF
KUWAIT
LEBANON
LIBERIA
LIBYAN ARAB REPUBLIC
LIECHTENSTEIN
LUXEMBOURG
MADAGASCAR
MALAYSIA
MALI
MEXICO
MONACO
MONGOLIA
MOROCCO
NETHERLANDS
NEW ZEALAND
NIGER
NIGERIA
NORWAY
PAKISTAN
PANAMA
PARAGUAY
PERU
PHILIPPINES
POLAND
PORTUGAL
ROMANIA
SAUDI ARABIA
SENEGAL
SIERRA LEONE
SINGAPORE
SOUTH AFRICA
SPAIN
SRI LANKA
SUDAN
SWEDEN
SWITZERLAND
SYRIAN ARAB REPUBLIC
THAILAND
TUNISIA
TURKEY
UGANDA
UKRAINIAN SOVIET SOCIALIST REPUBLIC
UNION OF SOVIET SOCIALIST REPUBLICS
UNITED KINGDOM OF GREAT BRITAIN AND NORTHERN IRELAND
UNITED STATES OF AMERICA
URUGUAY
VENEZUELA
VIET-NAM
YUGOSLAVIA
ZAIRE, REPUBLIC OF
ZAMBIA

The Agency's Statute was approved on 23 October 1956 by the Conference on the Statute of the IAEA held at United Nations Headquarters, New York; it entered into force on 29 July 1957. The Headquarters of the Agency are situated in Vienna. Its principal objective is "to accelerate and enlarge the contribution of atomic energy to peace, health and prosperity throughout the world".

Printed by the IAEA in Austria
May 1974

PROCEEDINGS SERIES

PHYSICS AND CHEMISTRY OF FISSION
1973

PROCEEDINGS OF THE THIRD IAEA SYMPOSIUM
ON THE
PHYSICS AND CHEMISTRY OF FISSION
HELD BY THE
INTERNATIONAL ATOMIC ENERGY AGENCY
IN ROCHESTER, NEW YORK, 13-17 AUGUST 1973

In two volumes

VOL. II

INTERNATIONAL ATOMIC ENERGY AGENCY
VIENNA, 1974

PHYSICS AND CHEMISTRY OF FISSION 1973
IAEA, VIENNA, 1974
STI/PUB/347

FOREWORD

This third international Symposium on the Physics and Chemistry of Fission, held in Rochester, N.Y., from 13 to 17 August 1973, was a worthy successor to the important symposia held in Salzburg (1965) and in Vienna (1969). Although there may not have been in Rochester quite the excitement that prevailed in Vienna (where the beautiful verification of the structured fission barrier provided by the Strutinsky calculations was presented), the present meeting reaped the benefits of this revolutionary discovery. The first direct experimental verifications of the deformed fission isomers have also only recently been achieved.

The present Symposium, somewhat more than previous ones, concentrated on theoretical concepts and calculations concerning the fission process itself, and only on those new experimental results most pertinent to the theoretical development. Contained in these two volumes are the full texts and discussions of the 62 papers presented at the Symposium, and abstracts of those contributions that, because of time limitations, could not be presented.

These Proceedings of course do not represent the *last* word on this obviously complex topic. It is apparent that even the liquid drop features of the fission process have not yet been fully, or even adequately, worked out, the most obvious deficiency still being a reliable treatment of the dynamics, where a better knowledge of the 'viscosity' is obviously needed. The importance of quantum mechanical, single particle effects in the fission process is emphasized in these Proceedings, and a number of advances in microscopic calculations are included.

It is clear, in view of the large participation and the quality of the work presented, that scientists throughout the world find these meetings a valuable international forum for the exchange of information and welcome the Agency's initiative in promoting this continuing series of symposia.

EDITORIAL NOTE

The papers and discussions incorporated in the proceedings published by the International Atomic Energy Agency are edited by the Agency's editorial staff to the extent considered necessary for the reader's assistance. The views expressed and the general style adopted remain, however, the responsibility of the named authors or participants.

For the sake of speed of publication the present Proceedings have been printed by composition typing and photo-offset lithography. Within the limitations imposed by this method, every effort has been made to maintain a high editorial standard; in particular, the units and symbols employed are to the fullest practicable extent those standardized or recommended by the competent international scientific bodies.

The affiliations of authors are those given at the time of nomination.

The use in these Proceedings of particular designations of countries or territories does not imply any judgement by the Agency as to the legal status of such countries or territories, of their authorities and institutions or of the delimitation of their boundaries.

The mention of specific companies or of their products or brand-names does not imply any endorsement or recommendation on the part of the International Atomic Energy Agency.

CONTENTS OF VOL. II

MASS, CHARGE AND KINETIC ENERGY DISTRIBUTIONS IN FISSION

(Session VI)

Chairman: S.S. Kapoor (India)

SYMMETRIC AND ASYMMETRIC FISSION OF Ra- AND Ac-ISOTOPES

E. KONECNY, H.J. SPECHT, J. WEBER
Beschleunigerlaboratorium der
Universität und Technischen Universität München,
Munich, Federal Republic of Germany

Abstract

SYMMETRIC AND ASYMMETRIC FISSION OF Ra- AND Ac-ISOTOPES.

Fission probabilities and fragment anisotropies have been investigated at low excitation for fission of ^{226}Ac, ^{227}Ac, ^{228}Ac and ^{225}Ra, ^{227}Ra induced on a ^{226}Ra target by direct reactions with a 23.5-MeV ^{3}He beam and an 18-MeV d beam. These results show that the triple-humped character of the mass distribution pertains to low excitation energies where second- and higher-chance fission are energetically excluded. More important, they reveal different thresholds for symmetric and asymmetric fission. In addition, the angular anisotropies for both components close to the fission barrier seem to be different, also suggesting that asymmetric and symmetric fission of the nuclei investigated proceed over different saddle points. The fission probability Γ_f/Γ_n increases exponentially for both components, with a much bigger slope for the symmetric one. For ^{227}Ra and ^{228}Ac the fission probability for symmetric fission even exceeds that for asymmetric fission already at some few MeV above the barrier.

The average kinetic energy is lower for the symmetric than for the asymmetric component and does not change significantly with excitation energy of the fissioning nucleus. On the contrary, for asymmetric fission it decreases with excitation, as observed for fission of actinide nuclei.

1. INTRODUCTION

One of the important problems in nuclear fission has been to understand the existence of two types of fragment mass distributions, symmetric and asymmetric. Low excitation fission of higher-Z actinide nuclei is typically asymmetric (for a review see, e.g. ref.[1]), characterized by a double humped mass distribution. On the contrary, nuclei near Pb and Bi exhibit a symmetric mass distribution [2,3]. For fission of nuclei in the intermediate region (Ra, Ac, Th, Pa) a triple humped mass distribution with well-established minima between the three mass yield peaks is observed[4-11].

It has been suggested that the triple humped mass distribution is the result of a superposition of two different fission components, a symmetric one which has similar features like the symmetric fission of lighter nuclei and is appropriately described by the liquid drop model[12] and an asymmetric component, which shows the same characteristic features like fission of U or Pu, the energetics of which is explained to very great detail by the influence of shells in the nascent heavy fragment [13].

Briefly summarized, the evidence for two separate components is the following: (a) The average total fragment kinetic energy for symmetric fission is about 5 MeV smaller than for asymmetric fission; the average values for the

asymmetric and symmetric component follow separately the kinetic energy systematics of asymmetric fission for nuclei with higher Z and of symmetric fission for lower-Z nuclei, respectively[5]. (b) The dependence of the fragment kinetic energy on the excitation energy of the fissioning nucleus is very different for the two components (see below). (c) If analyzed as a function of fragment mass, the width of the kinetic energy distribution shows clear maxima for those fragment masses for which the contribution of both components is about equal; apparently, another contribution is added to the "intrinsic" energy width of each component which results from the difference in average values[5,9]. (d) The fragment excitation energy as represented by the number of evaporated neutrons shows independent evidence for the superposition of two components, becoming especially visible in the number of emitted neutrons as a function of fragment kinetic energy for constant mass ratio. A full and quantitative description is given in ref.[9].

Although there are hints for two components even for U and Pu fission at moderate excitation energies[6] they become most clearly visible for Ra or Ac. Since so far all experiments exhibiting evidence for two-component fission were carried out at higher excitation energies, it remained experimentally undecided whether the two components are associated with two different fission barriers. According to recent calculations on the deformation-dependent nuclear potential energy surface[14-18], the character of the fragment mass split is, in fact, explained as a consequence of either an asymmetrically (pear shape like) or a symmetrically distorted outer fission barrier, with slight hints even for two different saddles in the same nucleus[14,15].

It therefore seemed desirable to measure the fission probability and the fragment anisotropy (presumed to be determined at the barrier) close to the fission threshold, separately for the two mass components. Such a study is not feasible for higher-Z actinide nuclei both because of the inner barrier being the higher one[15] and the extremely low relative yield ($< 10^{-3}$) of the symmetric component close to the barrier; earlier attempts in this direction[19,20] have, in fact, been unsuccessful. In the present experiment, we have therefore investigated fission of Ac and Ra isotopes for which the outer barrier is presumably the higher one. In order to obtain sufficiently low excitation energies, we have investigated fission of ^{226}Ac, ^{227}Ac, ^{228}Ac and of ^{225}Ra, ^{227}Ra induced by the reactions (^{3}He,t), (^{3}He,d), (^{3}He,α), (d,p), on a ^{226}Ra target respectively. It has been proved [21] by cross bombardments and by a comparison with neutron induced fission that indeed direct reactions provide a reliable tool for determining fission thresholds.

2. EXPERIMENT AND DATA ANALYSIS

The experiments were carried out with 23.5-MeV ^{3}He and 18-MeV d beams from the Munich MP accelerator on a 50 μg/cm^2 ^{226}Ra target evaporated on a 20 μg/cm^2 carbon backing. The outgoing light particles from the direct reactions were identified by a ΔE - E telescope mounted at 108° with respect to the beam axis. In coincidence with these, the fission fragments were

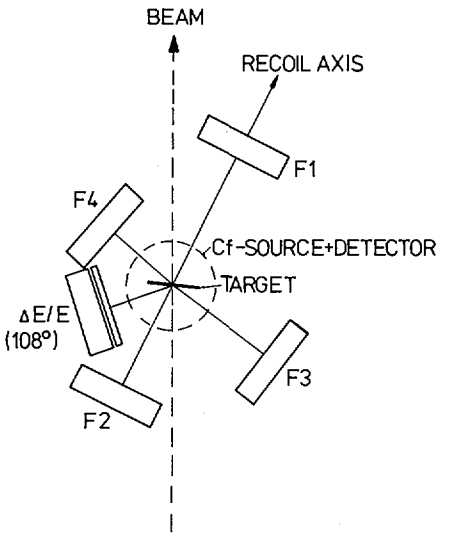

FIG. 1. Diagram of the detector arrangement. The dashed circle indicates the position of a ^{252}Cf source mounted on a Si-detector above the reaction plane for on-line calibration and stabilization of the fission detectors F1 to F4.

measured in two pairs of semiconductor detectors at approximately 0° and 90° with respect to recoil axis in very close geometry. A geometrically correct diagram of the detector arrangement is given in fig.1. On-line calibration and stabilization of the fragment detectors was done by additional coincidences with a further detector placed behind a ^{252}Cf spontaneous fission source. Fast-slow techniques with constant fraction triggers were used throughout, with pile-up rejection in addition for the ΔE-detector. The pulses from the 6 detectors and their time relationship were digitized in 7 ADCs, fed into the Munich PDP8/10 computer system and stored event-by-event on magnetic tape. The incoming data were sorted into four types of events: (a) ΔE-E telescope coincidences; (b) triple coincidences of ΔE/E with either F2 or F4, the closer fission fragment detectors in each direction; (c) quadruple coincidences of ΔE/E with either F1/F2 or F3/F4; (d) events in each of the fission detectors F1 to F4 in coincidence with the ^{252}Cf detector mentioned above.

The data were then analyzed on-line according to excitation energy of the final nucleus, fragment mass and total kinetic energy using the Schmitt calibration method[22] and including corrections for recoil effects, prompt neutron emission and target absorption. Chance coincidences could be exactly corrected for using the time spectra of the coincidences and the singles particle energy spectra.

From the data, the fission anisotropies $\sigma_f(0°)/\sigma_f(90°)$ and the fission probabilities

$$P_f = \frac{\sigma(^3He,pf)}{\sigma(^3He,p)} = \frac{\Gamma_f}{\Gamma_n} \qquad \text{for } \Gamma_f \ll \Gamma_n$$

(and equivalent for the other reactions used) were determined as a function of excitation energy. The denominator $\sigma(^3He,p)$ is obtained from the ΔE-E singles but must be corrected for contaminants from the C-target backing and, specifically in this case, for break-up of the ^3He particle into p+p+n in the Coulomb field of the target nucleus which was investigated separately with coincidences between pairs of $\Delta E/E$ telescopes. The break-up correction influences only the data obtained for the highest excitation energies. In all cases, the "true" singles spectrum has been checked by additional runs with ^3He and d on ^{238}U, assuming that the fission-particle coincidence spectra represent the shape of the reaction singles spectrum, since Γ_f / Γ_n is nearly constant over a wide energy region for the corresponding compound nuclei [21,23] (taking into account the second-chance fission effects and small differences in the Coulomb field between Ra and U). Throughout the paper, the indicated error bars refer to statistical errors only; the systematic error is of the order of 20%.

For $^{226}Ra(^3He,\alpha)^{225}Ra \rightarrow f$ a further correction must be applied for ternary fission of the ^{229}Th compound nucleus formed after ^3He capture. A good quantitative estimate of this correction can be obtained from the observation of α-particle-fission coincidences in the reaction d+ ^{226}Ra, for which the reaction $^{226}Ra(d,\alpha)^{224}Fr \rightarrow f$ is ruled out energetically for the deuteron energy used. The shape of this α spectrum as well as its relative yield are in agreement with similar data on ^{252}Cf spontaneous ternary fission [24]. For the total energy range covered in the experiment, the total amount of this correction is about 20% of the observed events with an estimated relative error of 0.2 included in the error bars for the ^{225}Ra data.

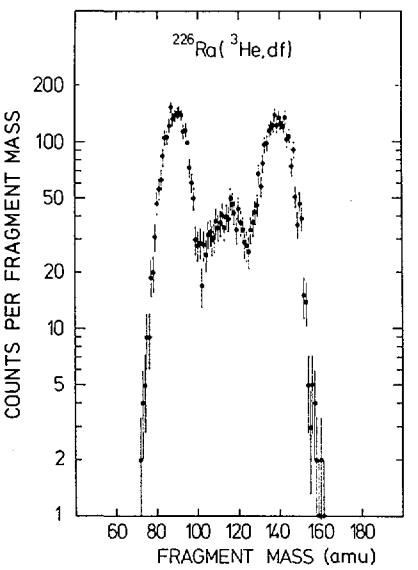

FIG. 2. Fragment mass distribution for fission of ^{227}Ac at excitation energies between 7 and 13 MeV.

The fission probabilities and fragment anisotropies were analyzed both for events of type (b), and for the asymmetric and symmetric component separately (using coincidences of type (c)). Fig.2 shows, for example, the fragment mass spectrum for fission of ^{227}Ac at 0° corresponding to excitation energies between 7 and 13 MeV. The symmetric component was determined from a narrow mass window (in this case $105 < A < 123$) and its corresponding yield multiplied by a scale factor (~ 1.4) transforming the window observed to the area corresponding to a symmetric mass distribution with Gaussian shape [9]. Because of the steeper angle with respect to the target surface for the fission fragments detected, the pair of detectors F1/F2 had a better mass resolution, i.e. no tails from the asymmetric yield in the symmetric window; for F3/F4 a small correction (3% of the asymmetric yield) for such tails had to be subtracted. The sum of the counts for the symmetric and asymmetric components observed in correlated detector pairs F1/F2 or F3/F4 were normalized to the corresponding number of counts observed in F2 or F4 alone, to avoid errors from misalignment of the detectors.

For the two nuclei investigated with the highest statistical accuracy (^{227}Ac and ^{228}Ac) the data were also completely analyzed with respect to the correlated three parameters: nuclear excitation energy, fragment kinetic energy and fragment mass.

3. FISSION PROBABILITY FOR ASYMMETRIC AND SYMMETRIC FISSION

The mass distribution for ^{227}Ac for $7 \leq E_x \leq 13$ MeV as given in fig.2 shows a triple humped curve with clear minima between the three mass yield peaks. Since second-chance fission is excluded here for energetical reasons, we can conclude that both fission modes really occur in the same nucleus, contrary to speculations that one of them is due to fission of another isotope after neutron emission from the originally excited nucleus.

Figs 3 and 4 show fission probabilities and fragment anisotropies as a function of excitation energy in the fissioning nuclei ^{226,227,228}Ac and ^{225,227}Ra, respectively, separately for the symmetric and asymmetric fission modes. In all cases the data presented for the (in most cases dominant) asymmetric component were obtained by subtraction of the curve indicated in the figs. for the symmetric component from the data points for total fission which were measured with higher statistical accuracy (events of type (b)). Only for ^{225}Ra in fig.4 the total fission probability is given in addition, for clarity displaced by a factor of 10.

Several interesting features are directly visible in figs. 3 and 4.

1. Most important, symmetric and asymmetric fission appear, in fact, to be associated with different fission barriers; for all cases except ^{225}Ra the symmetric barriers appear to be higher than the asymmetric ones. This is definitely true for ^{227}Ac and ^{228}Ac, the two cases with the highest statistical accuracy (8.5 MeV compared to 7.3 for ^{227}Ac, 9.2 compared to 7.2 for ^{228}Ac respectively). In these cases, the upper limit for a

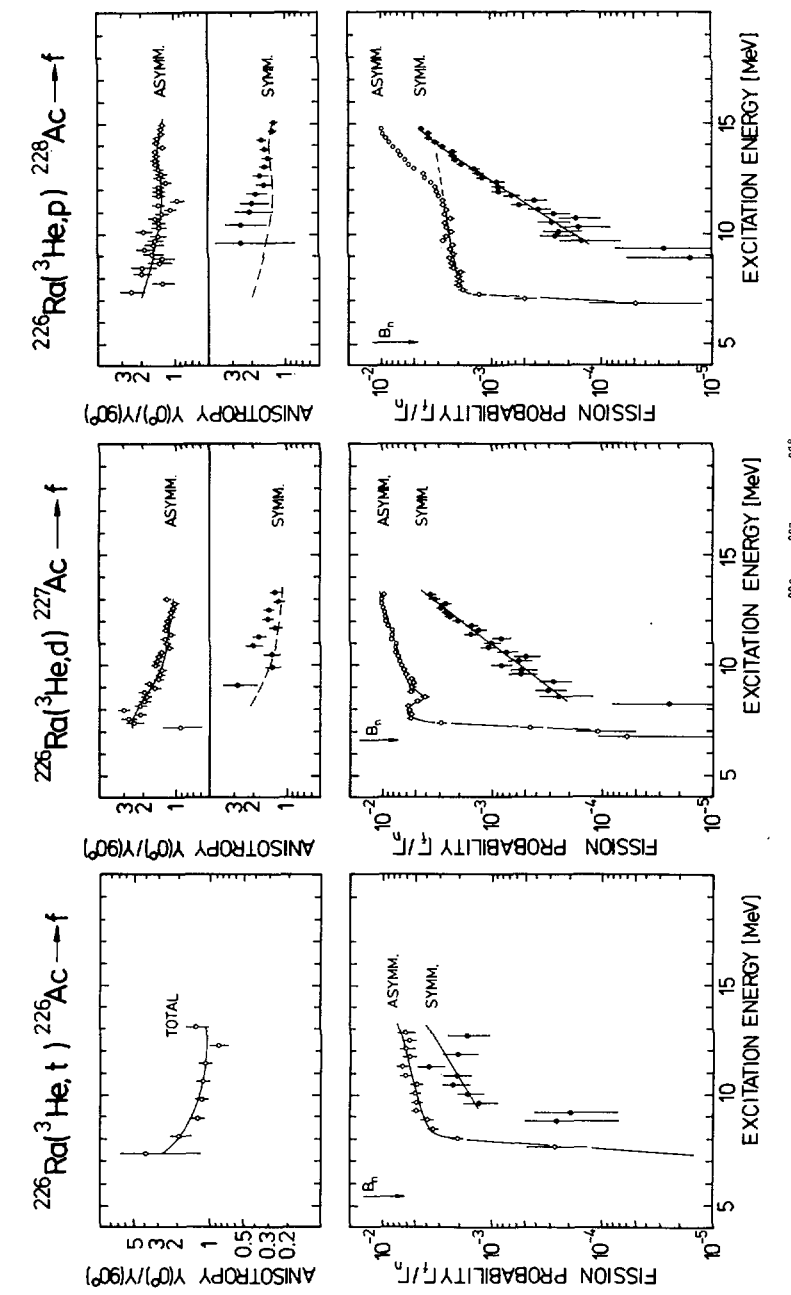

FIG. 3. Fission probabilities and fragment anisotropies for ^{226}Ac, ^{227}Ac and ^{228}Ac as a function of the excitation energy in the fissioning nuclei. Arrows mark the neutron binding energies. Solid lines fitting the asymmetric anisotropy data are repeated as dashed lines in the field showing the symmetric data.

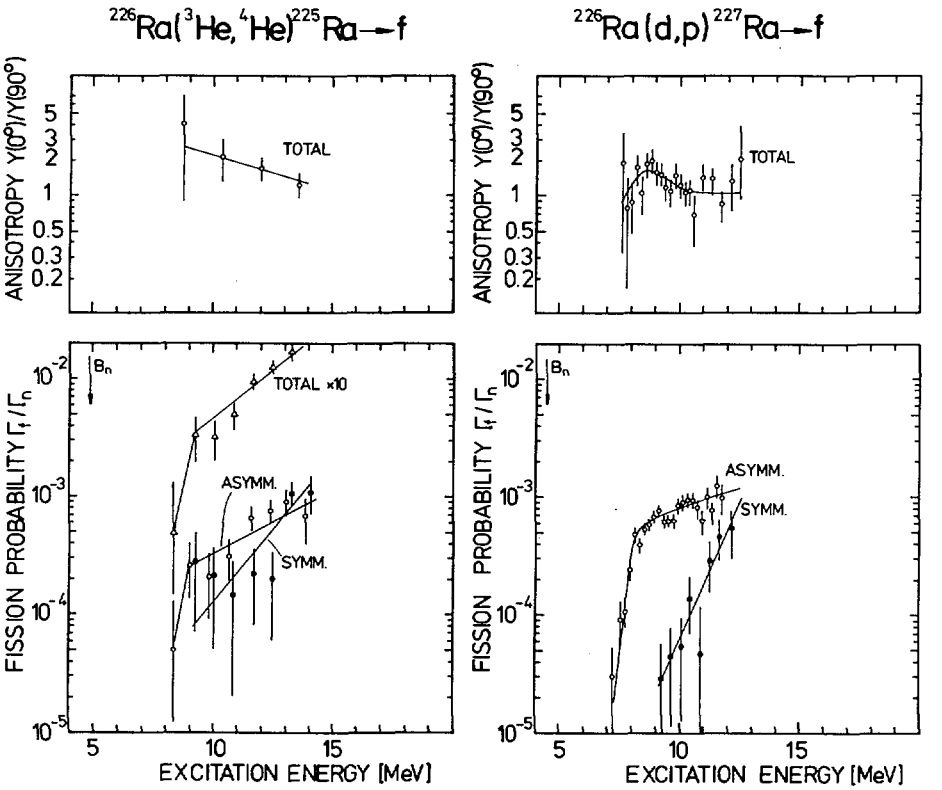

FIG. 4. Fission probabilities and fragment anisotropies for ^{225}Ra and ^{227}Ra as a function of the excitation energy in the fissioning nuclei. Arrows mark the neutron binding energies.

possible symmetric yield averaged over the region between the two thresholds relative to the symmetric yield just above the symmetric threshold is 6% (95% confidence limit). The fragment angular anisotropies also seem to be different for the two mass components; the dashed line in the plots for symmetric fission (top of fig.3) marks the anisotropy for the asymmetric component. This difference further supports the interpretation of the different threshold behaviour as really being due to separate barriers.

2. Following the well-known trend at the lower-Z actinides, the atomic number of the fissioning nucleus appears to have a predominant influence on the total fission probability. From Ra to Ac, adding one single proton increases the fission probability near the threshold by almost a factor of 10. Nevertheless, the absolute fission probabilities, especially for symmetric fission, are extremely small, which, of course, presents the major difficulty of these experiments.

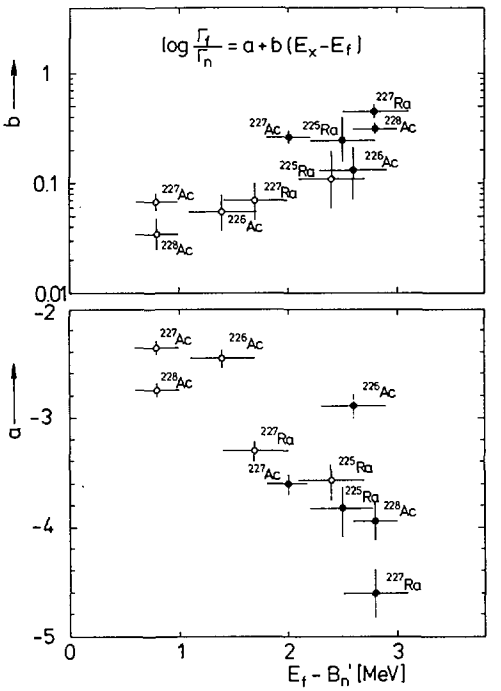

FIG. 5. Intercept a and slope b of the function $\log(\Gamma_f/\Gamma_n) = a + b(E_x - E_f)$ as a function of $E_f - B_n'$ for all nuclei investigated, plotted separately for the asymmetric (open circles) and symmetric (filled circles) components. The quantities E_x, E_f and B_n' are explained in the text.

3. The competition of symmetric and asymmetric fission seems to be governed more by the neutron number. Clearly, both for Ra and Ac the nuclei investigated with the smallest neutron numbers (^{225}Ra and ^{226}Ac) reveal the biggest relative contributions of symmetric fission.

4. The fission probability for both the symmetric and asymmetric component rises exponentially with increasing excitation energy, generally for the symmetric component much steeper than for the asymmetric one. In the logarithmic plots of figs. 3 and 4, the slope of the fission probability $\partial(\log(\Gamma_f/\Gamma_n))/\partial E_x$ for both fission modes remains constant for at least 5 MeV above the barrier (the increase above the dotted line for ^{228}Ac in fig. 3 is caused by the onset of second-chance fission) and is much smaller than expected on the basis of simple statistical model considerations [25]. However, it seems to be influenced by the same parameters used in ref. [25] to describe the statistical aspects of neutron evaporation vs. fission competition. Fig. 5 shows the slope b and the intercept a of the function $\log(\Gamma_f/\Gamma_n) = a+b(E_x-E_f)$ as a function of E_f-B_n', E_f being the fission barrier and B_n' the neutron binding energy of the daughter nucleus after neutron evaporation, corrected for even-odd neutron number

effects ($B_n' = B_n + \Delta$; $\Delta = 0$ for odd N and equal to the neutron energy gap for even-N daughter nuclei [25]; for a nucleus (Z,N) it has been deduced by interpolating differences in the neutron binding energies [26] for the nuclei (Z,N), (Z, N-1) and (Z,N), (Z,N+1)). Although the observed slopes are higher and the fission probabilities are lower for symmetric compared to asymmetric fission, both components seem to follow the same trend.

5. Most surprisingly, however, the yield of the symmetric component even exceeds that of the asymmetric component already a few MeV above the threshold, as is evident for ^{227}Ra and ^{228}Ac within the range of our data and has been observed also for ^{227}Ac [8-10]. This result cannot be due to second-chance fission as has been speculated before [27]. Nor can it be explained [27] as due to a washing-out of shell effects with increasing excitation energy, which, according to recent calculations [28], should be negligible at these low energies. In a simple statistical model for the competition of symmetric and asymmetric fission, level density considerations to be valid would require the level density parameter a_s for levels associated with the symmetric saddle to exceed that for level densities above the asymmetric saddle, a_f, by more than 30% for ^{227}Ra and ^{228}Ac.

6. The fission probability for the asymmetric component of ^{227}Ac shows a definite structure in the region of the fission threshold. Although the minimum in the structure might be correlated with the onset of symmetric fission, it could more likely be caused by the competing neutron channel (the difference between fission threshold and neutron binding energy being only 0.7 MeV in that case), since similar effects are not observed for the other reactions in Figs 3 and 4. A similar structure (a "plateau") observed in the ^{226}Ra(n,f) reaction at $8.5 \leq E_x \leq 9.5$ MeV in ^{227}Ra [29] is not confirmed in our ^{226}Ra(d,pf) data.

In conclusion, we have found experimentally the existence of different barriers for symmetric and asymmetric fission in the same nucleus, suggesting that the character of the fragment mass split is already predetermined at the saddle stage of the fission process. Although this seems to be in accord with the expectations from shell model calculations [14, 15], a deeper understanding specifically of the rapid increase of the symmetric fission probability above the asymmetric one has to await further detailed analysis.

4. FRAGMENT MASS AND ENERGY DISTRIBUTIONS

Aside from the fundamental question on different barriers for symmetric and asymmetric fission, the observed data contain a rather comprehensive information on the fragment mass and kinetic energy distributions as a function of excitation energy of fissioning Ac-nuclei. Although much has been known on this subject before [5,8-10] a more detailed presentation of our data on the reactions observed with the highest statistical accuracy, i.e. ^{226}Ra(^{3}He,pf) and ^{226}Ra(^{3}He,df), seems reasonable since only the present data allow one to exclude influences from second- and higher-chance fission.

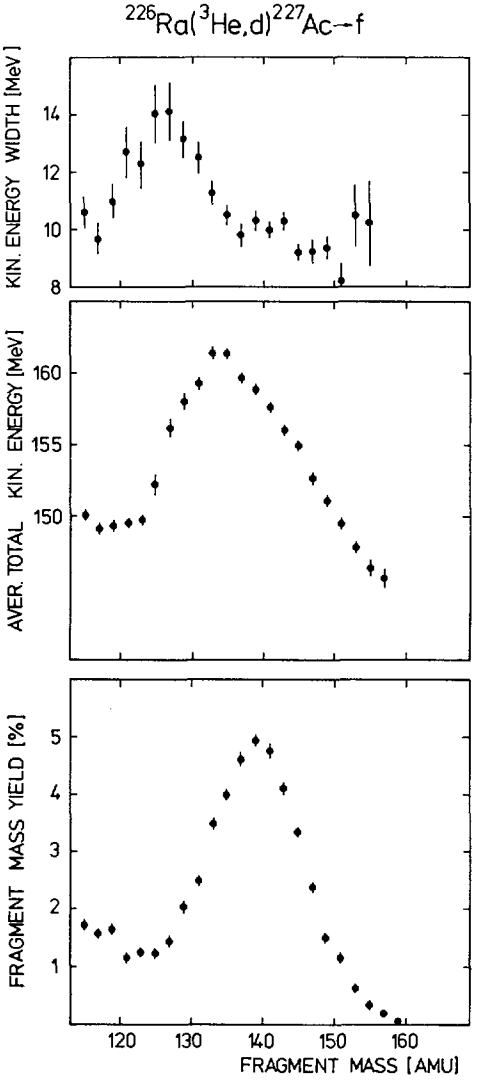

FIG. 6. Mass yield, average total kinetic energy and width of the kinetic energy distribution as a function of the heavy fragment mass for the reaction ^{226}Ra (^{3}He, df), the data for fragment masses A and 227-A being averaged. Data shown refer to excitation energies in ^{227}Ac between 7 and 13 MeV (first-chance fission only).

Fig.6 shows the fragment mass yield, the average total kinetic energy and the width of the kinetic energy distribution as a function of fragment mass for all events observed in the reaction ^{226}Ra(^{3}He,df). Although this sum is weighted in a complicated way by the fission probability and by the energy-dependent (^{3}He,d) cross-section (high deuteron energy corresponds to low excitation energy), it contains only data for

excitation energies in ^{227}Ac(7 MeV $\leq E_x \leq$ 13 MeV) and therefore refers to first-chance fission only, E_x second-chance fission being ruled out by energy considerations. The data show the same features as those known for higher-energy fission of ^{227}Ac[9,10] and similar nuclei:

a minimum in the mass distribution around fragment mass A=125;

an average fragment kinetic energy being about 10 MeV lower for near symmetric mass splits (A≈114) with respect to A=134 to 136 and the subsequent decrease for higher fragment masses, well known for asymmetric fission and explained by shell effects in the nascent fragment nuclei[1];

a distinct maximum of the width of the kinetic energy distribution for fragment masses A=128 to 130, which can be interpreted as strong evidence for the existence of two components as outlined in section 1. For ^{226}Ra(^{3}He,pf), the data observed look rather similar. For $E_x >$ 12 MeV they contain contributions of second-chance fission E_x(see fig.3).

In figures 7 and 8, the average kinetic energy is analyzed for the symmetric and asymmetric component separately as a function of excitation energy in the fissioning nuclei ^{227}Ac and ^{228}Ac, respectively. (The squares in fig.8 refer to data corrected for second-chance fission using the data of figs.7 and 3). The average values for both components not only appear to be different in absolute value, indicating that the distances of the charge centres of the nascent fragments at scission are different for the two components. They also change with excitation energy in a different way. For asymmetric fission, the fragment energy decreases with excitation energy by

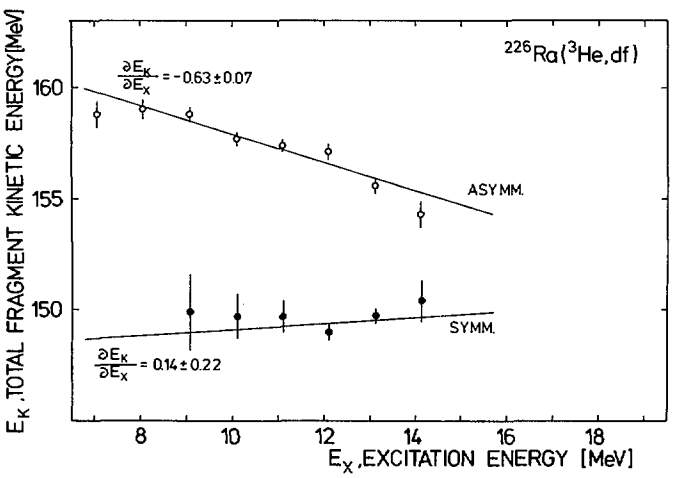

FIG. 7. Average total fragment kinetic energy for the asymmetric and symmetric component as a function of excitation energy in the fissioning nucleus ^{227}Ac. Lines represent least squares fits.

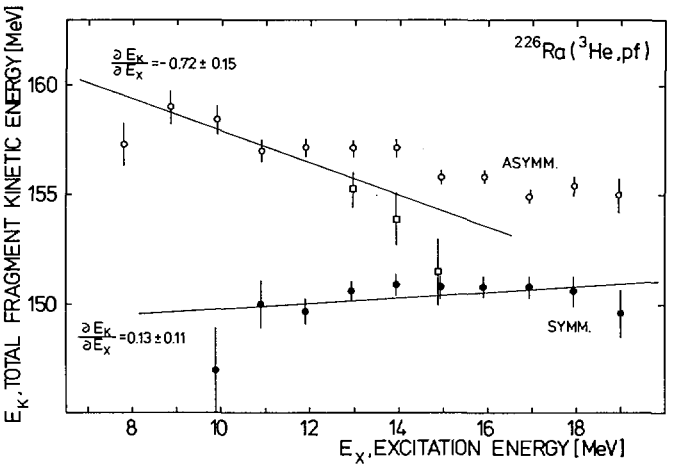

FIG. 8. Average total kinetic energy for the asymmetric and symmetric component as a function of excitation energy of the fissioning nucleus ^{228}Ac. Open squares represent data for the asymmetric component corrected for second-chance fission. Lines represent least squares fits (in the case of asymmetric fission, for the corrected data points).

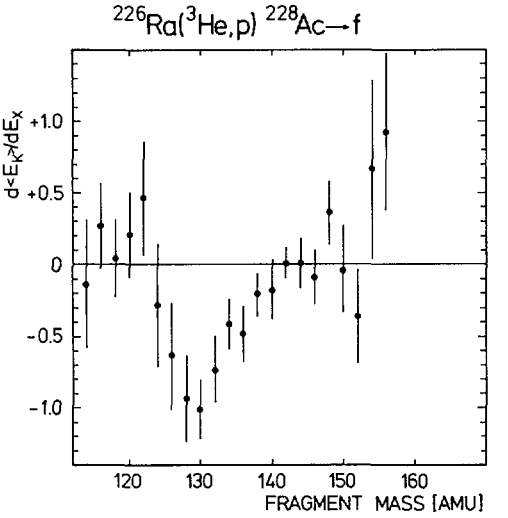

FIG. 9. Slope of the average fragment kinetic energy vs. excitation energy in ^{228}Ac, $\partial\langle E_k\rangle/\partial E_x$, plotted as a function of heavy fragment mass, the data for fragment masses A and 228-A being averaged (not corrected for effects of second-chance fission).

$\partial E_k/\partial E_x = -0.72 \pm 0.15$ for ^{228}Ac and $\partial E_k/\partial E_x = -0.63 \pm 0.07$ for ^{227}Ac (corrected for second-chance fission), very similar to $\partial E_k/\partial E_x = -0.54 \pm 0.04$ found for the (asymmetric) fission reaction ^{239}Pu(d,pf) [30]. In particular, this decrease is greatest for the near magic heavy fragments with A ≈ 132-134. This is more clearly shown in fig.9, where for ^{228}Ac the average slope $\partial E_k/\partial E_x$ is plotted as a function of fragment mass (not corrected for second-chance fission effects). This trend is consistent with earlier measurements [30-32] and explicitely discussed in refs. [31,33]. Contrary to asymmetric fission, the fragment kinetic energy for the symmetric component does not change significantly with excitation energy (if at all, it rather increases than decreases; the comparative values for $\partial E_k/\partial E_x$ are 0.14 ± 0.22 and 0.13 ± 0.11 for ^{227}Ac and ^{228}Ac, respectively). The different behaviour for symmetric and asymmetric fission also in this respect is another piece of evidence for the existence of two separate fission modes.

Thus it seems that after the gross determination of the symmetric or asymmetric character of fission made already at the barrier, the two components follow a different path with no or little overlap in the development from the barrier to the scission configuration.

REFERENCES

[1] SCHMITT, H.W., Proc. 2nd IAEA Symp. on Physics and Chemistry of Fission, Vienna 1969, p.67.
[2] PLASIL, F., BURNETT, D.S., BRITT, H.C., THOMPSON, S.G., Phys. Rev. 142 (1966) 696.
[3] PLASIL, F., SCHMITT, H.W., Phys. Rev. C5 (1972) 528.
[4] JENSEN, R.C., FAIRHALL, A.W., Phys. Rev. 109 (1958) 942; Phys. Rev. 118 (1960) 771.
[5] BRITT, H.C., WEGNER, H.E., GURSKY, J.C., Phys. Rev. 129 (1963) 2239.
[6] BRITT, H.C., WHETSTONE Jr., S.L., Phys. Rev. 133 (1964) B 603.
[7] UNIK, J.P., HUIZENGA, J.R., Phys. Rev. 134 (1964) B 90.
[8] FERGUSON, J.M., READ, P.A., Phys. Rev. 139 (1965) B 56.
[9] KONECNY, E., SCHMITT, H.W., Phys. Rev. 172 (1968) 1213 and 1226.
[10] PERRY, D.G., FAIRHALL, A.W., Phys. Rev. C4 (1971) 977.
[11] HOLUBARSCH, W., PFEIFFER, E., GÖNNENWEIN, F., Nucl. Phys. A171 (1971) 631.
[12] NIX, J.R., SWIATECKI, W.J., Nucl. Phys. 71 (1965) 1.
[13] MUSTAFA, M.G., MOSEL, U., SCHMITT, H.W., Phys. Rev. C7 (1973) 1519.
[14] MÖLLER, P., Nucl. Phys. A192 (1972) 529.
[15] PAULI, H.C., Physics Reports 7C (1973) No.2.
[16] MOSEL, U., SCHMITT, H.W., Phys. Rev. C4 (1971) 2185.
[17] BOLSTERLI, M., FISET, E.O., NIX, J.R., NORTON, J.L., Phys. Rev. C5 (1972) 1050.
[18] PASHKEVICH, V.M., Nucl. Phys. A169 (1971) 275.
[19] KIVIKAS, T., FORKMAN, B., Nucl. Phys 64 (1965) 420.
[20] VANDENBOSCH, R., UNIK, J.P., HUIZENGA, J.R., IAEA Symp. on the Physics and Chemistry of Fission, Salzburg 1965, Vol I., p. 547.
[21] BRITT, H.C., CRAMER, J.D., Phys. Rev. C2 (1970) 1758.

[22] SCHMITT, H.W., KIKER, W.E., WILLIAMS, C.W., Phys. Rev. 137 (1965) B837.
[23] BRITT, H.C., RICKEY Jr., F.A., HALL, W.S., Phys. Rev. 175 (1968) 1525.
[24] FRAENKEL, Z., Phys. Rev. 156 (1967) 1283.
[25] HUIZENGA, J.R., VANDENBOSCH, R., in Nuclear Reactions, edited by P.M.Endt and P.B.Smith (North Holland Publ. Co., Amsterdam 1962), Vol II., p. 42.
[26] WAPSTRA, A.H., GOVE, N.B., Nucl. Data Tables 9 (1971) 303.
[27] TSANG, C.F., WILHELMY, J.B., Nucl. Phys. A184 (1972) 417.
[28] JENSEN, A.S., DAMGAARD, J., Nucl. Phys. A203 (1973) 578.
[29] BABENKO, Yu.A., IPPOLITOV, V.T., NEMILOV, Yu.A., SELITSKII, Yu.A., FUNSHTEIN, V.B., Yad. Fiz. 10 (1969) 233 [Sov. J. Nucl. Phys. 10 (1969) 133].
[30] MILTON, J.C.D., FRASER, J.S., SPECHT, H.J., Journ. de Physique 33 (1972) C5-I-15.
[31] KONECNY, E., NÖRENBERG, W., SCHMITT, H.W., Nucl. Phys. A139 (1969) 513.
[32] BURNETT, S.C., FERGUSON, R.L., PLASIL, F., SCHMITT, H.W., Phys. Rev. C3 (1971) 3023.
[33] NÖRENBERG, W., Proc. 2nd IAEA Symp. on Physics and Chemistry of Fission, Vienna 1969, p. 51.

DISCUSSION

H. C. BRITT: Your Γ_f/Γ_n results show structures that look very much like subbarrier resonance structures, especially in the case of ^{227}Ac, and I am curious to know what the experimental energy resolution was in these experiments. If the structures are subbarrier resonances, then it seems possible that the estimated asymmetric barrier heights might be too low, as was the case for ^{240}Pu before we took resonance phenomena into account.

E. KONECNY: The experimental energy resolution was about 100 keV FWHM. For statistical reasons, however, we have summed over 200-keV energy intervals. The structure observed is not broadened by insufficient resolution. It is very interesting that the dip in the structure for ^{227}Ac occurs exactly at the position where the symmetric fission sets in. We have therefore looked for similar structures in the data for the other nuclei investigated and have not found any with statistical significance.

H. J. SPECHT: We have discussed three possible explanations for the structure in the case of ^{227}Ac. First of all, one might suspect transmission resonances below the barrier, as Mr. Britt has pointed out. However, the width of the structure is of the order of 1 MeV, which is much more than the instrument resolution, but also much more than the width normally observed for such resonances. As in the other cases, the fission probability increases extremely rapidly at the barrier, in accordance with the behaviour of a single rather than a double barrier.

Secondly, as Mr. Konecny has already said, the minimum in the structure coincides exactly with the onset of symmetric fission. This looks very much like a destructive interference between two coupled channels, and, in fact, the size of the dip even agrees quantitatively with such an exciting speculation. Unfortunately, however, we just do not find this phenomenon in the other nuclei investigated.

The third and I think the most likely explanation at the moment is the presence of some structure in the competing neutron channel. In the case of ^{227}Ac, the difference between the fission threshold and the neutron binding energy is only about 1 MeV, whereas in all the other cases this difference amounts to 2-3 MeV.

C.F. TSANG: I should just like to raise again the idea that Dietrich suggested in Session IV in the discussion on Bjørnholm's paper[1]. One can perhaps understand the behaviour of Γ_f/Γ_n for asymmetric and symmetric fission based on Bjørnholm's enhancement of Γ_f/Γ_n for asymmetric shapes. The observation that initially the asymmetric Γ_f/Γ_n is much larger than the symmetric one may be due in part to this enhancement. Then the rate of increase of Γ_f/Γ_n as a function of excitation energy for the asymmetric case being much less than that for the symmetric case may be explained by the washing-out of this enhancement.

H. GROENING: The data for ^{226}Ra seem to indicate that the fission barrier for symmetric fission would be much thinner than that for asymmetric fission. I understand that Nix has mapped the potential energy surface for Ra and I wonder if the calculations bear this out.

Also, I do not think that the data which you obtained differ greatly from those of Babenko and co-workers[2] in the ^{226}Ra(n,f) reaction. Both show a plateau at roughly the same energies with a subsequent sudden increase. Your data for ^{225}Ra seem to show an analogous phenomenon.

E. KONECNY: The statistical accuracy of our ^{227}Ra data is too small to establish the slope of the symmetric threshold. From the data on ^{227}Ac and ^{228}Ac, however, we find no significant differences in the steepness of the symmetric and asymmetric threshold. The subsequent rise in fission probability for the symmetric component is attributed to the neutron emission vs fission competition and not to the penetration of a barrier.

The hint of a (statistically non-significant) "plateau" in our data on ^{227}Ra relates to excitation energies of about 9.4 to 10 MeV compared to the plateau observed by Babenko and co-workers at about 8.5 to 9.5 MeV. At these latter energies we observe a fairly steep rise in the fission probability instead. For ^{225}Ra our data are statistically not precise enough to deduce any structure.

D.G. PERRY: Would you comment as to why, in the case of ^{228}Ac, one sees a rise attributed to second-chance fission in the asymmetric component, but not a corresponding increase in the symmetric component?

E. KONECNY: At the onset of second-chance asymmetric fission at an excitation energy of about 12.5 MeV in ^{228}Ac the first-chance asymmetric fission probability is about 2.5×10^{-3}, compared to an asymmetric fission probability of about 5×10^{-3} in ^{227}Ac; thus second-chance effects become very clearly visible. For symmetric fission, second-chance fission effects may be expected at about 14 MeV in ^{228}Ac (very close to the end of the energy range covered in the experiment), where the first-chance symmetric fission probability is also about 2.5×10^{-3}. The symmetric fission probability for ^{228}Ac near the threshold, however, is only about 3×10^{-4}. Therefore second-chance effects for symmetric fission do not become observable in our data.

---

[1] BJØRNHOLM, S., BOHR, A., MOTTELSON, B.R., Paper IAEA-SM-174/205, these Proceedings, Vol. 1.

[2] BABENKO, Yu.A., et al., Sov. J. Nucl. Phys. 10 (1969) 133.

S. BJØRNHOLM: Do you still see the bump around 8 MeV in ^{227}Ac when you sum the symmetric and asymmetric fission probabilities?

E. KONECNY: Yes.

H. J. SPECHT: One should distinguish between an interference effect and simple competition between uncoupled channels. In the first case, the sum will still show structure, whereas in the latter it will not.

S. S. KAPOOR (Chairman): I should like to point out that your results showing a larger anisotropy for symmetric mass divisions are in agreement with the results of some of our measurements carried out about eight years ago for the 4-MeV neutron-induced fission of ^{235}U. These results seem to imply that not only K_0^2 but also mass division should be determined at the fission transition point.

E. KONECNY: You are correct. The differences in anisotropies for symmetric and asymmetric fission support the theory that the two fission channels proceed over different barriers associated with different K-distributions. As far as correlations between fragment anisotropies and the finer details of the mass division are concerned, no conclusions can be drawn on the basis of our results.

FRAGMENT MASS AND KINETIC ENERGY DISTRIBUTIONS FOR FISSIONING SYSTEMS RANGING FROM MASS 230 TO 256*

J.P. UNIK, J.E. GINDLER, L.E. GLENDENIN, K.F. FLYNN,
A. GORSKI, R.K. SJOBLOM
Chemistry Division, Argonne National Laboratory,
Argonne, Ill., United States of America

Abstract

FRAGMENT MASS AND KINETIC ENERGY DISTRIBUTIONS FOR FISSIONING SYSTEMS RANGING FROM MASS 230 TO 256.

Pre-neutron-emission fragment mass and total kinetic energy (TKE) distributions, as well as mass-energy correlations, have been obtained for thermal-neutron-induced fission of ^{229}Th, ^{233}U, ^{235}U, ^{239}Pu, ^{245}Cm, ^{249}Cf, ^{254}Es and spontaneous fission of ^{246}Cm, ^{248}Cm, ^{250}Cf, ^{252}Cf, ^{254}Cf and ^{256}Fm using the double-energy method. Post-neutron-emission mass distributions of fragments formed in the thermal-neutron-induced fission of ^{251}Cf, ^{254}Es, ^{255}Fm and spontaneous fission of ^{253}Es, ^{254}Fm and ^{256}Fm have been obtained radiochemically. These data, covering a wide range of different fissioning systems, make possible detailed examinations of many aspects of the fission process. All the double-energy data were analysed in a self-consistent manner (identical energy calibration methods, corrected for neutron-emission effects, experimental resolution, fragment energy losses in target materials, etc.) so that the precision of reported $\overline{TKE}$ values and fragment masses, relative to the energy calibration method used, are believed to be better than ±0.5 MeV and ±0.2 amu, respectively. Several of the pre-neutron mass distributions, particularly for ^{229}Th(n, f), ^{235}U(n, f) and ^{248}Cm(sf), exhibit pronounced fine structure. This observed fine structure is discussed in terms of enhanced formation of even-Z fragments in fission, nuclear charge division and fragment shell structures at large deformations. The total kinetic energy released in the fission of ^{246}Cm and ^{250}Cf resulting from neutron capture is greater than in the respective cases of spontaneous fission. However, the fraction of initial excitation energy appearing as additional $\overline{TKE}$ in the fission of ^{250}Cf is substantially greater than for ^{246}Cm, consistent with existing neutron emission probability measurements. The neutron emission function $\bar{\nu}(A)$ for pre-neutron-emission fragment masses has been indirectly determined by comparison of cumulative pre- and post-neutron-emission mass yields for thermal-neutron-induced fission of ^{254}Es and spontaneous fission of ^{252}Cf and ^{256}Fm. The trends in $\bar{\nu}(A)$ and the characteristics of the mass distributions as a function of the fissioning nucleus and excitation energy are discussed.

1. INTRODUCTION

The large amount of data published in the past on fission fragment mass and kinetic energy distributions has contributed greatly toward our qualitative understanding of many aspects of the fission process. However, recent, rapid advancements in fission theory now require data of greater precision, studies of a wider range of fissioning systems (particularly the heaviest elements, such as fermium), and investigations of the many, finer details of the fission process. Unfortunately, complete post-neutron-emission (secondary) mass distributions of the fission products are presently known for only a few of the more readily available isotopes of uranium and plutonium and for ^{252}Cf. Physical measurements of the pre-neutron-emission (primary) mass and kinetic energy distributions and their various

* Work performed under the auspices of the US Atomic Energy Commission.

TABLE I. Summary of Pre-Neutron-Emission Fission Fragment Data[a]

Fissioning System	Source Preparation[b]	Events Analyzed (x 10^5)	$\bar{A}_L$	$\bar{A}_H$	σ_M^C	$\bar{E}_L$	$\bar{E}_H$	$\overline{TKE}$	σ_{TKE}^C
^{229}Th(n,f)	IS	1.0	89.6	140.4	4.7	99.8	63.8	163.6	8.2
^{233}U(n,f)[d]	V	3.7	95.0	139.0	5.6			172.1	9.9
^{235}U(n,f)	V	2.5	96.5	139.5	5.6	101.4	70.4	171.8	10.3
^{239}Pu(n,f)[d]	V	7.6	100.4	139.6	6.4			177.1	11.5
^{245}Cm(n,f)	IS	1.1	105.3	140.7	6.7	105.1	79.0	184.2	11.7
^{246}Cm(sf)	IS	4.3	106.0	140.0	6.3	104.5	79.4	183.9	10.6
^{248}Cm(sf)	IS	2.6	107.0	141.0	6.6	103.4	78.7	182.2[e]	10.5
^{249}Cf(n,f)	IS	2.6	108.2	141.8	7.4	107.0	82.0	189.1	13.0
^{250}Cf(sf)	IS	3.3	107.5	142.5	6.9	106.4	80.5	187.0	11.3
^{252}Cf(sf)	T	2.5	108.5	143.5	7.1	105.7	80.2	185.9	11.6
^{254}Cf(sf)	IS	2.5	110.6	143.4	7.2	105.3	81.5	186.9	11.8
^{254}Es(n,f)	IS	.5	112.7	142.3	8.1	108.1	86.2	194.3	15.9
^{256}Fm(sf)	IS	.1	113.9	142.1	7.6	109.6	88.3	197.9	14.4

[a] Estimated relative precision for $\bar{A}_{L,H}$, $\bar{E}_{L,H}$ and $\overline{TKE}$ are ±0.1 amu, ±0.2 MeV and ±0.5 MeV, respectively.

[b] IS = isotope separator, V = vacuum volatilization, T = self transfer

[c] Uncorrected for experimental resolution

[d] Data taken from ref. [1]

[e] Error ±0.9 MeV

correlations have been made for a much larger number of fissioning systems. However, much of this data is of limited value because of uncertainties associated with the different methods used for energy calibration, the corrections applied for neutron emission from the fragments, the quality of the sources, the experimental resolutions, etc.

A comprehensive program is currently underway to investigate fragment mass and kinetic energy distributions for a wide range of nuclides that fission either spontaneously (sf) or when irradiated with thermal neutrons (n,f). All data are collected and analyzed in a complete, self-consistent manner to attain the highest relative precision and absolute accuracy possible with available experimental methods. Secondary mass distributions are determined radiochemically, whereas primary mass distributions are obtained with solid-state detectors using the well-established double-energy method. These two methods are complementary since the radiochemical method can be used to obtain mass distributions for many fissioning systems where physical measurements are not feasible because of extremely low fission specific activities, low fission-to-alpha emission branching ratios, etc. On the other hand, for those fissioning systems where primary and secondary mass distributions are known, neutron emission probabilities, $\bar{\nu}(A)$, as a function of fragment mass can be indirectly obtained. The double-energy method provides a great deal of additional information, such as fragment kinetic energies and fragment mass and kinetic energy correlations. In the present investigation data have been obtained for fissioning nuclides ranging from ^{230}Th to ^{256}Fm. These results, combined with our earlier studies of nuclear charge distribution [1] and mass distribution fine structure [2] in fission, now make possible detailed examinations of many aspects of the fission process.

2. EXPERIMENTAL PROCEDURE

2.1. Double-Energy (Physical) Method

The fissioning systems studied by the physical method are listed in Table I. As indicated in this table, most of the sources were prepared by direct collection of de-accelerated isotope separator beams of the heavy-element isotopes onto thin (90 $\mu g/cm^2$) nickel foils. To avoid penetration of the heavy-element materials into the backings, collection voltages of only 300 volts were used. The ^{233}U, ^{235}U and ^{239}Pu targets were prepared by vacuum volatilization of the respective tetrafluorides onto the nickel backings, and ^{252}Cf sources were prepared by the self-transfer method. Source thicknesses were kept quite low to minimize uncertainties caused by fragment energy losses in the target materials. Calculated energy losses were used for the majority of the sources which had energy losses of less than 0.2 MeV based upon the measured thicknesses. Energy losses were measured directly for those few sources having energy losses greater than 0.2 MeV. As a result of these precautions and measurements the uncertainties associated with the energy losses of fragments in the target materials are generally less than ± 0.1 MeV.

Coincident fission fragments were detected by two 4-cm^2 gold-surface-barrier silicon detectors. The resultant pulse heights were recorded event-by-event onto magnetic tape for subsequent off-line data processing. All data were taken with an identical experimental arrangement and electronics, similar to those described in Ref. [1]. The fragment masses and kinetic energies were calculated event-by-event using an iterative technique. Post-neutron-emission kinetic energies of complementary fragments were first calculated from the recorded pulse heights using the mass-dependent energy calibration based on a ^{252}Cf fission fragment energy spectrum [3]. The post-neutron-emission kinetic energies were then transformed to pre-neutron-emission energies by a suitable correction for the average effects of neutron emission from the fragments. Published neutron emission functions, $\bar{\nu}(A)$, were used for the $^{233}U(n,f)$, $^{235}U(n,f)$, $^{239}Pu(n,f)$ and $^{252}Cf(sf)$ fissioning systems [4-6]. Neutron emission probabilities as a function of fragment mass are not known for the other cases studied. Therefore, the appropriate shape of the neutron function for $^{229}Th(n,f)$ was assumed to be the same as that measured for $^{235}U(n,f)$ [6], and the reported shape of the $^{252}Cf(sf)$ neutron function [4] was used in the fragment mass and energy computations for Cm, Cf, Es and Fm isotopes. Uncertainties introduced by these assumptions for the shapes of the $\bar{\nu}(A)$ functions are discussed in Sect. 5. In all cases, the neutron functions were normalized to give the appropriate measured average total neutron emission ($\bar{\nu}_T$) values [7] when averaged over the computed mass distributions,and corrections were included in these transformations for the dependence of $\bar{\nu}(A)$ on the total kinetic energy release. The primary fragment masses were then calculated from the pre-neutron-emission energies through the conservation laws of mass and linear momentum. The iteration procedure began with an estimate of the fragment masses and subsequently used results of the preceeding iteration until convergence criteria were met for the computed masses and kinetic energies.

By using the same experimental arrangement and electronic equipment, extremely thin targets and backing materials, a single consistent energy calibration method and neutron emission correction method, and by making the necessary second order corrections, the relative precision of reported average total kinetic energy values and fragment masses (relative to the energy calibration method used) are believed to be better than ± 0.5 MeV and ±0.2 amu, respectively. The absolute accuracies are more difficult to estimate since they are primarily dependent upon poorly understood inherent uncertainties in the energy calibration method used. However, an analysis of the data taken in this work for $^{235}U(n,f)$ and $^{252}Cf(sf)$ using a new, totally independent energy calibration method [8] yielded average values for the masses and total kinetic energies within 0.1 amu and 0.8 MeV, respectively, of those reported here. This new calibration procedure is based on the energy response of surface barrier detectors to heavy ions ranging from alpha particles to low-energy uranium ions and depends upon the mass, nuclear charge and energy of the ions. In comparison, the currently used calibration method [3] depends only on the mass and energy of the fragments. Although the new calibration method appears to be applicable over a wider range of energies and masses than the existing method, the parameterization of the new calibration

method must be more fully studied before it can be universally applied. However, since the two independent calibration methods yield almost identical results for low-excitation energy fission of the actinide elements (within their respective estimated errors), the results quoted here based on the existing calibration method are believed to have an absolute uncertainty of ± 0.2 amu and ± 1 MeV for the average masses of the light and heavy fragment groups and total kinetic energy release, respectively.

2.2. Radiochemical Method

Radiochemical measurements of the fission product mass distributions were made for the spontaneous fission of ^{253}Es, ^{254}Fm, ^{256}Fm and the thermal-neutron-induced fission of ^{251}Cf, ^{254}Es, and ^{255}Fm. Each of the above nuclides after chemical purification accounted for essentially all of the observed fission events with the exception of the ^{255}Fm samples for which corrections were made for growth of ^{251}Cf during the neutron irradiations. Chemical purification was achieved by separating the desired elements from other actinide elements on a cation exchange column using Dowex-50 resin in the ammonium form and α-hydroxyisobutyric acid as the elutriant [9]. Whenever purification from fission products or inert salts was required, a column of Aliquat-336 (a mixture of trioctyl and tridecyl methyl ammonium chloride) adsorbed on hydrophobic diatomaceous earth [10, 11] was used. Rare earth fission products were removed by elution with a 1M NH_4SCN - 0.01M H_2SO_4 solution. The desired element was then eluted with 0.02M H_2SO_4. Further purification was achieved by loading the 0.02M H_2SO_4 solution onto a column of di(2-ethyl hexyl) orthophosphoric acid (HDEHP) adsorbed on diatomaceous earth and eluting the column with various concentrations of hydrochloric acid [12].

Final samples of the isotopes were prepared by evaporating a tetraethylene glycol solution of the element as the nitrate or chloride on a 0.005-inch-thick platinum plate. This gave samples that were well-distributed and thin enough to collect recoiling fission fragments on catcher foils. Aluminum catcher foils were used for spontaneously fissioning samples, whereas polyethylene catcher foils were used for thermal-neutron-induced fission to avoid interference by neutron-activated impurities in aluminum. In most cases, the catcher foils were in intimate contact with the fissioning source. In a few cases, a 0.00025-inch mylar film was interposed between the fissioning source and catcher foil to prevent transfer of the actinide source material and thus avoid possible contamination of lanthanide fission products with alpha activity.

Neutron irradiations were made in the large pneumatic tube (rabbit) of the Argonne heavy water reactor, CP-5, in a flux of $\approx 2 \times 10^{13}$ neutrons cm^{-2} sec^{-1}. The irradiations were from thirty to sixty minutes duration.

After an irradiation or collection period the catcher foils were either counted in a standard position of a Ge(Li) γ-ray spectrometer or dissolved (in HCl or NaOH for aluminum and in $HClO_4$-HNO_3 for polyethylene) in the presence of carriers for the fission product elements. The fission products were

isolated using conventional radiochemical techniques and counted in a beta proportional counter with a low background. Fission yields were calculated from the measured activities using the appropriate Bateman equations to correct for growth and decay.

3. FRAGMENT MASS DISTRIBUTIONS

3.1. Double-Energy (Physical) Method

The first moments of the fragment pre-neutron-emission mass ($\overline{A}_{L,H}$), kinetic energy ($\overline{E}_{L,H}$) and total kinetic energy ($\overline{TKE}$) distributions as well as the root-mean-square widths of these distributions are listed in Table I for all of the fissioning systems studied. The subscripts L and H refer to the light and heavy fragment mass groups,respectively. The pre-neutron-emission mass distributions for thermal-neutron-induced fission and spontaneous fission are shown in Figs. 1 and 2, respectively. All of the distributions shown have been corrected for the effects of experimental mass dispersion caused by neutron evaporation from the fragments, the energy resolution of the detectors and the energy loss of the fragments in the target materials [1]. The calculated mass resolutions for the fissioning systems studied here range typically from σ = 1.22 to 1.78 amu.

Many qualitative features of mass division in low-energy fission are evident in Figs. 1 and 2. For example, the average masses of the heavy fragment groups are nearly constant over the entire range of fissioning nuclides studied, whereas the average masses of the light fragment groups increase with increasing mass of the fissioning nuclides. There is an appreciable increase in the yield of symmetric fission fragments for the very heaviest fissioning systems, particularly for ^{254}Es(n,f) and ^{256}Fm(sf). Furthermore, it is quite apparent that a great deal of fine structure exists in the mass distributions, most notably for the lighter fissioning nuclides. This fine structure has previously been shown to be the result of a preferential formation of fragments with even nuclear charges in low-energy fission [2, 13, 14]. The shaded vertical bars in Figs. 1 and 2 indicate the calculated masses corresponding to the formation of fragments with the designated even nuclear charge numbers. The most probable or average nuclear charge, $\overline{Z}_{L,H}$, associated with a fragment of mass, $A_{L,H}$, was found in earlier charge division studies [1] of ^{233}U(n,f), ^{235}U(n,f), ^{239}Pu(n,f) and ^{252}Cf(sf) to be $\approx$0.5 ± 0.2 proton greater for the light fragment and $\approx$ 0.5 proton less for the heavy fragment than calculated on the basis that the fragments are formed with the same charge density (Z_F/A_F) as the fissioning nuclide. From this observation the average fragment masses corresponding to given even nuclear charges, as indicated in Figs. 1 and 2, were calculated using the relationships,

$$\overline{A}_L = (A_F/Z_F)(Z_L - 0.5) \qquad (1)$$

$$\overline{A}_H = (A_F/Z_F)(Z_H + 0.5) \qquad (2)$$

As can be seen in Figs. 1 and 2, there is generally excellent agreement between masses corresponding to the maxima of the

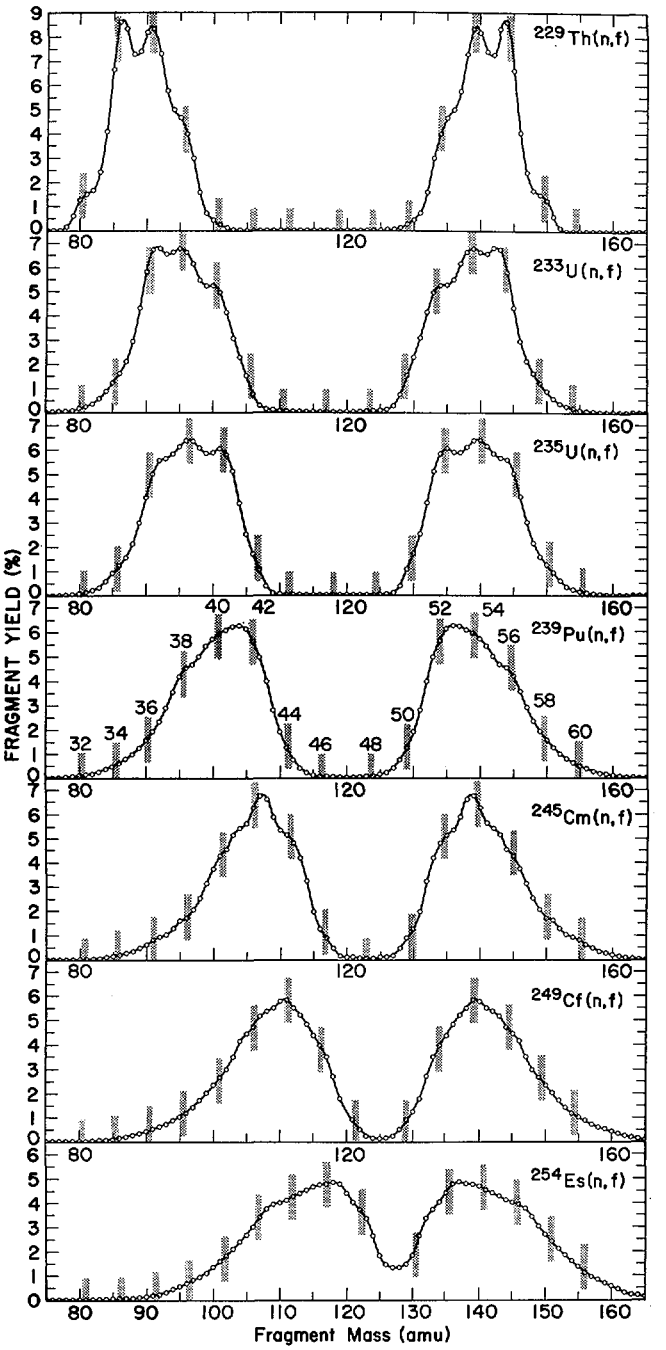

FIG. 1. Primary fragment mass distributions obtained for thermal-neutron-induced fission. All distributions have been corrected for experimental dispersions. The shaded vertical bars indicate the calculated fragment masses associated with the even nuclear charges shown in the figure for ^{239}Pu(n, f).

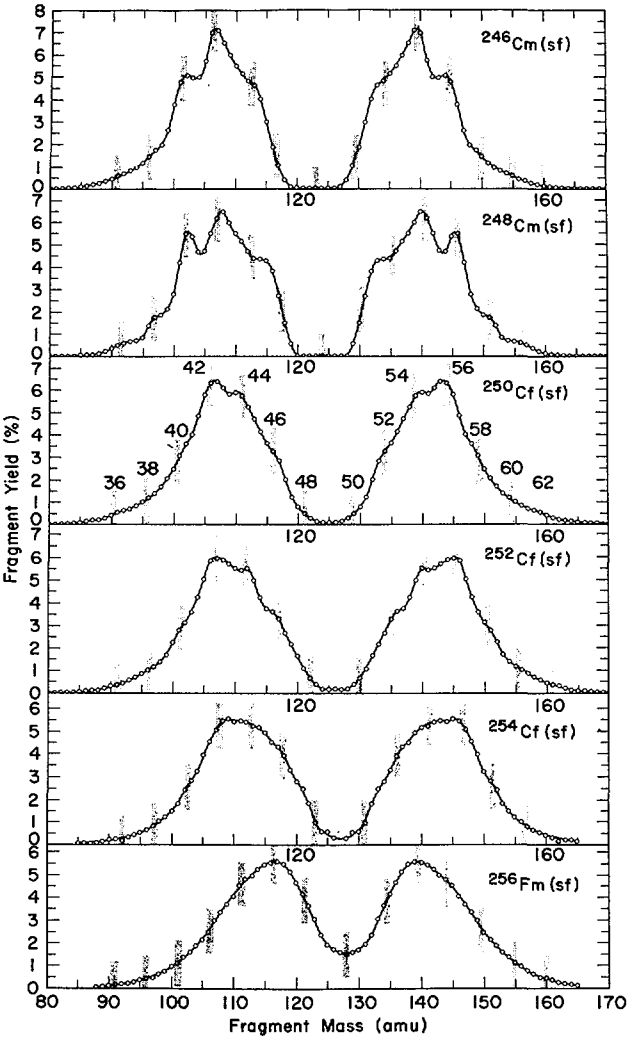

FIG. 2. Primary fragment mass distributions obtained for spontaneous fission. All distributions have been corrected for experimental dispersions. The shaded vertical bars indicate the calculated fragment masses associated with the even nuclear charges shown in the figure for ^{252}Cf(sf).

mass-distribution fine structure and the calculated masses associated with fragments possessing even nuclear charges. The widths of the shaded bars shown in Figs. 1 and 2 reflect an estimated ± 0.2 proton uncertainty in the calculation of average masses associated with even-charge fragments.

By closer examination of the mass distributions shown in Figs. 1 and 2, there appears to be a strong preference in these

fissioning systems for mass and charge divisions that yield heavy-fragment groups containing 52 to 58 protons. Major fractions of the yields for all these fissioning systems are associated with heavy fragments formed within this range of protons numbers. Furthermore, there appears to be a preference for divisions in which the light fragment contains 42 protons and is complementary to a heavy fragment with 52, 54 or 56 protons. For thorium and uranium isotopes where the Z = 42 light fragments are not complementary to these proton numbers, these charge-mass divisions occur in very low yields. However, for fissioning nuclides of plutonium, curium and californium the divisions corresponding to (Z_L, Z_H) = (42, 52), (42, 54), and (42, 56), respectively, generally occur with the highest or nearly highest yields. It is not immediately obvious that, in the act of fission, fragments formed with these protons numbers have special, stabilizing properties which strongly influence the fission mass and charge distributions or whether the neutron numbers associated with these proton numbers are the more important, controlling factors.

Wilkins and Steinberg [15] have been somewhat successful in reproducing the qualitative features of mass distributions over a wide range of fissioning nuclides using a static potential-energy surface calculation. The total potential energy of two nearly tangent spheroids was calculated as the sum of three deformation-dependent terms: 1) a liquid-drop term, 2) a Strutinsky-type deformed-shell and pairing correction term, and 3) a Coulomb interaction correction term between the fragments. The minima in the potential energy surfaces were found to be critically dependent on the fragment deformations and the size of the deformed-shell correction terms. In their model, Wilkins and Steinberg calculate the relative potential energies for all mass divisions at the value of the deformations for light and heavy fragments corresponding to the minimum in the surface and relate these potential energies to the observed fission yields. Examination of the various contributions to the total potential energy at these deformations reveals that the minima are strongly influenced by sizable negative shell corrections occurring for neutron numbers in the vicinity of ≈66 and ≈88, and for proton numbers of ≈44 for large fragment deformations. These shell corrections, taken from the work of Strutinsky [16], are shown in Fig. 3. In this figure, a deformation parameter of $\eta \approx 9$ would correspond to the deformation at which the deepest minima in the calculated potential energy surface occur. As can be seen in Fig. 3 for this region of fragment deformations, there are no sizable negative proton shell corrections corresponding to the large fission yields observed for $52 \leq Z \leq 58$. However, a large netative shell correction exists for fragments having ≈80-90 neutrons. These fragments have proton numbers associated with them which are within the Z = 52 to 58 range. Sizable shell corrections also occur at these deformations for $Z \approx 44$ and $N \approx 66$, nucleon numbers that are quite close to those of the Z = 42 fragments which also seem to play a role in determining fragment mass distributions in fission.

Therefore, on the basis of simple, static potential energy considerations, the neutron shell corrections (level densities) for deformed fragments near 88 neutrons seem to be important in determining the relative constancy of the heavy fragment mass

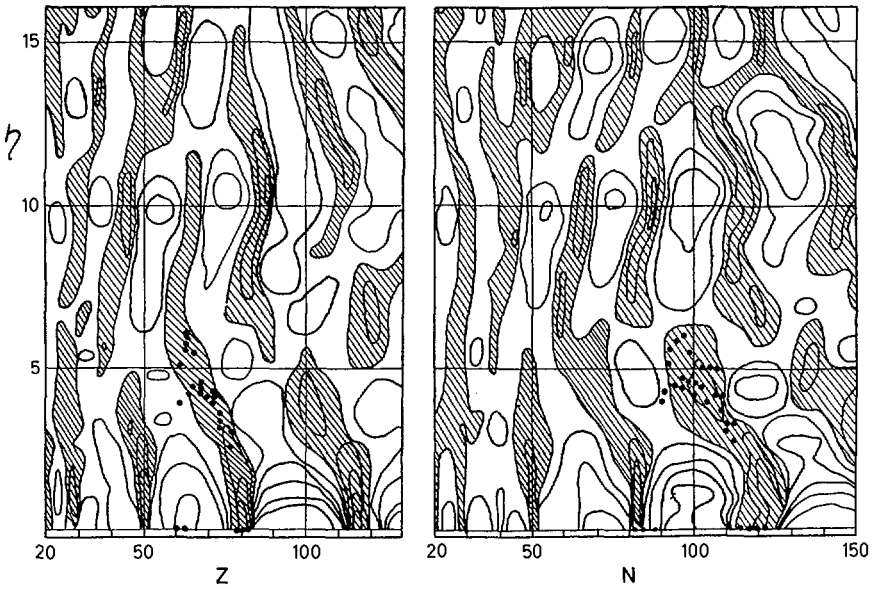

FIG. 3. Contour diagrams of Strutinsky shell corrections as a function of nucleon number and nuclear deformation [16]. Negative shell corrections are shaded. Contour lines correspond to increments of 5 $(\hbar\omega_0)^{-1}$.

group near $A_H \approx 140$ for a wide range of fissioning nuclides. In addition, neutron and proton shell corrections near $N \approx 66$ and $Z \approx 44$ also contribute to the shapes of the fragment mass distributions. Further refinements in the calculation of these potential-energy surfaces including shell corrections which are calculated more precisely [17] may lead to a more quantitative interpretation of many aspects of mass and charge division in fission.

3.2. Radiochemical Method

Fission yields for the various mass chains determined in this work are presented in Table II and plotted as mass-yield curves in Fig. 4. Included in both the table and figure are the fission yields determined previously at this laboratory for ^{256}Fm(sf) [18]. The errors for the values given in Table II were evaluated on the basis of the number of measurements, the statistical error in the counting rate determination, and any uncertainties in the decay scheme of the particular nuclide measured. The measured yields of the isomers 53.5-h ^{115g}Cd and 27-h ^{121g}Sn were converted to total chain yields by using values for the isomer ratio, (m+g)/g, reported for ^{235}U(n,f) as 1.072 ± 0.02 [19] and 1.156 ± 0.05 [20], respectively. However, the reported isomer ratio of 2.5 ± 0.2 [20] for ^{125g}Sn in ^{235}U(n,f) does not appear to be applicable to the heaviest fissioning systems, ^{255}Fm(n,f) and ^{256}Fm(sf) (see Table II and Fig. 4). This leads to some uncertainty in estimating the peak-to-valley ratios

TABLE II. Summary of Fission Yields

Fission Product	Fission Yield (%) ^{251}Cf(n,f)	^{254}Es(n,f)	^{255}Fm(n,f)	^{253}Es(sf)	^{254}Fm(sf)	^{256}Fm(sf)
^{83}Br				0.061±0.006		
^{89}Sr		0.053±0.01		0.37±0.04		
^{91}Sr	0.54±0.04	0.28±0.03	0.50±0.10	0.53±0.04	0.40±0.04	0.22±0.03
^{93}Y			0.30±0.10	0.67±0.07	0.48±0.05	
^{95}Zr	1.0±0.1	0.72±0.07		1.3±0.2	0.54±0.08	
^{97}Zr	1.7±0.1	0.99±0.1	0.83±0.13	1.8±0.1	1.3±0.1	0.70±0.14
^{99}Mo	3.4±0.2	2.3±0.2	1.8±0.3	3.1±0.2		
^{103}Ru		3.2±0.3		5.8±0.3	3.1±0.3	
^{105}Ru	5.0±0.4	4.3±0.4	2.9±0.3	7.7±1.2		2.9±0.4
^{106}Ru		4.1±0.4		6.5±0.5	5.8±0.6	
^{109}Pd	5.4±0.4	3.8±0.6		5.5±0.5	5.7±0.6	3.4±0.9
^{111}Ag	5.2±0.3	4.2±0.2	3.3±0.4	4.7±0.2	5.5±0.3	5.0±0.4
^{112}Pd	5.5±0.4	4.4±0.4	3.6±0.4	3.8±0.4	5.1±0.5	4.4±0.6
^{115g}Cd	4.3±0.2	5.3±0.3	5.2±0.6	2.6±0.2	4.5±0.4	5.2±0.5
^{115m}Cd		0.30±0.03		0.21±0.02	0.58±0.06	
^{115} total	4.6±0.2[a]	5.6±0.3	5.6±0.6[a]	2.8±0.2	5.1±0.4	5.6±0.6
^{118}Cd						5.3±0.9
^{121g}Sn	0.48±0.04	2.5±0.2	3.2±0.3	0.14±0.01	0.66±0.07	2.1±0.2
^{121} total[a]	0.55±0.05	2.9±0.3	3.7±0.4	0.16±0.02	0.76±0.08	2.5±0.3
^{125g}Sn	0.20±0.02	0.45±0.03	1.6±0.2	0.009±0.001	0.066±0.007	0.56±0.2
^{127}Sb	0.62±0.06	0.95±0.1	2.4±0.3	0.064±0.005	0.24±0.02	0.41±0.07
^{129}Sb	0.95±0.09	2.0±0.2	2.4±0.3	0.31±0.03	0.79±0.08	0.82±0.14
^{131}I	1.9±0.15	3.8±0.2	3.4±0.4	1.2±0.1	2.7±0.3	2.4±0.5
^{132}Te	4.4±0.4	4.8±0.5	5.3±0.5	2.4±0.2	3.0±0.3	3.6±0.5
^{133}I	4.0±0.4	5.1±0.8	5.7±0.6	2.7±0.3	3.4±0.3	3.6±0.7
^{135}I	4.3±0.4	5.3±0.8	6.3±0.6	3.9±0.4		5.0±0.9
^{139}Ba				5.9±0.6		5.8±0.8
^{140}Ba	4.6±0.2	4.0±0.2	5.2±0.5	5.6±0.3	5.7±0.3	5.6±0.5
^{141}Ce	5.0±0.5	4.6±0.3		5.8±0.6	6.3±0.5	6.6±1.3
^{143}Ce	5.2±0.3	4.8±0.4	3.7±0.4	6.5±0.3	5.7±0.3	5.7±0.5
^{144}Ce		3.9±0.4		5.2±0.5	5.1±0.5	
^{145}Pr						4.8±0.9
^{149}Pm			1.9±0.3	3.2±0.3		2.5±0.4
^{151}Pm		1.7±0.3	1.4±0.2	1.9±0.2		2.0±0.3
^{153}Sm		1.6±0.3	1.1±0.2	1.5±0.2	1.4±0.1	1.3±0.3
^{156}Sm		0.80±0.16				0.65±0.2
^{157}Eu		0.76±0.11	0.42±0.06	0.75±0.08	0.63±0.06	0.49±0.07
^{159}Gd				0.57±0.06	0.44±0.04	0.47±0.07

[a]Total chain yield calculated from isomer ratio for ^{235}U(n,f).

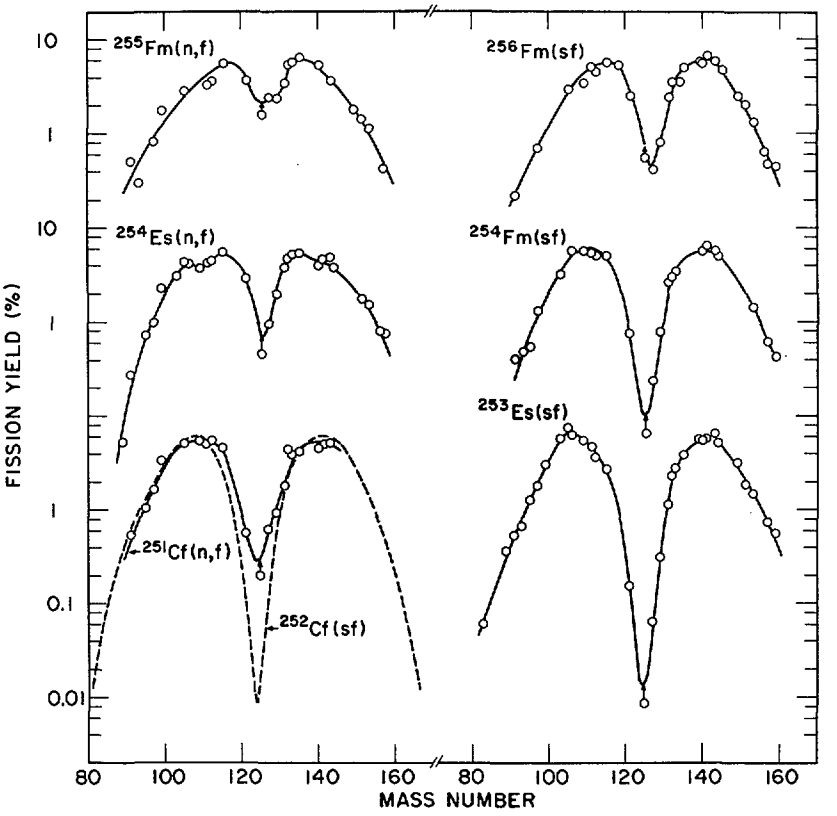

FIG. 4. Radiochemically determined mass-yield curves for several fissioning systems.

for the other fissioning systems (Table III). An isomer ratio of ≈1.5 for ^{129g}Sn is suggested by the mass-yield curve for ^{255}Fm (n,f) and was used to establish approximate valley positions for the other cases (arrowheads in Fig. 4). Summations of the mass-yield curves for the six fissioning systems were normalized to 200%.

It is interesting to note the marked decrease in the peak-to-valley ratios of the mass distributions (enhancement of symmetrical fission) with increasing mass of the fissioning nucleus for both spontaneous and neutron-induced fission. Of particular interest is the nearly symmetrical fission in the case of ^{255}Fm (n,f) (with a peak-to-valley ratio of only ≈2.5) in view of the reported symmetrical fission for ^{257}Fm(n,f) [21]. Enhancement of symmetrical fission with the increased excitation energy of ≈ 6 MeV from neutron absorption is also apparent in comparisons of ^{251}Cf(n,f) with ^{252}Cf(sf) and of ^{255}Fm(n,f) with ^{256}Fm(sf). Shigin [22] has predicted on the basis of a statistical approach

TABLE III. Summary of Radiochemically Determined Mass Distribution Characteristics

Fissioning System	$\bar{M}_L$ (amu)	$\bar{M}_H$ (amu)	$\bar{\nu}_T$	Peak-to-Valley Ratio
^{229}Th(n,f)	87.6	139.9	2.5	500
^{233}U(n,f)	93.3	138.2	2.5	440
^{235}U(n,f)	94.9	138.6	2.5	620
^{239}Pu(n,f)	98.9	138.1	3.0	150
^{245}Cm(n,f)	102.8	139.2	4.0	155
^{249}Cf(n,f)	105.8	139.8	4.4	$\gtrsim$30
^{251}Cf(n,f)	107.3	140.7	4.0	$\approx$20
^{252}Cf(sf)	106.1	142.1	3.8	$\gtrsim$600
^{253}Es(sf)	105.9	142.4	4.7	$\approx$450
^{254}Es(n,f)	110.6	140.2	4.2	$\approx$8
^{254}Fm(sf)	108.8	141.5	3.7	$\approx$60
^{255}Fm(n,f)	113.2	138.8	4.0	2.5
^{256}Fm(sf)	111.8	141.0	3.2	12

that symmetrical fission of ^{252}Cf will decrease with an increase in excitation energy. The results presented here for ^{251}Cf(n,f) clearly do not support this hypothesis. Also in evidence in Fig. 4 is the shift of the light mass peak and the relative constancy of the heavy mass peak. The characteristics of the six mass distributions are summarized in Table III together with the characteristics of several other mass distributions determined previously.

The variation with fissioning mass in the mean masses (first moments) of the light and heavy groups for both primary (solid curve) and secondary (dashed curve) mass distributions is shown in Fig. 5. Previous papers (e.g.,Ref. [18]) have considered the variation of the mean secondary masses, $\bar{M}_L$ and $\bar{M}_H$, to be essentially linear functions of the fissioning mass (A_F) with only ^{252}Cf(sf) deviating from this pattern. However, with the new data presented in this paper it is clear that these functions (for both primary and secondary masses) are not quite linear and that there is a distinct deviation in the region of $A_F \approx 250$ to 255.

Values of the average total emission of neutrons per fission ($\bar{\nu}_T$) presented in Table III and Fig. 5 are those derived by the mass-balance relationship

$$\bar{\nu}_T = A_F - (\bar{M}_L + \bar{M}_H) \qquad (3)$$

These values agree fairly well with values of $\bar{\nu}_T$ measured directly [7] (depicted by the dashed-dot curve in Fig. 5) and seem to indicate a leveling off of $\bar{\nu}_T$ for $A_F > 245$.

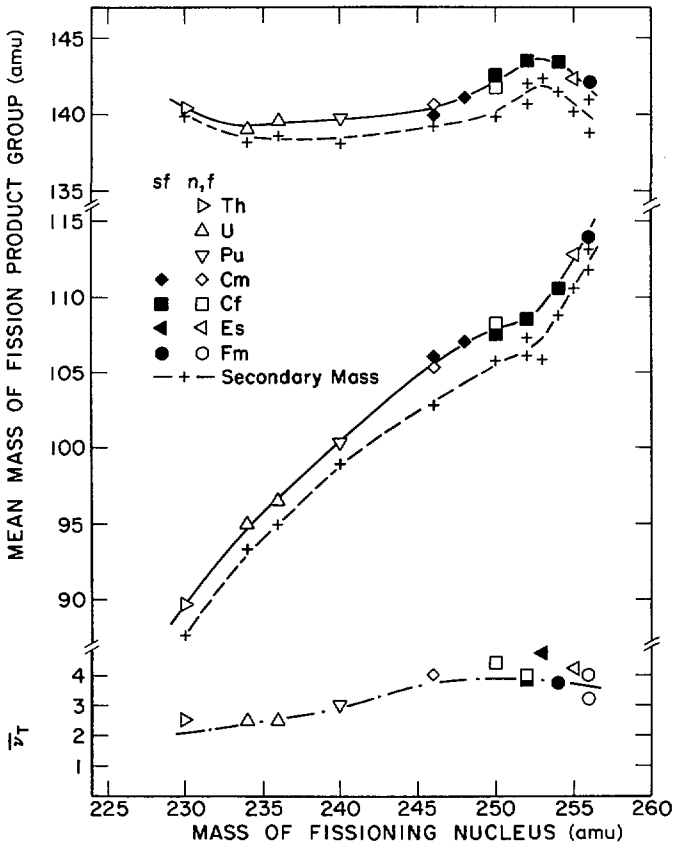

FIG. 5. Average primary masses (solid curves) and secondary masses (dashed curves) of the fission product groups and total average neutron emission $\bar{\nu}_T$ (dot-dash curve) as a function of the mass of the fissioning nucleus.

4. FRAGMENT TOTAL KINETIC ENERGY CORRELATIONS

The average total kinetic energy release for many fissioning systems has in the past been correlated with the symmetric-fission Coulomb repulsion parameter $Z_F^2/A_F^{1/3}$, i.e.,

$$\overline{TKE} = B\ (Z_F^{\,2}/A_F^{\,1/3}) + C \qquad (4)$$

However, in previous correlations, e.g.,Ref. [23], $\overline{TKE}$ values with large uncertainties were included as well as data for fissioning systems with widely different excitation energies and angular momentum distributions. The total kinetic energy has previously been shown to be slightly dependent on both excitation energy as well as angular momentum [24]. The $\overline{TKE}$ values obtained in this work are correlated with the Coulomb repulsion

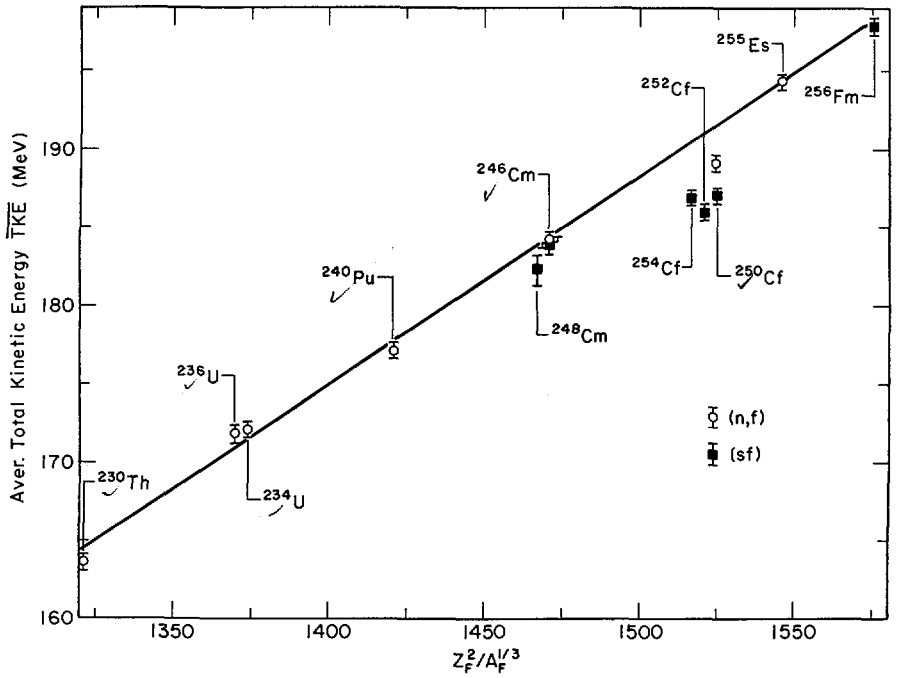

FIG. 6. Correlation of measured average total kinetic energies ($\overline{TKE}$) with the symmetric-fission Coulomb repulsion parameter $Z_F^2/A_F^{1/3}$. Data for thermal-neutron-induced fission are shown as open circles, data for spontaneous fission are shown as solid squares. The fissioning nuclides are indicated for each data point.

parameter in Fig. 6. The line in this figure is the result of a least-squares fit of the (n,f) data (open circles) to Eq. (4) yielding B = 0.13323 and C = -11.64. For fission data taken at nearly the same low excitation energy and with no angular momentum, it is seen that $\overline{TKE}$ data can be adequately represented by Eq. (4), generally to within ± 1 MeV. However, in fitting the data, the $\overline{TKE}$ value for ^{249}Cf(n,f) was omitted since it is considerably lower than expected from such a linear fit. The $\overline{TKE}$ values measured in this work as well as in the work of others (e.g., Ref. [25]) indicate a deviation for californium isotopes from this general linear dependence. The first moments of the fragment mass groups for californium fission also deviate from the smooth dependence with fissioning mass based upon isotopes of other elements as shown in Fig. 5.

The $\overline{TKE}$ values measured for spontaneous fission are in almost all cases less than those measured or interpolated from (n,f) data, as seen in Table I or Fig. 6. Fragment mass and kinetic energy correlations have been obtained for spontaneous fission as well as fission following neutron capture for two fissioning nuclides, ^{246}Cm and ^{250}Cf. In the case of ^{246}Cm there is little difference between the $\overline{TKE}$ for ^{245}Cm(n,f) as compared with ^{246}Cm(sf). However, ^{250}Cf(n,f) has a substantially

TABLE IV. Energy Balance Comparison: Spontaneous vs Thermal-Neutron-Induced Fission

Fissioning System	$^{246}_{96}Cm$	$^{250}_{98}Cf$
$E^*(n,f)$ (MeV)	6.450	6.617
$\bar{\nu}_T(n,f)$	3.832 ± 0.034	4.06 ± 0.04
$\bar{\nu}_T(sf)$	2.86 ± 0.06	3.53 ± 0.09
$\Delta\bar{\nu}_T$	0.972 ± 0.07	0.53 ± 0.10
$\overline{TKE}(n,f)$ (MeV)	184.2 ± 0.5	189.1 ± 0.5
$\overline{TKE}(sf)$ (MeV)	183.9 ± 0.5	187.0 ± 0.5
$\Delta\overline{TKE}$ (MeV)	0.3 ± 0.7	2.1 ± 0.7
$\bar{B}_n$ (MeV/n)	6.3 ± 0.8	8.5 ± 2.1

greater $\overline{TKE}$ value than $^{250}Cf(sf)$. The difference in behavior of $\overline{TKE}$ of the two fissioning nuclides for (sf) compared with (n,f) can be directly correlated with the measured neutron emission probabilities, since the difference in initial excitation energy between (n,f) and (sf) must appear primarily as additional internal excitation energy of the fragments (resulting in increased neutron emission) or additional kinetic energy of the fragments. The energy balances of neutron emission and $\overline{TKE}$ for these two fissioning nuclides are summarized in Table IV. For ^{246}Cm fission there is little difference in $\overline{TKE}$ between (n,f) and (sf), and most of the initial excitation energy appears as additional internal excitation energy of the fragments resulting in increased neutron emission. For ^{250}Cf there is a substantial difference of $\overline{TKE}$ (2.1 MeV) for (n,f) compared to (sf). Consequently, less of the initial excitation energy is available for eventual neutron emission. The energy balance can be put into quantitative terms by assuming that the initial excitation energy (E^*) must be distributed between additional neutron emission ($\Delta\bar{\nu}_T$) and additional kinetic energy ($\Delta\overline{TKE}$) according to the relationship

$$E^* = (\Delta\bar{\nu}_T)\bar{B}_n + \Delta\overline{TKE} \qquad (5)$$

An average energy required to emit a neutron, $\bar{B}_n \approx 7$ MeV/neutron, is obtained from this correlation using the available data. This is quite consistent with the generally accepted value for $\bar{B}_n$.

Comparison of spontaneous fission with fission taking place above the barrier as in (n,f) for the same fissioning nuclide can, in principle, provide information regarding dynamic, dampening effects in fission. However, the meager amount of information available at present indicates that interpretations will be very complex. As seen from the ^{246}Cm and ^{250}Cf data presented here, there are differences in $\overline{TKE}$ between (sf) and (n,f).

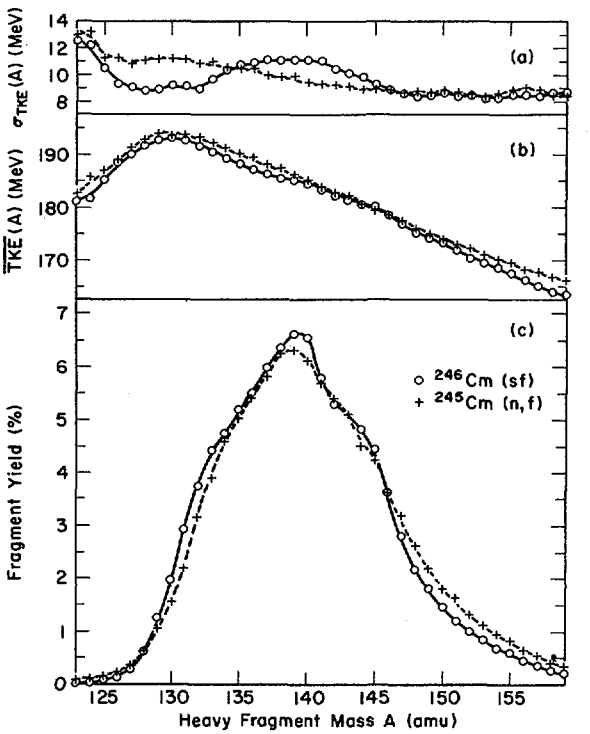

FIG. 7. (a) rms of total kinetic energy distribution, (b) kinetic energy data and (c) primary fragment mass distribution for ^{246}Cm(sf), shown as circles, and for ^{245}Cm(sf), shown as crosses. All distributions are uncorrected for experimental dispersion.

However, the differences are variable from one fissioning nuclide to another, and furthermore they are dependent on the fragment masses. Figs. 7 and 8 show comparisons of the mass distributions and $\overline{TKE}$ values as a function of fragment mass for spontaneous fission and fission following neutron capture for ^{246}Cm and ^{250}Cf, respectively. The data shown in these two figures have not been corrected for experimental resolutions. The mass distributions for ^{246}Cm(sf) and ^{245}Cm(n,f) are very similar, with the ^{245}Cm(n,f) mass distribution being slightly more asymmetric. On the other hand, the mass distributions for ^{250}Cf(sf) and ^{249}Cf(n,f) are quite different, with the ^{249}Cf(n,f) case being more symmetric, contrary to the results for ^{246}Cm. For both fissioning nuclides, the major differences in $\overline{TKE}$ between (sf) and (n,f) occur for fragment masses more symmetric than the average masses as shown in Figs. 7b and 8b. Correction for the poorer mass resolution of the (n,f) cases (because of increased neutron emission) would slightly increase the observed differences in $\overline{TKE}$ for (n,f) and (sf) cases in mass regions more symmetric than the average masses and decrease the observed small differences for very asymmetric mass divisions.

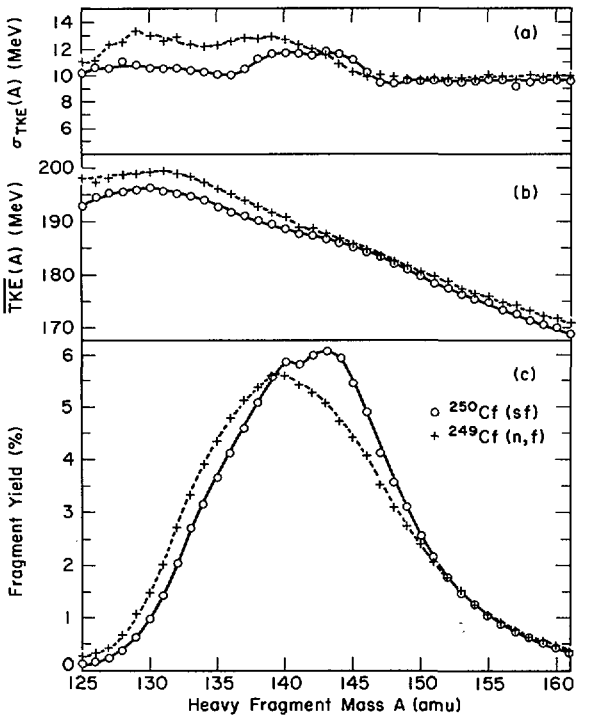

FIG. 8. (a) rms of total kinetic energy distribution, (b) kinetic energy data and (c) primary fragment mass distribution for ^{250}Cf(sf), shown as circles, and for ^{249}Cf(n, f), shown as crosses. All distributions are uncorrected for experimental dispersion.

Results for the total kinetic energy release as a function of fragment mass are shown in Fig. 9 for the (n,f) cases studied. As can be seen, the well known decrease in $\overline{TKE}$ near symmetric fission (indicated by vertical lines) becomes less pronounced for heavier fissioning systems. While most of the distributions are essentially structureless, the $\overline{TKE}$ distribution for ^{229}Th(n,f) contains a great deal of structure. Fig. 10b shows an expanded version of $\overline{TKE}$(A) for ^{229}Th(n,f). For comparison the $\overline{TKE}$(A) distribution (normalized by an arbitrary factor of 0.944) for the nearest fissioning system measured, ^{233}U(n,f), is shown by a dashed line. This normalized $\overline{TKE}$(A) distribution is shown here as being representative of previously measured, structureless distributions. The difference between the measured $\overline{TKE}$(A) distribution for ^{229}Th(n,f) and that representative of a typical smooth distribution is shown in Fig. 10a. As can be seen, this difference is of the order of a few MeV. Furthermore, the masses corresponding to the maxima in Fig. 10a are identical to those associated with the mass distribution fine structure shown in Fig. 1. This correlation with masses associated with even-Z fragments suggests that in ^{229}Th(n,f) mass divisions containing even-Z fragments have a greater $\overline{TKE}$ release than odd-Z fragments.

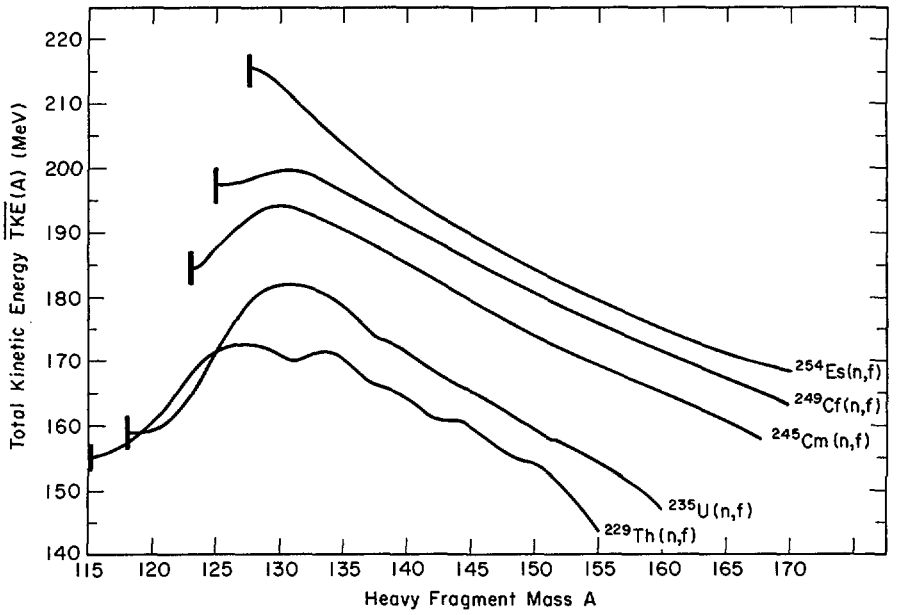

FIG. 9. Average total kinetic energy as a function of primary heavy-fragment mass for cases of thermal-neutron-induced fission. The vertical lines indicate the symmetric fission masses for each fissioning nuclide.

There are several possible explanations for this observation, none of which are conclusive. However, the interpretation must be related to the fact that the energy released in ^{229}Th(n,f) is low and smaller than in all fissioning systems studied here. For example, if the energy required to break a proton pair for formation of two odd-Z fragments came totally at the expense of $\overline{TKE}$, then one would expect the even-Z fragments to have ~2.5 MeV more total kinetic energy than odd-Z fragments. It may also be that in this case the energy available for internal excitations during the transition from the saddle point to the scission configuration is insufficient to break nucleon pairs. A larger fraction of any existing pre-scission kinetic energy may then survive dissipation into excitation energy for even-even paired fragments as opposed to odd-A or odd-odd fragments. The effect could also be caused simply by a smaller charge separation (of the order of 2%) of the fragments at scission for even-Z totally paired fragments as opposed to odd-Z fragments.

5. DETERMINATION OF NEUTRON EMISSION FUNCTIONS

No information is presently available on neutron emission probabilities as a function of fragment mass, $\overline{\nu}(A)$, for the heaviest fissioning systems ($A_F > 252$). However, these functions can be obtained indirectly for ^{254}Es(n,f) and ^{256}Fm(sf)

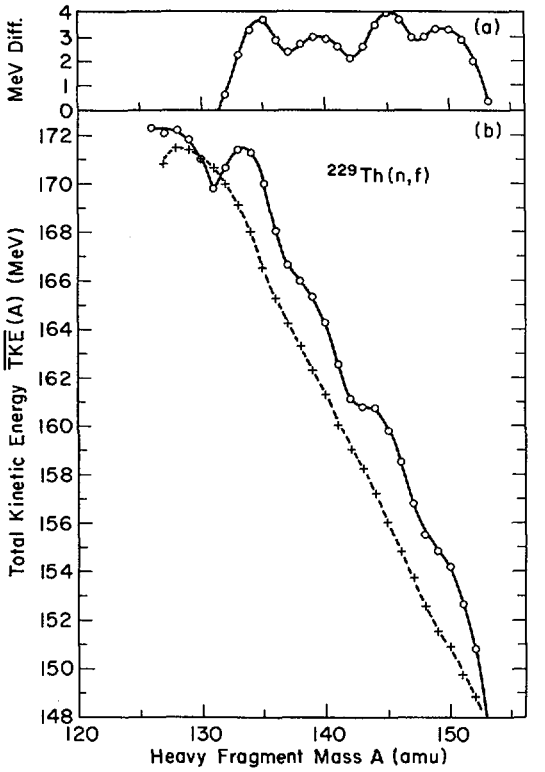

FIG. 10. Average total kinetic energy for ^{229}Th(n, f) as a function of primary heavy-fragment mass. The dashed curve in (b) shows the $\overline{TKE}$(A) values obtained for ^{233}U(n, f) multiplied by 0.944. The curve shown in (a) represents the difference between the two curves shown in (b).

from the primary and secondary mass distributions which have been determined in the present work and in earlier work [18], since these distributions are interrelated by the $\bar{\nu}$(A) function. For this purpose an iterative method was used to derive neutron emission functions.

Initially the $\bar{\nu}$(A) function was assumed to have the same shape as the measured ^{252}Cf(sf) neutron emission function [4]. This function was used to derive a provisional primary mass distribution as described in Sect. 2.1. The provisional mass distribution was corrected for experimental mass resolution and then transformed into a secondary mass distribution using the assumed neutron function and dispersing the transformed secondary mass yields with a Gaussian distribution of average variance $\langle\sigma^2(\bar{\nu}(A),A)\rangle$. The variances were obtained by interpolating or extrapolating as a function of $\bar{\nu}_T$ the average variances deduced by Terrell [26] for ^{235}U(n,f), ^{239}Pu(n,f) and ^{252}Cf(sf). The transformed, secondary mass distribution was then compared with

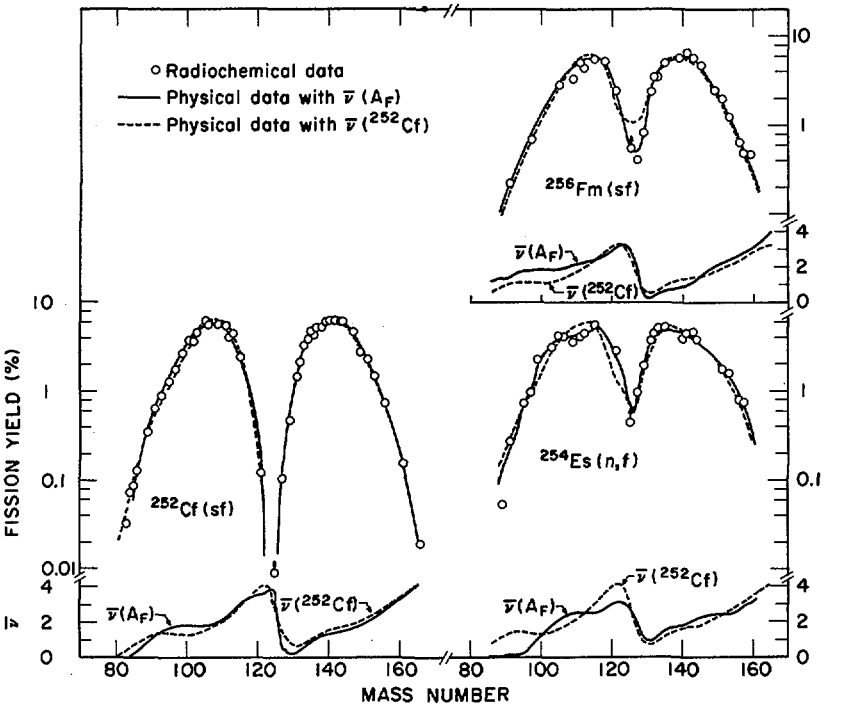

FIG. 11. Comparison of radiochemical mass yield data with secondary mass distributions obtained by transformation of physically determined primary mass distributions using the known $\bar{\nu}(A)$ function for $^{252}Cf(sf)$ (dashed curves) and empirical functions $\bar{\nu}(A_F)$ (solid curves) derived by an iterative method.

the secondary mass distribution obtained radiochemically to determine the accuracy of the transformation. If the two distributions did not agree, a new approximation to the neutron emission function was calculated. This was done following closely the method of Terrell [26]. The provisional primary mass yields were summed to give a cumulative primary mass-yield distribution as a function of primary mass. The same was done for the radiochemical mass yields using a smooth curve drawn through the data points. This gave a cumulative secondary mass-yield distribution as a function of secondary mass. The lateral displacement between these two cumulative distributions when plotted as a function of mass was equated to the average number of neutrons emitted from a given primary mass. The $\bar{\nu}(A)$ function so obtained was used to calculate new provisional primary masses, and the entire procedure was repeated until convergence was achieved.

The results of this iterative method are shown in Fig. 11. The physical data, transformed with various $\bar{\nu}(A)$ functions, are given as curves through the radiochemical data (open circles). The $\bar{\nu}(A)$ functions used in the transformations are given as corresponding solid or dashed curves. In all cases, the initial transformed curves obtained with a $^{252}Cf(sf)$-shaped $\bar{\nu}(A)$ function are shown as dashed curves.

The $^{252}Cf(sf)$ system provides an excellent test for the iterative method since the $\bar{\nu}(A)$ function has been determined directly by experiment [4], and a large number of fission product yields have been determined as well. As might be expected, the transformed physical data using the experimental $\bar{\nu}(A)$ function fits the radiochemical data very well (see Fig. 11). There is, however, an indication of some discrepancy in the fit on the light side of the light peak (from $M \approx 90$ to 106) and in the valley where the radiochemical yields are <0.5%. The latter small discrepancy may be attributed,at least in part, to uncertainties existing in corrections for the experimental mass resolution applied to the physical data and poorly known radiochemical yields in the valley. On the other hand, the directly determined $\bar{\nu}(A)$ values [4] in regions of low yields also have a relatively large uncertainty because of mass resolution corrections, etc. The saw-toothed neutron emission function derived by the iterative method for $^{252}Cf(sf)$ and shown in Fig. 11 is similar to that measured directly [4], thus confirming the

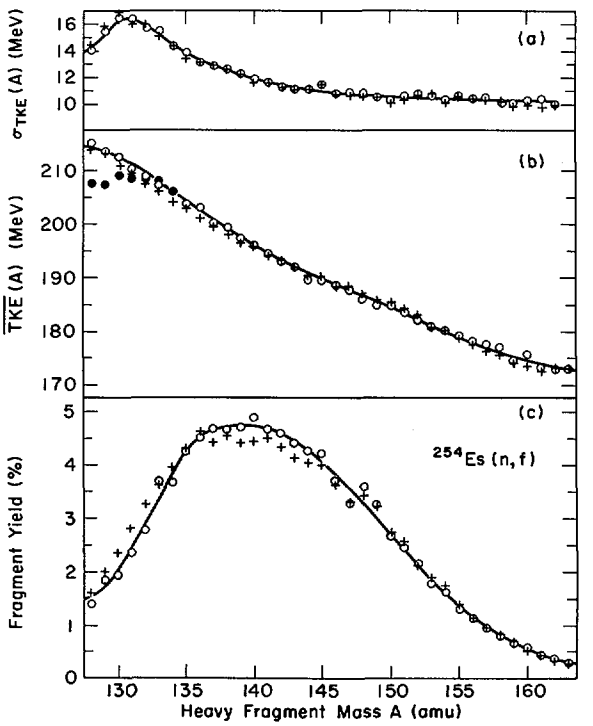

FIG. 12. (a) rms of total kinetic energy distribution, (b) kinetic energy data and (c) primary fragment mass distribution for $^{254}Es(n, f)$. Data points indicated by open circles were calculated assuming that the $\bar{\nu}(A)$ function had the same shape as that directly measured for $^{252}Cf(sf)$ (Ref. [4]). Data points shown as crosses were calculated using the $\bar{\nu}(A)$ function derived indirectly in this work and shown in Fig. 11.

validity of the method used here. Other than the region near symmetry, the most obvious difference between the experimental and derived $\bar{\nu}(A)$ functions is in the mass region of A $\tilde{\sim}$ 95 to 105 where the derived function indicates greater neutron emission.

Since the radiochemical mass distributions for ^{254}Es(n,f) and ^{256}Fm(sf) are considerably less complete than the one for ^{252}Cf(sf), the uncertainties associated with the derived $\bar{\nu}(A)$ functions shown in Fig. 11 are correspondingly greater. The most significant conclusions that can be drawn from these results is that the derived $\bar{\nu}(A)$ functions are definitely saw-toothed in character and the shapes of the functions are most likely different from the shape of the ^{252}Cf(sf) function. Thus, for the spontaneous and thermal-neutron-induced fission of nuclides heavier than ^{252}Cf, shell effects continue to play an important role in determining the relative fragment deformation energies.

The primary mass and kinetic energy distributions presented for the fission of Cf, Es and Fm isotopes in Sects. 3.1 and 4 were calculated assuming that the $\bar{\nu}(A)$ functions for these systems have the same shape as the $\bar{\nu}(A)$ function measured [4] for ^{252}Cf(sf). However, the $\bar{\nu}(A)$ functions derived here for ^{254}Es (n,f) and ^{256}Fm(sf) have slightly different shapes than that for ^{252}Cf(sf). It is therefore important to establish what effect different $\bar{\nu}(A)$ functions have on the calculated primary mass and kinetic energy distributions. Such a comparison is shown in Fig. 12 for ^{254}Es(n,f) which seems to have a $\bar{\nu}(A)$ function most different from that of ^{252}Cf(sf). The open circles indicate the results calculated with a ^{252}Cf(sf)-shaped $\bar{\nu}(A)$ function, and the crosses indicate the results calculated with the derived $\bar{\nu}(A)$ function. As can be seen in Fig. 12, the mass distribution calculated with the latter $\bar{\nu}(A)$ function is shifted slightly toward symmetry compared with the distribution calculated with the ^{252}Cf(sf)-shaped $\bar{\nu}(A)$ function. However, the results of the two calculations are in very good agreement. Also the results of total kinetic energy calculations using the two $\bar{\nu}(A)$ functions agree well. Thus, for the purpose of calculating primary mass and kinetic energy distributions, a normalized ^{252}Cf(sf)-shaped $\bar{\nu}(A)$ function is a sufficiently good approximation for the heavier fissioning systems investigated in this work.

ACKNOWLEDGEMENTS

It is a pleasure to acknowledge the cooperation of the Transplutonium Program Committee of the USAEC and the Chemical Technology Division at ORNL in supplying the nuclides used in this work. The authors also wish to thank personnel at the HFIR(ORNL) and CP-5 (ANL) reactors and those at the ANL cyclotron for the neutron and alpha-particle irradiations. Special thanks are due Mr. J. Lerner for preparation of the mass-separated sources, Dr. E. P. Horwitz for discussions on chemical separations, and Dr. I. Ahmad for actinide identification by γ-ray spectrometry. Dr. R. G. Clark participated in some preliminary phases of the work on ^{248}Cm(sf) and ^{256}Fm(sf). The

authors wish also to acknowledge many valuable discussions with Drs. B.D. Wilkins and E. P. Steinberg concerning their potential-energy calculations.

REFERENCES

[1] REISDORF, W., UNIK, J. P., GRIFFIN, H. C., GLENDENIN, L. E., Nucl. Phys. A177(1971)337.
[2] REISDORF, W. N., UNIK, J. P., GLENDENIN, L. E., Nucl. Phys. A205(1973)348.
[3] SCHMITT, H. W., NEILER, J. H., WALTER, F. J., Phys. Rev. 141(1966)1146.
[4] BOWMAN, H. R., MILTON, J. C. D., THOMPSON, S. G., SWIATECKI, W. J., Phys. Rev. 129(1963)2133.
[5] APALIN, V. F., GRITSYUK, Yu.N., KUTIKOV, I. E., LEBEDEV, V. I., MIKAELIAN, L. A., Nucl. Phys. 71(1965)553.
[6] MILTON, J. C. D., FRASER, J. S., in Physics and Chemistry of Fission 2, IAEA, Vienna (1965)39.
[7] MANERO, F., KONSHIN, V. A., Atomic Energy Rev. 10(1972)637.
[8] KAUFMAN, S. G., STEINBERG, E. P., WILKINS, B. D., UNIK, J. P., GORSKI, A. J., FLUSS, M. J., Nucl. Inst. Meth. (1973) to be published.
[9] MILSTED, J., BEADLE, A. B., J. Inorg. Nucl. Chem. 3(1956) 248.
[10] HORWITZ, E. P., SAURO, L. J., BLOOMQUIST, C. A. A., J. Inorg. Nucl. Chem. 29(1967)2033.
[11] BARBANO, P. G., RIGALI, L., J. Chromat. 29(1967)309.
[12] SOCHACKA, R. J., SIEKIERSKI, S., J. Chromat. 16(1964)376.
[13] THOMAS, T. D., VANDENBOSCH, R., Phys. Rev. 133(1964)B976.
[14] WAHL, A. C., NORRIS, A. E., ROUSE, R. A., WILLIAMS, J. C., in Physics and Chemistry of Fission, IAEA, Vienna (1969) 183.
[15] WILKINS, B. D., STEINBERG, E. P., Phys. Letters 42B(1972) 141.
[16] STRUTINSKY, V. M., Nucl. Phys. A122(1968)1.
[17] WILKINS, B. D., STEINBERG, E. P., CHASMAN, R. R., private communication (1973).
[18] FLYNN, K. F., HORWITZ, E. P., BLOOMQUIST, C. A. A., BARNES, R. F., SJOBLOM, R. K., FIELDS, P. R., GLENDENIN, L. E., Phys. Rev. C5(1972)1725.
[19] WAHL, A. C., BONNER, N. A., Phys. Rev. 85(1952)570.
[20] ERDAL, B. R., WILLIAMS, J. C., WAHL, A. C., J. Inorg. Nucl. Chem. 31(1969)2993.
[21] JOHN, W., HULET, E. K., LOUGHEED, R. W., WESOLOWSKI, J. J., Phys. Rev. Letters 27(1971)45.
[22] SHIGIN, V. A., Soviet J. Nucl. Phys. 7(1968)506.
[23] VIOLA, V., Nucl. Data 1(1966)391.
[24] UNIK, J. P., CUNINGHAME, J. G., CROALL, I. F., in Physics and Chemistry of Fission, IAEA, Vienna (1969)717.
[25] BRANDT, R., THOMPSON, S. G., GATTI, R. C., PHILLIPS, L., Phys. Rev. 131(1963)2617.
[26] TERRELL, J., Phys. Rev. 127(1962)880.

DISCUSSION

M. S. MOORE: What do the closed circles represent in the last figure?

J.P. UNIK: The closed circle data points in the last figure were obtained using a neutron function which had the same shape as that measured for ^{252}Cf(sf) but assuming $\bar{\nu}$(A) to be independent of $\overline{TKE}$ (A).

M. S. MOORE: Is it really fair to include ^{230}Th and Fm in the figure showing average total kinetic energy vesus $Z_F^2/A_F^{1/3}$ (Fig. 6), when we know that these distributions show anomalous behaviour?

J. P. UNIK: For the purpose of this figure, namely to be able to interpolate and extrapolate unmeasured $\overline{TKE}$ values, I think it is perfectly satisfactory to include these data points.

S. BJØRNHOLM: I was struck by the amount of structure in the mass and kinetic energy distributions of ^{229}Th(n, f) and ^{246}Cm(sf) showing a preference for even fragments. Extrapolating, you should expect even more structure in ^{240,242}Pu(sf). Have you studied that?

J. P. UNIK: I would expect appreciable fine structure in the mass distribution for spontaneous fission of ^{240}Pu and ^{242}Pu. We are currently studying ^{240}Pu(sf) but have no data available at this time. However, Deruytter will show mass distributions obtained for ^{240}Pu(sf) in a paper to be presented later in this session.[1]

J. C. D. MILTON: In your work you have found that the fragment total kinetic energy increases with the excitation energy of the fissioning system (i. e. dE_k/dE^* is positive) yet previous direct reaction studies by many workers[2] have shown the reverse effect. Moreover, Konecny has just shown us (Fig. 9 of paper IAEA-SM-174/20) that dE_k/dE^* is most negative near mass 130, whereas it is most positive at the same point in your Fig. 8. Do you have an explanation for this discrepancy?

J. P. UNIK: No, I do not have a conclusive explanation for this difference However, the effect observed in this work is experimentally real and, I believe, consistent with the observations of Deruytter for fission of ^{240}Pu. All the cases you cite are for systems above the fission barrier, with angular momentum, whereas I am comparing systems well below the barrier with those slightly above the barrier.

M. ASGHAR: It seems that your ^{239}Pu(n, f) data show less structure than the neighbouring nuclei, ^{235}U(n, f) and ^{245}Cm(n, f). Could you enlarge on this?

J. P. UNIK: I have no comment to make on this.

M. ASGHAR: The data show that the peak-to-valley ratio goes down as the mass of the fissioning nucleus goes up. Have you tried to correlate this ratio to something like $Z_F^2/A_F^{1/3}$, as you did for the $\overline{TKE}$?

J. P. UNIK: We are at present trying to correlate and compare measured peak-to-valley ratios with various theoretical predictions.

P. FONG: I should like to report some recent calculations on asymmetric mass distributions, which is still one of the major problems in fission theory. The starting point of these calculations is the potential

---

[1] DERUYTTER, A.J., WEGENER-PENNING, G., Paper IAEA-SM-174/35, these Proceedings, Vol. 2.

[2] KONECNY, E., SPECHT, H.J., WEBER, J., Paper IAEA-SM-174/20, these Proceedings, Vol. 2; MILTON, J.C.D., SPECHT, H.J., FRASER, J.S., European Conf. on Nucl. Phys., Aix-en-Provence, June-July 1972, J. Phys. (Paris) Colloque 5, Supplement to Vol. 33, No. 8-9 (1972) 17; also earlier work by Schmitt and others.

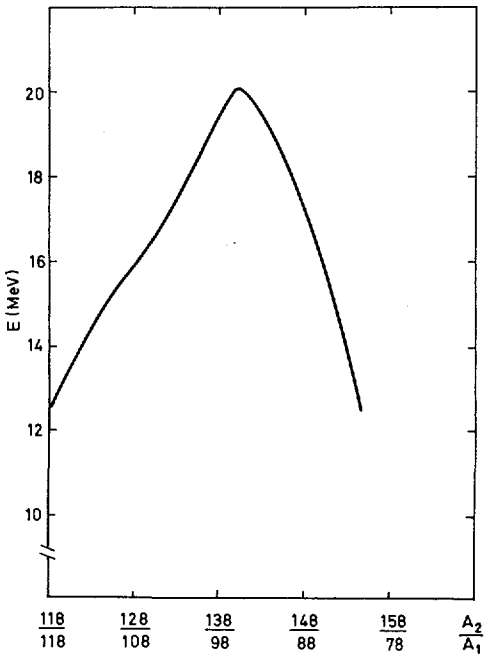

FIG. A. Calculated energy release between saddle and scission for ^{236}U as a function of fragment mass ratio.

energy surface of Mustafa, Mosel and Schmitt. As the ^{236}U nucleus moves from saddle to scission, the potential energy decreases. Figure A shows the amount of energy released as a function of the mass ratio of division. This energy may be transformed to heat excitation energy or kinetic energy of the collective modes of motion. Two alternative calculations are carried out. One assumes that all the energy becomes heat excitation energy, this being the statistical theory which I originated a long time ago. The other assumes that all the energy becomes kinetic energy and this will be referred to as the dynamical theory. The results are shown in Fig. B. The statistical-theory prediction of asymmetric mass distribution is as good as can be expected. This agreement removes one serious difficulty in the statistical theory.

If we examine the current status of the statistical theory, we see that there is no single set of calculations that explains all distributions. On the other hand, within one systematic consistent framework, there do exist separate calculations on mass distribution, charge distribution, kinetic energy distribution, prompt neutron distribution, energy dependence of distributions, LRA fission rate, LRA energy and angular distributions, spontaneous fission distributions and so on. These calculations are reasonably successful and at the present time there are no serious problems.

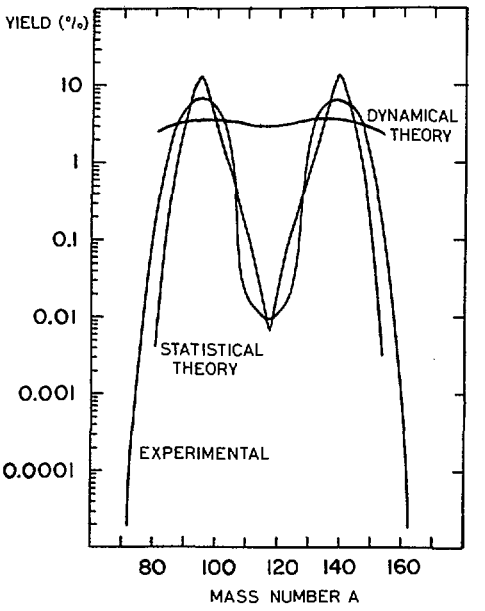

FIG. B. Fragment mass distribution for thermal neutron fission of ^{235}U, calculated assuming energy release all goes into excitation of the fragments (statistical theory) or energy release all goes into kinetic energy of the fragments (dynamical theory).

The fact that the calculations are not combined into one single set is a reflection of the enormous mathematical complexity rather than any intrinsic fundamental difficulty. With the development of more powerful theoretical tools, such as the Strutinsky prescription, BCS calculation, viscosity studies and so on I am optimistic that a single set of calculations for all distributions may eventually emerge.

MEASUREMENT OF THE KINETIC ENERGY DISTRIBUTIONS IN THE THERMAL-NEUTRON-INDUCED FISSION OF ^{255}Fm AND ^{251}Cf

R.C. RAGAINI, E.K., HULET, R.W. LOUGHEED
Lawrence Livermore Laboratory,
University of California,
Livermore, Calif.,
United States of America

Abstract

MEASUREMENT OF THE KINETIC ENERGY DISTRIBUTIONS IN THE THERMAL-NEUTRON-INDUCED FISSION OF ^{255}Fm AND ^{251}Cf.

The kinetic energy distributions of coincident fission fragments from the thermal-neutron-induced fission of ^{255}Fm and ^{251}Cf have been measured with phosphorus-diffused silicon detectors. The most probable value of the post-neutron total kinetic energy is 192.5 ± 2.9 MeV for ^{255}Fm and 182.1 ± 2.7 MeV for ^{251}Cf. Fragment mass distributions were calculated with no neutron emission corrections. The resultant mass and kinetic energy distributions for ^{255}Fm show characteristics indicating predominantly asymmetric fission with appreciable symmetric fission. Fragments near mass symmetry are unusually energetic, which is a feature in common with symmetric fission in ^{257}Fm and ^{258}Fm.

The thermal-neutron-induced fission cross-sections were measured as 3400 ± 170 barns for ^{255}Fm and 4800 ± 250 barns for ^{251}Cf.

The complete text of this paper has been published as:
RAGAINI, R.C., HULET, E.K., LOUGHEED, R.W., Phys. Rev. C9 (1974) 399.

DISCUSSION

M.S. MOORE: Perhaps I misunderstood your comment that the changes you observe do not seem to be very dependent on excitation energy. To my mind, the changes between ^{256}Fm spontaneous fission and (^{255}Fm + n) prompt fission appear quite pronounced.

E.K. HULET: I believe you must be comparing the ^{256}Fm(sf) mass distribution determined by radiochemistry with our distribution measured by counters. Because of the large difference in mass resolution between the two experiments, a comparison of peak-to-valley ratios is not very meaningful. Our conclusion concerning the effect of excitation energy is based partially on the small changes in the mass distribution we observed in ^{251}Cf(n,f) compared with ^{252}Cf(sf). The main point is that we do not find any evidence that excitation energy can be blamed for the very large amount of symmetric fission found in ^{257}Fm(n,f).

M.S. MOORE: Can you extract $\bar{\nu}$ for ^{256}Fm prompt fission using these data and the radiochemical results?

E.K. HULET: Yes, in principle $\bar{\nu}$ can be derived from these experiments, but it would be quite inaccurate.

D.C. HOFFMAN: Firstly, I should like to confirm that the counter experiments do not have as good a mass resolution. For example, the peak-to-valley ratio for ^{252}Cf is ≅ 700 from radiochemical measurements, while ≅ 10 is a good value for counter experiments. In addition, if a $\bar{\nu}$ correction is made for Fm, this can deepen the valley obtained from counter measurements.

Secondly, as you have pointed out, the highest TKE is observed for mass symmetric splits both for ^{255}Fm(n,f) and ^{257}Fm(sf) but, in addition, the variance of the TKE is large and some symmetric fission has rather low TKE. Would you comment on whether this may be another type of symmetric fission or is it a tailing of asymmetric peaks, in other words, why is there such a large distribution of TKE at symmetry?

E.K. HULET: Since we can distinguish symmetric fission by the unusually high kinetic energies of the fragments, the mass-kinetic energy distributions have the appearance of a symmetric fission mode superimposed upon a normal asymmetric one. It looks as if there are two fission modes present in ^{255}Fm(n,f), ^{257}Fm(sf) and ^{257}Fm(n,f). The low kinetic energies from fragments near mass symmetry would then arise from the asymmetric mode of fission – that is a symmetric scission of asymmetrically deformed nuclei.

B.D. WILKINS: We have calculated potential energy surfaces for the fermium isotopes using a static model. For the ligher fermium isotopes the calculations show a deepest minimum in the potential energy, asymmetric in mass, occurring at quite large deformations. As one adds neutrons, a second minimum, occurring at small deformations, rapidly comes down in energy as one approaches ^{264}Fm. This minimum is symmetric in mass and because of its small deformations would be expected to yield significantly higher TKE values than the asymmetric component.

When one looks at the experimental data for ^{255}Fm(n,f), it is clear that the asymmetric component is quite dominant even at symmetry, where one expects it to have a TKE release of about 215 MeV. However, a small yield from the symmetric minimum giving a TKE of ~240 MeV is readily apparent.

At ^{258}Fm the situation has changed with the symmetric minimum becoming dominant. Thus, in addition to the high TKE release, one expects a much greater variance in TKE at symmetry owing to the contributions from both minima.

F. PLASIL: I would like to disagree with Mr. Hulet's comment that his results seem to indicate the existence of two modes of fission in the neutron-induced fission of ^{255}Fm. First, I think that the term "fission mode" should be reserved for situations where it is clearly demonstrated that two qualitatively different processes are involved, such as could be the case if the barriers were to be different. What we should consider is the question whether there is justification for decomposing the measured distributions into symmetric and asymmetric components. The decision to decompose and to talk about two different components is largely arbitrary, but it does not seem to be suggested by the fragment total kinetic energy versus fragment mass contour diagram just shown. There is no hint of a separate peak in the distribution as is the case in the fission of nuclei near radium. All that seems to be indicated is a preference for higher kinetic energies when the mass divisions are close to symmetry.

This effect can be understood, as Mr. Hulet pointed out, in terms of the expected near-spherical shape of the fragments in that mass region.

K. DIETRICH: I should like to mention that when Dickmann and I recalculated the Vandenbosch model using the Strutinsky method some years ago, we always obtained two minima for a given mass split. They corresponded to different fragment deformations at scission and this would therefore also imply different kinetic energy components. These calculations were done for uranium and it is conceivable that similar results could be obtained for fermium.

U. MOSEL: In the case of the ligher actinides, one of the two minima you obtained in your recalculation would be due to the liquid drop behaviour, whereas the other one would be due to the shell effects. Since fission becomes symmetric again in the fermium region and both the LDM and the shell corrections tend to favour symmetric splits, there is little reason to expect two fission modes based on this explanation for the most dominant decay mode.

COMPARISON OF THE FISSION CHARACTERISTICS OF THERMAL-NEUTRON-INDUCED FISSION OF ^{239}Pu AND THE SPONTANEOUS FISSION OF ^{240}Pu

A.J. DERUYTTER
CBNM, Euratom, Geel

G. WEGENER-PENNING*
SCK-CEN, Mol,
Belgium

Abstract

COMPARISON OF THE FISSION CHARACTERISTICS OF THERMAL-NEUTRON-INDUCED FISSION OF ^{239}Pu AND THE SPONTANEOUS FISSION OF ^{240}Pu.

The thermal-neutron-induced fission of ^{239}Pu and the spontaneous fission of ^{240}Pu were compared to study the influence of the excitation energy on the fission characteristics. A two-dimensional coincident fragment pulse-height analysis was performed with a 4π Pu source viewed by a surface barrier detector on each side of the foil. The Pu source was a mixture of about 90% ^{240}Pu and 10% ^{239}Pu. The thermal neutron measurements were performed with a well-thermalized beam of the BR1 graphite reactor. The ^{240}Pu spontaneous fission experiments were performed with the reactor shut down. In such a method the systematic errors cancel in the comparison. Kinetic energy and mass distributions were obtained for both systems. The average pre-neutron total kinetic energy is found to be higher for thermal-neutron-induced fission, i.e. 177.9 ± 0.04 MeV, than the value 176.8 ± 0.14MeV for spontaneous fission. The indicated errors are statistical. The mass distributions are similar. However, the peak-to-valley ratio is larger, and the peaks are narrower and shifted towards the symmetric point over 1 mass unit for spontaneous fission. Mass distributions for several groups of total kinetic energies of the fragments indicate that with increasing toral kinetic energy the mass peaks become narrower, the average heavy mass approaches 132 and apparent fine structure at lower kinetic energies disappears. The fine structure effects in the mass distributions at low total kinetic energies are more pronounced in spontaneous fission. This effect may be due to the fact that in thermal-neutron-induced fission of ^{239}Pu, 0^+ and 1^+ channels are open.

1. INTRODUCTION

The mass and kinetic energy distributions of the fission fragments show many peculiarities such as asymmetry of the fragment mass division, fine structure at well-defined masses and a maximum of the total kinetic energy for a heavy fragment mass equal to 132.

Until now one could not predict the influence of the excitation energy on all these peculiarities, because knowledge is lacking on the fission process between the saddle point and the scission point.

Several fast neutron fission experiments have been carried out for nuclei with mass number varying from ^{232}Th to ^{241}Pu. In those experiments the probability for the reaction (n, n'f) is real and may cause trouble in the correct interpretation of the results.

We carried out a double energy experiment with the compound nucleus ^{240}Pu. We compared the thermal-neutron-induced fission of ^{239}Pu with the spontaneous fission of ^{240}Pu. In the first case the excitation energy of the

* Research sponsored by I.W.O.N.L., Belgium

compound nucleus was 6.4 MeV higher than in the second. The relatively short half-life for spontaneous fission of ^{240}Pu and its very low fission cross-section at thermal neutron energies permitted the use of one source containing ^{240}Pu as well as ^{239}Pu. The thermal neutron fission of ^{239}Pu (large cross-section) is measured with the reactor beam on; ^{240}Pu spontaneous fission with the reactor shut down. So the same experimental arrangement could be used for both.

An analogous experiment was carried out a long time ago by Mostovaya [1] with a double ionization chamber. Toraskar and Melkonian [2] also studied the spontaneous fission of ^{240}Pu and the low-energy neutron induced fission of ^{239}Pu, but this was done in two separate experiments with a different source and another set of detectors. Recently, analogous experiments were done on the compound nuclei ^{242}Pu [3], ^{250}Cf and ^{246}Cm [4].

2. EXPERIMENTAL PROCEDURE

The fission source was prepared at CBNM-Geel and consisted of 60 $\mu g/cm^2$ Pu acetate electrosprayed on a gold-coated VYNS film. It contained about 8.3% of ^{239}Pu and about 90% of ^{240}Pu. The exact isotopic composition is given in Table I.

Care was taken to keep the Cf- and Cm-impurities below the detection limit. Two large gold-silicon surface barrier detectors were placed face-to-face at opposite sides of the target. Detectors and fission source were mounted parallel to the direction of the neutron beam in a vacuum fission chamber constructed with thin Al windows for entrance and exit of the neutron

TABLE I. ISOTOPIC COMPOSITION OF THE Pu-TARGET

Isotope	Abundance (%)
^{238}Pu	0.006
^{239}Pu	8.261
^{240}Pu	90.820
^{241}Pu	0.853
^{242}Pu	0.060
^{241}Am	1.07
Cm	$\ll$ 0.01
Cf	$\ll$ 0.01

beam. A well-thermalized and collimated neutron beam of the Belgian reactor BR 1 was used. The electronic apparatus for this two-parameter correlation experiment consisted of two charge-sensitive preamplifiers and two double-delay-line clipped amplifiers with a clipping time of 2 μs to avoid distortion of the pulse-height spectra by α pile-up. We further used a fast-slow coincidence unit with a resolution time of 6 ns, and a double analogue-to-digital converter of 128 x 128 channels. Coincident pulse heights were registered event by event on paper tape. We registered alternatively the thermal fission with the reactor on, and the spontaneous fission with the reactor shut down, to avoid background. The data were collected during a period of several weeks. About 10^5 thermal and about 10^4 spontaneous fission events were registered.

With such an experimental procedure, systematic errors cancel in the comparison of the results and we only have to take the statistical errors into account for the comparison.

3. DATA ANALYSIS

From the coincident pulse heights of the two complementary fragments, post-neutron kinetic energy values were calculated with the simple linear equations

$$E_i = A_i x_i + B_i \qquad i = 1, 2 \text{ (detectors)} \qquad (1)$$

where E_i and x_i are the energy and the pulse height of the fragment, and A_i and B_i are the calibration constants.

The use of the mass-dependent calibration formula of Schmitt [5] is not appropriate here because the detectors suffer from a large α-flux.

The constants A_i and B_i from Eq. (1) are determined by identification of the average light pulse height and the average heavy pulse height with the corresponding post-neutron kinetic energies obtained by Schmitt [5].

For each thermal fission run, the calibration constants were determined. They varied slowly with time and we fitted a linear function of the time through the experimental values of $A_i(t)$ and $B_i(t)$. This method permitted us to obtain accurately the values of the calibration constants for the spontaneous fission runs by interpolation.

A first approximation of the fragment masses, μ_i, was obtained from the relations

$$\mu_1 E_1 = \mu_2 E_2 \qquad (2)$$

$$\mu_1 + \mu_2 = 240 \qquad (3)$$

E_1 and E_2 are the post-neutron energies from Eq. (1). Equation (2), the law of conservation of impulse, is only rigorously valid for the fragments before neutron evaporation. To correct these preliminary energy and mass values for neutron emission we used the distribution of emitted neutrons as a function of the fragment mass as obtained by Milton and Fraser [6]. For spontaneous fission of ^{240}Pu, such a distribution is not available in the literature, but it is well known that for all fissioning isotopes the general features of these distributions are similar. So we multiplied the whole distribution of

(^{239}Pu + n_{th}) with the ratio between the average number of emitted neutrons per fission [7] for spontaneous fission of ^{240}Pu and for thermal-neutron-induced fission of ^{239}Pu.

In this way neutron emission corrections were carried out for spontaneous as well as for thermal fission, event by event. From these event-by-event calculated values the mass and the total kinetic energy distributions were obtained and the correlation between mass and energy was studied. We obtained mass distributions for several discrete groups of total kinetic energy values, as well as the variation of the total kinetic energy as a function of the heavy fragment mass.

4. RESULTS AND DISCUSSION

4.1. Total kinetic energy and mass distributions

The total pre-neutron kinetic energy for the thermal-neutron-induced fission of ^{239}Pu is 177.95 ± 0.04 MeV. This value is 1.1 ± 0.2 MeV larger than that for the spontaneous fission of ^{240}Pu. In the latter case we obtained 176.84 ± 0.14 MeV. This difference is caused mainly by the difference in kinetic energy of the light fragment (cf. Table II).

A normal distribution was fitted to the experimental total kinetic energy distributions. The areas of these distributions shown in Figs 1 and 2 are normalized to make the comparison easier.

The distribution for spontaneous fission differs from that for thermal fission in a few respects:

(a) The right side of the distribution in Fig. 1 shows a deviation from the normal shape.
(b) The distribution is slightly broader.
(c) The whole distribution is shifted to the low-energy side (see Fig. 2).

TABLE II. PRE-NEUTRON ENERGY AND MASS VALUES

	^{239}Pu + n_{th}	^{240}Pu sp.f.
$< E^*_{tot.kin.} >$	177.9 ± 0.04 MeV	176.8 ± 0.14 MeV
$< E^*_L >$	103.4 ± 0.04 MeV	102.4 ± 0.14 MeV
$< E^*_H >$	74.5 ± 0.04 MeV	74.3 ± 0.14 MeV
$< m^*_L >$	100.76 ± 0.04 amu	101.55 ± 0.14 amu
$< m^*_H >$	139.24 ± 0.04 amu	138.45 ± 0.14 amu

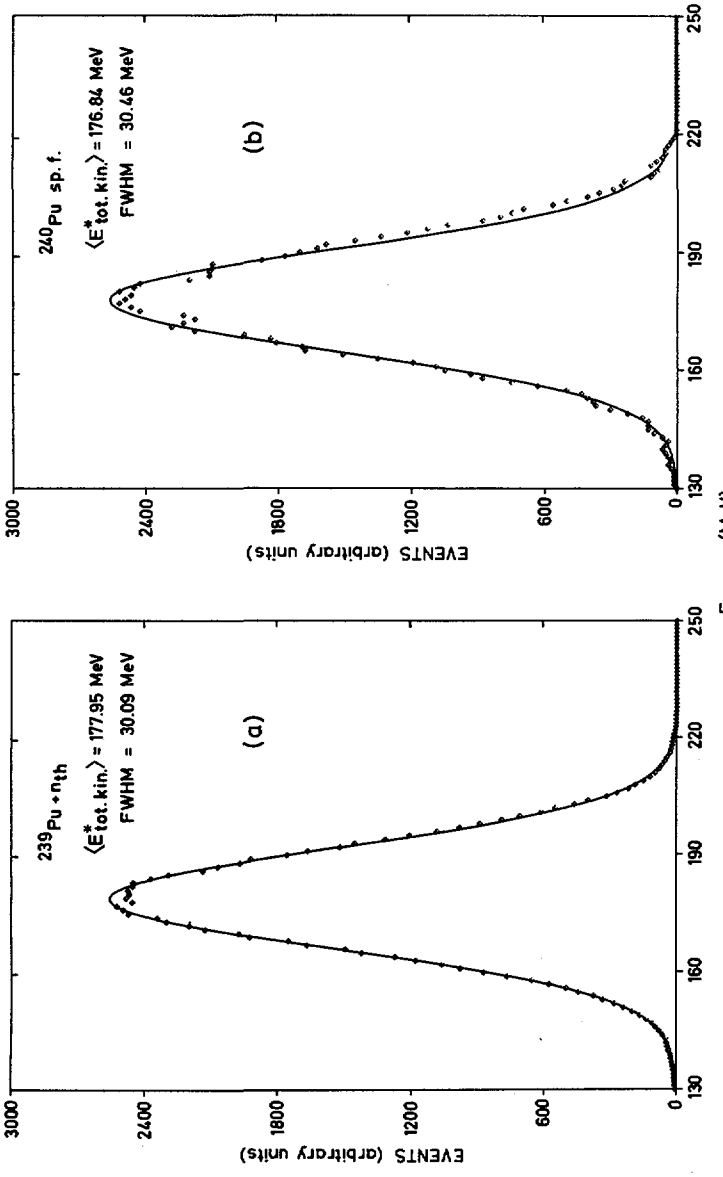

FIG.1. Distribution of the total pre-neutron kinetic energy of the fission fragments for (a) ^{239}Pu + n_{th} and (b) ^{240}Pu spontaneous fission. The full lines represent the normal distribution fitted through the experimental points, represented by dots.

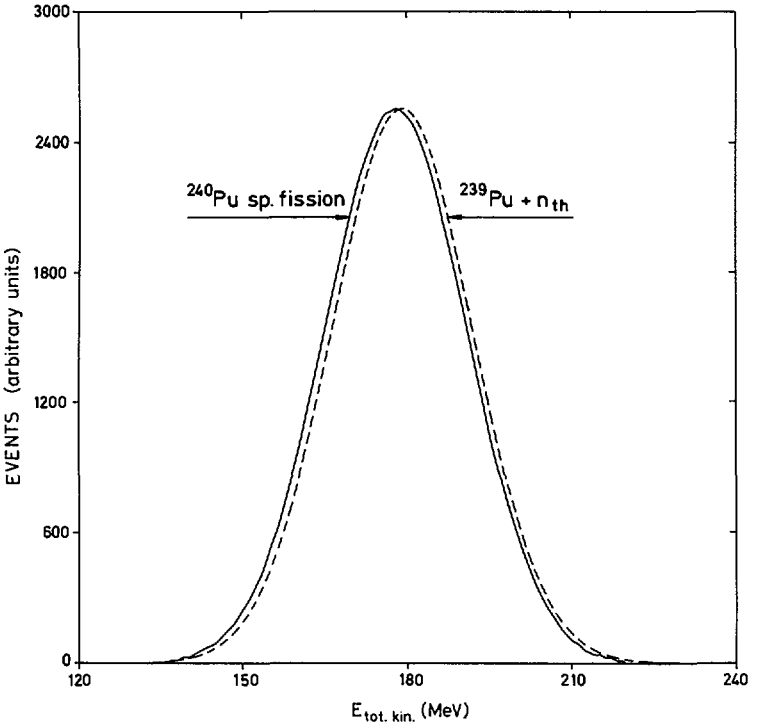

FIG. 2. Comparison of the fitted energy distributions for $^{239}Pu + n_{th}$ (dotted line) and for ^{240}Pu spontaneous fission (full line).

The mass distributions are shown in Fig. 3. Again the areas of the distributions are normalized. Only the heavy fragment side is shown on the figure; the light fragment side is identical but reflected with respect to the symmetric point M = 120.

There are again some differences between the spontaneous and induced fission results:

(a) There is a shift over about one mass unit of the peak to the point M = 120 for spontaneous fission (see also Table II).
(b) The peak is broader for induced fission.

There is in general good agreement between our results and those of Mostovaya [1]. There are however considerable disagreements between our results and those of Toraskar and Melkonian [2]. They obtained a total kinetic energy which is about 3.7 MeV higher for spontaneous fission, where we found a difference in the opposite direction of 1.1 MeV. The shapes of the mass and energy distributions show significant differences from all such distributions known until now: they detected a pronounced shoulder in the mass distribution near $M_H = 142$ and also one in the energy distribution near $E^*_{tot.\,kin.} = 186$ MeV.

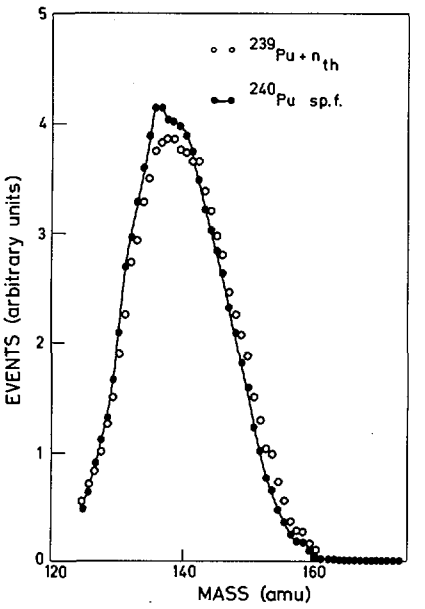

FIG.3. Mass distributions for spontaneous and induced fission (only the heavy fragment mass is represented).

The results of Toraskar and Melkonian are obtained from two separate experiments, so in the comparison of the results the systematic errors do not cancel. An additional uncertainty is introduced by the different calibration procedures used in the two cases: for induced fission, the mass-dependent Schmitt formula for ^{239}Pu was used, but for spontaneous fission of ^{240}Pu the same formula was used utilizing ^{252}Cf spontaneous fission data. The total error (systematic and statistical) on the total energy difference is about 3 MeV, whereas the statistical accuracy of our result is 0.2 MeV.

Recently Dyatchenko and co-workers [3] carried out an analogous experiment on the compound nucleus ^{242}Pu. They also obtained a higher total kinetic energy for the spontaneous fission compared with their value for induced fission, but the general characteristics of the kinetic energy and mass distributions obtained by this group are in agreement with our results.

Unik and co-workers [4] also performed analogous experiments. They compared the thermal-neutron-induced fission of ^{245}Cm and ^{249}Cf with the spontaneous fission of ^{246}Cm and ^{250}Cf, respectively. There is good agreement between our results and those of Unik. The total kinetic energy is higher for induced fission then for spontaneous fission. Also the general shape of the distributions shows the same trends.

4.2. Total energy balance

The compound nucleus ^{240}Pu formed by capture of a thermal neutron in the nucleus ^{239}Pu has an excitation energy which is 6.4 MeV – the binding energy of the neutron – higher than the nucleus ^{240}Pu fissioning spontaneously in its ground state.

TABLE III. TOTAL ENERGY BALANCE

	$^{239}Pu + n_{th}$	^{240}Pu sp.f.
$< E^*_{tot.kin.} >$	177.95 ± 0.04 MeV	176.8 ± 0.14 MeV
$< E_{neutr.} >$	21.2 ± 0.4 MeV	15.8 ± 0.5 MeV
$< E_\gamma >$ [9]	8 ± 1.5 MeV	8 ± 1.5 MeV
$< Q >$	207.1 ± 1.9 MeV	200.6 ± 2.1 MeV

There should be about the same 6.4-MeV difference between the $\langle Q \rangle$ values of both systems – $\langle Q \rangle$ is the average total energy released per fission. $\langle Q \rangle$ is composed of the total kinetic and the total excitation energy of the fragments. We assume the average released gamma energy to be equal for both cases, then only neutrons account for the difference in total excitation energy. We calculated from our mass distributions, and using the neutron distributions of Milton and Fraser [6] and the neutron binding energy tables of Milton [8], that about 5.3 MeV of the initial supplementary excitation energy goes into neutron emission in the case of induced fission (see Table III). Together with the total kinetic energy difference of 1.1 MeV, we obtain a $\Delta\langle Q \rangle$ value of about 6.5 MeV, almost exactly the difference in initial excitation energy. We obtained the same conclusion as Unik [4] for the compound nuclei ^{246}Cm and ^{250}Cf, i.e. the additional excitation energy is distributed between additional kinetic energy and additional neutron emission.

4.3. The mass distribution correlation with kinetic energy

The variation of the total kinetic energy as a function of the heavy fragment mass is shown in Fig. 4. In general, the energy curve for spontaneous fission lies below that for induced fission. But at the broad maximum situated between $M_H = 130$ and $M_H = 135$ the energy for both systems is about equal, within the statistical error limits.

There is also a slight deviation from a monotonic decrease in the region $136 < M_H < 150$ near a heavy mass value $M_H = 142$.

Analogous features are found by Unik and co-workers [4] and Dyatchenko and co-workers [3] for other isotopes. Toraskar and Melkonian [2] found that the entire energy curve for spontaneous fission lies higher than that for induced fission in the case of ^{240}Pu. Owing to limited statistical accuracy in the curve, no further conclusions may be drawn.

In Figs 5 and 6, mass distributions are shown for increasing total kinetic energy, ranging from 152 MeV to 207 MeV in steps of 5 MeV, for spontaneous and induced fission respectively. With increasing kinetic energy the peaks of the distributions become narrower and shift to the symmetric point, the symmetric yield decreases and the average heavy mass

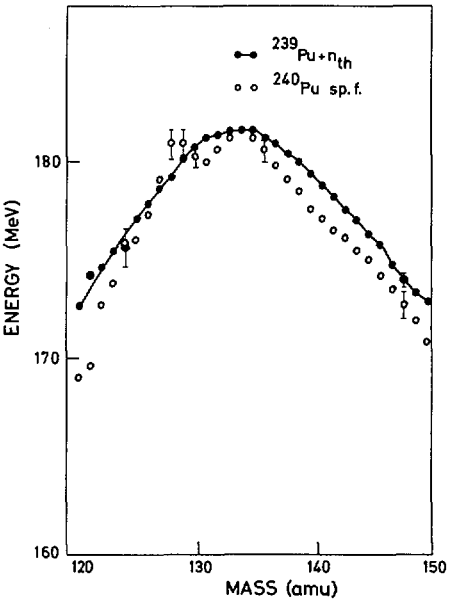

FIG.4. Comparison of the variation of the total kinetic energy with the heavy fragment mass for both fissioning systems.

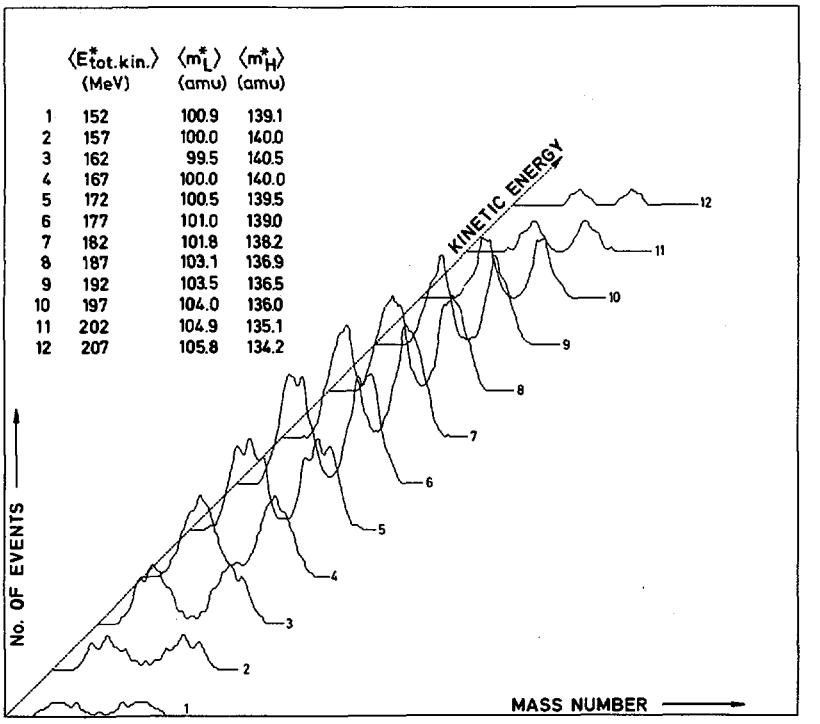

FIG.5. Mass distributions for the spontaneous fission of ^{240}Pu for increasing total kinetic energy of the fragments, ranging from 152 MeV to 207 MeV in steps of 5 MeV.

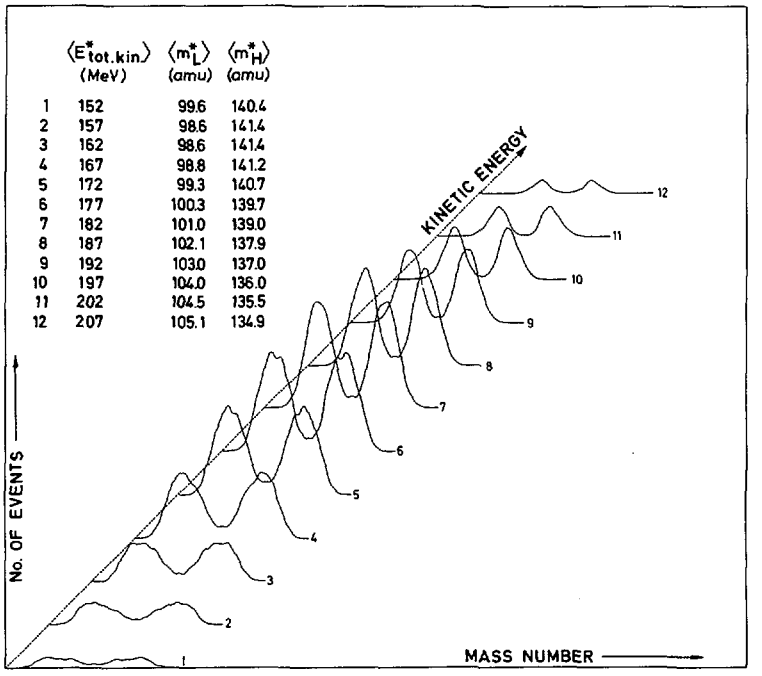

FIG. 6. Mass distributions for the thermal-neutron-induced fission of ^{239}Pu for increasing total kinetic energy of the fragments, ranging from 152 MeV to 207 MeV in steps of 5 MeV.

approaches $M_H = 132$. These trends are illustrated in the tables in Figs 5 and 6. Although the statistical errors in the spontaneous fission experiments are large, especially for the spectra away from the maximum yield, and call for some reserve, the mass distributions seem to show more structure than in the case of induced fission. This may be because more fission channels are open in the latter case, leading to slightly different mass and kinetic energy divisions.

From the previous discussion it follows that the difference of 6.4 MeV in excitation energy of the compound nucleus leads to a difference of 1.1 MeV in kinetic energy of the fragments and 5.3 MeV in internal excitation energy of the fragments. This result supports the relatively strong damping during the first part of the descent from the saddle point to the scission point in the picture proposed by Bjørnholm [10].

ACKNOWLEDGEMENTS

The authors thank Dr. V. Verdingh and Dr. P. De Bièvre of CBNM, Geel, Belgium, for the target preparation and the isotopic analysis, respectively, Dr. W. Wegner, Mr. E. Mies and Mr. R. Boden of SCK, Mol, Belgium for programming, electronic assistance and chemical analysis of the target, respectively.

REFERENCES

[1] MOSTOVAYA, T.M., in Peaceful Uses of Atomic Energy (Proc. Conf. Geneva, 1958) 15, UN, New York (1958) 433.
[2] TORASKAR, J., MELKONIAN, E., Phys. Rev. C4 (1971) 267 and Phys. Rev. C4 (1971) 1391.
[3] DYATCHENKO, N.P., KABENIN, V.N., KOLOSOV, N.P., KUZMINOV, B.D., SERGATCHEV, I., Institute of Physics and Energetics, Obninsk (USSR) Rep. 366. (1973).
[4] UNIK, J.P., GINDLER, J.E., GLENDENIN, L.E., FLYNN, K.F., GORSKI, A., SJOBLOM, R.K., Paper IAEA-SM-174/209, these Proceedings, Vol.2.
[5] NEILER, J.N., WALTER, F.J., SCHMITT, H.W., Phys. Rev. 149 (1966) 897.
[6] MILTON, J.C.D., FRASER, J.S., Annu. Rev. Nucl. Sci. 16 (1966) 894.
[7] BROOKHAVEN NATIONAL LABORATORY, Rep. BNL 325, Suppl. 2 (1965).
[8] MILTON, J.C.D., Rep. UCRL-9883 (1962).
[9] JAMES, M.F., J. Nucl. Energy 23 (1969) 517.
[10] SWIATECKI, W.J., BJØRNHOLM, S., Phys. Reports 4 (1972) 325.

DISCUSSION

H.J. SPECHT: With the aid of Fig. A I should like to present some experimental information on the dependence of the average total kinetic energy $\langle E_k \rangle$ on excitation energy in ^{240}Pu. In addition to the two points indicated by crosses for spontaneous and thermal neutron fission reported by Mr. Deruytter, I have included the excitation energy dependence found in the ^{239}Pu (d, pf) reaction by Milton and co-workers[1]. I have also added a point for fission from the well-known 4-ns isomeric state in ^{240m}Pu which we have measured in Munich. The error bars given include possible systematic errors, which I do not think is the case with Mr. Deruytter's points. (These are normalized to Schmitt's thermal neutron value, which in turn is indicated by the solid point and large error bar.) It is remarkable that this value still seems to follow the trend observed for fission above the barrier, whereas the point for spontaneous fission from the ground state is definitely lower.

J.P. UNIK: The excitation energy dependence of the total kinetic energy for fission of ^{240}Pu is more complex than indicated in this figure. Several years ago we reported the negative slope observed for ^{239}Pu (d, pf). However, we also observed at that time that the negative slope ($d\overline{TKE}/dE^*$) was approximately three times larger for the case of ^{240}Pu ($\alpha, \alpha' f$), indicating a strong angular momentum dependence.

A.J. DERUYTTER: It would certainly be very dangerous to extrapolate the curve shown in this figure to zero excitation energy, because this would lead to quite a high value for the kinetic energy, one that would be hard to explain.

M. ASGHAR: According to the data presented in Mr. Deruytter's paper, most of the 1.1-MeV difference in the total kinetic energy between ^{239}Pu (n, f) and ^{240}Pu (sf) appears to be taken up by the light fragment. I wonder why this should be so?

S. BJØRNHOLM: I believe that the preferential increase in the kinetic energy of the lighter fragment is related by conservation of momentum to the shift towards higher mass asymmetry in the neutron-induced fission experiment.

---

[1] MILTON, J.C.D., et al., in European Conf. on Nuclear Physics (Aix-en-Provence, June-July 1972), J. Phys. (Paris) Colloque 5, Supplement to Vol. 33, No. 8-9 (1972) 17.

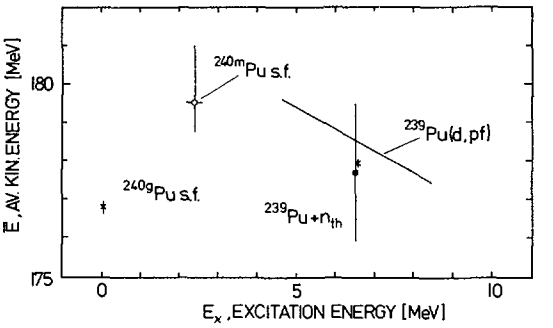

FIG. A. Average total fragment kinetic energy versus excitation energy for excitation below 10 MeV. See discussion for a description of symbols in figure.

A. J. DERUYTTER: It is certainly clear from the experimental evidence presented in the paper that the major part of the difference is taken up by the light fragment and I agree with Mr. Bjørnholm's observation.

S. BJØRNHOLM: The advantage of your experiment is that you can in principle compare fission from 0^+ states exclusively. How much does fission from the 1^+ resonances in ^{239}Pu (n_{th}, f) contribute in practice?

A. J. DERUYTTER: In the case of thermal-neutron-induced fission of ^{239}Pu, about 51% of the fissions result from a bound level resonance (0^+), 42% from the 0.297-eV resonance (1^+) and the remaining fraction from higher energy resonances (mixture of 0^+ and 1^+). However, as has been shown by Melkonian and co-workers at Columbia University, the difference in kinetic energy between these two channels is only 0.7 MeV and cannot explain the observed difference. However this remark does not affect the experimental 1.1-MeV difference observed here between spontaneous fission of ^{240}Pu and the thermal-neutron-induced fission of ^{239}Pu.

E. MELKONIAN: In our measurements at Columbia University we used Be and Sm filters to isolate the negative 0^+ energy level and the 0.3-eV 1^+ level, respectively. The Be-filtered data give a more direct comparison with the SF case. The total kinetic energy difference between the two levels is 0.7 MeV, a correction for which would reduce, but not eliminate, your effect.

I should like to ask a question concerning the use of 128 channel ADCs. Such a small number of channels leads to grid fluctuations, as pointed out by J. C. D. Milton and others many years ago. How did you handle this problem?

A. J. DERUYTTER: The grid fluctuations are indeed real if you want to make a two-dimensional mass surface starting from two energy values, but we simply plotted the mass distributions for groups of 5-MeV total kinetic energies. Furthermore, as I stressed in the oral presentation, we have a greater interest in the more general characteristics of the behaviour of these distributions as a function of total kinetic energy. Statistical fluctuations are present, especially for ^{240}Pu spontaneous fission.

T. GOZANI: The ambiguity in the angular momentum states excited in fissions that are induced in direct reactions with charged particles, mentioned now and on several occasions before, emphasizes again the desirability of performing more photofission studies in the threshold and subthreshold regions. The experimental problems involved in the unfolding of the bremsstrahlung data should be more than compensated for by the fact that no more than two states (E1 and E2) are excited for even-even nuclides.

A SYSTEMATIC ODD-EVEN EFFECT IN THE INDEPENDENT YIELD DISTRIBUTIONS OF NUCLIDES FROM THERMAL-NEUTRON-INDUCED FISSION OF ^{235}U

S. AMIEL, H. FELDSTEIN
Nuclear Chemistry Department,
Soreq Nuclear Research Centre,
Yavne, Israel

Abstract

A SYSTEMATIC ODD-EVEN EFFECT IN THE INDEPENDENT YIELD DISTRIBUTIONS OF NUCLIDES FROM THERMAL-NEUTRON-INDUCED FISSION OF ^{235}U.

A detailed analysis of experimental data was found to exhibit a systematically consistent odd-even effect in the independent yield distributions of the nuclides in thermal-neutron-induced fission of ^{235}U.

The odd-even effect in the element yield distribution for elements at the fission peaks appears as a saw-tooth structure, in which the amplitudes between the enhanced even-Z yields and the less favoured odd-Z yields are $\pm$ 25% of the mean values. The elements examined constitute ~75% of the fission yield.

The distribution of the isotopic yields in many cases was found to have a saw-tooth pattern superimposed on a Gaussian-like shape, where the amplitudes between the high even-N and low odd-N values are on the average $\leq \pm$ 8% of the mean values. This effect at the light peak nuclides seemed to be unresolved while pronounced at the heavy peak nuclides.

The isobaric dispersions were studied in 24 mass chains (14 at the heavy mass peak and 10 at the light peak) and were found to follow the general pattern of a Gaussian with widths varying between 0.45 and 0.8 charge units. The detailed description of the isobaric dispersion is represented by a saw-tooth structure fluctuating with amplitudes of $\geq$ 30% around a constant-width Gaussian in which the even-Z nuclides are consistently enhanced. The only appearance of a significant closed shell effect is observed in ^{134}Te.

The fact that the neutron pairing effect in the yields as compared with that of the protons is much smaller is attributed to the evaporation of neutrons during the de-excitation of the fragments, a process which is responsible for "washing out" part of the original neutron pairing effect in the primary fragment formation in fission.

The present set of experimental data indicates the relative importance of the individual properties of the fragments versus the collective behaviour of the fissioning nucleus, as described by the calculations of deformations of shell-corrected liquid drop potential energy surfaces. One is also led to conclude that nucleon transfer, visualized by the different charge density of the fragments, takes place before scission and that at scission there is a smaller probability, consistent with energy considerations, of breaking pair configurations.

INTRODUCTION

Much of the phenomenology of fission has recently been described satisfactorily using Strutinsky's method of calculating deformed shell structured potential energy surfaces (1). Calculations based on this approach rendered a qualitatively correct picture of most mass distributions in fission of both symmetric and asymmetric modes (2-6). However, a more detailed comparison between the theoretical and experimental results indicates that the fine structures experimentally observed (e.g., in the mass yields and kinetic energy distributions) are not explained by the theory at this stage. Such structure has been found experimentally in thermal neutron fission of doubly even nuclides, indicating a pronounced preference for the formation of doubly even fission fragments at low excitation energies (7-9). This may be explained by the greater stiffness of doubly

even fragments, being less deformed and hence formed preferably when the available energy is low (8). Another possible explanation is obtained by referring to the proton and neutron pairs in the fissioning nucleus; since low-energy fission may be sufficiently adiabatic there is a reduced probability for breaking of pairs at scission and doubly even fragments should thus be more frequent than those of odd mass, while doubly odd ones should be further reduced (10).

Wahl has given a satisfactory approximation for the calculation of independent yields in thermal neutron fission in ^{235}U by using the experimental mass yields, an empirical Z_p function and assuming a Gaussian distribution of constant width of $\sigma = 0.56 \pm 0.06$ charge units applicable to the whole range of fission products (11). The correlation of those yields, which he referred to as the "normal" ones, with the experimental values, revealed an enhancement in yields of even-Z elements (12) and depression of those of odd-Z.

Recent experimental data, based on isotopic separation of fission products, substantiated Wahl's suggestion and clearly showed an enhancement of yields of some even-Z elements as compared with the depressed yields of odd-Z elements (12-16). However, measurement of K X-rays in coincidence with fission fragments from thermal neutron fission of ^{235}U, ^{233}U and ^{239}Pu revealed only a weak proton pairing effect (9).

The neutron pairing effect has been found in the mass-separated cesium and rubidium isotopes, the effect being greatest for the heavy isotopes and diminishing towards the peak of the isotopic yield distributions (17). Adopting the "pair breaking" argument one should expect a higher fission yield of fragments with a paired number of the same nucleon. This seems to be true for the proton pairing but does not seem as prominent for the neutrons.

Some experiments based on mass and kinetic energy selection showed an effect of closed shells on the yield distribution (15), but radiochemical experiments did not substantiate it [1](31,33).

The purpose of this work is to elucidate the odd-even systematics by a rigorous treatment of the available experimental data and to establish quantitatively the magnitude of the pairing and shell effects in the overall distribution of nuclides in low-energy neutron fission of ^{235}U.

EVALUATION OF EXPERIMENTAL FISSION YIELDS

The experimental independent yields of thermal-neutron-induced fission products of ^{235}U are given in Tables I and II. The data were taken from the literature (12, 18-40) and from recent experimental results from this laboratory obtained by on-line isotope separations (13,25). Fractional independent and cumulative fission yields are given in the tables as they are quoted in the various sources and the "normal" fractional independent yields (hence, FIY) were those calculated by Wahl (12). The "corrected" fractional independent yields in the tables are based on the experimental data wherever such were available. When several different values were published, the "corrected" one was chosen considering the distribution of yields of the neighboring isobars in the chain and of isotopes of the same elements in

[1] Denschlag reports that by selecting longer-range recoils followed by radiochemical separation he was able to observe some enhancement of ^{132}Sn.

view of the generally prevailing odd-even proton number systematics, discussed below. In a few cases, "corrected" values derived by the above considerations have been substituted for the published values. Where fission yields have not yet been established experimentally, they were calculated from other FIY's in the isobaric chain, satisfying the requirement that the sum of fractional independent yields should be unity.

Table III summarizes the isotopic yields of some complementary light and heavy elements, which constitute about 75% of the fission products. The column, "experimental yield", was calculated by multiplying the "corrected" FIY's from Tables I and II by the corresponding chain yields. Since comparison of the total element yield with the predicted "normal" value indicated a systematic enhancement of the yields of even-Z elements by approximately 25% and the same decrease for the odd-Z yields, we adopted a multiplication factor of 1.25 x "normal" or 0.75 x "normal" according to proton pairing, in order to calculate a few missing "corrected" FIY's in Tables I and II which otherwise could not be calculated.

SYSTEMATICS OF ELEMENT YIELDS

Table III demonstrates clearly the proton pairing effect of the isotopic chain yields, which is about ± 25% relative to the predicted Wahl's "normal" values. The latter seem to serve as an excellent average value for all the experimental yields. The effect is apparent in Fig. 1 where the yields fit well the curves obtained by multiplying the "normal" distribution by a factor of 1.25 or 0.75 for even or odd proton number, respectively. This finding is in good agreement with Wahl's previous observation (12) and the experimental results (13-16); the only exception being the

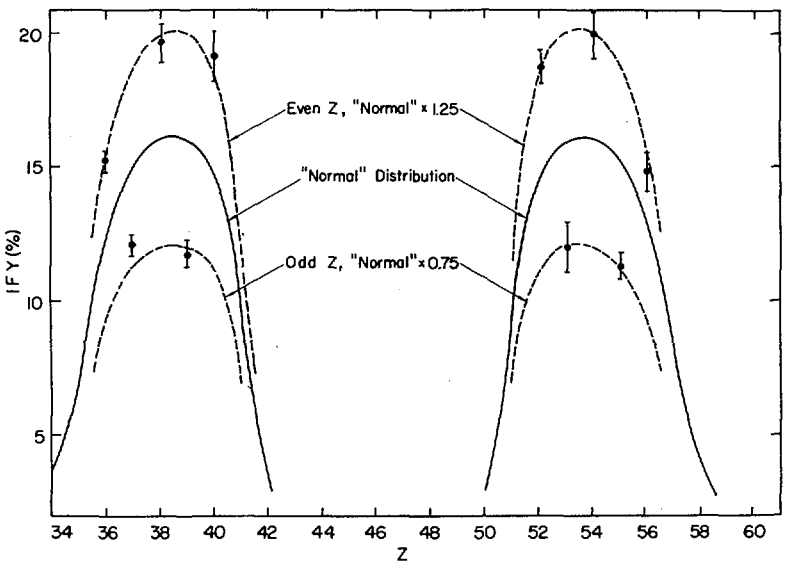

FIG. 1. Element yield distribution in thermal-neutron-induced fission of ^{235}U.

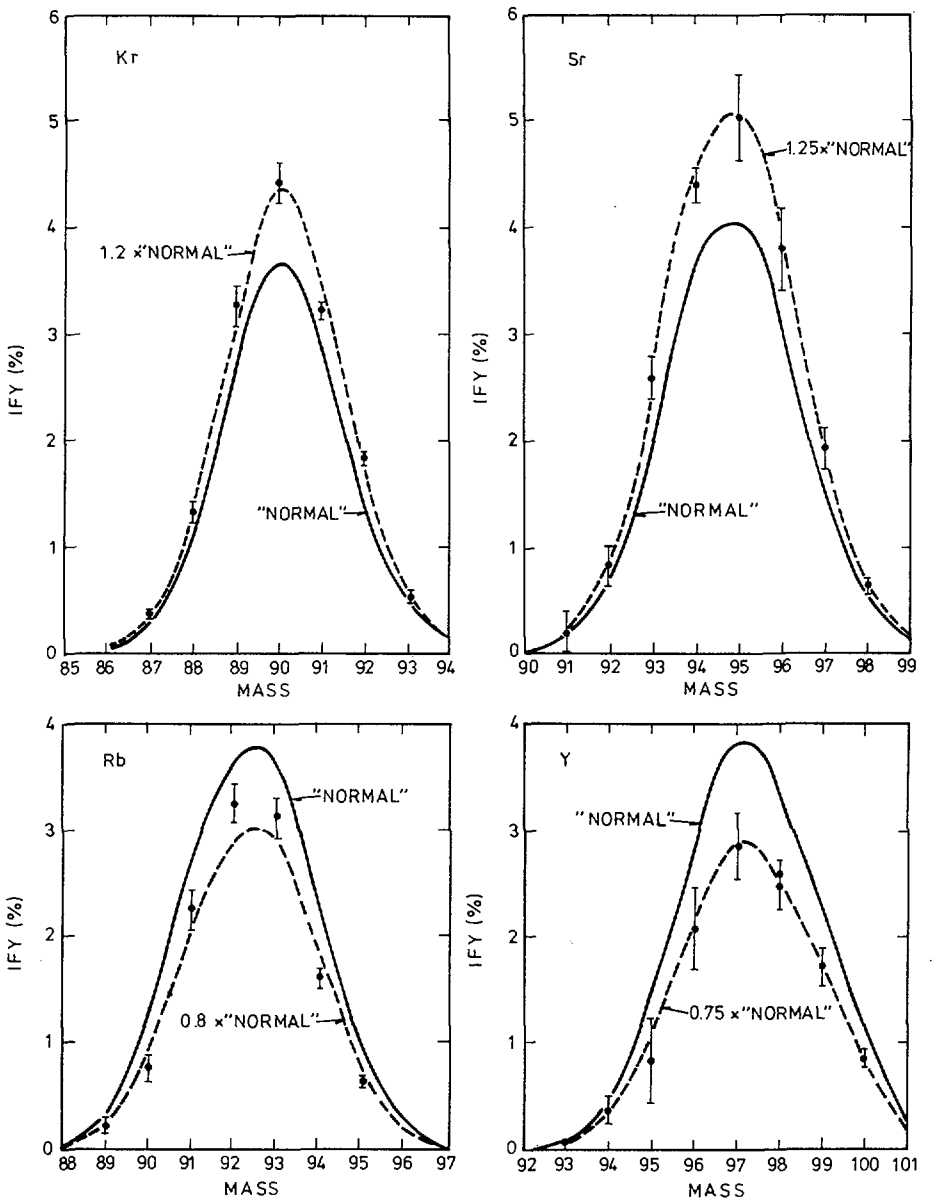

FIG. 2. Isotopic yield distributions of krypton, rubidium, strontium and yttrium in thermal-neutron-induced fission of ^{235}U.

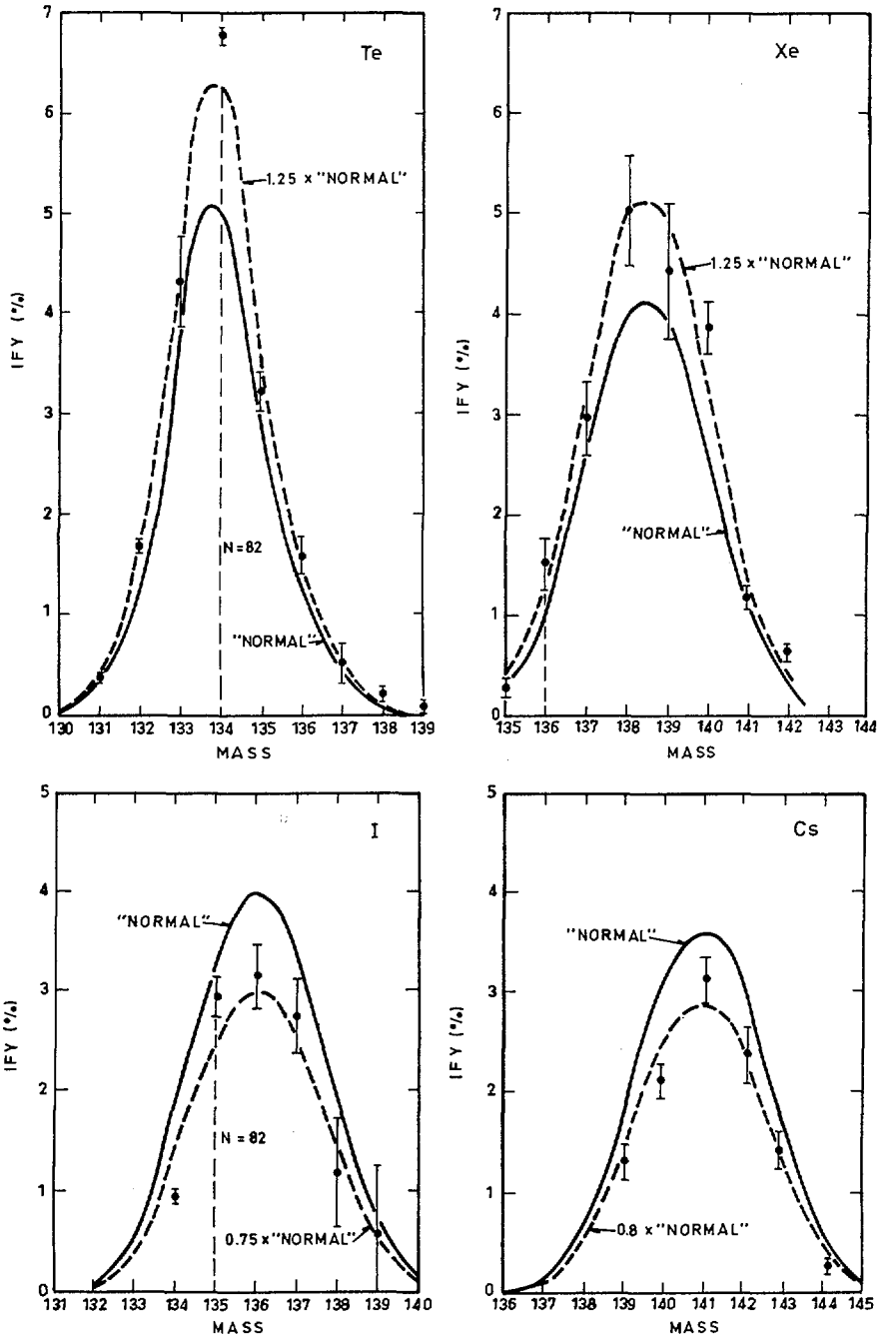

FIG.3. Isotopic yield distributions of tellurium, iodine, xenon and caesium in thermal-neutron-induced fission of ^{235}U. (The closed shell of 82 neutrons is emphasized by a dashed line.)

work based on K X-ray measurements (9). In that case an "inverse" effect due to the low K X-ray yields of even-Z fragments was observed, which after correction for the K X-ray yields rendered an elemental yield curve almost coinciding with the "normal" one. The applied correction was probably insufficient, and in a later discussion dealing with those experimental results, the same authors allow for a proton pairing effect as high as $\pm$ 20% (41).

SYSTEMATICS OF ISOTOPIC YIELDS

The isotopic yields seem to fluctuate around an average distribution curve obtained by multiples of 1.25 (for even Z) or 0.75 (for odd Z) of Wahl's "normal" curve (Figs. 2,3). The neutron pairing effect which is expected to cause these fluctuations does not seem as prominent as the proton pairing in the element yields, although it seems to be consistent in many cases. Relating the neutron pairing effect to the multiplied "normal" distribution (hence, "corrected normal") the consistency is masked in many cases by the relatively large experimental errors (Δ' values in Table III), with the exception of the closed shell of 82 neutrons where the effect is clearly observed for all the isotones (Fig. 3).

Tracy et al. (17) reported a neutron pairing effect in the yields of rubidium and cesium isotopes in thermal neutron fission of ^{235}U and in medium to high energy proton fission of ^{232}Th, ^{238}U, Ta, V and Ir. They calculated the effect by a numerical differentiation of a hypothetical Gaussian passing through any four consecutive points (third differences) and found systematic odd-even fluctuations of 10%-15% for rubidium and cesium, both at the neutron-richest part of the isotopic distribution. The effect decreased gradually down to a few percent at the peak of the isotopic distribution. The neutron pairing effects at the peaks of the isotopic distribution of most elements given in Table III generally agree with the above findings, i.e., indicating an average systematic effect of a few percent.

Maximum energy release considerations favor both even proton and neutron configurations to almost the same extent (8). Alternatively it can be stated that the same argument holds for breaking either proton pairs or neutron pairs (10) (both neutron and proton pairing energies are about 2.5 MeV at the region of mass 130 (42)). Thus the neutron pairing effect should be as prominent as that of the protons (i.e., $\pm$ 25%). The smallness of the neutron pairing effect can be attributed to the evaporation of neutrons during the de-excitation of the fragments, a process which is responsible for washing out part of the original effect in the primary fragment formation in fission.

Tracy et al. (17) attributed the higher value of the neutron pairing effect resulting from their calculations to the primary effect, using a rough estimate based on a Poisson distribution of neutron emission probabilities (which implies a relatively high probability for no neutron emission). In that way the original structure is preserved at the heavy end of the isotopic distribution, where the yields drop steeply as the mass number increases. If this argument can be substantiated by more realistic calculations of the de-excitation of fission fragments, one may conclude that the neutron pairing in the primary (i.e., pre-neutron emission) fragments is of a magnitude close to that of protons.

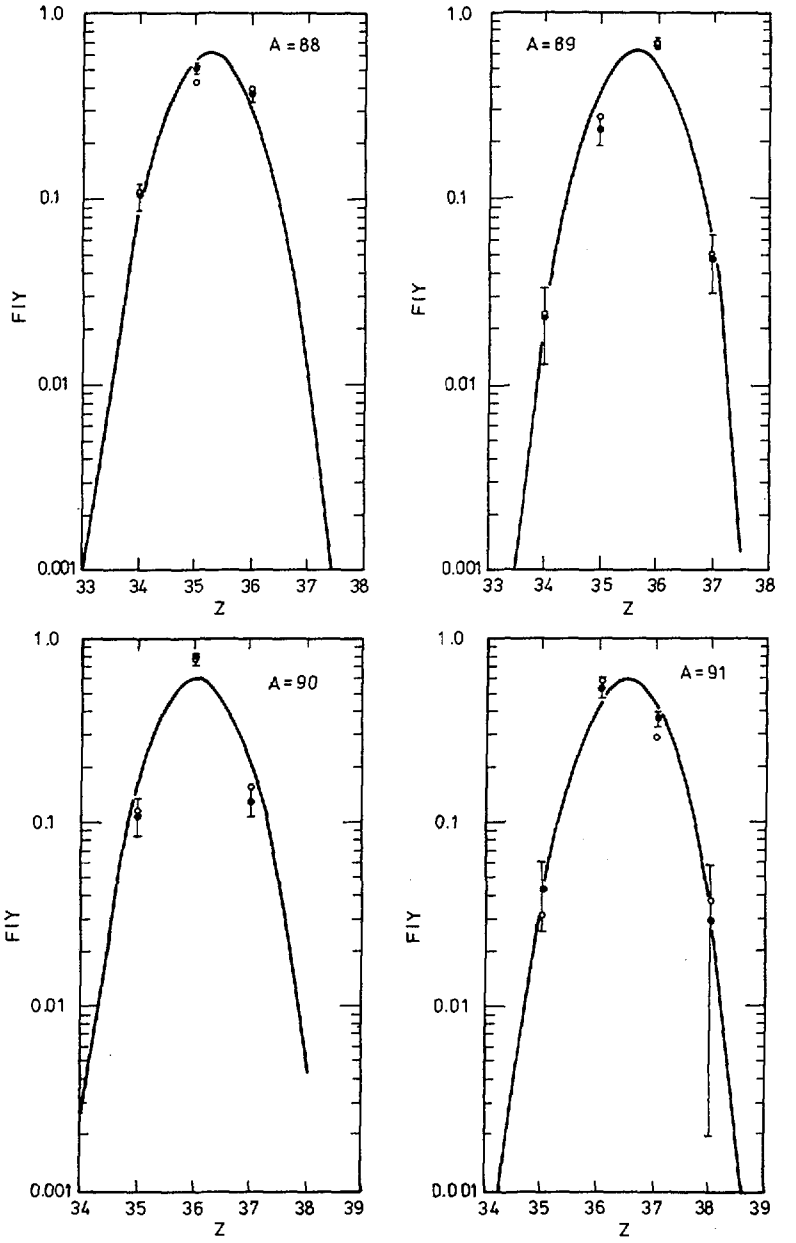

FIG.4. Fractional independent yields of isobars in mass chains 88-91, in thermal-neutron-induced fission of ^{235}U. ——— : Wahl's normal distribution, ●: experimental values, ○: "normal" values multiplied by 1.25 for even-Z elements and by 0.75 for odd-Z elements.

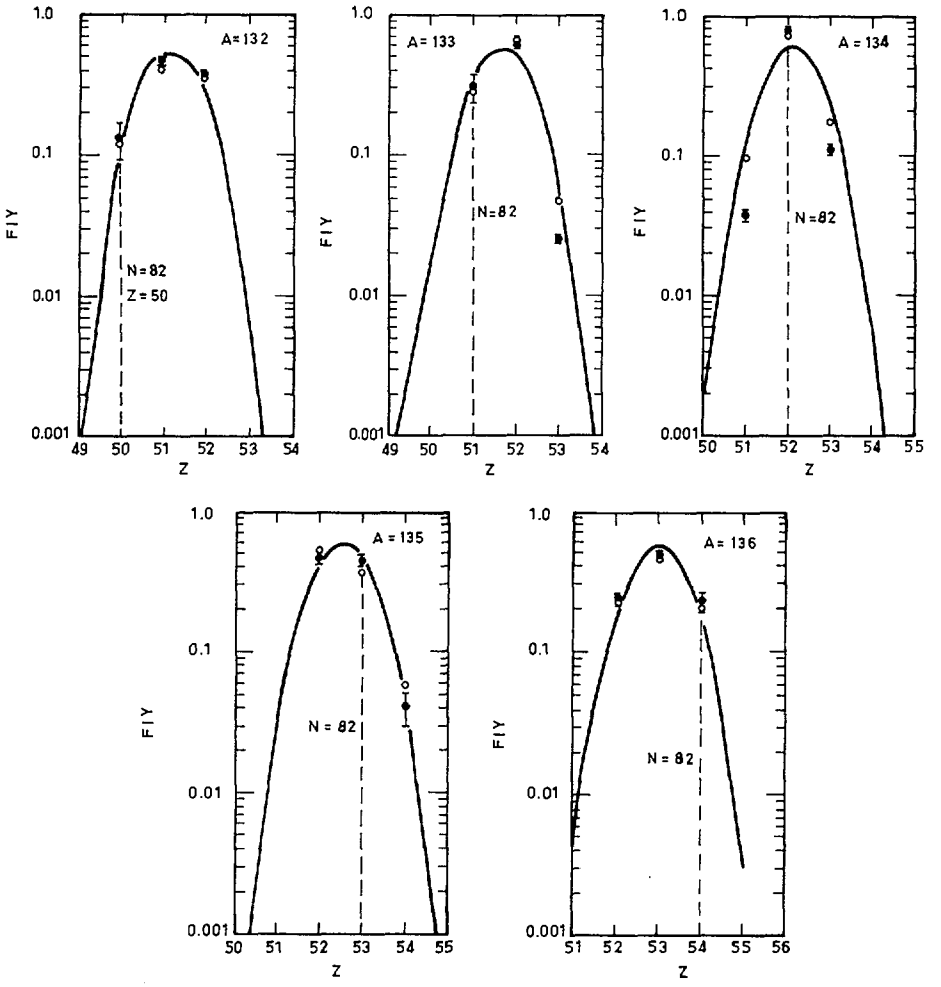

FIG.5. Fractional independent yields of isobars in mass chains 132-136, in thermal-neutron-induced fission of ^{235}U. ——: Wahl's "normal" distribution, ●: experimental values, ○: "normal" values multiplied by 1.25 for even-Z elements and by 0.75 for odd-Z elements; closed nuclear shells of 82 neutrons and 50 protons are emphasized by dashed lines.

SYSTEMATICS OF ISOBARIC DISTRIBUTIONS AND CHARGE DIVISION

The isobaric distributions (Tables I, II; Figs. 4,5) display a distinct proton pairing effect which appears as a sawtooth structure superimposed on the "normal" distribution curve. The neutron pairing effect related to the "corrected normal" values is preserved in some mass chains like 90, 91, 134, 135, 136 (Figs. 4,5), while not clearly detectable (within experimental errors) in other mass chains. As mentioned above, the only consistent neutron pairing effect appears in the closed shell of 82 neutrons (Fig. 5). This can be related to the high neutron binding energy and the

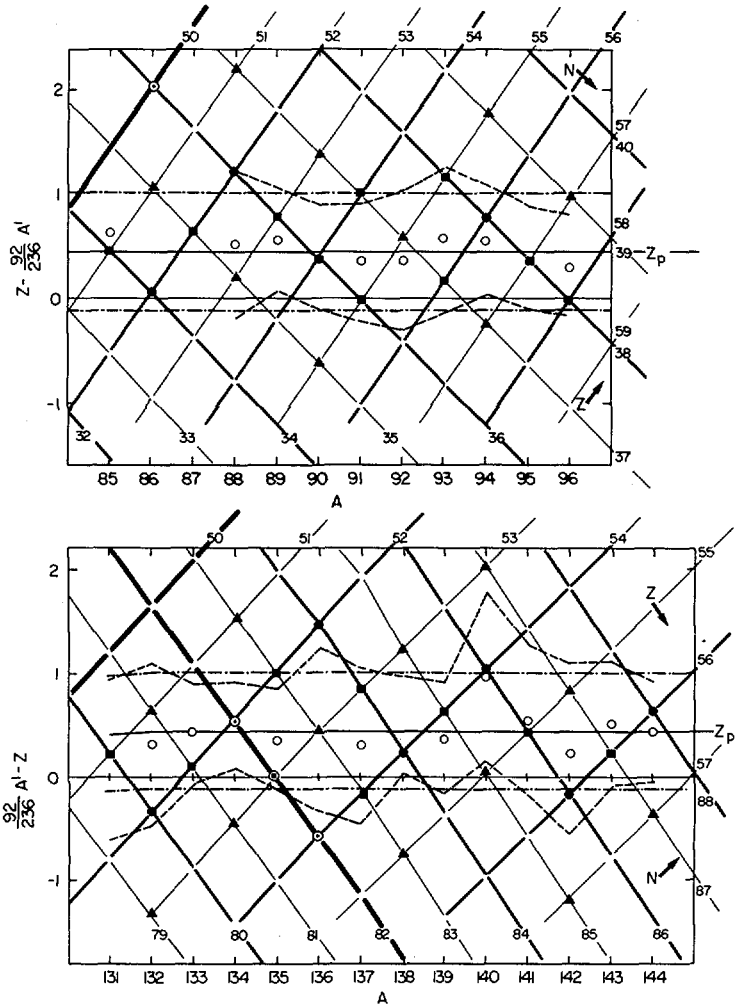

FIG.6. Most probable charge distribution and the widths of isobaric dispersions in thermal-neutron-induced fission of ^{235}U. Z_p: Wahl's calculated Z_p, O: experimental Z_p, ——— : odd number of protons or neutrons, ——— : even number of protons or neutrons, ▬▬ : closed nuclear shell, ●: even-even nuclei, ▲: odd-odd nuclei, ■: odd A nuclei, ⊙: closed shell, -----: experimental width of isobaric dispersion, -·-·-: Wahl's standard isobaric dispersion, $(92/236)A'$: unchanged charge dispersion (pre-neutron emission).

resulting smaller neutron evaporation. Measuring mass distribution of energy-selected fragments, Thomas and Vandenbosch (8), Reisdorf et al. (9) and Andritsopoulos (45) revealed an increasing enhancement of even-even nuclei as excitation energy becomes lower. At lower energies the pairing effect is expected to prefer the more stable species and diminish the neutron evaporation effect.

The FIY of the doubly even nuclide $^{132}_{50}Sn_{82}$, with closed proton and neutron shells, is not enhanced more than predicted by the proton and neutron pairing systematics (Fig. 5), although the experimental value (based on counting of beta-tracks of mass- and energy-separated fragments collected on a photographic plate) reported by Konecny et al. (21) is extremely high (~50% of the isobaric chain yield). They found a dip in Wahl's Z_p line at mass 132, as well as a high yield of ^{132}In and a negligible yield of ^{132}Te. This is in disagreement with radiochemical findings (Table II). The high enhancement of the formation of ^{132}Sn can be explained by the experimental conditions where high kinetic energies (low excitation energy) were selected; this is consistent with previous findings (7-9). However, this is not substantiated for the average energy distribution in fission. In the case of ^{132}Sn the lower range of the experimental results was taken for the "corrected" value, since it is in good agreement with the published radiochemical yields of antimony and tellurium. Thus the influence of the doubly magic configurations is well within the limits of the proton and neutron pairing effect.

A Gaussian fit through the three highest points of the yield distributions of individual chains resulted in Z_p values which were found to fluctuate with a maximum amplitude of $\pm$ 0.2 charge units around Wahl's Z_p values (of $\sigma = 0.56 \pm 0.06$) which were calculated assuming a constant deviation of 0.45 charge units from the unchanged charge distribution (UCD) in fission (12) (Fig. 6). The constant deviation of Z_p from the UCD distribution was also measured by Armbruster et al. (43) and explained as a result of a polarization effect causing protons to move before scission (44). The widths, σ, of the individual experimental Gaussians lie within the range of 0.45 to 0.8 charge units. The distribution is narrow when Z_p is close to an even integer and increases for Z_p passing close to an odd integer (Fig. 6, Table IV). The narrowest isobaric dispersion is found at A=134. The only disagreement is in the case of mass 140 where a large σ value was obtained for Z_p values corresponding to an even-Z nuclide at the peak of the isobaric dispersion. The neutron pairing does not influence the σ values as could be expected, as a result of the neutron evaporation. The general insensitivity of the Z_p values to nuclear structure considerations is well approximated by various theoretical calculations (2,44).

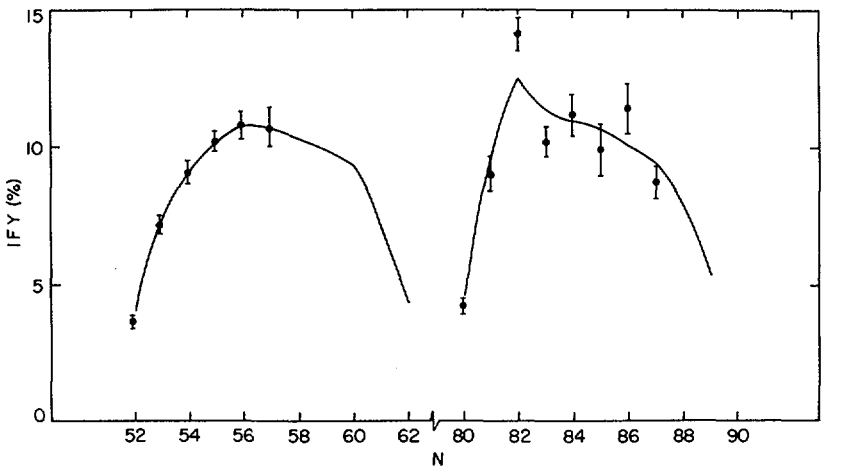

FIG.7. Isotonic yields in thermal-neutron-induced fission of ^{235}U. ——— : Wahl's normal curve, ●: experimental points.

SYSTEMATICS OF ISOTONIC YIELDS

The average neutron pairing effect can be demonstrated clearly by summing the independent yields of the isotones (Table V and Fig. 7). From Fig. 7 it is evident that the average effect relative to the "normal" yields in the light mass peak can hardly be resolved while in the heavy mass peak a sawtooth structure having an average amplitude of $\pm$ 8% is observed.

The neutron pairing in the closed shell of 82 neutrons is about 60% more than the average effect ($+[12.7 \pm 4.8]\%$), but the normal value in this particular case is strongly influenced by the high chain yield of mass 134, which is mainly represented by ^{134}Te of N=82. A "smoothened" normal curve would reveal a $\sim$30% effect, viz. several times larger than the average neutron pairing effect. This is due to a shell effect which is also better preserved than in the higher isotones where neutron emission is more prominent. This latter argument is supported by the observation of a low neutron emission from tin, antimony and tellurium as reported by Reisdorf et al. (9).

CONCLUSIONS

The above observations of the systematics of yield distributions of thermal neutron ^{235}U fission products leads to the following conclusions.

a. The "normal" distribution as proposed by Wahl is a good average of all the actual cases and is a very convenient reference for the experimental results and for revealing the nuclear structure systematics of the yields.

b. There is a consistent proton pairing effect with an average value of +25% relative to "normal" for even-Z nuclides and -25% for odd-Z nuclides.

c. The neutron pairing effect, expected to be as high as that of protons, is mostly "washed out" by neutron evaporation and therefore the average residual effect in the heavy mass peak is only $\sim \pm$ 8% and in the light mass peak it is not resolved beyond the experimental error. Without an accurate account of the neutron evaporation from individual fragments it is impossible to say what is the primary neutron pairing effect, especially as compared with the constant $\pm$ 25% proton pairing effect.

d. The shell effect is pronounced only in the case of $^{134}_{52}Te_{82}$ where the Z_p is 52.1. In other cases of N=82 where nuclides are on the lower parts of the isobaric dispersion slopes, this effect is not seen and the only observation is the one accounted for by the systematic neutron and proton pairing.

e. The widths of the individual Gaussians drawn through the experimental FIY varies with respect to the value of Z_p, being about 0.45 for Z_p close to an even integer and 0.8 for Z_p values close to an odd integer, which is another expression of the sawtooth structure of $\sim$30% superimposed on the "normal" Gaussian curve. These fluctuations can be related to scission when the nuclear structure effects take place.

f. The nearly constant average deviation of the charge division between the fragments from that of the fissioning nucleus suggests that this is a result of a process which is already over at scission, and can be ascribed either as a polarization effect during deformation (44) or preferably to a two-neutron transfer process (a nuclear Josephson effect) through the neck (10,46). This seems more reasonable than referring to individual nuclear properties of the fragments.

We believe that the above systematics may offer fairly accurate predictions for yields which have not been established as yet experimentally, with an average error within the uncertainty in the residual neutron pairing effect, which is evaluated as ± 10%.

REFERENCES

1. STRUTINSKY, V.M., Nucl. Phys. A 95 (1967) 420, A 122 (1968) 1.
2. WILKINS, B.D., STEINBERG, E.P., Argonne National Laboratory, preprint (1972).
3. TSANG, C.F., WILHELMY, J.B., Nucl. Phys. A 184 (1972) 417.
4. MOSEL, U, SCHMITT, H.W., Phys. Rev. C 4 (1971) 2185.
5. DICKMANN, F, DIETRICH, K., Nucl. Phys. A 129 (1969) 241.
6. NÖRENBERG, W., in Physics and Chemistry of Fission (Proc. Symp. Vienna, 1969), IAEA, Vienna (1969) 51.
7. MILTON, J.C.D., FRASER, J.S., Can. J. Phys. 40 (1962) 1626.
8. THOMAS, T.D., VANDENBOSCH, R., Phys. Rev. 133 (1964) B976.
9. REISDORF, W., UNIK, J.P., GRIFFIN, H.C. GLENDENIN, L.E., Nucl. Phys. A 177 (1971) 337.
10. DIETRICH, K., Proceedings of Minerva Symp. on Physics, Rehovot (Apr. 1973), Weizmann Institute of Science, Israel (1973).
11. WAHL, A.C., FERGUSON, R.L., NETHAWAY, D.R., TROUTNER, D.E., WOLFSBERG, K., Phys. Rev. 126 (1962) 1112.
12. WAHL, A.C., NORRIS, A.E., in Physics and Chemistry of Fission (Proc. Symp. Vienna, 1969), IAEA, Vienna (1969) 813.
13. EHRENBERG, B., AMIEL, S., Phys. Rev. C6 (1972) 618.
14. CHAUMONT, J., Ph.D. thesis, Faculté des Sciences Orsay (1970) (unpublished).
15. KONECNY, E., GUNTHER, H., SIEGERT, G. WINTER, L. Nucl. Physics A 100 (1967) 465. See also GUNTHER, H., SIEGERT, G., FERGUSON, R.L. EWALD, H., KONECNY, E., Nucl. Phys. A 196 (1972) 401.
16. TROUTNER, D.E., HARBOUR, R.M., Abstracts, 161st National Meeting of the American Chem. Soc. (Apr. 1971).
17. TRACY, B.L., CHAUMONT, J., KLAPISCH, R., NITSCHKE, J.M., POSKANZER, A.M., ROECKL, E., THIBAULT, C., Phys. Rev. C5 (1972) 222.
18. DELUCCHI, A.A., GREENDALE, A.E., STROM, P.O., Phys. Rev. 173 (1968) 1159.
19. MEEK, M.E., RIDER, B.F., General Electric Report, NEDO 12154 (1972).
20. BRAUN, C., AMIEL, S., Israel AEC Ann. Rept. 1968, IA-1190, 102.
21. KONECNY, E., OPOWER, H., GUNTHER, H., GOBEL, H., in Physics and Chemistry of Fission (Proc. Symp. Salzburg, 1965) 1, IAEA, Vienna (1965) 401.
22. KONECNY, E., GUNTHER, H. SIEGERT, G. Arkiv Physik 36 (1966) 319.
23. WUNDERLICH, F. Radiochim. Acta 7 (1967) 105.
24. FASHING, J.L., CORYELL, C.D., Rept. MIT-905-108 (1967) 21.
25. VENEZIA, A., Ph.D. Thesis, Hebrew University, Jerusalem (1973).
26. TOMLINSON, L., HURDUS, M.H. J. Inorg. Nucl. Chem. 33 (1971) 3609.
27. del MARMOL, P., PERRICOS, D.C., J. Inorg. Nucl. Chem. 32 (1970) 705.
28. KRATZ, J.V., HERRMANN, G. J. Inorg. Nucl. Chem. 32 (1970) 3713.
29. NIECE, L.H., TROUTNER, D.E., Phys. Rev. C1 (1970) 312.
30. HARBOUR, R.M., TROUTNER, D.E., J. Inorg. Nucl. Chem. 33 (1971) 1.
31. DELUCCHI, A.A., GREENDALE, A.E., Phys. Rev. C1 (1970) 1491.
32. FORMAN, L., BALESTRINI, S.J., WOLFSBERG, K., JETER, T.R., Inter. Conf. on the Properties of Nuclei Far from the Region of Beta-Stability, CERN 70-30 (1970).
33. NAEUMANN, R., FOGLER, H., DENSCHLAG, H.O., J. Inorg. Nucl. Chem. 34 (1972) 1785.

34. WAHL, A.C., DENIG, R., J. Inorg. Nucl. Chem. 34, (1972) 2413.
35. REEDER, P., Private communication (1972).
36. FOWLER, M., WAHL, A.C., Submitted to J. Inorg. Nucl. Chem. (June 1973).
37. del MARMOL, P., J. Inorg. Nucl. Chem. 30 (1968) 2873.
38. STROM, P.O., LOVE, D.L., GREENDALE, A.E., DELUCCHI, A.A., SAM, D., BALLOU, N.E., Phys. Rev. 144 (1966) 984.
39. WAHL, A.C., Phys. Rev. 99 (1955) 730.
40. OKAZAKI, A., Can. J. Phys. 44 (1966) 237.
41. REISDORF, W.N., UNIK, J.P., GLENDENIN, L.E., Preprint (1973).
42. GOVE, N.B., WAPSTRA, A.H., Nucl. Data Tables 11, No. 283 (1972).
43. SISTEMICH, K., ARMBRUSTER, P., EIDENS, J., ROECKL, E., Nucl. Phys. A 139 (1969) 289.
44. ARMBRUSTER, P., Nucl. Phys. A 140 (1970) 385.
45. ANDRITSOPOULOS, G., Nucl. Phys. A 94 (1967) 537.
46. GAUDIN, M., Nucl. Phys. A 144 (1970) 191.

TABLE I. THERMAL NEUTRON FISSION YIELDS OF ^{235}U LIGHT MASS PEAK

Mass	Chain Yield %[12]		Yields				
			$_{32}Ge$	$_{33}As$	$_{34}Se$	$_{35}Br$	$_{36}Kr$
83	0.543±0.011 ν_{83}= 0.90	FCY		0.8 ±0.08 (37)		.939[19]	
		FIY					
		Corrected FIY					
		Normal	0.1178	0.6085	0.2365	0.008344	1.467×10^{-5}
		Δ%					
			$_{32}Ge$	$_{33}As$	$_{34}Se$	$_{35}Br$	$_{36}Kr$
84	0.96 ±0.02 ν_{84}= 0.96	FCY		0.17 ±0.02[37]		0.964±0.067[19]	
		FIY					
		Corrected FIY					
		Normal	0.02791	0.4222	0.5014	0.04810	2.84×10^{-4}
		Δ%					
			$_{33}As$	$_{34}Se$	$_{35}Br$	$_{36}Kr$	$_{37}Rb$
85	1.3 ±0.03 ν_{85}= 1.01	FCY		0.8115±0.273[19]			
		FIY	0.04846±0.0097[19]				
		Corrected FIY	0.048±0.01	0.7630±0.27	0.185±0.27	0.003	
		Normal	0.1916	0.6278	0.1732	0.003	3.401×10^{-6}
		Δ%	-[74.60 ±5.2]	+[21.50 ±43.0]	+[7.10 ±156]	0	

			34^{Se}	38^{Br}	36^{Kr}	37^{Rb}	38^{Sr}
86	2.00±0.04 ν_{86}= 1.08	FCY					
		FIY				$(1.4 \pm 0.2)\times10^{-5}$	
		Corrected FIY					
		Normal	0.5169	0.4044	0.02466	8.843×10^{-5}	1.554×10^{-8}
		Δ%					
			33^{As}	34^{Se}	35^{Br}	36^{Kr}	37^{Rb}
87	2.37±0.05 ν_{87}= 1.17	FCY		0.48±0.1 (12) 0.28±0.05 (26) 0.266 (27) 0.41 (28)			
		FIY			0.3075±0.0768 (19) 0.3497±0.0593 (19)	0.152±0.013 (13)	
		Corrected FIY	0.01	0.49±0.07	0.346±0.06	0.152±0.013	0
		Normal	0.009191	0.2746	0.6038	0.111	0.001349
		Δ%		+[78.4±25.5]	-[42.7±10.0]	+[36.9 ± 11.7]	
			33^{As}	34^{Se}	35^{Br}	36^{Kr}	37^{Rb}
88	3.56±0.07 ν_{88}= 1.27	FCY		0.109±0.013 (26) >.24 (4)			
		FIY				0.371±0.028 (13)	
		Corrected FIY	0	0.109±0.013	0.51±0.03	0.371±0.028	0.01
		Normal	8.886×10^{-4}	0.08935	0.5821	0.3148	0.01277
		Δ%		+[22.4±19.5]	-[12.4±5.1]	+[18.1±8.9]	

TABLE I. (cont.)

Mass	Chain Yield % (12)		Yields				
			$_{34}Se$	$_{35}Br$	$_{36}Kr$	$_{37}Rb$	$_{38}Sr$
89	4.71±0.09 ν_{89}= 1.32	FCY	0.023±0.01 (26)		0.96±0.004 (12)		
		FIY		0.581±0.145 (19) 0.823±0.049 (20)	0.692±0.04 (13)	0.047±0.016 (12) 0.0403 (35)	
		Corrected FIY	0.023±0.01	0.238±0.044	0.692±0.04	0.047±0.016 (12)	
		Normal	0.0191	0.3684	0.5456	0.0663	5.085×10^{-4}
		Δ%	+[20.4±52.36]	-[35.4±11.94]	+[26.83±7.33]	-[29.11±24.13]	
			$_{35}Br$	$_{36}Kr$	$_{37}Rb$	$_{38}Sr$	$_{39}Y$
90	5.84±0.12 ν_{90}= 1.35	FCY		0.86±0.02 (12)			
		FIY	0.625±0.026 (20)	0.633±0.082 (13)	0.13±0.02 (12) 0.13±0.02		>8×10^{-5} (12)
		Corrected FIY	0.109±0.025**	0.761±0.032	0.13±0.02		
		Normal	0.156	0.6253	0.2110	5.057×10^{-3}	6.593×10^{-6}
		Δ%	-[30.17±16.39]	+[21.7±5.1]	-[38.39±9.47]		
			$_{35}Br$	$_{36}Kr$	$_{37}Rb$	$_{38}Sr$	$_{39}Y$
91	5.91±0.12 ν_{91}= 1.38	FCY		0.59±0.01 (12)			
		FIY		0.546±0.015 (13)	0.40±0.02 (12)	0.03±0.03 (12)	<0.01 (12)
		Corrected FIY	0.044±0.018	0.546±0.015	0.38±0.032	0.03±0.03	
		Normal	0.04301	0.4852	0.4399	0.03151	1.348×10^{-4}
		Δ%	0	+[12.53±3.09]	-[13.62±7.27]	0	

			$_{35}Br$	$_{36}Kr$	$_{37}Rb$	$_{38}Sr$	$_{39}Y$
92	5.91±0.12 ν_{92} = 1.41	FCY		0.31±0.01 (12)			
		FIY		0.25±0.012 (13)	0.55±0.03 (12) 0.414±0.04 (35)		$(1.3\pm0.2)\times10^{-3}$ (12)
		Corrected FIY		0.31±0.01	0.55±0.03	0.14±0.031	
		Normal	7.567×10^{-3}	0.2526	0.6133	0.1248	1.701×10^{-3}
		Δ%		+[22.72±3.96]	-[10.32±4.89]	+[12.18±24.84]	

			$_{35}Br$	$_{36}Kr$	$_{37}Rb$	$_{38}Sr$	$_{39}Y$
93	6.35±0.13 ν_{93} = 1.46	FCY		$0.078^{+0.012}_{-0.002}$ (12)			
		FIY		$0.083^{+0.011}_{-0.004}$ (13)	0.498±0.03 (35) 0.48 ±0.03 (12)		0.016±0.002 (12)
		Corrected FIY	0	0.083±0.008	0.49±0.03	0.41±0.03	0.016±0.002
		Normal	7.866×10^{-4}	0.08378	0.5748	0.3266	0.014
		Δ%		0	-[14.75±5.22]	+[25.53±9.18]	+[14.28±14.28]

			$_{36}Kr$	$_{37}Rb$	$_{38}Sr$	$_{39}Y$	$_{40}Zr$
94	6.60±0.13 ν_{94} = 1.49	FCY	$0.015^{+0.009}_{-0.002}$ (12)				
		FIY	0.39±0.003 (13)	0.262±0.015 (35) 0.23±0.01 (12)		0.06±0.02 (12)	
		Corrected FIY	0.027	0.246±0.015	0.667±0.025	0.06±0.02	
		Normal	0.01829	0.3624	0.5501	0.06861	5.417×10^{-4}
		Δ%		-[32.1±4.1]	+[21.2±4.5]	-[12.5±29.1]	

TABLE I. (cont.)

Mass	Chain Yield % (12)		Yields				
			$_{36}Kr$	$_{37}Rb$	$_{38}Sr$	$_{39}Y$	$_{40}Zr$
95	6.52±0.13 ν_{95} = 1.52	FCY	$1.1\ ^{+5.0}_{-0.1} \times 10^{-3}$ (12)				
		FIY		0.122±0.009 (35) 0.098±0.005 (12)		0.13 ± 0.06 (12)	$(6\pm3)\times10^{-4}$ (29) $(4\pm0.6)\times10^{-3}$ (12)
		Corrected FIY		0.098±0.005	0.772±0.06	0.13 ± 0.06	
		Normal	2.389×10^{-3}	0.1478	0.6232	0.2213	5.603×10^{-3}
		Δ%		-[33.7±3.4]	+[23.9±9.6]	-[42.3±27.1]	
			$_{36}Kr$	$_{37}Rb$	$_{38}Sr$	$_{39}Y$	$_{40}Zr$
96	6.36±0.13 ν_{96} = 1.54	FCY					
		FIY		0.03 ±0.0045 (35) 0.021±0.001			
		Corrected FIY		0.021±0.001			
		Normal	2.175×10^{-4}	0.04141	0.04797	0.4457	0.03279
		Δ%		-[49.3±2.4]			

			$_{37}Pb$	$_{38}Sr$	$_{39}Y$	$_{40}Zr$	$_{41}Nb$
97	6.26 ± 0.13 $\nu_{97} = 1.55$	FCY					
		FIY	0.016 ± 0.006 (35) $(5.6\pm0.7)\times10^{-3}$ (12)				$(1.7\pm0.8)\times10^{-3}$ (12)
		Corrected FIY	$(5.6\pm0.7)\times10^{-3}$				
		Normal	7.202×10^{-3}	0.2472	0.6153	0.1285	1.802×10^{-3}
		Δ%	$-[22.2\pm9.7]$				

FIY - Fractional independent yield

FCY - Fractional cumulative yield

ν - Number of prompt neutrons emitted per mass chain (12)

Normal - Normal FIY calculated by Wahl (12)

$$\Delta = \frac{\text{Corrected FIY} - \text{"normal" FIY}}{\text{"normal" FIY}} \times 100$$

** - Corrected value calculated according to the odd-even systematics.

TABLE II. THERMAL NEUTRON FISSION YIELDS OF ^{235}U HEAVY MASS PEAK

Mass	Chain (12) Yield %		Yields				
			$_{49}In$	$_{50}Sn$	$_{51}Sb$	$_{52}Te$	$_{53}I$
130	1.43 ± 0.18 (36) $\nu_{130}=0.30$	FCY		0.63 ± 0.07 (36)			
		FIY					$(1.6\pm0.2)\times10^{-4}$ (12)
		Corrected FIY					
		Normal	0.05563	0.5219	0.3984	0.02365	8.234×10^{-5}
		Δ%					
			$_{49}In$	$_{50}Sn$	$_{51}Sb$	$_{52}Te$	$_{53}I$
131	2.97 ± 0.6 $\nu_{131}=0.38$	FCY		0.437 ± 0.072 (31)	0.875 ± 0.14 (31)	0.998 (31)	
		FIY		0.39 ± 0.08 (12)	0.567 ± 0.137 (31)	0.124 ± 0.014 (12)	$(1.4\pm0.2)\times10^{-3}$ (12)
		Corrected FIY	0.01	0.39 ± 0.08	0.476 ± 0.08	0.124 ± 0.014	
		Normal	0.01011	0.2859	0.5983	0.1044	1.199×10^{-3}
		Δ%		$+[36.5\pm28.0]$	$-[20.4\pm13.4]$	$+[18.8\pm13.4]$	
			$_{49}In$	$_{50}Sn$	$_{51}Sb$	$_{52}Te$	$_{53}I$
132	4.43 ± 0.09 $\nu_{132}=0.49$	FCY		0.33 ± 0.05 (12) 0.135 ± 0.039 (31) 0.137 ± 0.008 (33)	0.80 ± 0.023 (31)	0.99603 ± 0.00025 (31)	
		FIY	0.22 ± 0.06 (21)	0.51 ± 0.09 (21)	0.63 ± 0.08 (31) 0.487 ± 0.01 (33) 0.22 ± 0.08 (21)	0.2 ± 0.03 (12) 0.376 ± 0.015 (33)	$(3.9\pm0.3)\times10^{-3}$ (12)
		Corrected FIY	0	0.136 ± 0.04	0.487 ± 0.01	0.376 ± 0.015	0
		Normal	0.00113	0.1013	0.5953	0.2917	0.0106
		Δ%		$+[34.2\pm39.5]$	$-[18.2\pm1.7]$	$+[35.7\pm5.1]$	

			$_{50}Sn$	$_{51}Sb$	$_{52}Te$	$_{53}I$	$_{54}Xe$
133	6.70±0.13 ν_{133}=0.65	FCY	< 0.002 (12)	0.404±0.045 (31)	0.9734±0.0014 (31)		
		FIY		0.33±0.1 (12) 0.455 (38)	0.644±0.068 (31) 0.57 (38)	0.025±0.003 (12) 0.0266±0.0014 (31)	$<10^{-3}$ (12)
		Corrected FIY	~0.02	0.31±0.07	0.644±0.068	0.026±0.002	
		Normal	0.01995	0.3744	0.5411	0.06405	4.772×10^{-4}
		Δ%		-[17.2±18.7]	+[19.0±12.6]	-[59.4±3.1]	
134	8.13±0.16 ν_{134}=0.85		$_{50}Sn$	$_{51}Sb$	$_{52}Te$	$_{53}I$	$_{54}Xe$
		FCY		0.03±0.01 (12)	0.88 (39)		
		FIY	0.08±0.03 (21)	0.039±0.004 (18) 0.11±0.06 (21)	0.54±0.09 (21)	0.11±0.01 (12) 0.117±0.01 (31)	0.05±0.02 (22)
		Corrected FIY	0	0.039±0.004	0.834±0.011	0.117±0.01	0.01
		Normal	0.001907	0.1322	0.6172	0.2418	0.006854
		Δ%		-[70.5±3.0]	+[35.1±1.8]	-[51.6±4.1]	
135	6.56±0.13 ν_{135}=0.99		$_{51}Sb$	$_{52}Te$	$_{53}I$	$_{54}Xe$	$_{55}Cs$
		FCY		0.52±0.07 (19)	0.97 (40)		
		FIY			0.46±0.03 (12) 0.44±0.07 (31)	0.04±0.01 (12)	
		Corrected FIY	0.02	0.49±0.03	0.45±0.03	0.04±0.01	
		Normal	0.02907	0.4281	0.496	0.04635	2.658×10^{-4}
		Δ%		+[14.5±7.0]	-[9.3±6.0]		

TABLE II. (cont.)

Mass	Chain Yield %[12]		Yields				
			$_{51}Sb$	$_{52}Te$	$_{53}I$	$_{54}Xe$	$_{55}Cs$
136	6.33±0.13 ν_{136}=1.07	FCY			0.65±0.15[12] 0.759±0.17[34]		
		FIY	0.02±0.02[21]	0.1±0.03[21]	0.1736±0.067[23] 0.67 ±0.25[21]	0.24±0.18[34] 0.21±0.04[21]	$(9.3\pm0.5)\times10^{-4}$[12]
		Corrected FIY	0	0.25**	0.51±0.11[25]	0.24±0.04	$(9.3\pm0.5)\times10^{-4}$
		Normal	0.004106	0.1916	0.6278	0.1732	3.318×10^{-3}
		Δ%		+30.5	-18.8	+[38.6±23.1]	-[72±1.5]
			$_{52}Te$	$_{53}I$	$_{54}Xe$	$_{55}Cs$	$_{56}Ba$
137	6.37±0.13 ν_{137}=1.11	FCY			0.978±0.003[12]		
		FIY	0.08±0.03[21]	0.53±0.06[21] 0.28±0.06[25]	0.466±0.063[13] 0.33 ±0.05[21]	0.05±0.03[21]	
		Corrected FIY	0.08±0.03	0.434±0.06	0.466±0.056	0.02	
		Normal	0.05563	0.5219	0.3984	0.02365	8.234×10^{-5}
		Δ%	+[43.8±53.9]	-[16.8±11.5]	+[17.0±14.1]		
			$_{52}Te$	$_{53}I$	$_{54}Xe$	$_{55}Cs$	$_{56}Ba$
138	6.75±0.14 ν_{138}=1.14	FCY					
		FIY	0.03±0.01[22]	0.2387±0.015[20] 0.16±0.04[35] 0.124±0.025[25]	$0.7452^{+0.0918}_{-0.0741}$[13] 0.46±0.09[22]	0.047±0.002[12] 0.0477±0.011[32] 0.25±0.07[22]	0.1±0.4[22]
		Corrected FIY	0.03±0.01	0.178±0.08	0.745±0.08	0.047±0.002	
		Normal	0.0106	0.2917	0.5953	0.1013	0.00113
		Δ%		-[39.0±27.4]	+[26.1±13.4]	-[53.6±2.0]	

			$_{52}Te$	$_{53}I$	$_{54}Xe$	$_{55}Cs$	$_{56}Ba$
139	6.51±0.14 ν_{139}=1.17	FCY			0.83±0.02 (1)		
		FIY	0.01±0.01 (22)	0.072±0.038 (25) 0.18695±0.01 (20) 0.02±0.01 (22)	$0.7926^{+0.0768}_{-0.0614}$ (13) 0.13±0.03 (22)	0.184±0.018 (35) 0.24±0.04 (12) 0.195±0.03 (32)	$(1.1^{+0.5}_{-0.3})\times10^{-2}$ (12) 0.35±0.05 (22)
		Corrected FIY	0.01±0.01	0.093±0.103	0.681**±0.103	0.206±0.03	$(1.1^{+0.5}_{-0.3})\times10^{-2}$ (12)
		Normal	0.001272	0.1077	0.6011	0.2803	9.642×10^{-3}
		Δ%		-[13.65±25.64]	+[13.3±17.1]	-[26.51±10.7]	+[14.6±41.7]
			$_{53}I$	$_{54}Xe$	$_{55}Cs$	$_{56}Ba$	$_{57}La$
140	6.43±0.13 ν_{140}=1.19	FCY		0.596±0.01 (12)			
		FIY		0.4591±0.0669 (13)	0.31±0.04 (12) 0.3297±0.0264 (35)	(4.6±3)x10^{-2} (12)	(7±1)x10^{-4} (12)
		Corrected FIY	0.02	0.604±0.04	0.33±0.03	0.046±0.03	
		Normal	0.02571	0.4104	0.5118	5.176×10^{-2}	3.239×10^{-4}
		Δ%		+[47.2±9.7]	-[35.5±5.9]	-[11.1±58]	
			$_{53}I$	$_{53}Xe$	$_{55}Cs$	$_{56}Ba$	$_{57}La$
141	5.79±0.12 ν_{141}=1.21	FCY		$0.205^{+0.019}_{-0.004}$ (12)			
		FIY		$0.205^{+0.023}_{-0.008}$ (12)	0.55±0.04 (12) 0.445±0.071 (32) 0.5457±0.0414 (35)	0.26±0.05 (12)	(3.7±1.3)x10^{-3} (12)
		Corrected FIY	∿0	0.205±0.02	0.546±0.04	0.26±0.05	(3.7±1.3)x10^{-3}
		Normal	3.894×10^{-3}	0.1869	0.628	0.1777	3.501×10^{-3}
		Δ%		+[9.7±9.7]	-[13.1±6.4]	+[46.3±28.1]	

TABLE II. (cont.)

Mass	Chain Yield % (12)		Yields				
			$_{54}Xe$	$_{55}Cs$	$_{56}Ba$	$_{57}La$	$_{58}Ce$
142	5.86 ± 0.12 $\nu_{142}=1.23$	FCY	$(5.9^{+0.8}_{-0.3})\times10^{-2}$ (12)				
		FIY	$0.1075^{+0.017}_{-0.012}$ (13)	0.41 ± 0.05 (12) 0.512 ± 0.041 (35) 0.249 ± 0.066 (32)		$(1.7\pm0.4)\times10^{-2}$ (12)	
		Corrected FIY	$0.1075^{+0.017}_{-0.012}$	0.41 ± 0.05	0.465 ± 0.052	$(1.7\pm0.4)\times10^{-2}$	
		Normal	5.563×10^{-2}	0.5219	0.3984	0.02365	8.234×10^{-5}
		Δ%	$+[93.2\pm27]$	$-[21.4\pm9.6]$	$+[16.7\pm13.0]$	$-[28.1\pm16.9]$	
			$_{54}Xe$	$_{55}Cs$	$_{56}Ba$	$_{57}La$	$_{58}Ce$
143	5.80 ± 0.11 $\nu_{143}=1.25$	FCY	$(8.5^{+0.7}_{-0.5})\times10^{-3}$ (12)		0.88 ± 0.06 (12)		
		FIY	$0.0465^{+0.0137}_{-0.0121}$ (13) $0.0085^{+0.0007}_{-0.0005}$ (12)	0.25 ± 0.03 (12) 0.3 ± 0.026 (35) $0.169+0.029$ (32)			$(5.3\pm2.6)\times10^{-3}$ (12) 0.122 ± 0.0263 (24)
		Corrected FIY	$(8.5^{+0.7}_{-0.5})\times10^{-3}$	0.25 ± 0.03	0.62 ± 0.07	0.115 ± 0.06	$(5.3\pm2.6)\times10^{-3}$
		Normal	1.111×10^{-2}	0.2974	0.5922	0.09821	1.065×10^{-3}
		Δ%		$-[15.9\pm10.1]$	$+[4.7\pm11.8]$	$+[17.1\pm61.1]$	

			$_{54}Xe$	$_{55}Cs$	$_{56}Ba$	$_{57}La$	$_{58}Ce$
144	5.37 ± 0.11 $\nu_{144}=1.27$	FCY	$(1.1^{+0.5}_{-0.1})\times10^{-3}$ (12)		0.78 ± 0.04 (12)		
		FIY		0.223 ± 0.028 (35) 0.053 ± 0.016 (12)			<0.023 (24)
		Corrected FIY	$(1.1^{+0.5}_{-0.1})\times10^{-3}$	0.052 ± 0.016	0.727 ± 0.06	0.197 ± 0.05	0.023
		Normal	1.349×10^{-3}	0.111	0.6038	0.2746	9.191×10^{-3}
		Δ%		$-[53.1\pm14.4]$	$+[20.4\pm9.9]$	$-[28.3\pm18.2]$	
			$_{55}Cs$	$_{56}Ba$	$_{57}La$	$_{58}Ce$	$_{59}Pr$
145	3.85 ± 0.08 $\nu_{145}=1.30$	FCY					
		FIY	$0.026^{+0.014}_{-0.012}$ (32) 0.0727 ± 0.018 (35)			0.61 (24)	
		Corrected FIY	0.026 ± 0.013				
		Normal	0.02679	0.4163	0.5066	0.0499	3.033×10^{-4}
		Δ%					

FIY - Fractional independent yield.

FCY - Fractional cumulative yield.

ν - Number of prompt neutrons emitted per mass chain (12).

Normal - Normal FIY calculated by Wahl (12).

Δ - $\frac{\text{Corrected FIY} - \text{"normal" FIY}}{\text{"normal" FIY}} \times 100$.

** - Corrected value calculated according to the odd-even systematics.

TABLE III. Z AND N PAIRING EFFECT IN INDEPENDENT YIELDS OF COMPLEMENTARY ELEMENTS (Z and 92-Z)

Mass	Independent Yield %	"Normal" Yield %	1.2 x"Normal" Yield %	Δ% Odd N	Δ% Even N	Mass	Independent Yield %	"Normal" Yield %	1.2 x"Normal" Yield %	Δ% Odd N	Δ% Even N
	Krypton						Barium				
86	0.05	0.049	0.059			139	0.07±0.03	0.063	0.075	-[6.7±40]	
87	0.36±0.03	0.263	0.316	+[14.0±9.5]		140	0.30±0.19	0.333	0.399		-[24.8±47.6]
88	1.32±0.10	1.121	1.345		-[1.8±7.4]	141	1.50±0.29	1.029	1.235	+[21.4±23.5]	
89	3.26±0.19	2.570	3.084	+[5.7±6.2]		142	2.72±0.30	2.335	2.802		-[2.9±10.7]
90	4.44±0.18	3.652	4.382		+[1.3±4.1]	143	3.60±0.41	3.435	4.122	-[12.7±9.9]	
91	3.23±0.09	2.868	3.441	-[6.1±2.6]		144	3.90±0.32	3.242	3.891		+[0.2±8.2]
92	1.83±0.06	1.493	1.791		+[2.2±3.3]	145	**1.91±0.27	1.603	1.923	**-[0.8±14.1]	
93	0.53±0.05	0.532	0.638	-[17.0±7.8]		146	**0.64±0.06	0.534	0.641		+[0.6±9.0]
94	0.18	0.121	0.145			147	**0.11±0.01	0.094	0.113	-[0.8±14.1]	
95	0.02	0.016	0.019			148	**0.01±0.00	0.011	0.013		+[0.6±9.0]
Σ%	15.22±0.31	12.685	15.22				14.76±0.75	12.679	15.21		
	Δ_{Σ}% = +[20.0±2.4]						Δ_{Σ}% = +[16.4±5.9]				

Mass	Independent Yield %	"Normal" Yield %	0.8 x "Normal" Yield %	Δ% Odd N	Δ% Even N	Mass	Independent Yield %	"Normal" Yield %	0.8 x "Normal" Yield	Δ% Odd N	Δ% Even N
	Rubidium						Cesium				
88	0.04	0.045	0.036			136	0.01±0.00	0.021	0.017	-[40±0]	
89	0.22±0.07	0.312	0.250		-[11.9±28]	137	0.13	0.151	0.120		+[7.9]
90	0.76±0.12	1.232	0.986	-[22.9±12.2]		138	0.32±0.01	0.684	0.547	- [41.5±1.8]	
91	2.25±0.19	2.510	2.080		+[8.2±3.1]	139	1.34±0.19	1.825	1.460		-[8.2±13.0]
92	3.25±0.18	3.625	2.900	+[12.1±6.2]		140	2.12±0.19	3.291	2.632	-[19.5±7.2]	
93	3.11±0.19	3.650	2.920		+[6.5±6.5]	141	3.16±0.23	3.636	2.909		+[8.6±7.9]
94	1.62±0.10	2.392	1.913	-[15.3±5.2]		142	2.40±0.29	3.058	2.446	-[1.9±11.8]	
95	0.64±0.03	0.963	0.771		-[17.0±3.9]	143	1.45±0.17	1.725	1.380		+[5.1±12.3]
96	0.13±0.01	0.263	0.211	-[38.2±4.7]		144	0.28±0.09	0.596	0.477	-[41.2±18.2]	
97	0.03±0.00	0.045	0.036			145	0.10±0.05	0.103	0.082		+[21.4±61]
98		0.005				146		0.011			
Σ%	12.05±0.37	15.042	12.01			Σ =	11.31±0.50	15.101	12.01		
	Δ_{Σ}% = -[20.3±2.4]						Δ_{Σ}% = -[25.1±3.3]				

TABLE III. (cont.)

Mass	Independent Yield %	"Normal" Yield %	1.25 x "Normal" Yield %	Δ%		Mass	Independent Yield %	"Normal" Yield %	1.25 x "Normal" Yield %	Δ%	
	Strontium			Odd N	Even N		Xenon			Odd N	Even N
90		0.029	0.037			134		0.056	0.070		
91	0.18±0.18	0.186	0.233	-[22.6±77.2]		135	0.26±0.07	0.304	0.380	-[31.6±18.4]	
92	0.83±0.18	0.738	0.922		-[10.0±1-.5]	136	1.52±0.25	1.097	1.371		+[10.9±18.2]
93	2.60±0.19	2.074	2.592	+[0.3±7.3]		137	2.96±0.36	2.538	3.172	-[6.7±11.3]	
94	4.40±0.16	3.631	4.538		-[3.0±3.5]	138	5.03±0.54	4.018	5.023		+[0.1±10.7]
95	5.03±0.39	4.063	5.079	-[1.0±7.7]		139	4.44±0.67	3.913	4.892	-[9.2±13.7]	
96	**3.81±0.38	3.051	3.814			140	3.88±0.26	2.639	3.298		+[17.6±7.9]
97	**1.93±0.19	1.547	1.934			141	1.18±0.12	1.082	1.353	-[12.7±11.1]	
98	**0.63±0.06	0.501	0.626			142	0.63±0.09	0.326	0.407		+[54.7±22.1]
99	**0.15±0.01	0.124	0.155			143	0.05±0.00	0.064	0.080	-[38.1±0]	
100	**0.03±0.00	0.023	0.028			144	0.006±0.001	0.007	0.009		
Σ =	19.59±0.68	15.967	19.959			Σ =	19.96±1.01	16.044			
	Δ_{Σ}% = +[22.7±4.2]						Δ_{Σ}% = +[24.4±6.3]				

Mass	Independent Yield %	"Normal" Yield %	0.75x"Normal" Yield %	Δ%		Mass	Independent Yield %	"Normal" Yield %	0.75 x"Normal" Yield %	Δ%	
	Yttrium			Odd N	Even N		Iodine			Odd N	Even N
93	0.10±0.01	0.089	0.067		+[49.7±14.9]	132	0.02±0.001	0.047	0.035	-[43.6±2.8]	
94	0.40±0.13	0.453	0.340	+[17.8±38.2]		133	0.17±0.01	0.429	0.322		-[47.1±3.1]
95	0.85±0.39	1.441	1.081		-[21.3±36.1]	134	0.95±0.08	1.966	1.475	-[35.6±5.4]	
96	**2.10±0.38	2.835	2.126	-[1.2±17.9]		135	2.95±0.20	3.254	2.440		+[20.9±8.2]
97	**2.88±0.31	3.852	2.889			136	3.16±0.32	3.974	2.980	+[6.0±10.7]	
98	**2.51±0.23	3.350	2.512			137	2.76±0.38	3.324	2.493		+[10.7±15.2]
99	**1.74±0.17	2.321	1.741			138	1.20±0.54	1.969	1.476	-[18.7±36.6]	
100	**0.87±0.09	1.159	0.869			139	0.60±0.67	0.701	0.526		+[14.1±127.4]
101	**0.22±0.02	0.294	0.220			140	0.13	0.165	0.124		
102	**0.04	0.052	0.039			141		0.022	0.017		
Σ =	11.71±0.5	15.847	11.884			Σ =	11.94±1.02	15.851	11.888		
	Δ_{Σ}% = -[26.1±3.2]						Δ_{Σ}% = -[24.7±6.4]				

TABLE III. (cont.)

Mass	Independent Yield %	"Normal" Yield %	1.25 x "Normal" Yield %	Δ' %		Mass	Independent Yield %	"Normal" Yield %	1.25 x "Normal" Yield %	Δ' %	
	Zirconium			Odd N	Even N		Tellurium			Odd N	Even N
95		0.036	0.046			130	0.0	0.035	0.044		
96	**0.32	0.208	0.261		+22	131	0.37±0.04	0.310	0.388	-[4.6±10.3]	
97	**1.39±0.36	0.804	1.005	+[38.2±35.9]		132	1.67±0.07	1.292	1.615		+[3.4±4.3]
98	**2.58±0.23	1.857	2.321		+[11.1±9.9]	133	4.31±0.46	3.625	4.531	-[4.9±10.1]	
99	**4.19±0.42	3.355	4.194			134	6.78±0.09	5.018	6.272		+[8.1±1.4]
100	**5.12±0.51	4.094	5.117			135	3.21±0.20	2.809	3.511	-[8.6±5.7]	
101	**3.36±0.34	2.687	3.359			136	**1.58±0.19	1.213	1.516		+[4.2±12.5]
102	**1.61±0.16	1.291	1.614			137	0.51±0.19	0.354	0.443	+[15.1±42.9]	
103	**0.48±0.05	0.381	0.476			138	0.20±0.07	0.072	0.090		
104	**0.09±0.01	0.074	0.092			139	0.06±0.06	0.008	0.010		
105	**0.01	0.007	0.009								
Σ =	19.15±0.87	14.794				Σ =	18.72±0.59	14.736			
	Δ_Σ% =	+[29.4±5.9]					Δ_Σ% =	+[27.03±4.1]			

** - Values assumed according to the odd-even systematics.

Δ_Σ - Deviation of the elemental yield from "normal" distribution according to Wahl[1].

Δ' - Deviation of the experimental value from corrected "normal" distribution.

TABLE IV. THE MOST PROBABLE ISOBARIC CHARGE, Z_p, AND THE GAUSSIAN WIDTH, σ, FOR EXPERIMENTAL INDEPENDENT YIELDS OF THERMAL-NEUTRON-INDUCED FISSION OF ^{235}U

Mass	Z_p	2 σ(Charge Units) Central Nuclide*			
		Even N, Even Z	Odd N, Odd Z	Even N, Odd Z	Odd N, Even Z
		LIGHT MASS PEAK			
88	35.32		1.41		
89	35.78				0.99
90	36.02	1.0			
91	36.37				1.13
92	36.79		1.34		
93	37.41			1.37	
94	37.79	1.04			
95	38.03				1.04
96	38.35	1.01			
	mean 2σ	1.02±0.02	1.37±0.03	1.37	1.05±0.07
		HEAVY MASS PEAK			
131	50.63			1.55	
132	51.33		1.55		
133	51.68				0.97
134	52.07	0.83			
135	52.48				0.97
136	52.99		1.59		
137	53.54			1.51	
138	53.84	0.94			
139	54.12				1.08
140	54.06	1.64			
141	55.07			1.46	
142	55.6		1.74**		
143	55.85				1.19
144	56.17	0.97			
	mean 2σ	0.91±0.07 (without A=140) (see text)	1.57±0.02	1.51±0.04	1.05±0.10

* By central nuclide we mean the nuclide present at or near the peak of the charge distribution.

**In this case the peak of the charge distribution falls between an odd-odd and an even-even nuclide.

TABLE V. NEUTRON PAIRING EFFECT IN ISOTONIC CHAINS FOR THERMAL-NEUTRON-INDUCED FISSION OF ^{235}U

Neutron Number	Isotonic Yield %		Relative Deviation from "Normal" %	
	Experimental	"Normal"	Odd N	Even N
52	3.66±0.24	4.15		-[11.7±5.8]
53	7.18±0.35	6.71	+[7.0±5.2]	
54	9.13±0.38	9.04		+[1.0±4.2]
55	10.22±0.34	10.02	+[2.0±3.4]	
56	10.77±0.48	10.68		+[0.8±4.5]
57	10.73±0.66	10.70	+[0.3±6.2]	
80	4.14±0.28	4.30		-[3.7±6.5]
81	8.92±0.53	9.48	-[5.9±5.6]	
82	14.06±0.60	12.48		+[12.7±4.8]
83	10.17±0.52	11.27	-[9.8±4.6]	
84	11.16±0.74	10.92		+[2.2±6.8]
85	9.87±0.95	10.69	-[7.7±8.9]	
86	11.35±0.89	10.00		+[13.5±8.9]
87	8.7 ±0.6	9.4	-[7.4±6.4]	

DISCUSSION

H.O. DENSCHLAG: You restricted your analysis to the high-yield fission products. Could you comment on the ΔZ values that would be obtained in the very asymmetric and the symmetric fission regions using your formalism?

S. AMIEL: We account for ~75% of the fission products. So far, owing to the scarcity and dispersion of experimental results in the valley and far wings, I would not dare to commit myself to any statement. I hope we shall know more about it shortly.

H.O. DENSCHLAG: I think, in principle, you should be able to obtain a value of ΔZ for any chain for which at least one experimental yield value is known. Am I right?

S. AMIEL: I believe so. We shall know more when we extend the systematics to all cases left out so far.

M. ASGHAR: This odd-even effect of ~25% on the mass yields is impressive. Mr. Fong showed a slide of the mass distribution during the discussion on Unik's paper[1] and his calculated values tie up with the measured values of P(M). I wonder if he could say how much this effect would affect the yields in his theory?

P. FONG: The statistical theory previously developed considers the even-odd effect to be an aberration peculiar to the ground state which is washed out at excited states. Therefore it predicts no even-odd effect. However, this treatment of the even-odd effect is now antiquated. When replaced by an up-to-date treatment, the statistical theory will predict an even-odd difference in mass yield. An effect of 25% is not beyond expectation.

[1] UNIK, J.P., et al., Paper IAEA-SM-174/209, these Proceedings, Vol.2.

YIELDS OF SHORT-LIVED FISSION PRODUCTS IN THE 50-NEUTRON-SHELL REGION IN THERMAL-NEUTRON-INDUCED FISSION OF ^{235}U

J.-V. KRATZ*, G. HERRMANN,
Institut für Kernchemie der Universität Mainz,
Mainz, Federal Republic of Germany

Abstract

YIELDS OF SHORT-LIVED FISSION PRODUCTS IN THE 50-NEUTRON-SHELL REGION IN THERMAL-NEUTRON-INDUCED FISSION OF ^{235}U.

Radiochemical charge distribution measurements have shown a strong influence of the 50-proton shell on low-energy fission reactions. The possible influence of the 82-and 50-neutron shells on charge distribution is still subject to experimental work. Especially little data on charge distributions have been published in the 50-neutron-shell region. This is mainly because the half-lives of fission products around N=50 are as short as a few seconds or less, and suitable fast chemical separations have not been developed until recently. The rapid volatilization of arsenic and selenium as hydrides from aqueous solutions has been used to identify new short-lived isotopes of germanium, arsenic and selenium with half-lives down to a few tenths of a second, e.g. 0.3-s ^{87}As and 0.9-s ^{86}As. Half-lives were determined directly by following the decay of prominent γ-ray peaks, by delayed neutron counting, or indirectly by milking of known daughter or granddaughter activities. These techniques were also applied to determine branching ratios (a) within a given β^--decay chain (in the case of isomerism) and (b) from one chain to another (via delayed neutron emission) by measuring delayed neutron yields. Taking these data into account, fractional cumulative yields of arsenic and selenium isotopes were determined via their bromine daughter activities in the chains 83, 84, 85, 87 and 88. The isobaric yield distributions have the same width as the Gaussian distributions found far from closed shells. However, the distributions around mass number 84 are shifted if compared to the position expected by interpolation of adjacent distributions. This shift could indicate a preferential formation of closed-shell fragments in the fission process. It can be shown, however, that this effect can also be explained by a shell-dependent evaporation of prompt neutrons.

1. INTRODUCTION

Charge distribution in low-energy fission reactions has been investigated with similar overall results by radiochemical and physical methods [1]. Purely instrumental methods are (a) the determination of the kinetic energies of complementary fragments with solid state detectors and a simultaneous detection of their K X-rays [2], (b) an on-line mass separation followed by the determination of the β^--decay-chain length [3] and (c) the measurement of the intensity of prompt γ-ray transitions from the first 2^+-level of the 0^+-ground state in even-even nuclei [4]. In principle, these methods are able to give complete information on the charge distribution over the whole mass range in one experiment. This is a very important advantage over the usually very time-consuming radiochemical investigations. However, owing to their limited resolution, the instrumental methods can only show an average trend of the most probable charge versus fragment mass.

---

* Present address: Lawrence Berkeley Laboratory, Berkeley, Calif., United States of America.

Radiochemical methods separate single elements from the mixture of fission products, and this separation determines the nuclear charge Z; afterwards the mass number A of the fission product is determined, e. g. via decay characteristics of a daughter nuclide. Theoretically, the resolution of radiochemical yield determinations is unlimited. In practice, however, the determination of the fractional yields of two or three isotopes in a given mass chain requires specific chemical separations for just as many (i. e. two or three) different elements and these separations should be extremely fast as the nuclide under investigation should be eliminated out of its β^--decay – chain before β^--decay alters the yields markedly. If these requirements are fulfilled, radiochemical yield determinations are particularly reliable and they should especially be applied to those mass regions where structures in the charge distribution function may occur which cannot be detected by physical methods.

Among the mass regions where the formation of closed-shell nuclei might cause structures in the trend of the charge distribution function, the region of the closed 50-neutron shell is the one most poorly investigated. Besides several determinations of the independent yield of the shielded isotope ^{82}Br [5], the only yield measurements were performed on ^{83}As and ^{84}As by del Marmol [6]. In this work an unusually low yield for ^{84}As (51 neutrons) was reported and interpreted as an effect of the closed 50-neutron shell on local charge distribution.

We have found it worthwhile to re-investigate the charge distribution in that region by measuring arsenic and selenium fractional yields with mass numbers $83 \leq A \leq 88$. Nuclides in these mass chains are characterized by half-lives as short as a few seconds or tenths of a second. It was therefore to be expected that even in a very fast chemical separation the need for decay- and growth-corrections could not be avoided. For such corrections one requires rather accurate half-life values. Also it is necessary to study branching ratios into and from isomeric states. Finally, delayed neutron emission had to be investigated as this decay mode results in branching from one mass chain to another and thus affects yield measurements of very neutron-rich isotopes. Therefore, in this paper we will mention some of the aspects of the half-life determinations, branching ratio determinations and mass assignments before proceeding to the yield measurements and the conclusions that we would draw from it.

2. CHEMICAL SEPARATIONS

Our methods for rapid volatilization of selenium and arsenic hydrides from fission product solutions have already been described in detail [7-9]. The hydrides are formed by action of finely divided zinc powder on conc. HCl and are selectively absorbed in liquid or solid absorbents. The separations are completed within 5.0 and 2.5 s after irradiation, respectively. The absorption traps serve directly as samples for measuring γ-ray spectra of arsenic and selenium isotopes and their decay products and for delayed neutron counting. The mid-time of the arsenic-selenium separation, which is important for the evaluation of milking experiments and yield determinations, is as early as 0.8 ± 0.3 s after irradiation [8, 9]. For the yield measurements, slight modifications of the published separation schemes were applied.

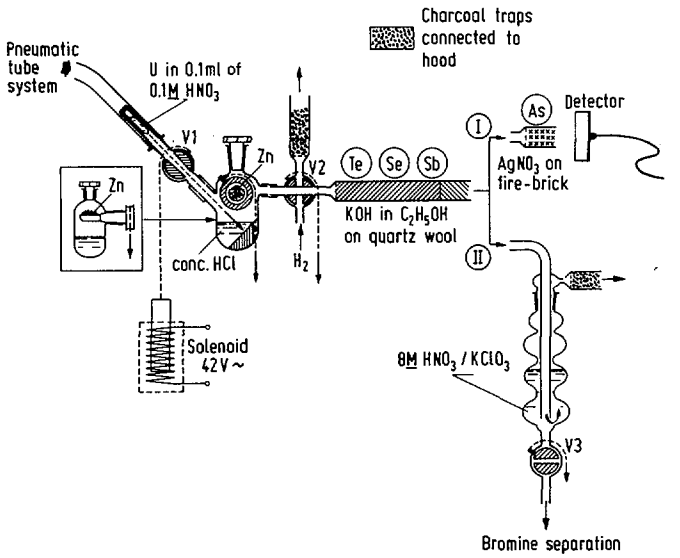

FIG. 1. Apparatus for fast automatic separation of arsenic from fission products. Absorption of AsH_3 on $AgNO_3$/fire-brick (I) in the counting position is used for direct γ-ray spectroscopy and delayed neutron counting. Decomposition of AsH_3 in $HNO_3/KClO_3$ (II) followed by a standard bromine separation is used for yield measurements.

Figure 1 shows the arsenic procedure. Short irradiations (typically 0.1 s duration at about 10^{14} neutrons/cm^2 · s maximum flux) of uranium solutions sealed in small glass capsules take place in a fast pneumatic tube system of the Mainz Triga reactor. After irradiation the capsule is transported to the separation apparatus and smashed inside the reaction vessel containing 12M HCl. A surplus of zinc powder is added by turning a spoon (Fig. 1). The hydrogen burst sweeps the hydrides through a tube containing quartz wool impregnated with a saturated solution of KOH in ethanol. This trap absorbs efficiently the hydrides of antimony, tellurium and selenium, whereas arsenic hydride is absorbed in 8M $HNO_3/KClO_3$ solution. This solution is allowed to stand until total decay of the arsenic and selenium isotopes under investigation is ensured. Bromine is then separated from this fraction using a standard procedure [10] after adding a known amount of bromide carrier and holdback carrier for arsenic, selenium and iodine. Bromine is finally precipitated and mounted as AgBr and counted on a 3 x 3 in. NaI(Tl) scintillation spectrometer or in a proportional counter. The chemical yield of bromine is later determined via neutron activation. The chemical yield of arsenic and selenium is determined by comparing the activity of 17.7-d ^{74}As or 120-d ^{75}Se recovered in the water phase of the first CCl_4-extraction with the activity added to the uranium solution prior to irradiation. Small changes in the amount of ^{235}U in the samples were determined by γ-ray counting before irradiation. The integrated neutron fluxes were recorded with a fission chamber. The necessary corrections for changes in the neutron flux were in no case larger than ± 3%.

For yield measurements the bromine activities recovered in the arsenic or selenium fraction were compared to the bromine activities obtained from so-called "unseparated samples". These samples were prepared and irradiated under the same conditions as the other samples, but no chemical separation of arsenic or selenium was carried out. After decay of the isotopes under investigation into their bromine daughters, bromine was separated from these samples using the above-mentioned procedure. For yield determinations in the mass chains 87 and 88 [8, 9] a chemical separation of bromine from separated and unseparated samples was not necessary. The bromine members of these chains are strong delayed neutron precursors [11] which can be determined selectively without chemical separation by delayed neutron counting.

To improve our knowledge of the half-lives of neutron-rich germanium isotopes which had been detected indirectly via the growth of their arsenic daughters (see Section 3), a few experiments with a fast separation of germanium from fission product solutions were also performed. These separations are based on the volatility of $GeCl_4$ from 12M HCl when air is bubbled through the solution. Yields of 50% were achieved within 10 s. Volatilization of arsenic as $AsCl_3$ under these conditions may be inhibited by adding a strong oxidizing agent, e. g. $K_2S_2O_8$, to the solution.

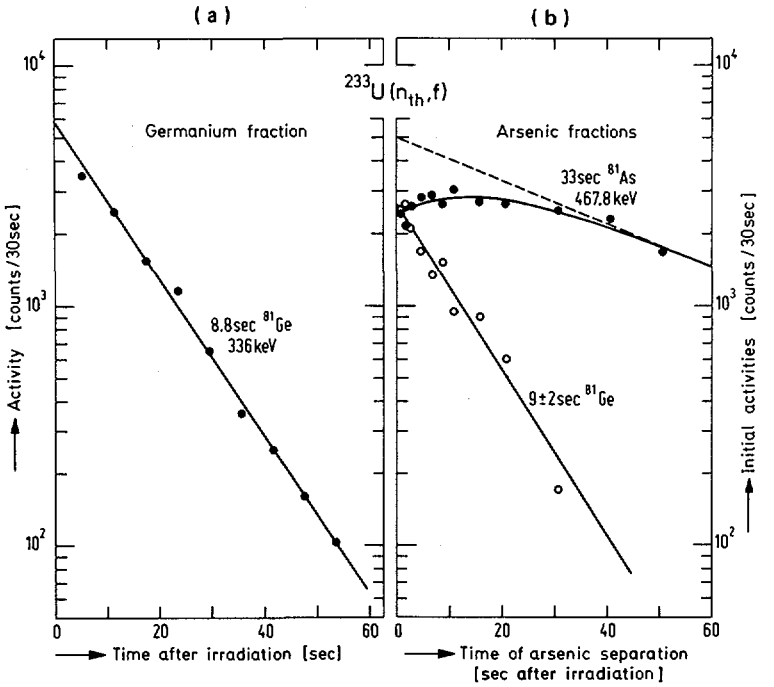

FIG. 2(a) Decay-curve of the 336-keV peak of the germanium fraction. (b) Initial activities of the 467.8-keV peak of ^{81}As growing in arsenic fractions separated after increasing delay times between irradiation and separation.

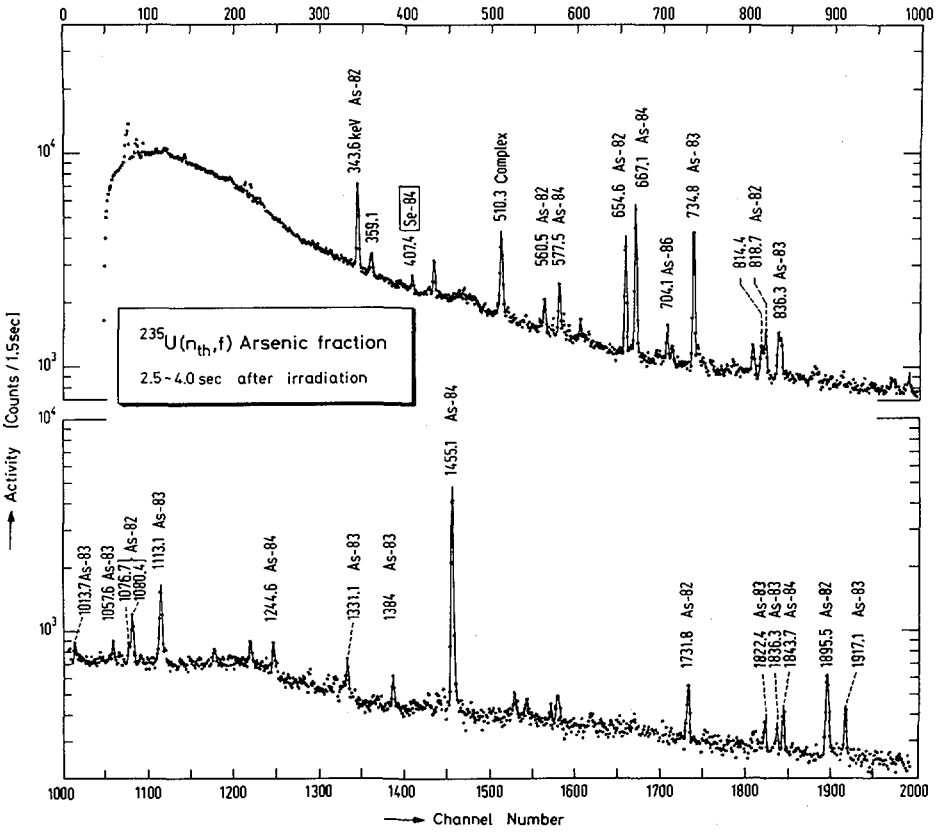

FIG. 3. Low-energy part of the γ-ray spectrum of the arsenic fraction, 2.5 to 4.0 s after irradiation, obtained by summing the spectra of 117 single experiments.

3. HALF-LIVES AND MASS ASSIGNMENTS

At the beginning of this work, information on half-lives and the main decay characteristics of neutron-rich germanium, arsenic and selenium isotopes was rather limited. We have applied our fast separations to a total of 19 nuclides in the mass region $79 \leq A \leq 88$. Some of these isotopes were previously unknown, many others had not been observed directly before. Parallel studies in this field have been performed by del Marmol and co-workers [6, 12, 13] and Tomlinson and Hurdus [14].

Wherever possible, we measured half-lives directly by following the decay of prominent γ-ray peaks or by delayed-neutron counting. In addition, indirect half-life determinations were carried out in a series of separations with increasing delay times between irradiation and separation. These "milking experiments" served also to show the genetic relationship of the observed activities with known daughter or granddaughter activities. A few examples are given for illustration.

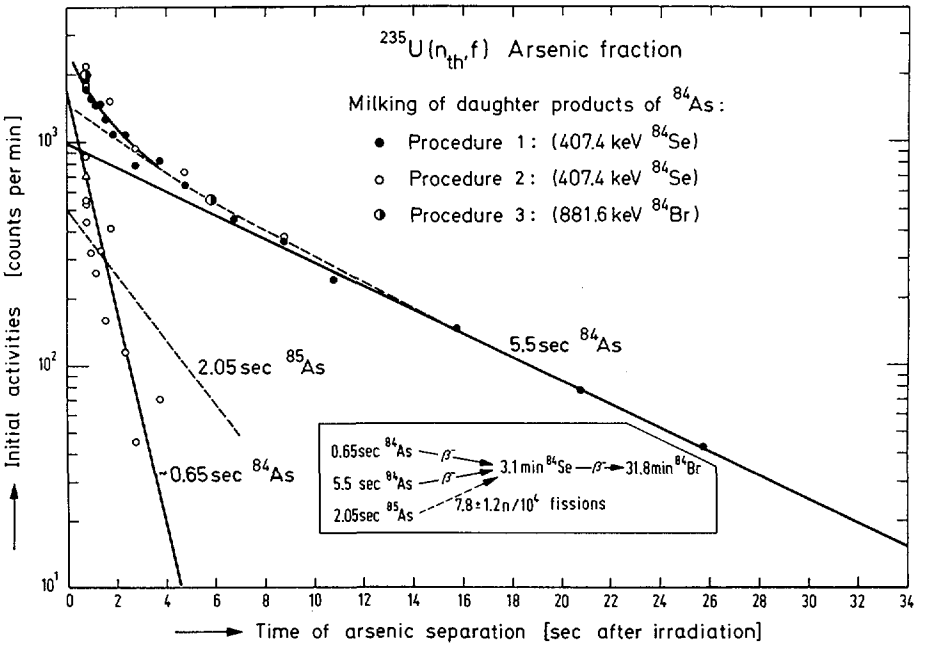

FIG. 4. Activities of 3.10-min ^{84}Se and 31.8-min ^{84}Br in delayed separations of the arsenic fraction. ^{84}Se has three parents: a previously unknown 0.65-s state of ^{84}As, 5.5-s ^{84}As and 2-s ^{85}As.

Figure 2a shows the decay curve of the 336-keV γ-ray peak of the germanium fraction. In Fig. 2b we have plotted the growth of the initial activities at 467.8 keV of 33-s ^{81}As, observed in arsenic fractions separated after increasing delay times between irradiation and hydride volatilization. The growth of ^{81}As from its parent results in a half-life of 9 ± 2 s which agrees with the directly observed half-life of 8.8 s. Thus the γ-ray transition at 336 keV and a half-life of 8.8 ± 1.1 s are assigned to ^{81}Ge. Similar results have recently been reported by del Marmol and Fettweis [13].

Figure 3 shows the low-energy part of the γ-ray spectrum of the arsenic fraction obtained in 117 experiments shortly after the chemical separation. The spectrum includes strong γ-ray peaks of ^{80}As, ^{81}As, of the two states of ^{82}As, of ^{83}As, ^{84}As and ^{86}As. In the decay of 2.05-s ^{85}As, γ-ray transitions could not yet be detected. Of special interest for the following discussion is the peak at 407.4 keV. It belongs to 3.10-min ^{84}Se and is the strongest peak in the late spectra of the arsenic fractions.

Figure 4 illustrates the result of milking experiments in the mass chain 84. Arsenic was separated from the mixture of fission products after various delay times. One set of data was obtained by determining the initial activities of the above-mentioned 407.4-keV line of the daughter product ^{84}Se growing in the arsenic fractions when the arsenic hydride was absorbed on $AgNO_3$/firebrick directly in the counting position. In a second series of delayed separations the arsenic fraction was further purified by an extraction chromatography step improving the decontamination from germanium and was again

TABLE I. HALF-LIVES AND PRINCIPAL DECAY CHARACTERISTICS OF ISOTOPES NEAR N=50

Isotope	Half-life*)	Nuclide counted	Technique+)	Production mode	Half-life [literature]
^{79}Ge	47 ±2 sec	^{79}Ge	γ(230.5, 542.2, ...)	^{82}Se(n,α)	50 ±5 sec /a/
				^{233}U(n,f)	40 ±4 sec /b/
					41.1 ±4.3 sec /c/
^{80}Ge	28 ±4 sec	^{80}As	γ(666.2)	^{233}U(n,f)	24.5 ±1.0 sec /c/
		^{80}Ge	γ(266)		
^{81}Ge	8.8 ±1.1 sec	^{81}As	γ(467.8)	^{233}U(n,f)	10.1 ±0.8 sec /c/
		^{81}Ge	γ(336)		
^{82}Ge	5 ±1 sec	^{82}As	γ(654.6)	^{233}U(n,f)	4.60±0.35 sec /c/
^{83}Ge	≤1.6 sec	^{83}As	γ(734.5)	^{233}U(n,f)	1.9 ±0.4 sec /c/
^{84}Ge					1.2 ±0.3 sec /c/
^{80}As	15.2 ±0.2 sec	^{80}As	γ(666.2, 782.4, 1207.2, 1448.8, ...)	^{80}Se(n,p)	15.3 ±0.2 sec /d/
				^{233}U(n,f)	16.5 ±0.3 sec /e/
^{81}As	34 ±2 sec	^{81}As	γ(467.8)	^{233}U(n,f)	33 sec /c/
^{82a}As	19.1 ±0.5 sec	^{82a}As	γ(654.6, 1731.3, ...); β$^-$	^{235}U(n,f)	19.0 ±1.5 sec /b/
				^{82}Se(n,p)	22.6 ±1.4 sec /c/
^{82b}As	14.0 ±0.5 sec	^{82b}As	γ(343.5, 560.5, 654.6 ...)	^{235}U(n,f)	13.0 ±0.6 sec /b/
				^{82}Se(n,p)	
^{83}As	13.3 ±0.6 sec	^{83}Br	β$^-$	^{235}U(n,f)	14.1 ±1.1 sec /f/
		^{83m,g}Se	γ(356.5, 987.9, 1030.3 ...)		
		^{83}As	γ(734.5, 1113.1, 1331.1, 1917.3, ...)		

TABLE I. continued

Isotope	Half-life*)	Nuclide counted	Technique+)	Production mode	Half-life [literature]
^{84a}As	5.3 ±0.4 sec	^{84}Br	γ(881.6)	$^{235}U(n,f)$	5.5 ±0.6 sec /f/
		^{84}Se	γ(407.4)	$^{233}U(n,f)$	
		^{84a}As	γ(1455.1, 667.1, 577.5, 1244.6,..)		
			n		
^{84b}As	0.65 ±0.15sec	^{84}Br	γ(881.6)	$^{235}U(n,f)$	
		^{84}Se	γ(407.4)	$^{233}U(n,f)$	
$^{85}As^{‡}$)	2.05 ±0.05sec	^{85}Se	γ(345.1)	$^{235}U(n,f)$	2.028±0.012 sec /g/
		^{85}As	n		2.15 ±0.15 sec /h/
		$^{84}Se^{++}$)	γ(1455.1, ...)		
$^{86}As^{‡}$)	0.9 ±0.2 sec	^{86}Br	γ(1564.9)	$^{235}U(n.f)$	
		^{86}As	γ(704.1), n		
$^{87}As^{‡}$)	~ 0.3 sec	^{87}Br	n	$^{235}U(n,f)$	
^{83m}Se	69 ±2 sec	^{83m}Se	γ(356.5, 673.9, 987.9, ...)	$^{82}Se(n,γ)$ $^{233}U(n,f)$	70 ±1 sec /i/
^{83g}Se	22.4 ±0.2 min	^{83g}Se	γ(365.5, ...)		22.6 ±0.2 min /i/
^{84}Se	3.10±0.10min	^{84}Br	γ(881.6, ...)	$^{235}U(n,f)$	3.1 ±0.2 min /j/
		^{84}Se	γ(407.4)		
^{85}Se	33 ±2 sec	^{85}Se	γ(345.1)	$^{235}U(n,f)$	39 ±4 sec /k/
^{86}Se	16.1 ±0.6 sec	^{86}Br	γ(1564.9, ...)	$^{235}U(n,f)$	
		^{86}Se	γ(2441.5, ...)		
$^{87}Se^{‡}$)	5.85±0.15sec	^{87}Br	γ(1419.9)	$^{235}U(n,f)$	16 ±3 sec /k/
			n		5.9 ±0.2 sec /l/
		^{87}Se	n		5.41±0.1 sec /m/

TABLE I. continued

Isotope	Half-life*)	Nuclide counted	Technique+)	Production mode	Half-life[literature]
^{88}Se‡)	1.4 ±0.3 sec	^{88}Br	n	$^{235}U(n,f)$	1.3 ±0.3 sec /l/
		^{88}Se	n		1.53±0.06 sec /m/
^{89}Se			n		0.41±0.04 sec /m/

*) Some of these results were obtained in cooperation with H. Franz and N. Kaffrell

+) γ: from γ-ray spectra (γ-ray transitions [keV] are given in parentheses); the ... symbol means that there are more γ lines than the ones indicated

β^-: from β^--counting

n: from neutron decay curves

++) Excited levels in ^{84}Se are fed in the delayed-neutron decay branch of ^{85}As

‡) Data on these isotopes have previously been published by the authors in Refs. /8,9/

/a/ Blachot et al. /15/

/b/ Van Klinken et al. /16/

/c/ del Marmol and Fettweis /13/

/d/ Mathew et al. /17/

/e/ McMillan and Pate /18/

/f/ del Marmol /6/

/g/ Tomlinson and Hurdus /19/

/h/ del Marmol and Nêve de Mêvergnies/20/

/i/ Marlow and Waggoner /21/

/j/ Rengan and Griffin /22/

/k/ Sattizahn et al. /23/

/l/ del Marmol and Perricos/12/

/m/ Tomlinson and Hurdus /14/

counted for the 407.4-keV peak of ^{84}Se. In a third series the granddaughter ^{84}Br was extracted from the arsenic fractions and counted for its 881.6-keV line. There is no systematic deviation to be seen between these three independent series (Fig. 4). The result is a complex decay-curve consisting of three components:

(1) 5.5-s ^{84}As, indicated by the solid line. Its decay has also been observed directly via a number of γ-ray transitions in ^{84}Se, the strongest one being the ($2^+ \rightarrow 0^+$) transition at 1455.1 keV with a half-life of 5.3 ± 0.4 s.

(2) A 2-s component, indicated by the lower dashed line. (For clarity, activities are not plotted here.) It is assigned to that part of the known 2-s arsenic isotope of mass number 85 which decays into ^{84}Se by emission of delayed neutrons after β^--decay. The initial activity of this 2-s component corresponds exactly to what should be expected from the delayed neutron yield of ^{85}As [9] and the fission yield of 5.3-s ^{84}As (see Section 5).

(3) The sum of the 5.5-s and the 2-s components (top dashed line in Fig. 4) does not yet explain the very early activities. Further curve analysis gives evidence for a third activity of about 0.65-s half-life. We assign this activity to a hitherto unknown β^--unstable second state in ^{84}As. It should be emphasized that the extremely low fission yield of ^{84}As reported by del Marmol [6] did not include the yield of this state.

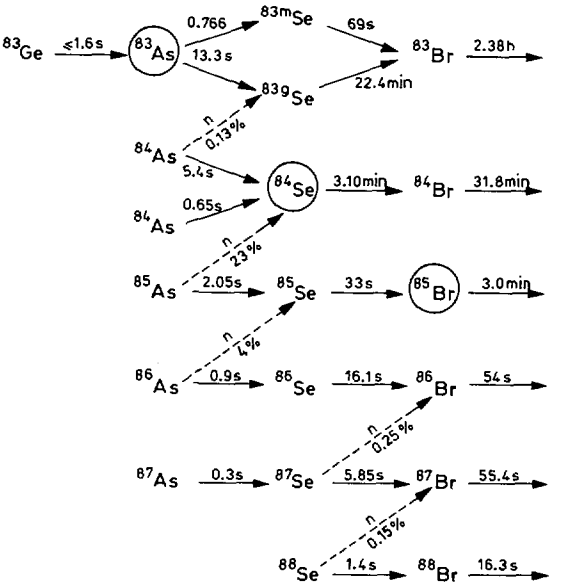

FIG. 5. Isobaric chains near N = 50. Half-lives, branching ratios and delayed neutron emission probabilities shown are the results of the present work. → = β^--decay; - - → = delayed neutron emission. Magic nuclei are encircled.

A summary of our results on half-lives, mass assignments and principal decay characteristics of germanium, arsenic and selenium isotopes is given in Table I together with the results of other authors. As far as they are relevant for the yield measurements, these data are collected again in Fig. 5, demonstrating more clearly the genetic relationships in the mass chains.

4. DETERMINATION OF DECAY BRANCHES

It is evident from Fig. 5 that besides precise half-life determinations two more features have an influence on the final evaluation of our yield data. These are the branching of the β^--decay chains into two states in the mass chains 83 and 84 and the branching from one mass chain to another by delayed neutron emission.

The isomeric ratio of the two states in ^{84}As can directly be taken from Fig. 4: the yield of the 0.65-s ^{84}As is 1.6 ± 0.3 times the yield of the 5.3-s ^{84}As.

The decay branch of 13.3-s ^{83}As into 69-s ^{83m}Se was determined indirectly using a value from the literature on the ratio of (n,γ) formation cross-sections of the two states of ^{83}Se [24]. We have measured the intensity of the 22.4-min and 69-s components in the decay of the 356.5-keV peak of ^{83m}Se and ^{83g}Se respectively, both in the ^{82}Se (n,γ) reaction and in the β^--decay of 13.3-s ^{83}As. We can normalize our activity ratio observed in the (n,γ) reaction to the reported ratio of (n,γ) formation cross-sections. Then, the activity ratio of the isomers observed after β^--decay of ^{83}As leads to a branching ratio of 76.6 ± 8.8% from ^{83}As into ^{83m}Se. This value is not contradictory to the value 64 ± 8% reported earlier by del Marmol [6]. The higher value, however, is more consistent with our observation [25] that about half of the cumulative yield of 22.4-min ^{83g}Se stems from β^--decay of ^{83}As.

Delayed neutron emission from short-lived selenium and arsenic isotopes (indicated by dashed arrows in Fig. 5) has also been investigated [8, 9]. In general, neutron emission probabilities in the interesting mass region turned out to be low and their branching to the next lower mass chain may thus be neglected. However, this does not hold for the 2-s ^{85}As, where a delayed neutron yield of 0.078 ± 0.012 n/10^2 fissions of ^{235}U was observed. Consequently, corrections to the fractional cumulative yields of ^{84}As and ^{85}Se had to be applied.

5. FRACTIONAL CUMULATIVE YIELDS OF ARSENIC AND SELENIUM ISOTOPES

By taking into consideration the decay and branching data that are shown in Fig. 5, fractional cumulative yields were determined for ^{83}As, ^{83}Se, ^{84}As, ^{84}Se, ^{87}As, ^{87}Se, ^{88}Se. Nuclides with the magic number of 50 neutrons are ^{83}As, ^{84}Se and ^{85}Br. As already mentioned, the bromine activities separated from arsenic or selenium fractions were compared to the bromine activities obtained directly from "unseparated samples" after complete decay of the early members of the chain. The bromine activities were corrected for the chemical yield of arsenic or selenium, for the chemical yield of bromine, for self-adsorption in the β^--counting (^{83}Br), and for small changes in the neutron flux, and were then extrapolated back to irradiation time. The relations between these initial

TABLE II. SUMMARY OF FRACTIONAL YIELD DATA

Isotope	Fractional cumulative yield [%]	
	This work	Literature
^{83}As	76.0 ± 6.3	80 ± 8 /a/
$^{83m,g}Se$	≥ 93	
^{84a}As	15.3 ± 1.2	17 ± 2 /a/
$^{84a,b}As$	39.8 ± 5.5	
^{84}Se	96.6 ± 2.1	
^{85}Se	81.8 ± 6.6	
^{87}As +)	1.8 ± 0.9	
^{87}Se +)	40.7 ± 7.1	45.6 ± 6.3 /b/
		29 ± 5 /c/
		25 ± 5 /d/
^{88}Se +)	22.2 ± 5.6	13 ± 2 /d/
^{89}Se		3 ± 0.5 /c/

+) These values have previously been published by the authors in Refs. /8,9/

/a/ del Marmol /6/

/b/ Grimm /26/

/c/ Tomlinson and Hurdus /14/

/d/ del Marmol and Perricos /12/

activities and the fractional yields were derived from the standard equations of radioactive decay. In these calculations the fractional cumulative yields of ^{83}Br and ^{84}Br were first assumed to be equal to the chain yields. Once the cumulative yields of ^{83}Se and ^{84}Se had been calculated in this way, the independent yields of ^{83}Br and ^{84}Br could be estimated and inserted into more developed expressions. The final yield values were then obtained by iterations. In the mass chains 87 and 88, estimated fractional cumulative yields of 95 ± 4% and 80 ± 5% for ^{87}Br and ^{88}Br [26] were used for normalization of our data. The reference value for ^{88}Br is slightly different from the one

used in Ref. [8]; thus the yield for ^{88}Se given in the present paper differs somewhat from our previous publication. A summary of our results is given in Table II, which contains results from other authors too. Our values are in good agreement with the published data on ^{83}As and 5.3-s ^{84}As [6]. For the yields of ^{87}Se and ^{88}Se some spread in the values occurs. The cumulative yield of ^{83}Se could not be distinguished from the total chain yield. Thus the error in our determination sets a lower limit at ≥ 93%. The cumulative yield of ^{85}Se was not determined experimentally. In 1960, when Sattizahn and co-workers [23] identified ^{84}Se and ^{85}Se via their bromine daughters, they obtained the ratio of their absolute cumulative fission yields from the β^--activities of ^{84}Br and ^{85}Br growing in the selenium samples. Since we have measured the cumulative yield of ^{84}Se, a calculation of the ^{85}Se yield is now possible; chain yields of 1.31 ± 0.03% and 1.01 ± 0.02% [27] were used in this calculation and a correction for the delayed neutron emission of the precursor ^{85}As was applied.

TABLE III. DETERMINATION OF THE CHARGE DISTRIBUTION PARAMETERS σ AND ΔZ

Mass chain	Nuclide	Fractional cumulative yield	σ	Z_p	Z_{UCD}	ΔZ
83	As	76.0±6.3	a)	33.10±0.16	32.69	+0.41±0.16
	Se	≥ 93				
84	As	39.8±5.5	$0.50^{+0.09}_{-0.10}$	33.63±0.075	33.10	+0.53±0.08
	Se	96.6±2.1				
85	Se	81.8±6.6	a)	33.99±0.20	33.51	+0.48±0.20
87	As	1.8±0.9	$0.53^{+0.10}_{-0.11}$	34.62±0.10	34.34	+0.28±0.11
	Se	40.7±7.1				
	Br	95 ±4 +)				
88	Se	22.2±5.6	$0.61^{+0.16}_{-0.12}$	34.98±0.11	34.76	+0.22±0.11
	Br	80 ±5 +)				

+) Reference values /26/

a) Average value σ = 0.56±0.06 /5/ used for determination of Z_p

6. CHARGE DISTRIBUTION IN THE 50-NEUTRON-SHELL REGION

Nuclear charge distribution in a fission product chain can be described by a Gaussian charge dispersion curve with a width parameter σ and by the deviation ΔZ of the maximum (Z_p) of this curve from a fragment charge (Z_{UCD}), calculated assuming unchanged charge density (UCD) of compound nucleus and fragments [5, 28]. Table III shows the results of the analysis of our data with respect to these two parameters. The width parameters σ of the Gaussian charge dispersion curves fitted to our fractional yield data agree within the errors with the average value $\sigma = 0.56 \pm 0.06$ given by Wahl [5]. Hence we conclude that the closed 50-neutron shell does not significantly influence this parameter. In Table III, Z_{UCD} is calculated according to

$$Z_{UCD} = (A + \bar{\nu}) Z_F / A_F$$

where Z_F and A_F are the nuclear charge and mass of the fissioning nucleus ^{236}U, $\bar{\nu}$ is the average number of neutrons emitted from the initial fragments. A mean value for $\bar{\nu}$ was taken from Refs [5] and [29]. It should be emphasized that the actual number of neutrons emitted from a single fragment is not known: All available neutron data are average numbers for groups of fragments. The correction for prompt neutron evaporation must therefore be considered as a rough approximation. It may even be definitely wrong in the region of closed neutron shells. We shall come back to this point.

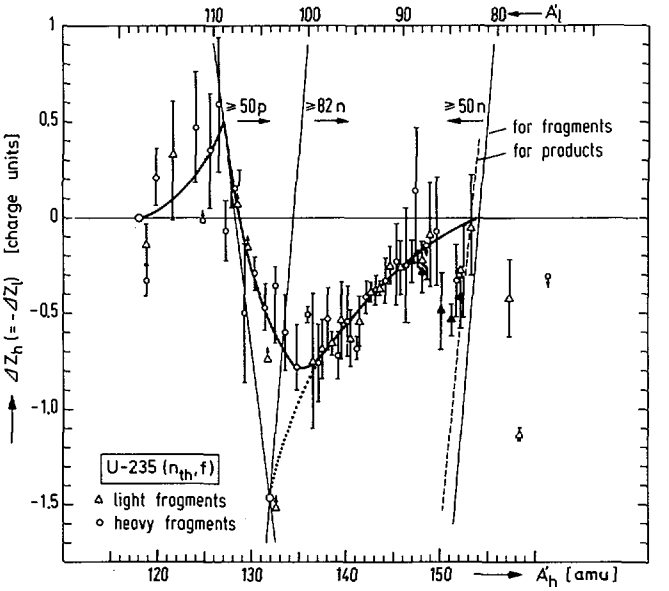

FIG. 6. Deviation ΔZ of the most probable nuclear charge from Z_{UCD} versus fragment mass number. Data (open circles and triangles) from Ref. [30]. Results of the present work: black triangles. For further explanation of figure, see Ref. [30].

The last column in Table III gives the deviation ΔZ of the most probable nuclear charge Z_p from the prediction of the UCD-rule. These values indicate a slight enrichment of protons in the light fragments which is in agreement with the known trend of charge distribution in low-energy fission reactions.

In Fig. 6 the deviation ΔZ is plotted versus fragment mass number for heavy and light fragments. In this plot negative values of ΔZ refer to an enrichment of neutrons in the heavy fragments and an enrichment of protons in the complementary light ones. ΔZ values of the present work are plotted as black triangles. The straight lines indicate what ΔZ values should be expected if magic fragments were generally formed with the highest fractional yield possible within a Gaussian charge dispersion curve. We are fully aware of the problems inherent in this kind of plot (Fig. 6). However, the fact that the data do show a correlation rather than a wild scatter gives us confidence that one can learn something from it, e. g. that the 50-proton shell has a strong influence on charge distribution. A combination of mass and charge distribution data makes the influence of closed shells in thermal-neutron-induced fission of ^{235}U even clearer: the 50-proton and 82-neutron shells are conserved in more than 99% of all fission channels. All three shells are conserved in more than 90% of the fission events. This led to the assumption of a dumb-bell configuration of the fissioning nucleus [31] where closed-shell fragments are pre-formed before scission. From the rather well-established trend of the radiochemical ΔZ values between mass numbers 132 and 82 (Fig. 6) Denschlag and Qaim [31] concluded that the dumb-bell configuration includes the magic clusters ^{132}Sn and ^{82}Ge, connected by a neck of high charge density. The prediction of this picture for the isobars of mass chain 82 would be no deviation from the UCD rule, as ^{82}Ge has the same charge density as ^{236}U. The experimental ΔZ value for mass 82 gives support to such considerations. Also our data for mass chains 87 and 88 fit well into the ascending band of radiochemical data.

As Fig. 6 shows, the experimental ΔZ values for the isobaric chains 83, 84 and 85 deviate from the general trend. Considering this structure as significant, one could interpret it as a local tendency of the fissioning nucleus to form its light fragments around A = 84 with the magic number of 50 neutrons. However, the dashed line in Fig. 6, representing the closed 50-neutron shell after neutron evaporation, is in a better agreement with the experimental data than the pre-neutron emission line.

This observation suggested that one could ask whether the observed structure in the ΔZ values around mass number 84 could be the result of a disturbance in the dispersion of prompt neutron evaporation caused by the jump in neutron binding energies at the shell, rather than the result of a primary local shell-effect in fission.

Our considerations are outlined in Fig. 7. We have assumed that charge distribution of the fragments (before prompt neutron emission) follows the trend which is drawn on the left-hand side and have calculated the respective fragment yields Y. The width parameter of the fragment Gaussian charge dispersion curves was assumed to be $\sigma = 0.41$, as measured in ^{252}Cf fission by Glendenin and co-workers [2]. For simplification, the average number of neutrons in assumed to be 1.0 for all mass chains investigated. This is correct only for mass number 87, but the error is less than 20% in the other isobaric chains. The equation in Fig. 7 shows how the different fission fragments contribute by neutron evaporation to the independent yield of ^{84}As. P_0

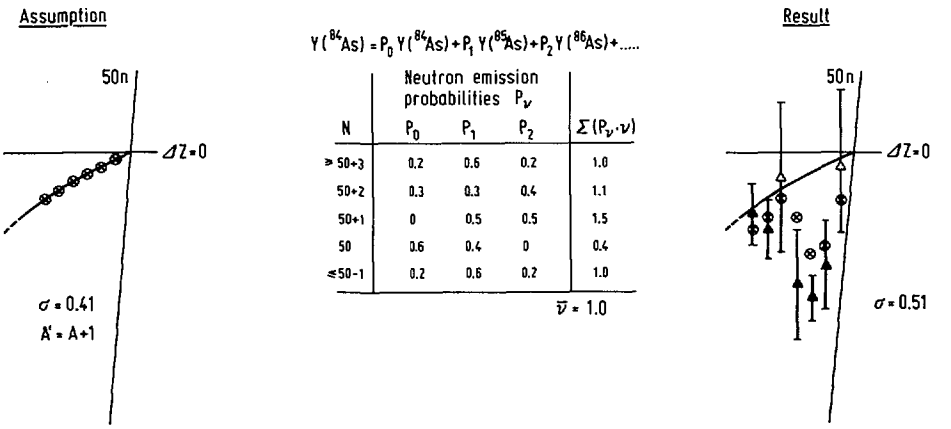

$$Y(^{84}As) = P_0\,Y(^{84}As) + P_1\,Y(^{85}As) + P_2\,Y(^{86}As) + \ldots$$

N	Neutron emission probabilities P_ν P_0	P_1	P_2	$\Sigma(P_\nu \cdot \nu)$
≥ 50+3	0.2	0.6	0.2	1.0
50+2	0.3	0.3	0.4	1.1
50+1	0	0.5	0.5	1.5
50	0.6	0.4	0	0.4
≤50-1	0.2	0.6	0.2	1.0
			$\bar{\nu}$ =	1.0

FIG. 7. Considerations on prompt neutron evaporation from fragments near the closed 50-neutron shell. Experimental data (right-hand side) are given as triangles: ▲ this work, △ Denschlag [30]. The crossed circles ⊗ are assumed (pre-neutron emission) and calculated (post-neutron emission).

is the probability that the fragment ^{84}As evaporates no neutrons, P_1 is the probability that ^{85}As emits one neutron, and P_2 is the probability that the fragment ^{86}As emits two neutrons, etc. Neutron emission probabilities for three and more neutrons are neglected.

The neutron emission probabilities listed below the equation are chosen to obtain a preference of P_2 at 52 neutrons, P_1 at 51 neutrons and P_0 at 50 neutrons. Despite this preference, the average number of neutrons has been kept at 1.0 in each chain.

Simulating the prompt neutron evaporation this way leads to isobaric yield distributions whose width parameters and ΔZ values overlap in all cases with the error bars of the experimental points, as is shown on the right-hand side of Fig. 7.

The assumptions on the neutron emission probabilities are certainly rather extreme, and they should, of course, be checked by more serious theoretical work. Nevertheless, they show clearly what qualitative consequences a shell-dependent disturbance of prompt neutron evaporation would have.

Whether there is a primary shell effect or a secondary effect caused by neutron evaporation can only be detected by measuring fission yields of complementary products in the region of heavy cerium, praseodymium and neodymium isotopes. However, this would require the development of a rapid separation technique for lanthanide elements.

It is interesting to note in this context that Gäggeler and von Gunten [32] have very recently performed a measurement of the fractional yield of the shielded isotope ^{150}Pm ($5.4 \pm 0.3 \times 10^{-4}$). Although this yield is rather low – which results in a large uncertainty in the Z_p value – the deviation ΔZ (about -0.53) agrees closely with the value of the complementary light fragment. Certainly, more experimental data are needed to clarify the situation.

ACKNOWLEDGEMENTS

We gratefully acknowledge the assistance of Mrs. A. Bode and the financial support from the Bundesministerium für Bildung und Wissenschaft.

REFERENCES

[1] INTERNATIONAL ATOMIC ENERGY AGENCY, Physics and Chemistry of Fission (Proc. Symp. Vienna, 1969), IAEA, Vienna (1969).
[2] GLENDENIN, L.E., UNIK, J.P., GRIFFIN, H.C., REISDORF, W., ibid., p. 781.
[3] See for example ARMBRUSTER, P., MEISTER, H., Z. Phys. 170 (1962) 274.
[4] CHEIFETZ, E., WILHELMY, J.B., JARED, R.C., THOMPSON, S.G., Phys. Rev. C4 (1971) 1913.
[5] WAHL, A.C., NORRIS, A.E., ROUSE, R.A., WILLIAMS, J.C., in Physics and Chemistry of Fission (Proc. Symp. Vienna, 1969), IAEA, Vienna (1969) 813.
[6] del MARMOL, P., J. Inorg. Nucl. Chem. 30 (1968) 2873.
[7] FOLGER, H., KRATZ, J.-V., HERRMANN, G., Radiochem. Radioanal. Lett. 1 (1969) 185.
[8] KRATZ, J.-V., HERRMANN, G., J. Inorg. Nucl. Chem. 32 (1970) 3713.
[9] KRATZ, J.-V., FRANZ, H., HERRMANN, G., J. Inorg. Nucl. Chem. 35 (1973) 1407.
[10] GLENDENIN, L.E., EDWARDS, R.R., GEST, H., in Radiochemical Studies: The Fission Products (CORYELL, C.D., SUGARMAN, N., Eds) 2, McGraw-Hill, N.Y. (1951) 232.
[11] SCHÜSSLER, H.D., AHRENS, H., FOLGER, H., FRANZ, H., GRIMM, W., HERRMANN, G., KRATZ, J.-V., KRATZ, K.-L., in Physics and Chemistry of Fission (Proc. Symp. Vienna, 1969), IAEA, Vienna (1969) 591.
[12] del MARMOL, P., PERRICOS, D.C., J. Inorg. Nucl. Chem. 32 (1970) 705.
[13] del MARMOL, P., FETTWEIS, P., Nucl. Phys. A194 (1972) 140.
[14] TOMLINSON, L., HURDUS, M.H., J. Inorg. Nucl. Chem. 33 (1971) 3609.
[15] BLACHOT, J., BENABED, A., HERMENT, J., MONNAND, E., CEN-Grenoble Rep. CEA-R-3678 (1968).
[16] VAN KLINKEN, J., TAFF, L.M., DIJKSTRA, H.T., DE HAAN, A.M., HANSON, H., KOENE, B.K.S., MÅRING, J.M., SCHUURMAN, J.J., YANO, F.B., Nucl. Phys. A157 (1970) 385.
[17] MATHEW, P.J., McCALLUM, G.J., FREEMAN, R.M., Phys. Lett. 28B (1968) 106.
[18] McMILLAN, D.K., PATE, B.D., Nucl. Phys. A174 (1971) 593.
[19] TOMLINSON, L., HURDUS, M.H., J. Inorg. Nucl. Chem. 30 (1968) 1649.
[20] del MARMOL, P., NEVE DE MEVERGNIES, J. Inorg. Nucl.Chem. 29 (1967) 273.
[21] MARLOW, K.W., WAGGONER, M.A., Phys. Rev. 163 (1967) 1098.
[22] RENGAN, K., GRIFFIN, H.C., J. Inorg. Nucl. Chem. 30 (1968) 2887.
[23] SATTIZAHN, J.E., KNIGHT, J.D., KAHN, M., J. Inorg. Nucl. Chem. 12 (1960) 206.
[24] IYER, R.S., RAMANIAH, M.V., J. Inorg. Nucl. Chem. 29 (1967) 181.
[25] KRATZ, J.-V., Doctoral Dissertation, Mainz (1971).
[26] GRIMM, W., Doctoral Dissertation, Mainz (1971).
[27] FARRAR, H., FICKEL, H.R., TOMLINSON, R.H., Can. J. Phys. 40 (1962) 1017.
[28] WAHL, A.C., FERGUSON, R.L., NETHAWAY, D.R., TROUTNER, D.E., WOLFSBERG, K., Phys. Rev. 126 (1962) 1112.
[29] MASLIN, E.E., RODGERS, A.L., CORE, W.G.F., Phys. Rev. 164 (1967) 1520.
[30] DENSCHLAG, H.O., Habilitationsschrift, Mainz (1971).
[31] DENSCHLAG, H.O., QAIM, S.M., Z. Naturforsch. 24A (1969) 2000 and references quoted therein.
[32] GÄGGELER, H., VON GUNTEN, H.R., Private communication.

DISCUSSION

H. O. DENSCHLAG: We did some experiments in order to find out whether prompt neutron emission can have an influence on charge distribution, as has just been discussed by Mr. Kratz.

We chose chain 132, which is especially interesting because it contains the doubly magic nucleus tin-132, and because in this chain we have a large

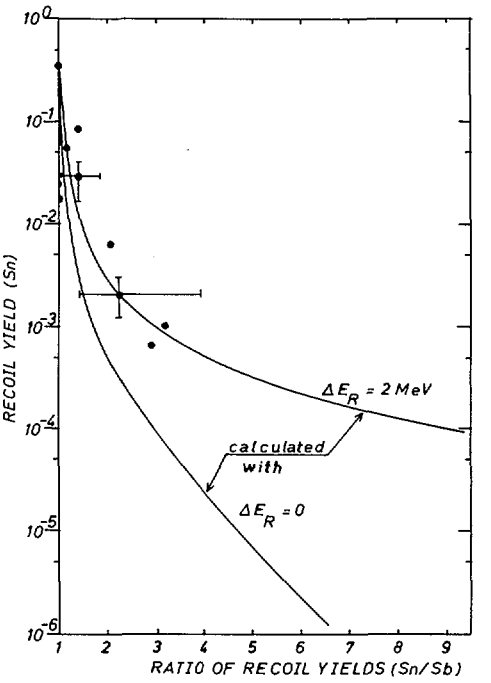

FIG. A. Dependence of the charge distribution, as measured by the observed ratio of ^{132}Sn to ^{132}Sb yields, as a function of absorber thickness (in the form of the recoil yield of ^{132}Sn).

discrepancy between radiochemical measurements[1] and a physical measurement performed by Konecny and co-workers[2]. We wanted to check whether this discrepancy was related to a prompt neutron effect.

In order to check whether the charge distribution is different before and after prompt neutron emission, we measured the ratio of ^{132}Sn to ^{132}Sb in fission fragments that had penetrated increasing amounts of absorber foil.

Thick absorber foils are penetrated only by fragments of high recoil energy which are known to emit practically no prompt neutrons.

The results are shown in Fig. A, in which absorber thickness (in the form of the recoil yield of ^{132}Sn) is plotted against the Sn/Sb yield ratio.

As can be seen from the experimental points (dots – with typical error bars in two cases), there is indeed an increase in the ratio of Sn/Sb, from 1 at about 40% recoil yield, to 3 to 4 at around 0.1%.

We have compared the experimental results with a calculated curve. This curve, marked $\Delta E_R = 0$, assumes no effect of prompt neutron emission on charge distribution and, therefore, no difference in the recoil energy between Sn and Sb.

---

[1] NAEUMANN, R., FOGLER, H., DENSCHLAG, H.O., J. Inorg. Nucl. Chem. 34 (1972) 1785.

[2] KONECNY, E., et al. Z. Phys. 271 (1970) 59.

This curve deviates from a ratio of the recoil yields Sn/Sb = 1 only because the interaction of Sb (Z = 51) with the absorbers is stronger than that[3] of Sn (Z = 50).

We find that the experimental points, even though statistically inaccurate, lie on the right-hand side of this curve, signifying that the charge distribution is altered by prompt neutron emission.

To make quantitative conclusions, we require more accurate data and these are being prepared. However, it would already appear that the effect is too small to fully explain the discrepancy between the radiochemical and Konecny's measurements.

M. ASGHAR: We have heard that neutron emission tends to demolish the structure due to pairing and shell effects. I feel that this could be avoided if one chooses those events where the fragment kinetic energy is so high that no neutrons could have been emitted. One would then have fragments with primary nuclear charge (Z) and neutron number (N).

S. AMIEL: When carrying out experiments involving fragment kinetic energy selection, one should be careful about drawing conclusions concerning nucleon pairing effects. As we go to lower excitation energies (i.e. higher kinetic energies), two simultaneous changes take place – without our knowing the rate of change and function of each: one being the drop in neutron evaporation, the other the enhancement of the primary even-odd effect associated with the decrease in the formation of odd-configurations. Unless we know more about the function of one of these with respect to the excitation energy, we should refrain from making any conclusive statements about the other. Of course this is a general statement; isolated cases may exist where it would not matter.

H. O. DENSCHLAG: The measurements of pre-neutron-emission charge distribution carried out by Glendenin and co-workers[4] show that the second effect you mention is pretty small. Therefore, what we see here is due mainly to prompt neutron evaporation. This is naturally only true within the limited accuracy of our and Glendenin's values.

---

[3] NORTHCLIFFE, L.L., SCHILLING, R.F., Nucl. Data Tables 17 (1970) 233.

[4] REISDORF, W., UNIK, J.P., GRIFFIN, H.C., GLENDENIN, L.E., Nucl. Phys. A 177 (1971) 337.

PROMPT NEUTRONS AND RADIATION FROM FISSION FRAGMENTS

(Session VII)

Chairman: P. Ribon (France)

Review Paper

NEUTRON AND GAMMA EMISSION IN FISSION*

H. NIFENECKER**
Lawrence Berkeley Laboratory,
University of California,
Berkeley, Calif.,
United States of America

C. SIGNARBIEUX, R. BABINET, J. POITOU
Centre d'études nucléaires de Saclay,
France

Abstract

NEUTRON AND GAMMA EMISSION IN FISSION.

Some of the characteristics of neutron and gamma emission in fission are reviewed. Recent measurements of the average number of neutrons as a function of fragment masses m and total kinetic energy E_k show distinctive differences from previous measurements. The reasons for these discrepancies are analysed and it is shown that, at present, the use of large neutron detectors gives more reliable results than those of small neutron detectors. The energy necessary for the emission of one additional neutron is discussed and shown to be of the order of 8 MeV, in the case of the ^{252}Cf spontaneous fission. This includes the effect of the observed correlation between neutron multiplicity and total γ-ray energy. This correlation cannot be explained on the basis of neutron binding energy variations alone and is interpreted as an effect of the spins of the fragments.

The gross features of γ-ray emission by fission fragments (time, energy, angular distributions) are summarized. These features appear to be in agreement with a statistical de-excitation of the fragments provided angular momentum effects are suitably taken into account.

The variances of the excitation energies of the fission fragments as a function of m and E_k are obtained from the observation of neutron number distributions. Here again it is shown that, at present, the use of large neutron detectors is the safer technique. Knowledge of these variances allows an improved estimation of the difference between the total energy release in fission and the minimum potential energy of the scission configuration. This difference is found to be at most of the order of 7 MeV in the ^{252}Cf of spontaneous fission.

One of the basic assumptions of the "fission band" model of Nörenberg is strongly supported by the observation of a 1.6-MeV difference in the total kinetic energy of fission which gives rise to odd Z-odd Z compared with fission which yields even Z-even Z pairs of fragments. This model also accounts for many of the aspects of the neutron and gamma emission in fission.

INTRODUCTION

Rather than being a general survey of all experimental evidence on neutron and gamma emission in the fission process, this paper will focus on some of the recent detailed measurements relative to this subject. In the first section we shall examine the average neutron number measured as a function of both mass and kinetic energy of the fission fragments. Although recent measurements do not show new qualitative features, they quantitatively differ from previous ones, especially with respect to the value of the energy carried away per neutron. The disagreement may be traced to different experimental approaches; one set of experiments makes use of low-efficiency plastic scintillators and the other uses high-efficiency loaded liquid scintillators.

* Work performed under the auspices of the US Atomic Energy Commission.

** On leave from CEN Saclay.

We shall discuss the relative advantages and drawbacks of these two techniques. In the second section we shall examine some of the detailed measurements of γ-ray energy, γ-ray multiplicity and γ-ray angular anisotropy which have been carried out as a function of the energy, mass or charges of the fragments. Combining the neutron, gamma and fragments kinetic energy measurements, the measured energy release in fission can be compared with predictions of mass tables. We shall present evidence for even-odd effects in the dependence of neutron and gamma emission and fragment kinetic energies on the charges of the fragments. We conclude this section with a discussion of the angular momenta of the fragments. In the third section we shall discuss the detailed measurements of the variances of the neutron number distribution in view of the large discrepancies observed between the results obtained in experiments using low-efficiency and high-efficiency neutron detectors, respectively. We show how the variances of the neutron number can be transformed into variances of the excitation energies of the fragments. In the last section we shall discuss the significance of the even-odd effects and the possible use of the variance measurements for testing different theories of fission.

1. VARIATIONS OF THE AVERAGE NEUTRON NUMBER AS A FUNCTION OF MASS AND KINETIC ENERGY OF THE FISSION FRAGMENTS

At the time of the Salzburg Symposium most of our knowledge of the average neutron number variations as a function of mass and kinetic energy of the fragments was obtained using low-efficiency neutron detectors [1-3], with the noticeable exception of the measurement made by Whetstone [4] on the spontaneous fission of californium. In an effort to resolve the existing discrepancies between some of those experiments in the case of the neutron induced fission of ^{236}U, Maslin and co-workers [5] and Boldeman and co-workers [6] used a large gadolinium loaded scintillator as a high-efficiency neutron detector. On the other hand, we have obtained [7] the neutron number distributions in the spontaneous fission of ^{252}Cf and, thereby, their first moments; our results are to be compared to those of Whetstone [4] and Bowman and co-workers [1]. Figure 1 shows the variations of the average neutron number $\bar{\nu}(m)$ as a function of the mass of the fragments as obtained in these experiments. Although the general trends of the representative curves $\bar{\nu}(m)$ are similar in all measurements, quantitative discrepancies as high as 30% can be noticed on the figure. The situation is hardly better when one considers the variations of the average total neutron number $\bar{\nu}_T(E_k)$ as a function of total kinetic energies of the fragments, as can be seen on Fig. 2 where the results obtained by Bowman and co-workers [1], Whetstone [4], and ourselves are compared. This situation gives rise to a wide range of values of the energy carried away per neutron from the 6.6 MeV/n advocated by Bowman and co-workers [1] to the 18.5 MeV/n claimed by Maslin [5]. The origin of these discrepancies seems to be mostly in the different methods used to take into account the following factors:

(a) The assumed geometrical efficiency of the detector which depends, sometimes critically, on the assumptions made regarding the neutron energies and angular distributions.

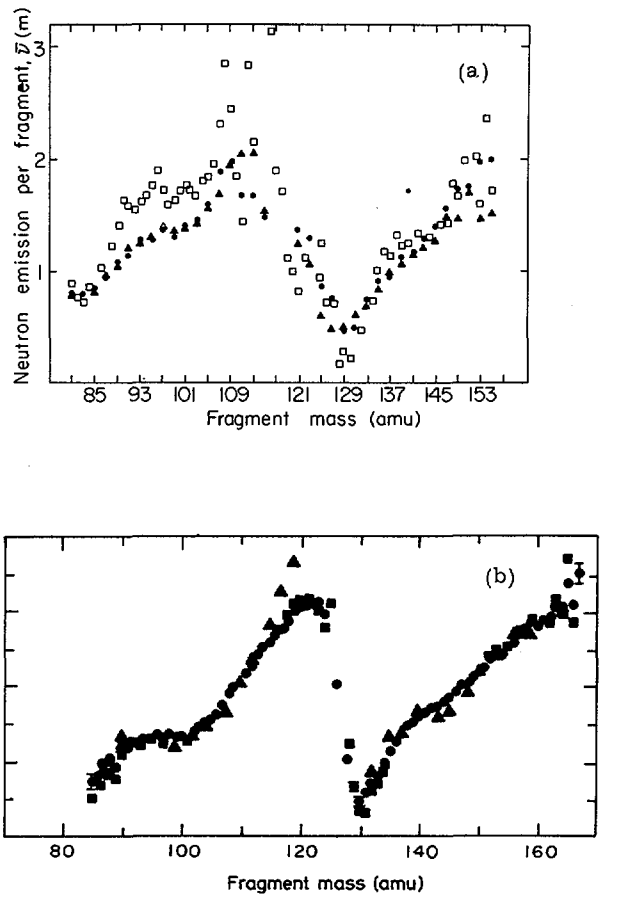

FIG. 1. Variations of the average neutron number $\bar{\nu}$(m) with the fragment mass as obtained in different experiments. (a) For the slow neutron induced fission of ^{235}U [6]. Δ: Maslin, et al.[5], ●: Boldeman, et al.[6], □: Milton and Fraser [2]. (b) For the spontaneous fission of ^{252}Cf. ▲: Bowman, et al.[1], ●: Signarbieux, et al. [7].

(b) The efficiency of detection of neutrons penetrating the detector.
(c) The energy and mass resolution and possible asymmetry of the fission fragments detection system.
(d) For the large liquid scintillator, the dead-time corrections and the possible multiple firing of the phototubes.
(e) The recoil correction which has to be used for the determination of the masses and kinetic energy of the fragments. This correction has recently been studied in detail by Gavron [8] and found to be most sensitive for small-efficiency detectors.

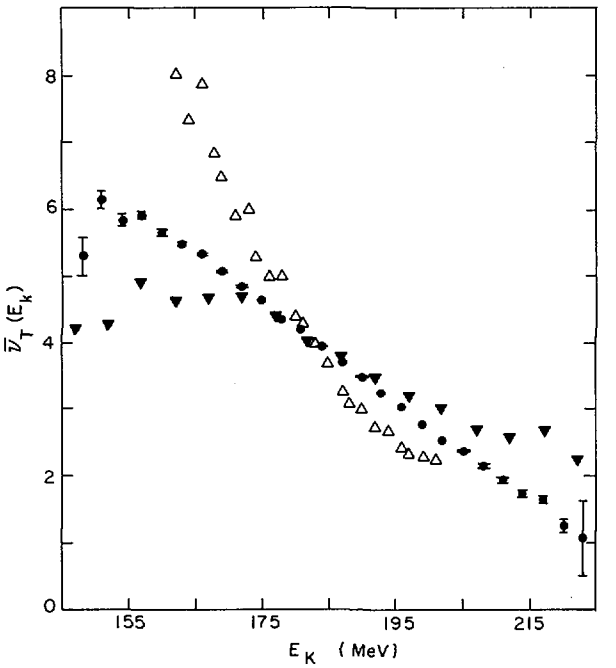

FIG.2. Variations of the total neutron number $\bar{\nu}_T(E_k)$ with fragments' total kinetic energy E_k for the ^{252}Cf spontaneous fission. Δ : Bowman, et al. [1], ▼ : Whetstone [4], ● : our results.

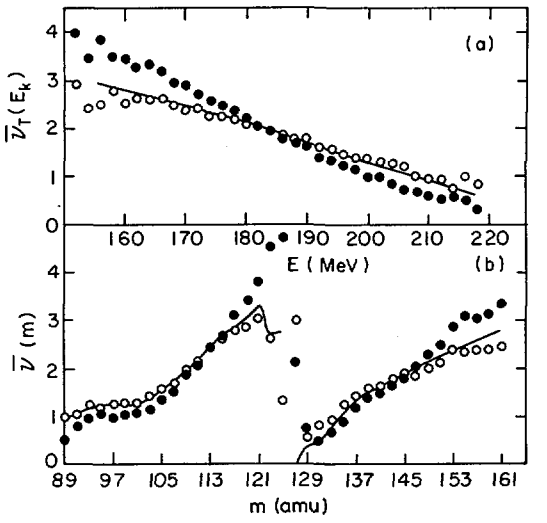

FIG.3. Effects of neutron recoil correction on the average neutron number measured with low-efficiency detectors. Effects on (a) $\bar{\nu}_T(E_k)$ results, (b) $\bar{\nu}$(m) results. ● : uncorrected results, ○ : corrected results. The continuous line denotes the input data. Figure taken from Ref.[8].

As shown by Terrell [9] the low-efficiency neutron detector experiments are much more sensitive to the first two factors. When a large liquid scintillator is used in a 4π geometry to measure total number of neutrons, the efficiency problem is obviously minimized, being reduced to the question of neutron detection efficiency. Monte-Carlo simulations have shown that, as expected, the neutron detection efficiency is itself almost insensitive to centre-of-mass energy spectra provided the radius of the detector is greater than approximately 30 cm. It therefore appears that, provided the last two factors of possible systematic errors could be satisfactorily dealt with, the total number of neutron measurements carried out with large 4π detectors should be used to check the more error-prone determinations of average number of neutrons emitted per fragment.

Gavron has recently [8] shown that the very fact that a neutron is detected in a preferential direction requires that the masses and kinetic energies of the fragments be corrected for recoil effects. This recoil correction appears to be especially important when the kinetic energy dependence of neutron numbers is studied. The magnitude of this correction is shown in Fig. 3 and appears to be able to account for most of the differences observed between the high- and low-efficiency measurements. In 4π neutron counting this correction does not exist and in the high-efficiency 2π measurements it is drastically reduced.

It is outside the scope of this paper to go into details about dead-time corrections and optimization of the large liquid scintillator operation. As pointed out by several authors [10, 11] it is possible to confirm that the dead-time and background corrections have been made properly and that the detector worked correctly. Let $\bar{\nu}$ and $\sigma^2(\nu)$ be the mean value and the variance of the neutron number distribution of the source. Let $\bar{q}$ and $\sigma^2(q)$ be the same quantities relative to the distribution obtained after correction of the experimental one for background and dead-time but before the efficiency correction. Let ϵ be the efficiency of the detector. Then

$$\bar{q} = \epsilon\bar{\nu}$$

and

$$\sigma^2(q) = \epsilon^2\,\sigma^2(\nu) + \epsilon(1 - \epsilon)\,\bar{\nu} \qquad (I.1)$$

Substituting for ϵ

$$\frac{\sigma^2(q)}{\bar{q}^2} - \frac{1}{\bar{q}} = \frac{\sigma^2(\nu)}{\bar{\nu}^2} - \frac{1}{\bar{\nu}} \qquad (I.2)$$

From the form of Eq. (I. 2) one sees that the left-hand side must then be independent of the efficiency of the neutron detector. Figure 4 shows to what extent this condition can be realized in an actual system. It is fulfilled for efficiencies lower than 80%. For higher efficiencies the influence of afterpulses in the phototubes and of multiple-firing of the discriminators

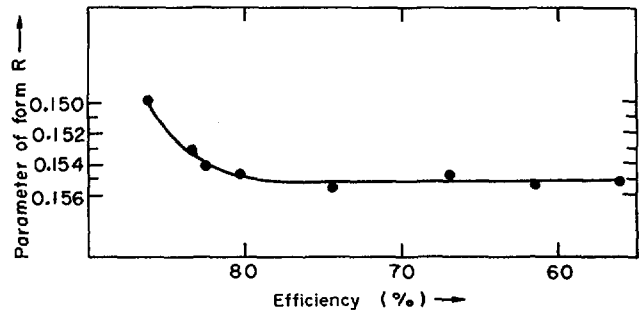

FIG.4. Variations of the "invariant" $R = \frac{\sigma^2(q)}{\bar{q}^2} - \frac{1}{\bar{q}}$ as a function of efficiency in an actual 4π neutron detection system.

starts to be felt. It is noteworthy that the observed invariance of expression (I.2) is an indication that delayed γ-rays from the fission fragments do not impair the measurements. In a more detailed check of the operational and correction procedures in the total number of neutrons measurements we found that the results obtained for the values of both the means $\bar{\nu}_T(m, E_k)$ and the variances $\sigma^2(\nu_T: m\ E_k)$ of the neutron number distribution measured as a function of the mass and total kinetic energy of the fragments agreed within statistical accuracy for two experiments where the detector efficiency was 80% and 55%, respectively. Finally, an independent check of the validity of the measurements of total number of neutrons with 4π high-efficiency liquid scintillators is provided by the agreement between those measurements and those recently [12] carried out with ^{3}He counters placed in a paraffin moderator. This rather lengthy justification of the use of large neutron detectors for measurements of total number of neutrons was felt useful in view of recent doubts [13] which have been raised in their behalf. In particular, it has been argued that these experiments gave unreasonably high values of the energy necessary to emit one additional neutron. The variation of the average total number of neutrons emitted by both fragments as a function of their total kinetic energy is very nearly linear. The inverse of the slope of this variation $\langle d\nu_T/dE_k \rangle^{-1}$ has been found to be 16.7 MeV/n by Boldeman and co-workers [6] in the thermal neutron induced fission of ^{236}U and, by us, to be 13.0 MeV/n in the case of the spontaneous fission of ^{252}Cf. However, these quantities should not be interpreted as the energy necessary for a given pair of fragments to emit one more neutron. This is mostly because different mass distributions are obtained for different total kinetic energies. The argument can be put on a more quantitative basis with the help of relations similar to those already used by Terrell [9]. First, the slope $\langle d\nu_T/dE_k \rangle$ can be expressed as a function of the variance $\sigma^2(E_k)$ of the total kinetic energy and of the co-variance of ν_T and E_k

$$\left\langle \frac{d\nu_T}{dE_k} \right\rangle = \frac{C(\nu_T, E_k)}{\sigma^2(E_k)} \qquad (I.3)$$

Then, up to first order in the variations of E_k and ν_T as a function of fragments masses, the overall co-variance $C(\nu_T, E_k)$ can be expressed as a function of the mass-averaged value of the conditional co-variances $C(\nu_T, E_k: m)$ of ν_T and E_k for a fixed mass by

$$C(\nu_T,E_k) = < \frac{d\nu_T}{dm} > < \frac{dE_k}{dm} > \sigma^2(m) + \overline{C(\nu_T,E_k: m)} \qquad (I.4)$$

Owing to the small variation of ν_T as a function of m, the first term of the right-hand side of equation (I.4) can be neglected so that

$$C(\nu_T,E_k) = \overline{C(\nu_T,E_k: m)} \qquad (I.5)$$

A relation similar to Eq. (I.3) holds between quantities measured at a fixed mass ratio of the two fragments, so that

$$C(\nu_T,E_k: m) = \left\langle \frac{d\nu_T}{dE_k} \right\rangle_m \sigma^2(E_k: m) \qquad (I.6)$$

Assuming a negligible correlation between the values of $\langle d\nu_T/dE_k \rangle_m$ and $\sigma^2(E_k: m)$ for different mass values, one can then write that

$$\left\langle \frac{d\nu_T}{dE_k} \right\rangle_m^{-1} = \left\langle \frac{d\nu_T}{dE_k} \right\rangle^{-1} \frac{\overline{\sigma^2(E_k: m)}}{\sigma^2(E_k)} \qquad (I.7)$$

In the case of ^{252}Cf using resolution-corrected values of $\sigma(E_k: m) = 9.2$ MeV and $\sigma(E_k) = 11.33$ MeV one obtains an approximate value of

$$\left\langle \frac{d\nu_T}{dE_k} \right\rangle_m^{-1} = 8.6 \text{ MeV/neutron}$$

This figure can be considered to be a determination of the energy necessary to emit one additional neutron and can be compared with estimates based on neutron binding energies, kinetic energies and, as will be seen later, on gamma-neutron competition. We shall make this comparison in the next section using the more detailed values of $\langle d\nu_T/dE_k \rangle_m^{-1}$ computed for each mass of the heavy fragment. Figure 5 shows the result of this comparison.

Compared with measurements of the total number of neutrons, the study of neutron emission by each individual fragment presents the added difficulty

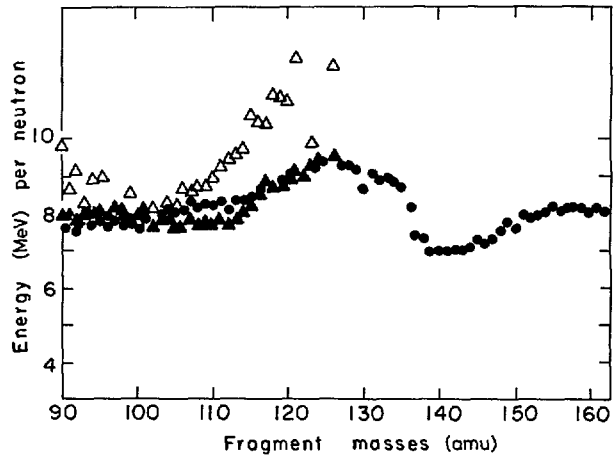

FIG. 5. Experimental and calculated energies carried away per neutron. The experimental values were obtained from $\left\langle \frac{d\nu}{dE_k} \right\rangle^{-1}$. The calculated values were obtained from $\bar{B}+\bar{\eta}+0.75$, where $\bar{B}$ = mean binding energy of the neutron, $\bar{\eta}$ = centre-of-mass neutron kinetic energy. ● : calculated values for each fragment mass, ▲ : calculated values for a fragment pair, △ : experimental values for a fragment pair.

of detector efficiency variations with the angular and energy distributions of the neutrons. We shall assume that the fission events are sorted out according to the mass m of the fragment flying towards the neutron detector and the total kinetic energy E_k of the two complementary fragments. The average number of detected neutrons for a given fission configuration is then equal to

$$\bar{q}(m,E_k) = \epsilon(m,E_k)\,\bar{\nu}(m,E_k) + r(M-m,E_k)\,\bar{\nu}(M-m,E_k) \qquad (I.8)$$

where $\bar{\nu}(m,E_k)$ and $\bar{\nu}(M-m,E_k)$ are the average number of neutrons emitted by the fragments moving towards and away from the neutron detector, respectively. $\epsilon(m,E_k)$ and $r(M-m,E_k)$ are the probabilities of detection of these neutrons. A similar relation holds when the fragment of mass M - m moves towards the detector, namely

$$\bar{q}(M-m,E_k) = \epsilon(M-m,E_k)\,\bar{\nu}(M-m,E_k) + r(m,E_k)\,\bar{\nu}(m,E_k) \qquad (I.9)$$

Provided the set of forward and backward efficiencies $\epsilon(m,E_k)$ and $r(m,E_k)$ are known, the average number of neutrons emitted per individual fragment $\bar{\nu}(m,E_k)$ can be obtained. The sets of efficiencies can be computed by means of a Monte-Carlo simulation [14]. They depend on the fragment velocity and the centre-of-mass neutron energy spectrum. We have already

noticed that, in the case of large neutron detectors, the forward efficiencies were not sensitive to the assumption made for the centre-of-mass neutron energy distribution. However, in this case, the ratio of the backward to the forward efficiencies can be as high as 20% and the quantities $r(m, E_k)$ cannot, by any means, be neglected.

The values of the average neutron number per fragment, $\bar{\nu}(m, E_k)$, were found to vary by less than 2% over their entire range when two different assumptions were made on the neutron spectra: in one case we assumed a constant-temperature Maxwellian spectrum, and in the other we used the actual spectra as determined by Bowman and co-workers [1]. The sum $\bar{\nu}(m, E_k) + \bar{\nu}(M - m, E_k)$ of the average neutron number emitted by two complementary fragments should be equal to the average total neutron number $\bar{\nu}_T(m, E_k)$ as determined in the 4π geometry experiments. This agreement was obtained by Whetstone [4], and by Maslin and co-workers [5]. In our experiment the agreement is better than 2% for the entire range of masses and kinetic energies. This seems to be a good check of the efficiency correction procedure.

Up to now we have not considered the possible existence of an isotropic component in the neutron angular distribution. This component was first suggested by Skarsväg and co-workers [15], Fraser and co-workers [2], and Kapoor and co-workers [16]. It is shown in Appendix I that, in the case of a large detector subtending a 90° angle from the neutron source and assuming a constant detection efficiency for all neutrons entering the detector,

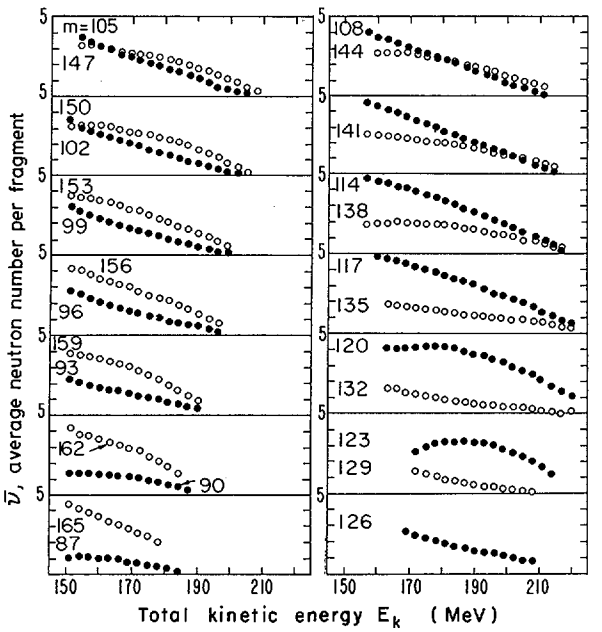

FIG.6. Variations of the average number of neutrons emitted per fragment as a function of the total kinetic energy of the fragments for a range of fragments masses. ● : light fragment, ○ : heavy fragment.

the neglect of the isotropic component is equivalent to the sharing of it equally between the two fragments. However, with a small neutron detector, the sharing will depend on the fragment and neutron velocities. This could give rise to differences of up to 5% between the results of the large and small detectors.

The variations of the average number of neutrons emitted by complementary fragments of selected masses as a function of their total kinetic energy E_k are shown in Fig. 6. It can be seen that, while the variations of the total number of neutrons with E_k are very nearly linear, this is not so for the number of neutrons emitted by one of the fragments. Therefore, for a given mass split, the fraction of excitation energy taken up by one of the fragments cannot be assumed constant.

2. γ-RAY EMISSION AND ENERGY BALANCE IN FISSION

The emission of γ-rays by fission fragments is not as well known as their neutron emission. This is the consequence of several experimental difficulties:

(a) The need to discriminate between fission γ-rays and γ-rays produced following neutron capture or inelastic scattering.
(b) The time distribution of fission γ-rays, which covers a wide range, from less than 10^{-11} s to several microseconds. This circumstance makes the comparison between experiments using different arrangements difficult.
(c) The moderate amount of anisotropy in the angular distribution of the fission γ-rays, which makes it much more difficult to measure the relative contribution of each fragment to the γ-emission than to the neutron emission. The first difficulty is usually overcome by the conjunction of a time discrimination between the γ-rays originating from the fission fragments and those produced in neutron capture or inelastic reactions, and by a careful collimation of the γ-ray beam. For total γ-ray energy measurements, large liquid scintillators of the type described in Section 1 can also be used with the advantage of a very high efficiency; in this case a satisfactory correction for neutron parasitic effects can be made, provided a simultaneous measurement of neutron multiplicity is made [17].

To deal with the two last difficulties a knowledge of both distribution in time and angular distribution of the fission γ-rays is needed. In the following we first summarize this knowledge.

2.1. Angular distribution of fission γ-rays

There are two causes of anisotropy in the fission γ-ray angular distribution. The first one is a Doppler effect similar to what is observed in the neutron case. This Doppler anisotropy obviously disappears when the two fragments are not distinguished by the experimental setup or when they are stopped before the γ-emission takes place. On the other hand, it can be used to determine the share taken by each of the two complementary fragments [18, 19]

in the total γ-ray emission and to obtain information on the time dependence of that emission [20].

The other cause of anisotropy of the fission γ-rays is a consequence of a preferential orientation of the fragments' spins with respect to their direction of flight. Wilhelmy and co-workers [21] have measured the angular distribution of several $2^+ \rightarrow 0^+$ transitions in the ground state bands of several even-even fission isotopes. They found a preferential emission of the E2 radiations along the direction of the fragment with anisotropies ranging between 8.3% and 33.4%. Because of possible attenuation effects in the platinum catcher they used, these values are to be considered as lower limits for the actual anisotropies. These anisotropies can only be explained if the initial spins of the fragments are preferentially oriented perpendicular to the fragments' paths, in agreement with the results of the early analysis of the gross angular distribution of fission γ-rays by Hoffman [22]. In more recent experiments the anisotropy of the whole fission γ-ray spectrum has been studied as a function of fragment kinetic energies, mass ratios, masses and as a function of γ-ray energy. These experiments all dealt with the slow neutron induced fission of ^{235}U. Figure 7 shows the results obtained by Ivanov and co-workers [23] in their study of fission γ-anisotropy as a function of total kinetic energy and mass ratio of the fragments. The figure shows a definite increase of anisotropy with the total kinetic energy of the fragments for all mass ratios studied. On the other hand, the anisotropy seems insensitive to the mass ratio of the two fragments. This last result has been confirmed by Armbruster and co-workers [20]. Using the collimator technique pioneered by Johansson [24] these authors have been able to study the anisotropy of the γ-rays emitted between 10 and 100 ps after

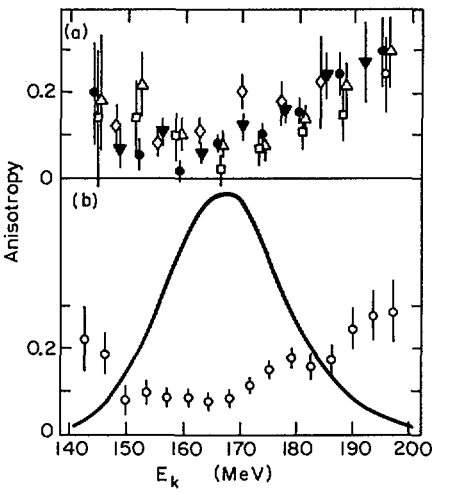

FIG. 7. Anisotropy of the γ-ray yield versus fragment kinetic energy in the fission of ^{235}U (a) for different fragment mass ratios. □ : $(m_1/m_2) = 1.1 - 1.25$, △ : $(m_1/m_2) = 1.25 - 1.35$, ● : $(m_1/m_2) = 1.35 - 1.45$, ▼ : $(m_1/m_2) = 1.45 - 1.65$, ◇ : $(m_1/m_2) = 1.65 - 1.9$. (b) for all realized mass ratios; the solid curve shows the fragment kinetic energy distribution. Figure taken from Ref.[23].

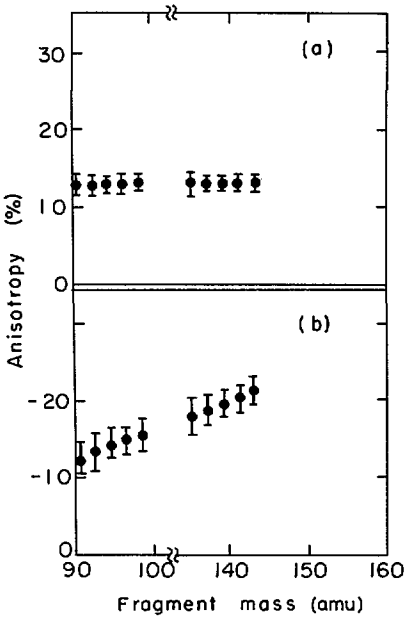

FIG. 8. Anisotropy of the prompt gammas as a function of fragment mass. (a) anisotropy without collimator: the contributions of the two fragments are not separated; (b) anisotropy with collimator selecting gammas in the time region 10-100 ps after fission. Figure taken from Ref. [20].

fission as a function of the fragment's mass. Their results are shown in Fig. 8; they show some structure but no definite trend except for a tendency to higher anisotropies in the heavy fragment mass range, which averages around 20% as compared to 14% for the light fragment. When measured as a function of γ-ray energy between 0.1 and 1.2 MeV, the anisotropies [20] do not show strong departure from an average value of 13%. This is only slightly less than the values obtained by Wilhelmy and co-workers [21] for pure E2 transitions. It therefore appears that measured anisotropies of fission γ-rays indicate that those γ-rays are mostly of the E2 type with a possible admixture of between 10% and 20% of dipole radiation. This conclusion holds for γ-energies between 0.1 and 1.2 MeV as quoted above. As a concluding remark concerning the question of anisotropy of γ-ray emission by the fission fragments it is worthwhile noting that neglecting this effect in some of the measurements of γ-ray energy emitted in fission could lead to errors of about 5%; this holds not only for absolute values but also for relative ones, especially when the fragment's kinetic energy is retained as a parameter in the measurement.

2.2. Time dependence of γ-ray emission by the fission fragments

The gross time dependence of γ-emission by the fission fragments of ^{235}U has been most thoroughly investigated by Albinsson [25]. Using the collimator technique that author studied the rate of production of fission

γ-rays between 10 and 200 ps. He found that the corresponding decay curve could be well represented by the sum of three exponentials corresponding to half-lives of 7.5 ps, 18 ps, and 60 ps with intensities, relative to the total gamma radiation emitted within 1 ns after fission, of 35%, 25%, and 10%, respectively. Armbruster and co-workers [20], by a comparison of observed γ-ray anisotropy when both fragments were allowed to fly and when one of them was stopped in the fission source backing, concluded that in the latter case the average velocity of the stopped fragment had to be reduced to 27% of its original value to account for the observed residual Doppler anisotropy. They show that, assuming a single time constant T for the decay curve of the γ-emission, the reduction factor f is equal to

$$f = \frac{t_c}{T + t_c}$$

where t_c is the characteristic slowing-down time in the source backing. In their experiment Armbruster and co-workers [20] estimated this slowing-down time to be approximately 1.7 ps. One then finds that if the fastest time components were those reported by Albinsson the reduction factor would amount to approximately 4%. To explain the observed reduction factor one is then led to assume the existence of a fast component with minimal relative intensity of 23% corresponding to an infinitely short half-life. This component is most probably responsible for the attenuation of the γ-ray anisotropy for measurements carried out between 0 to 1 ns after fission with respect to those relative to the 10 ps-100 ps range. It is thus probably of the dipole type. Albinsson [26] has measured the gross features of the γ-ray energy spectra corresponding to the three decay constants reported earlier. The bulk of the γ-rays corresponding to the 7.5-ps half-life has an energy centered around 1 MeV. At this energy both the single particle lifetime estimates for E1 and M1 transitions and the collective estimates for E2 transitions are much shorter than 7.5 ps. On the other hand, this value lies very close to the single particle estimate for E2 transitions. The same can be said about the energy spectra associated with the 18-ps time component. The 60-ps component displays a strong peak around 200 keV which very probably corresponds to E2 rotational transitions similar to those reported in the work of Cheifetz and co-workers [27] in the californium fission case.

From the preceding and the average multiplicity of about four γ-rays per fragment, a qualitative picture can be drawn of the average cascade of γ-rays emitted by the fragments. A first transition, mostly of the electric dipole type with an average energy greater than 1 MeV, is followed by two E2 transitions of a non-collective types; the cascade then terminates with an average of about one transition in the ground state rotational band, when this band exists.

In some cases, after what can be considered as the prompt γ-emission, delayed γ-rays can be emitted. John and co-workers [28] estimated that approximately 20% of the total γ-ray number or 7% of the total γ-ray energy was emitted between approximately 100 ns and 2000 ns after fission of ^{252}Cf.

The picture for γ-ray emission by fission fragments presented above is certainly oversimplified; it should be modified, in particular, according to the measured photon-multiplicities and total γ-ray energies, which are now reviewed.

TABLE I. TOTAL AND AVERAGE γ-ENERGY

Type of fission	E_γ(total) (MeV)	Average energy per photon (MeV)	γ-multiplicity	$\bar{\nu}_T$
$^{235}U + n$	6.51	0.97	6.69	2.42
$^{239}Pu + n$	6.82	0.94	7.25	2.83
^{252}Cf Spontaneous L.R.A.	5.99	0.88	6.7	3.052
^{252}Cf Binary spontaneous	6.84	0.88	7.75	3.756

TABLE II. AVERAGE γ-MULTIPLICITIES AND TOTAL γ-ENERGIES AS A FUNCTION OF TIME AFTER THE SLOW NEUTRON INDUCED FISSION OF ^{235}U

γ-energy (MeV)	Time interval (ns)	$\bar{N}_{\gamma T}$ (γ/fission)	$\bar{E}_{\gamma T}$ (MeV/fission)
0.09-10	~ 5	6.51	6.43 ± 0.3
0.03-10.4	~ 70	8.1	7.0 ± 0.7
0.03-10.4	275	8.6	7.4 ± 0.7

2.3. Multiplicities and energies of the fission γ-rays

A very careful measurement of total γ-energy and average photon energy in the fission of ^{252}Cf, ^{240}Pu, and ^{236}U was reported at the Vienna Symposium by Verbinsky and co-workers [29]. Their results are shown in Table I, together with the average neutron numbers. The values relative to the long-range particle accompanied (L. R. A.) fission in Table I are taken from the work of Mehta and co-workers [30] except for the average energy per fission which has been assumed equal in binary and ternary fission. The measurements of Verbinsky and co-workers [29] refer to a period extending up to approximately 10 ns after fission and a γ-energy range from 0.14 to 10 MeV. Pleasonton and co-workers [19] report measurements of total γ-ray energies and multiplicities in time ranges of 5 ns, 70 ns, and 275 ns after the slow induced fission of ^{235}U. Their values are shown in Table II and are in very good agreement with the ^{235}U figures of Verbinsky. From Table II it can be seen that the delayed-γ contribution in the case of the induced fission of ^{235}U would account for approximately 24% of the total number of γ-rays and 14% of the total γ-ray energy. The last figure is more than twice the corresponding one reported by John and co-workers [28] for the spontaneous fission of californium 252. In summary, we find that the total γ-ray energy emitted

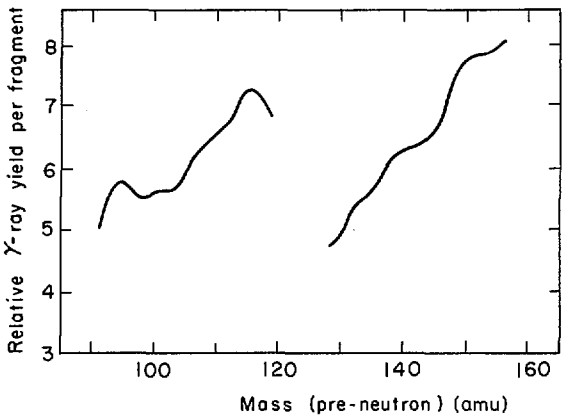

FIG. 9. γ-ray yield per fragment versus fragment mass in the ^{252}Cf spontaneous fission. Figure taken from Ref.[24].

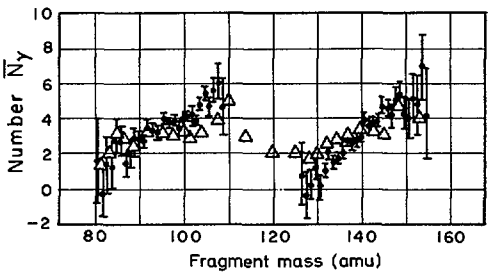

FIG. 10. γ-ray yield per fragment versus fragment mass in the slow neutron induced fission of ^{235}U. ● : data taken from Ref.[19], △ : data taken from Ref.[32].

in fission lies around 7.5 MeV with an absolute uncertainty of about 0.5 MeV for most of the known cases. This value of 7.5 MeV can be compared with that obtained in statistical computations such as the recent one by Nardi and co-workers [31] of approximately 6 MeV in the ^{252}Cf spontaneous fission case. Although the difference between the expected value and the observed one is much less than some years ago it is still significant. Table I shows that positive correlation exists between the γ-ray multiplicities and the total number of neutrons per fission.

Such a correlation had been observed by Johansson [24] when he first determined the γ-multiplicity as a function of the mass of the emitting fission fragments of ^{252}Cf. John and co-workers [28] added a delayed component to Johansson's results and obtained the curve shown in Fig. 9. Similar data have been obtained in the slow neutron induced fission case by Albinsson and co-workers [32] using the same collimator technique as Johansson and by Pleasonton and co-workers [19] using the Doppler anisotropy technique. The results obtained by both groups are shown on Fig. 10. Although the two

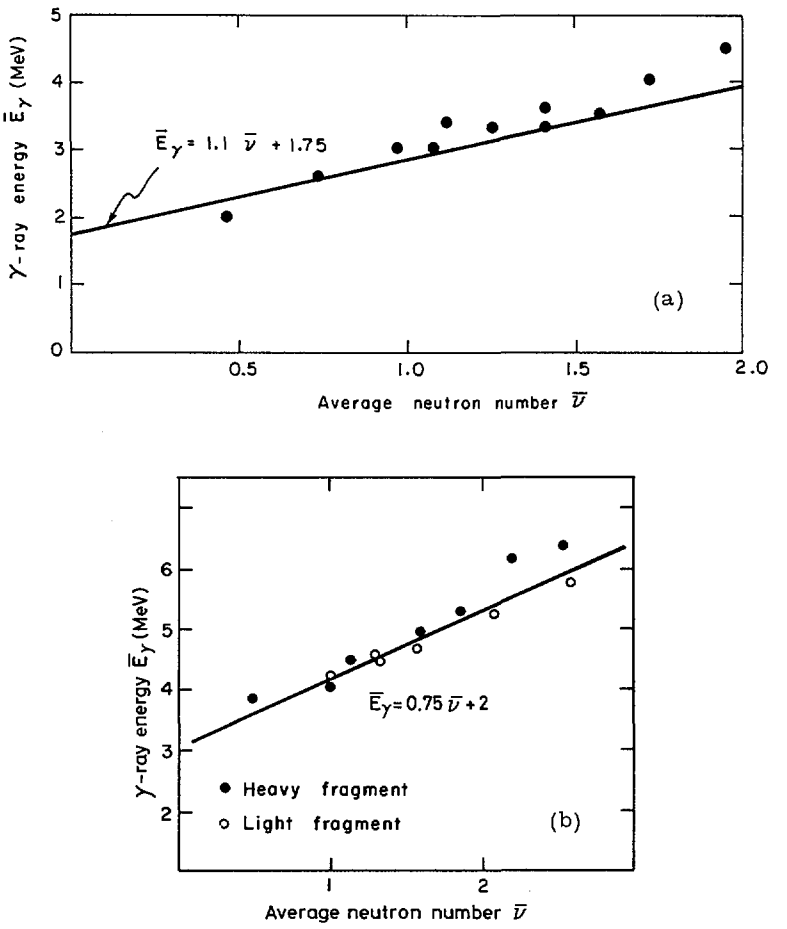

FIG. 11. Observed correlation between the values of gamma ($\bar{E}_\gamma$(m)) and neutron ($\bar{\nu}$(m)) multiplicities (a) for induced fission of ^{236}U, (b) for spontaneous fission of ^{252}Cf.

experiments agree qualitatively and both show a pronounced sawtooth structure, the rates of variation of the γ-multiplicities as a function of fragment mass are different. This difference cannot be attributed in its entirety to the different time range after fission studied in the two experiments, since, if it were so, the values obtained by Pleasonton should always be greater than those obtained by Albinsson. The correlation between γ-ray and neutron emission is best visualized by plotting the points corresponding to the various pairs of values of $(\bar{E}_\gamma(m), \bar{\nu}(m))$ on the $(\bar{E}_\gamma, \bar{\nu})$ plane. This is done in Fig. 11 for both the californium and ^{236}U cases. In preparing Fig. 11 we have transformed the γ-multiplicities reported by Albinsson for ^{236}U and by John for ^{252}Cf into total γ-ray energies.

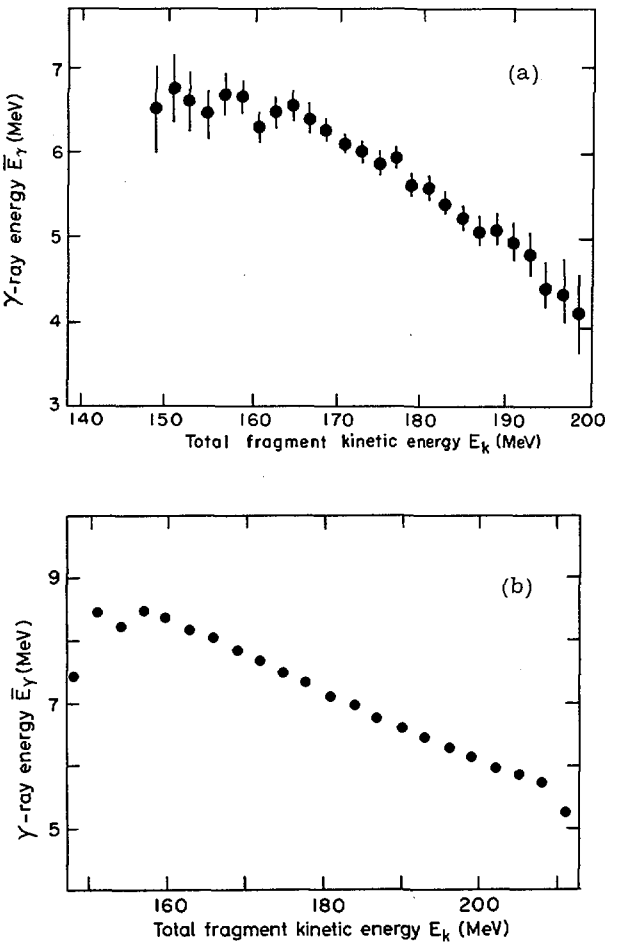

FIG. 12. Variations of total γ-energy $\bar{E}_\gamma(E_k)$ as a function of total fragment kinetic energy (a) in the induced fission of ^{236}U, (b) in the spontaneous fission of ^{252}Cf.

The variations of total γ-energy or yields as a function of the total kinetic energy of the fragments have been measured by Albinsson [33], Pleasonton and co-workers [19], and Val'skii and co-workers [34] in the slow neutron induced fission of ^{235}U. Good agreement is observed between the results obtained by the three groups. We show in Fig. 12 the results obtained by Albinsson. Using a large liquid scintillator as a 4π γ-ray detector [35] we obtained the variations of total γ-ray energy as a function of total fragment kinetic energy for the spontaneous fission of ^{252}Cf. These variations are also shown on Fig. 12. The correlation between the total γ-ray energy and the average total number of neutrons measured as a function of total fragment kinetic energy can be examined as done before for the fragment's mass. This is done in Fig. 13. This figure and Fig. 12

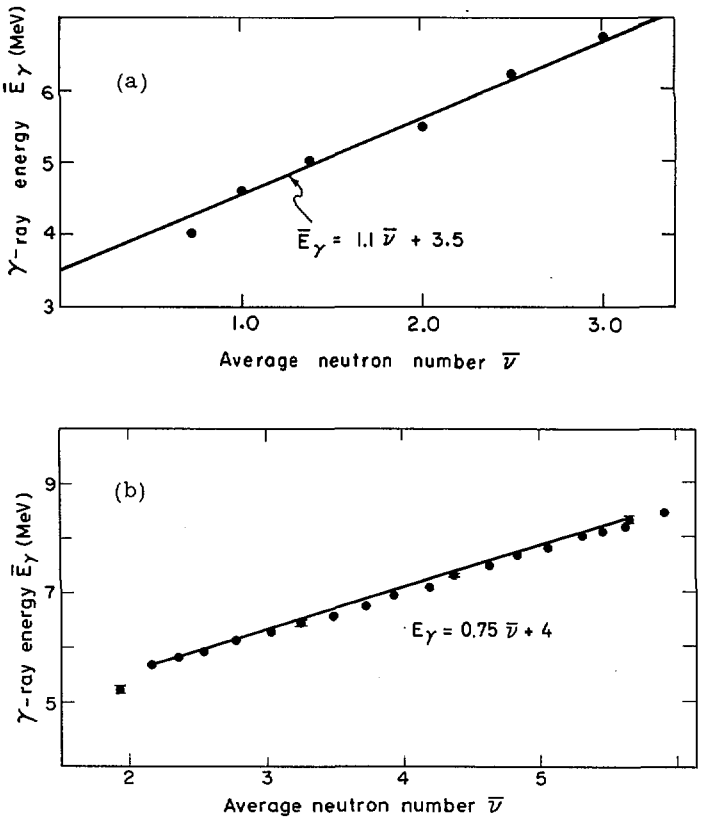

FIG. 13. Correlation between the total γ-ray energy $\bar{E}_\gamma(E_k)$ and the neutron multiplicity $\bar{\nu}(E_k)$ (a) in the induced fission of ^{236}U, (b) in the spontaneous fission of ^{252}Cf. It should be noted that the constant term in the relation $\bar{E}_\gamma = a\bar{\nu} + b$, obtained when the correlation with average total number of neutrons is considered, has twice the value of that obtained with average number of neutrons per fragment.

strongly suggest that a linear relation exists between the total γ-ray energy and the number of neutrons emitted in fission. The straight lines appearing in Figs 11 and 13 correspond in the ^{252}Cf case to the assumption that

$$\bar{E}_\gamma(m,E_k) = [0.75\ \bar{\nu}(m,E_k) + 2]\,(\mathrm{MeV}) \qquad \text{(II. 1)}$$

and

$$\bar{E}_\gamma(m,E_k) = [1.1\ \bar{\nu}(m,E_k) + 1.75]\,(\mathrm{MeV}) \qquad \text{(II. 2)}$$

in the ^{236}U case. The extent to which such relations are accurate can be estimated from more detailed measurements where the γ-ray energies or multiplicities are studied as a function of both the masses and the kinetic

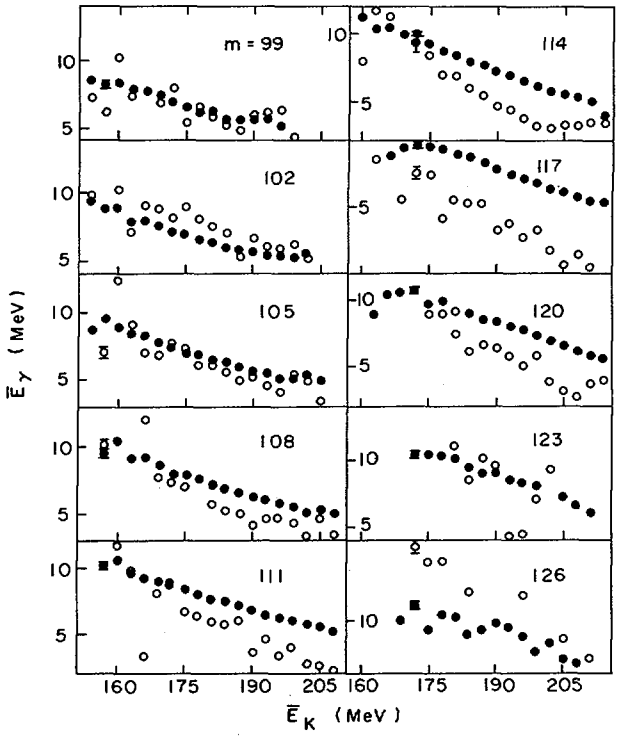

FIG.14. Variations of the total γ-ray energy as a function of the total kinetic energy of the fragments for different light fragment masses of ^{252}Cf fission. ● : direct measurement, ○ : results obtained from energy balance considerations.

energies of the fragments. Using the large liquid scintillator we have measured [35] the total γ-energy emitted in fission as a function of total kinetic energy and mass ratio of the fragments. The results are shown in Fig. 14 where the variations of total γ-energy as a function of the fragment's total kinetic energy are displayed for a choice of mass ratios (M = mass of the light fragment). It can be seen from the figure that the variations are very nearly linear. In Fig. 15 we show the variations of the average total γ-energy and of the slopes $\langle dE_\gamma/dE_k \rangle$ of the above-mentioned linear variations as a function of mass ratio (or mass of the light fragment). It can be seen that the variations of those quantities are less than 10% except at symmetry. Since the variations in the slopes $\langle d\nu_T/dE_k \rangle$ as a function of fragment mass as shown in Fig. 5 are themselves less than 10%, it follows that Eq. (II. 1) could be accurate within 20% for the whole mass and kinetic energy range. However, this conclusion might be an oversimplification and the results obtained by Pleasonton and co-workers [19] seem to indicate that this is the case. Figure 16 taken from the work of these authors shows the variations of the γ-energy emitted by one fragment as a function of the

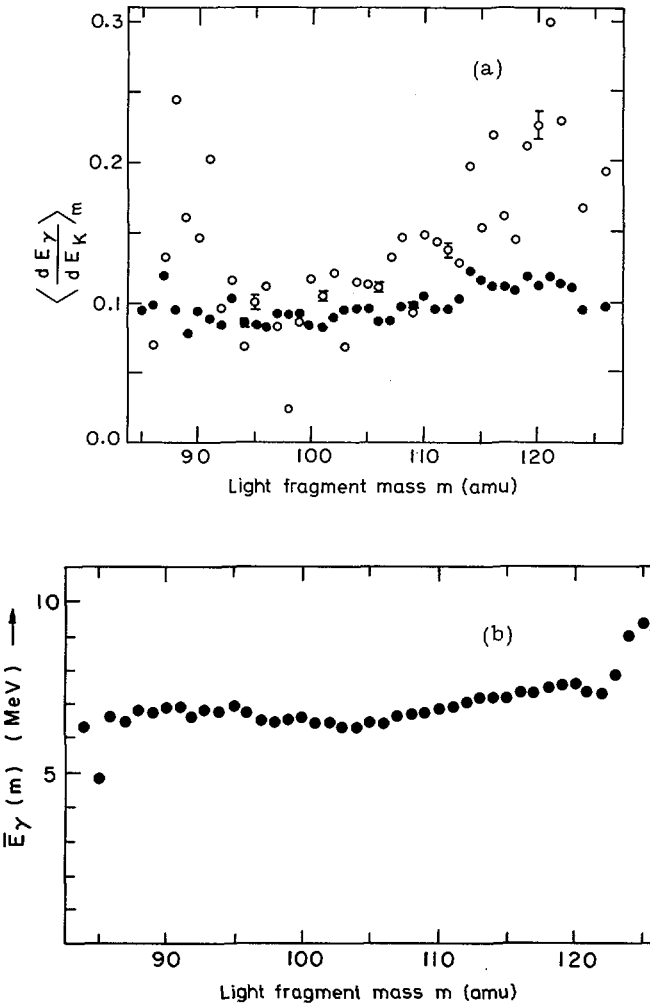

FIG. 15. (a) Slopes $\left\langle \frac{dE_\gamma}{dE_k} \right\rangle_m$ of the variations of the total γ-ray energy versus the total kinetic energy of the fragments as a function of m, the light fragment mass (^{252}Cf). • : direct measurement, O : results obtained from energy balance considerations. (b) Total γ-ray energy as a function of the light fragment mass (^{252}Cf).

total kinetic energy for various masses of the fragment. It can be seen on the figure that for some heavy fragments the emitted γ-energy tends to increase with kinetic energy and is, thereby, anticorrelated with the number of neutrons emitted by this fragment. This tendency sometimes leads to values of γ-ray energy emitted by one fragment well under half the neutron binding energy for fission events where the fragment emits about two neutrons. Such behaviour is very difficult to understand.

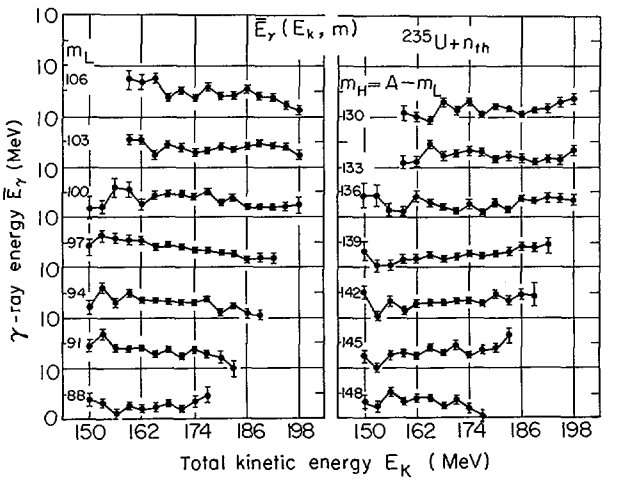

FIG. 16. Slice plots at constant mass m in the 3 MeV × 3 amu array $\bar{E}_\gamma(E_k, m)$. Figure taken from Ref. [19].

2.4. Energy balance in fission

The observed variations of total γ-ray energy as a function of the total kinetic energy of the fragment have a bearing on the computation of energy balance in fission. For example, from Eq. (II. 1) one sees that the energy necessary to emit one supplementary neutron will be approximately 0.75 MeV higher than the sum of the neutron binding and centre-of-mass kinetic energies. A comparison between the computed and observed energies carried away per neutron is made on Fig. 5. The agreement is fair and the energy carried away per neutron ranges around 8.5 MeV. It is seen, however, that the experimental value lies consistently higher than the computed one especially for light fragment masses higher than 105. This will be explained in the following section in terms of a tailing of the kinetic energy resolution function which has not been accounted for. The detailed measurements of average neutron numbers $\bar{\nu}(m, E_k)$, of total γ-ray energies $E_\gamma(m, E_k)$ and of the centre-of-mass neutron kinetic energies $\bar{\eta}(m, E_k)$ as a function of mass and kinetic energies of the fragments allow equally detailed computations of the total energy $Q(m, E_k)$ released in fission:

$$Q(m,E_k) = E_k + \bar{\nu}_1(m,E_k)[\bar{B}(m,E_k) + \bar{\eta}(m,E_k)]$$

$$+ \bar{\nu}_1(M - m,E_k)[\bar{B}(M - m,E_k) + \bar{\eta}(M - m,E_k)] + \bar{E}_\gamma(m,E_k)$$

where $\bar{\nu}_1(m, E_k)$ is the average number of neutrons emitted by a fragment of mass m, $\bar{\eta}(m, E_k)$ is the average centre-of-mass kinetic energy of these

neutrons, $\bar{B}(m, E_k)$ is the mean binding energy of these neutrons as obtained from a suitable averaging of tabulated values, $\bar{E}_\gamma(m, E_k)$ is the total γ-ray energy emitted by the two complementary fragments, m is the mass of one of the fragments, M-m the mass of the complementary one.

The values of $Q(m, E_k)$ should be independent of the total kinetic energy E. The extent to which this condition is fulfilled provides a very useful check of the coherency of the experimental data. This check can be made in the case of the spontaneous fission of ^{252}Cf with the help of Fig. 14. On this figure both the γ-ray energies obtained from direct measurement and those obtained with the assumption of energy balance are displayed for several masses. The condition that total energy release be independent of E_k is equivalent to the requirement that the variations of the above quantities be parallel. This appears to be the case, for most masses, within statistical accuracy. However, although the two quantities plotted on Fig. 14 display parallel variations, their absolute values differ. The experimental values [35] are 1 to 2 MeV higher than the ones computed from the mass tables of Garvey and co-workers [36]. Recent evidence [37] seems to indicate that fragment total kinetic energies could indeed be overestimated by such an amount.

2.5. Even-odd effects on fission energetics

The energy release in fission can be expressed from the masses of the fissile species and of the fragments. For example, in the case of the spontaneous fission of ^{252}Cf

$$Q(N,Z) = M(154,98) - M(N,Z) - M(154-N,98-Z)$$

expresses the total energy release for a fission giving rise to a fragment with Z protons and N neutrons. When the fissile nucleus has an even charge the fragments have both either an odd or an even charge. Because of the pairing energy of the protons it then follows that a fission giving rise to two even-charge fragments will be, on the average, 2.5 MeV more energetic than a fission giving rise to two odd-charge fragments. Studies of the variations of average total kinetic energies as well as neutron and gamma emission as a function of the fragment charges can therefore provide information on the partition of this even-odd energy difference; such information cannot be obtained from mass measurements. We have measured the average total γ-ray energy, total neutron number emitted in the fission of ^{252}Cf as well as the fragment total kinetic energy as a function of the charges of the fragments. Since no detailed report of this work has been made earlier, we now briefly describe the experimental technique involved as well as some aspects of the data analysis.

In the neutron multiplicity and total γ-ray energy measurements, a californium fission source was placed near a silicon/lithium drifted X-ray detector at the centre of a cylindrical hole through the centre of a large spherical gadolinium-loaded liquid scintillator. For each detected fission event the pulse height of the coincident pulse produced in the scintillator was analysed as well as the pulse height delivered by the X-ray detector; the number of neutrons detected by the scintillator was counted between

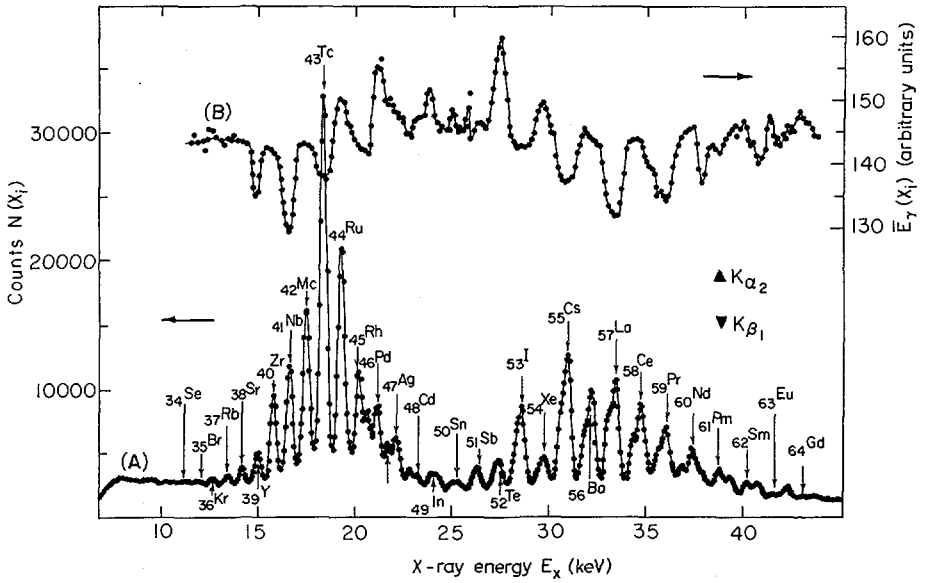

FIG. 17. (A) : Fission X-ray spectrum $N(X_i)$, (B) average value of the γ pulse height as a function of X-ray detector pulse height $\bar{E}_\gamma(X_i)$ (^{252}Cf fission).

1 μs and 36 μs after fission. The three quantities were then stored on an event-by-event basis on a magnetic tape. The fission events were detected either by the requirement of a coincidence between an auxiliary fragment detector and the X-ray detector or by the requirement of a coincidence between the X-ray detector and the liquid scintillator. In the latter case it was also required that at least one neutron be counted in the 35-μs gate. We have been able to show that the two techniques for detecting fission events were equivalent. In the latter case, both fragments could be stopped in the source and the Doppler broadening of the X-rays emitted by the fragments was thereby minimized. In that case the resolution of the X-ray detector was 350 eV at 35 keV.

The fission fragment X-ray spectrum obtained in this experiment is shown in Fig. 17.

The kinetic energy determination made use of data obtained by Cheifetz and co-workers [27] in the course of their study of γ-rays emitted by fission fragments. In one of their experimental setups the ^{252}Cf source was deposited on a solid state detector, which detected one of the fragments. The other fragment was detected in another solid state counter. Both fragment detectors were operated in coincidence with an X-ray detector positioned behind the source. The pulse heights delivered simultaneously by the three detectors were stored on event-by-event basis on a magnetic tape. When the data were processed, only events where the X-ray had been emitted by the stopped fragments were considered. From the two pulse heights provided by the fragment detectors, the total kinetic energy of the

fission event was obtained using the calibration scheme first proposed by Schmitt [38]. In this experiment the resolution of the X-ray detector was approximately equal to 1 keV.

The data from the two experiments were processed in a similar way. The number of counts corresponding to each X-ray amplitude bin was determined, as well as the corresponding average values of the interesting quantities (γ-ray energy, neutron multiplicity and total kinetic energy). Thus, if X_i is a particular X-ray bin, we obtained

$$N(X_i), \quad \overline{E}_\gamma(X_i), \quad \overline{\nu}(X_i), \quad \overline{E}_k(X_i)$$

In the following we shall denote by $\overline{A}(X_i)$ the measured average value of the quantity A corresponding to the X-ray amplitude X_i. Let $y(Z,A)$ be the number of fissions producing a fragment of charge Z and a value A of the quantity under study. Let $Y(X_i,A)$ be the number of fissions producing an X-ray pulse in channel X_i and the same value A of the quantity under study. For each fission producing a fragment of charge Z we assume that we count a pulse in the X-ray channel X_i with the probability $R(Z,X_i)$ which corresponds to the elemental response of the detector. Then the charge yields $y(Z,A)$ can be obtained from the observed channel yields $Y(X_i,A)$ by minimizing the sum of squares

$$\chi^2 = \sum_{i=1}^{n} W_i \left(Y(X_i,A) - \sum_Z R(Z,X_i)\, y(Z,A)\right)^2$$

The solution of the least-squares equation then expresses the charge yields as linear functions of the channel yields

$$y(Z,A) = \sum_i B(Z,X_i)\, Y(X_i,A) \tag{II. 3}$$

The matrix elements $B(Z,X_i)$ depend exclusively on the weights W_i and the response matrix elements $R(Z,X_i)$; they do not depend on A.

A relation similar to Eq. (II. 3) obviously holds for any linear function of the yields

$$L(y(Z,A)) = \sum_i B(Z,X_i)\, L(Y(X_i,A))$$

In particular if

$$N(X_i) = \sum_A Y(X_i,A) \qquad Y(Z) = \sum_A y(Z,A)$$

$$N(X_i)\,\overline{A}(X_i) = \sum_A A\, Y(X_i,A) \qquad Y(Z)\overline{A}(Z) = \sum_A A\, y(Z,A)$$

we can write that

$$Y(Z) = \sum_i B(Z,X_i)\, N(X_i) \tag{II. 4}$$

$$Y(Z)\, \bar{A}(Z) = \sum_i B(Z,X_i)\, N(X_i)\, \bar{A}(X_i) \tag{II. 5}$$

Equations (II. 4) and (II. 5) are identical to those which would result from a least-squares analysis of the quantities $N(X_i)$ and $N(X_i)\bar{A}(X_i)$, respectively.

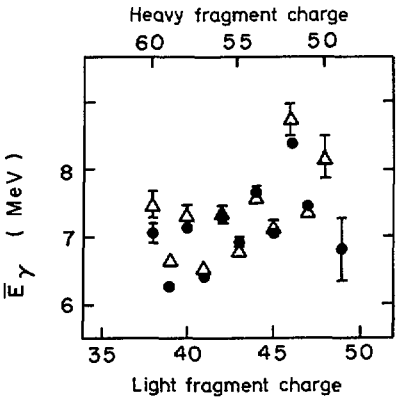

FIG. 18. Average total γ-ray energy emitted as a function of the light fragment's charge (●) and of the heavy fragment's charge (△) (^{252}Cf fission).

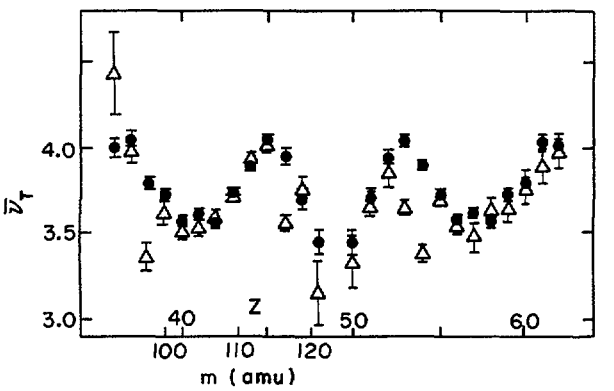

FIG. 19. Average neutron number as a function of the mass of the fragments (●) and of the charge of the fragments (△)(^{252}Cf fission).

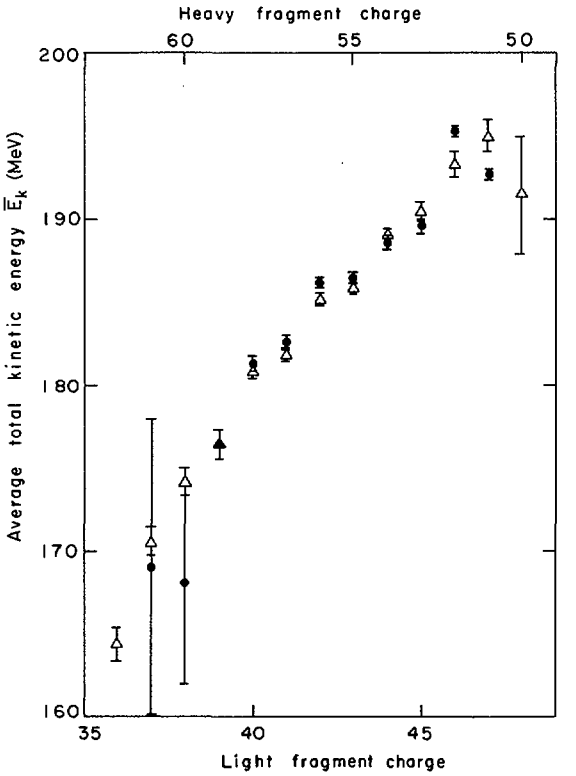

FIG. 20. Average kinetic energies as a function of the light fragment's charge (●) and of the heavy fragment's charge (Δ).

Thus, the charge yields y(Z) and average values $\bar{A}(Z)$ can be obtained from only two least-squares treatments operating on the channel yields $N(X_i)$ and on the products $N(X_i)\bar{A}(X_i)$ of the channel yields by the channel average values. This analysis was applied to the experimental data in order to obtain the charge dependent yields Y(Z), average total γ-ray energies $\bar{E}_\gamma(Z)$, neutron multiplicities $\bar{\nu}(Z)$ and average total kinetic energies $\bar{E}_k(Z)$.

Since the K X-rays emitted by fission fragments are mostly produced by electron conversion processes, their yields are expected to depend strongly upon the nuclear characteristics of the fragments, and this has been confirmed in numerous experiments. The question then arises as to the extent to which the values of average γ-energies, neutron multiplicities and total kinetic energies obtained in experiments such as those described above are not seriously biased. If such a bias exists, it is not probable that it acts identically on different fragments; therefore it is possible to check its existence by comparing the values of $\bar{E}_\gamma(Z)$, $\bar{\nu}_T(Z)$, and $\bar{E}_k(Z)$ obtained for a pair of complementary charges Z and 98-Z. This comparison can be made on Figs 18 - 20. Figure 18 shows the variation of the measured total

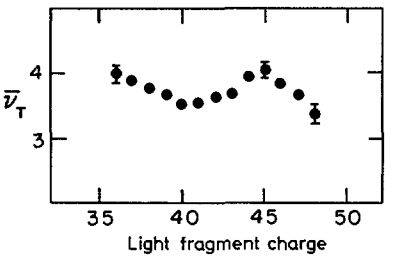

FIG. 21. Best average neutron number as a function of charge of the binary fission fragments (^{252}Cf fission).

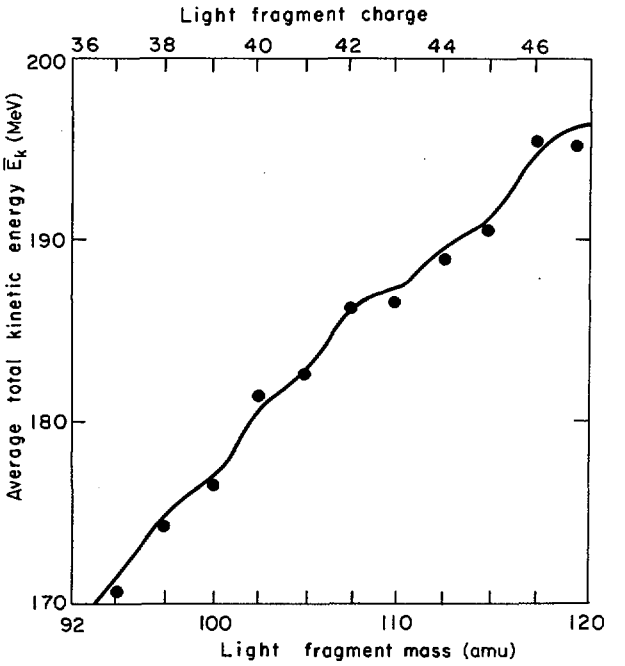

FIG. 22. Best average total kinetic energy as a function of charge of the fission fragments. The continuous line shows the value of average total kinetic energy as a function of mass of the fragments. The mass and charge scales reflect the charge-to-mass ratios of the fragments.

γ-energy as a function of the charges of the fragments. It can be seen that the complementarity condition (non-existence of bias) is fulfilled within statistical accuracy for almost all charges. Also apparent on the figure is a clear even-odd effect on $\bar{E}_\gamma(Z)$. As can be seen on Fig. 19, the complementarity condition is not always fulfilled for the variations of total number of neutrons $\bar{\nu}_T(Z)$. We have superimposed on Fig. 19 the variations of the total

number of neutrons as a function of mass $\bar{\nu}_T(m)$ as obtained in experiments such as those referred to in Section 1. The mass and charge scales of the figure reflect the charge-to-mass ratios of the fission fragments. It can be seen that, whenever the complementarity condition is fulfilled, the values of $\bar{\nu}_T(Z)$ lie close to the corresponding values of $\bar{\nu}_T(m)$. The complementarity condition is not fulfilled for the charge pairs 45-53, 44-54, 46-52 and several pairs with the light fragment's charge smaller than 39. It appears that in those pairs one of the values of $\bar{\nu}_T(Z)$ lies close to the corresponding value of $\bar{\nu}_T(m)$ while the other is smaller. We have assumed that the value closer to $\bar{\nu}_T(m)$ was not biased by the X-ray emission process. Figure 21 shows the values of $\bar{\nu}_T(Z)$ obtained when keeping the highest of the two observed values of $\bar{\nu}_T(Z)$ and $\bar{\nu}_T(98-Z)$. No even-odd effect is apparent on the figure.

The values of $\bar{E}_k(Z)$ show an even-odd effect for both heavy and light fragments. Values for complementary charges differ by 0.5 to 1 MeV. This is mostly a consequence of the existence of a high background under the X-ray peaks, due to interactions of high-energy γ-rays with the detector. Figure 22 shows the values of $\bar{E}_k(Z)$ obtained when keeping the highest of the two observed values of $\bar{E}_k(Z)$ and $\bar{E}_k(98-Z)$. Also shown for comparison are the values of $\bar{E}_k(m)$ obtained in a double fragment kinetic energy measurement. It is clear that the even-odd effect observed on the values of $\bar{E}_k(Z)$ reflects itself in the modulations appearing on the $\bar{E}_k(m)$ curve.

In summary, while the calculated difference in energy release between fission events with two even-charge fragments and those with two odd-charge fragments is

$$\Delta Q = Q_e(Z) - Q_o(Z) = 2.7 \text{ MeV}$$

it is found experimentally that: (1) the difference $\Delta\nu_T$ in the total number of neutrons is less than 0.04, corresponding to a difference in excitation energy smaller than 0.3 MeV, (2) the difference in total γ-ray energy amounts to $\Delta\bar{E}_\gamma = 0.66 \pm 0.05$ MeV and (3) the difference in fragment total kinetic energy amounts to $\Delta\bar{E}_k = 1.58$ MeV $\pm$ 0.1 MeV. The sum $\Delta\bar{E}_\gamma + \Delta\bar{E}_k$ is then equal to 2.24 $\pm$ 0.45 MeV. Within statistical accuracy it is in agreement with the computed value of 2.7 MeV.

2.6. De-excitation mechanism of the fission fragments

We should like, in the following, to summarize the experimental results on fragment de-excitation which have been presented above and discuss whether these results can be explained within a coherent theoretical framework. We shall mostly concentrate on the features of γ-ray emission by the fission fragments. However, we must bear in mind that the neutron energy spectra appear to be satisfactorily accounted for by a standard evaporation theory, provided the level densities used in the calculation properly include shell effects. Such calculations have been performed, among others, by Nardi and co-workers [31] and Fig. 23 shows a comparison between the experimental and computed values of the average centre-of-mass kinetic energies of the neutrons. Those computations made use of the technique developed by Moretto [39], where both shell effects and pairing are taken into account for the determination of level densities.

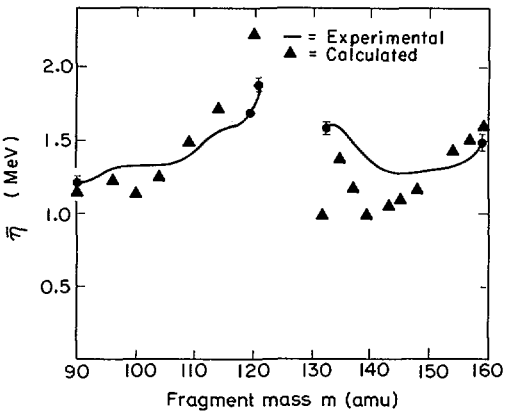

FIG. 23. Experimental and calculated values of the average centre-of-mass kinetic energy of the neutrons, $\bar{\eta}$. Typical experimental errors are shown by full dots with error bars. The theoretical values were obtained including pairing in the level densities. Figure taken from Ref. [31].

In an attempt to explain the striking correlation between γ and neutron emissions by the fission fragments, Johansson [24] made the hypothesis that the γ-rays corresponded mainly to vibrational transitions through which the fragments could lose the deformation they had at scission. The high proportion of E2 radiation in the fission γ spectrum seemed to confirm this point of view. However, there are very strong objections to this hypothesis. It seems to be well-established experimentally that at least 70% of the total γ-ray energy is emitted more than one picosecond after fission while the neutrons are emitted in a time shorter than 10^{-14} s. We have shown earlier that the fastest γ-ray transitions were probably E1 in character since they tend to decrease the angular anisotropy. It thus appears that the collective γ-ray transitions, if they exist, occur after neutron emission. The γ-ray emission should reflect the state of the system at this time and not at the time of scission. The hypothesis assumes that most of the initial excitation energy of the fragments is tied into deformation. After neutron emission most of this deformation energy has been dissipated and the remaining fraction, if it exists, has no reason to be proportional to the initial value. Furthermore, the success of the evaporation theory of neutron spectra points to an effective damping of the deformation energy of the fragments in times less than 10^{-18} s. The last objection to Johansson's hypothesis is that the lifetimes of the possible vibrational transitions should be at least an order of magnitude shorter than the observed ones, which, as stated earlier, are close to E2 single particle estimates.

The alternative to Johansson's hypothesis is to assume that the de-excitation of fission fragments is governed by the statistical theory. Using the shell plus pairing model, Nardi and co-workers [31] were not able to reproduce the variations of the γ-ray energy as a function of fragment mass. Their model did not fully include the influence of the spin on the level density. Such models predict some correlation between the neutron and the γ-ray emissions by the fragments. This correlation reflects mostly the increase

in the binding energy of the last emitted neutron when the number of neutrons emitted by the fragment increases. From the mass tables it is seen that, in the fission fragments region, an increase of one unit in the number of emitted neutrons produces an increase of approximately 0.3 MeV in the binding energy of the last neutron, which should be reflected by an increase of 0.15 MeV of the γ-ray energy. This effect is certainly present in the experimental data, but it leaves unexplained, in the case of ^{252}Cf, an increase of γ-ray energy of approximately 0.6 MeV for each additional emitted neutron.

Statistical computations which treat the influence of pairing in a phenomenological way by introducing the effective excitation energy have had some success in reproducing the trend of the variation of the γ-ray energy emitted as a function of the fragment's mass. Such a calculation has also been performed by Nardi and co-workers [31]. However, the physical justification of such phenomenological models is not clear and it is possible that the introduction of an effective excitation energy simulates the effect of the spins of the fission fragments, which will be discussed later. Furthermore, these models cannot account for the observed increase in γ-ray energy with excitation energy for fragments of given masses.

That spin considerations should enter into statistical computation of γ-ray emission by the fission fragments stems from the following considerations:

(1) Most evaluations of the spins of the fragments before neutron emission indicate that these spins are approximately $6\hbar$ to $8\hbar$ higher than the ground state spins. Neutron emission is not expected to decrease that spin by more than one unit of angular momentum. When the fragments are left with an energy only slightly higher than a neutron binding energy, they still have from 5 to $7\hbar$ units of angular momentum to dissipate. Further neutron emission which would leave the residual nucleus in the vicinity of its ground state is thus expected to be strongly inhibited except for odd-odd nuclei. To obtain a level with spin differing from that of the ground state by more than five units of angular momentum requires the coupling of at least two unpaired nucleons, and thus the breaking of a pair in both even-even and odd-A nuclei. The observed even-odd difference in total γ-ray energy emitted in fission is easily explained in that context. From the experimental value of 0.66 MeV for this difference, we can derive the increase of γ-ray energy emitted in fission induced by angular momentum effects. If we assume that there is no increase for odd-odd fragments and that the increases are equal in the other cases, we find that angular momentum effects should add 1 MeV to the γ-ray energy release in fission. The total γ-ray energy emitted in fission would then lie between 7.0 and 7.5 MeV, in reasonable agreement with experiment.

(2) The dominant E2 character of the fission γ-rays as well as their relatively high multiplicity cannot be understood when compared with the features of neutron capture γ-ray spectra without the assumption that γ-emission by the fission fragment is strongly influenced by the absence of available states for El transitions.

After neutron emission has taken place the residual fragment is left with an average energy of approximately 4 MeV, and an average spin of approximately $6\hbar$. Under these conditions electric dipole emission should not be

inhibited and we can assume it takes place with an average energy of approximately 1.5 to 2 MeV. This emission should not reduce the spin of the fragment significantly and thereby leaves it with an excitation energy of approximately 2 to 2.5 MeV and an average spin exceeding $5\hbar$, that is, in the region of the "yrast" line. However, the "yrast" line should not be considered as the ground state rotational band but rather as the "yrast" region of the intrinsic levels at which energy it becomes possible to treat the density of levels of given spin and parity statistically. In this "yrast" region E2 transitions dominate, because of spin and parity limitations, until the ground state band is reached. In this picture the E2 transitions reduce the spin of the fragment by the maximum possible amount, that is, by two units of angular momentum. The average energy of the E2 transitions of approximately 1 MeV thus represents the average energy which is necessary to reduce the spin of the fragment by 2 units along the path followed by the system in the (E,I) representation.

This deexcitation should be similar for fission frogments and for the products of (charged particle, xn) reactions with comparable initial spins. That this is the case has been shown by Wilhelmy and co-workers [21].

The consequence of this oversimplified model of the γ-deexcitation of fission fragments is that the increase of γ-ray energy with excitation energy which has been reported would be the consequence of an increase of the average spin of the fragments with their excitation energy. Using the experimentally determined increase of 0.6 MeV in γ-energy for each additional neutron, a value of 8 MeV for the energy necessary to emit one more neutron and a difference of 2 spin units for 1 MeV additional γ-energy, one finds that the average spin of the fission fragments should increase by one unit for an increase of excitation energy of approximately 7 MeV. Such a result does not contradict that of Wilhelmy and co-workers [21] who found that the increase in spin of the fragments was less than 2 for a decrease of the total kinetic energy of approximately 15 MeV.

Armbruster and co-workers [20] have pointed out that such a behaviour of the spins of the fragments could be explained in the framework of the collective model of fission suggested by Nörenberg [40, 41]. This model also predicts the observed preferential orientation of the fragments' spins in the plane perpendicular to the fission direction.

3. VARIANCES OF THE EXCITATION ENERGIES OF THE FISSION FRAGMENTS

With the exception of the pioneering work of Whetstone [4] it is only recently that detailed measurements of the variances of the number of neutrons emitted in fission have been carried out. In the following we shall assume that the neutrons are all emitted by the fragments, after fission has taken place. One should, however, bear in mind the possible existence of an isotropic component in the fission neutrons which could seriously impair the results and interpretation of variances measurements. With that assumption we write the probability that ν_1 neutrons are emitted by one of the fragments and ν_2 by the other as a bi-variate distribution $P(\nu_1, \nu_2)$. We have shown elsewhere [42] how it is possible, in principle, to derive this distribution from the probability $Q(g_1, g_2)$ that g_1 and g_2 neutrons are detected simultaneously by two suitably arranged detectors. Such a program is not feasible,

however, because of the statistical errors in the definition of the observed distribution $Q(g_1, g_2)$ and because of our uncertain knowledge of the efficiencies of the neutron detectors. We must therefore content ourselves with the extraction of some significant features of the distribution $P(\nu_1, \nu_2)$ from the experimental data. Such features are, for example, the five lowest moments of this distribution defined as follows:

$$\bar{\nu}_1 = \iint \nu_1 \, P(\nu_1,\nu_2) \, d\nu_1 \, d\nu_2$$

$$\bar{\nu}_2 = \iint \nu_2 \, P(\nu_1,\nu_2) \, d\nu_1 \, d\nu_2$$

$$\sigma^2(\nu_1) = \iint (\nu_1 - \bar{\nu}_1)^2 \, P(\nu_1, \nu_2) \, d\nu_1 \, d\nu_2$$

$$\sigma^2(\nu_2) = \iint (\nu_2 - \bar{\nu}_2)^2 \, P(\nu_1, \nu_2) \, d\nu_1 \, d\nu_2$$

$$C(\nu_1, \nu_2) = \iint (\nu_1 - \bar{\nu}_1)(\nu_2 - \bar{\nu}_2) \, P(\nu_1, \nu_2) \, d\nu_1 \, d\nu_2$$

We have dealt with the determination of the two first moments in Section 1. We have seen that, as soon as the masses of the fragments are measured, a single measurement with one neutron detector provided the values of the two average numbers of neutrons. Similarly only two independent measurements are necessary to determine the three second-moments. As in Section 1. two different techniques have been used for that purpose. The low-efficiency technique makes use of two small neutron detectors in conjunction with two fragment detectors [43]. When the two neutron detectors are on the same side of the fission source, the ratio of the rate of quadruple coincidences to the square of the rate of triple coincidences is equal to:

$$\frac{< \varepsilon \, \nu_1 \, \varepsilon(\nu_1 - 1) >}{< (\varepsilon \, \nu_1) >^2}$$

where it is assumed that both neutron detectors have the same efficiency ϵ. It is further assumed that this efficiency does not depend on the neutron multiplicity, at least when the fragment mass and kinetic energies are specified. One then obtains:

$$\frac{< \nu_1(\nu_1 - 1) >}{< \nu_1 >^2} = \frac{< \nu_1^2 >}{\bar{\nu}_1^2} - \frac{1}{\bar{\nu}_1} = \frac{\sigma^2(\nu_1)}{\bar{\nu}_1^2} - \frac{1}{\bar{\nu}_1} + 1$$

A similar relation holds when the complementary fragment flies in the direction of the neutron detector, allowing one to obtain $\sigma^2(\nu_2)$.

When the two neutrons are situated on opposite sides of the source, one then obtains, in the same manner as above

$$\frac{\langle \varepsilon_1 \nu_1 \varepsilon_2 \nu_2 \rangle}{\langle \varepsilon_1 \nu_1 \rangle \langle \varepsilon_2 \nu_2 \rangle} = \frac{\langle \nu_1 \nu_2 \rangle}{\bar{\nu}_1 \bar{\nu}_2} = \frac{C(\nu_1 \nu_2)}{\bar{\nu}_1 \bar{\nu}_2} + 1$$

This technique assumes a complete separation of the neutrons emitted by the two fragments, owing to the fragments velocity. It is subject to the same causes of uncertainty that have been mentioned for the measurements of the average number of neutrons. The consequences of these uncertainties are, however, amplified here. We show that this is so for the co-variance measurement. Let M be the measured ratio of coincidence rates. Then

$$C(\nu_1, \nu_2) = \bar{\nu}_1 \bar{\nu}_2 (M - 1)$$

The relative error is thus approximately given by

$$\frac{\Delta C(\nu_1, \nu_2)}{C(\nu_1, \nu_2)} = \frac{\Delta \bar{\nu}_1}{\bar{\nu}_1} + \frac{\Delta \bar{\nu}_2}{\bar{\nu}_2} + \frac{\Delta M}{M - 1} \qquad \text{(III. 1)}$$

The first two terms of the right-hand side of Eq. (III. 1) do not lead to unacceptable errors on the co-variance; they include effects such as errors in the efficiency determination or in the mass and kinetic energy resolution corrections. The last term includes principally two effects: the first effect is related to the fragment recoil correction, which was found by Gavron [8] to be very important in average neutron number measurements. Starting from Gavron's considerations we show in Appendix II that the dominant term in the error on the co-variance is

$$\Delta C(\nu_1, \nu_2) \sim - 0.56 + 0.14 (E_k - \bar{E}_k)$$

where E_k is the total kinetic energy. This correction is of the same order of magnitude as the co-variances themselves.

The second important cause of error in the co-variance measurements stems from the dependence of the efficiencies on the neutron multiplicities. It is also shown in the appendices that if one assumes a linear dependence of the efficiency on ν_1

$$\varepsilon_1 = \bar{\varepsilon}_1 + (\nu_1 - \bar{\nu}_1) k_1 \varepsilon_1$$

$$\varepsilon_2 = \bar{\varepsilon}_2 + (\nu_2 - \bar{\nu}_2) k_2 \varepsilon_2$$

the co-variance is given by the modified equation

$$\frac{C(\nu_1, \nu_2)}{\bar{\nu}_1 \bar{\nu}_2} \left(1 + k M \nu_T \right) = M - 1$$

where we have assumed

$$k = k_1 = k_2$$

Since

$$M \sim 1$$

we obtain

$$\Delta C(\nu_1, \nu_2) \sim k \nu_T \; C(\nu_1, \nu_2)$$

For higher multiplicities the average neutron energy decreases so that the efficiency decreases and k is negative. The magnitude of k depends on the experimental setup and is difficult to evaluate; however, a value of k of around 0.1 could be found and would lead to a 40% error on the co-variance. Since published results [43] on the variances of the neutron multiplicity distributions which made use of low-efficiency detectors do not account for the above two causes of error they appear strongly in doubt. However, if an accurate treatment of the experimental data became available, the small neutron detector technique would be the easiest and most elegant way of measuring the moments of the neutron number distributions.

The measurements making use of large neutron detectors, although rather cumbersome, are essentially free from the errors mentioned in the case of small neutron detectors. They require a knowledge of both backward and forward neutron detection efficiencies. Two independent measurements are necessary to obtain the three second-moments of the neutron number distributions, but, in contrast with the low-efficiency case, the two measurements must be considered together; this is a consequence of the finite values of the backward efficiencies.

The first measurement uses a 4π geometry and provides the variance of the total number of neutrons for the different kinetic energy and mass ratios of the fragments.

The second measurement uses a geometry such that the neutron detector subtends less than a 2π solid angle as viewed from the fission source.

As a more detailed account of both the experimental technique involved and the results is given in another contribution to this Symposium [44], we shall now deal only with two specific questions, namely the comparison between total kinetic energy variances and total number of neutrons variances and the extraction of excitation energy variances from the neutron multiplicity measurements.

3.1. Variances of the distributions of the total number of neutrons

The variances of the total number of neutrons have been measured as a function of both the mass of one of the fragments and the total kinetic energy. The values obtained are written $\sigma^2(\nu_T:\ m\ E_k)$. For a given mass split we define the average value of these quantities as

$$\overline{\sigma^2(\nu_T:\ m\ E_k)} \equiv \underset{E_k}{\mathcal{M}}\ \sigma^2(\nu_T:\ m\ E_k) = \int_{E_k} \sigma^2(\nu_T:\ m\ E_k)\ p(E_k)\ d\ E_k$$

The variance of the total number of neutrons measured for a given mass split and for all possible kinetic energies is given by [45]

$$\sigma^2(\nu_T:\ m) = \left\langle \frac{d\nu_T}{d\ E_k} \right\rangle_m^2 \sigma^2(E_k:\ m) + \overline{\sigma^2(\nu_T:\ m\ E_k)} \qquad \text{(III. 2)}$$

the quantities $\sigma^2(\nu_T:\ m)$ and $\sigma^2(\nu_T:\ m\ E_k)$ as obtained from the experiment are plotted on Fig. 24 for the case of the spontaneous fission of ^{252}Cf. It is possible to use Eq. (III. 2) to compute the values of the kinetic energy variance $\sigma^2(E_k:\ m)$. If the values of $\langle d\nu_T/dE_k \rangle_m$ obtained in the experiment and shown on Fig. 5 were used, one would then obviously obtain values of $\sigma^2(E_k:\ m)$ equal to those that can be determined from the fission yield curves alone. This is because Eq. (III. 2) stands as an identity in such a case, provided only that the regression of ν_T on E_k is linear. If, on the other hand, one uses the values of $\langle d\nu_T/dE_k \rangle_{calc.}$ which have been calculated from the neutron binding and kinetic energies and from the rate of change in γ-ray energy as a function of E_k one obtains another set of values for $\sigma^2(E_k:\ m)$. Both sets are shown on Fig. 25. It can be seen that the two sets diverge, especially for masses which range between the most probable mass and symmetry. This divergence reflects the one observed on Fig. 5 for the two corresponding sets of values of $\langle d\nu_T/dE_k \rangle_m$. Figure 25 suggests that kinetic energy resolution effects were not completely accounted for; inspection of the fragment yields shows that a low-energy tailing appears for the masses where the experimental and calculated values of $\langle d\nu_T/dE_k \rangle_m$ diverge. It is probable that such a tailing has an experimental origin. If this is true, the values of $\sigma^2(E_k:\ m)$ computed from the values of $\sigma^2(\nu_T:\ m)$ as indicated above would be better estimates of the true total kinetic energy variances than the values obtained directly from the fragment yields curves. It is interesting to see that the rise of $\sigma^2(E_k:\ m)$ near symmetry does not occur for the calculated values, which stay remarkably constant. On the other hand, it is well known that tailing of the fragment energy resolution functions will result in a shift of the experimental masses towards symmetry and in an increase of the variance of the total kinetic energy for the more symmetrical fragments pairs. Since the neutron and γ-ray results should not be very sensitive to this tailing, it is possible that, in the future, they will be used to correct the kinetic energy data.

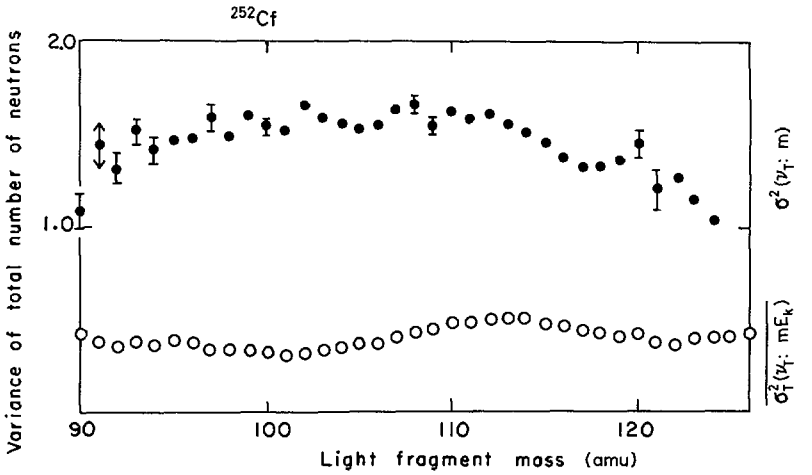

FIG. 24. ● : Variations of the variance of the total number of neutrons $\sigma^2(\nu_T:\ m)$ as a function of mass of the light fragment. ○ : Average value over the total kinetic energy of the conditional variances $\overline{\sigma^2(\nu_T:\ m\ E_k)}$ as a function of the mass of the light fragment.

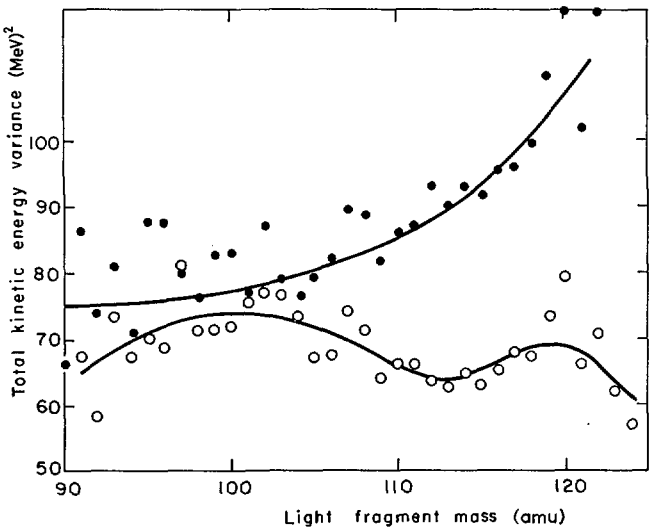

FIG. 25. Variances of the total kinetic energy as obtained directly from the kinetic energies (●) and as obtained from the neutron variances (○). The full lines give an idea of the errors on the experimental values.

3.2. Variances of the excitation energies of the fission fragments

Experiment provides the values of the variances $\sigma^2(\nu_1:\ m\ E_k)$, $\sigma^2(\nu_2:\ m\ E_k)$ and the co-variances $C(\nu_1\nu_2:\ m\ E_k)$ of the neutron distributions for selected values of one fragment mass and of the total kinetic energy. These quantities cannot be immediately transformed into fragment excitation energy variances because of the neutron evaporation process. Even if a fragment is produced with a given mass, charge and excitation energy, a finite variance of the number of neutrons will be observed owing to the statistical nature of this evaporation process.

Since, as will be shown below, we are chiefly interested in the excitation energy variances for fixed masses and charges of the fragments and since the experimental quantities are measured as a function of masses or charges alone, it is also necessary to determine in what respect the experimental data are representative.

We first examine this question. Assuming linear regressions [45] we can write that

$$\sigma^2(\nu_1:\ m\ E_k) = \left\langle \frac{d\nu_1}{dZ} \right\rangle^2_{m,E_k} \sigma^2(Z:\ m\ E_k) + \mathcal{M}_Z\, \sigma^2(\nu_1:\ m\ Z\ E_k)$$

$$\sigma^2(\nu_2:\ m\ E_k) = \left\langle \frac{d\nu_2}{dZ} \right\rangle^2_{m,E_k} \sigma^2(Z:\ m\ E_k) + \mathcal{M}_Z\, \sigma^2(\nu_2:\ m\ Z\ E_k)$$

$$C(\nu_1\ \nu_2:\ m\ E_k) = \left\langle \frac{d\nu_1}{dZ} \right\rangle_{m,E_k} \left\langle \frac{d\nu_2}{dZ} \right\rangle_{m,E_k} \sigma^2(Z:\ m\ E_k) + \mathcal{M}_Z\, C(\nu_1\ \nu_2:\ m\ Z\ E_k) \qquad \text{(III. 3)}$$

We shall assume that the isotopic widths $\sigma^2(Z:\ m\ E_k)$ and the slopes $\langle d\nu_1/dZ\rangle_{m,E_k}$ and $\langle \partial\nu_2/\partial Z\rangle_{m,E_k}$ do not depend sensitively on the total kinetic energies so that Eqs (III. 3) would also hold when the total kinetic energy variable is disregarded.

Neutron emission is very sensitive to shell effects so that it has more physical basis to express the rates of variation of the average number of neutrons as a function of the charge and neutron number of a nucleus than as a function of its mass number. Let us then consider the slopes $\langle d\nu_1/dZ\rangle_N$ and $\langle d\nu_1/dN\rangle_Z$ which express the rate of variation as a function of charge (or neutron number) of the average number of neutrons emitted by a fragment having a fixed number of neutrons (or of protons). Then, since $m = N+Z$

$$\left\langle \frac{d\nu_1}{dZ} \right\rangle_m = \left\langle \frac{d\nu_1}{dZ} \right\rangle_N - \left\langle \frac{d\nu_1}{dN} \right\rangle_Z \qquad \text{(III. 4)}$$

and, for example

$$\sigma^2(\nu_1:\ m) = \left(< \frac{d\nu_1}{dZ} >_N - < \frac{d\nu_1}{dN} >_Z \right)^2 \sigma^2(Z:\ m) + \underset{Z}{\mathcal{M}}\ \sigma^2(\nu_1:\ m\ Z) \qquad \text{(III. 5)}$$

On the other hand, the slope of the representative curves $\bar{\nu}_1(m)$ which have been presented in Section 1 can be written as

$$< \frac{d\nu_1}{dm} > = < \frac{d\nu_1}{dZ} >_N \frac{dZ}{dm} + < \frac{d\nu_1}{dN} >_Z \frac{dN}{dm}$$

assuming that the charge density is the same in the fragments as in the fissile nucleus, we obtain for ^{252}Cf fission

$$< \frac{d\nu_1}{dm} > = 0.39 < \frac{d\nu_1}{dZ} >_N + 0.61 < \frac{d\nu_1}{dN} >_Z$$

Typical values of $\langle d\nu_1/dm \rangle$ range around 0.1. It appears reasonable to assume that for most of the cases $\langle d\nu_1/dZ \rangle_N$ and $\langle d\nu_1/dN \rangle_Z$ have the same sign since the closed shells at 50 protons and 82 neutrons occur in the same mass region. Then the first term of the right-hand side of Eq. (III. 5) is maximum for

$$< \frac{d\nu_1}{dN} >_Z = 0$$

and

$$< \frac{d\nu_1}{dZ} >_N \sim 0.25$$

Taking a value of $\sigma^2(Z:\ m) \sim 0.25$ [46] we obtain for

$$\left(< \frac{d\nu_1}{dZ} >_N - < \frac{d\nu_1}{dN} >_Z \right)^2 \sigma^2(Z:\ m)$$

a maximum value of 0.015. This value is approximately 1% of the observed values of $\sigma^2(\nu_1:\ m)$ and less than 10% of the values of $\sigma^2(\nu_1:\ m\ E_k)$. We conclude that for most masses the existence of a charge distribution for the fragments should not impair the conclusions which could be drawn from the study of the variances of neutron number measured only as a function of total kinetic energy and masses.

We now turn to the extraction of the excitation energy variances. Assuming, again, that linear regression analysis applies, we can write

$$\sigma^2(\nu_1:\ m\ E_k) = < \frac{d\nu_1}{dE_1} >^2_{m,E_k} \sigma^2(E_1:\ m\ E_k) + \underset{E_1}{\mathcal{M}}\ \sigma^2(\nu_1:\ m\ E_k\ E_1)$$

$$\sigma^2(\nu_2:\ m\ E_k) = \left\langle \frac{d\nu_2}{dE_2} \right\rangle^2_{m,E_k} \sigma^2(E_2:\ m\ E_k) + \mathop{\mathcal{M}}_{E_2} \sigma^2(\nu_2:\ m\ E_k\ E_2)$$

$$C(\nu_1\ \nu_2:\ m\ E_k) = \left\langle \frac{d\nu_1}{dE_1} \right\rangle_{m,E_k} \left\langle \frac{d\nu_2}{dE_2} \right\rangle_{m,E_k} C(E_1\ E_2:\ m,E_k)$$

$$+ \mathop{\mathcal{M}}_{E_1 E_2} C(\nu_1\ \nu_2:\ m\ E_k\ E_1\ E_2) \qquad \text{(III. 6)}$$

The second terms of the right-hand side of Eqs (III. 6) represent the contribution of the evaporation process to the neutron number variances and co-variances. In particular, the term $C(\nu_1\nu_2:\ m\ E_k E_1 E_2)$ measures the correlation between the numbers of neutrons emitted by two complementary fragments of fixed masses and excitation energies. Except for possible weak spin effects, the two evaporation processes should not be correlated and therefore

$$C(\nu_1\ \nu_2:\ m\ E_k\ E_1\ E_2) \sim 0$$

The inverses of the slopes $\langle d\nu_1/dE_1\rangle_{m,E_k}$ and $\langle d\nu_2/dE_2\rangle_{m,E_k}$ are the energies necessary for the fragment to emit one additional neutron. These can be computed, as indicated previously, from the mass tables, average neutron numbers and kinetic energies, and from the variations of the γ-ray energy with neutron number.

The two excitation energies E_1, E_2 and the total kinetic energy E_k are obviously related by the energy conservation requirement:

$$Q(m) - E_k = E_1 + E_2 \qquad \text{(III. 7)}$$

The value of Q is not strictly defined by knowledge of the masses of the fragments because of their charge distribution. Using again linear regression analysis [45], one can write

$$\sigma^2(E_1:\ m,E_k) = \left\langle \frac{dE_1}{dQ} \right\rangle^2_{m,E_k} \sigma^2(Q:\ m) + \mathop{\mathcal{M}}_{Q} \sigma^2(E_1:\ m\ E_k\ Q)$$

$$\sigma^2(E_2:\ m\ E_k) = \left\langle \frac{dE_2}{dQ} \right\rangle^2_{m,E_k} \sigma^2(Q:\ m) + \mathop{\mathcal{M}}_{Q} \sigma^2(E_2:\ m\ E_k\ Q)$$

$$C(E_1\ E_2:\ m\ E_k) = \left\langle \frac{dE_1}{dQ} \right\rangle_{m,E_k} \left\langle \frac{dE_2}{dQ} \right\rangle_{m,E_k} \sigma^2(Q:\ m)$$

$$+ \mathop{\mathcal{M}}_{Q} C(E_1\ E_2:\ m\ E_k\ Q) \qquad \text{(III. 8)}$$

Because of Eq. (III. 7) we have

$$< \frac{dE_1}{dQ} > + < \frac{dE_2}{dQ} > = 1$$

We assume that

$$< \frac{dE_1}{dQ} > = < \frac{dE_2}{dQ} > = \frac{1}{2}$$

in order to estimate the first terms of the right-hand sides of Eqs (III. 8). This choice maximizes this correction term for the third equation. Using the mass tables and the data relative to the charge distribution of the fission fragments one can see that $\sigma^2(Q: m)$ fluctuates between 1 MeV^2 and 12 MeV^2 [45]. Retaining this last number one sees that the correction terms

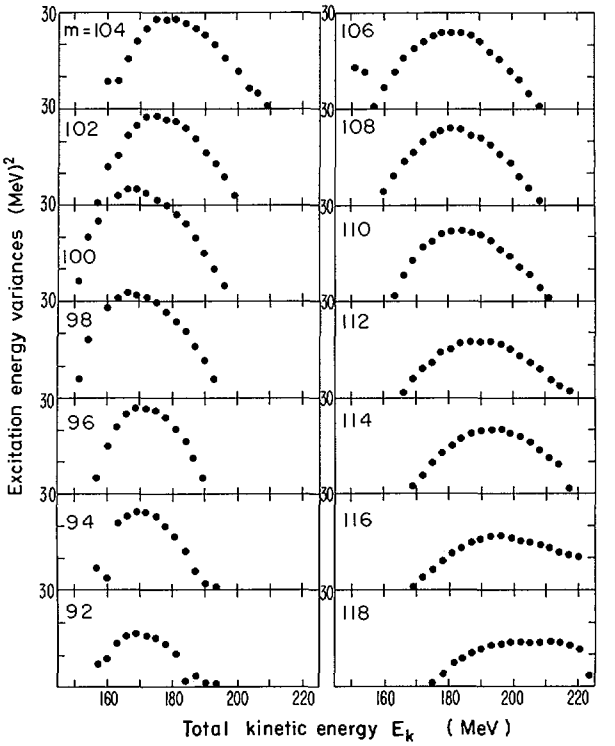

FIG. 26. Variations of the excitation energy variances $\sigma^2(E_1 : m E_k)$ as a function of E_k for various masses of the light fragment.

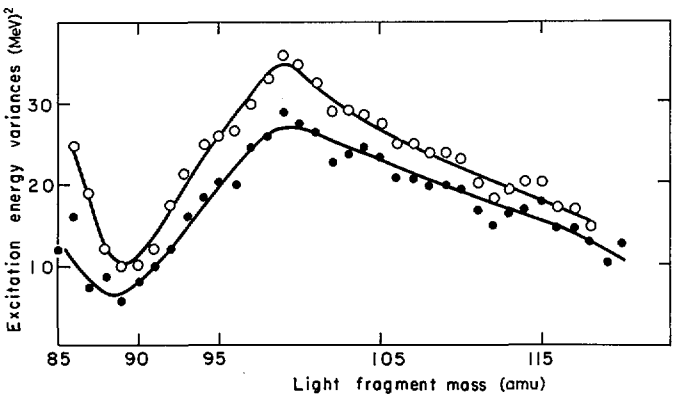

FIG 27. ● : Variations of the excitation energy variances $\overline{\sigma^2(E_1 : m E_k)}$ averaged over E_k as a function of light fragment mass. ○ : Variations of the maximum observed energy variance as a function of fragment mass. The full lines give an idea of the errors.

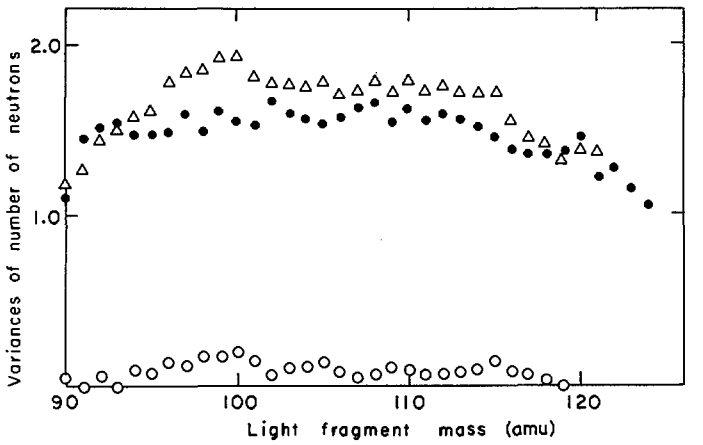

FIG. 28. ● : Variations of the variances of the total number of neutrons $\sigma^2(\nu_T : m)$ as a function of the light fragment mass. △ : Variations of the sum of the two neutron variances for complementary fragments $\sigma^2(\nu_1 : m) + \sigma^2(\nu_2 : m)$ as a function of the light fragment mass. ○ : Variation of the co-variance of the neutron distribution as a function of the light fragment mass.

$$C(\nu_1 \nu_2 : m) = \tfrac{1}{2}[\sigma^2(\nu_T : m) - \sigma^2(\nu_1 : m) - \sigma^2(\nu_2 : m)]$$

The quantity shown on the figure is $-C(\nu_1 \nu_2 : m)$ for the sake of convenience.

in the co-variance are at most equal to 3 MeV^2. Expressed in terms of the neutron number these quantities are approximately equal to 0.05 n^2 which is of the order of 10% of the observed values. In the following we have neglected this effect, and have therefore assumed that for a given value of m and E_k the total excitation energy $E_1 + E_2$ was determined. In that case one has evidently

$$\sigma^2(E_1:\ m\ E_k) = \sigma^2(E_2:\ m\ E_k) = -\ C(E_1\ E_2:\ m\ E_k)$$

and the system III. 8 can be solved. Figure 26 shows the variations of the variances $\sigma^2(E_1:\ m\ E_k)$ obtained as explained above with the total kinetic energy E_k for a choice of masses of the light fragment. The experimental data had been smoothed before the background and efficiency corrections were made. The estimated errors on the curves presented in Fig. 26 are of the order of 20%. The parabolic behaviour of the variances appear to be well established. Figure 27 shows the variations of the variances averaged over E_k as a function of m as well as the value of the maximum variance for each mass. Lastly, Fig. 28 which is taken from Ref. [47] shows the values of the variances and co-variances of the neutron number as a function of mass alone. These quantities are related to the previous ones by relations such as

$$C(\nu_1\ \nu_2:\ m) = \left\langle \frac{d\nu_1}{dE_k} \right\rangle \left\langle \frac{d\nu_2}{dE_k} \right\rangle \sigma^2(E_k) + \underset{E_k}{\mathcal{M}}\ C(\nu_1\ \nu_2:\ m\ E_k)$$

From Fig. 28 it can be seen that the co-variances $C(\nu_1 \nu_2:\ m)$ almost vanish except for masses between 95 and 105.

4. SOME THEORETICAL CONSEQUENCES OF THE EXPERIMENTAL RESULTS

We should like to conclude this review of neutron and gamma emission in fission by an evaluation of the information which the experimental results provide for a theory of nuclear fission. We shall first deal with the knowledge of the potential energy surface of the system undergoing fission, which can be obtained from the study of the de-excitation of the fragments.

4.1. Potential energy surface

Studies of the properties of the fission fragments can only provide information on the potential energy near the scission stage of the fission process. It is convenient, at that stage, to split the potential energy of the system into three parts:

Mutual Coulomb interaction energy C
Deformation energies of the two nascent fragments D_1 and D_2

Since the potential energy surface can be considered as the adiabatic ground state of the system for fixed values of a set of shape parameters, the potential energy does not absorb the whole available energy. The remaining energy can also be split into three parts

Pre-scission kinetic energy ϵ
Intrinsic excitation energies of the fragments X_1 and X_2

If one neglects the post-scission Coulomb effect, the experimentally measured quantities can be expressed as a function of the "scission" ones: the total fragment kinetic energy as

$$E_k = C + \epsilon \tag{IV.1}$$

and the fragment excitation energies as

$$E_1 = D_1 + X_1$$
$$E_2 = D_2 + X_2 \tag{IV.2}$$

The comparisons [48-51] between potential energy computations and experiment have been based on the average values of kinetic and excitation energies of the fragment. Thus it was necessary to make assumptions on the magnitude of the pre-scission kinetic energy and intrinsic excitations of the fragments. Those assumptions were, in fact, related to a picture of the dynamics of the fission process. Knowledge of the variances of the fragment excitation energies avoids the necessity of such ambiguous assumptions. We can see from Fig. 26 that the representative curves of these variances can be extrapolated to zero. For each mass ratio there are two resulting points characterized by two values of the kinetic energies $E_k^{(1)}(m)$ and $E_k^{(2)}(m)$. For those points the variance $\sigma^2(E_1 : m E_k)$ vanishes. From Eq. (IV. 2) we can write

$$\sigma^2(E_1) = \sigma^2(D_1) + 2C(D_1, X_1) + \sigma^2(X_1)$$

Since

$$|C(D_1, X_1)| \leqslant \sigma(D_1)\ \sigma(X_1)$$

the variance $\sigma^2(E_1)$ can only vanish if both $\sigma^2(D_1)$ and $\sigma^2(X_1)$ vanish, or if the deformation and intrinsic energies D_1 and X_1 were totally anticorrelated. The last possibility is obviously unphysical.

When the total intrinsic excitation energy of the system is non-vanishing, one expects that it will be shared in a random manner between the two fragments; this random sharing will produce a non-vanishing value of the variance $\sigma^2(X_1)$. Thereby the vanishing value of $\sigma^2(X_1)$ implies that both intrinsic excitation energies X_1 and X_2 vanish.

Assuming that linear regression analysis applies, one can write that

$$\sigma^2(D_1:\ E_k\ m) = \left\langle \frac{dD_1}{d\varepsilon} \right\rangle_{m,E_k} \sigma^2(\varepsilon:\ E_k\ m) + \mathop{\mathcal{M}}_{\varepsilon}\ \sigma^2(D_1:\ E_k\ m) \qquad \text{(IV. 3)}$$

Since we have shown that, for the kinetic energies $E_k^{(1)}(m)$ and $E_k^{(2)}(m)$, $\sigma^2(D_1:\ E_k\ m) = 0$, the two terms of the right-hand side of Eq. (IV. 3) should cancel. The slope

$$\left\langle \frac{dD_1}{d\varepsilon} \right\rangle_{m,E_k} = - \left\langle \frac{dD_1}{dC} \right\rangle_{m,E_k}$$

has no reason to vanish, so that we obtain the result that

$$\sigma^2(\varepsilon:\ E_k^{(1,2)}{}_m) = 0$$

An argument similar to that used for the intrinsic excitation energies shows that this condition can only be fulfilled if $\epsilon = 0$.

An intuitive understanding of the preceding arguments can be obtained from consideration of Fig. 29.

On the figure we have schematically drawn the minimum potential energy of the system along the scission line (curve A). This curve has been labelled according to the potential Coulomb interaction at each point. We also show the horizontal line corresponding to the total energy available to the system. The shaded area corresponds to the excess energy in the system which can be split more or less at random into pre-scission kinetic

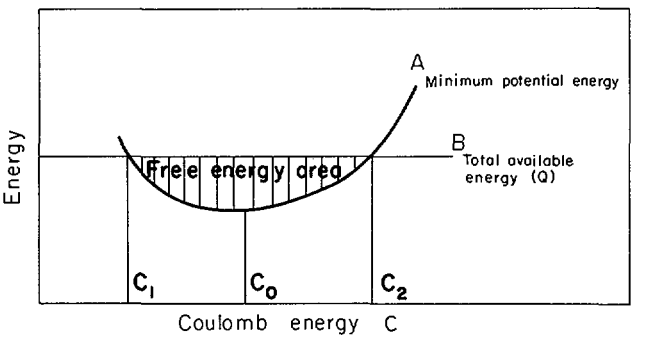

FIG. 29. Schematic representation of the minimum potential energy and "free energy" along the scission line. Abscissa: Coulomb interaction energy C. Curve A: minimum potential energy. Curve B: total energy of the fissioning system. Points 1 and 2: points where the minimum potential energy is equal to the total available energy. The shaded area shows the amount of free energy.

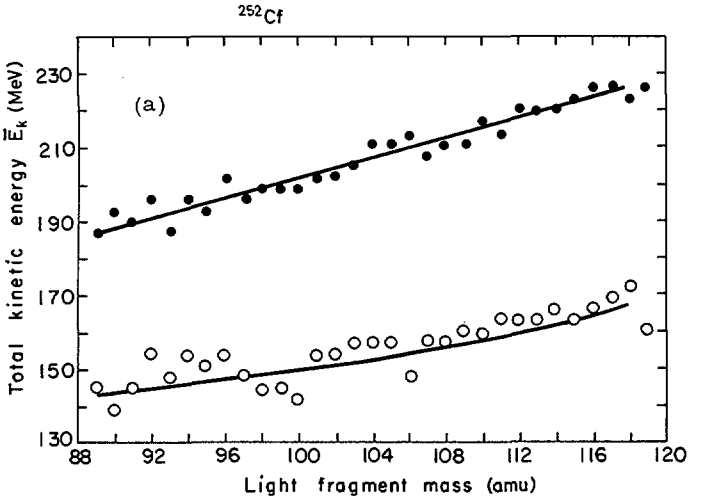

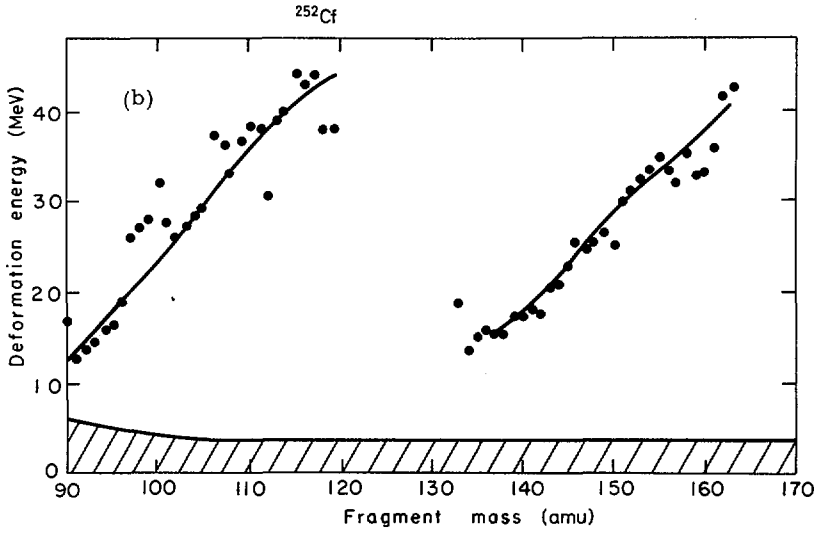

FIG. 30. (a) ● : Values of the maximum Coulomb energy at scission $E_k^{(1)}$ (m) as a function of light fragment mass. ○ : Values of the minimum Coulomb energy at scission $E_k^{(2)}$(m) as a function of light fragment mass. (b) ● : Values of the deformation energies of the fragments corresponding to the minimum Coulomb energy. The shaded area represents the range of possible values of the deformation energies for the maximum Coulomb energy configuration. The full lines give an idea of the errors.

energy, additional potential energy or intrinsic excitation energy. For all points between 1 and 2 the system can occupy a whole range of states and thereby the variances of the excitation energies of the fragments should not vanish. At points (1) and (2) all the available energy is necessary to provide the necessary potential energy, and the system has no additional freedom. At these points we can therefore write that

$$C_1 = E_k^{(1)}(m) \qquad D_1^{(1)} = E_1^{(1)}(m) \qquad D_2^{(1)} = E_2^{(1)}(m)$$

$$C_2 = E_k^{(2)}(m) \qquad D_1^{(2)} = E_1^{(2)}(m) \qquad D_2^{(2)} = E_2^{(2)}(m)$$

The above treatment therefore provides, for each mass ratio of the fragments, two points along the minimum potential energy scission line where the Coulomb interaction energy and the fragment's deformation energies are known. Figure 30 displays the values for these quantities as obtained from the experiment on the spontaneous fission of ^{252}Cf. It would be interesting to study the behaviour of the variances of the excitation energy as a function of the excitation of the nucleus undergoing fission. Such studies could perhaps provide additional points on the potential energy surface. Some additional information can also be obtained using a slightly modified two-spheroid model. We assume that the potential energy P along the scission line has a minimum for a value C_0 of the Coulomb potential. We further assume that the potential energy can be satisfactorily approximated by a parabola so that

$$C_o = \frac{C_1 + C_2}{2}$$

The potential energy can therefore be written as

$$P = C + D = P_o + a(C - C_o)^2$$

which gives for the deformation energy

$$D = P_o + a(C - C_o)^2 - C$$

If Q is the energy released in fission, we can also write

$$Q = P_o + a(C_1 - C_o)^2 = P_o + a(C_2 - C_o)^2 = P_o + a\Delta C^2$$

since the points (1) and (2) are such that the potential energy is equal to the energy release, as shown earlier.

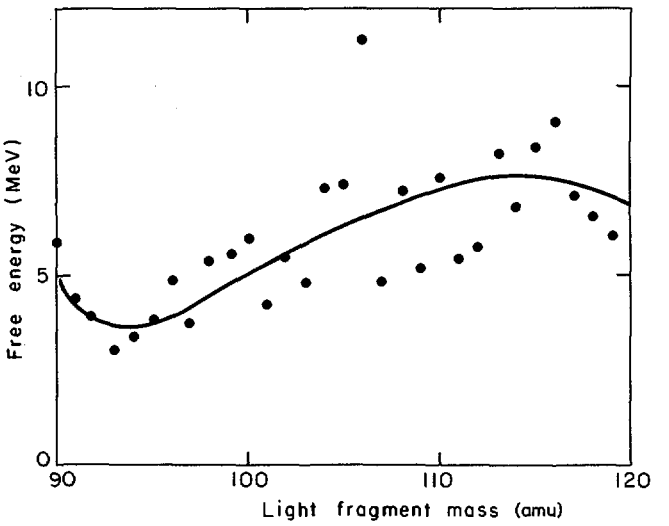

FIG. 31. Maximum "free energy" available at scission as a function of light fragment mass.

We make the further assumption, as in the two-spheroid model, that there exists a value C^* where both

$$D(C^*) = 0 \quad \text{and} \quad \left(\frac{dD(C)}{dC}\right)_{C=C^*} = 0$$

These conditions are written:

$$C^* - C_o = \frac{1}{2a}$$

$$4a^2 \Delta C^2 - 4a(Q - C_o) + 1 = 0$$

We make the further assumption that $C^* > Q$ (this is equivalent to the assumption that the fragments are always elongated at scission) and obtain

$$P = Q + \frac{[(C - C_o)^2 - \Delta C^2]}{2 \Delta C^2} \times [Q - C_o - \sqrt{(Q - C_o)^2 - \Delta C^2}]$$

The maximum energy of the system which is not tied up in potential energy is obtained for $C = C_0$ and amounts to

$$Q - P(C_o) = \frac{1}{2}((Q - C_o) - \sqrt{(Q - C_o)^2 - \Delta C^2})$$

The variations of this quantity as a function of the mass of the light fragment are shown in Fig. 31. It is an upper limit for both the pre-scission kinetic energy and total intrinsic excitation energy.

It can be seen on Fig. 30, that the values of the maximum energy which is not tied up in potential energy are surprisingly small. They rise slightly from the most asymmetric splits to the most probable ones where it reaches a value of approximately 7 MeV. Although the error on that number is difficult to estimate, it should not exceed 50%. It appears doubtful that the statistical approach of Fong [52] could be justified with excitation energies of the fragments as low as 4 MeV. On the other hand, pre-scission kinetic energies of 40 MeV which have been obtained in some computations [53, 54] seem to be ruled out. In that respect it is worth recalling that the early α-accompanied fission experiments [55] which seemed to confirm this high figure have been improved and yield much smaller values [56, 57]. The study of the even-odd effect reported in Section 2 provides an additional experimental approach to fission dynamics.

4.2. Even-odd effects and quasiparticle excitations in the fission process

The production of two odd-charge fragments in the fission of an even-charge nucleus requires the breaking of at least one proton-pair bond. For low excitation fission where the nucleus can be considered as cold at the saddle point as well as for spontaneous fission the corresponding two quasi-particle excitation must occur somewhere between saddle and scission. If the time difference between the instant when this excitation takes place and the instant of scission is longer than the characteristic time of a nucleon in the nucleus (approximately 2×10^{-22}s) the two unpaired protons can be freely exchanged between the two nascent fragments before scission takes place. At scission the positions of the two protons can be considered to be uncorrelated. The probabilities to observe two odd-charge or two even-charge fragments will therefore be equal. If two even-charge fragments are observed one of them would have at least one two-quasiparticle excitation. While the excitation energies of the even-Z fragments will be higher by approximately 2.5 MeV than those of the odd-Z ones, the observed total kinetic energies should not differ for the two cases. The experimental results show that approximately two-thirds of the pairing energy appears as fragment's kinetic energy, in contradiction with the above prediction. We conclude that most of the even-Z fragments are produced in the absence of quasiparticle excitation.

It is known that the yields of odd-Z fragments do not differ markedly from those of even-Z ones. The radiochemical measurements [58] appear to show a slight enhancement by approximately 30% of the even-charge elements. In the following we shall assume that this enhancement is 50%. If we again make the hypothesis that the two-quasiparticle excitation required to produce odd-Z fragments occurs at a relatively long time before scission, and that the energy of approximately 2.5 MeV necessary to break the proton-proton bond comes entirely from the kinetic energy of the fragments, an average difference of 1.25 MeV in kinetic energy should be observed between odd-Z and even-Z fragments. This is because half of the even-Z fragments should be formed with at least one two-quasiparticle excitation as explained above. Since the experimental figure is again higher than the predicted one, itself an upper limit, the hypothesis that the quasiparticle excitations occur a

long time before scission must be abandoned. It, therefore, appears that quasiparticle excitations occur only at the very late stage of the fission process with a probability close to 0.5.

These findings are contradictory to the basic assumptions of the statistical model of Fong [52]. They agree well with the calculations of Nörenberg [41] who found that the probability of level-slippage at the crossing of two levels differing by their number of particle-hole excitations was close to unity. This means that the structure of the level is conserved and therefore that the probability for quasiparticle excitations from saddle to scission is small.

An interesting check on the ideas just outlined would be to study the even-odd effect on fragment kinetic energies as a function of the excitation energy of the fissile nucleus. As soon as quasiparticle excitations would be possible at the saddle point, this even-odd effect should decrease markedly and eventually vanish.

4.3. Variances of the excitation energies

We have noticed the remarkable experimental result that the co-variance of the excitation energies for a fixed mass ratio $C(E_1, E_2: m)$ was very close to zero. We now show that this can be expected on the basis of a very schematic two-spheroid model with the assumption of equipartition of the energy.

Let α and β be the deformation parameters of the two fragments. The deformation energies of these fragments are assumed to be

$$D_1 = d_1 \alpha^2$$

$$D_2 = d_2 \beta^2$$

We further assume that around the minimum potential energy of the system the Coulomb energy is a linear function of α and β

$$C = V - K(\alpha + \beta)$$

The potential energy is then equal to

$$P = V - K(\alpha + \beta) + d_1 \alpha^2 + d_2 \beta^2$$

and can be written around the minimum

$$P - P_{min} = 2\, d_1(\alpha - \alpha_M)^2 + 2\, d_2(\beta - \beta_M)^2$$

If we assume thermal equilibrium, the probability to observe a deformation couple α, β is

$$p(\alpha,\beta) = \exp \frac{P(\alpha,\beta) - P(\alpha_M,\beta_M)}{T} = p(\alpha)\, p(\beta)$$

It follows that the two deformations behave independently and that

$$C(\alpha,\beta) = 0$$

and also that $C(D_1, D_2) = 0$.

We had previously assumed [59] that the variances of the deformation energies for a fixed value of the total kinetic energy

$$\sigma^2(D_1 : \ m\ E_k)$$

could be neglected. The above result shows that this cannot be the case since we have

$$0 = C(D_1,D_2 : \ m) = < \frac{dD_1}{dE_k} > < \frac{dD_2}{dE_k} > \sigma^2(E_k) + \underset{E_k}{\mathcal{M}}\ C(D_1,D_2 : \ m\ E_k)$$

and

$$\underset{E_k}{\mathcal{M}}\ C(D_1,D_2 : \ m\ E_k) = - < \frac{dD_1}{dE_k} > < \frac{dD_2}{dE_k} > \sigma^2(E_k)$$

Therefore, contrary to our original assumption [59], we find that the variances of the deformation energies are more important than those of the intrinsic excitation energies. Assuming that

$$C(E_1,E_2 : \ m) = C(D_1,D_2 : \ m) = 0$$

we obtain an average value of $C(E_1, E_2 : \ m\ E_k)$ of approximately

$$-\frac{\sigma^2(E_k)}{4} = -20\ \text{MeV}^2 = \overline{C(E_1,E_2 : \ m\ E_k)} = -\overline{\sigma^2(E_1 : \ m, E_k)}$$

in good agreement with the experimental values shown on Fig. 26.

The above treatment implied that the fluctuations of the intrinsic excitation energies were small. This is to be expected if the system behaves statistically except when the fluctuations become critical.

While in the previous sub-section we have shown that almost no quasi-particle excitations occurred in the descent from saddle to scission, we had not ruled out the possibility of a strong coupling of collective states within what Nörenberg [41] defines as a fission band. Nörenberg predicts that such a strong coupling should exist and that a statistical treatment of the system near scission should be adequate. We have shown above that such a treatment predicts, at least qualitatively, the values of the variances of the excitation energy. We have not shown, however, that other models would fail to predict these values. It appears, at this time, that the strongest argument in favour of the "fission band" model comes from another kind of experiment where the total kinetic energies obtained in induced and spontaneous fission of the same nucleus are compared [60]. It appears that only a small fraction of the increase in excitation energy of the fissioning system appears as additional kinetic energy. This suggests a strong damping of the fission mode on the first part of the way from saddle to scission.

CONCLUSION

In conclusion, we should like to summarize the information which appears to us relevant to fission theory and which has been explained in detail previously. We also wish to suggest some possible future developments as regards experiments.

The γ-ray emission by fission fragments can be explained within the framework of the theory of statistical decay of excited nuclei provided angular momentum effects are included. The anisotropy of the fission γ-rays, as well as the correlation between total γ-ray energies and excitation energies, can be explained in the framework of the "fission band" model of Nörenberg [41].

The experimentally determined variances of the excitation energies of the fragments yield values of the minimum potential energy of the system near scission which are surprisingly high, allowing for less than 10 MeV in pre-scission kinetic energy or internal excitation.

The study of the even-odd fluctuations of the total kinetic energy of the fragments points to a very small probability for two-quasiparticle excitations in the descent from saddle to scission. On the other hand, the comparison between total kinetic energy in induced and spontaneous fission is easily explained in terms of a strong damping of the fission mode into other excitation modes. Those two features are reconciled in the "fission band" model which predicts the right order of magnitude for the variances of the excitation energies.

As far as the experimental situation is concerned, we have seen that some some discrepancies remain with respect to a satisfactory account of the energy balance in fission. The main cause of uncertainty lies in the kinetic energy measurements; our knowledge of the energy resolution and tailing obtained with fragment detectors needs to be improved. The availability of heavy-ion beams or of separated beams of fission fragments should help to obtain this information.

The better accuracy obtained in measurements of average neutron numbers has not been accompanied by similar progress in obtaining the average neutron kinetic energies; the time has perhaps come to improve on the measurements of Bowman and co-workers [1]. In particular, the

question of the isotropic component in neutron emission remains mostly open not only with respect to its behaviour as a function of the masses and kinetic energies of the fragments but also regarding its very existence. A better knowledge of the neutron kinetic energy and angular distributions could in turn allow an improvement of the neutron variance measurements; it could also help resolve the present discrepancies between variance measurements using large and small detectors, respectively. It is important that this discrepancy be resolved so that the less cumbersome small detector method could be used safely.

The neutron variance measurements, if carried out at varying excitation energies of the fissile nucleus, could provide more points on the potential energy surface and perhaps more sensitive tests of models for fission dynamics.

Regarding the γ-ray measurements, it has usually been assumed that their angular distribution was not significantly perturbed by the hyperfine interaction. It appears [61] that such an assumption might not be justified since deorientation effects are very important for highly ionized rare-earth nuclei.

Finally, the study of even-odd effects on kinetic energy as a function of excitation energy of the compound nucleus should be a useful test of the conclusions we have reached here and eventually provide information on the number of two-quasiparticle excitations at the saddle point.

APPENDIX I

EFFECT OF AN ISOTROPIC COMPONENT ON THE DETERMINATION OF THE AVERAGE NUMBER OF NEUTRONS EMITTED BY FISSION FRAGMENTS

We consider a fission event in which ν_1 neutrons are emitted by fragment 1, ν_2 by fragment 2 and assume ν_a scission neutrons. When fragment 1 flies towards the neutron detector the average number of detected neutrons will be

$$g_1 = \varepsilon\, \nu_1 + r\, \nu_2 + a\, \nu_a$$

where ϵ is the efficiency for neutrons emitted by fragments flying towards the detector, r the efficiency for neutrons emitted by the complementary fragment and a the efficiency for detecting scission neutrons. We assume that ϵ and r are independent of the fragment's characteristics. Then, when fragment 2 flies towards the neutron detector we have

$$g_2 = \varepsilon\, \nu_2 + r\, \nu_1 + a\, \nu_a$$

and

$$g_1 + g_2 = (\varepsilon + r)(\nu_1 + \nu_2) + 2a\, \nu_a$$

When we neglect the pre-scission component we assume that n_1 and n_2 neutrons are emitted by the two fragments so that

$$g_1 = \epsilon' n_1 + r' n_2$$

$$g_2 = \epsilon' n_2 + r' n_1$$

The efficiencies ϵ' and r' are assumed to be proportional to ϵ and r

$$\epsilon' = \alpha \epsilon \qquad r' = \alpha r$$

As explained in the text the proportionality constant is determined by writing

$$g_1 + g_2 = (\epsilon' + r')(n_1 + n_2) = \alpha(\epsilon + r)(n_1 + n_2)$$

with

$$n_1 + n_2 = \nu_1 + \nu_2 + \nu_a = \nu_T$$

so that

$$\alpha(\epsilon + r)(\nu_1 + \nu_2 + \nu_a) = (\epsilon + r)(\nu_1 + \nu_2) + 2a\,\nu_a$$

from which we obtain

$$\alpha = 1 + \frac{\nu_a}{\nu_T}\left(\frac{2a}{\epsilon + r} - 1\right)$$

and

$$n_1 = \frac{1}{2}\left[\nu_1\left(1 + \frac{1}{\alpha}\right) + \nu_2\left(1 - \frac{1}{\alpha}\right) + \nu_a\right]$$

$$n_2 = \frac{1}{2}\left[\nu_2\left(1 + \frac{1}{\alpha}\right) + \nu_1\left(1 - \frac{1}{\alpha}\right) + \nu_a\right]$$

We now consider two limiting cases. In the first one a large neutron detector is seen from the source through an angle of 90°. Then, if one assumes that all efficiencies are proportional to the related solid angles, one can see that

$$\frac{2a}{\varepsilon + r} = 1 \quad \text{and} \quad \alpha = 1$$

so that

$$n_{(1,2)} = \nu_{(1,2)} + \frac{\nu_a}{2}$$

We see that in this case, the assumption that all neutrons are emitted by the fragments is equivalent to an equal sharing of the pre-scission component between the two fragments. Furthermore, the condition $n_1 + n_2 = \nu_T$ is always fulfilled. In the second case we consider a low-efficiency detector. We therefore can neglect r and

$$\alpha = 1 + \frac{\nu_a}{\nu_T}\left(\frac{2a}{\varepsilon} - 1\right) \qquad \text{(A.I.1)}$$

Assuming a Maxwellian shape for the centre-of-mass fragment neutron spectrum we have

$$\frac{\varepsilon}{a} = 2\sqrt{\frac{E_\rho}{\pi T}}\, e^{-\frac{E_\rho}{T}} + \left(1 + P\left(\sqrt{\frac{2E_\rho}{T}}\right)\right)\left(1 + \frac{2E_\rho}{T}\right) \qquad \text{(A.I.2)}$$

where E_ρ is the energy per nucleon of the fission fragment, T is the neutron spectrum temperature and

$$P\left(\sqrt{\frac{2E_\rho}{T}}\right) = \frac{1}{\sqrt{2\pi}} \int_{-\sqrt{\frac{2E_\rho}{T}}}^{+\sqrt{\frac{2E_\rho}{T}}} e^{-\frac{t^2}{2}}\, dt$$

Typical values of E_ρ/T are around 0.5. Then

$$\frac{\varepsilon}{a} \sim 4$$

and

$$\alpha \sim 1 - \frac{\nu_a}{\nu_T} \times 0.5$$

From Eq. (A.I.1) it can be seen that the value of α which ensures that the condition $n_1 + n_2 = \nu_T$ is fulfilled will depend on the fission event's characteristics with respect to both the value of ν_a/ν_T and that of a/ϵ. Alternatively,

if one uses the value of α obtained for the average characteristics of the fission fragments, one obtains

$$n_1' + n_2' = \nu_T + 2\,\nu_a a\left(\frac{1}{\epsilon} - \frac{1}{\epsilon'}\right)$$

where $n_1'+n_2'$ represents the average total number of neutrons as obtained with the assumption that there are no pre-scission neutrons, ϵ and ϵ' are the efficiencies computed for the average and the specific fission events, respectively. In particular, one obtains for the slopes with respect to E_k

$$< \frac{d(n_1' + n_2')}{dE_k} > = < \frac{d\nu_T}{dE_k} > + 2\,\frac{\nu_a\, a^2}{\epsilon^2} \; < \frac{d\epsilon(E_k)/a}{dE_k} >$$

With typical values of the variations of E_ρ/T in Eq. (A.I.2), one obtains a relative increase of a few per cent in the slopes of the variation of the average total number of neutrons as a function of E_k. The error on ν_T itself is of the order of 0.1 neutron.

APPENDIX II

A STUDY OF TWO CAUSES OF SYSTEMATIC ERRORS IN THE MEASUREMENT OF NEUTRON NUMBER VARIANCES

1. Recoil effect

Gavron [8] has pointed out that the hypothesis of isotropic emission of the neutrons, usually made to obtain pre-neutron masses and kinetic energies from the post-neutron energies of the fission fragments, was no longer valid when the neutrons were detected with small detectors. We first present the treatment given by Gavron for the case of average neutron number measurements. We then extend his treatment to the measurement of covariances of the neutron distributions.

Using Gavron's notation, V_F is the velocity of the fragment before the detected neutron is emitted, V_F' its velocity after emission of the neutron, V' and θ' are the velocities and angle of emission of the neutron in the fragment frame, V and θ the corresponding quantities in the laboratory system.

The final energy of the fragment when a neutron is detected at the angle θ will differ from that of the isotropic case, when no neutron is detected, by

$$e_{1F}(\theta) - e_{1F}(is) = -\frac{2e_1}{m_1}\left(\frac{V\cos\theta}{V_F} - 1\right)$$

where $e_{1F}(\theta)$ is the final energy of the fragment when a neutron is detected at angle θ, e_{1F} (is) the same energy in the isotropic case, e_1 and m_1 the pre-neutron emission kinetic energy and mass of fragment 1.

The pre-neutron energy of the fragment is then equal to

$$e_1' = e_{1F}\left(1 + \frac{\bar{\nu}_1(m_1, e)}{m_1}\right) - \frac{2\, e_{1F}}{m_1}\left(\frac{V \cos\theta}{V_F} - 1\right)$$

When the recoil effect is not taken into account the pre-neutron energy is written

$$e_1 = e_{1F}\left(1 + \frac{\bar{\nu}_1(m_1, e)}{m_1}\right)$$

$\bar{\nu}_1(m_1, e)$ is the average number of neutrons emitted by the fragment of mass m_1 and for a total kinetic energy $e = e_1 + e_2$.

The average neutron number is given by the ratio of two counting rates. The numerator $N_C(e, m_1)$ is proportional to the number of triple coincidences between the fragment and neutron detectors, the denominator $N_T(e, m_1)$ to the number of double coincidences between the fragment detectors. When the recoil correction is not included one obtains

$$\bar{\nu}_1(e) = \frac{N_C(e, m_1)}{N_T(e, m_1)}$$

when it is included one should write

$$\bar{\nu}_1'(e) = \frac{N_C(e', m_1')}{N_T(e, m_1)}$$

Gavron has shown that the error made in assuming that $m = m'$ was not great; therefore, in the following we will not consider the m dependence. If we make a first-order expansion in e we obtain

$$\bar{\nu}_1' - \bar{\nu}_1 = \frac{1}{N_T(e)}(e' - e)\frac{d\, N_C(e)}{de} = \frac{1}{N_T(e)}(e' - e)\frac{d\, \bar{\nu}_1 N_T(e)}{de}$$

$$= (e' - e)\frac{d\bar{\nu}_1}{de} + \frac{1}{N_T(e)}\bar{\nu}_1(e' - e)\frac{dN_T(e)}{de}$$

We now assume that $N_T(e)$ is a Gaussian function of the total kinetic energy so that

$$\frac{dN_T/de}{N_T} = - \frac{(e - \bar{e})}{\sigma^2}$$

where $\bar{e}$ is the most probable value of e, and σ^2 is the variance of $N_T(e)$.

The difference e' - e arises only from the difference between e_1 and e_1'. We then obtain

$$\Delta\bar{\nu}_1 = \bar{\nu}_1' - \bar{\nu}_1 = \frac{-2m_2 e}{m_1(m_1+m_2)} \left(\frac{V\cos\theta}{V_F} - 1\right)\left(\frac{d\bar{\nu}_1}{de} - \frac{\bar{\nu}_1(e-\bar{e})}{\sigma^2}\right) \qquad \text{(A. II. 1)}$$

This expression also allows the study of the difference in slope between the corrected and uncorrected data. We neglect the second derivative $d^2\bar{\nu}_1/de^2$, so that:

$$\frac{d\bar{\nu}_1'}{de} - \frac{d\bar{\nu}_1}{de} = \frac{-2m_2}{m_1(m_1+m_2)}\left(\frac{d\bar{\nu}_1}{de} - \frac{\bar{\nu}_1(e-\bar{e})}{\sigma^2} - \frac{\bar{\nu}_1 e}{\sigma^2} - \frac{e(e-\bar{e})}{\sigma^2}\frac{d\bar{\nu}_1}{de}\right)\left(\frac{V\cos\theta}{V_F} - 1\right)$$

(A. II. 2)

the dominant term in the parenthesis is $-\bar{\nu}_1 e/\sigma^2$. In Eq. A. II. 2, setting $\cos\theta = 1$, $V/V_F = 2$ and writing the same equation for the complementary fragment, one obtains an estimate of the difference in the slopes of the variations of the total number of neutrons

$$\overline{\frac{d\bar{\nu}_T'}{de} - \frac{d\bar{\nu}_T}{de}} = - 0.07$$

For example, if the true value $(d\bar{\nu}_T'/de)^{-1}$ is -8.3 MeV, the uncorrected value would yield -5.26 MeV.

In the small neutron detector measurements of the co-variances the quantity

$$M(e) = \frac{N_4(e)}{N_1^C(e)\, N_2^C(e)}$$

is provided by the experiment, the co-variance being given by

$$\frac{C(\nu_1\, \nu_2)}{\bar{\nu}_1\, \bar{\nu}_2} = M - 1$$

Here the quantity $N_4(e)$ is proportional to the number of quadruple coincidences between two neutron detectors and two fragment detectors while

$N_1^C(e)$ and $N_2^C(e)$ are proportional to the number of triple coincidences between one of the neutron detectors and the two fragment detectors. Using the definitions of $\bar{\nu}_1$ and $\bar{\nu}_2$ we also can write that

$$C(\nu_1\ \nu_2) = \frac{N_4(e)}{N_1^C(e)\ N_2^C(e)}\ \bar{\nu}_1\ \bar{\nu}_2 - \bar{\nu}_1\ \bar{\nu}_2 = \frac{N_4(e)}{N_T^2(e)} - \bar{\nu}_1\ \bar{\nu}_2$$

We define

$$P(e) = \frac{N_4(e)}{N_T^2(e)}$$

The errors made in neglecting the recoil effect will then be

$$\Delta P = \frac{N_4(e') - N_4(e)}{N_T^2(e)}$$

and

$$\Delta C = \Delta P - \bar{\nu}_1\ \Delta\ \bar{\nu}_2 - \bar{\nu}_2\ \Delta\ \bar{\nu}_1$$

where $\Delta\bar{\nu}_1$ and $\Delta\bar{\nu}_2$ have been computed above.
We express ΔP as

$$\Delta P = \frac{1}{N_T^2(e)}\ \frac{dN_4(e)}{de}\ (e' - e) = \frac{1}{N_T^2}\ \frac{d'P(e)\ N_T^2(e)}{de}\ (e' - e)$$

$$= \left[\frac{d\ P(e)}{de} - 2P(e)\frac{e - \bar{e}}{\sigma^2}\right]\left[e_1' + e_2' - e_1 - e_2\right]$$

The quantity P(e) is very nearly equal to $\bar{\nu}_1\bar{\nu}_2$ since $C(\nu_1, \nu_2)$ is a small quantity so that:

$$\Delta P = \left[\bar{\nu}_1\ \frac{d\nu_2}{de} + \bar{\nu}_2\ \frac{d\nu_1}{de} - 2\bar{\nu}_1\bar{\nu}_2\ \frac{e - \bar{e}}{\sigma^2}\right]\left[e_1' + e_2' - e_1 - e_2\right]$$

From Eq. A. II. 1 we also have

$$\Delta \nu_1 = \left[\frac{d\nu_1}{de} - \frac{(e - \bar{e})\bar{\nu}_1}{\sigma^2} \right] (e'_1 - e_1)$$

and

$$\Delta \nu_2 = \left[\frac{d\nu_2}{de} - \frac{(e - \bar{e})\bar{\nu}_2}{\sigma^2} \right] (e'_2 - e_2)$$

We then obtain:

$$\Delta C = \frac{e'_1 - e_1}{e'_2 - e_2} \bar{\nu}_1 \Delta\bar{\nu}_2 + \frac{e'_2 - e_2}{e'_1 - e_1} \bar{\nu}_2 \Delta\bar{\nu}_1$$

and inserting typical values of V, V_F and σ^2 we obtain

$$\Delta C \sim -0.56 + (e - \bar{e})\, 0.14$$

The correction is of the same order of magnitude as the co-variances themselves. It usually has a tendency to yield positive correlations.

2. Variations of the efficiencies with neutron multiplicity

We shall consider, as an example, the obtaining of co-variances with small neutron detectors. The measured quantity M ($\equiv$ M(e)) is equal to

$$M = \frac{\overline{\varepsilon_1 \nu_1 \varepsilon_2 \nu_2}}{\overline{\varepsilon_1 \nu_1}\ \overline{\varepsilon_2 \nu_2}}$$

and it is assumed that ϵ_1 and ϵ_2 do not depend on ν_1 and ν_2. In that case

$$M = \frac{\overline{\nu_1 \nu_2}}{\bar{\nu}_1\, \bar{\nu}_2}$$

However, even for fixed masses and total kinetic energies of the fragments it must be expected that the centre-of-mass velocities of the neutrons will depend on their multiplicity. Therefore, the efficiencies should themselves depend on the neutron multiplicity. To first order we write

$$\varepsilon_1(\nu_1) = \varepsilon_1 + k_1 \varepsilon_1 (\nu_1 - \bar{\nu}_1)$$

and similarly

$$\varepsilon_2(\nu_2) = \varepsilon_2 + k_2\varepsilon_2(\nu_2 - \bar{\nu}_2)$$

It is expected that the values of the efficiencies should decrease with neutron numbers so that k_1 and k_2 should be negative. For the sake of simplicity we assume that $k_1 = k_2$. Then, to first order

$$M = \frac{\overline{\varepsilon_1(1 + k(\nu_1 - \bar{\nu}_1))\nu_1 \; \nu_2(1 + k(\nu_2 - \bar{\nu}_2))\varepsilon_2}}{\overline{\varepsilon_1(1 + k(\nu_1 - \bar{\nu}_1))\nu_1} \; \overline{\varepsilon_2(1 + k\,\varepsilon_2(\nu_2 - \bar{\nu}_2))\nu_2}}$$

$$= \frac{\overline{\nu_1\nu_2} + k[\overline{\nu_1\nu_2(\nu_1 - \bar{\nu}_1)} + \overline{\nu_1\bar{\nu}_2(\nu_2 - \bar{\nu}_2)}]}{\bar{\nu}_1\,\bar{\nu}_2 + k[\overline{\nu_1(\nu_1 - \bar{\nu}_1)}\bar{\nu}_2 + \overline{\nu_2(\nu_2 - \bar{\nu}_2)}]\bar{\nu}_1}$$

We assume that, since the total kinetic energy and masses of the fragments are fixed, $\nu_1 + \nu_2 = \nu_T = \bar{\nu}_1 + \bar{\nu}_2$ and one has

$$M = \frac{\overline{\nu_1\nu_2}}{\bar{\nu}_1\,\bar{\nu}_2\left(1 + k\left(\frac{\sigma^2(\nu_1)}{\bar{\nu}_1} + \frac{\sigma^2(\nu_2)}{\bar{\nu}_2}\right)\right)}$$

and since $\nu_1 + \nu_2 = \nu_T$

$$\sigma^2(\nu_1) = \sigma^2(\nu_2) = -C'(\nu_1,\nu_2)$$

so that

$$M = \frac{\overline{\nu_1\nu_2}}{\bar{\nu}_1\,\bar{\nu}_2\left(1 - k\,\frac{C'(\nu_1,\nu_2)\nu_T}{\bar{\nu}_1\,\bar{\nu}_2}\right)}$$

which leads to

$$\frac{C'(\nu_1\,\nu_2)}{\bar{\nu}_1\,\bar{\nu}_2}\;(1 + k\,M\,\nu_T) = M - 1$$

If the variations of the efficiency had not been taken into account we would have

$$\frac{C\ (\nu_1,\nu_2)}{\bar{\nu}_1\ \bar{\nu}_2} = M - 1$$

The quantity M is close to 1 and ν_T to 4. Values of k of the order of -0.2 appear possible and in that case $C' = 5C$.

This is again of the same order of magnitude as the observed quantities.

ACKNOWLEDGEMENTS

One of us, H. Nifenecker, has greatly benefitted from the hospitality of the Lawrence Berkeley Laboratory. He is deeply indebted to S. G. Thompson, who made available the data used in the study of even-odd effects on the fragments' total kinetic energy, and whose continuous interest has been of great help. It is also a pleasure to thank R. C. Jared for his help in sorting out the kinetic energy data. Most fruitful discussions with J. J. Griffin, S. S. Kataria, M. Kleber, H. Krappe, L. Moretto, W. Myers, G. Sussmann, W. Swiatecki, C. F. Tsang, and J. B. Wilhelmy have very much helped in writing this review.

REFERENCES

[1] BOWMAN, H.R., THOMPSON, S.G., MILTON, J.C.D., SWIATECKI, W.J., Phys.Rev. 126 (1962) 2120.
[2] MILTON, J.C.D., FRASER, J.S., in Physics and Chemistry of Fission (Proc.Symp.Salzburg, 1965) 2, IAEA, Vienna (1965) 39.
[3] APALIN, V.F., GRITYUK, Y.N., KUTIKOV, I.E., LEBEDEV, V.I., MIKAELYAN, L.A., Nucl.Phys. 55 (1964) 249.
[4] WHETSTONE, S.L., Phys.Rev. 100 (1956) 1016.
[5] MASLIN, E.E., RODGERS, A.L., CORE, W.G.F., Phys.Rev. 164 (1967) 1520.
[6] BOLDEMAN, J.W., MUSGROVE, A.R.L., WALSH, R.L., Aust.J.Phys. 24 (1971) 821.
[7] SIGNARBIEUX, C., NIFENECKER, H., POITOU, J., RIBRAG, M., J.Phys. 33 8-9, Suppl.C-5 (1972) I.23.
[8] GAVRON, A., Correction of Experimental Results in Fission Experiments, to be published.
[9] TERRELL, J., Phys.Rev. 127 (1962) 880.
[10] RIBRAG, M., POITOU, J., SIGNARBIEUX, C., MATUSZEK, J., Etude d'un ensemble de détection destiné à mesurer la multiplicité de l'émission neutronique dans les réactions nucléaires, CEA, Internal Rep., SMPNF/853/71 (1971).
[11] BOLDEMAN, J.W., DALTON, A.W., Rep. AAEC/E172 (1962).
[12] MACKLIN, R.L., GLASS, F.M., HALPERIN, J., ROSEBERRY, R.T., SCHMITT, H.W., STOUGHTON, R.W., TOBIAS, M., Nucl. Instrum. Methods 102 (1972) 181.
[13] GAVRON, A., FRAENKEL, Z., unpublished.
[14] POITOU, J., NIFENECKER, H., SIGNARBIEUX, C., unpublished.
[15] SKARSVÄG, K., BERGHEIM, K., Nucl.Phys. 45 (1963) 72.
[16] KAPOOR, S.S., RAMANNA, R., RAMA RAO, D.N., Phys.Rev. 131 (1963) 283.
[17] NIFENECKER, H., SIGNARBIEUX, C., RIBRAG, M., POITOU, J., MATUSZEK, J., Nucl.Phys. A189 (1972) 285.
[18] MAIER-LEIBNITZ, H., SCHMITT, H.W., ARMBRUSTER, P., in Physics and Chemistry of Fission (Proc.Symp.Salzburg, 1965), 2, IAEA, Vienna (1965) 143.
[19] PLEASONTON, F., FERGUSON, R.L., SCHMITT, H.W., Phys.Rev. C 6 3 (1972) 1023.

[20] ARMBRUSTER, P., LABUS, H., REICHELT, K., Z.Naturforsch. A 26 (1971) 512.
[21] WILHELMY, J.B., CHEIFETZ, E., JARED, R.C., THOMPSON, S.G., BOWMAN, H.R., RASMUSSEN, J.O., Phys.Rev. C5 6 (1972) 2041.
[22] HOFFMAN, M.M., Phys.Rev. B 133 (1964) 714.
[23] IVANOV, O.I., KUSHNIR, Y.A., SMIRENKIN, G.N., Zh.Ehksp.Teor.Fiz.Pis'ma 6 10 (1967) 898.
[24] JOHANSSON, S.A.E., Nucl.Phys. 60 (1964) 378.
[25] ALBINSSON, H., Phys.Scr. 3 (1971) 113.
[26] ALBINSSON, H., Energies and Yields of Prompt Gamma Rays from Fragments in Slow Neutron Induced Fission of ^{235}U, Internal Rep.AE-420 (1971).
[27] CHEIFETZ, E., JARED, R.C., THOMPSON, S.G., WILHELMY, J.B., Phys.Rev.Lett. 25 (1970) 38.
[28] JOHN, W., WESOLOWSKI, J.J., GUY, F., Phys.Lett. 30B (1969) 340.
[29] VERBINSKY, V.V., WEBER, H., SUND, R.E., in Physics and Chemistry of Fission (Proc.Symp.Vienna, 1969), IAEA, Vienna (1969) 929.
[30] MEHTA, G., POITOU, J., RIBRAG, M., SIGNARBIEUX, C., Phys.Rev. C 7 (1973) 373.
[31] NARDI, E., MORETTO, L.G., THOMPSON, S.G., Phys.Lett. 43B (1973) 259.
[32] ALBINSSON, H., LINDOW, L., Prompt Gamma Radiation from Fragments in the Thermal Fission of ^{235}U, Internal Rep.AE-398 (1971).
[33] ALBINSSON, H., Yield of Prompt Gamma Radiation in Slow Neutron Induced Fission of ^{235}U as a Function of the Total Fragment Kinetic Energy, Internal Rep.AE-417 (1971).
[34] VAL'SKII, G.V., PETROV, G.A., PLEVA, Y.S., Sov.J.Nucl.Phys. 8 (1969) 171.
[35] NIFENECKER, H., SIGNARBIEUX, C., RIBRAG, M., POITOU, J., MATUSZEK, J., Nucl.Phys. A189 (1972) 285.
[36] GARVEY, G.T., GERACE, W.J., JAFFEE, R.L., TALMI, I., KELSON, I., Rev.Mod.Phys. 41 4 (1969) 81.
[37] WILKINS, B.D., FLUSS, M.J., KAUFMAN, S.B., GROSS, C.E., STEINBERG, E.P., Nucl.Instrum. Methods 92 (1971) 381.
[38] SCHMITT, H.W., PLEASONTON, F., Nucl.Instrum.Methods 40 (1966) 204.
[39] MORETTO, L.G., Nucl.Phys. A182 (1972) 641.
[40] RASMUSSEN, J.O., NÖRENBERG, W., MANG, H.J., Nucl.Phys. A136 (1969) 465.
[41] NÖRENBERG, W., "Zur mikroskopischen Beschreibung der Kernspaltung", Habilitationsschrift, Heidelberg University (1970).
[42] NIFENECKER, H., Nucl.Instrum.Methods 81 (1970) 45.
[43] GAVRON, A., FRAENKEL, Z., Phys.Rev.Lett. 27 (1971) 1148.
[44] BABINET, R., NIFENECKER, H., POITOU, J., SIGNARBIEUX, C., Paper IAEA-SM-174/41, these Proceedings, Vol.2.
[45] NIFENECKER, H., Thesis, CEA R4121 (1970).
[46] REISDORF, W., UNIK, J.P., GRIFFIN, H.C., GLENDENIN, L.E., Nucl.Phys. A177 (1971) 337.
[47] SIGNARBIEUX, C., POITOU, J., RIBRAG, M., MATUSZEK, J., Phys.Lett. 39B (1972) 503.
[48] TERRELL, J., in Physics and Chemistry of Fission, (Proc.Symp.Salzburg, 1965) 2, IAEA, Vienna (1965) 3.
[49] VANDENBOSCH, R., Nucl.Phys. 46 (1963) 129.
[50] DICKMANN, F., DIETRICH, K., Nucl.Phys. A129 (1969) 241.
[51] SCHMITT, H.W., in Physics and Chemistry of Fission (Proc.Symp.Vienna, 1969), IAEA, Vienna (1969) 67.
[52] FONG, P., Phys.Rev. 102 (1956) 434.
[53] NIX, J.R., SWIATECKI, W.J., Nucl.Phys. 71 (1965) 1.
[54] HASSE, R.W., in Physics and Chemistry of Fission (Proc.Symp.Vienna, 1969), IAEA, Vienna (1969) 33.
[55] BONEH, Y., FRAENKEL, Z., NEBENZAHL, I., Phys.Rev. 156 (1962) 1305.
[56] RAJAGOPALAN, M., THOMAS, T.D., Phys.Rev. C5 (1972) 2064.
[57] FLUSS, M.J., KAUFMAN, S.B., STEINBERG, E.P., WILKINS, B.D., Phys.Rev. C7 (1973) 353.
[58] WAHL, A.C., in Physics and Chemistry of Fission (Proc.Symp.Salzburg, 1965) 1, IAEA, Vienna (1965) 317.
[59] NIFENECKER, H., BABINET, R., SIGNARBIEUX, C., J.Phys. 33 8-9, Suppl.C-5 (1972) II.24.
[60] DERUYTTER, A.J., WEGENER-PENNING, G., Paper IAEA-SM-174/35, these Proceedings, Vol.2.
[61] STEPHENS, F., private communication.

ETUDE EXPERIMENTALE DE LA CORRELATION ENTRE LES NOMBRES DE NEUTRONS PROMPTS EMIS PAR LES DEUX FRAGMENTS COMPLEMENTAIRES DANS LA FISSION SPONTANEE DE ^{252}Cf

C. SIGNARBIEUX, R. BABINET, H. NIFENECKER, J. POITOU
CEA, Centre d'études nucléaires de Saclay,
Gif-sur-Yvette, France

Abstract–Résumé

EXPERIMENTAL STUDY OF THE CORRELATION BETWEEN THE NUMBERS OF PROMPT NEUTRONS EMITTED BY THE TWO COMPLEMENTARY FRAGMENTS IN SPONTANEOUS FISSION OF ^{252}Cf.

The large liquid scintillator method was used to measure the mean values $\bar{\nu}_1$ and $\bar{\nu}_T$ and the variances $\sigma^2(\nu_1)$ and $\sigma^2(\nu_T)$ of the distributions of the number of neutrons emitted per fragment and per fission as a function of the mass A of one of the fragments and the total kinetic energy E_K of both. The data on the mean values $\bar{\nu}_1(A, E_K)$ agree well qualitatively with earlier measurements of Bowman and co-workers except for the mass region above A = 150. On the reasonable assumption that the de-excitation modes of the two complementary fragments are independant, the correlation between the excitation energies of these fragments can be determined very simply from the variance data. For each mass ratio an anticorrelation is observed when the E_K value is fixed; the magnitude of this anticorrelation is maximum around the most probable E_K value and tends towards zero at the limits of the distribution $p(E_K)$. Moreover, the overall correlation of the excitation energy distribution (integrated over all the E_K values) is practically zero for all mass ratios. These results show clearly that the degree of freedom associated with the elongation of the nucleus towards fission is strongly coupled with other degrees of freedom of the system, which means that the rate of evolution of the system could be slow enough to justify the hypothesis of a state of quasi-equilibrium at the scission point.

ETUDE EXPERIMENTALE DE LA CORRELATION ENTRE LES NOMBRES DE NEUTRONS PROMPTS EMIS PAR LES DEUX FRAGMENTS COMPLEMENTAIRES DANS LA FISSION SPONTANEE DE ^{252}Cf.

La méthode du gros scintillateur liquide a été utilisée pour mesurer les valeurs moyennes $\bar{\nu}_1$ et $\bar{\nu}_T$ et les variances $\sigma^2(\nu_1)$ et $\sigma^2(\nu_T)$ des distributions du nombre de neutrons émis par fragment et par fission en fonction de la masse A de l'un des fragments et de l'énergie cinétique totale E_K des deux. Les données sur les valeurs moyennes $\bar{\nu}_1(A_1, E_K)$ sont en bon accord qualitatif avec les anciennes mesures de Bowman et al., à l'exception toutefois de la région des masses supérieures à A = 150. Si l'on fait l'hypothèse raisonnable que les modes de désexcitation des deux fragments complémentaires sont indépendants, les données sur les variances permettent de déterminer très simplement la corrélation des énergies d'excitation de ces deux fragments. Pour chaque rapport des masses, on observe une anticorrélation qui est maximale au voisinage de la valeur la plus probable de E_K et qui tend vers zéro aux bornes de la distribution $p(E_K)$. Par ailleurs la corrélation globale de la distribution des énergies d'excitation (intégrée sur toutes les valeurs de E_K) est pratiquement nulle pour tous les rapports des masses. Ces résultats montrent clairement que le degré de liberté associé au mouvement d'élongation du noyau vers la fission est fortement couplé à d'autres degrés de liberté du système, de telle sorte que la vitesse d'évolution du système pourrait être assez basse pour justifier l'hypothèse d'un état de quasi-équilibre au point de scission.

INTRODUCTION

Dans la fission des noyaux lourds pour lesquels les configurations de scission sont plus allongées que les configurations de point-selle, l'évolution du système entre le point-selle et la scission procède d'un mouvement

continu d'élongation du noyau. L'étude de cette «descente» vers la scission pose le problème du couplage entre le degré de liberté associé à ce mouvement d'élongation et les autres degrés de liberté du système. Dans le cas d'un couplage faible, la différence d'énergie potentielle entre le point-selle et la scission se retrouvera principalement sous forme d'énergie cinétique de translation des fragments et les énergies d'excitation de ces fragments proviendront de la déformation acquise dans ce mouvement d'élongation; il est alors raisonnable de penser que les énergies d'excitation de deux fragments de masses complémentaires sont fortement corrélées. Au contraire, un couplage fort entraînera un amortissement du mouvement d'élongation; l'énergie dissipée dans les autres degrés de liberté se retrouvera alors sous forme d'énergie d'excitation des fragments et tendra à diminuer la corrélation attendue dans le cas du couplage faible.

Nous ne possédons jusqu'à présent que quelques données fragmentaires et plutôt contradictoires [1-3] sur la valeur de la corrélation des énergies d'excitation de deux fragments complémentaires. Le but de la présente expérience était d'obtenir dans le cas de la fission spontanée de ^{252}Cf un ensemble complet de données sur les distributions d'énergies d'excitation et la corrélation de ces énergies en fonction des masses des fragments. Des résultats préliminaires ont déjà fait l'objet d'une courte publication [4].

1. METHODE EXPERIMENTALE

Nous allons montrer que si l'on fait des hypothèses raisonnables sur le mécanisme de désexcitation des fragments, la corrélation entre les énergies d'excitation E_{x_1} et E_{x_2} de deux fragments de masses complémentaires peut être déduite assez directement de la mesure de la corrélation entre les nombres de neutrons prompts ν_1 et ν_2 émis respectivement par chacun des deux fragments.

Pour une distribution de probabilité $P(E_{x_1}, E_{x_2}, \nu_1, \nu_2)$, on peut écrire en toute généralité une relation entre les covariances de la forme

$$\mathrm{COV}(\nu_1, \nu_2) = \mathrm{COV}(\bar{\nu}_1(E_{x_1}, E_{x_2}), \bar{\nu}_2(E_{x_1}, E_{x_2})) + \iint \mathrm{COV}(\nu_1, \nu_2 : E_{x_1}, E_{x_2})\, P(E_{x_1}, E_{x_2})\, dE_{x_1}\, dE_{x_2} \qquad (1)$$

Si l'on fait l'hypothèse que le mécanisme d'émission des neutrons prompts par un fragment est indépendant de l'état quantique du fragment complémentaire, la relation (1) s'écrit alors

$$\mathrm{COV}(\nu_1, \nu_2) = \mathrm{COV}(\bar{\nu}_1(E_{x_1}), \bar{\nu}_2(E_{x_2})) \qquad (2)$$

Si l'on fait l'hypothèse supplémentaire que, pour tous les fragments de même masse, il existe une régression linéaire de ν sur E_x de la forme

$$\nu = \lambda E_x + \mu \qquad (3)$$

la relation (2) appliquée à un couple de fragments de masses complémentaires A_1 et A_2 devient

$$\lambda_1 \lambda_2 \, COV(E_{x_1} \, E_{x_2} : A_1, \, A_2) = COV(\nu_1, \, \nu_2 : A_1, \, A_2) \qquad (4)$$

Pour chaque couple de masses, la valeur de $COV(\nu_1, \, \nu_2)$ peut être obtenue à partir de la mesure des variances des distributions $p(\nu_1)$, $p(\nu_2)$ et $p(\nu_1 + \nu_2)$ en utilisant la relation d'addition des variances:

$$2 \, COV(\nu_1, \, \nu_2) = \sigma^2(\nu_1 + \nu_2) - \sigma^2(\nu_1) - \sigma^2(\nu_2) \qquad (5)$$

Nous avons mesuré ces distributions à l'aide d'un scintillateur liquide de grand volume chargé au gadolinium et constitué de deux enceintes hémisphériques de 250 litres chacune qui étaient utilisées, soit juxtaposées pour constituer un détecteur 4π, soit séparément comme détecteur 2π.

En géométrie 4π (fig. 1) un tel détecteur de neutrons apparaît comme idéal pour mesurer la multiplicité des neutrons émis par fission, puisque son efficacité $\epsilon_{4\pi}$ est à la fois très élevée et pratiquement indépendante de l'énergie des neutrons.

Pour mesurer la multiplicité des neutrons émis par fragment, nous avons utilisé le fait que les neutrons prompts sont évaporés isotropiquement par les fragments totalement accélérés (l'existence d'une petite contribution de neutrons de scission — environ 10% — reste toujours controversée [5] et nous n'en avons pas tenu compte dans l'analyse de nos données). L'arrangement expérimental le plus satisfaisant consiste à placer un scintillateur hémisphérique en géométrie 2π par rapport à la direction de vol des fragments (fig. 1). Pour calculer les termes d'efficacité relatifs aux neutrons émis par chaque fragment, nous avons simulé par la méthode de Monte-Carlo le processus complet de détection des neutrons par le scintillateur en tenant compte des conditions géométriques exactes de l'expérience. Nous avons d'abord calculé les efficacités moyennes de détection $\bar{\epsilon}(e_n, \vec{V})$ et $\bar{\epsilon}(e_n, \overleftarrow{V})$ pour un neutron évaporé isotropiquement avec l'énergie e_n par un fragment animé d'une vitesse V (notée $\vec{V}$ ou $\overleftarrow{V}$ selon que le fragment se dirige dans la direction du détecteur ou dans la direction opposée). Etant donné

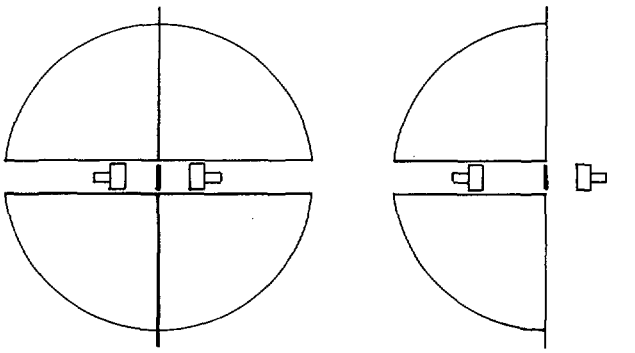

FIG. 1. Schéma de l'arrangement expérimental.

que le spectre d'émission d'un fragment dépend essentiellement du mode de scission (caractérisé par les vitesses V_1 et V_2 des deux fragments), nous avons calculé en fonction du couple (V_1 V_2) les termes d'efficacité $\bar{\epsilon}(\vec{V}_1)$, $\bar{\epsilon}(\overleftarrow{V}_1)$, $\bar{\epsilon}(\vec{V}_2)$ et $\bar{\epsilon}(\overleftarrow{V}_2)$ en pondérant les fonctions $\bar{\epsilon}(e_n, \vec{V})$ par les spectres d'énergie des neutrons prompts mesurés par Bowman et al. [6] pour la fission spontanée de ^{252}Cf. Typiquement, les valeurs de $\bar{\epsilon}(\vec{V})$ et $\bar{\epsilon}(\overleftarrow{V})$ ainsi calculées sont de l'ordre de 60% et 15% respectivement.

Si nous faisons la supposition que les termes d'efficacité sont indépendants de la multiplicité des neutrons émis (cette supposition, excellente dans la géométrie 4π, n'est qu'une approximation au premier ordre dans la géométrie 2π), les relations de corrections d'efficacité (démontrées dans la réf. [7]) s'écrivent comme suit:

$$\bar{q}_T = \epsilon_{4\pi}\ \bar{\nu}_T$$

$$\bar{q}_1 = \bar{\epsilon}(\vec{V}_1)\bar{\nu}_1 + \bar{\epsilon}(\overleftarrow{V}_2)\bar{\nu}_2$$

$$\bar{q}_2 = \bar{\epsilon}(\overleftarrow{V}_1)\bar{\nu}_1 + \bar{\epsilon}(\vec{V}_2)\bar{\nu}_2$$

$$\sigma^2(q_T) - \bar{q}_T = \epsilon_{4\pi}^2\,(\sigma^2(\nu_T) - \bar{\nu}_T) \qquad (6)$$

$$\sigma^2(q_1) - \bar{q}_1 = \bar{\epsilon}^2(\vec{V}_1)[\sigma^2(\nu_1) - \bar{\nu}_1] + \bar{\epsilon}^2(\overleftarrow{V}_2)[\sigma^2(\nu_2) - \bar{\nu}_2] + 2\bar{\epsilon}(\vec{V}_1)\,\bar{\epsilon}(\overleftarrow{V}_2)\,\mathrm{COV}(\nu_1, \nu_2)$$

$$\sigma^2(q_2) - \bar{q}_2 = \bar{\epsilon}^2(\overleftarrow{V}_1)[\sigma^2(\nu_1) - \bar{\nu}_1] + \bar{\epsilon}^2(\vec{V}_2)[\sigma^2(\nu_2) - \bar{\nu}_2] + 2\bar{\epsilon}(\overleftarrow{V}_1)\,\bar{\epsilon}(\vec{V}_2)\,\mathrm{COV}(\nu_1, \nu_2)$$

Les quantités notées q et ν se réfèrent respectivement aux distributions du nombre de neutrons détectés et émis.

Il est à noter que l'accord dans tout le domaine de variation de (V_1 V_2) entre les valeurs de $\bar{\nu}_T$, obtenues indépendamment dans les expériences 2π et 4π, constitue une excellente vérification de la validité des corrections d'efficacité.

L'installation expérimentale était la suivante: une source de ^{252}Cf de 10^4 fissions/minute, déposée sur un support de VYNS de 50 μg/cm^2, est placée au centre géométrique du détecteur de neutrons. Les deux fragments de fission sont détectés en coïncidence par deux détecteurs à barrière de surface de 3 cm^2, placés de part et d'autre de la source. Dans l'expérience 2π, la distance de ces détecteurs à la source était 1 cm et 4 cm respectivement de façon à orienter la direction de vol des fragments (à l'intérieur de ±20°) dans l'axe de révolution du scintillateur.

Les détails de notre détecteur et de l'électronique associée ont été publiés antérieurement [8]: pour caractériser la qualité de notre installation nous ne citerons que la valeur remarquablement faible du bruit de fond, qui était de 0,03 coup par porte de comptage de 35 μs pour une efficacité intrinsèque de détection des neutrons de 82%, ainsi qu'une excellente stabilité dans le temps de tous les paramètres mesurés.

2. ANALYSE DES DONNEES

Pour les deux expériences 2π et 4π, nous avons enregistré environ 10^6 événements tridimensionnels, à savoir les amplitudes des réponses

des deux détecteurs à semi-conducteur et le nombre de neutrons détectés dans le scintillateur.

L'analyse des données a été conduite selon les étapes suivantes:

– Calcul du nombre moyen de neutrons émis par fragment en fonction des paramètres μ et e_K(valeurs provisoires des masses et de l'énergie cinétique totale des fragments). Ces paramètres étaient calculés à partir des relations de calibration de Schmitt et al.[9].

– Calcul des valeurs moyennes et des variances des distributions de neutrons émis par fragment et par fission en fonction de A et E_K (masses et énergie cinétique totale des fragments primaires); les données neutroniques déterminées dans l'étape précédente permettent de calculer, pour chaque événement, les paramètres primaires à partir des paramètres provisoires selon les relations

$$A_1 = \frac{\mu_1 - \bar{\nu}_1(\mu_1, e_K)}{1 - \bar{\nu}_T(\mu_1, e_K)/A_0}$$

$$E_K = e_K\left(\frac{\mu_1}{A_1} + \frac{\bar{\nu}_2(\mu_1, e_K)}{A_2}\right) \qquad (7)$$

A étant la masse de ^{252}Cf.

– Calcul de la fonction de dispersion des paramètres A et E_K selon les relations

$$\sigma^2(A_1) = \frac{4}{3}\frac{\nu_T}{E_K}\bar{\eta}\frac{A_1 A_2}{A_0} + \frac{1}{4}\sigma^2(\nu_T) + \frac{A_1^2 + A_2^2}{E_K^2}\sigma^2(e_F)$$

$$\sigma^2(E_K) = 2\sigma^2(e_F) + \left(\frac{E_K}{A_0}\right)^2\left[\sigma^2(\nu_1)\left(\frac{A_1}{A_2}\right)^2 + \sigma^2(\nu_2)\left(\frac{A_2}{A_1}\right)^2\right] \qquad (8)$$

où $\bar{\eta}$ est l'énergie des neutrons dans le centre de masse du fragment et $\sigma^2(e_F)$ est la variance de la fonction de résolution des détecteurs à semi-conducteur [9], qui a été prise égale à 0,41 MeV^2.

– Correction des données neutroniques (obtenues dans la seconde étape) de la dispersion expérimentale sur A et E_K. Les données neutroniques étaient au préalable lissées par la méthode des moindres carrés.

Dans chacune des deux premières étapes, les données neutroniques expérimentales étaient successivement corrigées du temps mort de l'appareillage, du bruit de fond et de l'efficacité du scintillateur et normalisées sur une valeur de $\bar{\nu}_T$ de ^{252}Cf égale à 3,756.

3. RESULTATS ET DISCUSSION

L'ensemble des résultats sur les valeurs moyennes et les variances des distributions du nombre de neutrons prompts émis par fragment en fonction de leurs masses A et de leur énergie cinétique totale E_K est montré dans les figures 2a et 2b sous la forme de courbes de niveau. Nous avons

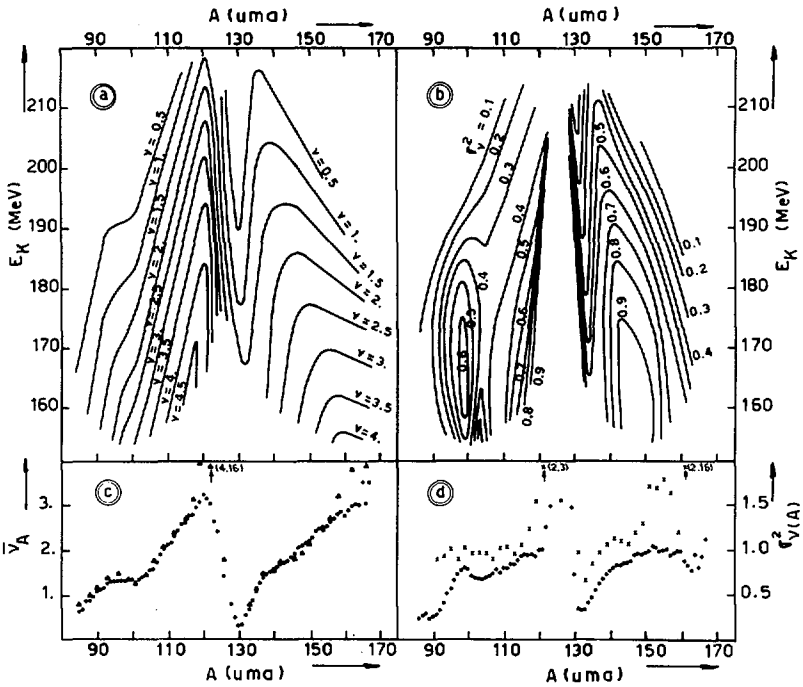

FIG. 2. Valeurs moyennes et variances des distributions du nombre de neutrons émis par fragment (données corrigées de la dispersion expérimentale sur les masses et les énergies cinétiques des fragments). Dans la figure 2c les triangles correspondent aux valeurs de Bowman et al. [6]; dans la figure 2d les croix correspondent aux valeurs de Gavron et Fraenkel [3].

comparé, dans les figures 2c et 2d, ces valeurs moyennes et variances en fonction de la masse – par intégration sur les distributions $p(E_K : A)$ – aux valeurs obtenues respectivement par Bowman et al. [6] et par Gavron et Fraenkel [3] qui utilisaient la méthode du petit scintillateur plastique pour mesurer la corrélation, dans le laboratoire, entre l'énergie et l'angle d'émission des neutrons par rapport à la direction des fragments.

En ce qui concerne les valeurs moyennes $\bar{\nu}_A$, le comportement en «dent de scie» est tout à fait similaire pour les deux expériences; néanmoins, les résultats diffèrent légèrement dans les régions de masses de faible probabilité et les différences sont beaucoup plus grandes en fonction de E_K. Gavron [10] a étudié en détail les causes d'erreur systématique dans la méthode du petit scintillateur; il a montré que les résultats de Bowman souffraient d'un manque de corrections nécessitées par l'aspect sélectif de la corrélation neutron-fragment; il a calculé que de telles corrections pouvaient rendre compte des différences observées entre les deux types d'expérience.

En ce qui concerne les variances $\sigma^2(\nu_A)$, la figure 2d montre que nos mesures sont en grand désaccord avec celles de Gavron et Fraenkel. On peut penser que les données obtenues par la méthode du petit scintillateur pourraient comporter des erreurs systématiques non contrôlées dans la

mesure où Gavron [10] a calculé, sur la base de ses résultats, que la variance $\sigma^2(\nu_T)$ de la distribution du nombre total de neutrons prompts émis dans la fission de ^{252}Cf était égale à 5,337, valeur considérablement plus élevée que la valeur de 1,56 déterminée à 3% près par de nombreux auteurs (voir réf. [8]). La variation de $\sigma^2(\nu_A)$ en fonction de A trouvée dans la présente expérience montre un comportement en dent de scie assez similaire à la variation de $\bar{\nu}_A$: ce résultat n'est pas surprenant, puisque la distribution $p(\nu_A)$ est le produit de la convolution de la distribution $p(E_{x_A})$ par une fonction de dispersion $g(\nu : E_{x_A})$ due à la nature statistique du nombre de neutrons évaporés, et que cette fonction est d'autant plus dispersive que l'énergie d'excitation E_{x_A} (et par conséquent $\bar{\nu}_A$) est plus élevée.

Comme on peut voir dans les figures 2b et 2d, il existe, dans la région des masses voisines de 100, un pic statistiquement significatif de la variance $\sigma^2(\nu_A)$; cette anomalie est clairement corrélée à un changement de la pente $d\bar{\nu}_A/dA$ dans la même région de masses. Dans la mesure où ce comportement particulier n'est pas observé dans la région des masses complémentaires, il semble légitime de l'attribuer aux propriétés liées à la désexcitation de ces fragments.

Dans la figure 3 sont montrées, pour le couple de masses (108-144), les variations de $\bar{\nu}$ et $\sigma^2(\nu)$ pour chaque fragment et de $COV(\nu_1, \nu_2)$ en fonction de l'énergie cinétique totale E_K des deux fragments. Les deux séries de résultats présentées sur la figure correspondent à deux analyses différentes de nos données; les ronds se réfèrent aux données de Bowman et al. [6], qui n'étaient pas corrigées de la dispersion expérimentale, les triangles se réfèrent à ces mêmes données, mais corrigées par nous de la dispersion. On peut constater que l'influence de cette correction est faible sur les valeurs moyennes et importante sur les valeurs des variances et de la covariance.

Pour discuter de la variation de $COV(\nu_1, \nu_2)$ en fonction de E_K, il est utile de montrer que cette covariance est proportionnelle aux variances des distributions des énergies d'excitation des deux fragments. En effet, pour un rapport de masses fixe, la valeur du Q de la réaction est égale à la somme des énergies d'excitation E_{x_1} et E_{x_2} et de l'énergie cinétique totale E_K des deux fragments, soit:

$$Q = E_{x_1} + E_{x_2} + E_K \tag{9}$$

En conséquence, pour une valeur de E_K fixée, E_{x_1} et E_{x_2} sont strictement anticorrélés, ce qui s'exprime par la relation

$$COV(E_{x_1}, E_{x_2} : A, E_K) = -\sigma^2(E_{x_1} : A, E_K) = -\sigma^2(E_{x_2} : A, E_K) \tag{10}$$

et on obtient, à partir de la relation (4),

$$COV(\nu_1, \nu_2 : A, E_K) = -\lambda_1 \lambda_2 \sigma^2(E_{x_1} : A, E_K) \tag{11}$$

En fait, l'existence de la distribution des charges des fragments tend à diminuer la valeur mesurée de $COV(\nu_1, \nu_2 : A, E_K)$, donc à sous-estimer légèrement la valeur de $\sigma^2(E_{x_1} : A, E_K)$.

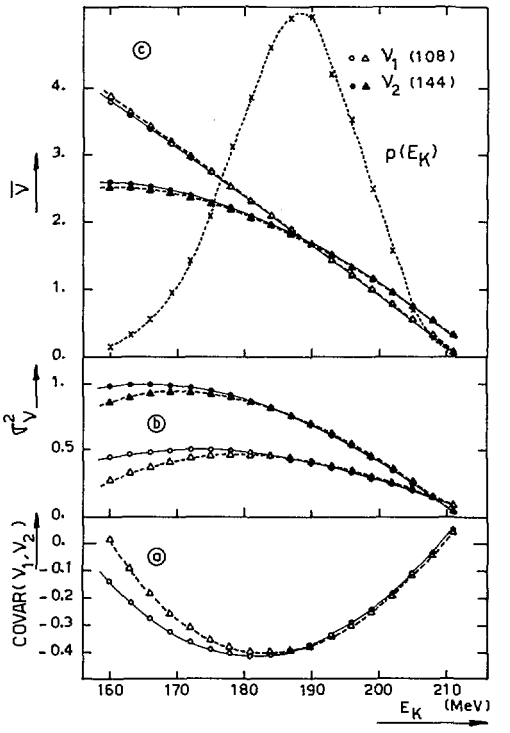

FIG. 3. Valeurs moyennes, variances et covariances de la distribution du nombre de neutrons émis par un couple de fragments complémentaires (A_1 = 108, A_2 = 144). Les données ont été lissées et corrigées de la dispersion expérimentale sur les masses et les énergies cinétiques des fragments. Les ronds et les triangles correspondent à deux analyses différentes des données (voir texte).

L'interprétation de la courbe présentée sur la figure 3a en termes de variances des énergies d'excitation est aisée: aux bornes de la distribution de $p(E_K)$, les variances tendent vers zéro, ce qui signifie qu'aux valeurs maximale et minimale de E_K correspondent deux configurations de scission complètement «froides», à savoir la moins allongée et la plus allongée. Au contraire, à la valeur E_K la plus probable correspond la distribution la plus large des configurations de scission. Un comportement similaire est observé quel que soit le rapport des masses des fragments.

Un autre résultat assez surprenant concerne les différences considérables entre les valeurs des variances $\sigma^2(\nu_A)$ des deux fragments complémentaires, ainsi qu'on peut l'observer pour le couple de masses 108-144 sur la figure 3b: par exemple pour la valeur de E_K la plus probable (où les nombres moyens de neutrons émis par chaque fragment sont pratiquement égaux), la variance du fragment lourd est presque deux fois plus grande que celle du fragment léger; cet effet s'accentue encore pour les faibles valeurs de E_K. Il est clair que ces différences doivent être interprétées en termes de désexcitation des fragments puisque, pour des valeurs de A et de E_K fixées, les distributions d'énergie d'excitation des deux fragments sont

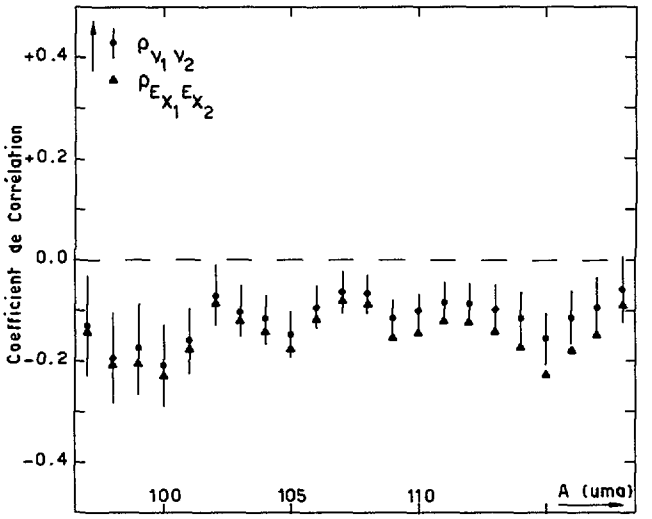

FIG. 4. Coefficient de corrélation de la distribution des nombres de neutrons $P(\nu_1, \nu_2)$ et des énergies d'excitation $P(E_{x_1}, E_{x_2})$ en fonction de la masse du fragment léger.

approximativement les mêmes (relation (10)). Des différences dans la dispersion des énergies de liaison des neutrons entre le fragment léger et le fragment lourd pourraient expliquer partiellement l'effet. Un autre type d'explication serait que le phénomène de compétition gamma-neutron (mis en évidence globalement pour les deux fragments [11]) affecterait préférentiellement l'un des deux fragments (le fragment lourd dans le cas du couple des masses 108-144).

Sur la figure 4 sont montrées les valeurs des coefficients de corrélation des distributions $P(\nu_1, \nu_2)$ et $P(E_{x_1}, E_{x_2})$ en fonction du rapport des masses des fragments. Rappelons que le coefficient de corrélation de deux variables aléatoires x et y est défini par

$$\rho(x, y) = \frac{COV(x, y)}{\sigma(x) \cdot \sigma(y)} \tag{12}$$

où $\sigma^2(x)$ et $\sigma^2(y)$ sont les variances des distributions marginales de $P(x, y)$ et $COV(x, y)$ la covariance de $P(x, y)$.

La covariance $COV(E_{x_1}, E_{x_2} : A_1, A_2)$ est déduite de la covariance $COV(\nu_1, \nu_2 : A_1, A_2)$ par la relation (4). Les variances $\sigma^2(E_{x_1} : A_1)$ et $\sigma^2(E_{x_2} : A_2)$ ont été calculées pour chaque masse en faisant l'hypothèse raisonnable d'une régression linéaire de E_x sur E_K, selon la relation suivante:

$$\sigma^2(E_{x_i} : A_i) = -\frac{1}{\lambda_i}\left(\frac{d\bar{\nu}_i}{dE_K}\right)_{A_i} \sigma^2(E_K : A_1, A_2) - \frac{1}{\lambda_1 \lambda_2} COV(E_{x_1}, E_{x_2} : A_1, A_2) \tag{13}$$

où $\sigma^2(E_K)$ est la variance de la distribution des énergies cinétiques totale et $(d\bar{\nu}_i/dE_K)A_i$ est la pente de la régression linéaire de ν sur E_K pour le fragment de masse A_i. Les paramètres λ_i ont été évalués à partir de nos données expérimentales; typiquement, pour le couple de masses (108-144), les valeurs de λ_1 et λ_2 étaient respectivement de 0,13 et 0,10 neutron/MeV.

Comme on peut l'observer sur la figure 4, la corrélation des énergies d'excitation des deux fragments de masses complémentaires est pratiquement nulle quel que soit le rapport des masses. Ce résultat prouve qu'au moment de la scission une partie importante de l'énergie gagnée par le système aux dépens de son énergie potentielle est dissipée dans d'autres degrés de liberté que la pure élongation et suggère que la vitesse d'évolution du système pourrait être suffisamment lente pour justifier l'hypothèse d'un état de quasi-équilibre au moment de la scission.

REMERCIEMENTS

Les auteurs ont plaisir à remercier MM. M. Ribrag et J. Matuszek pour la mise en œuvre du détecteur de neutrons, et le Bureau central de mesures nucléaires (EURATOM) pour la fabrication de la source de ^{252}Cf.

REFERENCES

[1] NIFENECKER, H., FREHAUT, J., SOLEILHAC, M., in Physics and Chemistry of Fission (C.r. Coll. Vienne, 1969), AIEA, Vienne (1969) 491.
[2] BLINOV, M.A., KUZARINOV, N.M., KRISYUK, I.T., KOVALEKO, S.S., Yad. Fiz. 10 (1969) 923 (Sov. J. Nucl. Phys. 10 (1970) 533).
[3] GAVRON, A., FRAENKEL, Z., Phys. Lett., B27 (1971) 1148.
[4] SIGNARBIEUX, C., POITOU, J., RIBRAG, M., MATUSZEK, J., Phys. Lett., B39 (1972) 503.
[5] TERRELL, J., in Physics and Chemistry of Fission (C.r. Coll. Salzbourg, 1965) 2, AIEA, Vienne (1965) 3.
[6] BOWMAN, H.R., MILTON, J.C.D., THOMPSON, S.G., SWIATECKI, W.J., Phys. Rev. 129 (1963) 2133.
[7] NIFENECKER, H., Nucl. Instrum. Methods 81 (1970) 585.
[8] RIBRAG, M., POITOU, J., MATUSZEK, J., SIGNARBIEUX, C., Rev. Phys. Appl. 7 (1972) 197.
[9] SCHMITT, H.W., GIBSON, W.M., NEILER, J.H., WALTER, F.J., THOMAS, T.D., in Physics and Chemistry of Fission (C.r. Coll. Salzbourg, 1965) 1, AIEA, Vienne (1965) 531.
[10] GAVRON, A., Communication personnelle.
[11] NIFENECKER, H., SIGNARBIEUX, C., RIBRAG, M., POITOU, J., MATUSZEK, J., Nucl. Phys., A 189 (1972) 285.

DISCUSSION

on Papers IAEA-SM-174/207 and 41

S. BJØRNHOLM: Since pairing is a long-range correlation, why should the rapid necking-in of a paired system necessarily lead to two doubly even fragments?

H. NIFENECKER: It is quite possible that pairs are broken in the necking-in process. The energy for breaking the pairs must then be obtained elsewhere. Very schematic calculations performed by M. Kleber show that this energy could indeed be obtained at the expense of the kinetic energy of the fragments.

K. DIETRICH: Let me try to answer Mr. Bjørnholm's question. The two nucleons in a Cooper pair are in magnetic substates of opposite sign, all other single particle quantum numbers being equal. Thus they differ in the direction of rotation around the axis of rotational symmetry but not in their localization in space.

Consider now the case where two fragments of different size move slowly away from each other. Then, as the distance between the fragment centres increases, the single particle states tend to be localized either in the small or in the large fragment. Thus both nucleons of a Cooper pair are expected to end up in the same fragment. The dynamical effects that Nifenecker mentioned have to be added to this picture.

P. ARMBRUSTER: Can you give an estimate of the pre-scission kinetic energy ϵ? Is ϵ smaller than the total free energy ($Q - P = X + \epsilon$) available, which is already much smaller (7 MeV) than previous estimates of ϵ (40 MeV).

H. NIFENECKER: Both the pre-scission kinetic energy and the internal heat of the fragments should be less than 7 MeV.

E. PIASECKI: Apart from extracting the second moments of the excitation energy distributions from your data, is it possible to deduce anything about the general shape of these distributions?

H. NIFENECKER: It is not possible at present to go beyond the second moments of the neutron distributions.

M. ASGHAR: It is thought that in alpha-particle ternary fission the alpha particle comes out from the region between the two fragments at or about the time of scission. By fitting the various distributions, such as the angular and energy distributions, with trajectory calculations, one can determine the pre-scission fragment kinetic energy. Over the years the accuracy of these distributions has been improved and we think that the pre-scission energy derived from the fits is around 7 to 10 MeV. This would tend to support Mr. Nifenecker's value.

M.J. FLUSS: I would just like to support the statement that one should not take too seriously the uniqueness of initial kinetic energies deduced from long-range alpha-particle angular distributions! The initial conditions of these calculations are not well defined and therefore the results are not unique.

PROMPT NEUTRONS FROM THE SPONTANEOUS FISSION OF ^{257}Fm[§]

J.P. BALAGNA, J.A. FARRELL, G.P. FORD, A. HEMMENDINGER,
D.C. HOFFMAN, L.R. VEESER, J.B. WILHELMY
Los Alamos Scientific Laboratory,
University of California,
Los Alamos, N. Mex.,
United States of America

Abstract

PROMPT NEUTRONS FROM THE SPONTANEOUS FISSION OF ^{257}Fm.

Prompt neutrons emitted following the spontaneous fission of ^{257}Fm were measured using a 75-cm-diam. Gd-loaded liquid scintillator (neutron detection efficiency = 66.5%). A chamber containing ^{257}Fm and ^{252}Cf sources, each facing a Si surface barrier detector, was placed in the centre of the tank. The average number of neutrons emitted for ^{257}Fm spontaneous fission $\bar{\nu}_T$ was found to be 3.77 ± 0.02 based on a value of $\bar{\nu}_T$ = 3.735 ± 0.014 for ^{252}Cf. The variance of the neutron multiplicity distribution is 2.49 ± 0.06 for ^{257}Fm compared with 1.57 ± 0.02 for ^{252}Cf. The variation of $\bar{\nu}_T$ as a function of single fragment kinetic energy was investigated. For ^{257}Fm, $\bar{\nu}_T$ is ≈ 1 for the highest 1% of the single fragment kinetic energies, while for ^{252}Cf the value is 3. The high kinetic energy fragments from the fission of ^{257}Fm are principally from symmetric mass splits, while in ^{252}Cf they are from asymmetric divisions. Low neutron emission from symmetric division in ^{257}Fm is consistent with the prediction of spherically stabilized fragments near the scission point due to the proximity of the ^{132}Sn doubly magic core.

INTRODUCTION

Previous studies of the kinetic energies of ^{257}Fm spontaneous fission products indicated for the first time that a low energy fission process can have a high yield for symmetric mass division [1]. Subsequent studies of fragment kinetic energy measurements on $^{255}Fm(n,f)$ [2] $^{257}Fm(SF)$ [3] and $^{257}Fm(n,f)$ [3], as well as radiochemical mass yield determinations for $^{255}Fm(SF)$ [4] and $^{255}Fm(n,f)$ [5] have substantiated that the low energy fission of these heavier Fm isotopes results in a higher yield of symmetric fission than has been observed in the low energy fission of other nuclei. These results have stimulated renewed interest in the problems associated with mass distributions in fission [6-8]. The accurate determination of the mass yields for symmetric division, however, requires knowing the number of neutrons evaporated as a function of fragment mass. Figure 1 (from ref. [1]) emphasizes this by showing two mass yield distributions calculated from the observed fragment kinetic energies following the spontaneous fission of ^{257}Fm; the first distribution is calculated with the assumption that the average number of neutrons emitted per fragment has a constant value of 2, while the second assumes the average number of neutrons emitted per fragment has a mass dependence the same as that observed in the spontaneous fission of ^{252}Cf. It is clear that the yield calculated for symmetric fission is dependent on the assumptions concerning the neutron multiplicities.

To elucidate this problem in the calculation of the symmetric fission yields we have measured the neutron multiplicities associated with the fission of ^{257}Fm.

§ Work performed under the auspices of the US Atomic Energy Commission.

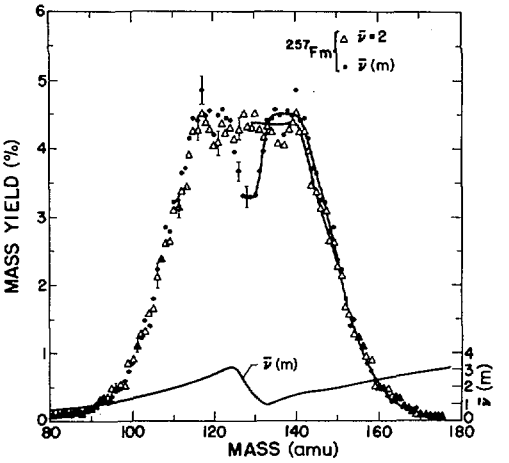

FIG. 1. Pre-neutron emission mass yield distributions for ^{257}Fm(SF). The two sets of points correspond to different assumptions on the variation of $\bar{\nu}$(m) (from Ref. [1]).

EXPERIMENTAL

The ^{257}Fm was produced by successive neutron capture in Cm targets irradiated in the high-flux isotope reactor (HFIR) and processed at the transuranium processing facility (TRU) at Oak Ridge National Laboratory. The ^{257}Fm was further purified at Los Alamos by standard cation column procedures involving elution with ethanol-HCl and hot α-hydroxy-isobutyrate to separate the Fm from other actinides. The principle contaminant before separation was $\approx 10^6$ dis/min of ^{253}Es. A solution of the purified source was evaporated on a 5×10^{-3}-in. Pt disk. This source was positioned ≈ 3 mm from a 1-cm-diam. by 30-μm-deep Si-surface-barrier detector. A ^{252}Cf source, prepared in a similar manner, was placed in the same position relative to a second surface barrier fission detector. The two sources, back-to-back, and their detectors were placed in a vacuum container in the center of a 75-cm-diam. spherical Gd-loaded liquid scintillator tank having a 15-cm-diam. cylindrical hole through the center.

The tank was divided optically into quadrants with each quadrant having two RCA-4522 photomultiplier tubes mounted on glass windows. The tank was filled with Nuclear Enterprise NE-323 liquid scintillator loaded with 0.5 wt.% gadolinium. The neutrons emitted in fission thermalized in the liquid and were captured by the gadolinium. The cascade gamma rays following neutron capture were detected by the photomultipliers after interaction with the scintillator liquid. The mean lifetime for the thermalization and capture of neutrons in the tank is about 10 μsec.

Detection in the solid state detectors of a fission fragment from either ^{252}Cf or ^{257}Fm opened a gate for 40 μsec following a 2 μsec delay to avoid counting the prompt fission gamma rays and the proton recoils resulting from the thermalization of the neutrons. During the open-gate period the sums of the dynode signals from the four photomultipliers on each half of the tank were fed into a dual discriminator. The discriminator levels determined the efficiency of the tank, and their 150-nsec output pulse lengths determined the dead time. A pulser was used to open the 40-μsec gate every 100 sec so that background counting rates of the system could be measured.

An on-line PDP-8/L computer recorded the outputs of fast scalers, which gave the neutron multiplicities, and of analog-to-digital converters (ADC) which measured the linearly amplified signals of the fission fragment solid state detectors.

The apparatus was placed in a low background room having thick concrete walls. During the experiment the average background rate was 0.1243 ± 0.0010 based on more than 125000 background gates. No more than three pulses were measured in any of the background gates and the frequency distribution of the various multiplicity events was consistent with a Poisson distribution. By having the ^{252}Cf source present in the tank it was possible to monitor continuously the efficiency of the system. The overall neutron detection efficiency was determined to be (66.49 ± 0.28)%, based on an average neutron multiplicity value of 3.735 ± 0.014 for the fission of ^{252}Cf [9].

RESULTS

Experimental data were collected for more than five months. During that time 10532 ^{257}Fm and 98659 ^{252}Cf fission events were detected. The ^{257}Fm fission detection rate varied from 5.5 SF/h at the start of the experiment to 1.8 SF/h at the conclusion. From a least squares fit to the observed decay rate we obtained a value of 99.3 ± 1.6 d for the half-life of ^{257}Fm, in good agreement with the recently published value of 100.5 ± 0.2 d [10]. Figure 2 presents the probability distribution of the observed multiplicity of neutrons from the fission of ^{257}Fm and ^{252}Cf. The probability of observing n events is

$$P_d(n) = \sum_{k=0}^{n} \sum_{\nu=n-k}^{\nu_{max}} \binom{\nu}{n-k} \epsilon^{n-k} (1-\epsilon)^{\nu-n-k} P_b(k) P_t(\nu) \qquad (1)$$

where ϵ = efficiency for neutron detection

$P_t(\nu)$ = probability that ν neutrons are emitted in a fission event, and

$P_b(k)$ = probability of measuring k background counts.

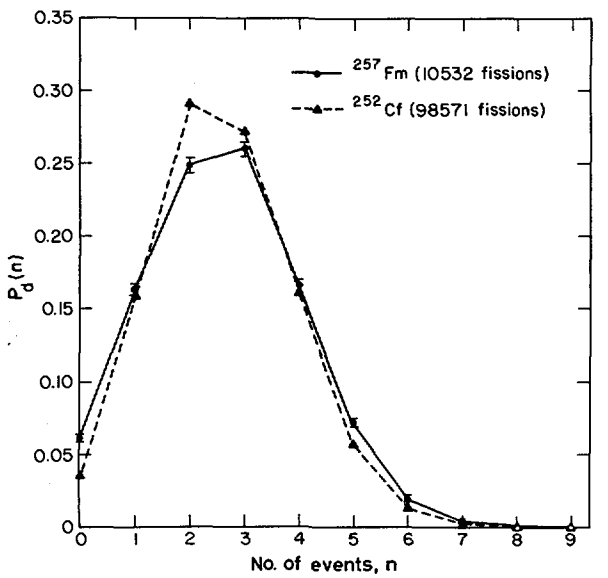

FIG.2. The experimentally observed distributions, $P_d(n)$, of events in the fission of ^{252}Cf and ^{257}Fm.

TABLE I. EXPERIMENTALLY DETERMINED NEUTRON PROBABILITY DISTRIBUTIONS FOR THE FISSION OF ^{257}Fm AND ^{252}Cf

	^{257}Fm (10532 fissions)		^{252}Cf (98571 fissions)	
n or ν	Observed $P_d(n)$	"Unfolded" $P_t(\nu)$	Observed $P_d(n)$	"Unfolded" $P_t(\nu)$
0	0.070 ± 0.003	0.022 ± 0.004	0.041 ± 0.001	0.003 ± 0.001
1	0.176 ± 0.004	0.078 ± 0.014	0.175 ± 0.001	0.021 ± 0.005
2	0.260 ± 0.005	0.077 ± 0.032	0.308 ± 0.002	0.140 ± 0.011
3	0.261 ± 0.005	0.259 ± 0.054	0.276 ± 0.002	0.264 ± 0.017
4	0.154 ± 0.004	0.211 ± 0.068	0.146 ± 0.001	0.307 ± 0.020
5	0.061 ± 0.003	0.259 ± 0.068	0.045 ± 0.001	0.191 ± 0.018
6	0.015 ± 0.002	0.039 ± 0.058	0.008 ± 0.0004	0.061 ± 0.013
7	0.003 ± 0.001	0.058 ± 0.032	0.001 ± 0.0002	0.008 ± 0.007
8	0.0001± 0.0002	-0.005 ± 0.015	0.0001 ± 0.00006	0.005 ± 0.003
9	0.0001± 0.0001	0.002 ± 0.004	0.00001 ± 0.00001	-0.0006 ± 0.0005
$\bar{n}(\bar{\nu})$	2.636 ± 0.014	3.769 ± 0.021	2.607 ± 0.004	(3.735 ± 0.014)
σ^2	2.068 ± 0.027	2.49 ± 0.06	1.651 ± 0.007	1.57 ± 0.02

TABLE II. SUMMARY OF NEUTRON EVAPORATION DATA FOR ^{257}Fm AND ^{252}Cf

^{257}Fm			
	No. of fissions	$\bar{\nu}_T$	$\sigma^2_{\bar{\nu}_T}$
Cheifetz et al. [1]	1499	3.97 ± 0.13	2.92 ± 1.40
This experiment	10532	3.77 ± 0.02	2.49 ± 0.06

^{252}Cf				
Ref.	[11]	[12]	[13]	[14]	This exp.
$\sigma^2_{\bar{\nu}_T}$	1.87 ± 0.08	1.55 ± 0.04	1.46 ± 0.14	1.46 ± 0.14	1.57 ± 0.02

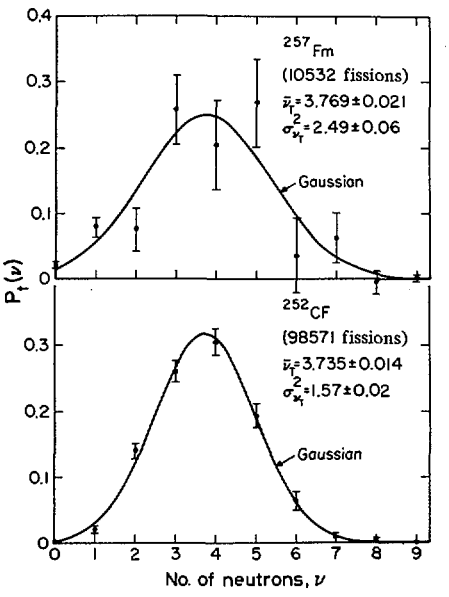

FIG.3. The "unfolded" frequency distribution, $P_t(\nu)$, of neutrons associated with the spontaneous fission of ^{257}Fm and ^{252}Cf. The solid curves represent Gaussian functions having the same first and second moments as the "unfolded" distributions.

Through a matrix inversion of Eq. 1 it is possible to determine the quantity $P_t(\nu)$, the multiplicity distribution of neutrons emitted in fission. Table I presents the observed and "unfolded" distributions for both ^{257}Fm and ^{252}Cf. The $\bar{\nu}$ value for ^{257}Fm is found to be 3.769 ± 0.021 which is less than 1% higher than the value of 3.735 ± 0.014 [9] for ^{252}Cf. The 2.49 ± 0.06 variance for ^{257}Fm is much larger than the value of 1.57 ± 0.02 measured for ^{252}Cf. In Table II we compare our current values of these quantities with those reported for ^{257}Fm by Cheifetz et al. [11] and with various reported results on ^{252}Cf [11-14].

A plot of our "unfolded" $P_t(\nu)$ distributions is presented in Fig. 3. The ^{252}Cf distribution is seen to be very nearly Gaussian. Although the ^{257}Fm results show more scatter, they are also represented reasonably well by a Gaussian function.

A notable feature in the fission of ^{257}Fm compared to ^{252}Cf is the higher probability of emission of 0 or 1 neutron. In fact, the whole neutron multiplicity distribution is much flatter for ^{257}Fm than for ^{252}Cf, as evidenced in their relative variances. This implies a broad distribution in excitation energies for ^{257}Fm fission products.

In this experiment only one fission fragment energy was recorded per fission. We have analyzed the variation of $\bar{\nu}_T$ and $\sigma^2_{\nu_T}$ as a function of single fragment energy. Figure 4 presents a histogram of the values of $\bar{\nu}_T$ and $\sigma^2_{\nu_T}$ for bins containing ≈10% increments of the single fragment kinetic energies. The variances for both ^{257}Fm and ^{252}Cf are seen to remain reasonably constant over the kinetic energy range. The $\bar{\nu}_T$ data for ^{257}Fm, however, show a dramatic decrease as the highest kinetic energy bins are selected, while no such strong effect is observed in the ^{252}Cf data. These results are presented in a cumulative manner in Fig. 5. We see that when all of the data are included (the 100% point on the far right of the graph) the ^{257}Fm and ^{252}Cf have, within 1%,

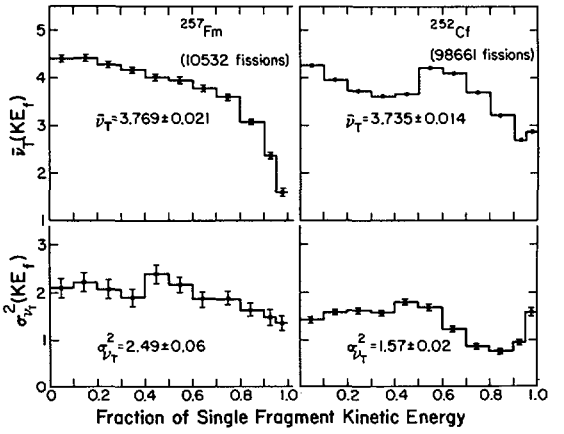

FIG.4. The average ($\bar{\nu}_T$) and variance ($\sigma^2_{\nu_T}$) of the neutron distributions for the fission of ^{257}Fm and ^{252}Cf as a function of single fragment kinetic energy. The data are presented in ≈ 10% bins corresponding to the lowest kinetic energy fraction on the left to the highest on the right.

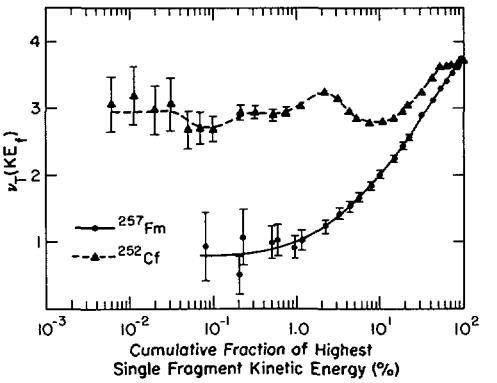

FIG.5. The variation of the average number of neutrons as a function of the cumulative fraction of single fragment kinetic energy. The value of the ordinate for abscissa value χ is the average number of neutrons for those events with the top χ per cent of single fragment kinetic energies.

the same value of $\bar{\nu}_T$, but when only the higher kinetic energy intervals are selected, the ^{257}Fm $\bar{\nu}_T$ results are substantially below the ^{252}Cf data. At the highest kinetic energy interval the ^{257}Fm multiplicity has decreased to less than 1 neutron per fission, whereas the ^{252}Cf data have asymtotically approached about 3 neutrons per fission. The low value of $\bar{\nu}_T$ for the high kinetic energy ^{257}Fm fission implies a very low fragment excitation energy for these events.

With only one fragment energy measured, definitive mass assignments are not possible. For ^{257}Fm fission, however, some selection of the mass distribution can be made by selection of single fragment kinetic energies. Figure 6 shows a mass distribution obtained by restricting one fragment to be within the top 5.3% of the kinetic energy range. These data, which were taken from the ^{257}Fm two-fragment kinetic-energy mass determination measurements of ref [1], show a preference for symmetric division when one fragment has a high

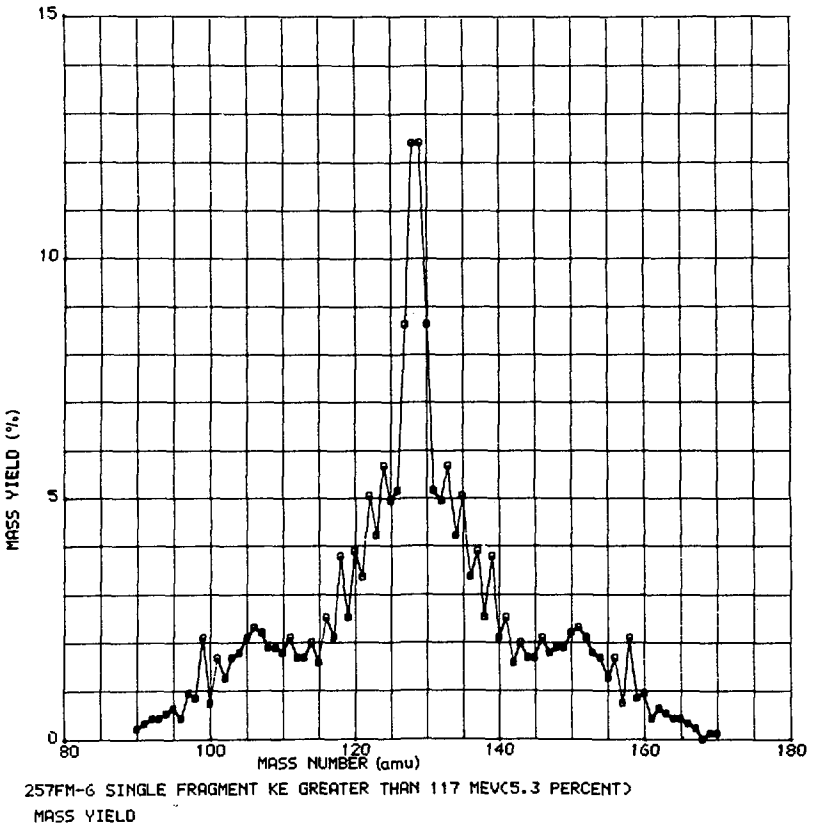

FIG.6. Mass distribution for ^{257}Fm(SF) obtained when one fragment is restricted to kinetic energy greater than 117 MeV (the top 5.3% of the single fragment kinetic energy distribution).

kinetic energy. Though not conclusive, the combination of the current neutron measurements with the previous mass determinations implies that the symmetric fission of ^{257}Fm results in fragments having very little internal excitation energy.

DISCUSSION AND CONCLUSIONS

We have repeated the ^{257}Fm neutron multiplicity measurements done by Cheifetz et al. [11] using a more efficient detection system (66.5% vs 51.5%). Our results, with smaller statistical uncertainties, are consistent with their values ($\pm 2\sigma$). With our higher efficiency we have been able to "unfold" the observed multiplicity distribution and obtain the true neutron distribution. Perhaps the most interesting observation is the strong decrease in $\bar{\nu}$ with increasing single fragment kinetic energy. These events are correlated with symmetric fission of ^{257}Fm. If we relate the neutron multiplicity to the post-scission fragment excitation energy, we have an estimate for the excitation energy for symmetric division. We present these data in Fig. 7, a graph containing the predictions of Schmitt and Mosel [7] for fragment excitation energy for symmetric [$Z_{f_1} = Z_{f_2} = Z/2$, $A/2$] and asymmetric [$Z_{f_1} = 50$, $A_{f_1} = 132$;

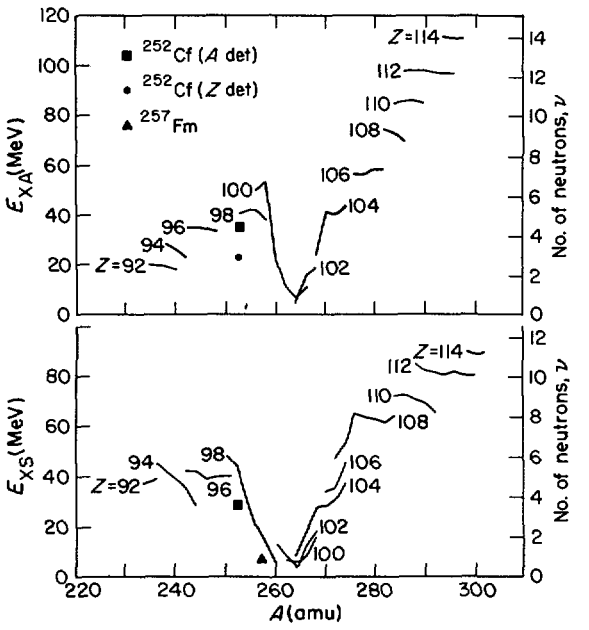

FIG.7. The solid curves represent calculated excitation energies (E_X) and neutron emission multiplicities (ν) for asymmetric (A) and symmetric (S) fission of nuclei from Z = 92 to 114 (from Schmitt and Mosel [7]). The points correspond to experimental values for the fission of ^{252}Cf and ^{257}Fm. See text for additional details.

Z_{f_2} = Z-50, A_{f_2} = A-132] division. Since the $\bar{\nu}$ value for any specific division is unknown, we can use only the measured $\bar{\nu}$ values for given mass or charge. For the fission of ^{252}Cf the neutron multiplicities have been determined both as a function of fragment mass [15] and charge [16] and both results are presented in Fig. 7. For asymmetric fission the mass determination method (i.e. A_{f_1} = 132, A_{f_2} = 120) gives a substantially higher $\bar{\nu}$ than does the charge determination (i.e. Z_{f_1} = 48, Z_{f_2} = 50) method [7]. For the symmetric fission the two ^{252}Cf methods give essentially the same value. For ^{257}Fm the symmetric mass division (as estimated from Fig. 5 for the highest kinetic energy events) has a $\bar{\nu}$ of $\approx$ 1. These results are in at least qualitative agreement with the Schmitt and Mosel predictions. The ^{257}Fm symmetric fission is expected to result in two fragments which are spherically stabilized by the proximity of the ^{132}Sn doubly magic core. Such fragments should be stiff against distortion and have nearly spherical scission configurations. These circumstances should result in high kinetic energy release (due to large coulomb energy from the compact spherical fragments) and low internal fragment excitation energy.

More definitive experiments in which neutron multiplicities are measured in coincidence with both fragment kinetic energies would improve our understanding of the energy division in the spontaneous fission of ^{257}Fm. We are currently attempting such an experiment with a slightly stronger source ($\approx$4 SF/min).

REFERENCES

[1] BALAGNA, J. P., FORD, G. P., HOFFMAN, D. C. and KNIGHT, J. D., Phys. Rev. Letters 26, 145 (1971).

[2] RAGAINI, R.C., HULET, E.K., LOUGHEED, R.W., WILD, J.W., Bull.Am.Phys.Soc. 18, 97 (1973). See also Paper IAEA-SM-174/72, these Proceedings, Vol.2.

[3] JOHN, W., HULET, E. K., LOUGHEED, R. W. and WESOLOWSKI, J. J., Phys. Rev. Letters 27, 45 (1971).

[4] FLYNN, K. F., HORWITZ, E. P., BLOOMQUIST, C. A., BARNES, R. F., SJOBLOM, R. K., FIELDS, P. R. and GLENDENIN, L. E., Phys. Rev. C 5, 1725 (1972).

[5] FLYNN, K. F., GINDLER, J. E., SJOBLOM, R. K. and GLENDENIN, L. E., private communication.

[6] TSANG, C. F. and WILHELMY, J. B., Nucl. Phys. A184, 417 (1972).

[7] SCHMITT, H. W. and MOSEL, U., Nucl. Phys. A186, 1 (1972).

[8] WILKINS, B. D. and STEINBERG, E. P., Phys. Letters 42B, 141 (1972).

[9] BOLDEMAN, J. W., "Prompt Neutron Yield from the Spontaneous Fission of ^{252}Cf" at Neutron Standards Reference Data Panel Meeting, Vienna (Nov. 20-24, 1972) IAEA.

[10] WILD, J. F., HULET, E. K. and LOUGHEED, R. W., J. Inorg. Nucl. Chem. 35, 1063 (1973).

[11] CHEIFETZ, E., BOWMAN, H. R., HUNTER, J. B. and THOMPSON, S. G., Phys. Rev. C 3, 2017 (1971).

[12] NIFENECKER, H., FREHAUT, J. and SOLEILHAC, M., Second Symposium on the Physics and Chemistry of Fission, Vienna (International Atomic Energy Agency, Vienna, Austria, 1969), p. 491.

[13] STOUGHTON, R. W., HALPERIN, J., BEMIS, C. E. and SCHMITT, H. W., Nucl. Sci. Eng. 50, 169 (1973).

[14] TERRELL, J., Phys. Rev. 108, 783 (1957).

[15] BOWMAN, H. R., MILTON, J. C. D., THOMPSON, S. G. and SWIATECKI, W. J., Phys. Rev. 126, 2120 (1962); Phys. Rev. 129, 2133 (1963).

[16] NIFENECKER, H., SIGNARBIEUX, C., BABINET, R., POITOU, J., Paper IAEA-SM-174/207, these Proceedings, Vol.2.

DISCUSSION

H. NIFENECKER: I should just like to point out that the maximum heat of less than one neutron reported by Mr. Wilhelmy in the case of fermium is of the order of the 7 MeV which I reported for spontaneous fission of ^{252}Cf.

MESURE DU NOMBRE MOYEN DE NEUTRONS PROMPTS ET DE L'ENERGIE MOYENNE DES RAYONS GAMMA PROMPTS EMIS LORS DE LA FISSION INDUITE PAR NEUTRONS DE RESONANCE DANS ^{235}U ET ^{239}Pu

J. FREHAUT
CEA, Centre d'études de Bruyères-le-Châtel, Montrouge

D. SHACKLETON
CEA, Centre d'études nucléaires de Saclay, Gif-sur-Yvette, France

Abstract-Résumé

MEASUREMENT OF THE MEAN NUMBER OF PROMPT NEUTRONS AND THE MEAN ENERGY OF PROMPT GAMMA RAYS EMITTED DURING RESONANCE NEUTRON INDUCED FISSION IN ^{235}U AND ^{239}Pu.

Using the 60-MeV linear accelerator at the Saclay Nuclear Research Centre as a pulsed neutron source, the authors measured the variations from resonance to resonance in the mean number $\bar{\nu}$ of prompt neutrons and the mean energy $\bar{E}_\gamma$ of line prompt gamma radiation emitted during induced by s-wave neutrons fission of ^{235}U and ^{239}Pu. Contrary to other published results, no clear-cut variation in $\bar{\nu}$ for ^{235}U was found. However, anticorrelated fluctuations of $\bar{\nu}$ and $\bar{E}_\gamma$ were observed in the case of ^{239}Pu. These fluctuations, which are independent of resonance spin, may be regarded as a contribution of the (n, γf) reaction.

MESURE DU NOMBRE MOYEN DE NEUTRONS PROMPTS ET DE L'ENERGIE MOYENNE DES RAYONS GAMMA PROMPTS EMIS LORS DE LA FISSION INDUITE PAR NEUTRONS DE RESONANCE DANS ^{235}U ET ^{239}Pu.

Les variations de résonance à résonance du nombre moyen $\bar{\nu}$ de neutrons prompts et de l'énergie moyenne $\bar{E}_\gamma$ du rayonnement gamma prompt ont été mesurées pour la fission de ^{235}U et ^{239}Pu induite pat neutrons s, en utilisant l'accélérateur linéaire d'électrons de 60 MeV du Centre d'études nucléaires de Saclay comme source pulsée de neutrons. Contrairement aux autres résultats publiés, les auteurs n'ont trouvé aucune variation nette de $\bar{\nu}$ pour ^{235}U. Ils ont observé des fluctuations anticorrélées de $\bar{\nu}$ et $\bar{E}_\gamma$ pour le ^{239}Pu. Ces fluctuations, indépendantes du spin des résonances, peuvent être interprétées comme une contribution de la réaction (n, γf).

I - INTRODUCTION

La théorie des états de transition de A. Bohr [1] permet de prévoir des corrélations entre le spin J^π du noyau fissionant et différents paramètres de la fission. Expérimentalement, pour la fission induite par neutrons "s" dans ^{239}Pu, de telles corrélations ont déjà été observées pour les largeurs de fission Γ_f [2] , ainsi que pour le rapport vallée-pic de la distribution en masse des fragments [3] . Cette corrélation pourrait également exister pour $\bar{\nu}$, le nombre moyen de neutrons prompts, puisque $\bar{\nu}$ dépend, entre autres, de la distribution en masse des fragments de fission.

Cependant les différentes mesures [4], [5], [6], [7] , [8] effectuées jusqu'alors étaient contradictoires et ne permettaient pas de conclure sur ce point.

C'est pourquoi nous avons récemment mesuré $\bar{\nu}$, ainsi que $\bar{E}_\gamma$, l'énergie moyenne du rayonnement γ prompt, pour la fission de ^{239}Pu [9] et ^{235}U induite par des neutrons "s", en utilisant l'accélérateur linéaire de 60 MeV de Saclay comme source pulsée de neutrons.

II - METHODE DE MESURE

Nous avons utilisé la technique de la chambre à fission rapide (temps de montée 6 ns) placée au centre d'un gros scintillateur liquide chargé au gadolinium [10] (fig. 1a). La fission était identifiée par une coïncidence entre une impulsion de la chambre à fission (détection d'un fragment de fission) et une impulsion du scintillateur liquide (détection des rayons γ prompts de fission). Les neutrons de fission, après thermalisation dans le liquide et capture par le gadolinium, étaient comptés pendant 30 µs après chaque fission.

Le bruit de fond enregistré en même temps que les neutrons de fission a été déterminé de façon précise en simulant un signal de fission décalé d'un intervalle de temps correspondant à une période de l'accélérateur (fig. 1b). De cette façon, le bruit de fond est déterminé dans des conditions pratiquement identiques à celles de la mesure proprement dite.

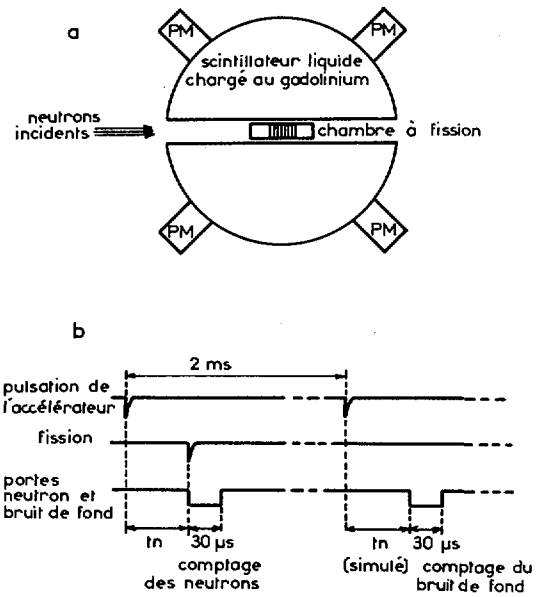

FIG.1. Schéma de principe de la mesure.

L'énergie des neutrons incidents a été déterminée par la méthode du temps de vol, en plaçant le détecteur à 30 m de la source de neutrons pulsée à la fréquence de 500 Hz. Chaque chambre à fission contenait environ 100 mg de matériau fissile répartis sur 8 sorties indépendantes (épaisseur des dépôts $\sim$ 1 mg/cm^2) et un dépôt de ^{252}Cf pour la normalisation des valeurs de $\bar{\nu}$ obtenues.

Les fluctuations de résonance à résonance de $\bar{E}_\gamma$ ont été obtenues en analysant la surface du signal prompt du scintillateur liquide. La calibration en énergie de ces fluctuations a été réalisée en mesurant la réponse du scintillateur pour le rayonnement γ obtenu par réaction (n,γ) sur ^{197}Au, ^{165}Ho, ^{167}Er, ^{182}W, ^{183}W, et pour le rayonnement γ de sources de ^{60}Co et ^{22}Na.

Pour chaque fission, les données expérimentales ($\bar{\nu}$, bruit de fond, $\bar{E}_\gamma$, temps de vol, N° de sortie de la chambre à fission) ont été enregistrées sur bande magnétique puis traitées sur ordinateur CDC 6600.

III - RESULTATS EXPERIMENTAUX

III-1 Généralités

Toutes les valeurs de $\bar{\nu}$ ont été normalisées à $\bar{\nu}$ = 3,782 pour la fission spontanée du ^{252}Cf.

Les valeurs de $\bar{E}_\gamma$ sont présentées en unités arbitraires et ne sont pas corrigées de l'énergie apportée par les protons de recul produits lors du ralentissement des neutrons de fission dans le scintillateur. La mesure de $\bar{E}_\gamma$ étant relative, cette correction, proportionnelle à $\bar{\nu}$, n'est nécessaire que si $\bar{\nu}$ varie de résonance à résonance.

III-2 Résultats pour ^{235}U

Les valeurs de $\bar{\nu}$ et de $\bar{E}_\gamma$ pour les résonances comprises entre 2 et 50 eV sont portées sur la figure 2.

Les largeurs de fission [11] et les spins des résonances [12] ont été portés au dessus des points expérimentaux lorsqu'ils sont connus.

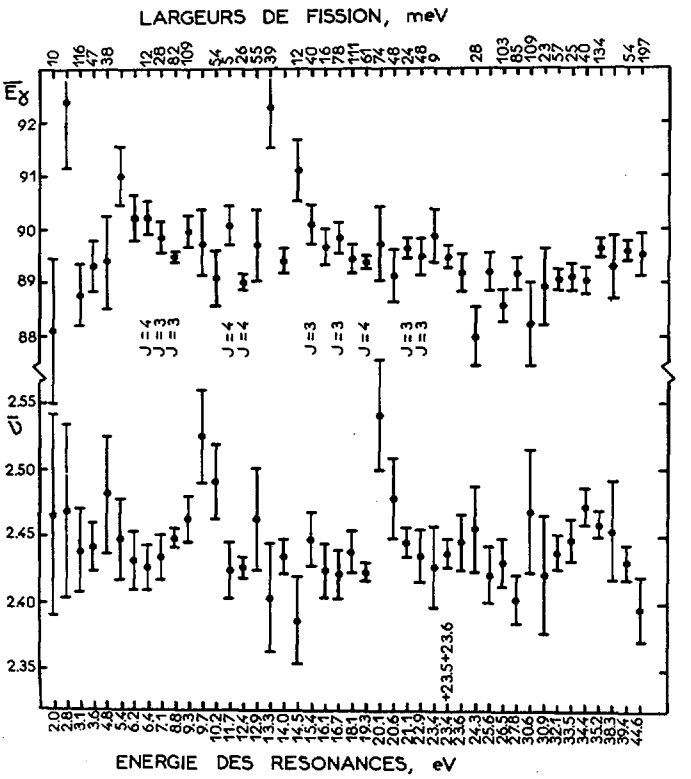

FIG.2. Valeurs de $\bar{\nu}$ et $\bar{E}_\gamma$ pour les résonances de ^{235}U.

Contrairement aux autres résultats publiés [4][5] , nous n'observons aucune variation nette de $\bar{\nu}$. Les fluctuations de $\bar{E}_\gamma$ semblent également être d'origine statistique.

III-3 Résultats pour ^{239}Pu

Nous avons analysé toutes les résonances de spin J connu jusqu'à une énergie de neutrons incidents de 250 eV et quelques résonances isolées entre 250 et 404 eV. Des résultats préliminaires ont déjà été publiés [13] [14] .

Les valeurs de $\bar{\nu}$ pour chaque état de spin sont portées sur la partie inférieure des figures 3 ($J^\pi = 1^+$) et 4 ($J^\pi = 0^+$). Elles sont en bon accord avec celles de Weston [6] [13] .

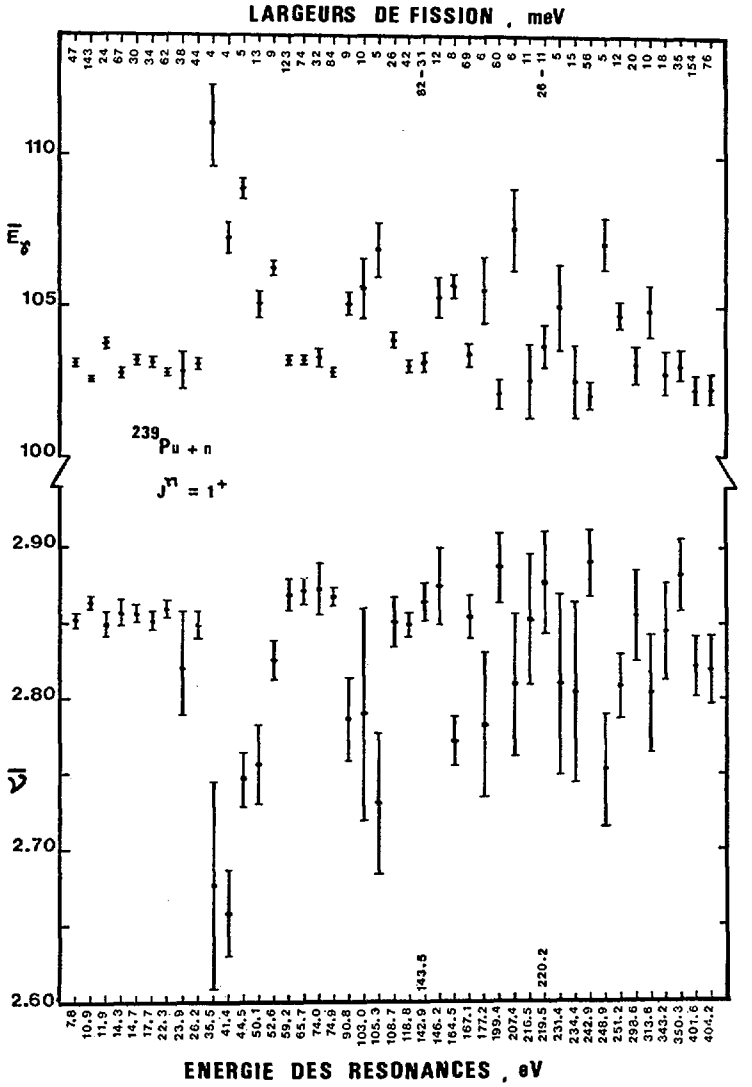

FIG.3. Valeurs de $\bar{\nu}$ et $\bar{E}_\gamma$ pour les résonances $J^\pi = 1^+$ de ^{239}Pu.

Sur la partie supérieure de ces 2 figures, nous avons porté les valeurs de $\bar{E}_\gamma$.

Les fluctuations de $\bar{\nu}$ et $\bar{E}_\gamma$ pour les résonances 1^+ (fig. 3) sont fortement anticorrélées. Les valeurs de $\bar{\nu}$ sont d'autant plus basses, et les valeurs de $\bar{E}_\gamma$ plus hautes, que les largeurs de fission Γ_f des résonances sont petites. Les valeurs de Γ_f de Blons et al [15] ont été portées au-dessus des points expérimentaux.

La correction de $\bar{E}_\gamma$ pour l'effet des protons de recul [16] entraînée par la variation de $\bar{\nu}$ (§ III-1) augmenterait légèrement l'anticorrélation observée.

En ce qui concerne les résonances 0^+, les fluctuations de $\bar{\nu}$ semblent d'origine statistique. Les valeurs de $\bar{E}_\gamma$ semblent plus élevées pour les résonances dont la largeur de fission est inférieure à 200 meV.

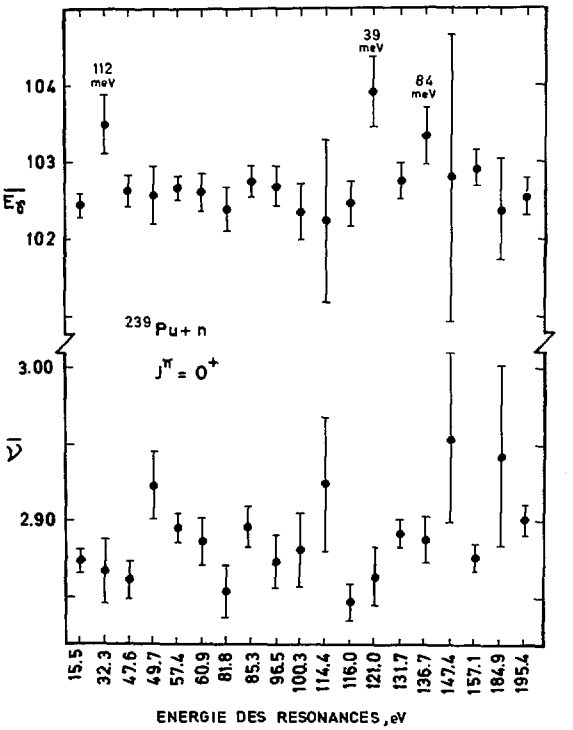

FIG.4. Valeurs de $\bar{\nu}$ et $\bar{E}_\gamma$ pour les résonances $J^\pi = 0^+$ de ^{239}Pu.

IV - INTERPRETATION DES RESULTATS

J. Trochon a proposé une interprétation des résultats obtenus pour le ^{239}Pu à partir de la réaction (n,γf) [17] [18] , dans laquelle des rayons γ sont émis par le noyau composé avant fission.

L'énergie des rayons γ de préfission s'ajoute alors à l'énergie du rayonnement γ prompt de fission, d'où une augmentation de $\bar{E}_\gamma$.

L'émission de rayons γ avant fission diminue l'énergie d'excitation du noyau composé, ce qui entraîne une réduction de l'énergie d'excitation des fragments de fission, donc une diminution du nombre de neutrons émis.

Expérimentalement, on observe un mélange de réactions (n,γf) et de réactions directes (n,f_d). L'influence de la réaction (n,γf) est d'autant plus importante qu'il y a moins de fissions directes, c'est-à-dire quand la largeur totale de fission Γ_f devient comparable à la largeur $\Gamma_{\gamma f}$ pour le processus (n,γf) (des valeurs de $\Gamma_{\gamma f}$ de ∿ 8 meV pour les résonances 0^+ et de ∿ 3 meV pour les 1^+ ont été calculées [19] [20]).

L'effet de la réaction (n,γf), très net pour les résonances 1^+ du ^{239}Pu, n'est pas observé pour les résonances 0^+ car la plupart de celles-ci ont une grande largeur de fission et le phénomène, alors très faible, est masqué par les erreurs expérimentales.

Les petites fluctuations de $\bar{\nu}$ et $\bar{E}_\gamma$ observées pour ^{235}U montrent que l'influence de la réaction (n,γf) est faible, ce qui tend à confirmer la valeur $\Gamma_{\gamma f}$ ∿ 1 meV calculée pour ce noyau [20] .

L'interprétation de nos résultats à partir de la réaction (n,γf) implique l'invariance d'une résonance à l'autre du produit $\Gamma_f.\Delta E$ de la largeur de fission Γ_f par l'accroissement en énergie ΔE de $\bar{E}_\gamma$. Cet accroissement ΔE se traduit par une diminution correspondante de l'énergie d'excitation du noyau composé, c'est-à-dire une diminution $\Delta\bar{\nu}$ de $\bar{\nu}$. [18]

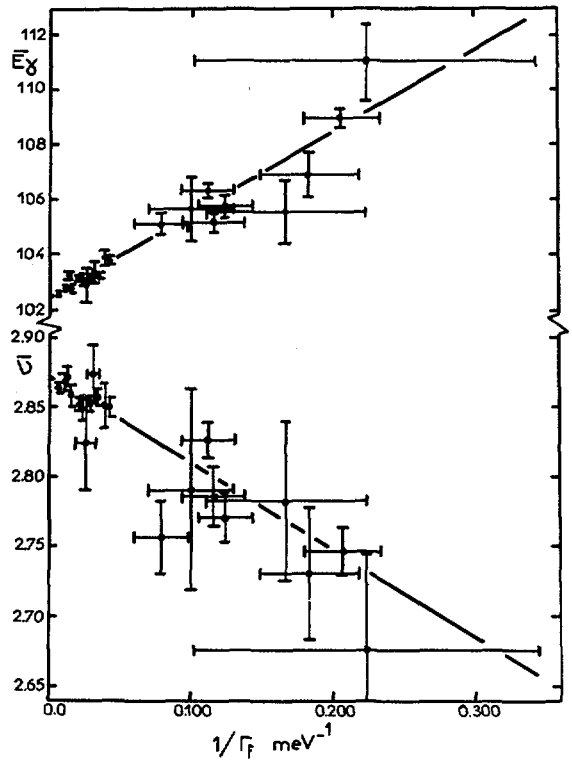

FIG.5. Lois $\bar{\nu} = f(1/\Gamma_f)$ et $\bar{E}_\gamma = f(1/\Gamma_f)$ pour les résonances 1^+ de ^{239}Pu. Les droites en traits pleins représentent des ajustements obtenus par la méthode des moindres carrés à partir des valeurs expérimentales.

Cette invariance est vérifiée expérimentalement :

Sur la figure 5, nous avons porté les valeurs de $\bar{\nu}$ et de $\bar{E}_\gamma$ obtenues pour les résonances 1^+ du ^{239}Pu en fonction de $1/\Gamma_f$.

Les lois $\bar{\nu} = f\ (1/\Gamma_f)$ et $\bar{E}_\gamma = f\ (1/\Gamma_f)$ sont des droites dont la pente permet de déduire la valeur du produit $\Gamma_f.\Delta E$.

Nous avons obtenu :

- à partir de $\bar{\nu} = f\ (1/\Gamma_f)$, $\Gamma_f.\Delta E = (4715 \pm 450)\ eV^2$,

en admettant que 0,13 neutrons sont émis en moyenne par MeV d'énergie d'excitation.

- à partir de $\bar{E}_\gamma = f\ (1/\Gamma_f)$, $\Gamma_f.\Delta E = (4807 \pm 400)\ eV^2$,

en utilisant la calibration directe en énergie de l'échelle $\bar{E}_\gamma$ (0,168 ± 0,010 MeV/canal) et en effectuant la correction pour l'effet des protons de recul [16] .

Les deux valeurs obtenues sont en bon accord, ce qui confirme l'interprétation des fluctuations de $\bar{\nu}$ et $\bar{E}_\gamma$ à partir de la réaction $(n,\gamma f)$.

V - CORRELATION ENTRE $\bar{\nu}$, $\bar{E}_\gamma$ ET LE SPIN DES RESONANCES DU ^{239}PU

L'extrapolation des droites $\bar{\nu} = f\ (1/\Gamma_f)$ et $\bar{E}_\gamma = f\ (1/\Gamma_f)$ pour $1/\Gamma_f = 0$ permet d'obtenir les valeurs de $\bar{\nu}$ et $\bar{E}_\gamma$ corrigées de l'effet de la réaction $(n,\gamma f)$ pour les résonances 1^+ du ^{239}Pu et de les comparer aux valeurs moyennes mesurées pour les résonances 0^+. On obtient :

	Résonances 0^+	Résonances 1^+	Différence
$\bar{E}_\gamma$: (canaux)	102,60 ± 0,07	102,45 ± 0,10	0,15 ± 0,12
$\bar{\nu}$:	2,882 ± 0,005	2,868 ± 0,005	0,014 ± 0,07

Les différences correspondent à 19± 20 keV pour $\bar{E}_\gamma$ (après correction pour l'effet des protons de recul) et à 110 ± 55 keV pour $\bar{\nu}$. Elles sont à peine significatives : contrairement à Weinstein [5] et à Ryabov [4], nous n'observons pas de corrélation nette entre $\bar{\nu}$ ou $\bar{E}_\gamma$ et le spin des résonances pour ^{239}Pu.

VI - CONCLUSION

La mesure simultanée de $\bar{\nu}$ et $\bar{E}_\gamma$ pour ^{235}U et ^{239}Pu semble avoir résolu les contradictions qui existaient entre les différentes mesures publiées.

Les fluctuations de $\bar{\nu}$ et $\bar{E}_\gamma$ que nous avons obtenues pour ^{239}Pu peuvent être interprétées comme une mise en évidence expérimentale de la réaction $(n,\gamma f)$.

Dans la limite de la précision statistique, nous n'observons aucune variation anticorrélée de $\bar{\nu}$ et $\bar{E}_\gamma$ pour ^{235}U, ce qui confirme les faibles valeurs de $\Gamma_{\gamma f}$ obtenues par le calcul.

Nous n'observons pas de corrélation supérieure à 0,5 % entre $\bar{\nu}$ ou $\bar{E}_\gamma$ et le spin des résonances pour ^{239}Pu et ^{235}U.

La différence de 110 ± 55 keV entre les valeurs de $\bar{\nu}$ pour les résonances 1^+ et les résonances 0^+ du ^{239}Pu semble correspondre à un effet de spin, elle est dans le sens prévu à partir de la théorie de Bohr.

REFERENCES

[1] BOHR, A., in Int. Conf. Peaceful Uses At. Energy (C.r. Conf. Genève, 1955) 2, ONU, New York (1956) 151.

[2] DERRIEN, H., BLONS, J., EGGERMAN, C., MICHAUDON, A., PAYA, D., RIBON, P., in Nuclear Data for Reactors (C.r. Conf. Paris, 1966) 2, AIEA, Vienne (1967) 195.

[3] COWAN, G., Phys. Rev. 114 (1966) 979.

[4] RYABOV, Yu.V., SO DON SICK, CICKOV, N., IANEVA, N., Rapport Doubna P 3-5297 (1970).

[5] WEINSTEIN, S., REED, R., BLOCK, R.C., in Physics and Chemistry of Fission (C.r. Coll. Vienne, 1969), AIEA, Vienne (1969) 477.

[6] WESTON, L.W., TODD, J.H., Proc. Conf. Neutron Cross Sections and Technology 2, University of Tennessee (1971) 861.

[7] TROCHON, J., LUCAS, B., MICHAUDON, A., PAYA, D., RYABOV, Yu., soumis pour publication dans J. Phys. Paris.

[8] THEOBALD, J.P., et al. Communication privée (1971).

[9] SHACKLETON, D., FREHAUT, J., LE BARS, M., C.r. Conf. Physique Nucléaire, Aix-en-Provence, Suppl. J. Phys. Paris 33 (1972) 24.

[10] SOLEILHAC, M., FREHAUT, J., GAURIAU, J., J. Nucl. Energy 23 (1969) 257.

[11] BLONS, J., DERRIEN, H., MICHAUDON, A., Proc. Conf. Neutron Cross Sections and Technology 2, University of Tennessee (1971) 829.

[12] MICHAUDON, A., Advances in Nuclear Physics 6, ch. Nuclear Fission, Plenum Publ. Corp. (1973).

[13] SHACKLETON, D., TROCHON, J., FREHAUT, J., LE BARS, M., Phys. Lett., B42 3 (1972) 344.

[14] FREHAUT, J., SHACKLETON, D., TROCHON, J., National Soviet Conference, Kiev, 1973.

[15] BLONS, J., DERRIEN, H., MICHAUDON, A., in Nuclear Data for Reactors (C.r. Conf. Helsinki, 1970) 1, AIEA, Vienne (1970) 513.

[16] NIFENECKER, H., et al., Nucl. Phys., A189 (1972) 285.

[17] RYABOV, Yu., TROCHON, J., SHACKLETON, D., FREHAUT, J., soumis pour publication dans Nucl. Phys.

[18] SHACKLETON, D., TROCHON, J., Résumé IAEA-SM-174/39, ces comptes rendus, vol.II.

[19] LYNN, J.E., Phys. Lett. 18 (1965) 31.

[20] LE COQ, G., Thèse, Paris, 1970 (non publiée).

DISCUSSION

J. TROCHON: An independent measurement of the multiplicity of prompt gamma rays from $^{239}Pu + n$ and $^{235}U + n$ fission was made at the Saclay linear accelerator; the results show the same variations from resonance to resonance as did the measurements of $\bar{E}_\gamma$.

This result can be explained very well in the case of ^{239}Pu as an effect of the $(n, \gamma f)$ process. The average number of prompt gamma rays varies only very little with the excitation energy of the fissioning nucleus, and consequently the total number of gamma rays emitted is increased by one unit, if the nucleus emits a pre-fission gamma ray.

In addition, we calculated[1] the width $\Gamma_{\gamma f}$ and the mean energy $\langle E_\gamma \rangle$ of the prompt gamma rays for the 1^+ resonances of ^{239}Pu from the experimental value for ^{239}Pu derived from measurements of $\bar{\nu}$

$$\Gamma_{\gamma f} \cdot \langle E_\gamma \rangle = (4715 \pm 400)\ eV^2$$

The calculation was performed with a simple barrier and on the assumption that only the gamma rays corresponding to the E1 transitions were emitted by the compound nucleus. The result we obtained was $\Gamma_{\gamma f_{1^+}} = 5.4 \pm 1.2$ meV,

[1] These Proceedings, Abstract IAEA-SM-174/39, Vol.2.

which is comparable with the calculations[2] of J. E. Lynn, who obtained $\Gamma_{\gamma f_{1+}} \sim 3$ meV. It is also in agreement with the limit $\Gamma_{\gamma f} \leq (4 \pm 1)$ meV obtained from an analysis of the effective (n, f) fission cross-sections. However, the value of $\langle E_\gamma \rangle = (850 \pm 100)$ keV which we find seems too high, for it corresponds to a height of the 1^- fission barrier much lower than that generally assumed. This could be due to the presence in the second well of the double-humped barrier of vibration states observed at around 1.2 MeV below the neutron binding energy in the effective cross-section of the (d, pf) reaction.

G. DE SAUSSURE: You said that you had performed measurements of $\bar{\nu}$ for ^{241}Pu. Do you have any results available?

J. FREHAUT: No, they are still being analysed.

T. GOZANI: Is your scale for $\bar{E}_\gamma$ in absolute or relative units?

J. FREHAUT: It is in relative units.

T. GOZANI: Do you have an absolute calibration for $\bar{E}_\gamma$ and $E_{\gamma 0}$ so that one can compare them with independent data?

J. FREHAUT: The calibration for $\bar{E}_\gamma$ is also relative and we do not obtain absolute values, neither for $\bar{E}_\gamma$ nor for $\bar{E}_{\gamma 0}$, the prompt gamma energy for (n, f) fission.

R. E. HOWE: At Livermore we also measured $\bar{\nu}$ for ^{235}U. We did not use the method of the Saclay group, nor that of the Rensselaer Polytechnic Institute group, but used instead two fast liquid scintillators with a near-critical spherical shell of ^{235}U surrounding our fission chamber. By using pulse-shape discrimination on the scintillators, we were able to separate secondary neutrons from the ^{235}U shell and miscellaneous gamma rays. Since the shell converts prompt fission neutrons, we eliminate any possible bias due to shifts in the spectrum of prompt neutrons.[3]

In brief, our results agree with those of the Saclay group, and fairly well with those of RPI, although our energy range is from 0.5 to about 300 eV. Using the spin assignments given by Keyworth[4], we definitely did not observe any spin dependence of $\bar{\nu}$. In particular, the 8.8 and 19.3 eV resonances differ in $\bar{\nu}$ values by almost 0.8%. The errors in these two points are slightly larger than 0.1%. Both of these resonances in ^{235}U have spin 4.

However, we did find some definite trends in $\bar{\nu}$ with energy. These are as follows: from 0.5 to 9 eV, $\bar{\nu}$ is high by about 0.4%; from 10 eV to 16 eV $\bar{\nu}$ descends smoothly to 0.5% below the mean; it remains 0.5% below the mean through 23 eV; from 24 eV to 55 eV, $\bar{\nu}$ remains flat within statistics; there is a brief decrease between 56 and 61 eV; finally $\bar{\nu}$ stays approximately flat at the mean value from 71 to 125 eV. Average data points are about 1.5 to 2.0 standard deviations from the mean. The spread in $\bar{\nu}$ values is roughly four times the width expected from the statistics of the data.

M. ASGHAR: I should like to ask Mr. Fréhaut two questions: firstly, what is the average multiplicity that you get from your data? Secondly, your data show no correlation between the $\bar{\nu}_r$ and the spin of the resonances. What is the situation when you add up the E_γ to $\bar{\nu}$?

J. FREHAUT: The multiplicity of the prompt gamma rays was measured by Trochon who will be able to answer that question. The fluctuations of $\bar{\nu}$ and $\bar{E}_\gamma$, expressed in energy, have the same amplitude but are of different

---

[2] LYNN, J.E., Phys. Lett. 18 (1965) 31.

[3] See Abstract IAEA-SM-174/65, these Proceedings, Vol.2.

[4] KEYWORTH, G.A., et al., Paper IAEA-SM-174/65, these Proceedings, Vol.1.

sign. The sum $\bar{\nu} + \bar{E}_\gamma$ is therefore constant for the 1^+ resonances and independent of Γ_f. Our results show that $\bar{E}_\gamma$ is 19 ± 20 keV greater and $\bar{\nu}$ is 110 ± 55 keV greater for the 0^+ resonances than for the 1^+ resonances, after correcting for the effect of the $(n,\gamma f)$ reaction. The sum $\bar{\nu} + \bar{E}_\gamma$ is therefore 129 keV greater for the 0^+ resonances, which may correspond to a spin effect.

J. TROCHON: The measurement we performed was a relative one and we have not normalized the results.

T. GOZANI: My remark pertains to all the papers which have dealt with $\bar{E}_\gamma$, ν_γ and related quantities. It seems to me that sometimes, when reference is made to prompt gamma rays from fission, there is an implicit assumption that the gamma ray multiplicity is independent of the energy spectra of the photons. While I do not presume that the possible invalidity of such an assumption would be at all detrimental to any of the quantities measured, I do feel that this question is a relevant one. Some years ago I conducted an experiment to see whether the multiplicity-energy function $\nu_\gamma(E)$ is separable, using a small ^{252}Cf source, large plastic scintillators for multiplicity determination, a fission detector and an NaI(Tl) spectrometer. The results indicated a small energy-multiplicity correlation for ^{252}Cf. More details can be found in the Abstract IAEA-SM-174/88 in these Proceedings.

H. NIFENECKER: One has to distinguish over-all measurements of the correlation between average photon energy and multiplicity with fixed total gamma-ray energy and those where the total gamma-ray energy varies. In my paper I assumed that the average energy of the photons did not vary strongly as a function of the total kinetic energy of the fragments (for example). This has been shown to be almost the case by F. Pleasonton and co-workers.

MEASUREMENT OF PROMPT GAMMA-RAY LIFETIMES OF FISSION FRAGMENTS OF ^{252}Cf[§]

R.C. JARED, H. NIFENECKER, S.G. THOMPSON
Lawrence Berkeley Laboratory,
University of California,
Berkeley, Calif.,
United States of America

Abstract

MEASUREMENT OF PROMPT GAMMA-RAY LIFETIMES OF FISSION FRAGMENTS OF ^{252}Cf.

The emission times of prompt gamma rays from the fission fragments of ^{252}Cf have been measured over a time range from approximately 1.0×10^{-10} to 2.0×10^{-9} seconds using the velocity and flight path of the fission fragment to determine the time. The ^{252}Cf source was deposited on a thin foil attached to a micrometer screw and located between two fission fragment detectors. The distance from the source to one of the fragment detectors was varied over a range from approximately 0.01 to 2.0 cm. A gamma-ray detector was located close to the reference fragment detector and operated in coincidence with the fission events. The gamma rays associated with the stopped fragments were distinguished from those of the moving fragments on the basis of the known Doppler shift. Measurements were taken at various distances between the source and the detector. The measured fission fragment kinetic energies were used to calculate the masses of the stopped fragments. Thus the gamma-ray spectra associated with the different fragment masses were obtained. The measured spectra were then used to obtain the intensities of the gamma lines at each distance. From these data it has been possible to obtain the energies and lifetimes of the electromagnetic radiation emitted by the fragments promptly after formation. Such data provide valuable information indicating values of the deformation parameters of the even-even isotopes; in particular the quadrupole moments calculated on this basis were found to agree with the theoretical values.

INTRODUCTION

In the recent past, interest in the neutron-rich isotopes near A = 100 has been generated by the observation of rotational-like energy levels which suggested a new region of deformation. The fission of ^{252}Cf produces isotopes in this region and thus is a convenient source for use in their study.

In this paper we report the results of a new series of experiments where the lifetimes of the high-yield gamma lines in the spontaneous fission of ^{252}Cf are measured by using their known velocities and defined flight paths. The length of the flight path is adjusted to six different positions. Each position corresponds to a well-defined average flight-path from fission until the fragments are stopped and thus to a known flight time of the fission fragments. Due to the high velocity of the fission fragments, the gamma rays emitted during flight are Doppler shifted and easily separated from those of the stopped fragments. At each position approximately 10^7 events were collected and mass sorted to obtain gamma-ray spectra as a function of the fragment mass. The intensities of the unshifted gamma lines are used along with the flight path length to obtain the lifetimes of the transitions. From the lifetimes and energies of the transitions, information on the deformation parameters of the even-even isotopes is obtained.

§ Work performed under the auspices of the US Atomic Energy Commission.

EXPERIMENTAL ARRANGEMENT

The experimental arrangement shown in Fig. 1 consists of five detectors. The fragment detector 1 is fixed in position and is parallel to the ^{252}Cf source and to the fission fragment detector 2(F2). The position of the ^{252}Cf source in respect of fragment (F1) detector can be varied by means of a micrometer screw in order to obtain different flight distances for the fission fragments. Since the velocity of the fragments is known, each distance corresponds to a particular time between fission and the instant when the fragment is stopped in the detector. The pulses produced by the gamma detector located behind the F2 detector are analyzed when they occur between 0 and 50 ns after a fission event is detected. The gamma rays emitted while the fragments are moving are Doppler shifted upwards by approximately 4%. This shift allows for an easy isolation of the gamma rays emitted after the fragment has stopped. Only the unshifted gamma rays from the stopped fragments are used to obtain the lifetimes. The gamma detector (3 cm^3 intrinsic germanium) is used to measure the intensities of the gamma lines from the stopped fragments. Fragment detector 2 is adjusted so that the variation in flight path over the finite acceptance angle is less than 10%. The alpha and NaI detectors operated in coincidence with the gamma detectors are used to provide gamma lines for digital gain stabilization and zero intercept corrections.

ELECTRONICS

A simplified diagram of the electronics is shown in Fig. 2. The signals from the fission and gamma detectors are transmitted to both the linear and logic sections. The linear section is composed of variable gain amplifiers, linear amplifiers, linear gates and units controlling the zero intercept. The variable gain amplifier and zero intercept units are controlled by the computer. The output from the linear circuitry feeds dimensions 1 to 4 of the analogue multiplexer and are defined as: dimension 1 fragment detector 1, dimension 2 fragment detector 2, dimension 3 low-energy gamma rays (< 400 keV) and dimension

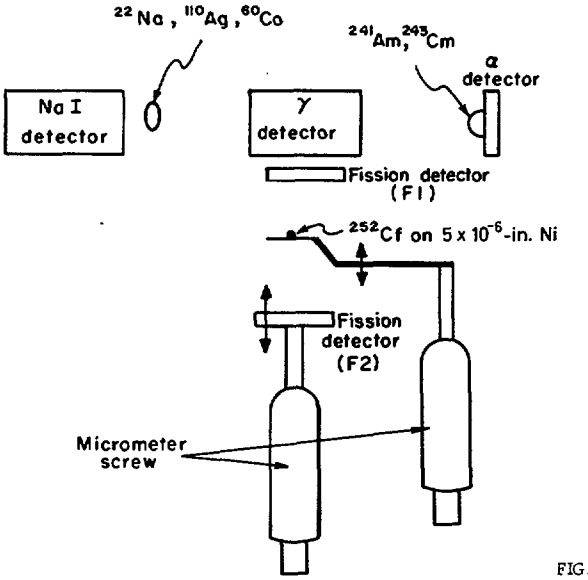

FIG. 1. The arrangement of the detectors.

4 high-energy gamma rays (< 1.2 MeV). The remaining two inputs to the analogue multiplexer are derived from the timing and logic sections. Dimension 5 is a marker which tells the computer what kind of event is being processed. Three different types of events can be processed: double coincidences between fragment detectors 1 and 2, triple coincidences between the two fragments and the gamma-ray detectors, and gamma stabilization events. One out of every twenty double coincidence events is used for digital gain stabilization and zero intercept correction of the fission fragment pulse height distribution.

The timing and logic circuitry that provides dimension 5 and the coincidence signal to the analogue multiplexer is fed by all 5 detectors and performs the normal coincidence (2τ = 100 ns) and logic functions. The sum of the fission stabilization events is used to give the number of fissions recorded during the data acquisition process and is used to determine the yields of the gamma lines per fission. The event-by-event data obtained from the analogue-to-digital converter are accepted by the computer and recorded on magnetic tape to be used for additional off-line sorting of the data, if necessary. In addition, the computer makes an on-line mass sort to obtain gamma-ray distributions as a function of mass. There are 32 such distributions, 4096 channels long, corresponding to adjacent mass windows of 2 amu. The gamma distributions are analyzed in a larger computer at the end of the experiment to obtain the gamma-ray intensities.

The mass calculation is performed by means of a table look-up procedure. An array containing masses indexed by the two fragments pulse height F1, F2 is precalculated and used as the table. The mass calculation is similar to that described by Watson et al. [1]. We differ in that we are using the neutron data from Nifenecker et al. [2]. Possible grid effects were removed by recording fission fragments pulse heights with 4096 channels.

DATA REDUCTION

The gamma-ray spectrum associated with each mass window is analyzed with the photopeak analysis code developed by Routti and Prussin [3] to obtain the gamma line intensities. Since the mass resolution (σ = 2-4 amu) is much broader than our mass windows (2 amu) it is necessary to fit the intensities of a particular gamma line as a function of mass assuming the shape of a gaussian in order (Fig. 3) to obtain the total yield at each position.

As mentioned above, six positions with respect to distance were used in the experiment: 0.008, 0.1250, 0.2500, 0.5000, 1.000, and 2.000 cm. Figure 3 shows an example of the intensities obtained for the 2 → 0 transition in ^{102}Zr. From these distances, the acceptance angle of the fission detectors and the velocities of the fission fragments, the lifetimes of the gamma lines were calculated. The average velocity of the fragments that produced a specific isotope after neutron emission was determined by first taking the Z of that isotope and using the experimental data of Reisdorf et al. [4] that gives the average preneutron mass (A^*) for the production of each charge. The mass of the isotope produced (A_F) is then subtracted from this mass to obtain the average number of neutrons emitted ($\bar{\nu} = A^* - A_F$). The number of neutrons emitted is then used along with the preneutron mass as indexes in the experimental data that gives the relationship of the total kinetic energy (E_K) of the fission fragments to $\bar{\nu}$ and A^* of Nifenecker et al. [2] to determine E_K. This value of E_K and A^* are then used in Eq. (1) to define the average value of the velocity

$$V_1 = \sqrt{\left(\frac{2}{A^*} - \frac{1}{126}\right)E_K} \qquad (1)$$

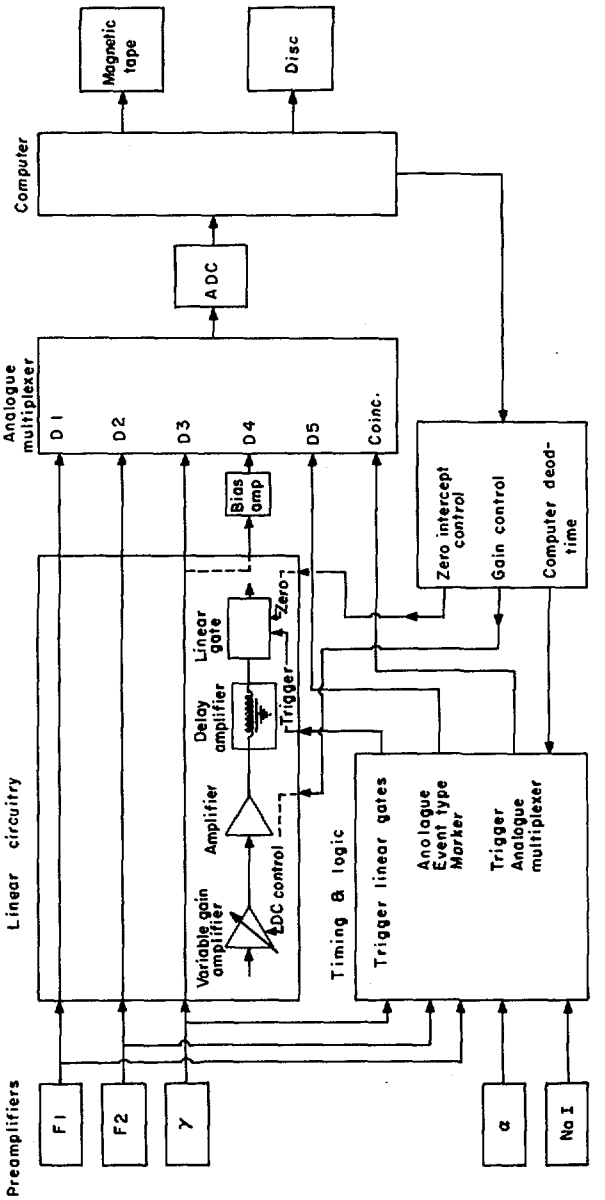

FIG. 2. Simplified diagram of the electronics.

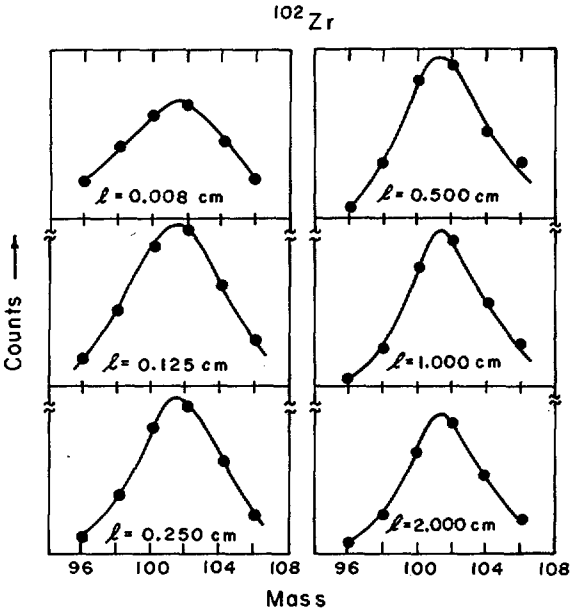

FIG.3. A composite plot of the intensity of ^{102}Zr $2^+ \rightarrow 0^+$ transition as a function of mass for each position. The counts are in arbitrary units and are not normalized to the number of fissions.

The lengths (ℓ) listed earlier for the distances from the source to the F1 detector are converted by Eq. (2) before calculating the lifetimes

$$\bar{\ell} = -\ell \left(\frac{\ell n |\cos \theta|}{1 - \cos \theta} \right) \qquad (2)$$

The angle θ is the acceptance angle of the fission fragment detectors. This correction was needed to define the length of the average flight path of the fragments. Using these distances and velocities of individual isotopes each position of the source is converted to a time between fission and the instant when a particular fragment of measured mass is stopped. This time is then used along with the gamma line yield at each position to determine the lifetime of each gamma transition.

The lifetimes of the gamma lines were then used to determine the reduced electric-quadrupole transition widths ($B(E2)_{ex}$), intrinsic electric quadrupole moments (Q_0) and β_2. These parameters which appear in Table I were obtained following the procedure of Stelson and Grodzins [5]. The isotopic assignments in Table I are taken from previous work of this group [6]. These isotopic assignments have since been confirmed by Khan et al.[7]partially. Figure 4 shows an example of the gamma-ray spectra for different distances, in this case centered around mass 148. The ^{148}Ce line position is marked in the upper left in Fig. 4. This line shows no significant Doppler-shifted component at short times but at longer times the Doppler-shifted component becomes equivalent to the unshifted one. A small amount of ^{146}Ba can also be seen in this figure. Figure 5 shows the results determining the total yield of these lines over the appropriate masses at each position. The figure shows one of the two examples of a 2-component decay curve observed in this experiment. The two cases of multiple decay curves are ^{146}Ba and ^{110}Ru.

TABLE I. SUMMARY OF RESULTS FROM MEASUREMENTS OF PROMPT GAMMA RAYS FROM FISSION FRAGMENTS OF ^{252}Cf

	Fragment Velocity (cm/nsec)	$t_{1/2}$ (nsec)	Energy (keV)	$B(E2)_{ex}$ ($cm^4 \times 10^{-51}$)	$\frac{B(E2)}{B(E2)_{sp}}$	β_2	$\lvert Q_0 \rvert$ ($cm^2 \times 10^{-24}$)	Q_0 Calculated[a]	
								Oblate	Prolate
^{100}Zr $2^+ \rightarrow 0^+$	1.39	0.714±0.03	212.7	845±40	62±3	0.32±0.02	2.9±0.2	-2.3	3.26
^{102}Zr $2^+ \rightarrow 0^+$	1.52	3.17±0.25	151.9	1275±100	91±8	0.38±0.02	3.6±0.2	-2.33	3.53
^{104}Mo $2^+ \rightarrow 0^+$	1.36	0.911±0.03	192.3	1060±40	74±3	0.32±0.02	3.26±0.2	-2.36	3.22
^{106}Mo $2^+ \rightarrow 0^+$	1.44	1.25±0.03	171.7	1300±40	88±3	0.35±0.02	3.61±0.2	-2.37	3.40
^{108}Ru $2^+ \rightarrow 0^+$	1.28	0.345±0.03	242.3	930±80	61±6	0.28±0.02	3.05±0.2	-2.42	2.88
^{110}Ru $2^+ \rightarrow 0^+$	1.38	0.34±0.04	240.8	970±120	62±7	0.28±0.02	3.12±0.2	-2.50	3.05
^{112}Ru $2^+ \rightarrow 0^+$	1.44	0.32±0.03	236.8	1120±110	70±7	0.32±0.02	3.35±0.2	-2.58	3.01
^{114}Pd $2^+ \rightarrow 0^+$	1.34	0.198±0.06	332.9	340±100	21±6	0.16±0.03	1.85±0.3	-2.42	2.73
^{116}Pd $2^+ \rightarrow 0^+$	1.40	0.106±0.03	340.6	570±170	34±10	0.20±0.03	2.39±0.3	-2.43	2.62
^{142}Ba $2^+ \rightarrow 0^+$	0.95	0.070±0.04	359.7	660±400	30±16	0.16±0.04	2.57±0.4		
^{144}Ba $2^+ \rightarrow 0^+$	1.08	0.070±0.03	199.4	1100±60	49±3	0.20±0.02	3.33±0.2	-2.17	2.20
^{146}Ba $2^+ \rightarrow 0^+$	1.09	0.86±0.06	181.0	1390±100	61±4	0.22±0.02	3.73±0.2		
^{146}Ce $2^+ \rightarrow 0^+$	0.93	0.26±0.05	258.6	880±180	39±8	0.17±0.02	2.97±0.2	-2.56	3.03
^{148}Ce $2^+ \rightarrow 0^+$	1.00	1.06±0.08	158.7	200±160	87±7	0.25±0.02	4.48±0.2	-3.30	4.56
^{150}Ce $2^+ \rightarrow 0^+$	1.03	3.60±1.0	97.1	3300±950	141±40	0.32±0.04	5.76±0.4		
^{154}Nd $2^+ \rightarrow 0^+$	0.97	7.7±2	72.8	2180±650	102±26	0.25±0.03	4.67±0.4		

[a] Q_0 calculated is from Ref. [7].

In $B(E2)_{ex}$ and $B(E2)_{sp}$, the subscripts ex and sp refer to experimental and single particle, respectively.

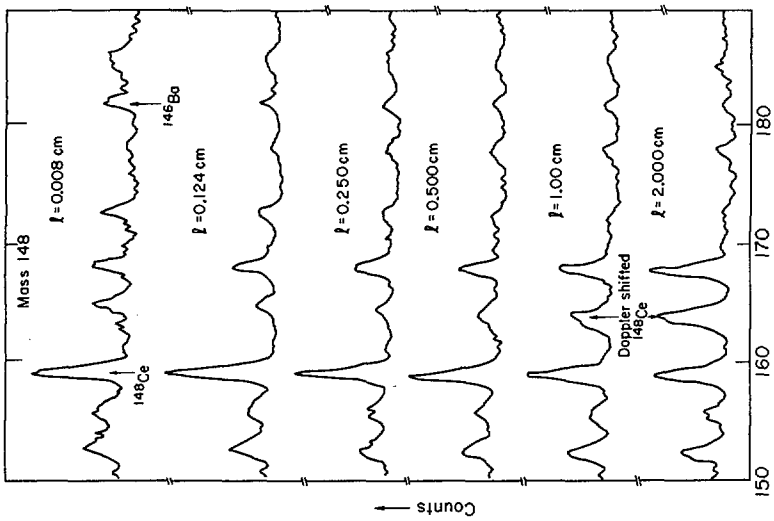

FIG. 4. Gamma spectra at different distances. The counts are in arbitrary units and are not normalized to the number of fissions.

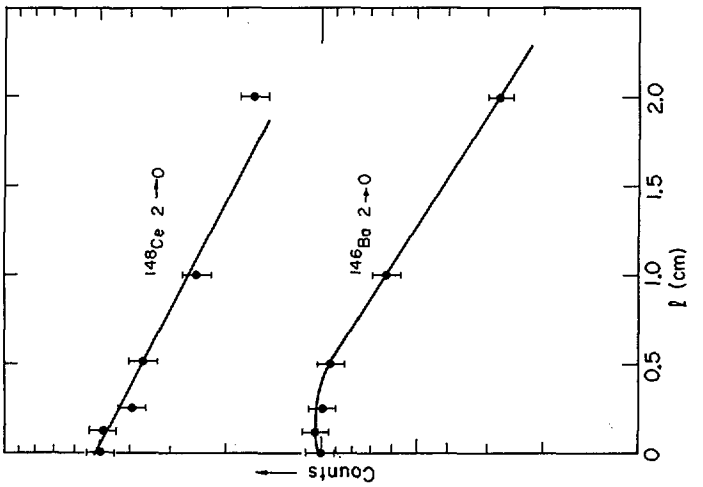

FIG. 5. Decay curves for ^{148}Ce and ^{146}Ba.

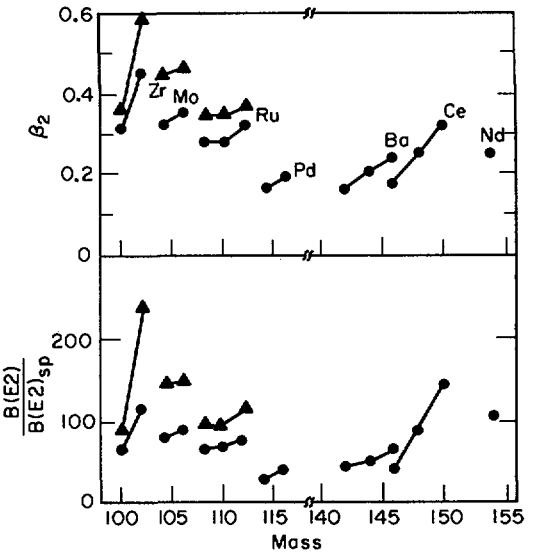

FIG.6. Comparison of the β_2 and $B(E2)/B(E2)_{sp}$ values of the experiment of Cheifetz and co-workers with those of this work. ▲: Cheifetz and co-workers, ●: this work.

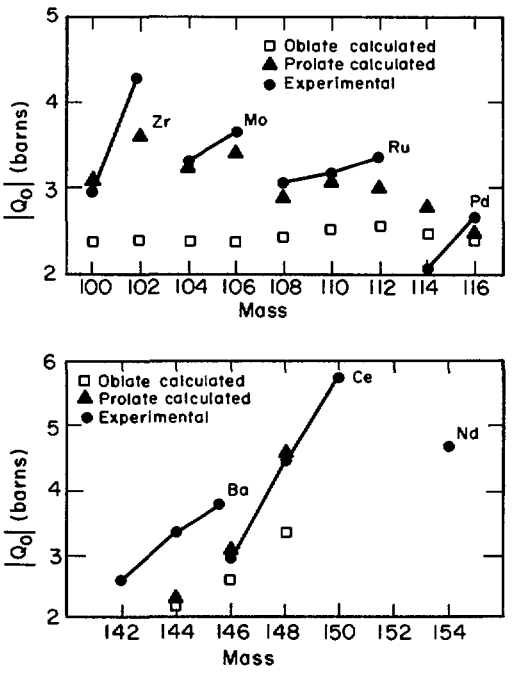

FIG.7. A comparison of the experimental and the calculated results of Ragnarsson [7].

No attempt has been made to correct the data for the hyperfine interaction (HFI) which couples the nuclear and the electronic spins of the fission fragments. This effect is expected to be strong for highly ionized fission fragments. This correction is such as to decrease the lifetimes as reported in this experiment. The magnitude of the correction could be as large as 20% if the destruction of the fission fragment alignment by the HFI occurred in a time comparable to the half-life of the gamma transition. It is expected, however, that the characteristic time for the spin deorientation should be much shorter than the half-lives reported here and, therefore, that such effects are probably negligible.

The results of this experiment do not agree well with the previous results of our group [6] using a two-point decay curve. Figure 6 shows the values of β_2 and $B(E2)/B(E2)_{sp}$ obtained from both experiments. It is seen that the half-lives measured in this experiment are approximately 50% longer than those reported earlier. The results of this experiment are also compared with the calculations of Ragnarsson et al. [8]. In Fig. 7 it can be seen that the agreement between calculated values for prolate shapes and the experimental ones is remarkably good. This of course does not prove that the system is prolate because we can not determine the sign of Q_0.

It should be noted that the previously reported large deformation ($\beta_2 \sim 0.6$) of zirconium 102 is disproved in this experiment.

ACKNOWLEDGMENTS

We wish to thank J. B. Hunter for help at various stages of the experiment and to J. Blachot for checking of numerical calculations.

REFERENCES

[1] WATSON, R. L., WILHELMY, J. B., JARED, R. C., RUGGE, C., BOWMAN, H. R., THOMPSON, S. G., RASMUSSEN, J. O., Nucl. Phys. A141 (1970) 449.
[2] NIFENECKER, H., SIGNARBIEUX, C., BABINET, R., POITOU, J., Paper IAEA-SM-174/207, these Proceedings, Vol. 2.
[3] ROUTTI, J. T., PRUSSIN, S. G., Nucl. Instr. Methods 72 (1969) 125.
[4] REISDORF, W., UNIK, J. P., GRIFFIN, H. C., GLENDENIN, Nucl. Phys. A177 (1971) 337.
[5] STELSON, P. H., GRODZINS, L., Nucl. Data A1 (1965) 211.
[6] CHEIFETZ, E., JARED, R. C., THOMPSON, S. G., WILHELMY, J. B., International Conference on the Properties of Nuclei Far from the Region of Beta-Stability, CERN, 7-30, 2 (1970) 883.
[7] KHAN, T. A., HOFMAN, D., HORSCH, F., to be published, Nucl. Phys. (1973).
[8] RAGNARSSON, International Conference on the Properties of Nuclei Far from the Region of Beta-Stability, CERN, 7-30, 2 (1970) 847.

FISSION FRAGMENT ISOMERS FROM SPONTANEOUS FISSION OF ^{252}Cf§

R.G. CLARK
University of Maryland,
Department of Chemistry,
College Park, Md.

L.E. GLENDENIN
Argonne National Laboratory,
Argonne, Ill.

W.L. TALBERT, Jr.
Iowa State University,
Ames, Iowa,
United States of America

Abstract

FISSION FRAGMENT ISOMERS FROM SPONTANEOUS FISSION OF ^{252}Cf.

Isomeric levels, populated before beta decay during the de-excitation of ^{252}Cf fission fragments, have been studied by observing the K X-rays and gamma rays from the isomeric decay. A six-parameter experiment with high-resolution Si(Li) and Ge(Li) detectors measured photon energies from 10-1500 keV and emission times from 1-3000 nsec after the detection of complementary fission fragment pairs by Si-Au surface barrier detectors. The photon intensity was studied as a function of fragment mass (computed from the complementary fragment kinetic energies), photon energy and emission time. Half-life and fragment mass assignments were made for all isomeric gamma rays. A four-parameter experiment, using two Ge(Li) detectors, observed coincidences between isomeric gamma rays, and the coincidence information was combined with the assignments and observed K X-ray intensities of the six-parameter experiment and with other work to assign 130 of the transitions to specific nuclei. Previously reported concentrations of the isomeric gamma-ray intensity around masses 98, 108 and 134 are discussed, along with feeding from isomeric levels into ground state rotational bands in the deformed rare-earth region.

1. INTRODUCTION

The neutron-rich, intermediate-mass nuclei far from stability have been for many years tempting, yet elusive, targets of nuclear spectroscopists, tempting because of their abundant availability as fission products, elusive because of the difficulty involved in studying the desired nucleus among the host of others produced in fission. Beta decay studies of fission products have been greatly facilitated by the advent of rapid chemical separation techniques and magnetic isotope separators operated on-line to reactors. However, progress in obtaining detailed spectroscopic information on fission fragment de-excitation before beta decay has been slow and difficult in spite of significant developments in the technology of semiconductor detectors and the advent of sophisticated multiparameter data acquisition systems.

§ Work performed under the auspices of the US Atomic Energy Commission.

The most significant studies of fission fragment spectroscopy are those reported by Watson et al. [1] in which fragment masses, atomic numbers, half-lives, multipolarities and energies of transitions were determined for gamma-ray and conversion-electron decay and those by Cheifetz et al. [2] and Wilhemy et al. [3] in which the systematics of the ground-state bands in even-even fragments are presented. The participants of the previous Fission Symposium at Vienna[1] were given preliminary reports of studies underway by John and collaborators at Livermore [4] and also by Armbruster and collaborators at Jülich [5] on isomeric states populated during fission fragment de-excitation. We wish to report here the results of two experiments dealing with fission fragment isomers carried out at Argonne National Laboratory.

2. EXPERIMENTAL PROCEDURE

The first of the two experiments was the six-parameter experiment illustrated in Fig. 1. A ^{252}Cf source (2 x 10^5 fissions/minute) was placed between two Si-Au surface barrier (SB) detectors of 4-cm^2 active area which detected the complementary fragment pairs from fission events. The SB detectors were cooled to -15°C during the experiment, and their mass calibration and resolution were checked by monitoring the mass spectra associated with prominent gamma rays from known masses. A planar Si(Li) detector of active volume 3 mm x 1.1 cm^2 and energy resolution of 560 eV full-width at half maximum (FWHM) at 26 keV was used to observe photons in the 10-100 keV range emitted by fragments after the first few millimeters of flight path. The prompt x-ray shield (1.7-mm-thick Cu) prevented detection of low-energy photons emitted by fragments near the source and of the Cm x-rays following alpha decay of ^{252}Cf. A planar Ge(Li) detector of active dimensions 1.0 cm x 2.0 cm x 2.7 cm and energy resolution varying from 2.0 keV (FWHM) at 122 keV to 2.9 keV (FWHM) at 1332 keV was placed on the opposite side of the source from the Si(Li) detector. By use of a Cu-lined Pb shield the Ge(Li) detector was permitted to view only those photons emitted by fragments near or stopped in Fragment Detector 1. The energy-dependent absolute detection efficiencies and linearities of the Si(Li) and Ge(Li) detector systems were determined by placing standardized sources on the face of a SB detector located in the same experimental geometry.

Fig. 2 illustrates the electronic signal processing used in the first experiment. The six ADC's were coincidence gated (OR GATE output) by one or both of two logic conditions: 1) there must have been a fast (2τ = 300 nsec) coincidence (FAST COINC) between the two SB detectors (F1, F2), undistorted by accidental pile-up with an alpha particle; and 2) this FAST COINC output must have been in slow coincidence (SLOW COINC) with both a time-to-amplitude converter (TAC) output and a photon-detector pulse-shape discriminator (PSD) output. The latter two outputs must have been associated with either the Si(Li) detector, Ge(Li) detector, or both. The PSD circuits

---

[1] INTERNATIONAL ATOMIC ENERGY AGENCY, Physics and Chemistry of Fission, (Proc. Symp. Vienna, 1969), IAEA, Vienna (1969).

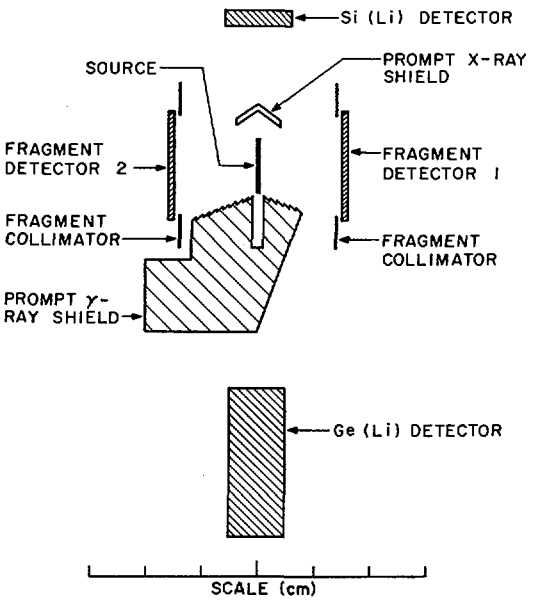

FIG 1. Schematic representation of the experimental geometry of the first fission fragment isomer experiment.

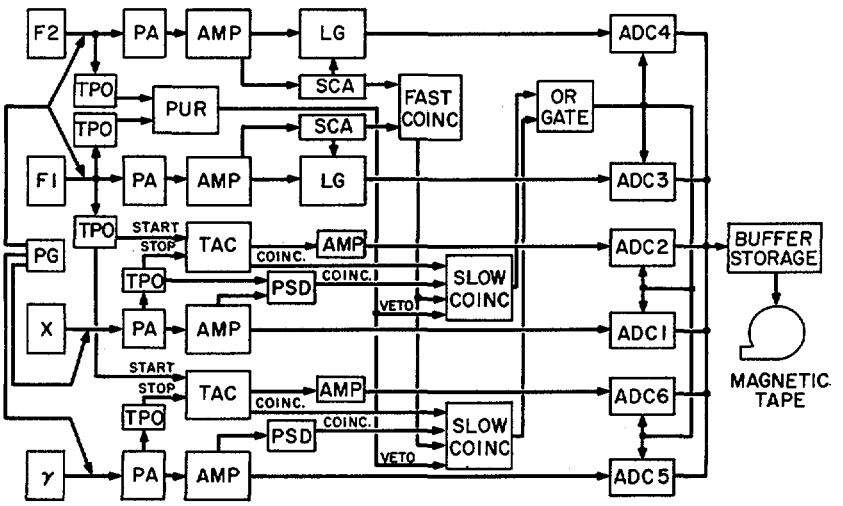

FIG.2. Block diagram of the electronics for the first experiment: F1, F2: fission-fragment detectors; X: Si(Li) detector; γ: Ge(Li) detector; PG: pulse generator; TPO: time pick-off; PA: preamplifier; AMP: linear shaping amplifer; PUR: pile-up rejector; TAC: time-to-amplitude converter; PSD: pulse shape discriminator; LG: linear gate; SCA: single-channel analyser; FAST COINC: fast-coincidence circuit; SLOW COINC: slow-coincidence circuit; ADC: analogue-to-digital converter.

were used to suppress photon detector pulses with anomalously slow rise times which cause spurious lifetime components in the TAC spectra [6]. A dual pulse generator (PG) was used at a low repetition rate to monitor instabilities in the electronic gains and baselines, and these pulser "events" were tagged by a special bit on the magnetic tapes. Changes in the gains and baselines were then corrected during subsequent data analysis by following the first moments of the pulser "event" peaks.

The electronic logic used here produced three types of real events on the data tapes: 1) F-F-G, a coincidence between a fission fragment pair and a photon in the Ge(Li) detector; 2) F-F-S, in which the photon detector is the Si(Li); and, 3) F-F-G-S, in which coincident photons are detected by both the Ge(Li) and Si(Li). Each F-F-G and F-F-S event had four parameters (F1, F2 and the pulse height and TAC output associated with its photon detector), while the F-F-G-S events had six parameters (F1, F2 and the pulse heights and TAC outputs of both photon detectors). In this experiment 8×10^6 F-F-G events, 5.5×10^6 F-F-S events and 8×10^4 F-F-G-S events were accumulated.

The objective of the data analysis was the determination of the energy of each gamma ray, the mass and charge number of the emitting nuclide, and the half-life and intensity of the activity, plus estimates of the associated errors. To obtain the mass, half-life, intensity and gamma-ray energy, the F-F-G and F-F-S events were treated in the following manner. The multiparameter data tapes were read, and the mass (after prompt neutron emission) of the fragment striking Fragment Detector 1 was computed from the two complementary fragment pulse heights using the previously established energy calibration method of Schmitt et al. [7] and correcting for prompt neutron emission [8]. The photon energy and TAC were corrected for electronic instability and the TAC parameter corrected for pulse-height-dependent timing walk. The data were then accumulated into photon energy spectra, sorted into time-after-fission intervals and 2-amu-wide mass intervals. For the Ge(Li) spectra, eight time regions were chosen with boundaries at 5, 9, 15, 29, 49, 99, 299, 999 and 3000 nsecs. Ten time regions were chosen for the Si(Li) spectra with boundaries at 7, 11, 15, 19, 27, 47, 99, 199, 299, 999 and 3000 nsec.

Each mass-time sorted photon energy spectrum was computer-analyzed by the Iowa State University PEAKFIND code [9] which located peaks using a method similar to that reported by Mariscotti [10]. After the peaks were located in a spectrum, PEAKFIND then fitted each peak intensity with a skewed Gaussian function (plus background) to obtain the photopeak centroid and intensity. The resulting ensemble of photopeak energies and intensities for all spectra was searched for peaks of the same energy appearing in adjacent mass and time regions, and those peaks were selected for the following analysis. The intensity distribution vs time and mass bin (from the previous step) was least-squares fitted with an appropriate functional form to determine the mass centroid, half-life and net intensity of the distribution for a particular gamma ray. The function used had a Gaussian shape in the mass direction and, in the time direction, was the integral between time boundaries of the convolu-

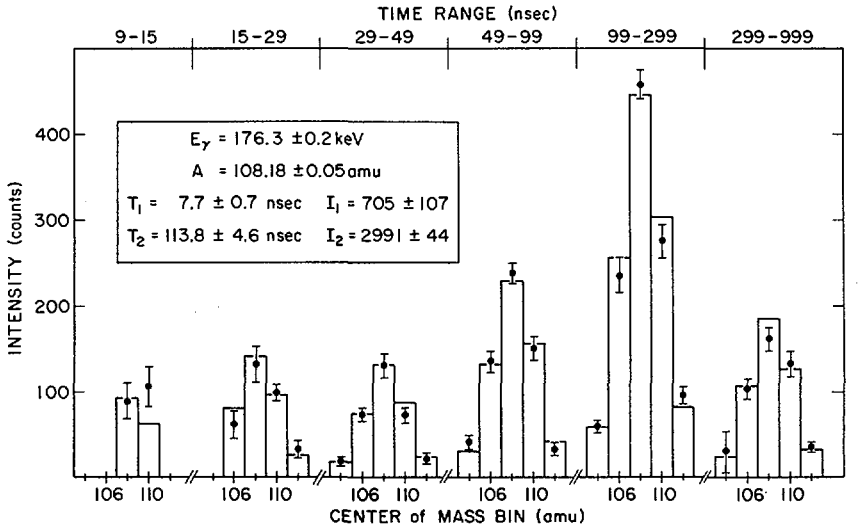

FIG.3. Resulting computer fit to PEAKFIND values of gamma-ray intensity versus (mass, time) regions for a two-time-component gamma ray. Solid circles with error bars are PEAKFIND intensities and histograms are least-squares-fit results. I_1 and I_2 are the total gamma-ray intensities of components 1 and 2 respectively of the two-time-component gamma ray. T_1 and T_2 are the half-lives of components 1 and 2 respectively of the two-time-component gamma ray.

ted exponential decay. The system prompt-time response functions used for the convolution lifetime analysis were experimentally determined beforehand. Fig. 3 shows the result of one such computer fit to a gamma ray with two lifetime components.

The portions of the F-F-S spectra containing the K x-rays were submitted to a least-squares computer program which resolved the spectra into individual contributions from elemental K x-ray groups. The K x-ray components (α_1, α_2, β_1', β_2') for each element were represented by the same skewed function used by PEAKFIND and the known relative intensities and energies [11] were kept fixed in the fitting procedure. The presence of gamma-ray interferences with K x-ray intensities in some regions was revealed by poor values of the resulting statistical goodness of fit and by observation of the graphical results of the fits in those regions. In such cases the fitting procedure was repeated with the gamma rays taken into account. A typical case of an interfering gamma ray, at 30.3 keV, is illustrated in Fig. 4.

The F-F-G-S events were sorted into a two-dimensional array of intensity vs Si(Li) energy and Ge(Li) energy, summed over the whole time range. The resulting array was then searched for

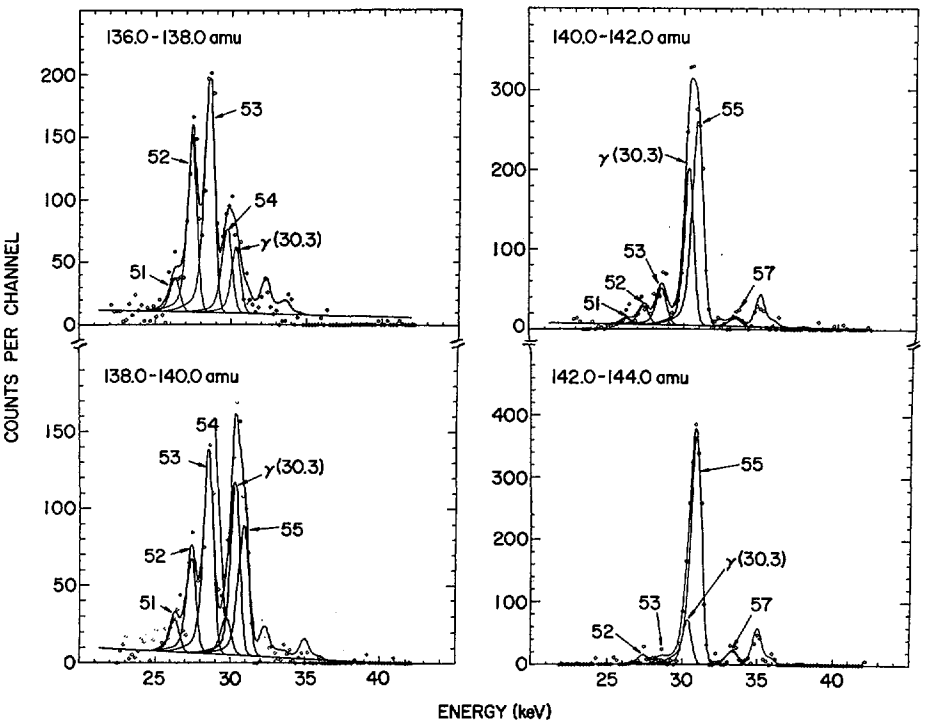

FIG.4. Least squares fits of K X-ray and 30.3-keV gamma-ray intensities for four consecutive mass bins in the 999-3000 nsec time range. Each resulting K_α peak is shown labelled with its elemental number.

coincidences between gamma rays and K x-rays. Due to the experimental geometry, a gamma ray could be detected in coincidence with a K x-ray from either the same fragment (due to internal conversion of cascading transitions) or the complementary fragment.

The final elemental identifications were made on the basis of the (gamma ray)-(K x-ray) coincidences, similar mass and half-life assignments for a gamma ray and K x-ray activity, and previous work on prompt gamma rays [1, 2, 3, 12], conversion electrons [1, 13] and (gamma ray)-(K x-ray) coincidence studies of fission product decays [14, 15]. Once the elemental identifications had been made, the mass number assignments were made based on local adjustments to the mass centroids of known ground-state band transitions in even-even fission fragments observed here and systematic deviations of the computed mass from the true mass scale [2, 3].

The second experiment, illustrated in Fig. 5, measured (gamma-ray)-(gamma ray) coincidences from de-excitation of the isomers. Ge(Li) Detector 1 was the same detector used in the first experiment. Ge(Li) Detector 2 was a coaxially drifted

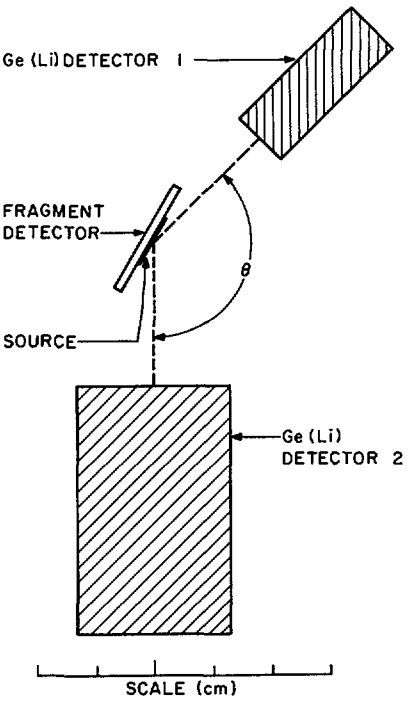

FIG.5. Geometrical arrangement used in the second fission fragment isomer experiment.

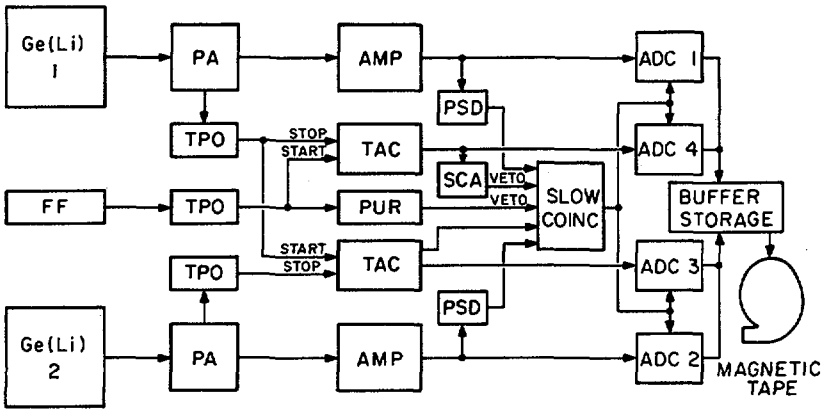

FIG.6. Block diagram of electronics for the second experiment. Nomenclature is identical to that of Fig.2 except that FF is the fission fragment detector.

detector with an active volume of 17 cm^3 whose resolution varied from 2.7 keV FWHM at 122 keV to 3.8 keV FWHM at 1332 keV. A block diagram of the electronics is shown in Fig. 6. Pulse shape discrimination was used on both Ge(Li) signals. The fission fragment detector (FF) was used to ensure that the two coincident gamma rays were themselves coincident with a fission event, and a pile-up rejection circuit was used to reject signals when two fission events occurred within 10 μsec. Four parameters were recorded for each event: 1) the photon energy from Ge(Li)-1, $E_{\gamma 1}$; 2) the photon energy from Ge(Li)-2, $E_{\gamma 2}$; 3) the time difference between Ge(Li)-1 and Ge(Li)-2 signals, $T_{\gamma\gamma}$; and the time difference between the fission event and detection of a photon in Ge(Li)-1, $T_{f\gamma}$. A single-channel analyzer window was set on the prompt region of $T_{f\gamma}$, and its output was used to veto coincidences between prompt gamma rays.

The 2.5×10^6 events collected from the second experiment were computer sorted into six correlation matrices of intensity vs ($E_{\gamma 1}$, $E_{\gamma 2}$). The six matrices represented six different $T_{f\gamma}$ regions with boundaries at 12, 28, 47, 97, 298, 999 and 3000 nsec. In order to facilitate the search of the correlation matrices for coincidences, a "similarity table" was constructed based on the results of the first experiment. The similarity table listed, for each isomeric gamma ray, those other isomeric gamma rays with similar half-life and mass centroid, and predicted the coincidence intensity for an assumed branching ratio of 1 with no internal conversion. For gamma rays emitted less than 50 nsec (the range of $T_{\gamma\gamma}$ parameter) after fission, the similarity table also displayed for each gating transition a list of gamma rays of the complementary masses which could appear to be coincident due to accidental detection of non-cascading gamma rays of short half-life, one from each fragment. The complementary mass list was used to negate otherwise apparent coincidences of similar gamma-ray energy.

3. RESULTS AND DISCUSSION

Table I presents those isomeric gamma rays which could be assigned to specific nuclei. Also listed are the coincidence data obtained from the second experiment, which were used in some cases to make the nuclear assignments. Those isomeric gamma rays for which a mass centroid could be determined, but no elemental assignment made, are listed in Table II. The initial mass centroids determined for F-F-S events were ambiguous with respect to the light vs heavy fragment assignment because of the Si(Li) detection geometry. In most cases the ambiguity was resolved by observing the same gamma ray in the F-F-G events or by mass and half-life similarity to a K x-ray activity. An assignment could be made to the heavy mass if the gamma-ray energy was below the K binding energy of the heavy fragment and the light fragment K x-rays showed no mass and half-life similarity, even though the K x-ray intensity was predicted to be observable in the most unfavorable case (i.e., E1 multipolarity). Figs. 7 and 8 show the regions of the chart of the nuclides in which the fission fragment nuclei occur. The solid curve in each region represents the line of most probable yield [16]. The nuclei determined in the

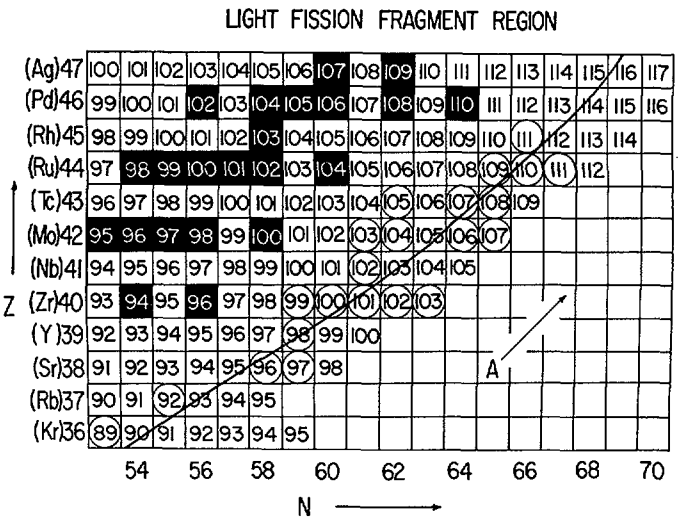

FIG. 7. Chart of the nuclides in the region of the light fission fragments.

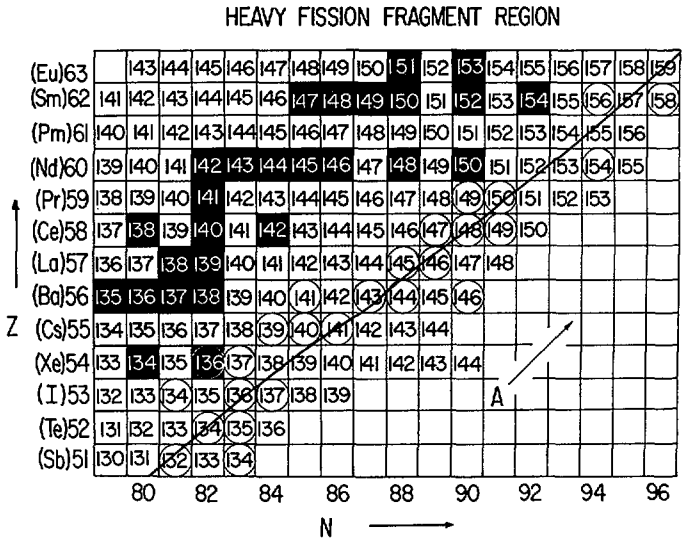

FIG. 8. Chart of the nuclides in the region of the heavy fission fragments.

present work to exhibit isomerism are circled; beta-stable nuclei are shaded.

There is generally good agreement between the results of the present work and the previous work of John et al. [17]. However, there are significant differences for half-lives and intensities of transitions below 150 keV and with half-lives $\lesssim$ 30 nsec. We believe the present work to be more accurate because of the pulse shape discrimination and convolution lifetime analysis used and the consistency of the present results for those gamma rays observed separately in the independently calibrated Ge(Li) and Si(Li) detectors. In addition, the Ge(Li) detection efficiency curve in the low-energy region was carefully calibrated with sources of ^{243}Cm and ^{249}Cf for which the relative gamma-ray intensities are well-known [18].

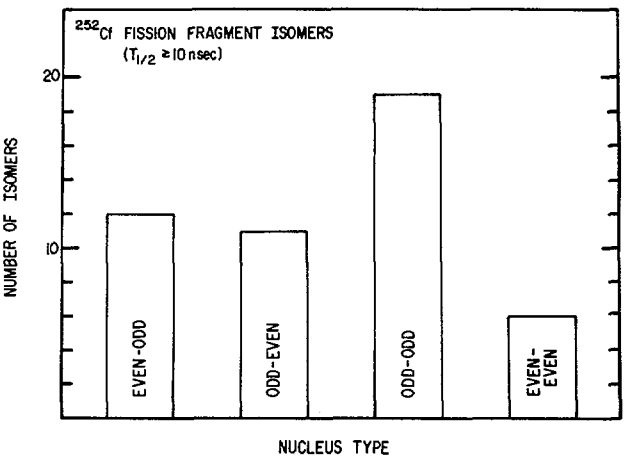

FIG. 9. Classification of isomers by type of nucleus for isomer half-lives $\geq$ 10 nsec. Data is taken from Table I.

Almost a hundred previously unknown isomeric gamma rays are reported here, most of which have energies below 100 keV. The addition of these new gamma rays do not significantly alter the general systematic features of the isomers as outlined in previous work [17, 19], namely the concentration of the isomeric intensity in certain mass regions and the range of multipolarities (E1, M1, E2) implied by the span of observed energy/half-life values. The gamma rays which could be assigned to specific nuclei represent 77% of the isomeric gamma-ray intensity. Figure 9 shows the data of Table I sorted according to the type of nucleus (even-odd, etc.) assuming that gamma rays from the same nucleus with the same half-life originate from one isomer.

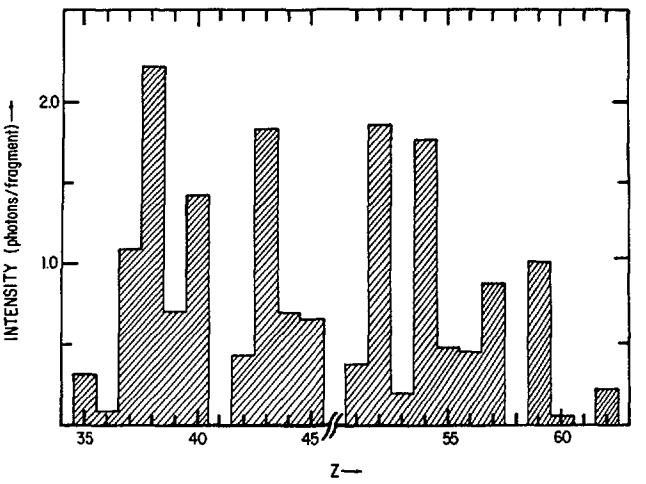

FIG.10. Fragment proton-number dependence of isomeric ($T_{\frac{1}{2}} \geq 10$ nsec) gamma-ray intensity. Data is taken from Table I.

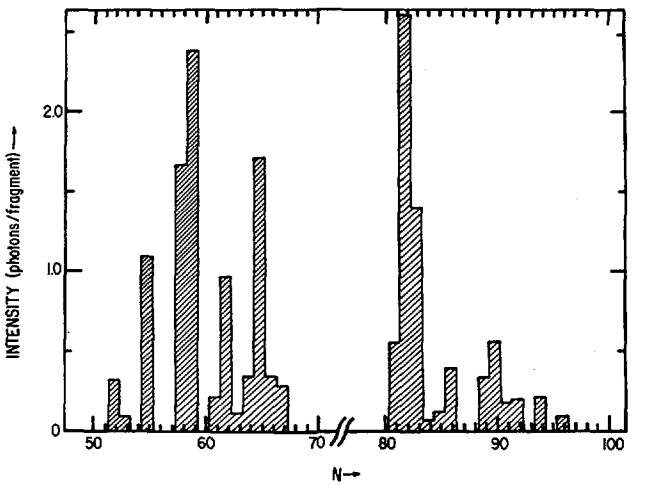

FIG.11. Fragment neutron-number dependence of isomeric ($T_{\frac{1}{2}} \geq 10$ nsec) gamma-ray intensity. Data is taken from Table I.

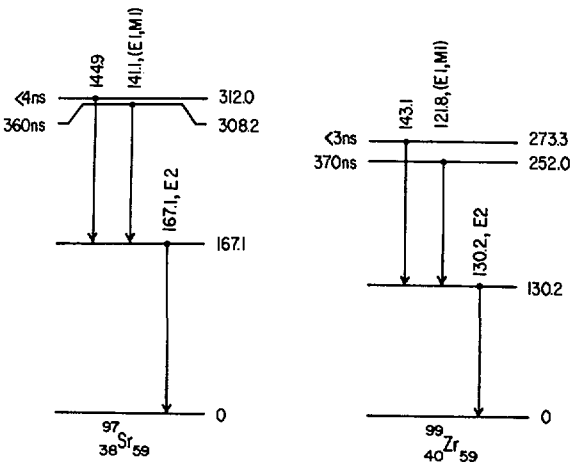

FIG. 12. Decay of isomeric levels in the even-Z isotones $^{97}_{38}Sr_{59}$ and $^{99}_{40}Zr_{59}$. Level and transition energies are in keV.

The data for half-lives of $\geq$ 10 nsec show the greatest preference for odd-odd nuclei while even-even nuclei are seen to be least preferred. The proton- and neutron- number dependence of the isomers is shown in Figures 10 and 11. The neutron dependence shows the most striking features and well illustrates the regions yielding more detailed information about the observed fission fragment isomers.

Figure 11 shows a peak at N = 55 which is due exclusively to $^{92}_{37}Rb_{55}$. A strong 142.2-keV gamma ray ($T_{\frac{1}{2}}$ = 57 nsec) was observed in the first experiment in coincidence with Rb K x-rays and was initially assumed to be the transition from the first excited state to the ground state of $^{92}_{37}Rb_{55}$ reported by Olson [9]. However, the second experiment revealed a strong coincidence between two gamma rays, each with energy 142 keV and half-life of 57 nsecs. We are unable to reconcile the 142-142 coincidence with the level scheme of Ref. 9 unless there exists an isomeric level at 284 keV or higher in $^{92}_{37}Rb_{55}$ which is not populated in the β decay of $^{92}_{36}Kr_{56}$.

The peak at N = 58, 59 is in a region of recent experimental and theoretical interest. Grüter et al. [12] reported six isomers in the microsecond lifetime region at N = 58, 59. Their elemental assignments were made on the basis of (gamma ray) - (K x-ray) coincidences and their mass assignments were taken from the results of John et al. [17]. The 141.1- and 167.1-keV gamma rays assigned by Grüter et al. [12] to $^{99}_{39}Rb_{59}$ are assigned in the present work to $^{97}_{38}Sr_{59}$ on the basis of half-life and mass centroid similarity to a Z = 38 K x-ray activity. The average half-life of these gamma rays was 360 nsecs but no Rb K x-rays with half-life greater than 60 nsecs were observed. The N=59 intensity is presently assigned to isotopes of Sr and Zr. The even-odd nuclei $^{97}_{38}Sr_{59}$ and $^{99}_{40}Zr_{59}$ are determined in the present work to

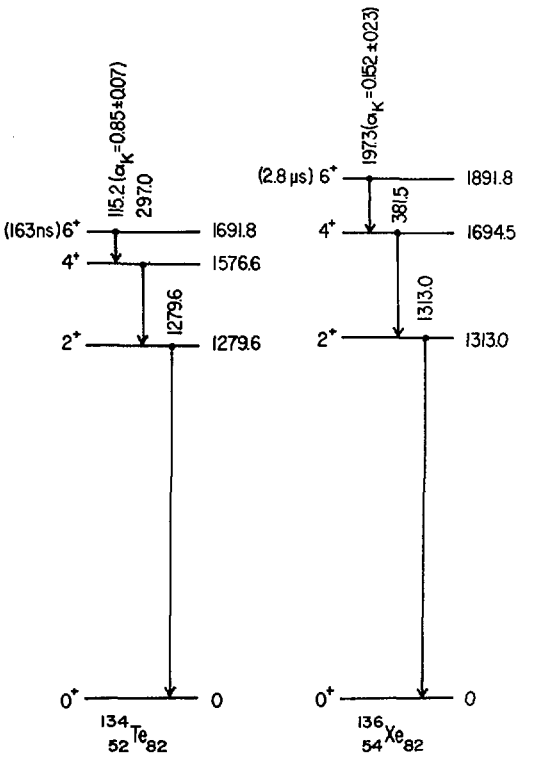

FIG.13. Decay of the $I^{\pi} = 6^+$ isomeric levels in the even-Z isotones $^{134}_{52}Te_{82}$ and $^{136}_{54}Xe_{82}$. Level and transition energies are in keV.

exhibit similar level structure, as shown in Fig. 12. The assignment of the lowest transition in each case was possible by virtue of its two-component decay curve. The multipolarities indicated in Fig. 12 were determined from K conversion coefficients, using the gamma-ray and K x-ray intensities from the first experiment. Since most of the K x-ray activity is due to conversion of the lowest transition, the K conversion coefficient determined in the present work for the isomeric transition has a large uncertainty, causing it to be consistent with either E1 or M1 multipolarity in both nuclei. The isomeric lifetime implies either an E1 transition hindered by a factor of 10^7 with respect to the single particle estimate or an M1 transition hindered by a factor of 10^5. Although the hindrance is within the range of experimental data for E1 transitions [20], the implied M1 hindrance is much larger than normal [21]. Recent work [22] indicates that reasonably stable, highly deformed structures exist for nucleon numbers 40 and 60, and suggestions have been made [12, 23] that there may be hindered transitions in this region between states of different deformation, i.e.,

shape isomerism. It is suggested experimentally [22, 24] that N = 59 is the transition between spherical and deformed ground states, analogous to N = 89 in the rare earth region. Future experiments are planned to clarify further the nature of the observed N = 59 isomerism.

The next large peak in Fig. 11 is located at N = 65 and is attributed to isotopes of Mo, Tc and Ru. The presence of weak unassigned gamma rays and the complexity of the K x-ray activities in this mass region prevented as detailed an analysis as

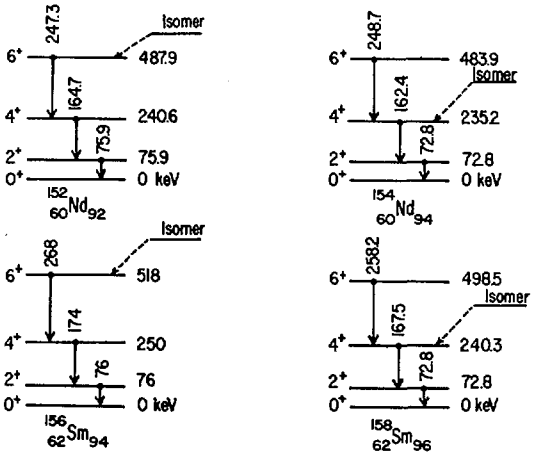

FIG. 14. Isomer de-excitation in the deformed, even-even rare-earth nuclei.

was possible for the N = 59 region. Nevertheless, these isomers may be caused by K forbiddenness since the N = 65 fission fragments are located well within a deformed region [2].

The region around N = 82 is distinctive because it contains the only isomeric gamma rays above 1 MeV. The N = 82 intensity is shared almost equally between two even-Z nuclei, $^{134}_{52}Te_{82}$ and $^{136}_{54}Xe_{82}$. The isomerism in these two nuclei is now believed to be well understood. Fig. 13 shows the similarity between the level structures of these nuclei. The calculations of Heyde et al. [25] indicate the isomer in both cases to be a $J^{\pi} = 6^+$ level of $(1g_{7/2})^2$ two quasi-particle (2QP) character decaying to the ground state via a $6^+ \rightarrow 4^+ \rightarrow 2^+ \rightarrow 0^+$ cascade and their calculations are in agreement with the isomeric transition probabilities. The present Ge(Li)-Ge(Li) coincidence experiment confirms the cascades. Furthermore, the K x-ray intensities were used with the gamma-ray intensities to compute the K conversion coefficients (α_K) shown in Fig. 13 for the presumed

$6^+ \rightarrow 4^+$ transitions, and the experimental α_K values are consistent with E2 multipolarities for the isomeric transitions. In addition, there is evidence in the decay curves of the present work for an 8-nsec isomer feeding both the 6^+ and 4^+ levels of $^{134}_{52}Te_{82}$, although gamma rays depopulating the 8-nsec isomer were not found.

The last detailed feature of the data concerns isomeric feeding into members of ground-state rotational bands in even-even, deformed rare-earth nuclei. In the earlier work, John et al. [17] searched their data for evidence of rotational band structure but could find none. The subsequent work of Wilhemy et al. [3] on ground-state bands in even-even fission fragments showed that several of the gamma rays observed as isomers in the earlier work [17] were assigned in the later work [3] to be $4^+ \rightarrow 2^+$ or $6^+ \rightarrow 4^+$ transitions in Nd and Sm isotopes. One of the objectives of the present work was to determine whether the observed isomerism [17] in these even-even nuclei was real or merely the result of no pulse shape discrimination in the photon detector timing circuitry. The present work confirms the existence of the ground-state rotational-band cascade members in the isomeric gamma rays as illustrated in Fig. 14.

It is apparent from the present results and the results of John et al. [17] that the ground-state rotational bands in $^{154}_{60}Nd_{94}$ and $^{158}_{62}Sm_{96}$ are populated at the $I^\pi = 4^+$ levels since the $6^+ \rightarrow 4^+$ transitions are not observed, whereas the $4^+ \rightarrow 2^+$ transitions are. The $6^+ \rightarrow 4^+$ transitions in $^{152}_{60}Nd_{92}$ and $^{156}_{62}Sm_{94}$ are observed among the isomeric gamma rays, but the isomers may be populating $I^\pi = 8^+$ levels or higher since the $8^+ \rightarrow 6^+$ or higher-lying (high-energy) transitions would not be detectable because of Ge(Li) detector efficiency considerations.

In α- and heavy ion-induced reaction studies of rare earth deformed nuclei [26, 27] the ground-state band is found to be populated in characteristic times of a few picoseconds due to "coherent" gamma-ray cascading along the yrast line. In fission fragment de-excitation the measured lifetimes of the $2^+ \rightarrow 0^+$ transitions imply that the bulk of the gamma-ray decay occurs within a few nanoseconds. The lifetimes of the isomers observed here are in the range of 70 to 2000 nsecs and their intensities imply that about 10% of the de-excitation proceeds through the isomers. At the opposite end of the deformed rare-earth region, a J^π, $K = 8^-$, 8 isomer is observed [28] in five $N = 106$, even-Z nuclei. This isomer decays into the 8^+ member of the ground-state band by a highly hindered E1 transition and accounts for 20-30% of the total population of the ground-state band 8^+ level. Thus, such behavior in the analogous fission fragment de-excitation process should not be completely unexpected, and we interpret the isomers to be low-lying 2QP states whose decay into the ground state band is K forbidden. From the available Nilsson single-particle levels near the Fermi level in this region [29] it is possible to construct 2QP levels with K^π values of 4^+, 4, 5^-, any of which could be the isomer decaying to the 4^+ level in $^{158}_{62}Sm_{96}$ or $^{154}_{60}Nd_{94}$. $K^\pi = 7^+$, 7^-, 2QP levels are also possible and could be the isomers in $^{152}_{60}Nd_{92}$ and $^{156}_{62}Sm_{94}$.

ACKNOWLEDGEMENTS

The authors wish to thank J. P. Unik for the many helpful suggestions on the experimental procedure and data analysis, W. Reisdorf for devising the mass calculation techniques used here, W. C. Schick, Jr. for supplying the PEAKFIND program, A. H. Jaffey for advice on statistical analysis, K. F. Flynn for preparation of the gamma-ray calibration sources, and R. R. Chasman for helpful discussions on interpretation of the data.

REFERENCES

[1] WATSON, R. L., WILHEMY, J. B., JARED, R. C., RUGGE, C., BOWMAN, H. R., THOMPSON, S. G., RASMUSSEN, J. O., Nucl. Phys. A141 (1970) 449.
[2] CHEIFETZ, E., JARED, R. C., THOMPSON, S. G., WILHEMY, J. B., Phys. Rev. Lett. 25I (1970) 38.
[3] WILHEMY, J. B., THOMPSON, S. G., JARED, R. C., CHEIFETZ, E., Phys. Rev. Lett. 25I (1970) 1122.
[4] JOHN, W., Physics and Chemistry of Fission (Proc. Conf. Vienna, 1969), IAEA, Vienna (1969) 535.
[5] ARMBRUSTER, P., Physics and Chemistry of Fission (Proc. Conf. Vienna, 1969), IAEA, Vienna (1969) 543.
[6] BALLAND, J. C., RIGNERET, J., SAMUELI, J. J., Nucl. Instr. Methods 52 (1967) 351.
[7] SCHMITT, H. W., KIKER, W. E., WILLIAMS, C. W., Phys. Rev. 137 (1965) B837.
[8] BOWMAN, H. R., MILTON, J. C. D., THOMPSON, S. G., SWIATECKI, W. J., Phys. Rev. 129 (1963) 2133.
[9] OLSON, R. J., "Gamma-ray decay schemes for ^{92}Kr, ^{92}Rb and ^{92}Sr", Ph.D. Thesis, Iowa State University, Ames, Iowa (1971).
[10] MARISCOTTI, M. A., Nucl. Instr. Methods 50 (1967) 309.
[11] WAPSTRA, A. H., NIJGH, G. J., VAN LIESHOUT, R., Nuclear Spectroscopy Tables, North-Holland, Amsterdam (1959).
[12] GRUTER, J. W., SISTEMICH, K., ARMBRUSTER, P., EIDENS, J., LAWIN, H., Phys. Lett. 33B (1970) 474.
[13] WATSON, R. L., USAEC Rep. UCRL-16798 (1966).
[14] HOPKINS, F. F., PHILLIPS, G. W., WHITE, J. R., MOORE, C.F., RICHARD, P., Phys. Rev. C4 (1971) 1927.
[15] HOPKINS, F. F., WHITE, J. R., PHILLIPS, G. W., MOORE, C.F., RICHARD, P., Phys. Rev. C5 (1972) 1015.
[16] REISDORF, W., UNIK, J. P., GRIFFIN, H. C., GLENDENIN, L. E., Nucl. Phys. A177 (1971) 337.
[17] JOHN, W., GUY, F. W., WESOLOWSKI, J. J., Phys. Rev. C2 (1970) 1451.
[18] AHMAD, I., WAHLGREN, M., Nucl. Instr. Methods 92 (1972) 333.
[19] JOHANSSON, S. A. E., Nucl. Phys. 64 (1965) 147.
[20] PERDRISAT, C. F., Rev. Mod. Phys. 38 (1966) 41.
[21] GROVE, N. B., "Nuclear transition rates", Nuclear Spin-parity Assignments (Grove, N. B., Robinson, R. L., Eds.) Academic Press, New York (1966) 76.
[22] SHELINE, R. K., RAGNARSSON, I., NILSSON, S. G., Phys. Lett. 41B (1972) 115.

[23] DIETRICH, K., Physics and Chemistry of Fission (Proc. Conf. Vienna, 1969), IAEA, Vienna (1969) 543.
[24] KHAN, T. A., HOFMANN, D., HORSCH, F., Nucl. Phys. A205 (1973) 488.
[25] HEYDE, K., WAROQUIER, M., BERGHE, G. V., Phys. Lett. 35B (1971) 211.
[26] WILLIAMSON, C. F., FERGUSON, S. M., SHEPHERD, B. J., HALPERN, I., Phys. Rev. 174 (1968) 1544.
[27] NEWTON, J. O., STEPHENS, F. S., DIAMOND, R. M., KELLY, W. H., WARD, D., Nucl. Phys. A141 (1970) 631.
[28] BURDE, J., DIAMOND, R. M., STEPHENS, F. S., Nucl. Phys. 85 (1966) 481.
[29] BUNKER, M. E., REICH, C. W., Rev. Mod. Phys. 43 (1971) 348.
[30] CHEIFETZ, E., JARED, R. C., THOMPSON, S. G., WILHEMY, J. B., USAEC Rep. UCRL-20426 (1971) 157.
[31] KAFFRELL, N., TRAUTMANN, N., private communication.
[32] WILHEMY, J. B., USAEC Rep. UCRL-18978 (1969).
[33] MOORE, P. A., RILEY, P. J., JONES, C. M., MANCUSI, M. D., FOSTER, J. L., Jr., Phys. Rev. C1 (1970) 1100
[34] MOORE, P. A., RILEY, P. J., Phys. Rev. 175 (1968) 1516.
[35] SCHICK, W. C., Jr., TALBERT, W. L., Jr., McCONNELL, J. R., Phys. Rev. C (1971) 507.
[36] TALBERT, W. L., Jr., private communication.

TABLE I. ISOMERIC GAMMA RAYS ASSIGNED TO SPECIFIC NUCLEI

Nucleus	E_γ[a] (keV)	$T_{\frac{1}{2}}$ (% error) (nsec)	Yield[b] Fission	Fragment	Remarks[c]
$^{87}_{35}Br_{52}$	110.8	2600(26)	12(20)	0.108	C(158.9?) } { Z[mt,12],
	158.9	4100[d] -	24(30)	0.216	C(110.8?) } { ΔA=±1
$^{89}_{36}Kr_{53}$	28.6[e]	22(6)	21(6)	0.091	Z[mt], ΔA=±1
$^{92}_{37}Rb_{55}$	142.2 } 142.2 }	57(2)	374(6)	1.016	[C(142.2), Z[Xγ,mt,9]
$^{95}_{38}Sr_{57}$	204.0	24(5)	605(6)	0.937	[C(352.0), Z[Xγ,mt,2]
	352.0	22(5)	467(11)	0.723	[C(204.0), Z[Xγ,mt,2]
$^{97}_{38}Sr_{59}$	141.1	380(30)	142(11)	0.317	[C(167,1), Z[mt], Z=37[12]
	144.9	< 4 -	123(30)	> 0.275	C(167.1?), Z[γγ]
	167.1	{ < 4 -	74(30)	> 0.165	C(144.9?) } { Z[mt],
		{ 340(6)	107(7)	0.239	C(141.1) } { Z=37[12]
$^{97}_{39}Y_{58}$	51.2[e]	509(12)	42(8)	0.030	[C(110.6?, 114.5, 119.7, 170.7?), Z[Xγ,mt,γγ]
	100.6	{ 176(50)	10(21)	0.008	C(114.5?), Z[mt,12]
		{1097(33)	48(12)	0.034	[C(110,6, 119.7(?), 130, 157.9?, 186.2?, 204,1?), Z[mt,12]
	110.6	758(16)	45(12)	0.033	[C(51.2?, 100.6, 119.7?, 130, 157.9?, 186.2?), Z[mt,γγ,12]
	114.5	270(50)	23(22)	0.017	[C(51.2, 100.6?), Z[γγ]
	119.7	1370(26)	126(16)	0.091	[C(51.2, 110.6?, 204.1), Z[mt,γγ,12]
	130	-	-	-	[C(100.6, 110.6, 114.5?, 157.9?), Z[γγ,12], not resolved in F-F-G spectra.
	157.9	596(14)	47(8)	0.033	[C(100.6?, 110.6?), Z[mt,γγ,12]
	170.7	1053(7)	190(7)	0.137	[C(51.2?, 204.1?), Z[mt,γγ,12]
	186.2	{ 300(39)	8(33)	0.007	Z[mt]
		{1004(22)	41(8)	0.030	[C(100.6?, 110.6?), Z[mt,γγ,12]
	204.1	> 3000[d]	200(30)	> 0.144	[C(119.7?, 170.7?), Z[mt,γγ,12]

TABLE I (cont.)

$^{99}_{40}Zr_{59}$	53.3 [e]	15(6)	134(10)	0.112	C(143.1?), Z[14]
	68.6	11(50)	106(20)	0.089	C(614.3), Z[γγ]
	121.8	427(27)	409(6)	0.342	C(130.2), Z[Xγ, γγ, 12, 14]
	130.2	< 4 -	90(50)	> 0.075	Z[14]
		370(3)	305(6)	0.255	C(121.8), Z[mt, γγ, 12, 14]
	143.1	< 3 -	352(30)	> 0.294	C(53.3?), Z[14]
	614.3	21(8)	400(8)	0.334	C(68.6), Z[15]
$^{100}_{40}Zr_{60}$	212.4	< 3 -	224(20)	> 0.128	C(91.6?, 106.1?), Z[1, 2(2⁺→0⁺), 15] M=100.81±0.19
$^{101}_{40}Zr_{61}$	91.6	< 4 -	40(30)	> 0.022	C(98.4, 106.1?, 212.4?)
		18(7)	180(6)	0.099	Z[γγ], Z=41[14] ΔA=+0, -1
	98.4	< 4 -	122(30)	> 0.067	C(91.6, 106.1) Z[1, 14, 30], ΔA=+0, -1
		16(26)	64(31)	0.035	
	106.1	20(37)	65(15)	0.036	C(91.6?, 98.4, 212.4?), Z[γγ] ΔA=+0, -1
	133.8	18(60)	39(60)	0.021	Z[14], ΔA=+0, -1
$^{102}_{40}Zr_{62}$	151.8	< 4 -	560(30)	> 0.422	Z[1, 2(2⁺→0⁺), 14] M=102.06±0.48
$^{103}_{40}Zr_{63}$	180.4	86(10)	72(8)	0.105	Z[15]
$^{102}_{41}Nb_{61}$	34.3 [e]	343(17)	36(9)	0.016	Z[mt]
$^{103}_{42}Mo_{61}$	102.8	< 4 -	600(50)	> 0.386	C(144.0, 251.1), Z[γγ, 14, 31]
	144.0	< 4 -	360(30)	> 0.232	C(102.8), Z[γγ, 14]
	251.1	3(50)	552(30)	> 0.355	C(102.8), Z[γγ, 14]
$^{104}_{42}Mo_{62}$	192.2	< 3 -	810(50)	> 0.288	Z[1, 2(2⁺→0⁺), 15, 32] M=105.12±0.15
$^{106}_{42}Mo_{64}$	94.9	< 4 -	320(50)	> 0.099	C(171.6?), Z[1, 14, 32]
	171.6	< 2 -	1260(50)	> 0.390	C(94.9?), Z[1, 2(2⁺→0⁺), 14], M=106.23±0.18
$^{107}_{42}Mo_{65}$	65.4 [e]	238(3)	895(6)	0.435	Z[14], ΔA=-0, +1
$^{105}_{43}Tc_{62}$	71.2 [e]	22(15)	360(6)	0.280	Z[14]
	85.2 [e]	23(10)	618(8)	0.480	Z[14]
$^{107}_{43}Tc_{64}$	45.5 [e]	6(38)	316(7)	0.093	C(81.8?, 103.9), ΔA=+0, -1 Z=42 or 43[14]
		194(18)	56(7)	0.016	
	81.8	< 8 -	350(50)	> 0.103	C(45.5?, 103.9), Z[14]
	103.9	10(38)	370(20)	0.109	C(45.5, 81.8), Z[14]

TABLE I (cont.)

Nucleus	E_γ[a] (keV)	$T_{\frac{1}{2}}$ (% error) (nsec)	Yield[b] Fission	Yield[b] Fragment	Remarks[c]
$^{108}_{43}Tc_{65}$	30.3	> 3000 [d] -	55(35)	> 0.017	Z[mt], ΔA=±1
	58.0 [e]	95(40)	176(8)	0.053	C(86.5?, 90.0, 106.1?, 153.9?, 176.3), Z[Xγ, γγ, 14]
	69.9 [e]	12(50)	109(10)	0.033	C(106.1, 153.9),
		235(22)	101(8)	0.031	Z[Xγ, γγ, 1, 14, 32]
	86.5	10(33)	80(60)	0.024	C(58.0?, 90.0, 153.9, 249.4?),
		177(32)	235(10)	0.071	Z[Xγ, γγ, 14]
	90.0	12(27)	35(15)	0.010	C(58.0, 86.5,
		117(7)	392(6)	0.119	153.9), Z[Xγ, γγ, 14]
	106.1	34(31)	44(15)	0.013	C(58.0?, 69.9, 153.9, 249.4?)
		128(9)	112(7)	0.034	Z[γγ, 14]
	116.0	14(10)	109(14)	0.033	C(119.8?), Z[γγ, 14]
	119.8	7(12)	106(16)	0.032	C(116.0?),
		126(12)	58(12)	0.018	Z[Xγ, 14]
	153.9	108(25)	725(6)	0.220	C(58.0, 69.9, 86.5, 90.0, 106.1, 176.3), Z[Xγ, γγ, 14]
	176.3	8(10)	65(16)	0.020	C(58.0, 153.9,
		114(4)	278(6)	0.084	249.4?), Z[Xγ, γγ, 14]
	249.4	11(8)	160(8)	0.049	C(86.5?, 106.1?, 176.3?), Z[γγ, 14]
$^{109}_{44}Ru_{65}$	60.2	192(42)	84(15)	0.028	C(96.2?), Z[mt, γγ]
	96.1	544(2)	1155(5)	0.386	C(60.2?), Z[Xγ, mt, 14]
	98.2	< 5 -	575(50)	> 0.191	C(132.0?), Z[30]
	132.0	< 3 -	340(30)	> 0.113	C(98.2?), Z[γγ]
$^{110}_{44}Ru_{66}$	240.8	< 2 -	390(30)	> 0.125	Z[1, 2(2⁺→0⁺), 14, 32] M=108.88±0.77
$^{111}_{44}Ru_{67}$	58.4 [e]	21(40)	265(8)	0.117	C(103.9, 150.3?), Z[γγ, 14], Z=44 or 45[14]
	62.7 [e]	11(21)	328(8)	0.165	C(103.9, 150.3?), Z[mt, 14, 17]
	103.9	< 4 -	900(30)	> 0.396	C(58.4, 62.7, 150.3) Z[γγ, 1, 14, 30]
	150.3	< 3 -	890(30)	> 0.392	C(58.4?, 62.7?, 103.9, 166.7?), Z[γγ, 14, 30]
	166.7	2.4(20)	275(14)	0.121	C(150.3?), Z[γγ, 14, 30]
	357.6	5(30)	95(19)	0.042	Z[30], A=111(J)
$^{109}_{45}Rh_{64}$	53.3 [e]	40(3)	255(15)	0.319	Z[14], ΔA=-0, +1
$^{111}_{45}Rh_{66}$	60.3	45(6)	798(8)	0.335	Z[mt, 14]

TABLE I (cont.)

$^{132}_{51}Sb_{81}$	91.1	104(5)	172(6)	0.143	C(163.0), Z[mt, 14]
	96.2	1794(34)	32(10)	0.030	Z[mt]
	163.0	100(4)	176(6)	0.168	C(91.1), Z[mt, 14]
$^{134}_{51}Sb_{83}$	125.2	107(4)	173(6)	0.380	Z[14]
$^{134}_{52}Te_{82}$	115.2	163(2)	596(5)	0.323	C(297.0, 1279.6), Z[Xγ, mt, γγ, 3($6^+ \rightarrow 4^+$), 12, 17], M=134.08±0.03
	297.0	8(20)	76(27)	0.041	C(115.2, 1279.6), Z[Xγ, mt, γγ, 3($4^+ \rightarrow 2^+$), 12, 17]
		167(3)	1016(5)	0.551	
	1279.6	154(13)	1010(16)	0.548	C(115.2, 297.0), Z[mt, γγ, 3($2^+ \rightarrow 0^+$), 12, 17($2^+ \rightarrow 0^+$)]
$^{135}_{52}Te_{83}$	50.0 [e]	300(19)	25(15)	0.017	C(324.8?), Z[mt, γγ]
	324.8	451(6)	268(7)	0.179	C(50.0?), Z[Xγ, mt, 15]
	1181.1	582(17)	286(11)	0.191	Z[mt]
$^{134}_{53}I_{81}$	59.9 [e]	98(24)	115(10)	0.105	C(182.4), Z[1, 14] ΔA=+0, -1
	182.4	16(12)	106(8)	0.097	C(59.9), Z[γγ, 14] ΔA=+0, -1
$^{136}_{53}I_{83}$	260.6	3.4(17)	209(7)	0.083	Z[15]
	288.3	2.8(20)	548(6)	0.217	Z[15]
$^{137}_{53}I_{84}$	117.7	< 4 -	167(30)	> 0.073	Z[14]
	154.7	< 4 -	280(30)	> 0.111	Z[14]
$^{136}_{54}Xe_{82}$	197.3	2775(6)	300(5)	0.279	C(381.5, 1313.0?) Z[mt, 12, 33], M=136.86±0.06
	381.5	> 3000 [d]	449	> 0.417	C(197.3), Z[mt, 12, 33]
	1313.0	3350(14)	490(9)	0.455	C(197.3?), Z[mt, 12, 33]
$^{137}_{54}Xe_{83}$	314.1	8.1(4)	344(6)	0.159	C(400.0), Z[15, 34]
	400.0	7.8(15)	464(10)	0.215	C(314.1), Z[15, 34]
	1221.0	5.1(11)	530(12)	0.245	Z[34]
$^{139}_{55}Cs_{84}$	68.8 [e]	186(18)	96(14)	0.051	Z[14], ΔA=-0, +1
$^{140}_{55}Cs_{85}$	13.9 [e]	521(2)	32(6)	0.011	Z[35]
	50.7 [e]	8(8)	243(10)	0.079	C(84.4?), Z[Xγ, 14, 35]
	84.4 [e]	< 8(25)	250(50)	> 0.082	C(50.7?), Z[γγ, 14, 35]
	103.0	11(11)	93(13)	0.031	Z[14, 35]
$^{141}_{55}Cs_{86}$	68.8 [e]	22(25)	114(22)	0.033	Z[14, 36]
	76.5 [e]	10(6)	496(10)	0.142	Z[1, 14], ΔA=±1
	89.9	12(10)	184(8)	0.053	Z[14, 36]
	96.1	12(22)	426(14)	0.123	Z[14], ΔA=±1
	105.8	14(7)	127(8)	0.036	Z[14, 36], ΔA=-0, +1
$^{141}_{56}Ba_{85}$	48.5	20(36)	103(20)	0.072	Z[14, 36]
$^{143}_{56}Ba_{87}$	117.3	6(30)	1340(30)	0.377	Z[mt, 14], ΔA=±1

TABLE I (cont.)

Nucleus	E_γ[a] (keV)	$T_{\frac{1}{2}}$ (% error) (nsec)	Yield[b] Fission	Fragment	Remarks[c]
$^{144}_{56}Ba_{88}$	199.2	< 2 -	346(30)	> 0.104	Z[1, 3(2⁺→0⁺), 14, 15, 32] M=143.94±0.27
$^{146}_{56}Ba_{90}$	180.8	< 2 -	188(30)	> 0.185	Z[1, 3(2⁺→0⁺)] M=145.63±0.32
$^{146}_{57}La_{89}$	46.6[e]	11(10)	150(17)	0.057	Z[14]
	66.0[e]	< 8 -	182(50)	> 0.070	C(158.7?), Z[1, 14], ΔA=±1
	81.9[e]	10(13)	296(10)	0.113	C(130.5, 158.7?), Z[14, 32]
	130.5	15(6)	276(6)	0.106	C(81.9, 158.7?), Z[1, 14]
	158.7	14(7)	141(6)	0.054	C(66.0?, 81.9?, 130.5?), Z[14, 32]
$^{147}_{57}La_{90}$	26.9[e]	60(21)	22(10)	0.012	Z[mt]
	56.0[e]	58(3)	305(7)	0.165	Z[mt, 14]
	167.5	11(10)	689(6)	0.374	Z[14]
$^{147}_{58}Ce_{89}$	117.4	8(25)	231(30)	0.142	C(283.4), Z[14]
	283.4	6.0(4)	682(6)	0.420	C(117), Z[15]
$^{148}_{58}Ce_{90}$	158.7	< 3 -	399(30)	> 0.214	Z[1, 3(2⁺→0⁺), 14, 32] M=147.33±0.43
$^{149}_{58}Ce_{91}$	135.6	3.5(5)	293(6)	0.194	Z[14], ΔA=±1
	142.2	3.9(5)	303(6)	0.200	Z[14], Z=59
$^{149}_{59}Pr_{90}$	54.7[e]	5.8(11)	183(15)	0.203	Z[14]
	58.0[e]	22.9(8)	421(7)	0.467	Z[14], 6-nsec precursor
$^{150}_{59}Pr_{91}$	27.7[e]	205(8)	20(9)	0.018	Z[mt]
	103.0	165(5)	99(6)	0.089	Z[mt, 14]
	130.7	165(27)	59(9)	0.053	Z[mt, 14]
$^{151}_{59}Pr_{92}$	96.8	20(40)	177(6)	0.183	Z[Xy]
$^{154}_{60}Nd_{94}$	162.6	1300(41)	31(14)	0.067	Z[mt, 3(4⁺→2⁺), 15] M=154.18±0.78
$^{156}_{62}Sm_{94}$	174.0	160(25)	33(9)	0.143	Z[mt, 3(4⁺→2⁺), 15]
$^{158}_{62}Sm_{96}$	167.7	164(15)	18(9)	0.083	Z[mt, 3(4⁺→2⁺)] M=157.74±0.27

Footnotes to Table I

[a] Energy uncertainty = 0.2 keV unless indicated by footnote e.

[b] Fission yield expressed as photons per 10^5 fissions with per cent uncertainty in parentheses. Fragment yield expressed as photons per fragment where the independent yield is computed from elemental yields and charge dispersion data of Reisdorf et al.[16].

[c] $C(E_{\gamma_1}, E_{\gamma_2}, \ldots)$ indicates gamma rays seen in coincidence, with less certain coincidences indicated by question marks. Mass number uncertainties, if not zero, are indicated by ΔA values. The methods of elemental identification are shown as Z[Xγ, mt, γγ, ..., i], where Xγ = (K X-ray)-(gamma ray) coincidence from the present work, mt = mass and half-life similarity between gamma-ray and K X-ray activity in the present work, γγ = (gamma ray) - (gamma ray) coincidence in the present work with a previously assigned gamma ray, and i = reference number of assignment from other work. Mass centroids (M) of transitions in even-even nuclei are given for reference.

[d] Half-life too long to be determined from computer fit. Value presented was obtained from relative intensities of last two time regions.

[e] Energy uncertainty = 0.1 keV.

TABLE II. UNASSIGNED ISOMERIC GAMMA RAYS

	Eγ (keV)	Half-life (nsec)		Photons/10^5 fissions	
Mass (amu)	(±0.2 keV)	Value	Sigma(%)	Value	Sigma(%)
87					
86.87±0.18	92.1	<4[a]	-	36	(50)
93					
93.00±0.94	108.7	16	(40)	88	(10)
93.40±0.30	111.0	69	(20)	36	(19)
93.46±0.28	217.1	<3[a]	-	56	(50)
		37	(28)	63	(19)
93.20±0.95	276.5	18	(40)	58	(20)
95					
95.03±0.98	129.2	10.1	(11)	30	(12)
95.23±0.89	191.4	113	(21)	29	(9)
97					
97.23±0.55	50.0[c]	815	(28)	21	(20)
99					
98.97±0.10	161.5	20	(33)	14	(31)
		109	(6)	92	(6)
98.59±0.35	228.6	7.1	(8)	92	(9)
100					
99.74±0.70[d]	10.8[c]	680	(6)	6.7	(8)
100.22±0.91	84.6	17	(33)	580	(10)
100.04±0.97	426.8	16	(24)	120	(17)
100.13±1.02	596.0	4	(25)	230	(25)
101					
100.65±0.73	11.2[c]	11	(20)	20	(23)
101.30±0.90	68.6	11	(50)	106	(20)
101.03±0.87	179.6	17	(10)	50	(15)

Mass (amu)	E_γ (keV) (±0.2 keV)	Half-life (nsec) Value	Sigma (%)	Photons/10^5 fissions Value	Sigma (%)
102					
102.34±0.30[d]	13.5[c]	271	(10)	10.9	(10)
103					
102.57±0.64[d]	39.2[c]	4	(25)	200	(38)
102.63±0.65[d]	61.8	12	(10)	131	(12)
103.28±0.07	163.9	4.8	(50)	409	(30)
103.17±0.91	237.8	4	(25)	145	(25)
104					
103.80±0.07[d]	16.2[c]	>3000[b]	-	>73	-
103.64±0.07[d]	28.9[c]	75	(13)	36.8	(9)
104.23±0.49	141.2	109	(21)	160	(7)
105					
105.14±0.71[d]	62.6[c]	4	(40)	140	(30)
105[d,e]	65.5	9	(22)	393	(12)
105[e]	204.6	15.0	(8)	71	(9)
106					
105.79±0.47	42.7[c]	318	(16)	23	(15)
106.04±0.89	72.1	<8[a]	-	860	(50)
105.63±0.21[d]	74.8[c]	10	(22)	403	(8)
107					
107.00±0.12	25.4[c]	10.5	(10)	84	(10)
107.15±0.18	35.4[c]	166	(14)	21	(12)
107.03±1.51	196.8	200	(33)	30	(24)
108					
108.28±0.45[d]	26.3[c]	7	(20)	69	(15)
109					
108.94±0.96[d]	42.8[c]	17	(20)	32	(30)
108.63±0.34	225.9	890	(26)	68	(9)
110					
109.95±0.26[d]	29.4[c]	16	(20)	77	(12)
110.43±0.15	222.0	7.2	(5)	234	(7)
111					
111.10±0.87	238.9	9	(10)	98	(10)
111[e]	303.7	4.1	(20)	405	(20)
		67	(32)	39	(20)
112					
111.80±0.91	74.2	780[b]	-	16	(25)
112.01±0.96	189.2	5.7	(19)	99	(17)

Mass(amu)	E_γ (keV) (±0.2 keV)	Half-life (nsec) Value	Sigma(%)	Photons/10^5 fissions Value	Sigma(%)
113					
113.42±0.60[d]	17.2	55	(11)	22	(21)
113.45±0.24	85.0[c]	72	(25)	134	(20)
114					
114[e]	373.8	2.5[b]	-	170	(19)
115					
115[d,e]	34.8[c]	65	(50)	8	(50)
114.88±0.12	38.7[c]	14	(3)	165	(6)
114.75±0.26	44.0[c]	136	(11)	39	(9)
115.08±0.92	48.6[c]	10	(17)	173	(6)
114.97±0.88	52.7[c]	10	(30)	72	(15)
114.89±0.79	126.0	30	(15)	37	(10)
116					
115.84±0.96	128.3	<4[a]	-	127	(30)
117					
116.97±0.92	155.5	7	(20)	34	(10)
118					
118.20±0.98	174.1	10	(40)	33	(20)
119					
118.70±0.89	73.5	<7[a]	-	90	(50)
129					
129.22±0.91	89.0	60	(9)	31	(8)
129.21±0.97	120.8	12	(24)	22	(10)
129.20±0.94	137.8	42	(13)	20	(10)
131					
131.21±0.92	173.4	560[b]	-	18	(30)
132					
131.96±0.27	85.1	11.4	(13)	94	(8)
133					
133[d,e]	34.8	64	(50)	8	(50)
132.94±0.19	103.2	96	(19)	45	(12)
		750	(30)	32	(17)
133.39±0.34	1151.1	79	(15)	344	(9)
134					
134.30±0.18	387.1	90	(28)	84	(12)

Mass (amu)	E_γ (keV) (±0.2 keV)	Half-life (nsec) Value	Sigma (%)	Photons/10^5 fissions Value	Sigma (%)
135					
134.86±0.60[d]	17.2	55	(11)	22	(21)
137					
137.12±0.32	67.9	997	(30)	40	(9)
138					
138.33±0.26[d]	29.4[d]	16	(20)	77	(12)
138.41±1.15	70.2	<9[a]	-	110	(30)
139					
139.34±0.96[d]	42.8[c]	17	(20)	32	(30)
139.15±0.92	218.8	<2[a]	-	190	(30)
140					
140.0±0.45[d]	26.3[c]	7	(20)	69	(15)
141					
141.28±0.12[d]	25.4[c]	10.5	(10)	84	(10)
143					
143.14±0.71[d]	62.6[c]	4	(40)	140	(30)
143[d,e]	65.5	9	(22)	393	(12)
142.65±0.21[d]	74.8	10	(22)	403	(8)
145					
144.48±0.07[d]	16.2[c]	>3000[b]	-	>73	-
144.64±0.28[d]	28.9[c]	75	(13)	36.8	(9)
144.97±0.89	48.2	84	(10)	324	(10)
144.85±0.87	155.0	<2[a]	-	135	(30)
145.13±0.95	250.4	5.0	(10)	114	(8)
145.50±0.16	288.0	13.5	(6)	187	(7)
145[e]	340.8	7.9	(3)	87	(9)
144.88	364.2	11.9	(11)	156	(8)
146					
145.94±0.30[d]	13.5[c]	271	(10)	10.9	(10)
145.71±0.64[d]	39.2[c]	4	(25)	200	(38)
145.65±0.65[a]	61.8	12	(10)	131	(12)
147					
146.64±0.69	26.9	60	(21)	21.5	(10)
146.92±0.63	105.2	8	(16)	150	(8)
148					
148.38±0.08	103.0	<4[a]	-	328	(6)

Mass (amu)	E_γ (keV) (±0.2 keV)	Half-life (nsec) Value	Sigma (%)	Photons/10^5 fissions Value	Sigma (%)
149					
148.81±0.90	85.0	<8[a]	-	113	(20)
148.95±0.76	92.5	12	(20)	50	(14)
150					
150.26±0.12	109.9	59.2	(3)	36	(9)
150.24±0.28	141.6	594	(18)	35	(10)
151					
150.85±0.91	87.1	<8[a]	-	64	(50)
152					
152.07±0.15	191.7	1293	(10)	133	(9)
154					
153.65±0.12	22.3	930	(6)	23.4	(7)
153.65±0.66	29.6	1470	(12)	41.4	(6)
154.05±0.97	71.5[c]	788	(16)	41	(10)
154.32±0.21	141.9	1507	(23)	42	(11)
153.90±0.92	169.9	1003	(37)	30	(9)
161					
161[e]	167.8	1500[b]	-	16	(20)

[a] Experimental time resolution prevents accurate half-life determination. Lower limit is ~0.1 nsec due to Pb shield.

[b] Determined from relative intensities in adjacent time bins; not varied in computer fit.

[c] Energy uncertainty = ±0.1 keV from analysis of Si(Li) spectra.

[d] Mass ambiguity due to Si(Li) geometry; also listed under the complementary mass.

[e] Computer fit would not converge properly due to interference by gamma-ray in neighboring energy, mass and lifetime region.

DISCUSSION

K. SISTEMICH: Many of the μs-isomers we found among the fission products of ^{235}U have N = 58, 59. Did you observe a similar concentration of isomeric states in this neutron region?

R. G. CLARK: Yes, very definitely. This feature is especially evident in Fig. 11, which shows the fragment-neutron number dependence of the isomers.

H. J. SPECHT: I did not quite understand the interpretation of the I = 6 isomeric states in the even-even nuclei which you have discussed.

R. G. CLARK: The calculation by Heyde and co-workers (Ref. [25] of the paper) was a normal quasiparticle calculation with Gaussian two-body interaction and the energy levels were derived using a two-quasiparticle basis set. The successful reproduction of the observed transition probability for the $6^+ \rightarrow 4^+$ transition in ^{136}Xe was obtained by demanding the occupation probability of the $(1g_{7/2})$ proton state to be 0.5, in agreement with a pure shell-model picture.

M. ASGHAR: The various microscopic calculations seem to show that the nuclei around mass number 100 may be "soft" as regards their shape and one may expect to find gamma-ray shape isomers (different from the spin isomers). You say that your data show some indication of this type of isomerism. How sure are you that the retardation of gamma-ray transitions is not caused by some factors other than the change of shape?

R. G. CLARK: The shape isomer hypothesis is only offered as a possible explanation. There are other possibilities as well, such as "ℓ" forbiddenness causing retardation of M1 transition rates.

J. B. WILHELMY: Just because nuclei are deformed, they need not be soft. We think the ^{100}Zr region is probably a region of rigid deformation.

In the de-excitation of the prompt products we see all (> 90%) of the yield of the products going through what we interpret to be the ground state band. If there were shape isomers, we would expect some fragmentation of the prompt de-excitation between the two bands in the separate wells.

MEASUREMENT OF PERTURBED ANGULAR DISTRIBUTION OF GAMMA RAYS FROM THE SPONTANEOUS FISSION OF ^{252}Cf

A. LAJTAI, L. JÉKI, Gy. KLUGE, I. VINNAY, F. ENGARD
Central Research Institute for Physics,
Budapest, Hungary

P.P. DYACHENKO, B.D. KUZMINOV
Institute of Physics and Power Engineering,
Obninsk, USSR

Abstract

MEASUREMENT OF PERTURBED ANGULAR DISTRIBUTION OF GAMMA RAYS FROM THE SPONTANEOUS FISSION OF ^{252}Cf.

The angular and energy distributions of the gamma rays emitted by fission fragments from the spontaneous fission of ^{252}Cf were measured using platinum or iron source backing and NaI(Tl) or Ge(Li) detectors. The average anisotropy of the gamma rays relative to the direction of fragment flight, expressed as $A = [I(180°) - I(90°)]/I(90°)$ is 11 ± 1% in the gamma energy interval 120 keV - 1.5 MeV, and 18 - 22% at energies from 350 to 850 keV if the platinum backing and NaI(Tl) detector are used. For iron backing the anisotropy value decreases under the same conditions to 5.2 ± 0.1% at energies from 120 keV to 1.5 MeV and to 5.1 ± 0.2% if a magnetic field is applied in the direction normal to the plane of fission in which the fragments and gamma rays are being counted.

Assuming a set of most plausible values for the lifetime of fission gamma rays and for the internal magnetic field at the iron site involved, average g-factors for the fission fragments were evaluated from the measured attenuation.

The measurements with the Ge(Li) detector show anisotropies which can be determined for about 30 gamma peaks and also the g-factors for specific gamma transitions seem to be evaluable. This work is still in progress.

INTRODUCTION

The angular distribution of the gamma rays emitted by fragments from spontaneous and thermal-neutron-induced fission has been investigated by several groups [1-12].

The average angular momentum of the fragments in the direction perpendicular to that of their flight was evaluated as $\sim 7\hbar$ from the anisotropy of the angular distribution of the gamma rays relative to the fragment flight. The angular anisotropy of the gamma rays can vary with the type of the emitter fragments and with the gamma energies [12]. Consequently the average value of the anisotropy and the average angular momentum of the fragments calculated from the former by use of various assumptions yield information only on the general tendency of these values.

The perturbed angular correlation measurements show that an attenuation effect can arise in the angular distribution measurements due to extranuclear perturbations occurring in the source backing [13].

In fact, for the evaluation of the angular momentum and the magnetic moment in specific states of a given fragment nucleus, the energies and angular distributions, the lifetimes, spin values and g-factors of the gamma transitions between the nuclear levels have to be known. These data, however, are only partly available for the fission products.

In the experiments reported in this paper the effects are studied which are produced by an applied magnetic field and by the extranuclear perturbations in the source backing on the angular correlation between the fission gamma rays and the direction of flight.

EXPERIMENTAL

The angular and energy distribution measurements on the gamma rays from the spontaneous fission of ^{252}Cf were performed in the first set of experiments by using Si semiconductor detectors for the fission fragments and a 4x4-inch NaI/Tl/ detector for the gamma rays /see Fig. 1/. The ^{252}Cf source was mounted on 0.2-mm-thick platinum or iron backing. One of the fission fragments was counted by the Si detector at 180° or 90° relative to the direction of the detected gamma-rays, while the other fission fragment was absorbed by the backing and stopped in less than 10^{-12} sec.

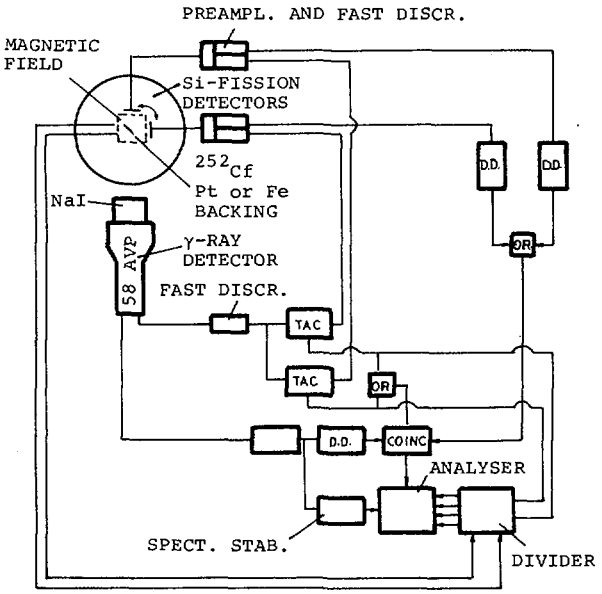

FIG 1. Schematic diagram of the experimental arrangement.

The electronic equipment is a 3-channel fast-slow coincidence system with a controller dividing the analyser into 4 parts, each comprising 256 channels which cover the gamma energies from 120 keV to 1.5 MeV at the two angular positions and in accordance with the changes in the direction of the applied magnetic field. The ^{252}Cf source is located at 5 cm from the fragment and at 80 cm from the gamma detector. This spacing, and the ±10-nsec time interval set for the prompt peak by the differential discriminator coupled to the time-to-pulse height converter, permitted suppressing the fast fission neutron and delayed gamma-ray counts.

In the same measuring arrangement with the Ge/Li/ detector, the gamma -ray analyser was divided into 4x1024 channels covering the fission gamma rays with energies from 120 keV to 850 keV.

The direction of the applied magnetic field in the case of iron backing was normal to the fission plane in which the fragments and gamma rays were being counted.

RESULTS

The angular and energy distributions of the fission gamma rays measured with NaI/Tl/ crystal simultaneously at 90° and 180° relative to the direction of the outflying fragments showed, for platinum backing, the anisotropy value A = 11±1% as averaged over the energy interval of 130 keV - 1.5 MeV. The value of A reached 18-22% in the interval 350 to 850 keV, as apparent from the anisotropy versus gamma energy curve /Fig. 2/. In the case of iron backing, the anisotropy was found to be lower, i.e. 5.2±0.1% or 10-15% in the energy interval from 350 to 850 keV /Fig. 3/. This decrease in anisotropy can be attributed to the substantial extranuclear perturbations caused by iron. When an external magnetic field was applied to the source with iron backing, the anisotropy was estimated as 5.1±0.2% /Fig. 4/. The measured anisotropy versus gamma energy curves are shown in Fig. 5.

The value of the attenuation due to iron backing permits the average g-factor of the fragments to be evaluated by making use of the following relationships.

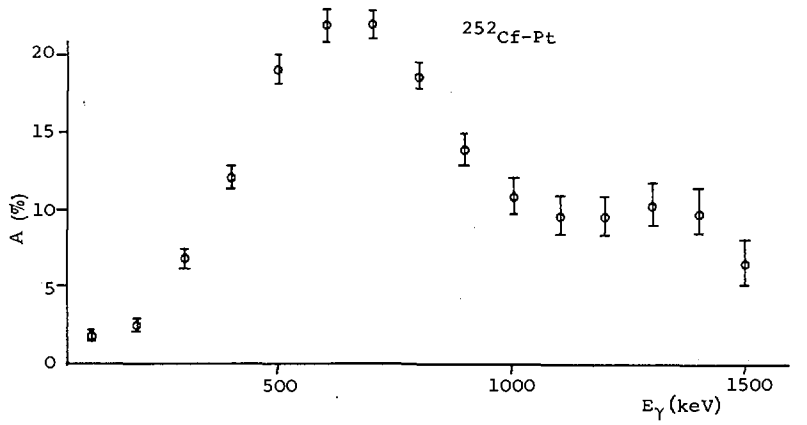

FIG.2. Anisotropy versus gamma energy from the measurements with Pt backing.

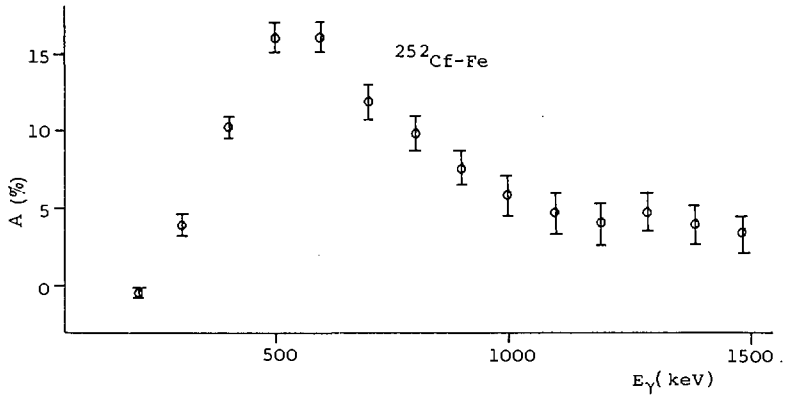

FIG.3. Anisotropy versus gamma energy from the measurements with Fe backing and turned-off external magnetic field.

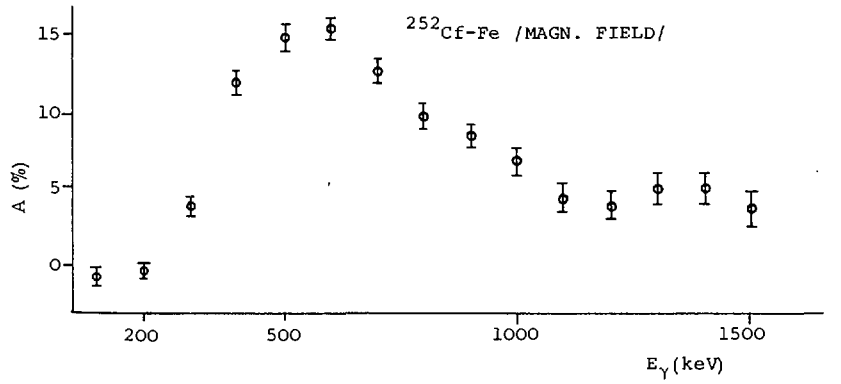

FIG.4. Anisotropy versus gamma energy from the measurements with Fe backing and turned-on external magnetic field.

The unperturbed angular distributions of the gamma rays can be approximated by a function of the form

$$W(\vartheta) \sim 1 + b_2 \cos 2\vartheta$$

while the angular distribution function perturbed by an applied magnetic field /this is the case of the iron backing aligned by an external field/ is given by

$$W(\vartheta, \pm B) \sim 1 + \frac{b_2}{\sqrt{1+(2\omega\tau)^2}} \cos\left(2\vartheta \pm \arctan\left(2\omega\tau\right)\right)$$

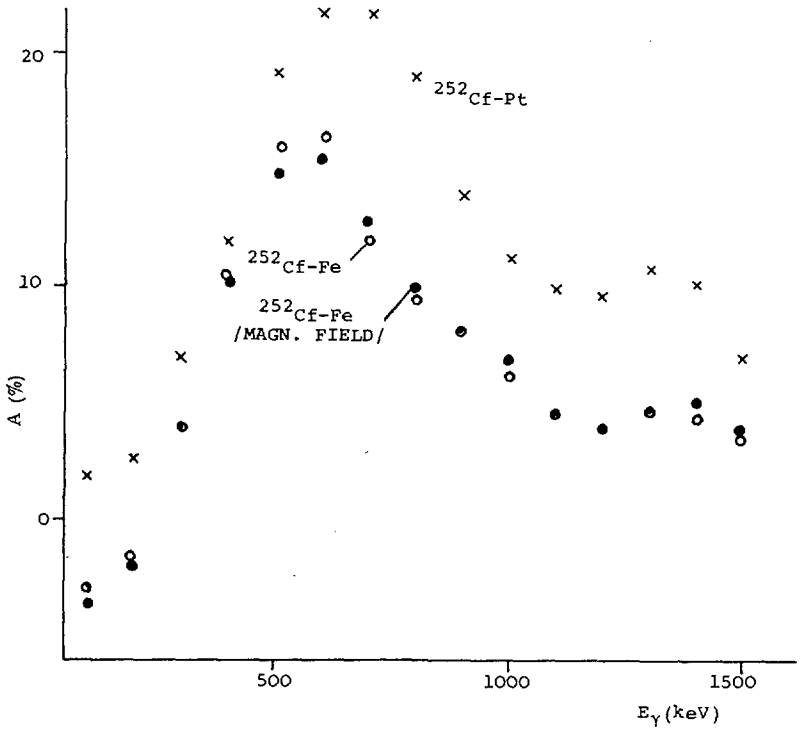

FIG.5. Measured anisotropy versus gamma energy.

If the different fragments are exposed to a magnetic field the direction of which is assumed to be randomly distributed /this is the case of the iron backing with the external magnetic field turned off/, the distribution function can be described as

$$W(\vartheta,B) \sim 1 + \frac{b_2 \arctan 2\omega\tau}{2\omega\tau} \cos 2\vartheta$$

where ϑ is the angle between the directions of the fragments and the gamma -rays and $\omega\tau$ is the angle of rotation which is related to the parameters /g-factor, lifetime τ and internal magnetic field B/ as

$$\omega\tau = g \frac{\mu_N}{\hbar} B\tau$$

Thus, for the evaluation of the g-factor, the lifetimes of the gamma transitions for fission fragments and the value of the internal magnetic field at the iron site at which the fragment has been stopped have to be known.

Choosing a set of most plausible values inferred from reported data [14, 15] for the lifetime and the internal magnetic field involved, the average g-factor of the fragments was calculated. The results of these calculations are presented below.

τ(sec)	B(G)	g
10^{-9}	5×10^{5}	0.15
5×10^{-10}	5×10^{5}	0.3
10^{-9}	10^{6}	0.07
5×10^{-10}	10^{6}	0.15
10^{-10}	10^{6}	0.77

The angular and energy distributions were measured also at the angles of 45° and 135° relative to the direction of fragment flight and the intensity and energy distributions of the gamma rays were observed while the direction of the applied magnetic field was varied up and down. The agreement between the counts and the energy spectra was considered to be an adequate test of the experimental equipment. In our case there is a complete symmetry relative to the plane normal to the direction of the fragment flight, thus, direction of angular rotation of the angular momenta and the magnetic moments could not be determined.

In the experiments with Ge/Li/ detector the measurements show very complex γ-spectra. Moreover some of the gamma lines appear above a large continuous background which makes the evaluation difficult. Preliminary estimations were made and the anisotropy values were determined for about 30 lines obtained with platinum backing. The variations in the intensities of these lines with the magnetic field applied up and down were measured at 45° and 135° in the case of iron backing.

The estimations of the g-factors of the gamma transitions in the specific fragments are in progress.

Strong magnetic fields due to non-compensated electron spins can be induced at the fragment nuclei flying in vacuum and thus unable to pick up electrons. For this reason measurements are made to study the effect of strong ionisation on the angular momentum alignment of the fission fragments. The fission gamma angular distribution is measured by letting the detected fragments fly through a gas at different low pressures or through VYNS foils of different thicknesses. In this way the counted fragments can pick up electrons and the perturbation of the magnetic field of non-compensated electron spins can be suppressed.

ACKNOWLEDGEMENTS

We gratefully acknowledge helpful discussions with L.Keszthelyi and Z.Szõkefalvy-Nagy and their stimulating interest.

REFERENCES

[1] Blinov, M.V., Kazarinov, N.M., Protapopov, A.N., Shiryayev, B.M., J. eksp. teor. Fiz., 43 /1962/ 1644.

[2] Dési, S., Graff, Gy., Lajtai, A., Nagy, L., Phys. Lett., 3 /1963/ 343.

[3] Kapoor, S.S., Ramanna, R., Phys. Rev., 133 /1964/ B598.

[4] Hoffman, M.M., Phys. Rev., 133 /1964/ B714.

[5] Skarsvåg, K., Singstad, I., Nucl. Phys., 62 /1965/ 103.

[6] Graff, Gy., Lajtai, A., Nagy, L., Physics and Chemistry of Fission 2, IAEA, Vienna /1965/ 163.

[7] Petrov, G.A., Yad. Fiz., 1 /1965/ 467.

[8] Skarsvåg, K., Nucl. Phys. A96 /1967/ 385.

[9] Val'skii, G.V., Petrov, G.A., Pleva, Yu.S., Yad. Fiz., 5 /1967/ 734.

[10] Val'skii, G.V., Petrov, G.A., Pleva, Yu.S., Yad. Fiz., 8 /1968/ 297.

[11] Val'skii, G.V., Aleksandrov, B.M., Baranov, I.A., Krivochatskii, A.S., Petrov, G.A., Pleva, Yu.S., Yad. Fiz. 10 /1969/ 240.

[12] Wilhelmy, J.B., Cheifetz, E. Jared, R.C., Thompson, S.G., Bowman, H.R., Phys. Rev., C5 /1972/ 2041.

[13] Perturbed Angular Correlations, North Holland, Amsterdam, 1964 /Edited by E.Karlsson, E.Matthias, K.Siegbahn/.

[14] Maier-Leibnitz, H., Armbruster, P., Specht, H.J., Physics and Chemistry of Fission 2, IAEA, Vienna /1965/ 113.

[15] Hyperfine Structure and Nuclear Radiation, North Holland, Amsterdam, 1968 /Edited by E.Matthias and D.A.Shirley/.

DISCUSSION

H. NIFENECKER: First of all a comment. The study of extranuclear effects on the fragments in a vacuum would be very relevant to studies such as that of Armbruster and co-workers on the angular anisotropies of gamma rays. However, those effects are expected to be small, since experiments with stopped fragments and flying fragments give similar values of the anisotropies.

Now a couple of questions. I find it difficult to understand the trend shown in your last figure. It appears that the anisotropies are proportionately more reduced for high-energy gamma rays than for ~400-keV gamma rays. This is contrary to what one would expect. Can you please comment? Also I think that the lifetimes you use in computing g-factors are longer than those measured by H. Albinsson. Is there a reason for this?

Gy. KLUGE: The last figure shows preliminary experimental results and at the moment we are not able to explain the trend of these curves.

As far as the gamma lifetimes are concerned, we used a number of possible lifetimes for evaluating the average g-factor values. Since the internal magnetic field is not very precisely known, these g-factor values have been computed only for the purposes of orientation.

P. ARMBRUSTER: I have two comments to make. First, the anisotropy of gamma emission for fragments stopped in a carbon or platinum backing does not differ significantly from the anisotropy measured for fragments flying in vacuum. This means the anisotropy is not destroyed by the internal fields of the solid backings used or by the internal intrinsic fields of the fission fragments.

Second, the g-factors depend on B and τ and neither of these quantities is accurately known. Consequently, the values you obtained for g may be wrong by a very large factor.

J.B. WILHELMY: The anisotropy of gamma rays at different energies may be affected by changes in the multipolarity of the predominant radiation in the spectrum (being E2 at lower energy and going towards E1 at higher). Such multipolarities will yield different anisotropies.

It would be good to have data on the anisotropies of transitions from fragments stopped in Pb or Cu, which are materials that should maintain the initial alignment.

S.S. KAPOOR: Have you corrected your data for the Doppler effect on the gamma anisotropies, to allow for the fact that one of the fragments is in motion.

Gy. KLUGE: No, these data are purely experimental results without any corrections.

H. NIFENECKER: This correction would go the other way, so I do not think it could explain those curves.

A STUDY OF THE PROMPT ELECTRONS EMITTED FROM INDIVIDUAL FRAGMENTS IN NEUTRON INDUCED FISSION

TASNEEM A. KHAN,
Pakistan Institute of Nuclear Science,
Nilore, Pakistan

F. HORSCH
Institut für Angewandte Kernphysik,
Kernforschungszentrum, Karlsruhe,
Federal Republic of Germany

Abstract

A STUDY OF THE PROMPT ELECTRONS EMITTED FROM INDIVIDUAL FRAGMENTS IN NEUTRON INDUCED FISSION.

A three-parameter experiment has been performed in which the energies of coincident fragment pairs and internal conversion electrons emitted within 1.8 ns after the thermal-neutron-induced fission of ^{235}U were recorded event by event. The fragment kinetic energies were used for mass identification. The self-consistency of the values of the electron energy, gamma-ray energy as determined in previous experiments and fragment charge, and the agreement with X-ray data, were used to identify the atomic numbers of the fragments. Analysis of the spectra has resulted in the assignment of many transitions to new isotopes as well as improvement in or confirmation of many assignments from the ^{252}Cf spontaneous fission data. Limited information on the multipolarities of the transitions in even nuclei is presented. The relative yield of electrons per fragment indicates softness to deformation in the mass region 100-110. An examination of the 2^+ to 0^+ level systematics of neighbouring even nuclei suggests a transition from vibrational to rotational behaviour in the light fragments between neutron numbers 58 and 60.

1. INTRODUCTION

There is an increasing interest in the study of nuclei away from the line of stability. Such studies help to explore the new regions of nuclear deformations and to extend nuclear theory to regions which were previously inaccessible. Primary fission fragments, with their large excess of neutrons, form a special class of such nuclei. Moreover they cover two very significant regions of nuclear deformation. The study of their nuclear properties is therefore of considerable interest.

Experimental studies of the de-excitation of the primary fission fragments are somewhat complicated by the fact that there is no way to study any one isotope without interfering radiation from numerous others formed in fission. However it is possible, using present-day techniques, to measure simultaneously the energy of the fission fragments as well as the energy of any radiation emitted by the fragments for individual fission events. Considerations of momentum and mass conservation then enable one to obtain the mass of the fragment giving rise to the radiation. Experiments of this type have been performed to study the gamma rays [1, 2] and conversion electrons [3] from the fragments of ^{252}Cf (sf). It was thought desirable to extend these measurements to thermal-neutron-induced fission firstly to investigate nuclei whose

yield in the spontaneous fission of ^{252}Cf is low and secondly to obtain more information on the mass region accessible to both ^{252}Cf (sf) and ^{235}U (n, f) and compare the results of the two fissioning systems. The first experiments were concerned with the spectra of gamma rays from the fragments produced in ^{235}U (n, f) [4, 5] . In the present experiment we have investigated the spectra of internal conversion electrons associated with intervals of fragment mass. These investigations are complementary to the gamma-ray measurements and, moreover, provide information on the important low-energy transitions in the regions of nuclear deformation. An attempt has been made to obtain the spectra with high enough resolution to obtain K/L ratios of the strongest transitions and thus assign multipolarities to them. By comparing the electron line energies with the energies of the corresponding gamma rays, assignment of the charge of the fragment was in many cases possible. The complete experimental procedures as well as the detailed results of the gamma-ray and conversion electron experiments are given elsewhere [5]. The present paper is concerned with some of the main features of these results and their bearing on current theories.

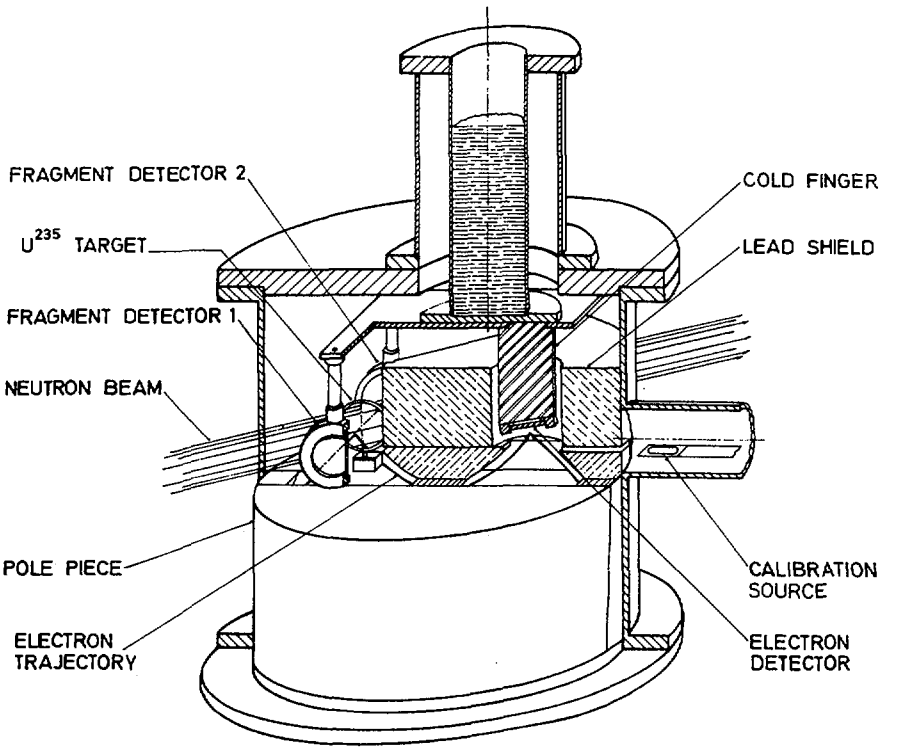

FIG. 1. Schematic diagram of the experimental arrangement.

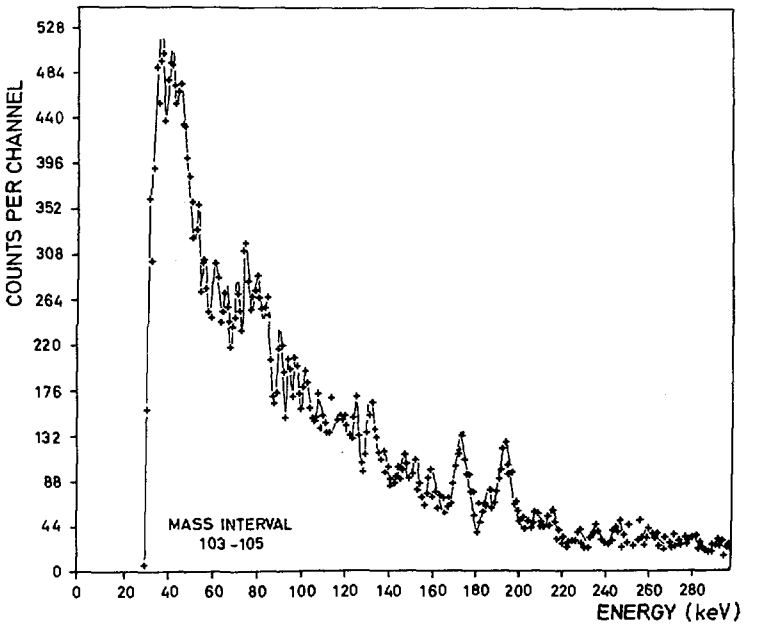

FIG.2. A mass-sorted electron energy spectrum from the light fragment group.

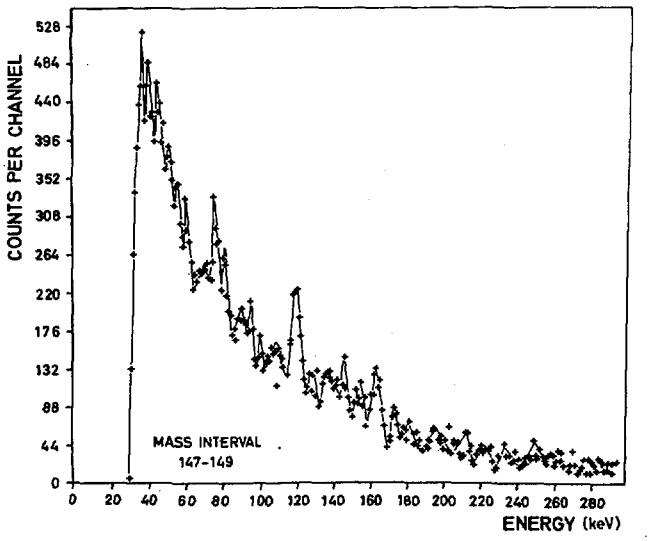

FIG.3. A mass-sorted electron energy spectrum from the heavy fragment group.

2. EXPERIMENTAL PROCEDURE

The experimental arrangement is shown in Fig. 1. A well-collimated beam from the FR-2 reactor impinged on a 100-$\mu g/cm^2$ target of ^{235}U. The energies of the fission fragments were measured by two silicon surface barrier detectors. The internal conversion electrons emitted by one of the fragments during the first 1.8 cm of its flight were focused onto a 200 $mm^2 \times 2$ mm-thick ion implanted detector by means of a magnetic field. The magnetic field steered the electrons around the lead shielding which protected the electron detector from the high fission correlated background. The electron detector, which was operated at liquid nitrogen temperatures, had a resolution of 3 keV in the region of interest. The angles of emission of the electrons with respect to the fragment flight path were restricted to around 90°. The serious losses of energy resolution due to Doppler broadening by the moving fragments were thus mitigated at the expense of a much lower count rate. Since only those electrons within a certain energy window were focused on the detector for a particular value of the magnetic field, the field was made to sweep back and forth continuously throughout the experiment. As the measurements were made over several months, digital stabilization was used on all three detectors. At the end of every 24 hours of measurement, calibration checks were made for stability and a two-parameter experiment was performed to obtain the correlated energies of the two fission fragments. This enabled one to obtain the calibration constants of the fission detectors as well as the mass yield for the neutron induced fission of ^{235}U. The data were processed by procedures described elsewhere [5] and electron spectra associated with fragment masses in 2-amu mass intervals were obtained. Figures 2 and 3 show two of the mass-sorted electron spectra.

3. RESULTS

Some general features of the results may be seen in Fig. 4 which shows the relative yield of electrons per fragment. The gross features of the yield as a function of mass may be understood in terms of the nuclear deformations beyond mass 144, the postulated deformations [6] of neutron-rich nuclei near mass 107, and the closed shell properties of nuclei near mass 132. In the regions of deformation, with low level spacing in the ground state rotational band, one would expect low-energy transitions which are highly converted and therefore high electron yields as seen in the yield curve. There also appears to be evidence of softness to deformation around mass 100. This is of interest in view of the calculations of Arseniev and co-workers [7] which predict deformation in this region.

A total of 131 lines have been analysed in the mass-sorted electron spectra out of which 63 belong to the light and 68 to the heavy fragments. The details of their energy, mass and charge assignments are given elsewhere [5]. The electron energies in the present experiment are estimated to have an error of ± 1 keV. The masses of the fragments were determined from the centroid of a plot of electron peak intensities as a function of mass [3].

Two complementary procedures were adopted to determine the charge of the fragments: (1) The results of the present experiment were compared with the work of Hopkins and co-workers [8, 9]. In their two-parameter experiment they have studied gamma rays in coincidence with X-rays from

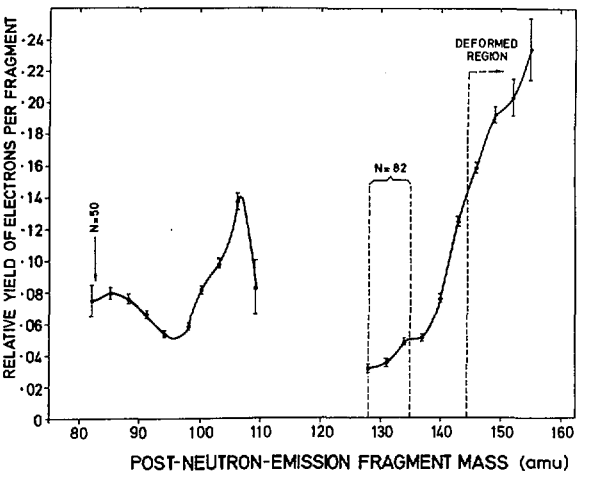

FIG.4. The relative yield of internal conversion electrons as a function of fragment mass.

the stopped fission fragments of ^{252}Cf. The energies of a large number of low-energy gamma rays are obtained and the coincident X-ray is used to restrict the charge of the fragment to a pair of complementary elements. In the present work, conversion electrons from only one fragment are observed and the spectra are sorted according to fragment mass. The procedure then was to calculate the K-electron energies from the gamma-ray energies of Hopkins and co-workers using the binding energies of both the proposed elements. By comparing the calculated K-line energies with the observed electron lines it was possible to ascertain the charge of the fragment as well as to assign a mass number to it. (2) As a further check on the above procedure and for those electron lines whose corresponding gamma rays were not observed in the work of Hopkins and co-workers, the binding energies of the elements around the most probable charge were used to calculate the corresponding gamma-ray energies for the electron lines observed. The results were compared with the energies of gamma rays measured in previous three-parameter gamma-ray experiments [5], and the element with the binding energy which gave the best fit was assigned.

Although a large number of lines have been assigned to the non-even nuclei [5], the present paper is concerned with transitions in the even nuclei and their bearing on current theory. Figures 5 and 6 show the mass and charge assignments for a number of lines which appear to be from the ground state rotational bands of even nuclei. Apart from the indications from their mass and charge assignments, several other features confirm their assignment to even fragments. For example, the relative intensities of the lines assigned as $2^+ \rightarrow 0^+$, after corrections for internal conversion, were found proportional to the independent yields of the assigned isotopes. This is to be expected since nearly all the de-excitation in the even fragments is channelled through the $2^+ \rightarrow 0^+$ transitions. Confirmation for the assignments is also provided by the K/L ratios observed, which are consistent with E2 transitions. In the

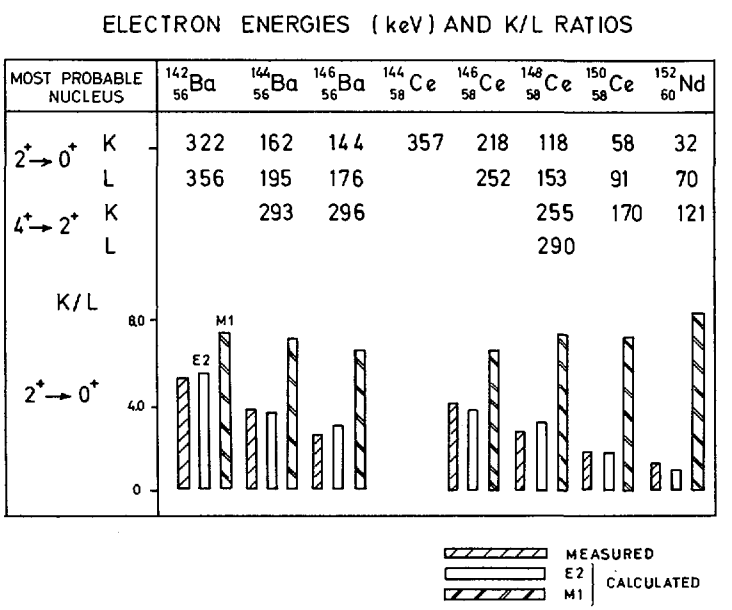

FIG. 5. Energy, K/L ratio and isotope assignment for transitions in the heavy fragment deformed region.

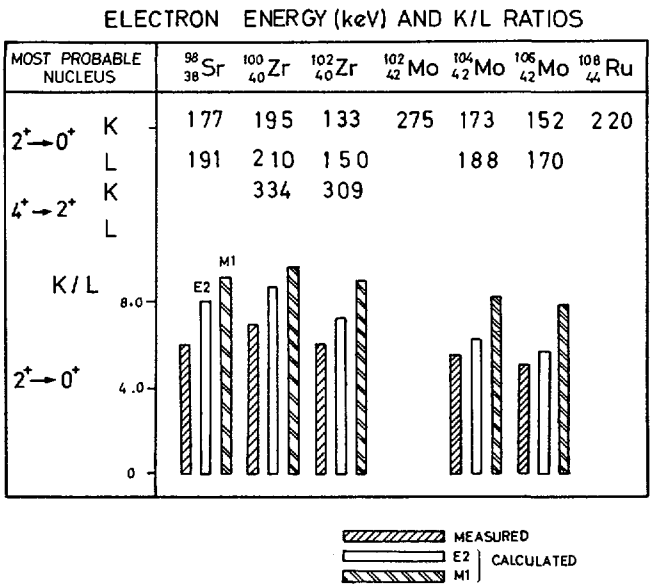

FIG. 6. Energy, K/L ratio and isotope assignment for transitions in the light fragment group in the region of postulated deformations.

light fragment group, where the K/L ratios are less unambiguous, the strong electron conversion of the lines further indicates E2 transitions since the conversion coefficients for E2 transitions are approximately five times higher in this region as compared with M1 and E1. Many of these transitions have been observed in the ^{252}Cf (sf) experiments of Cheifetz and co-workers [1, 2]. The present ^{235}U (n, f) measurements support their proposed assignments and the observed K/L ratios provide additional confirmation.

4. DISCUSSION OF RESULTS

An interesting aspect of the present results is their relationship to the deformed region in the light fragment group. Of particular interest is the region of transition from spherical to deformed nuclei. The first 2^+ levels of the even nuclei around the region of postulated deformation are shown in Fig. 7, which is based on present results and previous determinations [10]. Also plotted are the values of $(E_{2^+})_{crit.}$ $(= 13\hbar^2/\mathcal{I}_{rigid})$. This quantity is proposed as an approximate criterion for deformation by Adler and co-workers [11]. According to this criterion, nuclei having $E_{2^+} > (E_{2^+})_{crit.}$ are to be assumed spherical and those with $E_{2^+} < (E_{2^+})_{crit.}$ deformed.

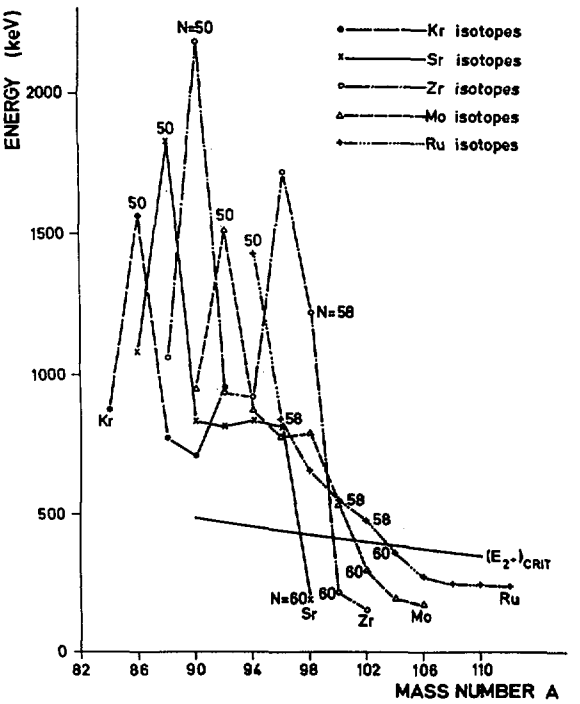

FIG. 7. The systematic variation of the first 2^+ excited states in the even-A isotopes of Kr, Sr, Zr, Mo, Ru.

TABLE I. DEFORMATION INDICATORS FOR THE TRANSITION NUCLEI IN THE LIGHT FRAGMENT GROUP

Nucleus	Neutron number	E_{2^+} (keV)	$[E_{2^+}]_{crit.}$ (keV)	$[E_{2^+}]_{crit.} - E_{2^+}$ (keV)	X	β'	$\beta_{theoretical}$[b]
^{98}Sr		193	422	229	0.92	0.30	-0.31
^{100}Zr	60	213	408	195	0.80	0.28	-0.29
^{102}Mo	60	296	395	99	0.56	0.23	-0.28
^{104}Ru	60	358[a]	383	25	0.45	0.21	-0.26
^{156}Gd		79.5[a]	192	112	1.0	0.24	

[a] See Ref. [10].

[b] See Ref. [7].

If strong charges in the energy of the first 2^+ levels may be regarded as indicative of transitions from vibrational to rotational modes and of a strong change in nuclear softness, then it appears that this transition occurs between neutron numbers 58 to 60 for the light fragments. This conclusion is also supported by the $(E_{2^+})_{crit.}$ criterion. Furthermore, although the transition in nuclear behaviour is analogous to that observed in the heavy fragment region between neutron numbers 88 and 90 [2], in the light fragments it is far more drastic. The most striking case is that of the zirconium isotopes (Z = 40) first observed by Cheifetz and co-workers [1]. The energy of the first 2^+ level changes from 1223 keV for ^{98}Zr to 213 keV for ^{100}Zr. In the neighbouring Mo (Z = 42) and Sr (Z = 38) isotopes, the changes in the first 2^+ level energies between N = 58 and 60 are much less abrupt and in Ru (Z = 44) the transition to rotational behaviour is relatively smooth and gradual. Sheline and co-workers [12] have recently suggested that the drastic changes in nuclear characteristics in the Zr and Mo isotopes may be due to a highly deformed secondary minimum (associated with the deformed shell structure at Z = 40) which moves down in energy with increasing N and becomes the ground state minimum at N = 60. Present results suggest that the behaviour of the Sr isotopes in the transition region may be similarly interpreted.

One transition of particular interest is the $2^+ \rightarrow 0^+$ transition in ^{98}Sr. The yield of this Sr isotope is very low in ^{252}Cf (sf) but in ^{235}U (n,f) it is produced in more significant quantities. The transition is of importance firstly because the change from ^{96}Sr to ^{98}Sr is across the transition region (N = 58 to 60) and secondly because the calculations of Arseniev and co-workers [7] predict that the strongest deformations should be in the heavier isotopes of strontium and it is of interest to compare the results with their predictions.

In the present experiment an electron line of energy 177 keV has been assigned to mass 98 ± 1 amu. The line appears to be the $2^+ \rightarrow 0^+$ transition in ^{98}Sr, firstly because a corresponding gamma-ray line at 193 keV and mass 98 ± 1 has also been observed in the complementary gamma-ray experiment [5] whose energy is in agreement with the assignment of the electron line to Sr and secondly because the relative intensity of the line was found compatible with its being the $2^+ \rightarrow 0^+$ line in ^{98}Sr.

At present the only information about the structure of ^{98}Sr is the energy of the first 2^+ level, if the proposed assignment is valid. Nevertheless, considerable understanding of the behaviour of a nucleus may be obtained by means of a number of indicators based on the energy of the first 2^+ level. It is therefore of interest to compare such indicators for neighbouring transition nuclei (i.e. nuclei with N = 60) in the light fragments. Three such indicators have been used. The first indicator is the deformation parameter χ [= $(79.51/E_{2^+}) \times (158/A)^{5/3}$] which gives an approximate mass-independent comparison of the energies of the first 2^+ states using the deformed nucleus ^{158}Gd as a comparison. The second indicator used is a relative value of the deformation β' extracted from the centrifugal stretching model of Diamond and co-workers [13] in which the moment of inertia $\mathcal{I}$ is assumed to be equal to $3B\beta^2$. The final indicator is the energy difference between E_{2^+} and $(E_{2^+})_{crit.}$ mentioned above. The values of these indicators for the four neighbouring transition nuclei and ^{158}Gd are given in Table I. Also given are the theoretical values of the deformation β from the calculations of Arseniev and co-workers [7], where the negative sign implies oblate deformations.

An examination of Table I shows that the values of the deformation indicators for the nuclei in the postulated region of deformation in the light fragments are quite comparable with the values for ^{158}Gd, which is known to be a good example of a deformed nucleus in the rare earth region. Furthermore, all three indicators suggest that of the four transition nuclei ^{98}Sr has the strongest tendency towards deformation, the tendency decreasing monotonically as one moves towards ^{104}Ru. This is in good agreement with the predictions of Arseniev and co-workers and, in particular, the values of β' derived from the centrifugal stretching model are very similar in magnitude and variation to the values for β predicted by Arseniev and co-workers. However, the actual values of β, for those nuclei whose B(E2) values are available [1, 14], are somewhat higher in magnitude.

5. CONCLUSION

The internal conversion spectra have made it possible to investigate the highly converted low-energy transitions and thus study the behaviour of nuclei in the regions of deformation.

Moreover the experiments have demonstrated the possiblity of the study of the structure of fission fragments using neutron induced fission. By using ^{233}U (n, f), mass regions which partly overlap those reached in (t, p) reactions could be investigated. Thus a large and continuous region on the neutron-rich side of the stability line is open to investigation.

REFERENCES

[1] CHEIFETZ, E., JARED, R.C., THOMPSON, S.G., WILHELMY, J.B., Phys. Rev. Lett. 25 (1970) 38.
[2] WILHELMY, J.B., THOMPSON, S.G., JARED, R.C., CHEIFETZ, E., Phys. Rev. Lett. 25 (1970) 1122.
[3] WATSON, R.L., WILHELMY, J.B., JARED, R.C., RUGGE, C., BOWMAN, H.R., THOMPSON, S.G., RASMUSSEN, J.O., Nucl. Phys. A141 (1970) 449.
[4] HORSCH, F., MICHAELIS, W., in Physics and Chemistry of Fission (Proc. Symp. Vienna, 1969), IAEA, Vienna (1969) 527.
[5] KHAN, T.A., HOFMANN, D., HORSCH, F., Kernforschungszentrum Karlsruhe Rep. KFK 1770 (1973).
[6] JOHANSSON, S.A.E., Ark. Fys. 36 67 (1966) 599.
[7] ARSENIEV, D.A., SOBICZEWSKI, A., SOLOVIEV, V.G., Nucl. Phys. A139 (1969) 269.
[8] HOPKINS, F.F., WHITE, J.R., PHILLIPS, G.W., MOORE, C.F., RICHARD, P., Phys. Rev. C4 (1971) 1927.
[9] HOPKINS, F.F., WHITE, J.R., PHILLIPS, G.W., MOORE, C.F., RICHARD, P., Phys. Rev. C5 (1972) 1015.
[10] WOOD, J.L., A Compilation and Survey of Data on Levels of Even-Even Nuclei, Kernforschungszentrum Karlsruhe Rep. KFK 1/71-1 (1971).
[11] ALDER, K., BOHR, A., HUUS, T., MOTTELSON, B., WINTHER, A., Rev. Mod. Phys. 28 (1956) 432.
[12] SHELINE, R.K., RAGNARSSON, I., NILSSON, S.G., Phys. Lett. 41B (1972) 115.
[13] DIAMOND, R.M., STEPHENS, F.S., SWIATECKI, W.J., Phys. Lett. 11 (1964) 315,
[14] JARED, R.C., NIEFENECKER, J., THOMPSON, S.G., Paper IAEA-SM-174/62, these Proceedings, Vol. 2.

ANGULAR MOMENTUM IN FISSION. HEAVY-ION-INDUCED FISSION

(Session VIII)

Chairman: Tasneem A. Khan (Pakistan)

CALCULATIONS OF THE CRITICAL ANGULAR MOMENTUM IN THE ENTRANCE REACTION CHANNEL

J. WILCZYŃSKI*
Niels Bohr Institute,
University of Copenhagen,
Copenhagen, Denmark

Abstract

CALCULATIONS OF THE CRITICAL ANGULAR MOMENTUM IN THE ENTRANCE REACTION CHANNEL.

A dynamic model, based on the force equilibrium concept, is proposed to estimate the critical angular momentum in the entrance channel for reactions between complex nuclei. The ion-ion force is derived from simple surface-energy considerations. Good agreement with the experimental data on complete-fusion cross-sections is obtained.

It is shown that, with the exception of heavy target nuclei, the equilibrium properties of the compound nucleus do not limit the cross-sections for complete fusion. A much stronger limitation, corresponding to lower angular momenta, arises in the entrance reaction channel before the compound nucleus can be formed.

For a particular compound system the critical angular momentum depends on the combination of target and projectile used for the production of this compound system. The calculated critical angular momenta are in good agreement with results of the experiment reported by Zebelman and Miller who measured the complete-fusion cross-sections in three different reactions leading to the formation of the same compound nucleus with the same excitation energy.

The critical angular momenta, acting in the entrance reaction channel, are calculated for all possible combinations of the target and projectile. It is shown that the cross-sections for complete fusion are drastically limited in the entrance reaction channel, especially for heavy colliding systems. Heavy compound nuclei in the region of the proposed "island of stability" around $Z = 114$, $N = 184$ can be produced only with very asymmetric combinations of target and projectile. It is suggested that the use of ^{48}Ca as a projectile and neutron-rich targets like ^{250}Cm or ^{252}Cf may be the most promising choice (among the conventional fusion reactions) to reach at least the neutron-deficient side of the "island".

The complete text of this paper has been published as:
WILCZYŃSKI, J., Nucl. Phys. A216 (1974) 386.

DISCUSSION

F. PLASIL: I agree with Mr. Wilczyński that in many cases the probability for the formation of the compound nucleus is governed by entrance channel considerations. In Fig. A (Fig. 4 of the paper) however, a curve for the zero fission barrier ($B_f = 0$) taken from calculations done by Cohen, Swiatecki and myself was shown, and the implication was that the curve does not compare well with experimental data. The $B_f = 0$ curve is not expected to compare with experimental measurements of compound nuclei that survive de-excitation (evaporation residues), because fission is expected to compete with particle emission when B_f is small, well before $B_f = 0$. Calculations that consider the competition between fission and particle emission for all

* On leave from the Institute of Nuclear Physics, Cracow, Poland.

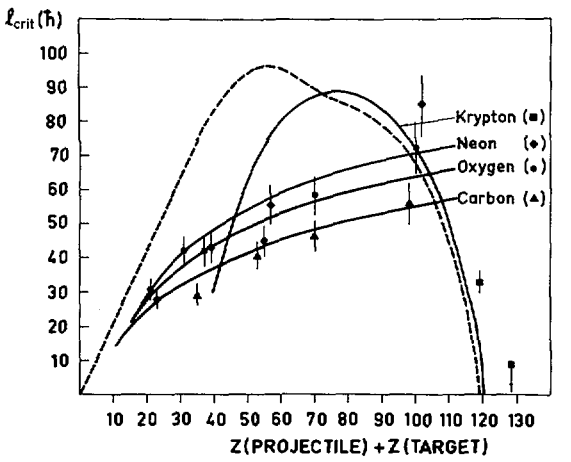

FIG. A. Critical angular momenta calculated from the measured (Refs [1-3, 9, 13] of the paper) values of σ_{CF} as a function of the Z of the compound system. The solid lines show the predictions of this model for C, O, Ne and Kr projectiles. The dashed line shows the limits of angular momentum for the compound system predicted by Cohen, Plasil and Swiatecki (Ref. [16] of the paper).

values of B_f were done by Blann and myself. When our calculations are compared with experimental results for evaporation residue cross-sections, the picture is much more favourable than shown in Fig. A.

J. WILCZYŃSKI: I should explain that when we talk about the cross-section for complete fusion we take into account both contributions — the evaporation residue cross-section and the fission cross-section. If you assume that the fusion cross-section is limited by the equilibrium properties of the compound system, then the sum of the two components σ (evaporation) + σ(fission) should correspond to the angular momentum limit for $B_f = 0$. In fact, experimental data show that the limit is much lower. The experimental data which have been taken for the comparison contain both parts of the fusion cross-section. The σ(fission) component was either measured independently or calculated. In many cases (especially at low energies and for light colliding systems) the contribution of σ(fission) is estimated to be very small.

J. R. NIX: I feel that your approach needs refining in three areas. First of all, the introduction of the finite range of the nuclear force would lead to a shift in the distance between the nuclear surfaces at which the maximum in the interaction barrier occurs. As shown by Krappe, this distance decreases for heavier systems because of the larger Coulomb repulsion relative to nuclear attraction. Secondly, as Sierk shows[1], when additional shape coordinates are introduced, heavy nuclei frequently undergo fission even after the system has passed over the maximum in the interaction barrier. Thirdly, the transition in the moment of inertia of the system from its two-point-mass value before interaction to a larger value, after the nuclei have fused, should be included. This last point is being studied by Tsang and Swiatecki at Berkeley.

[1] SIERK, A.J., NIX, J.R., Paper IAEA-SM-174/74, these Proceedings, Vol.2.

H. NIFENECKER: This is a very naive question, I am afraid, after such an illuminating talk. I understand that in your model you assume the radial velocity to be zero, when the two nuclei are touching. Is this the case and, if so, what is the justification for this assumption?

J. WILCZYŃSKI: This is a very important point. If ℓ_{crit} is significantly smaller than the angular momentum for peripheral collision, the radial component of relative velocity (at the touching point) will differ from zero in a wide range of the ℓ-values. However, we can assume that the motion in radial direction is very quickly damped due to the compression of nuclear matter in the area of overlap. Now the problem arises as to how the ion-ion force depends on the radial component of the relative velocity. In the model presented here it is assumed that the ion-ion force is energy-independent. Of course, this is a very rough assumption. We know from the heavy-ion scattering experiments (I mean from the measurements of excitation functions) that the real part of the optical potential increases slightly with energy. This implies that the critical angular momentum should also increase with energy. In fact, such an effect was observed experimentally by Natowitz.

J. B. NATOWITZ: With regard to Plasil's comment concerning the validity of comparisons between the Wilczyński calculations and the reported fusion cross-sections for the light elements, I would agree that the comparison should be made with complete-fusion cross-sections, which include all fusion processes regardless of the subsequent decay modes. We should note, however, that Blann and Plasil's model predicts very large fission cross-sections for the light elements, even when corrected for non-fusion reactions. But the experimental evidence is that the fission cross-sections are in fact much lower than calculated and therefore the available cross-sections based upon evaporated residue detection should be very close to the actual fusion cross-sections.

F. PLASIL: Apart from uncertainties in the parameters that could be considered adjustable, such as the level density parameters a_f and a_n, it should be stressed that we calculate primarily the cross-section for evaporation residues, that is to say compound nuclei that survive de-excitation by particle emission. Values for the actual fission cross-sections from our calculation can be believed only if the compound nucleus cross-section is known. If a large fraction of the total reaction cross-section does not involve compound nucleus formation, then the calculated fission cross-section will be small. This point is made in our paper on neon-induced fission of silver[2].

---

[2] PLASIL, F., FERGUSON, R.L., PLEASONTON, F., Paper IAEA-SM-174/71, these Proceedings, Vol. 2.

DYNAMICS OF FISSION AND FUSION WITH APPLICATIONS TO THE FORMATION OF SUPERHEAVY NUCLEI*

A.J. SIERK, J.R. NIX
Los Alamos Scientific Laboratory,
University of California,
Los Alamos, N. Mex.,
United States of America

Abstract

DYNAMICS OF FISSION AND FUSION WITH APPLICATIONS TO THE FORMATION OF SUPERHEAVY NUCLEI.

Within the framework of the liquid drop model various aspects of the dynamical evolution of nuclei are studied: the effects of viscosity on the separation of fission fragments, the fission of very large nuclei, and the fusion of two heavy ions. The effect of viscosity on the post-scission motion of fission fragments is calculated by assuming an irrotational flow pattern in spheroidal fragments. As the viscosity increases from 0 to ∞, the fission fragments remain prolate for a longer time, which increases the post-scission fragment kinetic energy. This increase is about 13 MeV for the symmetric fission of ^{236}U.

The dynamical path is calculated from an initially spherical configuration to scission for nuclei with fissility parameter x between 1.0 and 1.6 by use of the three-quadratic-surface shape parametrization. The inertias are calculated by means of the Werner-Wheeler approximation for irrotational flow. The motion is assumed nondissipative. As the Coulomb energy increases, the scission configuration becomes more and more elongated. As a specific example, the evolution of an initially spherical $^{476}184$ nucleus, formed from two ^{238}U nuclei, is calculated. It has been suggested that this system might form a superheavy nucleus by asymmetric fission. At scission the calculated length of this nucleus is about 14 times the diameter of the initial sphere. This result indicates that the nucleus would probably fission into three or more fragments if this were allowed by the shape parametrization. To complement this calculation, the static potential energy of two tangent spheroidal fragments of the $^{476}184$ nucleus corresponding to $^{300}116$ and ^{176}Er is computed. Configurations stable against fission of the $^{300}116$ nucleus have an energy over 100 MeV higher than the minimum energy of two tangent spheroids and the energy of the scission point in the dynamical calculation. Single particle effects lead to a small local minimum in the potential energy near the spherical heavy fragment with a barrier of about 4 MeV against prolate distortions. It is concluded from these results that the fusion-fission reaction of very heavy ions is not likely to produce superheavy nuclei.

The fusion reactions of two initially spherical tangent nuclei at various incident energies above the interaction-barrier height are studied. These calculations also do not contain viscosity and use the same shape parametrization as the fission study. This parametrization is deficient in that for most cases one is unable to follow the evolution to the point where the nuclei refission. The amount of incident energy necessary for symmetric systems to fuse to a configuration more compact than the liquid-drop-model saddle-point shape is calculated as a function of the fissility parameter x. As specific examples, the symmetric reactions $^{110}Pd + ^{110}Pd$ and $^{238}U + ^{238}U$ are considered.

1. INTRODUCTION

We have already seen in this symposium that dynamics plays an important role in many phenomena in fission and heavy-ion reactions. These include the division of the total energy released in fission into fission-fragment kinetic energy and internal excitation energy, and the amount of incident kinetic energy needed to cause fusion in a heavy-ion reaction.

* This work was performed under the auspices of the US Atomic Energy Commission.

The most fundamental way to study nuclear dynamics is of course to use a microscopic approach, as discussed earlier by Pauli [1] and others. However, because of the large amount of computing that is required, it is not yet feasible with such approaches to solve the equations of motion for the time evolution of the system. We therefore use a much simpler macroscopic approach, where the dynamics is treated in terms of classical hydrodynamical flow. Previous studies of this type [2-4] have been limited primarily to nonviscous irrotational flow and have been applied only to the fission of nuclei with fissility parameter x less than 1.0. (The fissility parameter is defined as the ratio of the Coulomb energy of a spherical sharp-surface drop to twice the spherical surface energy.) Natural extensions of this earlier work include the introduction of nuclear viscosity, the fission of heavier nuclei, and the study of fusion reactions. Certain aspects of these three extensions are considered in Secs. 2, 3, and 4, respectively.

In calculating the potential energy of the system, we include only the surface and Coulomb energies of the liquid-drop model. Although single-particle corrections to the potential energy are important in many specific phenomena, they have a small influence on the average trends of dynamical effects over the broad region of nuclei that we are considering. The equations of motion are solved classically because the DeBroglie wavelength of the motion is usually much smaller than distances over which the potential energy changes by an appreciable amount. Furthermore, we do not yet know how to incorporate dissipative effects into a quantum-mechanical equation of motion.

For small deformations, corresponding to the ground state and the region of the fission barrier, we know that the true nuclear inertia is several times the value corresponding to classical hydrodynamical flow, and in this region the treatment of nuclear dynamics in terms of classical hydrodynamical flow is seriously deficient. However, for larger distortions, such as those in the later stages of fission or near the point of first touching in heavy-ion reactions, experimental values for inertias are poorly known, and values calculated by use of the cranking model are close to the irrotational-flow values. This suggests that a classical hydrodynamical treatment may be sufficiently accurate for these larger distortions.

There are two general methods for computing hydrodynamical flow. One method is to solve the complete Navier-Stokes equations for a viscous fluid by means of finite-difference numerical techniques. A faster but more limited approach is to describe a nuclear shape by a small number of coordinates and to follow the time evolution of these coordinates. There have been some attempts in nuclear physics to use the first method but no results have appeared yet. We choose the second method because of its relative simplicity.

Because we are interested in both fission and fusion reactions, we choose a shape parametrization that describes shapes occurring in both processes. The shapes are restricted to axial symmetry and are formed by connecting smoothly two end spheroids with a central quadratic surface, which may be either a spheroid or a hyperboloid of revolution. This parametrization contains three symmetric and two asymmetric degrees of freedom, but is limited by not being able to describe either multi-fragment fission or many shapes encountered in heavy-ion fusion. However, even with these restrictions, we are able to learn several interesting properties of fission and fusion reactions.

2. EFFECTS OF VISCOSITY ON THE SEPARATION OF FISSION FRAGMENTS

One of our primary objectives is to study the effect of viscosity on nuclear dynamics. We introduce viscosity by means of the Rayleigh dissipation function

$$\mathcal{F} = \frac{1}{2} \sum_{i,j} \eta_{ij}(\vec{q})\, \dot{q}_i\, \dot{q}_j$$

where $\dot{q}_i$ is the time derivative of the shape coordinate q_i and where η_{ij} is an element of the viscosity tensor. The viscosity tensor, which is a function of the nuclear shape, is calculated by equating $\mathcal{F}$ to one-half the rate of energy dissipation from collective modes to internal energy. The equations of motion become the generalized Lagrange equations

$$\frac{d}{dt}\left(\frac{\partial \mathcal{L}}{\partial \dot{q}_i}\right) = \frac{\partial \mathcal{L}}{\partial q_i} - \frac{\partial \mathcal{F}}{\partial \dot{q}_i}$$

where the Lagrangian $\mathcal{L} = T - V$ is also a function of q_i and $\dot{q}_i$. The kinetic energy is T, and V is the potential energy. The introduction of viscosity adds to the equations of motion terms linear in the first time derivatives of $\vec{q}$. Most of the inertial effects are included in terms containing second time derivatives of $\vec{q}$, while the generalized forces are described primarily by terms involving the zeroth time derivative of $\vec{q}$.

Eventually we plan to solve the equations of motion with viscosity included for the descent from the saddle point to scission. Then by comparing the calculated most probable fission-fragment kinetic energies with experimental values, we should be able to deduce an average value for the coefficient of nuclear viscosity appropriate to large distortions, which is poorly known at present [5].

We have not yet computed $\mathcal{F}$ for our full parametrization but have studied instead the separation of two viscous fission fragments constrained to spheroidal shapes. Although we are able to treat a more general case (unequal fragments rotating in a plane formed by their symmetry axes), we present here results corresponding to the separation of equal collinear fragments. In this case the coordinates of interest are the center-of-mass separation r and the semi-symmetry axis c of the spheroids. The fragments are taken to be initially at rest in the configuration of tangent spheroids of minimum potential energy. The inertia and viscosity tensors are calculated by assuming incompressible, irrotational hydrodynamical flow. This approximation is discussed in the appendix.

The equations of motion for the symmetric spheroids are

$$\dot{p}_r = -\frac{\partial V}{\partial r}$$

and

$$\dot{p}_c = -\frac{\partial V}{\partial c} + \frac{p_c^2}{2M_c^2}\frac{dM_c}{dc} - \frac{4\pi R_0^3 \mu p_c}{M_c\, c^2}$$

where the two conjugate momenta are $p_r = M_r \dot{r}$ and $p_c = M_c \dot{c}$ and where the two elements of the diagonal inertia tensor are

$$M_r = \frac{1}{4} M_0$$

and

$$M_c = \frac{1}{5} M_0 [1 + \frac{1}{4} (R_0/c)^3]$$

The quantity M_0 is the mass of the original spherical nucleus, R_0 is its radius, and μ is the coefficient of nuclear viscosity.

We show in Fig. 1 the center-of-mass separation r and the fragment elongation σ of two symmetric fragments resulting from the fission of a nucleus with fissility parameter $x = 0.7$. The points are given at equal time intervals for varying values of viscosity. The coordinates r and σ [6] are generalizations of r and c which are useful for the more complex shapes that we consider later. If we bisect a reflection-symmetric shape at its center and define $\langle f \rangle$ as the average value of the function f over one-half the mass distribution, then $r = 2\langle z \rangle$ and $\sigma = (\langle z^2 \rangle - \langle z \rangle^2)^{\frac{1}{2}}$. For two separated spheroids, σ is exactly $c/\sqrt{5}$.

In Figs. 1 and 2 the viscosity is given in terms of the natural unit [2,3]

$$\mu_0 = \left[M_0 E_s^{(0)}\right]^{\frac{1}{2}} R_0^{-2}$$

When the second set of liquid-drop-model constants of Myers and Swiatecki [7] is used for a nucleus with fissility parameter $x = 0.7$ along Green's approximation to the line of beta stability [8], the resulting value is $\mu_0 = 6.73 \times 10^{17}$ MeV sec cm^{-3} $= 1.08 \times 10^{12}$ gm cm^{-1} sec^{-1} (poise). It is worth noting that a direct comparison of the magnitude of nuclear viscosity with that of familiar macroscopic systems is misleading because of scaling effects.

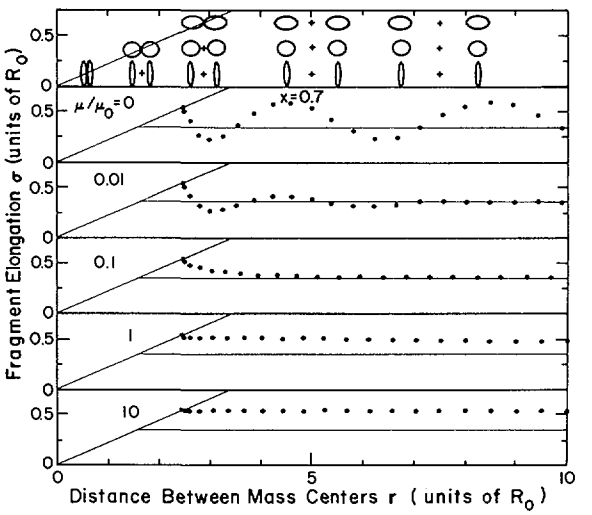

FIG. 1. Calculated fragment elongation σ and centre-of-mass separation r for spheroidal fission fragments for a nucleus with fissility parameter $x = 0.7$. The coordinate σ is $c/\sqrt{5}$, where c is the semi-symmetry axis of the spheroidal fragments. The paths are plotted at equal time intervals of $0.4\ T_0 \approx 1.8 \times 10^{-22}$ sec for five values of the viscosity μ. The natural unit of viscosity is $\mu_0 = [M_0 E_s^{(0)}]^{\frac{1}{2}} R_0^{-2}$, where $E_s^{(0)}$ is the surface energy of the original spherical nucleus. The shapes corresponding to selected values of these coordinates, indicated by the plus signs, are shown in the top part of the figure. The sloping lines give the configurations of two tangent spheroids, and the horizontal lines give the configurations of two separated spheres.

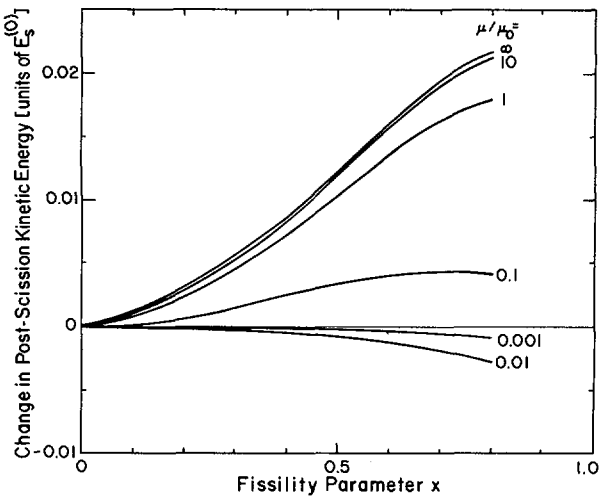

FIG.2. Calculated change in fragment kinetic energy due to viscosity as a function of the fissility parameter x for spheroidal fission fragments. The energy change is plotted as $[E(\mu) - E(0)]/E_s^{(0)}$ where $E_s^{(0)}$ is the surface energy of the original spherical nucleus. The natural unit of viscosity is $\mu_0 = [M_0 E_s^{(0)}]^{\frac{1}{2}} R_0^{-2}$.

The effect of viscosity on this system, as shown in Fig. 1, is qualitatively similar to that on a one-dimensional harmonic oscillator. For small values of viscosity, the shape oscillations continue with damped amplitude. As the viscosity increases to a critical value, the fragments approach spherical shape nearly exponentially. For very large values of viscosity the fragments approach the spherical shape much more slowly.

We show in Fig. 2 the change in post-scission kinetic energy relative to nondissipative motion for fragments with different amounts of viscosity. Because two prolate spheroids have a higher Coulomb interaction energy than two spheres with the same center-of-mass separation, the kinetic energy for very viscous fragments is larger than that for no dissipation. For small values of viscosity, the fragment energy is less than that for no viscosity because of the increased time the system spends with a significant oblate deformation relative to the time with a prolate shape.

3. FISSION OF VERY LARGE NUCLEI

Heavy-ion reactions that might produce superheavy nuclei lead to systems with fissility parameter x greater than 1. It is therefore important to know the fission properties of such systems, which are already being produced in heavy-ion reactions.

We calculate the dynamical evolution of nuclei with x greater than 1.0 by use of the three-quadratic-surface shape parametrization. The effective masses for irrotational flow are calculated by means of the Werner-Wheeler method, where the flow is approximated by circular layers of fluid which move along the symmetry axis and change their radii but do not lose

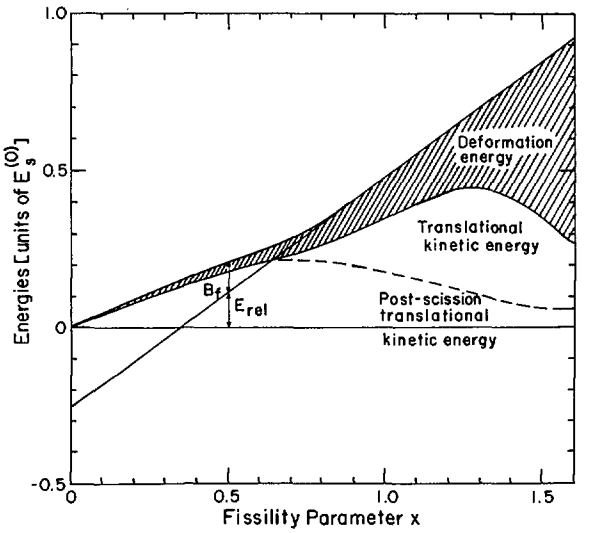

FIG. 3. Calculated division of the energy in fission for idealized nonviscous nuclei as a function of the fissility parameter x. The total energy available is the sum of the energy release E_{rel} and the fission-barrier height B_f. This energy is divided into pre-scission translational kinetic energy, post-scission translational energy, and fragment vibrational (excitation) energy at infinite separation. The results for $x < 1$ are taken from Ref. [3].

their disk-like shape [2,3]. Viscosity is not included. The initial conditions correspond to starting at a spherical shape with zero kinetic energy (at $t = -\infty$). In Fig. 3 we show the division of the energy released in fission as a function of x. The energy is divided into translational kinetic energy (acquired before and after scission) and deformation energy of the fragments at infinite separation. The Coulomb forces cause an increase in deformation energy at scission for large values of x, with more than half of the energy release going into deformation energy for x greater than 1.42. However, this large deformation energy is partly a result of our method of parametrizing the nuclear shape. Since we restrict the system to binary fission, it cannot reduce its large deformation energy by fissioning into three or more fragments.

As a specific example, we consider the $^{476}184$ system, which can be formed from the fusion of two ^{238}U nuclei. We investigate this problem from two complementary points of view: the dynamical evolution of an initially spherical $^{476}184$ nucleus, and the static potential energy as a function of fragment deformation for two tangent spheroidal fission fragments from the same nucleus.

In Fig. 4 we present the sequence of shapes followed by an initially spherical $^{476}184$ nucleus with 1 MeV of energy in the fission degree of freedom at time intervals of 10^{-21} sec. The Coulomb forces cause a very large fragment elongation, to a maximum length of more than 14 times the initial diameter of the sphere. This fact suggests that multi-body fission would occur in a less restricted shape parametrization. The fission of a ^{236}U nucleus, started from the liquid-drop-model saddle point with 1 MeV of

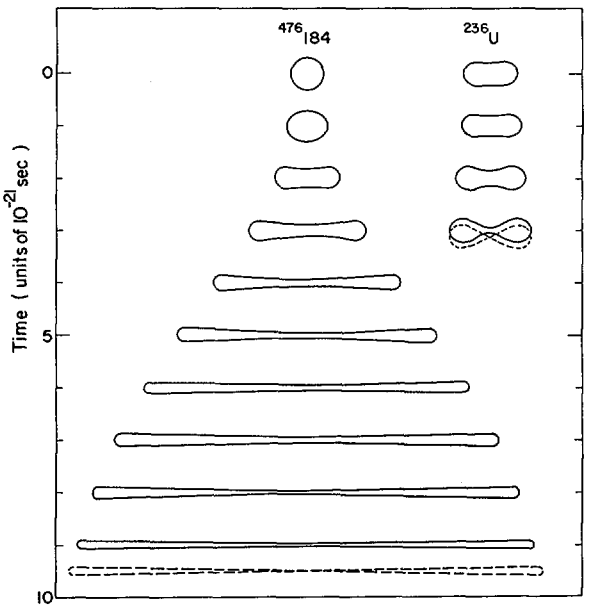

FIG.4. Calculated sequence of shapes at time intervals of 10^{-21} sec for the symmetric fission of $^{476}184$ and ^{236}U. The $^{476}184$ nucleus is initially spherical and the ^{236}U nucleus is initially at the liquid-drop-model saddle point. Both nuclei initially have 1 MeV of kinetic energy in the fission direction. The viscosity is zero. The shapes are constrained to binary fission in the three-quadratic-surface shape parametrization. The scission configurations are shown dashed.

kinetic energy in the fission direction is also shown in Fig. 4 for comparison with the result for $^{476}184$. The inclusion of viscosity in these calculations could cause the results to change significantly. In particular, large viscosity might cause the fragments to be much less elongated at scission.

In Fig. 5 we show a potential-energy map for two tangent spheroids, where the coordinates are the ratios c/a of the semi-symmetry to the semi-transverse axes for the two fragments. The energies are calculated by use of the droplet model [9], which contains primarily surface and Coulomb energies, but also includes higher-order corrections in $A^{-1/3}$ and $[(N-Z)/A]^2$ than are retained in the liquid-drop model; the constants are taken from the January 1973 analysis of Myers and Swiatecki [10]. The two fragments are taken to be $^{300}116$ and ^{176}Er, a division which approximately conserves the charge density of the $^{476}184$ parent system. The minimum energy of the system with the heavy nucleus spherical corresponds to a light-fragment semi-axis ratio c/a = 12.6 and is 126 MeV higher than the absolute minimum-energy configuration. This latter configuration corresponds to a light-fragment semi-axis ratio c/a = 2.1 and a heavy-fragment semi-axis ratio c/a = 11.9. Both of these minima are artifacts of the spheroidal shapes chosen, as the fragments would undergo fission if allowed to form a neck.

In Fig. 6 we show the potential energy of the tangent spheroids as a function of deformation of the superheavy fragment with the light fragment held fixed at the semi-axis ratio c/a = 12.6. To the droplet energy we add

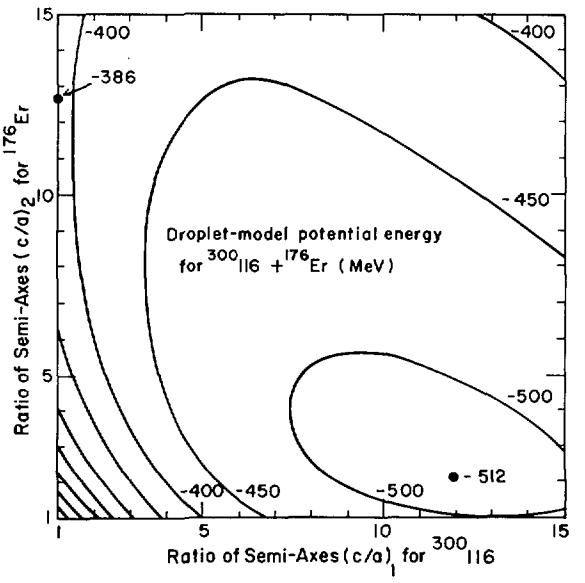

FIG. 5. Static potential energy of tangent spheroidal fragments calculated in the droplet model as a function of the ratios c/a of their semi-symmetry to semi-transverse axes. The fragments are $^{300}116$ and ^{176}Er formed from a $^{238}U + ^{238}U \rightarrow ^{476}184$ parent system. The black dot labelled -512 corresponds to an absolute minimum of the potential energy. That labelled -386 corresponds to the minimum energy configuration with the heavy fragment spherical.

the single-particle corrections calculated for the $^{300}116$ nucleus isolated from external interactions [11], which gives an estimate of the maximum effect of shell and pairing corrections. The single-particle effects lead to a local minimum in the potential energy, but the energy at this minimum is still more than 100 MeV higher than the energy of the configuration with the very elongated superheavy fragment and the energy of the scission configuration for the dynamical fission calculation described above. Because of this large energy difference, the probability for the large fragment to be formed with a semi-axis ratio less than the saddle-point value of 1.2 is extremely small.

In private discussions Vandenbosch has suggested that the presence of the Coulomb forces from the second fragment could possibly prevent the heavy fragment from undergoing fission by driving it toward a spherical shape. We estimate the importance of this effect by calculating the maximum elongation of the superheavy nucleus which could be driven to a spherical shape by a spherical light fragment initially in contact. This maximum elongation occurs at a semi-axis ratio for the $^{300}116$ fragment of $c/a = 2.0$. This value represents an upper limit because in this estimate the positions of the centers of mass of the fragments are held constant instead of being allowed to separate, and the light fragment is spherical instead of a more probable prolate spheroid.

We have shown that the production of superheavy nuclei from the asymmetric fission of nuclei with mass number $A \approx 500$ is highly improbable. This conclusion has been reached only for nonviscous motion; the result

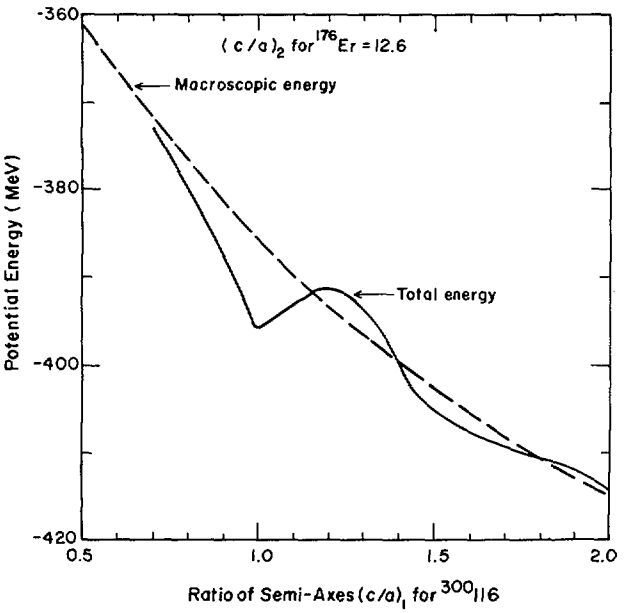

FIG. 6. Calculated potential energy of tangent spheroidal fragments as a function of the semi-axis ratio c/a of the $^{300}116$ fragment. The elongation of the ^{176}Er fragment is held constant at c/a = 12.6. The macroscopic contribution to the energy, which is calculated in the droplet model, is given by the dashed line. The total energy, which is obtained by adding shell and pairing corrections for a noninteracting $^{300}116$ nucleus, is given by the solid curve.

would be modified if very viscous flow resulted in fragment elongation at scission with a semi-axis ratio c/a significantly less than 2.0. For viscous flow the value would need to be less than 2.0 because the large fragment would not be able to respond quickly to the Coulomb restoring force of the lighter fragment before the two nuclei separate.

4. FUSION OF HEAVY IONS

We use the shape parametrization described in Sec. 3 and the dynamical equations in Ref. [3] to study the fusion of two initially spherical nuclei with zero relative angular momentum. In Fig. 7 we show the evolution of two ^{110}Pd nuclei interacting to form ^{220}U at various energies above the liquid-drop interaction barrier. (All energies are in the center-of-mass system.) Two ^{238}U nuclei are shown in Fig. 8 interacting at various energies to form a $^{476}184$ system. These two examples are qualitatively different: The ^{220}U system has a fission barrier with a liquid-drop-model saddle-point energy of about 5 MeV and would thus form a compound system for a significant range of collision energies (for nonzero viscosity), whereas the $^{476}184$ nucleus is unstable with respect to small spheroidal distortions and therefore has no fission barrier. In comparing Figs. 7 and 8 with Fig. 4 we see that the time scale for fusion reactions is much shorter than for fission.

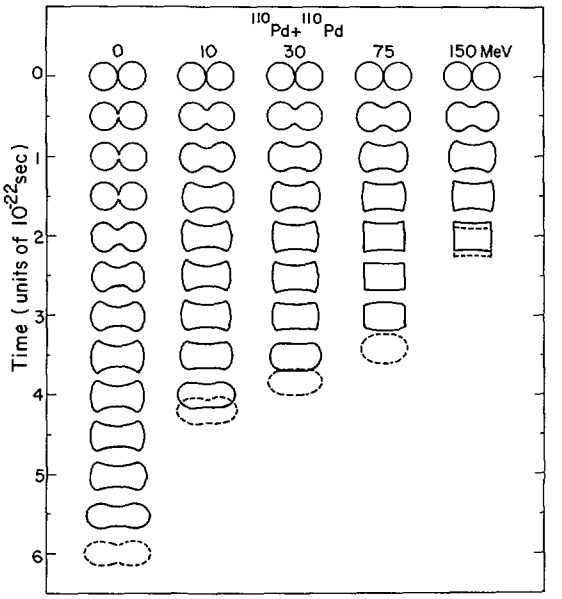

FIG. 7. Calculated sequence of shapes at time intervals of 5×10^{-23} sec for the fusion of ^{110}Pd + ^{110}Pd. The energies given are the incident kinetic energy (in the centre-of-mass system) of the ions above the liquid-drop-model interaction barrier. The nuclei are tangent spheres at t = 0.

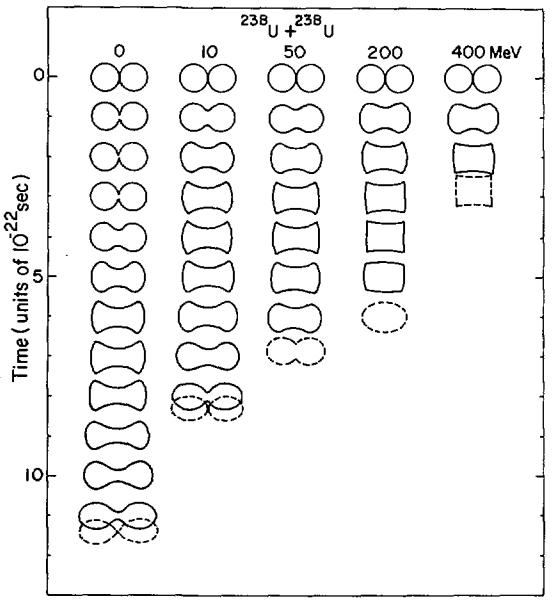

FIG. 8. Calculated sequence of shapes at time intervals of 10^{-22} sec for the fusion of ^{238}U + ^{238}U. The energies given are the incident kinetic energy (in the centre-of-mass system) of the ions above the liquid-drop-model interaction barrier. The nuclei are tangent spheres at t = 0.

These figures show the limitations of our shape parametrization for describing fusion reactions. For low energies, after the spheres touch the surface energy causes a rapid filling-in of the neck, which results in a shape with flattened ends and a high surface energy. This surface energy and the Coulomb forces cause the end bodies to rapidly become prolate and to intersect in a manner that forms a cusp at the middle of the shape. The inclusion of viscosity may slow down the motion to a point where this phenomenon does not occur. The situation would also be improved by including the effects of the finite range of the nuclear force on the macroscopic energy (instead of representing the energy in terms of surface tension), as discussed in this symposium by Krappe [12]. This improvement would greatly reduce the rapidity with which the neck grows after first contact. For higher energies the fusion continues until the system approaches a pure spheroidal form. Shapes close to a spheroid are not handled adequately by our parametrization, and the integration terminates when this condition occurs. For even higher energies, the end-flattening of the system, which is apparent at lower energies, proceeds to the point where the ends attempt to become concave, a type of shape that is not describable in any parametrization of the form $\rho = \rho(z)$. This end-flattening is a result of the rapid growth of the neck; the assumption of incompressible and nearly irrotational fluid flow requires that the material filling the neck comes primarily from the ends of the body. We conclude that a complete investigation of fusion reactions requires an unconstrained shape description.

Even within these limitations imposed by our coordinates, we learn a significant amount from these calculations. In a two-dimensional space described by the coordinates defined in Sec. 2 for reflection symmetric shapes (center-of-mass separation and the second central moment of the fragment shape), we present in Fig. 9 the paths followed by two colliding ^{150}Nd

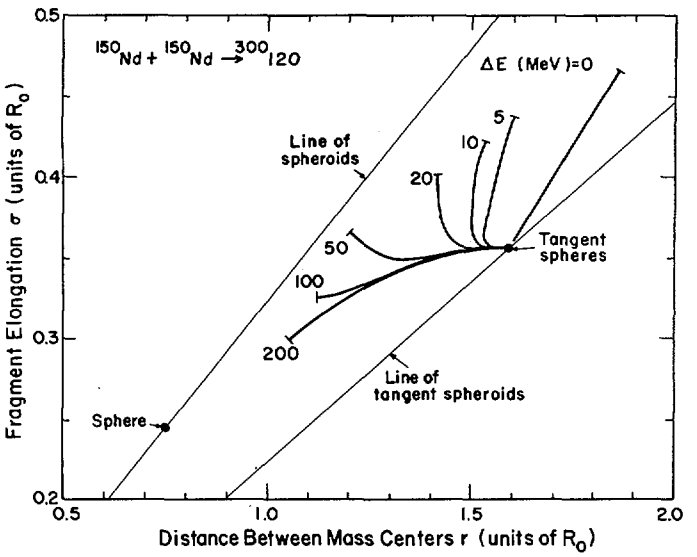

FIG.9. Calculated dynamical paths in the space of centre-of-mass separation r and fragment elongation σ (defined in Section 2) for two colliding ^{150}Nd nuclei. The nuclei are initially tangent spheres. The energies ΔE labelling the paths give the initial kinetic energy (in the centre-of-mass system) above the liquid-drop-model interaction barrier. The terminations of the paths are caused by deficiencies of the shape parametrization.

nuclei, which is a possible choice for producing the superheavy nucleus $^{300}120$ by a symmetric collision. We see that more than 100 MeV of energy over the interaction barrier (which is approximately 400 MeV high) is needed to drive the system to a nearly spherical shape, an indication of a lower limit to the additional energy required to produce a superheavy nucleus from such a collision, if such production is possible. Of course, for viscous flow even more energy would be required.

A recent paper by Lefort et al. [13] reports a very small probability for complete fusion when ^{209}Bi nuclei are bombarded with ^{84}Kr ions of 500-MeV energy, which is (35±9) MeV over the calculated interaction barrier in the center-of-mass system [12]. We have not yet calculated fusion reactions for such asymmetric systems, but some qualitative comparisons may be made. The $^{293}119$ system resulting from the above reaction is similar to the $^{300}120$ system considered in our symmetric dynamical calculation. For this calculation, more than 100 MeV of energy over the interaction barrier is required to bring the nuclei close enough for a long enough time to allow a significant mass transfer between the interacting nuclei. We expect the energy required for fusion to be somewhat less for an asymmetric system than for a symmetric one, but still of the same order of magnitude. The observed lack of fusion at the 35-MeV energy may be due either to the tendency of the nuclei to quickly re-fission because of the large Coulomb forces and the distribution of energy into degrees of freedom other than center-of-mass motion, as indicated in Fig. 9, or because large nuclear viscosity prevents mass transfer between the nuclei, or to a combination of these effects. The disruptive effect of angular momentum appears to be too small to account for the very small cross-sections observed [13].

By use of plots similar to the one in Fig. 9 for different nuclei we find the minimum-energy collision whose trajectory passes inside the liquid-drop-model saddle point. This gives an estimate of the lower limit to the energy needed to cause a complete fusion. In Fig. 10 we show this critical energy as a function of the fissility parameter. For values of x less than 0.72 no energy over the interaction barrier is needed. Above this value, the critical energy rises steeply to about 0.15 $E_s^{(0)}$, which is needed to reach the saddle-point shape for $x = 0.9$. For a nucleus along the line of beta stability, this energy is about 110 MeV above the interaction barrier. For larger values of x, we are not able to determine the critical energy because the calculated paths terminate before reaching the saddle point. This criterion of passing inside the liquid-drop-model saddle point is necessary but not sufficient to form a compound system. This is because a nonviscous system will ultimately re-fission since its total energy is higher than its saddle-point energy. Some dissipation must be present in order to form compound nuclei from heavy-ion reactions.

5. SUMMARY AND CONCLUSION

We have investigated several aspects of nuclear dynamics on the basis of the liquid-drop model, including the effect of viscosity on the separation of fission fragments, the fission of very large nuclei, and symmetric fusion reactions involving systems of different masses and interaction energies. We find that for small viscosities the often-suggested fusion-fission reaction method is highly unlikely to lead to the formation of superheavy nuclei. Although our nuclear shape parametrization has deficiencies for fusion reactions and the fission of large systems, it still provides some worthwhile information.

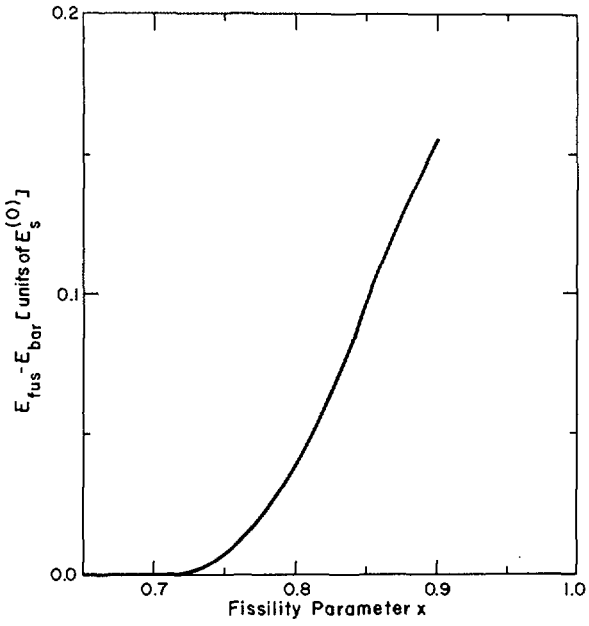

FIG. 10. Calculated incident kinetic energy (in the centre-of-mass system) above the liquid-drop-model interaction barrier necessary for complete fusion as a function of the fissility parameter x. The criterion adopted as necessary (but not sufficient) for complete fusion is that the trajectories of the fusing nuclei in the two-dimensional space defined by r and σ pass inside the liquid-drop-model saddle point. The centre-of-mass coordinate r and the fragment elongation coordinate σ are defined in Section 2.

A major objective of this type of study is to calculate cross-sections for fusion reactions. Ideally, one would like to do this by solving the full Navier-Stokes equations for unconstrained shapes, but even within our restricted shape parametrization there are three extensions to be made: the consideration of viscosity, the inclusion of angular momentum, and the calculation of the macroscopic energy by including the finite range of the nuclear force instead of by using surface tension. We are now in the process of calculating most-probable fission-fragment kinetic energies for viscous flow. By comparing these calculations with experimental results we hope to deduce an average value for the coefficient of nuclear viscosity that is appropriate to large distortions. Once the coefficient of viscosity is known, it should be possible to estimate fusion cross-sections for heavy systems by performing similar dynamical calculations with the inclusion of viscosity, angular momentum, and the finite range of the nuclear force in the macroscopic energy.

APPENDIX. EFFECT OF VISCOSITY ON THE INERTIA AND VISCOSITY TENSORS FOR THE SMALL OSCILLATIONS OF A CLASSICAL LIQUID DROP

The effect of viscosity on the inertia and viscosity tensors is computed from the exact solution to the Navier-Stokes equations for small motions about a spherical shape. For small values of viscosity the flow re-

mains nearly irrotational, so irrotational flow gives a very good approximation to the correct inertia and viscosity tensors. The normal modes for nearly-spherical shapes for all values of viscosity are the quantities α_i, where the surface of the axially symmetric drop is given by

$$R(\theta) = \frac{R_0}{\lambda}\left[1 + \sum_{i=2}^{\infty} \alpha_i(t)\, P_i(\cos\theta)\right]$$

The diagonal elements η_{ii} of the viscosity tensor are monotonically increasing functions of the coefficient of viscosity μ; the ratio η_{ii}/μ decreases from the irrotational flow value at $\mu = 0$ to a fraction of this number as $\mu \to \infty$. For the i = 2, 3, and 4 modes, respectively, the ratios η_{ii}/μ at infinite viscosity are 75%, 69%, and 63% of the values at $\mu = 0$. The elements of the inertia tensor are also monotonically increasing functions of μ; the i = 2, 3, and 4 elements reach 105%, 111%, and 117% of their nonviscous values as $\mu \to \infty$. We see that the irrotational-flow values provide a good estimate for the inertia and viscosity tensors for the small oscillations of classical liquid drops. The fragment distortions considered in Sec. 2 are somewhat larger than the small oscillations studied here, but the inaccuracies introduced by the larger distortions are no larger than those caused by viscosity. We re-emphasize that we are considering the effect of classical viscosity on the inertia and viscosity tensors, and not the potentially large changes caused by single-particle effects.

REFERENCES

[1] PAULI, H. C., LEDERGERGER, T., Paper IAEA-SM-174/206, these Proceedings.
[2] NIX, J. R., SWIATECKI, W. J., Nucl. Phys. 71 (1965) 1.
[3] NIX, J. R., Nucl. Phys. A130 (1969) 241.
[4] HASSE, R. W., Nucl. Phys. A128 (1969) 609.
[5] WIECZOREK, R., HASSE, R. W., SÜSSMANN, G., Paper IAEA-SM-174/2, these Proceedings.
[6] KOONIN, S. E., private communication (1972).
[7] MYERS, W. D., SWIATECKI, W. J., Ark. Fys. 36 (1967) 343.
[8] GREEN, A. E. S., Nuclear Physics, McGraw-Hill, New York (1955) 185, 250.
[9] MYERS, W. D., SWIATECKI, W. J., Ann. Phys. 55 (1969) 395.
[10] MYERS, W. D., SWIATECKI, W. J., private communication (1973).
[11] BOLSTERLI, M., FISET, E. O., NIX, J. R., NORTON, J. L., Phys. Rev. C 5 (1972) 1050.
[12] KRAPPE, H. J., NIX, J. R., Paper IAEA-SM-174/12, these Proceedings.
[13] LEFORT, M., NGÔ, C., PÊTER, J., TAMAIN, B., Orsay Preprint IPNO-RC-73-06 (1973).

DISCUSSION

R.W. HASSE: As we have learnt, for example from Krappe, the effect of the finite range of the nuclear forces is strongest at the scission or fusion point, because the usual definition of the surface energy breaks down at this point. Since you start your dynamical calculations just there, the motion of your fusioning system may proceed in an entirely different way, giving rise to very different results. Can you estimate the influence of this effect and do you plan to incorporate a more realistic surface energy at scission in your model?

A.J. SIERK: We are starting to modify the macroscopic surface energy calculation by including the finite range of nuclear forces, as discussed in this symposium by Krappe. We cannot estimate at the moment how much the reaction trajectories will be affected by this improvement.

C.Y. WONG: I would like to point out that for a nucleus with large fissility parameter, especially for $x > 1.0$, there is the possibility of fissioning through other topologies like tori and bubbles. There are many compelling reasons why they should be considered. Firstly, in the case of one water drop colliding with another in a nearly head-on collision, for some relative velocities, a torus is the very first shape the compound system assumes. This is an experimental fact. Secondly, for $x \geq 1.1$, while the spherical configuration is unstable, there is an equilibrium minimum for a toroidal shape lying at a lower energy which is stable against expansion and contraction degrees of freedom. Thirdly, for a highly charged compound system, the excessive charge has a tendency to exert a pressure to push the density outwards. The trajectory leading to the break-up of the nucleus might go through this channel. Finally, the question whether Wheeler's toroidal and bubble nuclei are stable because of nuclear shell effects is a fascinating subject which unfortunately cannot be discussed at this Symposium.

S. BJØRNHOLM: Your colliding spherical liquid drops fuse very quickly as you shoot them against each other. Real spherical nuclei seem to have much increased inertia compared to liquid drops and thus they will fuse on a slower time scale. This gives added significance to Wilczyński's considerations of the forces between colliding spheres. Unless the spheres start gravitating around their common centre-of-mass, there may not be sufficient time for the partial or complete fusion process to develop.

A.J. SIERK: It is certainly true that we do not claim our liquid drop inertias correspond to real nuclei. But one can likewise not readily maintain that the inertias of tangent spherical nuclei will be as large as those observed for individual spherical nuclei, and we feel that inertias for large deformations are closer to liquid drop values than to those seen in isolated spherical nuclei.

U. MOSEL: In your figures showing the evolution of nuclear shapes I see that quadratic nuclei appear soon after contact occurs. Is this a breakdown of the three-quadratic-surface shape parametrization and does that imply that your calculations become unrealistic soon after the point of contact?

A.J. SIERK: The three-quadratic-surface shape parametrization breaks down at the last shapes shown in the figures. However, we feel that the results previous to these terminations are realistic in so far as we claim to consider liquid drops and not real nuclei.

FISSION DE NOYAUX DE MASSE MOYENNE ET LOURDE INDUITE PAR IONS LOURDS Ar ET Kr

F. HANAPPE*, C. NGO, J. PETER, B. TAMAIN**
Institut de physique nucléaire,
Orsay, France

Abstract–Résumé

FISSION OF NUCLEI WITH MEDIUM AND HEAVY MASSES INDUCED BY HEAVY IONS (ARGON AND KRYPTON).

A series of targets with atomic numbers ranging from 42 to 92 were irradiated by an argon-ion and/or krypton-ion beam, of 150-300 MeV energy in the former case and 450-500 MeV in the latter. The fission fragments created by one and the same event are detected by two surface-barrier detectors. Knowledge of the relevant energies, emission angles relative to the direction of the beam, and the difference in the time-of-flight of the two fragments (used to check the validity of the analysed events) gives the fission cross-sections and the kinetic-energy and mass distributions of the fission products. The authors derived the excitation function for fission of the compound nucleus in the case of a Sb + Ar system. The function reveals a difference of about 10 MeV between the reaction and fission thresholds. This effect is interpreted in terms of the decrease in the fission barrier due to the high angular momentum of the compound nucleus. In the case of fission induced by 200-300 MeV argon ions in heavy holmium and uranium targets, the authors' results indicate that the fission cross-section of the compound nucleus represents 60% of the total reaction cross-section. On the other hand, in the case of 500-MeV krypton-ion-induced fission the proportion is as low as 5%. This effect can be interpreted either in terms of a fusion barrier greater than the interaction barrier or by assuming the existence of quasimolecular states for very heavy ion interactions. The variation of the mean total kinetic energy with respect to the mass of the compound nucleus at fission fragment symmetry is compared first with Nix's predictions, and then with the calculations of Schmitt and Mosel. The results reveal a monotonic variation compatible with Nix's data; the strong layer effect predicted by Schmitt and Mosel near Z = 106 was not observed, probably because of the high excitation energy involved in the present experiments. The characteristics of the mass and kinetic-energy distributions are compared with Nix's predictions for the following systems: (Mo + Ar), (Sb + Ar), (Pr + Ar), (Ho + Ar), (Au + Ar), (Bi + Ar), (Th + Ar) and (U + Ar). The observed mass distribution widths are generally higher than those envisaged by Nix. This effect is greater for high angular momenta.

FISSION DE NOYAUX DE MASSE MOYENNE ET LOURDE INDUITE PAR IONS LOURDS Ar ET Kr.

Une série de cibles de numéro atomique compris entre 42 et 92 ont été irradiées à l'aide d'un faisceau d'ions argon et (ou) d'ions krypton d'énergies comprises entre 150 et 300 MeV pour l'argon et 450 et 500 MeV pour le krypton. Les fragments de fission nés d'un même événement sont détectés dans deux détecteurs à barrière de surface. La connaissance des énergies correspondantes, des angles d'émission par rapport à la direction du faisceau et de la différence des temps de vol des deux fragments (utilisée pour contrôler la véracité des événements analysés) permet d'atteindre les sections efficaces de fission et les distributions en énergie cinétique et en masse des produits de fission. La fonction d'excitation pour la fission du noyau composé a été obtenue pour le système Sb + Ar. Elle fait apparaître une différence d'une dizaine de MeV entre les seuils de réaction et de fission. Cet effet est interprété à partir de l'abaissement de la barrière de fission dû au moment angulaire élevé du noyau composé. Dans le cas de la fission induite par des ions argon de 200 à 300 MeV sur des cibles lourdes d'holmium et d'uranium, les résultats font apparaître que la section efficace de fission du noyau composé représente 60% de la section efficace totale de réaction. Par contre, dans le cas de la fission induite par des ions krypton de 500 MeV ce pourcentage tombe à 5%. On peut interpréter ce résultat soit en terme de barrière de fusion supérieure à la barrière d'interaction, soit en admettant l'existence d'états quasi moléculaires pour les sytèmes ion lourd - ion lourd. La variation avec la masse du noyau composé de l'énergie cinétique totale moyenne à la symétrie des fragments de fission est comparée d'une part aux

---

* Chercheur IISN, détaché de l'Université libre de Bruxelles, Belgique.

** Détaché de l'Université de Clermont-Ferrand, France.

prévisions de Nix, d'autre part aux calculs de Schmitt et Mosel. Les résultats obtenus par les auteurs du mémoire font apparaître une variation monotone compatible avec les données de Nix; le fort effet de couche prévu par Schmitt et Mosel au voisinage de Z = 106 n'est pas observé, probablement à cause de l'énergie d'excitation importante mise en jeu dans les présentes expériences. Les caractéristiques des distributions en masse et en énergie cinétique sont comparées aux prévisions de Nix pour les systèmes (Mo + Ar), (Sb + Ar), (Pt + Ar), (Ho + Ar), (Au + Ar), (Bi + Ar), (Th + Ar), (U + Ar). Les largeurs des distributions de masses observées sont d'une façon générale très supérieures à celles prévues par Nix. L'effet obtenu est d'autant plus grand que le mouvement angulaire apporté est élevé.

INTRODUCTION

L'utilisation d'ions lourds pour induire la fission à énergie d'excitation moyenne présente plusieurs intérêts.

Le premier est de permettre l'étude de la fission de noyaux très lourds ($Z > 100$), formés soit par fusion complète entre une cible lourde et le projectile, soit par fusion partielle (transfert à la cible d'une partie importante du projectile). Ceci permettrait évidemment d'étendre la zone de noyaux pour lesquels on a actuellement des données expérimentales sur la fission (Z de ~ 75 à 100), et de vérifier si les théories concernant la fission établies à partir des données de cette zone sont applicables aux noyaux plus lourds. Par fusion complète entre ^{40}Ar et ^{238}U, on pourrait atteindre $^{278}_{110}X$, et $^{84}Kr + {}^{238}U$ donnerait $^{322}_{128}X$. Inversement, l'observation de la désexcitation par fission de ces noyaux est le moyen le plus simple de mettre en évidence qu'ils ont été effectivement formés.

Un second intérêt réside dans l'apport de moments angulaires très importants. Les théories actuelles de la fission ne prévoient pas l'effet du moment angulaire sur les distributions en masse et énergie des fragments, et des informations expérimentales peuvent déterminer quel peut être cet effet.

Nous avons donc entrepris deux séries d'expériences: la première a été menée à l'aide d'ions argon, la seconde à l'aide d'ions krypton. Dans les deux cas, nous avons obtenu les sections efficaces de fission du noyau composé sur une série de noyaux cibles. Pour les réactions induites par argon, des mesures ont pu être faites à plusieurs énergies de bombardement, et l'effet du moment angulaire sur la hauteur des barrières de fission a été étudié. Dans le cas du krypton, il est très difficile de former un noyau de fusion avec une cible lourde, et un nouveau type de réaction est apparu: fusion partielle entre le projectile et la cible, puis désintégration en deux fragments de masses voisines de celles du projectile et de la cible. Une étude de l'effet de la masse du noyau cible sur ce phénomène a été effectuée.

Enfin, dans le cas des réactions induites par argon, nous avons établi les spectres en masse et en énergie cinétique des fragments issus de la fission du noyau composé. Les valeurs des énergies cinétiques totales moyennes et des largeurs des distributions en masse et en énergie cinétique totale ont été comparées aux prévisions des différents modèles.

1. EXPERIENCES

La méthode expérimentale utilisée a été la même pour toutes les mesures discutées ici. Nous en donnons seulement une description sommaire; des détails peuvent être trouvés ailleurs [1, 2].

1.1. Dispositif expérimental

Trois détecteurs à barrière de surface, X, Y_1 et Y_2 sont placés aux angles θ_x, θ_{y1} et θ_{y2} par rapport à la direction du faisceau. Ils détectent en coïncidence (XY_1 ou XY_2) les fragments de fission ou autres produits de réaction (diffusion élastique, transfert) issus d'un même événement dans la cible. On enregistre sur bande magnétique la hauteur des impulsions linéaires correspondant à E_x, E_{y1} ou E_{y2}, ainsi que la différence de temps de vol entre les deux fragments (ΔTV_1 ou ΔTV_2). Cette différence de temps de vol est utilisée pour déterminer la contribution des événements fortuits [1]. Le bruit de fond des détecteurs est réduit au minimum: chacun est protégé par un champ magnétique et une feuille de nickel de 80 $\mu g/cm^2$ qui éliminent respectivement les électrons et rayons X mous dus au passage du faisceau dans la cible.

Le détecteur X est maintenu à un angle fixe et son ouverture angulaire $\Delta\theta_x$ dans le plan de la réaction est faible. Les détecteurs Y couvrent un domaine angulaire $\Delta\theta_y$ de 10° chacun et sont placés à 20° l'un de l'autre de manière à permettre l'exploration d'une large zone de corrélation angulaire en peu de mesures. Dans quelques cas $\Delta\theta_y$ a été réduit à 3°.

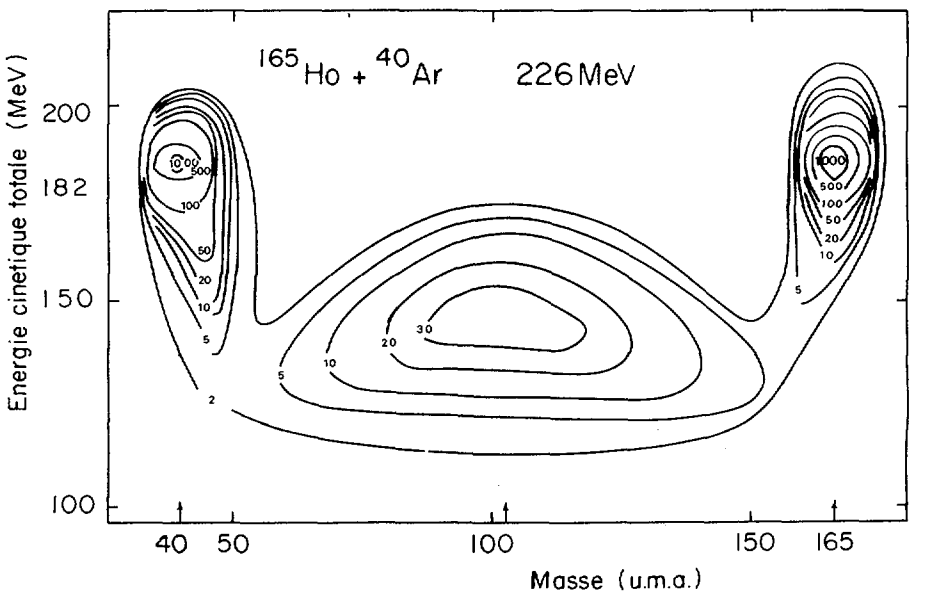

FIG.1. ^{40}Ar de 226 MeV (182 MeV centre de masse) sur cible ^{165}Ho. Tableau énergie cinétique totale dans le centre de masse – masse du produit reçu par le détecteur X placé à 59°. En plus des fragments de fission binaire, une zone d'argons diffusés et produits de transfert apparaît autour de 182 MeV – 40 uma, car l'angle maximal de diffusion élastique Rutherford pour le projectile est environ 60°. On a également Ho diffusé et des produits de transfert autour de 226 MeV – 165 uma, car l'angle minimal de diffusion Rutherford pour le noyau-cible est environ 54°.

Les corrélations angulaires ont été estimées préalablement en appliquant au noyau de fusion la quantité de mouvement initiale et en donnant aux fragments l'énergie cinétique prévue par la théorie de la goutte liquide [3]. Cette corrélation dépend du rapport des masses. Nous avons exploré une zone angulaire encadrant très largement la zone prévue.

L'évaporation de neutrons par les fragments a pour effet d'écarter du plan de la réaction les fragments issus d'un même événement. Afin de les recueillir, l'ouverture angulaire du détecteur X dans le sens perpendiculaire au plan de réaction ($\Delta\phi_x$, fig.1) était égale à $\pm 7,5°$, celle des détecteurs Y étant seulement de 2°. Le calcul des écarts angulaires possibles entre les fragments évaporant le plus grand nombre de neutrons indique que cette ouverture $\Delta\phi_x$ est suffisante pour ne pas perdre de fragments; ceci a été confirmé par des mesures de la corrélation dans la direction perpendiculaire au plan de réaction, mesures effectuées à l'aide d'un détecteur à localisation.

1.2. Traitement des données

On fait l'hypothèse que l'événement détecté ne comporte que deux produits finaux, dont la somme des masses est égale à celle des masses de la voie d'entrée (projectile + cible). La désexcitation par évaporation de neutrons ou particules chargées légères de ces deux produits de réaction peut modifier légèrement leurs masse, énergie et direction, mais il n'y a pas de troisième produit de masse importante créé au cours de la réaction. Le système formé de l'ensemble des nucléons du projectile et du noyau-cible qui donne naissance (par quelque processus que ce soit) aux deux produits finaux a donc la quantité de mouvement du projectile. De ce fait, les deux produits finaux doivent former, dans le laboratoire, un angle θ_{xy} très différent de 180° (chaque produit étant ramené vers l'avant). θ_{xy} variera, suivant les cas, de 140 à 60°. Les angles observés entre les produits de réaction ont bien des valeurs voisines de ces estimations. Par contre, l'écart dans la direction perpendiculaire au plan de réaction (ϕ) est faible; si une troisième particule de quantité de mouvement importante était créée, les deux produits détectés ne seraient qu'exceptionnellement coplanaires avec la direction initiale du projectile. On peut donc conclure que l'hypothèse faite est correcte.

A partir de cette hypothèse et des énergies et angles mesurés, nous pouvons calculer les masses des deux produits, leurs énergies et angles d'émission dans le système du centre de masse. Nous ne rappellerons pas les relations cinématiques utilisées [2].

Un premier problème de la méthode réside dans la réponse des détecteurs à barrière de surface aux ions lourds et énergiques. On sait en effet que cette réponse dépend de la masse des noyaux détectés. Les masses n'étant pas connues au départ, on est obligé de faire une série d'itérations pour aboutir à la détermination correcte à la fois des masses et des énergies cinétiques à partir des deux hauteurs d'impulsion mesurées. Ceci ne représente pas une source d'erreurs. Par contre, le fait que les énergies des produits détectés soient grandes (en raison en particulier de la quantité de mouvement importante de l'ensemble) peut entraîner une erreur systématique. En effet, les méthodes de calibration actuellement connues (Schmitt et al. [4], Wilkins et al. [5]) sont fondées sur la réponse des détecteurs à des ions d'énergies plus faibles que celles que nous avions à

mesurer. Les noyaux diffusés élastiquement (cible ou projectile ou les deux, suivant le cas), dont les masse et énergie sont connues, fournissaient un test aisé. Nous avons donc comparé les résultats obtenus pour la diffusion élastique avec les deux méthodes de calibration. De plus, nous avons étudié en détail le défaut d'ionisation des détecteurs utilisés pour des ions de masse et énergie élevées [6].

Dans le traitement des données, nous avons pris soin de tenir compte pour chaque produit détecté de ses pertes d'énergie dans la cible, éventuellement le support de cible, et la feuille de nickel qui protège le détecteur. Ceci a été réalisé à chaque étape du traitement itératif, à partir des pouvoirs d'arrêt de la table de Northcliffe et Schilling [7], dont la validité a été testée dans quelques cas [6].

La connaissance des angles θ_y est loin d'être précise puisque les ouvertures angulaires sont de 10°. Une correction par approximations successives a été là aussi nécessaire pour déterminer la véritable valeur de θ_y. Ceci a été réalisé en imposant aux deux produits d'être émis à 180° l'un de l'autre dans le centre de masse.

Un dernier point concerne non pas les caractéristiques d'un événement détecté, mais les proportions respectives des divers événements. En effet, un produit de masse M et vitesse V_x définies recueilli à l'angle θ_x correspond à un angle $\overline{\theta}_x$ et à une vitesse $\overline{v}_x$ dans le centre de masse. Les produits détectés à θ_x proviennent de différents $\overline{\theta}_x$ (selon $\overline{v}_x$). Si la distribution angulaire dans le système du centre de masse n'est pas isotrope (par exemple en $1/\sin\overline{\theta}$ pour la fission d'un noyau composé ayant un fort moment angulaire), certaines catégories d'événements se trouvent favorisées dans le laboratoire par rapport à leur contribution réelle dans le centre de masse. Pour limiter cette déformation, les mesures ont été faites à $\overline{\theta}$ voisin de 90°, angle pour lequel la section efficace différentielle $d\sigma/d\Omega$ ne dépend pratiquement pas de $\overline{\theta}$. D'autre part, le nombre de fragments recueillis dans l'angle solide $d\Omega$ est fonction du facteur de transformation centre de masse-labo dans lequel $\overline{\theta}_x$ et $\overline{v}_x$ interviennent. On a donc calculé ce facteur pour chaque événement détecté. De cette façon sont obtenus les spectres de masse et énergie corrects dans le centre de masse, aux défauts de résolution en angles et énergies près.

Les résultats ainsi obtenus ne tiennent pas compte de l'évaporation de neutrons, soit avant, soit après la fission. Nous avons calculé que dans tous les cas la possibilité d'évaporation de neutrons avant fission est très faible. Par contre, un grand nombre ν_T de neutrons peuvent être émis par les fragments. Ce nombre a été évalué à partir de l'énergie d'excitation disponible pour les fragments, et l'énergie cinétique totale moyenne de fission a pu être corrigée. Mais, faute de connaître la variation de ν avec la masse des fragments, les distributions de masse n'ont pu l'être.

2. CARACTERISTIQUES DES FRAGMENTS DE FISSION

Il est commode de présenter les résultats sous la forme d'un tableau (énergie cinétique totale dans le centre de masse – masse d'un des deux produits détectés). De tels tableaux sont présentés, en courbes de niveau, sur les figures 1, 2 et 8, où la masse est celle du produit reçu par le détecteur fixe X. Les fragments de fission, répartis autour de la masse

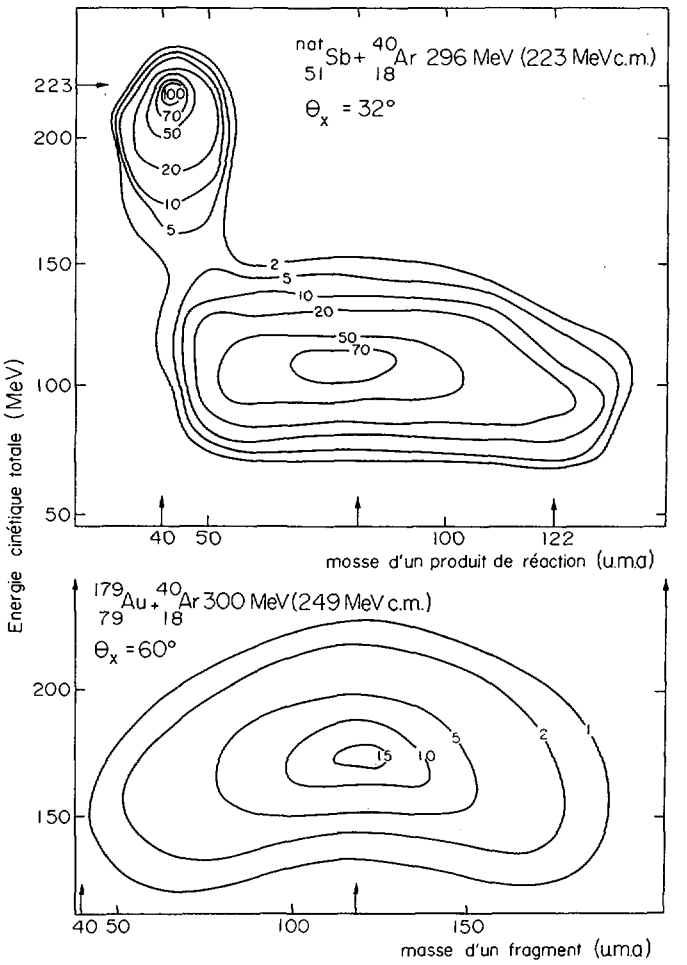

FIG.2. En haut: ^{40}Ar de 296 MeV (223 MeV centre de masse) sur cible ^{nat}Sb. Tableau énergie cinétique totale dans le centre de masse – masse du produit reçu par le détecteur X placé à 32°. En plus des fragments de fission binaire, Ar diffusé et produits de transfert apparaissent autour de 223 MeV – 40 uma, car l'angle maximal de diffusion élastique Rutherford pour le projectile est environ 30°. Il n'y a pas d'événements autour de 223 MeV – 122 uma, car l'angle minimal de diffusion Rutherford pour le noyau-cible est environ 70°.

En bas: ^{40}Ar de 300 MeV (249 MeV centre de masse) sur cible ^{197}Au. Le détecteur X placé à 60° reçoit seulement des fragments de fission, car les angles limites pour la diffusion élastique Rutherford sont respectivement 44° pour le projectile et 65° pour la cible.

moitié de celle du noyau de fusion, forment plus ou moins nettement les triangles à coins arrondis connus [8, 9].

De plus, il apparaît parfois des événements de diffusion élastique, inélastique ou transfert. Ces différents cas de figures apparaissent selon que l'angle de détection θ_x appartient aux ou est voisin des zones angulaires (0°, θ_{proj}) et (θ_{cible}, 90°) dans lesquelles respectivement le projectile et la cible sont diffusés élastiquement avec une section efficace différentielle importante voisine de celle de Rutherford. Dans ces zones, le paramètre d'impact est tel que la distance minimale d'approche est supérieure ou égale à la somme des rayons effectifs d'interaction du projectile et de la cible. Pour les paramètres d'impact plus petits se produisent des réactions de transfert, dont les produits se trouvent au voisinage de θ_{proj} et θ_{cible}.

Les figures 1 et 2 présentent trois cas différents. La distinction entre fragments de fission et diffusion élastique est aisée, mais ce n'est pas toujours le cas pour les produits de transfert ou de diffusion inélastique. Ainsi, pour le système Ar + Mo, les masses du projectile et de la cible sont assez proches pour que les événements de diffusion ou transfert perturbent les bords de la distribution de masse des fragments. Pour les cibles plus lourdes (Pr, Ho), ce problème ne se pose pratiquement plus. Pour les systèmes très lourds (Th ou U + Ar) à 250 MeV, les énergies cinétiques de fission sont voisines de celles de diffusion et les distributions en masse ont une largeur telle qu'elles sont perturbées par les transferts. Enfin, il n'est pas exclu que pour de tels systèmes il existe quelques événements du type de ceux observés pour le système Kr + Bi (fig. 8).

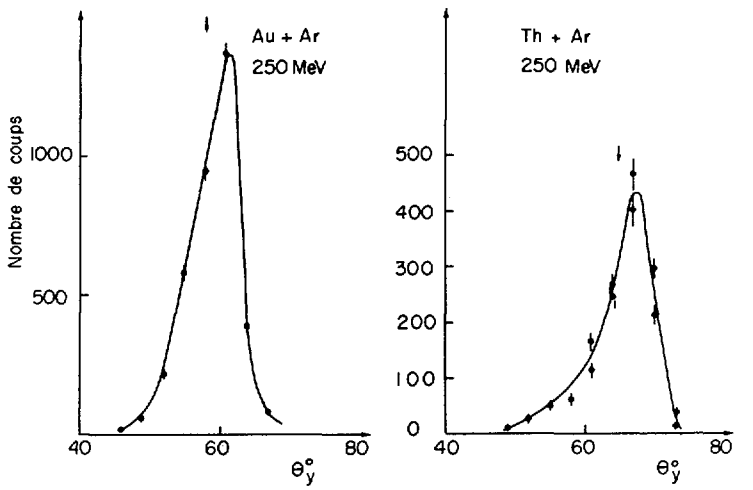

FIG. 3. Corrélations angulaires entre les fragments de fission des noyaux ^{237}Bk et ^{272}108 (cibles Au et Th bombardées par Ar de 250 MeV). La flèche verticale indique la corrélation attendue pour la fission symétrique d'après l'énergie cinétique totale prévue par Nix [3].

TABLEAU I. ENERGIES CINETIQUES TOTALES MOYENNES ET LARGEURS DES DISTRIBUTIONS DE MASSE ET D'ENERGIE CINETIQUE

Cible	Noy. Comp.	E_{argon} (MeV)	E^* (MeV)	<ECT'> (MeV)	<ECT> (Mev)	ECT_{Nix} (MeV)	$ECT_{Schmitt}$ (MeV)	θ (deg)	Γ_M (uma)	$\Gamma_{M(Nix)}$ (uma)	Γ_E (MeV)	$\Gamma_{E(Nix)}$ (Mev)
Mo	Nd	200	98	93	96	86		1,66	27	33	20	13
Mo	Nd	300	169	93	100	86		2,66	47	41	33	16
Sb	Tm	162	58	114	114	104,4		1,05				
Sb	Tm	179	72	111	113	104,4		1,36	31,5	27	18,5	14
Sb	Tm	199	86	111,8	114	104,4		1,58	34,5	29	22,5	15
Sb	Tm	226	106	111,7	116	104,4		1,87	36	32	26,5	16
Sb	Tm	300	164	108,9	116	104,4		2,4	55	36	36,5	18
Pr	Ir-181	226	95	131	135	122,8		1,75	47	27,5		17,5
Pr	Ir-181	300	150	125,7	133	122,8		2,31	55	31	36	19,5
Ho	As-205	226	97	145,5	152	142		1,74	46	24	29	18
Ho	As-205	300	160	143,4	154	142		2,35	60	28	38	20,5
Au	Bk-237	226	71	175,9	183	176,1	160	1,43	45	19	36	19
Au	Bk-237	250	89	181	190	176,1	160	1,63	66	21	39	20
Au	Bk-237	300	133	178,5	190	176,1	160	2,04	95	23	45	21,5
Bi	Md-249	250	80	183	193	188,6	185	1,49			45	
Bi	Md-249	250	80	193	203	188,6	185	1,49	~100			21,5
Th	108-272	250	83	207	218	212,2	246	1,49			46	
Th	108-272	250	83	214	224	212,2	246	1,49	90-110			
U	110-278	250	82	204,5	217	219,7	233	1,23				
U	110-278	300	125	203	218	219,7	233	1,53	100		65	

<ECT'> est l'énergie moyenne avant émission de neutrons. <ECT> est l'énergie corrigée pour l'émission de neutrons. Les valeurs d'énergie calculées par Nix [3], d'une part, Schmitt et Mosel [10] d'autre part, ainsi que les largeurs de distributions calculées par Nix sont indiquées.

2.1. Corrélations angulaires

Sur la figure 3 sont présentées quelques corrélations angulaires observées. Les angles les plus faibles correspondent aux rapports de masse élevés, car l'énergie cinétique totale est alors inférieure à celle qui correspond à la fission en deux fragments égaux. Ceux-ci sont les plus nombreux et forment les maximums des corrélations, à un angle plus grand. On a indiqué la corrélation prévue à partir de l'énergie cinétique moyenne pour la fission en deux fragments égaux, calculée selon Nix [3]. L'angle prévu est plus petit que l'angle observé, donc l'énergie cinétique prévue est inférieure à la valeur réelle.

2.2. Distributions en masse et en énergie cinétique

Sur le tableau I sont portés les résultats relatifs aux valeurs moyennes des énergies cinétiques totales et aux largeurs à mi-hauteur des distributions en masse et en énergie cinétique totale. Quelques exemples de distributions en masse et en énergie cinétique sont donnés sur la figure 4.

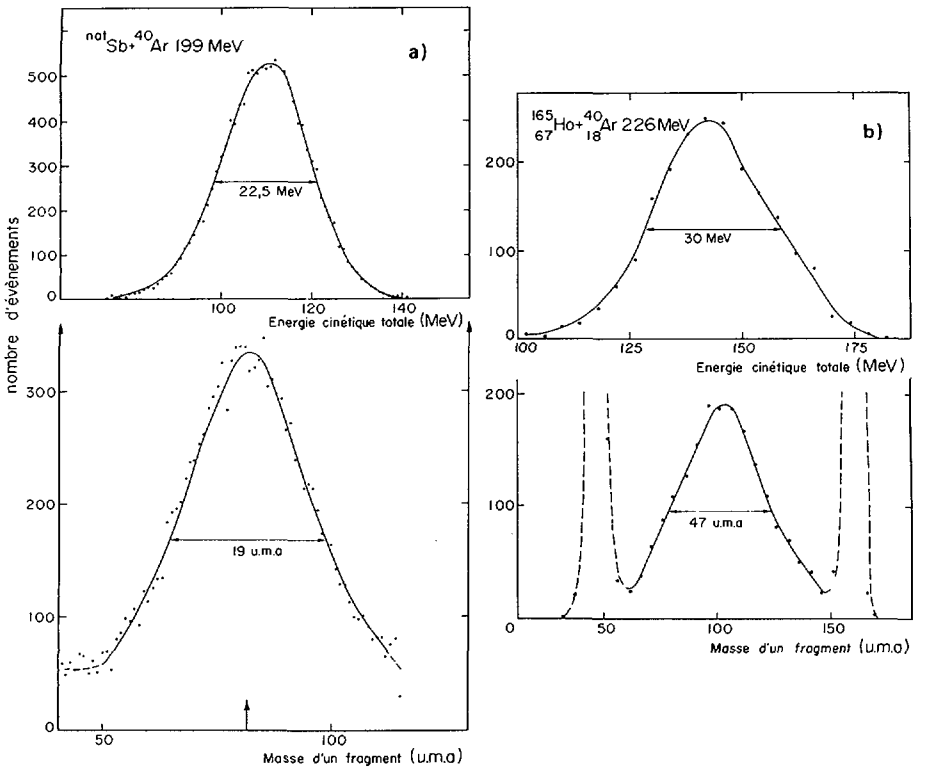

FIG.4. Spectres de masse et énergie cinétique totale pour les fragments de fission: a) de ^{161,163}Tm excité à 86 MeV (cible ^{nat}Sb, ion Ar de 199 MeV); b) de ^{205}At excité à 97 MeV (cible ^{165}Ho, ion Ar de 226 MeV).

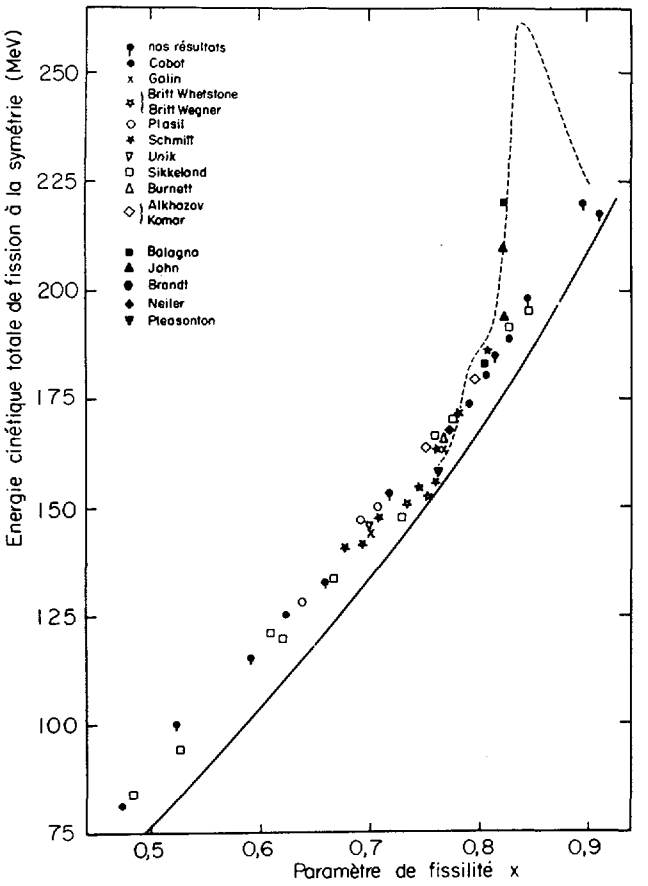

FIG.5. Variation de l'énergie cinétique totale pour la fission symétrique (fragments égaux) en fonction du paramètre de fissilité x. La courbe continue est la prévision de Nix [3]; la courbe pointillée est tracée d'après Schmitt et Mosel [10]. Les différents auteurs de la liste correspondent, dans l'ordre, aux références [21 à 36].

2.2.1. Energies cinétiques totales moyennes

Sur la figure 5, nos valeurs d'énergies cinétiques totales moyennes sont comparées à un ensemble de résultats obtenus par d'autres auteurs et aux prévisions théoriques de Nix d'une part [3], Schmitt et Mosel d'autre part [10]. Les énergies sont relatives à la fission en deux fragments égaux.

La théorie de Nix utilise le modèle de la goutte liquide et fait abstraction des effets de couche. Par contre, Schmitt et Mosel prévoient justement que ces effets sont très importants et se traduisent par une grande valeur de l'énergie cinétique quand les deux fragments obtenus sont presque magiques. Nos résultats expérimentaux se rapprochent beaucoup plus de ceux de Nix que de ceux de Schmitt et Mosel. On ne peut en conclure que le modèle

Schmitt et Mosel est inexact; plus probablement, aux grandes énergies d'excitation mises en jeu dans nos expériences (tableau I) les effets de couche deviennent négligeables. Ce résultat n'est pas surprenant si l'on note que, par exemple dans le cas de l'uranium excité à 40 MeV, la fission est déjà essentiellement de type symétrique; en particulier, l'énergie cinétique totale a des valeurs et une variation avec le rapport de masse des fragments différentes de celles obtenues pour la fission à basse énergie [9, 11].

L'effet prévu par Schmitt et Mosel étant très important, on espérait cependant qu'il en subsisterait une partie aux énergies d'excitation obtenues (tableau I).

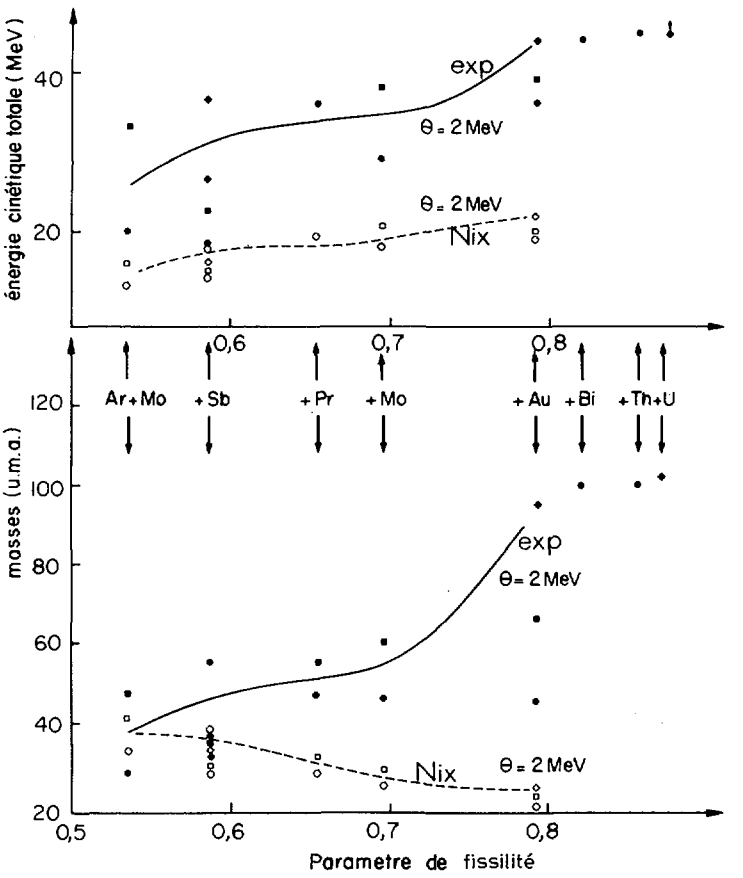

FIG.6. Largeurs des distributions en masse (en bas) et en énergie cinétique totale (en haut) pour la fission de différents noyaux composés, en fonction du paramètre de fissilité x. Les symboles noirs sont les résultats expérimentaux; les mêmes symboles ouverts sont les valeurs calculées d'après Nix [3] pour une même valeur de x. Les deux courbes montrent les variations avec x prévue et expérimentale, pour une même valeur de la température nucléaire au point-selle. (Les différents symboles correspondent à différentes températures nucléaires.)

TABLEAU II. SECTIONS EFFICACES DE FISSION DES NOYAUX DE FUSION COMPLETE FORMES AVEC LES PROJECTILES $^{40}_{18}Ar$

Cible	Noyau composé	x	Energie labo (MeV)	Energie c.m. (MeV)	Barrière d'interaction c.m. (MeV)	E^* (MeV)	B_f (MeV)	σ_F (mb)	σ_R (mb)	$\frac{\sigma_F}{\sigma_R}$	L_{max} ($\hbar$)	L_{crit} ($\hbar$)
Mo nat.	Nd	0,528	200	140	93,5	98	39	145 ± 30	1400	0,1	96	(82)
Mo nat.	Nd	0,528	300	209,5	93,5	169	39	163 ± 15	2350	0,07	151	(83)
Sb nat.	Tm	0,586	162	122	109	58	28,5	103 ± 1	450	0,02	53	(>53)
Sb nat.	Tm	0,586	179	135	109	72	28,5	187 ± 20	840	0,22	74	(>74)
			199	150	109	86	28,5	510 ± 80	1250	0,4	94	(94)
			226	170	109	106	28,5	535 ± 50	1620	0,32	114	(98)
			300	226	109	164	28,5	620 ± 60	2370	0,26	158	(108)
Ho-165	At-205	0,702	226	182	135	97	13	860 ± 90	1348	0,64	110	102
Ho-165	At-205	0,702	300	242	135	160	13	1430 ± 140	2300	0,62	166	139
Bi-209	Md-249	0,820	250	210	158	80	~0	1110 ± 200	1380	0,81	122	110
U-238	110-278	0,870	250	214	171	82	<0	766 ± 150	1230	0,62	117	92
U-238	110-278	0,870	300	257	171	125	<0	1220 ± 120	2043	0,60	166	128

Les erreurs indiquées sont des estimations.
Les valeurs entre parenthèses ont été obtenues à partir d'un modèle approximatif et les erreurs correspondantes peuvent atteindre 10 $\hbar$.

En ce qui concerne les prévisions de Nix, on note que comme pour les noyaux de Z inférieur à 95 les énergies calculées sont sous-estimées. De plus, les courbes expérimentale et théorique représentant la variation avec x (paramètre de fissilité) de l'énergie cinétique totale moyenne ont des pentes différentes, la courbe théorique croissant plus vite que la courbe expérimentale.

2.2.2. Largeurs des distributions en masse et en énergie cinétique

Puisque les effets de couche semblent être négligeables pour les réactions qui nous intéressent, il est bon de voir dans quelle mesure la théorie de la goutte liquide permet de rendre compte d'autres caractéristiques de la fission comme les largeurs Γ_M et Γ_E des distributions en masse et en énergie cinétique. On sait que la théorie de Nix [3] n'a de sens que pour des valeurs du paramètre de fissilité inférieures à 0,8. Dans le tableau I et sur la figure 6, on peut comparer les valeurs expérimentales et théoriques de ces largeurs quand cette condition est vérifiée.

Sauf dans le cas du molybdène, les largeurs calculées sont trop faibles, et cela d'autant plus que l'énergie d'excitation ou la masse du noyau composé est grande. De plus, la courbe calculée représentant la variation de Γ_M avec le paramètre de fissilité à température nucléaire constante décroît alors que la courbe expérimentale croît. La divergence entre des courbes équivalentes pour Γ_E est nette bien que moins importante. Dans tous les cas les températures nucléaires ont été calculées en ne déduisant de l'énergie d'excitation que la valeur de la barrière de fission augmentée de l'énergie minimale de rotation dont doit disposer le noyau pour fissionner (cf. paragr. 3). On a aussi considéré qu'aucun neutron n'était évaporé avant fission. Ces températures sont donc surestimées; un calcul plus correct ne ferait qu'augmenter la divergence théorie-expériences, particulièrement pour les grandes valeurs du paramètre de fissilité.

3. SECTIONS EFFICACES ET FONCTIONS D'EXCITATION DE FISSION INDUITE PAR ARGON

Les sections efficaces de fission dont il est question ici concernent uniquement la fission après transfert de moment complet, c'est-à-dire après fusion du projectile et de la cible. On a de plus admis que ce noyau de fusion atteignait l'état d'équilibre thermodynamique du noyau composé avant de fissionner. On a donc calculé les sections efficaces de fission en considérant que la distribution angulaire des fragments est proportionnelle à $1/\sin\theta$ en raison du moment angulaire important du noyau fissionnant [8, 9]. $1/\sin\theta$ est une limite supérieure, car au voisinage de 0° (ou 180°) la section efficace différentielle reste finie, mais même avec les moments angulaires moins importants apportés par des particules alpha de 150 MeV, la surestimation est inférieure à 5% [10].

Dans le tableau II sont regroupés nos résultats pour les différents couples cible + projectile à différentes énergies: paramètre de fissilité x, barrière d'interaction entre le projectile et la cible, énergie d'excitation du noyau composé, barrière de fission, section efficace de fission mesurée, section efficace de réaction calculée et, enfin, moment angulaire maximal possible pour le noyau composé et moment angulaire maximal atteint

réellement (critique). Les paramètres de fissilité sont calculés par la relation $x = Z^2/50,13\ A$. Les barrières d'interaction V ont été calculées en prenant un rayon d'interaction effectif r_e [11, 12] de 1,45 fm. Les énergies d'excitation sont obtenues à partir des défauts de masse de la table de Myers et Swiatecki [13], de laquelle sont également extraites les valeurs des barrières de fission du noyau composé. Les sections efficaces de réaction sont calculées par la relation

$$\sigma_R = \pi(R_1+R_2)^2\left(1-\frac{V}{E}\right)$$

où R_1 et R_2 sont les rayons des deux noyaux de la voie d'entrée, et E est l'énergie cinétique disponible dans le centre de masse.

Les erreurs indiquées sur les valeurs des sections efficaces de fission ont plusieurs sources: épaisseur des cibles, angles solides, mais surtout, dans certains cas, difficulté à distinguer les fragments provenant de fissions très asymétriques des produits de transfert (fig. 1 et 2).

Nous pouvons diviser ce tableau en deux parties. Pour les noyaux composés de masse inférieure à 200, la fission n'est pas le processus de désexcitation choisi par tous les noyaux. Par contre, pour les noyaux plus lourds, la quasi-totalité des noyaux résultant de la fusion du projectile et de la cible fissionnent à une étape de la chaîne de désexcitation.

3.1. Noyaux composés de masse inférieure à 200

Dans ces cas, la barrière de fission est grande (c'est-à-dire très supérieure à l'énergie de liaison du dernier neutron), ce qui implique que la fission n'est plus le processus dominant de désexcitation. En fait, il est même a priori surprenant d'observer des sections efficaces de fission aussi grandes quand les barrières correspondantes dépassent 20 MeV (cf. le cas de l'antimoine par exemple). Il s'agit là d'un effet du moment angulaire puisqu'on sait que celui-ci abaisse les barrières effectives de fission:

$$\Delta B_f = E_{R0} - E_{RS}$$

E_{R0} et E_{RS} sont les énergies de rotation des noyaux sphériques et au point-selle.

D'après Halpern et Strutinski [14]

$$\Delta B_f = \frac{\hbar^2}{2J_0} I\left(1-\frac{J_0}{J_\perp}\right) - \frac{\tau_s}{2}$$

où I est le moment angulaire du noyau fusionnant
J_0 et $J_\perp$ sont les moments d'inertie des noyaux sphériques, et au point-selle dans la direction perpendiculaire à l'axe de déformation
τ_s est la température nucléaire.

Les valeurs de $J_\perp/J_0$ ont été obtenues à partir des travaux de Cohen et Swiatecki [15].

Sur la figure 7, on a porté pour l'antimoine la variation avec l'énergie incidente de la section efficace expérimentale de fission, la section efficace totale de réaction et la section efficace de réaction correspondant aux ondes partielles de moment angulaire supérieur à $J_{B_f = S_n}$. $J_{B_f = S_n}$ est la valeur de

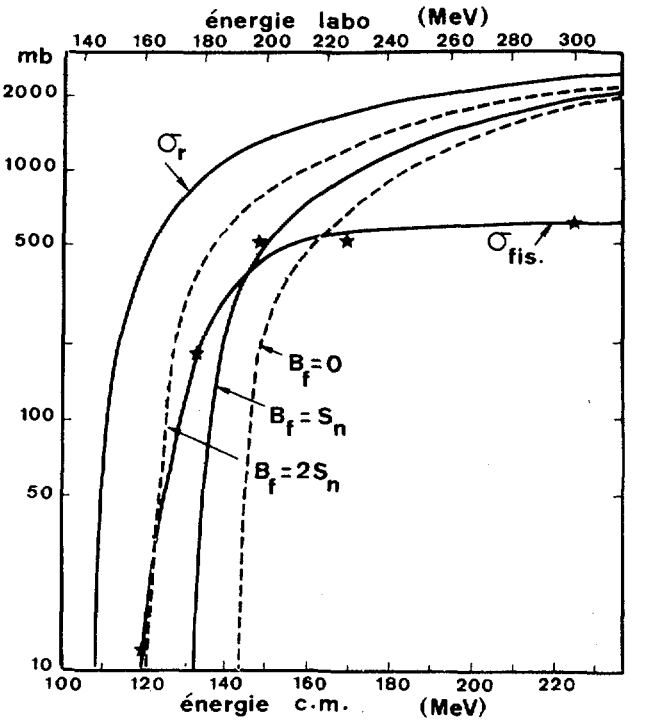

FIG.7. Fonction d'excitation pour la fission du noyau de fusion formé par Ar sur une cible ^{nat}Sb. Les courbes calculées correspondent à différentes hypothèses sur la valeur du moment angulaire à partir duquel les noyaux fissionnent (voir texte) et supposent qu'il n'y a pas de moment angulaire critique pour la formation du noyau de fusion.

moment angulaire pour laquelle l'abaissement de barrière est tel que la barrière effective de fission est égale à l'énergie de liaison du dernier neutron. On peut dire que les contributions à la section efficace de fission de moments angulaires inférieurs à $J_{B_f = S_n}$ sont nulles et que réciproquement tout noyau ayant acquis un moment angulaire supérieur à $J_{B_f = S_n}$ se désexcite à coup sûr en fissionnant. Ceci est évidemment très schématique et on a aussi porté sur la figure 7 (courbes en pointillés) les sections efficaces de réaction correspondant aux ondes partielles de moment angulaire supérieur à $J_{B_f = 0}$ et $J_{B_f = 2S_n}$. S'il n'existait pas de moment angulaire critique (comme c'est le cas pour les réactions induites par des ions plus légers) la courbe de la section efficace de fission se trouverait entre les deux courbes en pointillés de la figure 7 (avec toutefois la possibilité de dépasser la limite supérieure). On constate d'abord que la section efficace expérimentale de fission démarre bien dans cette zone. Ce résultat confirme la validité des calculs que nous avons effectués. Par contre, pour des valeurs plus grandes de l'énergie incidente, la section efficace de fission est inférieure

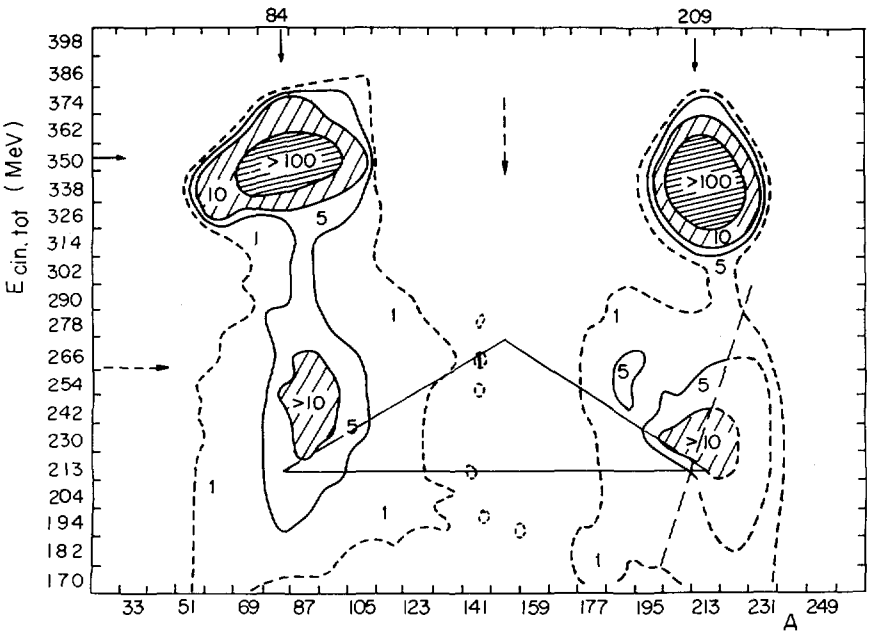

FIG.8. Kr de 500 MeV (357 MeV centre de masse) sur cible ^{209}Bi. Tableau énergie cinétique totale centre de masse – masse du produit reçu par le détecteur X placé à 54°. Des pics de diffusion élastique (courbe de niveau supérieur à 1000) et des produits de transfert apparaissent au voisinage de A = 84 et 209, ECT = 357 MeV. Les flèches en pointillés indiquent la place attendue des événements de fission binaire symétrique.

à la valeur attendue. Ce résultat est interprété en terme de moment angulaire critique et est développé ailleurs [16]. Rappelons que le moment angulaire critique est la valeur du moment angulaire au-delà de laquelle il ne serait plus possible de former un noyau de fusion.

Pour terminer nous ferons la remarque suivante: au fur et à mesure que la masse d'un noyau composé décroît, le moment angulaire critique décroît; par contre, le moment angulaire à partir duquel la probabilité de fission n'est plus négligeable croît (au moins jusqu'au molybdène) [17]. Il existe donc une masse de noyau composé au-dessous de laquelle la section efficace de fission est très faible (à énergie d'excitation moyenne). On peut situer cette masse au voisinage de 110 uma, c'est-à-dire une cible au voisinage du cuivre pour les réactions induites par argon.

3.2. Noyaux composés de masse supérieure à 200

Dans ce cas, la quasi-totalité des noyaux résultant de la fusion du projectile et de la cible fissionnent, soit immédiatement, soit après évaporation d'un neutron ou d'une particule chargée, ceci parce que la barrière de fission effective (compte tenu du moment angulaire) est inférieure à ou voisine de l'énergie de séparation du dernier neutron.

La mesure de la section efficace de fission après transfert de moment complet est donc une mesure de la section efficace de formation de noyau composé, ou plus généralement de la section efficace de formation de noyau de fusion complète entre le projectile et la cible.

On remarque que pour tous les cas cette section efficace est inférieure à σ_R. On en a déduit dans chaque cas la valeur du moment angulaire critique ℓ_{cr} au-delà de laquelle il n'y aurait plus fusion complète. Cette valeur augmente avec la masse du noyau de fusion et avec l'énergie d'excitation. La comparaison avec d'autres résultats a montré que ℓ_{cr} augmente également avec la masse du projectile, du moins jusqu'à l'argon [16]. Notons que ces résultats sont aussi en accord avec les résultats obtenus par Sikkeland pour la réaction Ar + U [18].

4. FISSION ET FUSION PARTIELLE INDUITES PAR KRYPTON

Nous voyons sur la figure 8 correspondant à l'interaction de ^{84}Kr de 500 MeV sur une cible de ^{209}Bi que très peu d'événements sont attribuables à la fission du noyau composé $^{293}_{119}X$. En effet, en prenant les quelques événements voisins du rapport de masse 1 et en supposant une distribution de masse des fragments de fission large de 100 uma, on obtient seulement environ 40 mb de fission suivant fusion complète entre Kr et Bi, soit moins de 5% de σ_R. Un résultat semblable concernant le noyau de fusion $^{322}_{128}X$ (obtenu par Kr + ^{238}U) indiquait une section efficace de fusion binaire inférieure à 10 mb [19] (tableau III). La valeur de ℓ_{cr} correspondante serait très petite.

Nous avons effectué les mêmes mesures avec des cibles ^{165}Ho et ^{186}W. Il apparaît que les sections efficaces de fission après fusion complète et la proportion de la section efficace de réaction sont plus importantes lorsque la masse de la cible est plus faible. Remarquons que dans nos expériences cela correspond également à des énergies plus élevées par rapport à la barrière d'interaction. Il est donc possible que le facteur décisif soit l'énergie nécessaire pour franchir une barrière de fusion éventuellement supérieure à la barrière d'interaction.

Ce résultat pourrait en fait signifier que la fission des noyaux composés excités super-lourds formés est essentiellement ternaire, et de ce fait inaccessible à nos mesures. Cette hypothèse n'apparaît pas injustifiée si l'on extrapole les résultats déjà connus pour des noyaux plus légers [20], mais trois faits la contredisent. D'une part, des noyaux de fusion complète de même Z et de A voisins ($^{278}_{110}X$ et $^{270}_{110}X$) ont été formés respectivement par les réactions ^{40}Ar + ^{238}U et ^{84}Kr + ^{186}W; aux deux réactions correspondent des valeurs très différentes du rapport σ_F/σ_R. D'autre part, pour les noyaux de fusion plus légers que $^{278}_{110}X$ et formés par Ar la proportion de fission ternaire n'est pas très importante [16]; or, ni l'énergie d'excitation, ni les moments angulaires apportés par les ions Kr ne sont supérieurs à ceux dus aux ions Ar de la réf. [19]. Enfin, il apparaît sur la figure 8 des événements autres que la fission ou des transferts.

La section efficace différentielle de ces événements est importante. Dans le cas de Kr + Bi, leur section efficace totale calculée en supposant une distribution angulaire isotrope dans le centre de masse serait égale à σ_R. C'est évidemment exagéré puisqu'il y a d'autres réactions (transferts)

TABLEAU III. SECTIONS EFFICACES DE FISSION BINAIRE σ_F ET SECTIONS EFFICACES DIFFERENTIELLES DE FUSION PARTIELLE $d\sigma/d\Omega$ OBSERVEES AVEC LES PROJECTILES $^{84}_{36}Kr$

Cible	Noyau composé	x	Energie labo (MeV)	Energie c.m. (MeV)	Barrière d'interaction c.m. (MeV)	Energie d'excitation (MeV)	σ_F (mb)	σ_R (mb)	$\frac{\sigma_F}{\sigma_R}$	ℓ_{max} ($\hbar$)	$d\sigma/d\Omega$ (mb/sr)
Ho-165	Lw-249	0,849	450	298	263	62	~200	800	~0,25	139	
Ho-165	Lw-249	0,849	493	327	263	91	(230)	1050	(0,22)	170	(20)
W-186	110-270	0,893	502	346	284	105	(150)	990	(0,15)	173	(15)
Bi-209	119-293	0,965	502	358	312	52	$\leqslant 40$	800	$\leqslant 0,05$	157	70
U-238	122-322	0,92	502	371	335	50	< 10	610	$< 0,02$	144	

Les valeurs entre parenthèses sont des résultats préliminaires. σ_R est la section efficace totale de réaction.

en nombre important et ceci suggère que leur distribution angulaire présente un maximum.

En examinant la distribution en masse et énergie cinétique totale de ces événements, on est frappé par le fait que leurs masses sont essentiellement voisines de celles de Kr et de la cible. D'autre part, leur énergie cinétique totale est de l'ordre de celle que l'on attend pour une fission très asymétrique. Ils pourraient résulter de la formation d'un état quasi moléculaire, entre la barrière d'interaction et la barrière de fusion, à courte durée de vie. La désintégration d'un tel état conduirait à des fragments de masses voisines de celles de la voie d'entrée puisque aucune configuration d'équilibre n'est atteinte.

REFERENCES

[1] CABOT, C., NGO, C., PETER, J., TAMAIN, B., Nucl. Instrum. Methods, à paraître.
[2] TAMAIN, B., Thèse en préparation, Orsay.
[3] NIX, J.R., UCRL-17958 (1968).
[4] SCHMITT, H.W., KIKER, W.E., WILLIAMS, C.W., Phys. Rev., B 137 (1965) 837.
[5] WILKINS, B.D., FLUSS, M.J., KAUFMAN, S.B., GROSS C.E., STEINBERG, E.P., Nucl. Instrum. Methods 92 (1971) 381; Ibid. 99 (1972) 320.
[6] BORDERIE, B., Thèse de 3e cycle, Orsay (1973).
[7] NORTHCLIFFE, L.C., SCHILLING, R.F., Nuclear Data Tables A7 (1970) 233.
[8] PLASIL, F., BURNETT, D.S., BRITT, H.C., THOMPSON, S.G., Phys. Rev., A 142 (1966) 696.
[9] GALIN, J., LEFORT, M., PETER, J., TARRAGO, X., CHEIFETZ, E., FRAENKEL, Z., Nucl. Phys., A 134 (1969) 513.
[10] SCHMITT, H.W., MOSEL, U., Nucl.Phys., A 186 (1972) 1.
[11] LEFORT, M., NGO, C., PETER, J., TAMAIN, B., Nucl. Phys., A 197 (1972) 485.
[12] WONG, C.Y., Phys.Lett., B 42 (1972) 186.
[13] MYERS, W.D., SWIATECKI, W.J., Nucl.Phys., A 81 (1966) 1.
[14] HALPERN, I., STRUTINSKI, V.M., 2nd Int. Conf. Peaceful Uses At. Energy (Proc. Conf. Geneva, 1958) 15, UN, New York (1958) 408.
[15] COHEN, S., SWIATECKI, W.J., Ann. Phys., N.Y. 22 (1963) 406.
[16] LEFORT, M., LE BEYEC, Y., PETER, J., IPNO-RC 73-04.
[17] PATE, B.D., PETER, J., Nucl. Phys., A 173 (1971) 520.
[18] SIKKELAND, T., Ark. Fysik 36 (1966) 539.
[19] BRANDT, R., Angew. Chem. 10 (1971) 890.
[20] PERE LYGIN, V.P., SHADLEVA, N.H., TRETLAKOVA, S.P., BOOS, A.M., BRANDT, R., Nucl. Phys., A 127 (1969) 577.
[21] CABOT, C., Thèse 3e cycle, Orsay (1972).
[22] GALIN, J., LEFORT, M., PETER, J., TARRAGO, X., CHEIFETZ, E., FRAENKEL, Z., Nucl. Phys., A 134 (1969) 513.
[23] BRITT H.C., WHETSTONE, S.L., Phys. Rev. 133 (1964) 603.
[24] BRITT, H.C., WEGNER, H.E., GURSKY, J.C., Phys. Rev. 129 (1963) 2239.
[25] PLASIL, F., BURNETT, D.S., BRITT, H.C., THOMPSON, S.G., Phys. Rev. 142 (1966) 696.
[26] SCHMITT, H.W., NEILLER, J.H., WALTER, F.J., Phys. Rev. 141 (1966) 1146.
[27] UNIK, J.P., CUNINGHAME, J.G., CROALL, I.F., Physics and Chemistry of Fission-1969 (C.r. Coll. Vienne, 1969), AIEA, Vienne (1969) 717.
[28] SIKKELAND, T., Phys. Lett., B 31 (1970) 451.
[29] BURNETT, S.C., FERGUSON, R.L., PLASIL, F., SCHMITT, H.W., Phys. Rev., C 3 (1971) 2034.
[30] ALKHAZOV, I.D., KOSTOCHKIN, O.I., KOVALENKO, S.S., MALKIN, I.Z., PETRZHAK, K.A., SHPAKOV, V.I., Sov. J. Nucl. Phys. 11 (1970) 281.
[31] KOMAR, A.P., BOCHAGOV, B.A., KOTOV, A.A., RANYUK, Yu.N., SEMENCHUK, G.C., SOLYALIN, G.E., SOROKIN, P.V., Sov. J. Nucl. Phys. 10 (1970) 30.
[32] BALAGNA, J.P., FORD, G.P., HOFFMAN, D.C., KNIGHT, J.D., Phys. Rev. Lett. 26 (1971) 145.
[33] JOHN, W., HULET, E.K., LOUGHEED, R.W., WESOLOWSKI, J.J., Phys. Rev. Lett. 27 (1971) 45.

[34] BRANDT R., THOMPSON, S.G., GATTI, R.C., PHILLIPS, L., Phys. Rev. 131 (1963) 2617.
[35] NEILER, J.H., WALTER, F.J., SCHMITT, H.W., Phys. Rev. 149 (1966) 894.
[36] PLEASONTON, F., Phys. Rev. 174 (1968) 1500.

An English translation of this paper can be obtained direct from the authors.

DISCUSSION

F. PLASIL: With regard to the high critical angular momenta (> 100 ħ) mentioned by you for the higher energy ^{40}Ar bombardments of Sb, I should like to point out that the calculations of Cohen, Swiatecki and myself predict that the fission barrier reaches zero at about 100 ħ. Thus it is possible that some of the fission you observe may in fact be from a process that does not involve the formation of a compound nucleus, namely a faster "direct" form of fission, which involves mass exchange but not full equilibrium. In such a case, full momentum would be transferred from the projectile to the composite system of target and projectile, and the observed fission fragments may not differ from those of compound nucleus fission in any way that could have been observed in your measurements.

I should also like to comment on the high fragment total kinetic energies predicted by Schmitt and Mosel for fissioning nuclei with mass near 264 amu. We have also attempted to check the Schmitt-Mosel prediction by means of the two systems $^{232}Th + ^{18}O \rightarrow [^{250}Cf^{*}] \rightarrow$ fission and $^{246}Cm + ^{18}O \rightarrow [^{264}104^{*}] \rightarrow$ fission. The average total fragment kinetic energies for the two systems are predicted to differ by more than 60 MeV. Like you, we did not find such a dramatic difference in fragment kinetic energy and we also attribute this to the disappearance of the shell effects at such a high excitation energy. A paper on this work by R.L. Ferguson, F. Plasil, H. Freiesleben, C.E. Bernis and H.W. Schmitt will appear in Phys. Rev., C shortly.

B. TAMAIN: With regard to your first point, it is true that we can only say that we have measured cross-sections for fission following full momentum transfer. The only possible way to establish whether our events correspond to fission following compound nucleus formation would be to measure the angular distribution of fission events, and we aim to do this.

FISSION AND COMPLETE-FUSION MEASUREMENTS IN ^{40}Ar BOMBARDMENTS OF ^{58}Ni AND ^{109}Ag§

H.H. GUTBROD
G.S.I. Darmstadt, Federal Republic of Germany

F. PLASIL
Oak Ridge National Laboratory, Oak Ridge, Tenn.

H.C. BRITT, B.H. ERKKILA, R.H. STOKES
Los Alamos Scientific Laboratory, Los Alamos, N. Mex.

M. BLANN
University of Rochester, Rochester, N.Y.,
United States of America

Abstract

FISSION AND COMPLETE-FUSION MEASUREMENTS IN ^{40}Ar BOMBARDMENTS OF ^{58}Ni AND ^{109}Ag.

Thin targets of ^{58}Ni and ^{109}Ag have been bombarded with 197- and 288-MeV ^{40}Ar ions from the Berkeley Super-HILAC. A particle telescope consisting of a gas proportional ΔE counter and a silicon surface barrier E detector was used to measure all reaction products ranging from elastically scattered argon ions to compound nucleus evaporation products. Fission fragments and transfer products were also detected. A good separation between fission fragments and other reaction products was possible in the case of the ^{109}Ag + ^{40}Ar reaction. Angular distributions were obtained from 4° to 40° in the laboratory system. Elastic scattering and a ^{252}Cf source were used to obtain energy and angular calibrations.

The fission fragment angular distribution is characterized by a 1/sinθ function, and the integrated fission cross-section was found to be 300 and 600 mb for Ar + Ag at 197 and 288 MeV.

Results have been interpreted in terms of a model in which fission competes with other modes of de-excitation of the compound nucleus, and in which the effects of angular momentum of the fission barrier are taken into account. The implications of this conclusion are discussed. Comparisons are also made with models for the complete-fusion cross-section which are based on the contact configuration for the interacting two-body systems.

1. INTRODUCTION

The work to be discussed is part of a broad program to measure as many of the main reaction channels as possible for heavy-ion-induced reactions. It is planned ultimately to do this for a number of target and projectile combinations, in the hope that these results will help provide the proving grounds for various macroscopic models of heavy-ion reactions.

The systems to be discussed are ^{40}Ar-induced reactions on targets of ^{58}Ni and ^{109}Ag at incident energies of 197 and 288 MeV. Beams were obtained from the Berkeley Super-HILAC. We will describe the experimental method used, the method of analyzing the data, and the results which consist

§ Work supported in part by the US Atomic Energy Commission and the Gesellschaft für Schwerionenforschung mbH.

of cross-sections for compound nucleus evaporation products (evaporation residues), fission cross-sections and angular distributions, a fission mass-yield distribution, and fission fragment kinetic energy distributions. Results will then be compared with several models which predict angular momentum limits for either the compound nucleus formation cross-section or for the evaporation residue cross-section.

2. EXPERIMENTAL METHOD

The results to be reported were obtained from angular distributions of reaction products measured with a gas/solid state ΔE×E counter telescope[1] with a ΔE thickness of $\sim 250 \mu g/cm^2$. Targets were $\leq 200 \mu g/cm^2$. Line targets on carbon backing were used for all measurements except the 197-MeV results in ^{109}Ag and the angular correlation result at 288 MeV. A self-supporting target was used for the latter. A contour plot of two spectra is shown as an example in fig. 1 (see caption). Energy resolution was ∿0.5% in the E plane and ∿6% in ΔE. The features to be noted in fig. 1 are the elastic scattering peak, the evaporation residue distribution, a fission-like distribution, and in some spectra a distribution which has been attributed to carbon backings or carbon target buildup. The latter is not evident in the examples of fig. 1. Low Z yields may also be seen in the contour from the ^{58}Ni target. Elastic scattering and use of ^{252}Cf sources were used in the calibration of the ΔE and E scales.

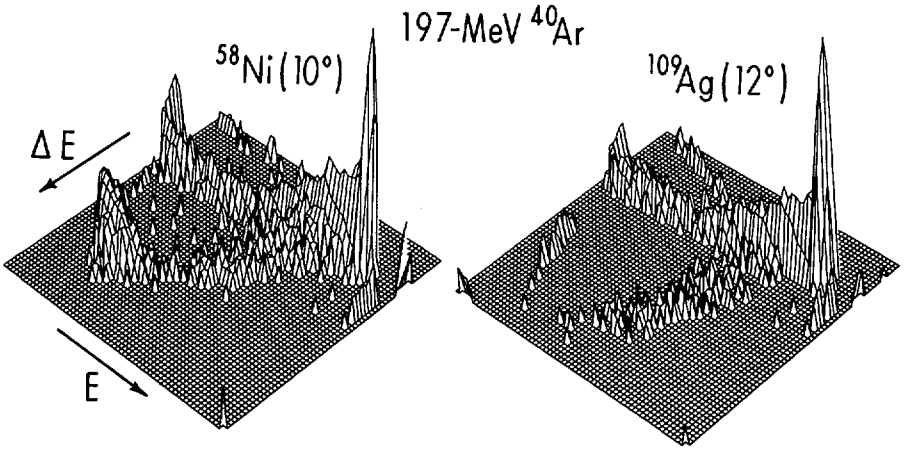

FIG. 1. Contour plots of counter-telescope data from ^{40}Ar (197 MeV) on ^{58}Ni and ^{109}Ag targets. The laboratory angles were 10° and 12° respectively. The ordinate is the logarithm of the number of counts. The high peaks at low ΔE and high E are the elastic ^{40}Ar peaks. A ridge due to inelastic events and slit-scattered ^{40}Ar may be seen at energies below the elastic peak. The peaks at high ΔE and relatively low E are the evaporation residues, and the group at medium E with a broad distribution in ΔE is the fission-like group.

Evaporation residue cross-sections have been obtained by integration over angle of the cross-sections from distributions such as shown in this example; fission angular distributions were obtained by integration of the fission-like products. The mass yield to be shown was deduced from the Z distribution of the fission-like fragments from a long run at 40° Lab; the kinetic energy distribution also was obtained from this run. Range energy results (dE/dX) due to Northcliffe and Schilling were used in identifying product atomic numbers[2]. Fission cross-sections were obtained from the angular distributions of the fission-like group. At 288-MeV ^{40}Ar + ^{109}Ag, a cross-section was also obtained from a measurement of the angular correlation of the two fragments.

3. RESULTS

Angular distributions for the evaporation residues are shown in fig. 2. These results were integrated to get total cross-sections. The largest source of error is thought to be the extrapolation of the measured distributions to 0°; total errors from all sources are believed to be $\leq$15%. Uncertainties in the extrapolation are reduced by the $\sin\theta$ factor which enters into the integration of the distributions of fig. 2. Results for fusion and fission cross-sections are summarized in Table I. Angular distributions of fission-like products are shown in fig. 3. Transformation to CM was made assuming symmetric binary fission. A $1/\sin\theta$ curve was fitted to the experimental results, and is shown as the solid line on this figure. Fission cross-sections were based on integration of the $1/\sin\theta$ distribution, corrected for the fraction of the mass yield estimated to be missing from the integration of each spectrum. This results in a very large uncertainty for the ^{40}Ar + ^{58}Ni system since the carbon backing made it undesirable to integrate below Z=22. The experimental results at 288 MeV on ^{109}Ag show some evidence of being more forward peaked than the $1/\sin\theta$ distribution. It is not clear if this is a statistically significant deviation. If it is, it could imply a contribution to the fission cross-section from a non-equilibrium system.

The charge yield deduced from the ΔE identification for the system ^{109}Ag + ^{40}Ar at 288 MeV is shown in fig. 4. The distribution is centered at $\sim$Z=30, which is consistent with the expectation for symmetric fission followed by particle evaporation. The mass yield implied by these results has FWHM of $\sim$40 amu. Spectra were not integrated below Z=22 when fig. 4 was prepared. Preliminary results indicate a distribution which is somewhat skewed to lower masses. Kinetic energy distributions for the light, medium and heavy fragments are shown in fig. 5. The shift to higher energies for lower mass in a manner consistent with binary fission may be seen. A fission correlation experiment was also performed during the run on which these data are based. The E counter used in the correlation subtended an angle of ±7.5°, which was estimated to record 47% of binary coincidence events. With the telescope at +40°, the E counter was placed at -57.5° giving a correlation angle of 97.5°. This may be compared with a predicted value of 101° for symmetric binary fission. The cross-section obtained in this measurement also agreed well with estimates from the singles measurements.

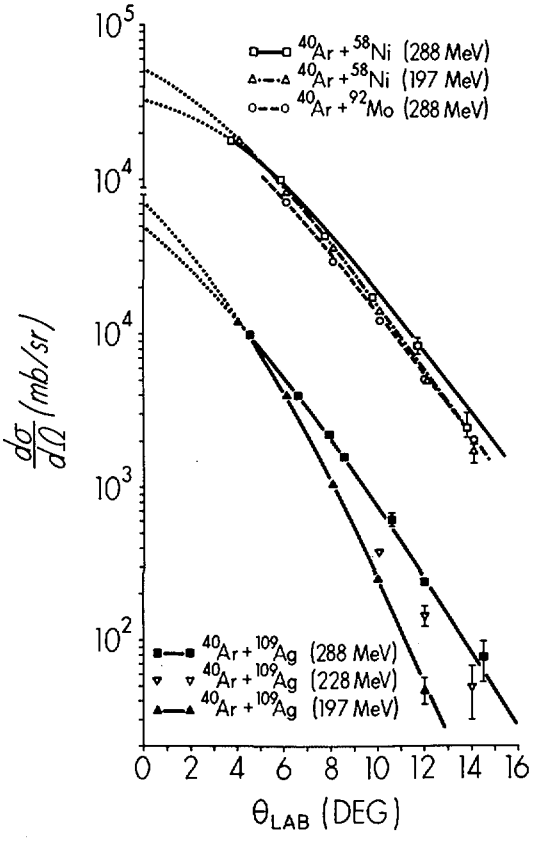

FIG.2. Angular distributions of evaporation residues following ^{40}Ar bombardment of ^{58}Ni, ^{92}Mo, and ^{109}Ag targets. The ordinate is broken to allow a double display. The solid line was drawn visually through the points before integration over angle. The dotted lines represent one set of extrapolations to 0°. Squares, triangles, and circles represent the experimental measurements.

Table I: Summary of cross-sections from ^{40}Ar bombardment

		Cross-sections (mb)	
Target	^{40}Ar Energy (MeV-Lab)	Evaporation Residue	Fission
^{58}Ni	288	900±120	
	197	880±120	(400±150)[a]
^{109}Ag	288	670±100	600±90
	197	620±90	300±45

[a] Rough estimate based on integration of less than half the mass-yield distribution.

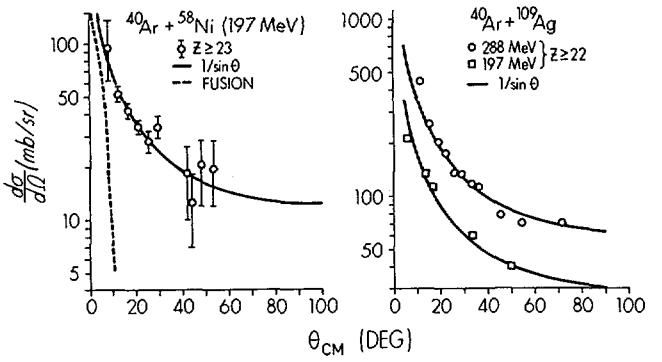

FIG. 3. Angular distributions of fission-like products. Points represent experimental measurements converted to CM assuming symmetric binary fission. Solid lines are best fit results of a 1/sinθ curve. For $^{40}Ar + ^{58}Ni$ the evaporation residue angular distribution is shown for comparison as a dashed curve.

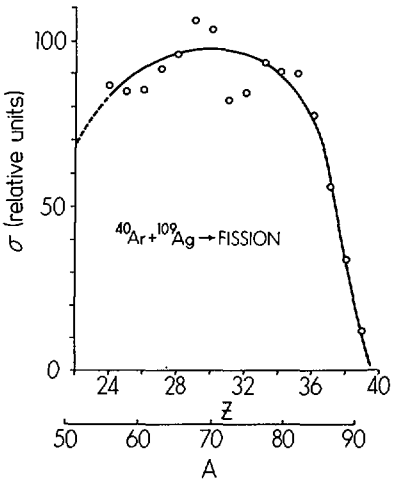

FIG. 4. Charge distribution curve deduced from ΔE of fission-like products measured at 40° (lab). The open points represent the experimental results converted to CM and integrated assuming a 1/sinθ angular distribution. The solid curve was arbitrarily drawn, and has been shown as a dashed curve below Z = 24 where it is extrapolated.

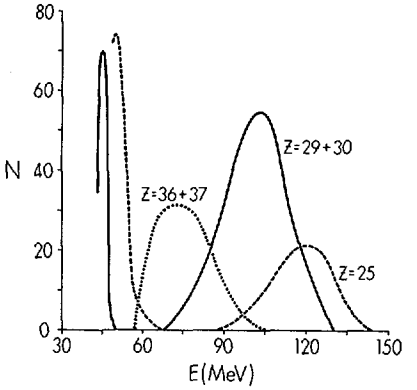

FIG.5. Kinetic energy distribution of fragments measured at 40°. The ordinate is number of counts, the abscissa is kinetic energy in the laboratory system. Counts from several Z were combined for statistical purposes. The peaks at low energy are thought to result from heavy transfer products which give a dE/dX similar to low-energy fission fragments. Those events were not included in the integrations of Fig. 4.

4. DISCUSSION

Experimental results of this work are compared with predicted angular momentum limits in fig. 6. The experimental evaporation residue cross-sections are shown and, for the ^{109}Ag targets, the sum of evaporation residue plus fission cross-sections are also indicated. The results show that at the higher energy in the Ar + Ag case, the sum of evaporation residue and fission cross-sections are still considerably less than the expected total reaction cross-section.

The lower solid curve is the predicted limit to the evaporation residue cross-sections due to application of the rotating liquid drop model[3]. The fission barriers and ground state rotational energies have been computed as a function of angular momentum by Cohen et al.[3]. These values were used in a Bohr-Wheeler[4]-type fission-evaporation competition calculation for each impact parameter for ^{40}Ar + ^{109}Ag. Multiple particle emission and multiple chance fission were included in the calculation[5]. This calculation should predict the cross-section of the evaporation residue if the compound nucleus is actually formed with partial waves higher than those which give highly fissionable nuclei. The comparison between calculated and experimental results in fig. 6 is quite satisfactory.

Models have been formulated to predict the angular momentum limits for the formation of a compound nucleus based on the potential energy surface for the initial contact configuration, or for related shapes.[6-9] These treatments are similar to one another in that they consider the surface attractive and Coulomb plus centrifugal repulsive terms in computing the potential energy.

The first such treatment to our knowledge was due to Kalinkin and Petkov[6], who considered ellipsoidal contact shapes. More recently Wilczyński has calculated the result

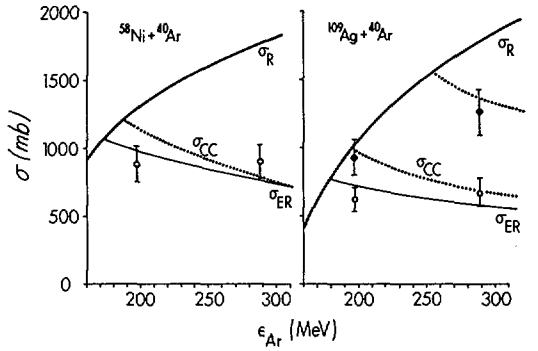

FIG. 6. Cross-sections versus ^{40}Ar bombarding energy. The heavy solid curve represents a calculated total reaction cross-section. Open points represent the experimentally measured evaporation residue cross-sections. Solid points represent the sum of measured fission plus evaporation residue cross-sections. The thin solid curves are calculated evaporation residue yields based on fission competition with a rotating liquid drop. The lower dotted curve represents predicted complete-fusion yields due to Wilczyński's formulation based on the contact configuration. The upper dotted curve represents the authors' interpretation of the limit due to a formulation of Tsang and Swiatecki, and also of Bass.

for a configuration of spherical target and projectile systems undergoing a grazing-like collision.[7] The predicted limit to the compound nucleus formation cross-section due to Wilczyński's formulation is shown by the lower dotted curve of fig. 6. If the experimentally observed fission yield results from fission of a compound nucleus, then the calculation with Wilczyński's model should be compared with the sum of fission plus evaporation residue cross-sections. In this case, Wilczyński's result seriously underestimates the fusion cross-section at 288-MeV ^{40}Ar + ^{109}Ag.

Tsang and Swiatecki are considering the problem of compound nucleus formation in a dynamic model with frictional effects, based also on a contact configuration for two spheres.[8] Their limits to the compound nucleus formation cross-section when the nuclear viscosity is high are shown as the upper dotted curve of fig. 6. A similar result follows from a related and in some ways similar treatment due to R. Bass.[9] The agreement between the limits of the Tsang-Swiatecki treatment and the experimental fission plus evaporation residue cross-section may be a preliminary indication of high nuclear viscosity for heavy-ion reactions in the energy range of these results.

5. CONCLUSIONS

The data discussed indicate that far less than the full reaction cross-sections are found in the evaporation residues. The evaporation residue cross-sections are in reasonably good agreement with values predicted by the rotating liquid drop model with fission competition, but the actual fission cross-sections can be much less than the difference between calculated evaporation residue and total reaction cross-sections.

Presumably the difference is to be found in direct reaction products, and evidence has been found for high transfer cross-sections at 288 MeV in γ-ray activation studies of ^{40}Ar + ^{109}Ag.[10] For the case Ag + Ar, the cross-section for the evaporation residue and fission is consistent with the predictions of a model based on the contact configuration with high friction as formulated by Tsang and Swiatecki. The fission product angular distributions are generally consistent with a $1/\sin\theta$ function, consistent with at least a major portion of the fission cross-section being due to equilibrium fission.

ACKNOWLEDGMENTS

The authors wish to express their appreciation to Dr. A. Ghiorso and the entire operating crew of the Berkeley Heavy Ion Accelerator. The programming assistance of Dr. R. Epple is similarly very much appreciated. We wish to thank Mrs. J. Gursky for preparing the targets. We have very much enjoyed helpful discussions with Drs. H. Krappe, W. D. Meyers, W. J. Swiatecki and C. F. Tsang.

REFERENCES

[1] K.D. HILDENBRAND, H.H. GUTBROD, W.V. OERTZEN and R. BOCK, Nucl. Phys. A157(1970)297.
[2] L.C. NORTHCLIFFE and R.F. SCHILLING, Nucl. Data Tables 7, No.3-4(1970).
[3] S. COHEN, F. PLASIL, and W.J. SWIATECKI, LBL Preprint LBL-1502(1972) submitted to Annals of Physics; Proceedings of the Third Conference on Reactions Between Complex Nuclei(ed. by A. GHIORSO, R.M. DIAMOND and H.E. CONZETT) Univ. of Calif. Press, Berkeley(1963) 325.
[4] N. BOHR and J.A. WHEELER, Phys. Rev. 56(1939)426.
[5] M. BLANN and F. PLASIL, Phys. Rev. Lett. 24(1972)303.
[6] B.N. KALINKIN and I.Z. PETKOV, Acta. Phys. Polon. 25(1964)265.
[7] J. WILCZYŃSKI "Calculations of the critical angular momentum in the entrance channel", Niels Bohr Institute Preprint(1973) unpublished.
[8] C-F. TSANG and W.J. SWIATECKI, private communication (1973).
[9] R. BASS, private communication(1973).
[10] M.E. HILLE, P. HILLE, and H.H. GUTBROD, private communication(1973).

DISCUSSION

J. MILLER: The calculation of the curve labelled σ_{ER} is one that assumes all the rest of the reaction cross-section is fission. This, of course, is contrary to the data that you have just presented. Thus the physical meaning of the theory behind σ_{ER} is obscure. There is, of course,

a considerable transfer-reaction cross-section. It would be remarkable if an equilibrium fission calculation also described a transfer reaction.

H.H. GUTBROD: The calculation for σ_{ER} is not based on the fact that all the rest of the reaction cross-section is fission. σ_{ER} is calculated for each partial wave, starting at $\ell = 0$. For low partial waves there might be no contribution to fission. At some higher value of ℓ the fission contribution becomes larger and finally no cross-section is left for the evaporation process. One has then obtained the σ_{ER} and can stop the calculations there. The angular momentum limit for the contact configuration, as pointed out by Tsang and Swiatecki and also by Bass, is the crucial gauge as to whether a composite system is formed or not, and whether therefore the Blann-Plasil-Swiatecki model can be applied or not.

S. BJØRNHOLM: It would perhaps be useful to distinguish between complete-fusion reactions leading to a spherical compound nucleus and complete-momentum-sharing reactions, where the two ions gravitate around each other, exchanging particles, energy etc., without necessarily fusing into a sphere. Both reactions can lead to fission, but they may differ in the angular distributions of the fragments. Would your measurements allow such a distinction to be made?

H.H. GUTBROD: I speculated on precisely this point in regard to the angular distribution of the fission-like events of $^{40}Ar + {}^{109}Ag$ at 288 MeV. The deviation from a $1/\sin\theta$ distribution at small angles might be an indication of a non-equilibrium fission process, as we like to call a reaction with full momentum transfer, and the nuclear matter exchange you mentioned.

NEON-INDUCED FISSION OF SILVER*

F. PLASIL, Robert L. FERGUSON, Frances PLEASONTON
Oak Ridge National Laboratory,
Oak Ridge, Tenn.,
United States of America

Abstract

NEON-INDUCED FISSION OF SILVER.

Thin targets of ^{107}Ag were bombarded at the Oak Ridge Isochronous Cyclotron with ^{20}Ne ions ranging in energy from 110.4 to 165.6 MeV. Silicon surface barrier detectors were used to detect coincident pairs of fission fragments and to measure fragment kinetic energies. The fission excitation function, relative to Rutherford scattering, was obtained. A fragment angular correlation measurement was made at 165.6 MeV, and, within the limits of our statistical uncertainties, the correlation was found to be symmetric with a full-width-at-half-maximum (FWHM) of 11°.

The fission cross-section, σ_f, was found to range from 1.06 mb at 110.4 MeV to 73.3 mb at 165.6 MeV. Calculations of σ_f have been made on the basis of a model in which fission competes with other modes of de-excitation of the compound nucleus, and in which the variation of the fission barrier B_f with angular momentum is taken into account. The barrier height and the ratio of the level density parameter for fission to the level density parameter for particle emission, a_f/a_n, were treated as adjustable variables. It was not possible to obtain a fit to our measured excitation function on the assumption that the compound nucleus formation cross-section, σ_{CN}, is equal to the total reaction cross-section σ_R. For $\sigma_{CN} < \sigma_R$, however, it was possible to fit our data with a wide range of B_f and a_f/a_n combinations.

At a bombarding energy of 165.6 MeV, fragment mass and total kinetic energy distributions were obtained from the data by means of an iterative centre-of-mass transformation. The mass distribution was found to be symmetric, and the average total kinetic energy to be 87 MeV. Measured widths of the mass and total kinetic energy distributions were compared with the liquid drop model, which predicts the mass distribution to be broad (38 amu FWHM), and the total kinetic energy distribution to be narrow (14 MeV FWHM). The measured width of the mass distribution (36 amu FWHM) was found to be in good agreement with the liquid drop prediction, but the width of the kinetic energy distribution (22 MeV FWHM), is somewhat greater than that predicted by the liquid drop theory.

I. INTRODUCTION

In undertaking a study of the fission of such relatively light nuclei as those in the region of silver, we have been motivated by several recent developments. First, there appears to be a widespread increase of interest in heavy-ion reactions in general, and in the way in which they can be used to form superheavy elements in particular. There is both experimental [1,2] and theoretical [3] evidence that high angular momenta encountered in heavy-ion reactions can lower the fission barrier drastically, and that this effect can influence both the formation and the decay of compound nuclei [4]. In the region of silver, where the fission barriers are very high (of the order of 40-50 MeV at zero angular momentum), it is possible to study fission only when angular momentum is used to lower the barrier to the point where the fission cross-section is in the millibarn region, and the fission counting rate is acceptable. By studying a system in which the angular-momentum-dependent lowering of the fission barrier is an essential ingredient, we hope to gain information that will also apply to other mass regions.

* Research sponsored by the US Atomic Energy Commission under contract with the Union Carbide Corporation.

A second motivation is the desire to understand the $^{20}Ne + ^{107}Ag$ reaction in general. Natowitz [5] has found that at a bombarding energy of 173 MeV the cross-section for evaporation residue products (i.e., compound nuclei that have de-excited by particle emission) is only about four-tenths of the estimated total reaction cross-section σ_R. Since the cross-section for transfer reactions is expected to account for only a small portion of the remaining six-tenths of σ_R, several hundred millibarns remain to be accounted for. Blann and Plasil [4] have shown that theoretical calculations are consistent with Natowitz's experimental result and have suggested that part of the "missing cross-section" can be accounted for by fission. In this work we have investigated the extent of the fission contribution.

Finally, the fragment mass and total kinetic energy distributions in this mass region are also of interest. For increasingly lighter fissioning systems, the so-called Businaro-Gallone [6,7] point is reached near rhodium. For elements lighter than rhodium, the saddle-point shapes are unstable against asymmetric distortions, with the result that at the Businaro-Gallone point Nix [7] predicts the fragment mass distribution to be infinitely broad. For fissioning systems such as ours, which are close to, but above, the Businaro-Gallone point, Nix predicts the mass distributions to be relatively broad, and the fragment total kinetic energy distributions to be relatively narrow. One of the purposes of this work is to check these liquid drop model predictions.

Earlier work in which heavy-ion-induced fission of silver was studied includes the glass-plate track detector experiment of Obukhov et al. [8] and the fragment energy and velocity measurements of Cabot [9]. Obukhov et al. have measured fission cross-sections from ^{20}Ne bombardments of silver at 168, 183 and 198 MeV. Unfortunately, their fragment detection technique was such that fragments with kinetic energies below an undefined limit did not register in the glass plates, and the cross-sections of reference [8] must, therefore, be regarded as lower limits. Cabot [9] has studied the fission of silver induced by 126 MeV ^{14}N ions. In this case, the angular momentum effects are relatively small, resulting in a low fission probability; consequently Cabot measured only about 400 fission events. She was, however, able to deduce crude mass and total kinetic energy distributions from her data.

Heavy-ion-induced fission of nuclei heavier than silver but lighter than gold has been studied by a number of authors [1,2,10,11]. Sikkeland and co-workers [2,11] have measured a large number of fission excitation functions for targets in the rare earth region and for projectiles ranging from ^{11}B to ^{22}Ne. The lightest system studied by Sikkeland was $Cs + ^{16}O$ [2]. Plasil, Burnett, Britt and Thompson [10] have measured fragment mass and total kinetic energy distributions for systems as light as $^{170}Er + ^{16}O$. Thus our investigation of fission from the $^{107}Ag + ^{20}Ne$ reaction extends both fission cross-section and mass distribution measurements to a region of nuclei that are considerably lighter than those studied previously. Our results consist of a fragment angular correlation measurement at 165.6 MeV bombarding energy, the fission excitation function from 110.4 MeV to 165.6 MeV, and a mass-total-kinetic-energy distribution at 165.6 MeV.

II. ANGULAR CORRELATION

The first part of our study consists of a measurement of the fragment angular correlation. Such measurements have been discussed fully by Sikkeland, Hanies and Viola, [12] and by Viola et al. [13]. The measurement makes use of two silicon surface-barrier detectors with small geometry. One detector (detector 1) is kept at a fixed laboratory angle relative to the beam axis, while the angle of the other detector (detector 2) is varied. The coincidence counting rate between fragments in the two detectors is measured

relative to the number of incident beam particles. In our experiment, we have followed the lead of Viola et al. [13] and have used a position-sensitive detector for detector 2. Thus it was not necessary to change the angle of detector 2, and the in-plane angular correlation was obtained in a single measurement.

The angular correlation data provides information on the forward linear momentum transfer from the projectile to the composite nucleus of target and projectile. Thus, for a given mass split and for given fragment kinetic energies in the center of mass system, it is possible to calculate the relationship between the two fragment angles in the laboratory system [14], based on the assumption of full momentum transfer. If the predicted angular correlation is observed, then it can be taken as evidence that fission was preceded by full momentum transfer. Should there be a component of fission following incomplete momentum transfer present, it would cause a tail in the angular correlation towards higher angles of detector 2 [12,13].

A. Experimental Details

A beam of 165.6 MeV $^{20}Ne^{6+}$ ions from the Oak Ridge Isochronous Cyclotron (ORIC) was incident on a self-supported ^{107}Ag target of about 200 μgm cm^{-2} thickness, oriented at 90° to the beam axis and located at the center of a scattering chamber. The beam collimation arrangement was such that the width of the beam incident on the target was approximately 2 mm. This was confirmed by examining a very faint burn pattern on the upstream side of the target at the termination of the experiment. Beam levels were held at about 30 nA, as measured with a Faraday cup at the exit of the chamber. Detector 1 was a silicon surface-barrier detector of the heavy-ion type (ORTEC). It was collimated by an aperture of 4 mm located at 7.64 cm from the center of the target. Detector 2 was a position-sensitive detector (ORTEC). It was located at 8 cm from the target and was collimated by a plate with 5 slits. Each slit was 0.14 cm wide and about 0.4 cm high. The spacing of the slits was 0.7 cm, on centers. Thus each slit subtended 1.0° at the center of the target, and detector 1 subtended 2.9°. Detector 1 was placed at an angle $\psi_1 = 60°$ to the beam axis, and the slits of detector 2 were located at angles ψ_2 ranging from 55° to 75°.

Four correlated parameters were recorded for each coincidence event. These were the energies of the two fragments, the position in detector 2 and the time difference between the two fragments. The data were sorted on a computer to yield, for each slit in detector 2, an array whose coordinates were the pulse heights in detectors 1 and 2. This array is related to an energy of fragment 1 vs. energy of fragment 2 array, and it was used to separate true fission events from other events and from accidental coincidences. The separation between the different types of events was found to be good.

B. Results and Discussion

The in-plane angular correlation obtained is shown in Fig. 1. About 1000 events were measured. The vertical error bars are due to statistical errors. The horizontal error bars take into account not only the finite apertures of the detectors, but also the finite effective target size. It was found that the data could easily be fitted with a symmetric Gaussian distribution of 10.9° FWHM. The position of the correlation peak at $\psi_2 = 62°$ (for a fixed angle of detector 1, $\psi_1 = 60°$) is consistent with full momentum transfer from the projectile to the fissioning system, for a symmetric mass split and for a center-of-mass total fragment kinetic energy E_K of 90 MeV. It will be shown in section IV that the mass distribution is indeed peaked at symmetric mass divisions, and that $\langle E_K \rangle$ is close to 90 MeV.

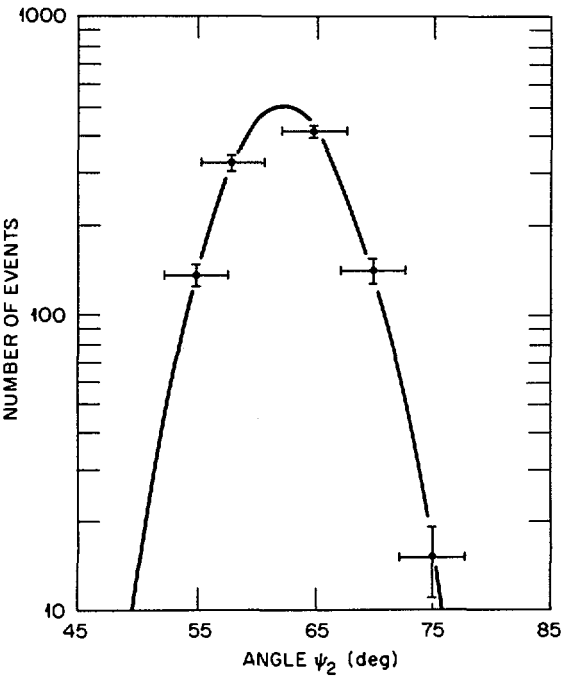

FIG. 1. Fission fragment angular correlation with angle of detector 1, ψ_1, fixed at 60° relative to the beam axis. ψ_2 is the angle of the various slits in the position-sensitive detector 2.

From the symmetric nature of the angular correlation, we conclude that there is not a large contribution present from fission following incomplete momentum transfer. This result is expected if all fission observed follows compound nucleus formation, as is likely to be the case. The width of the angular correlation, the position of its peak, the clean separation of fission events from other events, all seem to indicate that ^{20}Ne-induced fission of ^{107}Ag is a well-behaved process with few surprises, and that the observed fragments are due to the binary fission of the ^{127}La compound nucleus.

III. FISSION EXCITATION FUNCTION

The usual purpose in measuring a fission excitation function is to extract from the results a value for the fission barrier B_f of the fissioning nucleus [2,11]. This was also our goal, but as it turned out, it was not possible to obtain an unambiguous value of B_f for ^{127}La from our data. Furthermore, as a result of our analysis, we seriously question the validity of previous attempts [2,11] to extract B_f values from heavy-ion fission data.

Early analyses of heavy-ion fission excitation functions [2] involved the fitting at various bombarding energies of theoretical Γ_f/Γ_n ratios to σ_f/σ_{CN} ratios, where Γ_f and Γ_n are the fission and neutron widths, σ_f is the measured fission cross-section, and σ_{CN} is the calculated compound nucleus cross-section. This fitting was accomplished by means of adjusting various

parameters in the Γ_f/Γ_n expression, such as B_f and the level density parameters for fission and neutron emission, a_f and a_n. In reference 2 the Γ_f/Γ_n fits were made only for an average value of angular momentum. In a later paper [11] Sikkeland et al. have made fits of average values of Γ_f/Γ_n, where Γ_f/Γ_n was evaluated separately for each partial wave, and then averaged over the angular momentum distribution. Both in reference 2 and in reference 11, the angular momentum effects on the fission barrier were treated only approximately, by subtracting estimated rotational energies in the Γ_f and Γ_n expressions. These rotational energies were obtained from the moments of inertia of non-rotating (undeformed) ground and saddle-point shapes. Furthermore, in these analyses, the calculated compound nucleus cross-section σ_{CN} was obtained by assuming that it was some fraction of a calculated total reaction cross-section σ_R, and that the ratio σ_{CN}/σ_R was a function only of the projectile, and was independent of the target and of the bombarding energy. This assumption, which is inconsistent with recent measurements [5,15], can lead to particularly serious errors in the determination of B_f values, as we shall show.

In our analysis we have calculated σ_f values by the method of Blann and Plasil [4,16]. This method makes use of the variation of the fission barrier with angular momentum as given by the rotating liquid drop model [3] and allows for multiple-chance fission (i.e., fission following particle evaporation) and for competition from neutron, proton, and alpha particle emission. The fission cross-section is evaluated for each partial wave (i.e., for each integral value of the angular momentum J) and a final fission cross-section is obtained by summing over all J values. We will not describe these σ_f calculations here. A brief description can be found in reference 4, and a more detailed description will be available in the future [16].

A. Experimental Method

A $^{20}Ne^{6+}$ beam from ORIC was incident on a thin deposit (about 200 μg cm^{-2}) of ^{107}Ag on a 30 $\mu g\ cm^{-2}$ carbon backing. The deposit was a 1 mm by 3 mm rectangle, and the target was oriented perpendicular to the beam axis. Two silicon surface-barrier detectors were used to detect coincident fission fragments. At a bombarding energy E_L = 165.6 MeV, both detectors were placed at 61.5° relative to the beam axis. For other bombarding energies, the detector angles were calculated as indicated in reference 14. For the lowest energy studied, E_L = 110.4 MeV, $\psi_1 = \psi_2 = 66.2°$. Detector 1 was collimated with a 1.8 cm diameter aperture at 7.65 cm from target center and detector 2 was also collimated with a 1.8 cm diameter collimator, but was placed at 3.15 cm from the target. From our angular correlation (Section II) we estimate that, with this geometric arrangement, essentially all partners of fragments detected in detector 1 registered in detector 2.

The number of beam particles incident on the ^{107}Ag target was monitored by detecting elastically scattered ^{20}Ne particles in a monitor detector located at an angle of about 12.5° with respect to the beam. The effective aperture of the monitor detector was 0.2 cm by 0.04 cm, and it was located at a distance of 18.1 cm from the target center. The monitor detector's counting rate at each bombarding energy was corrected for the change of the Rutherford scattering cross-section with E_L. For the purpose of obtaining absolute fission cross-sections, Rutherford scattering of ^{20}Ne ions from the target was measured with fission detector 1 at 15° and 20° relative to the beam axis. For this purpose, detector 1 was collimated with an aperture of 0.4 cm diameter, but its distance remained fixed at 7.65 cm.

The ^{20}Ne energy was varied by means of insertion of aluminum foils into the beam ahead of the target. The beam energy was thus decreased, and the energy resolution was also decreased through straggling. The monitor detector provided a convenient means by which to measure the beam energy and

determine straggling effects. It was found that the undegraded elastic ^{20}Ne peak in the monitor detector had a FWHM of $\sim$ 1 MeV, while at our lowest degraded energy (110.4 MeV) the scattering peak had a FWHM of 2.3 MeV.

For each fission event, three correlated parameters were recorded on magnetic tape. These were the pulse heights X_1 and X_2, related to the kinetic energies of the fragments, and the difference in time between the detection of two fragments. Number-of-events $N(X_1,X_2)$ arrays were constructed for events falling within a specific window in the time parameter. True fission events were identified by inspection of the $N(X_1,X_2)$ arrays. There was little ambiguity in attributing events to fission or to other categories.

The fission cross-section σ_f at any particular bombarding energy E_L was obtained from our data as follows: The differential cross-section for fission at the laboratory angle ψ_1, was obtained from

$$\left(\frac{d\sigma_f}{d\Omega}\right)_{lab,\psi_1} = \frac{N_F\ N_{MR}\ G}{N_R\ N_{MF}} \left(\frac{d\sigma_{el}}{d\Omega}\right)_{lab,\psi_R}$$

where N_F is the number of fission events in a run in which N_{MF} monitor events were detected; N_R is the number of Rutherford scattered ^{20}Ne ions observed in detector 1 at a laboratory angle of ψ_R; N_{MR} is the number of monitor events observed during the Rutherford scattering run; and G is the factor by which the geometry of detector 1 was changed from the fission runs to the Rutherford scattering run. The differential Rutherford scattering cross-section in the laboratory system, $\left(\frac{d\sigma_{el}}{d\Omega}\right)_{lab,\psi_R}$ can be calculated easily. The differential fission cross-section in the center-of-mass system was obtained from

$$\left(\frac{d\sigma_f}{d\Omega}\right)_{cm,\theta_1} = \left(\frac{d\sigma_f}{d\Omega}\right)_{lab,\psi_1} \frac{\sin^2 \psi_1}{\sin^2 \theta_1} \cos\ (\theta_1 - \psi_1)$$

In our symmetric arrangement, $\theta_1 = 90^o$. The integrated cross-section was obtained from

$$\sigma_f = \pi \int_o^\pi \left(\frac{d\sigma_f}{d\Omega}\right)_{cm,\theta_1} \sin\ \theta\ d\theta$$

To perform this integration, the fragment angular distribution should be known. It was unfortunately, not possible to measure it due to problems associated with making measurements close to the beam axis. It is known, however, that fragment angular distributions from heavy-ion-induced fission follow a $1/\sin\ \theta$ function up to about $\psi_1 = 15^o$ [2]. If the $1/\sin\ \theta$ distribution were to hold at all angles, the above integral would be equal to π. Sikkeland [2] estimates that the integral is equal to $k\pi$, where k varies linearly from 0.95 at a bombarding energy of 208 MeV to 0.85 at 120 MeV. We have chosen to use this estimate. The final expression for σ_f is, therefore,

$$\sigma_f = k\pi^2 \frac{N_F\ N_{MR}\ G}{N_R\ N_{MF}} \frac{\sin^2 \psi_1\ \cos(\theta_1 - \psi_1)}{\sin\ \theta_1} \left(\frac{d\sigma_{el}}{d\Omega}\right)_{lab,\psi_R}$$

B. Results and Discussion

The excitation function was measured from E_L = 110.4 to E_L = 165.6 MeV. The results are shown in Fig. 2. On an absolute scale, we estimate that our errors from all possible sources may be as high as ± 20%. On a relative scale, however, the accuracy is considerably better, probably in the region of 5%. Our measured fission cross-section of 73.3 mb at 165.6 MeV can be compared with the result of Obukhov et al. [8] of 43.4 mb at 168 MeV. Considering the fact that the method of Obukhov et al. involved a low-energy detection cutoff and that their value is claimed to be a lower limit, the agreement between the two results is reasonable.

As was discussed earlier, we have attempted to fit our experimental excitation function with calculated σ_f values from a model that includes the variation of B_f with angular momentum, allows for multiple-chance fission, and includes competition from charged particle emission [4,16] in the de-excitation process. The calculation is an equilibrium model calculation,

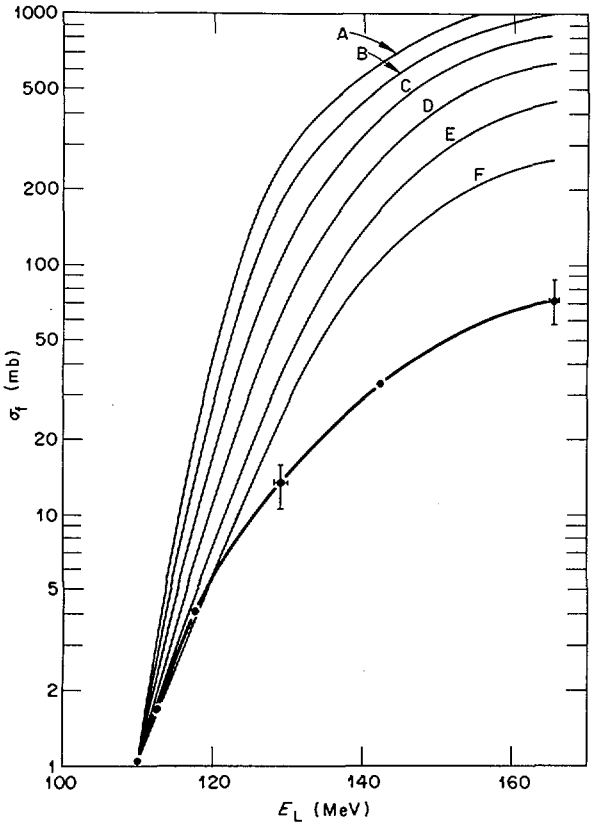

FIG.2. Measured fission excitation function (filled circles and heavy solid line), and attempted theoretical fits (light solid lines). The parameters for the curves are as follows: B_f/B_f^{LD} = 1.1, 1.0, 0.9, 0.8, 0.7 and 0.6 and a_f/a_n = 1.315, 1.220, 1.135, 1.060, 0.990 and 0.920 for curves A, B, C, D, E and F respectively.

predicting the decay modes of the compound nucleus. It is performed for each partial wave populating the compound nucleus. Partial-wave total reaction cross-sections were computed in the optical model, using Thomas' parabolic potential approximation [17] with parameters from reference 17. The two adjustable parameters in the σ_f calculation were the fission barrier B_f, and the ratio of the level density parameters for fission and particle (neutron, proton and alpha) emission, a_f/a_n. The variation of B_f was accomplished by setting $B_f = f\, B_f^{LD}$, where B_f^{LD} is the fission barrier from the rotating liquid drop model [3] and f is a scaling factor. Thus the functional variation of the barrier with angular momentum remains as prescribed by the liquid drop model, but the absolute magnitude can be adjusted. Since the calculation is sensitive to a_f/a_n but insensitive to the absolute values of the level density parameters, a_n was kept fixed at 15.9 MeV^{-1}.

Our initial fitting attempts were based on the assumption that at all bombarding energies the compound-nucleus cross-section σ_{CN} is equal to the total reaction cross-section σ_R, as calculated from the optical model. With this assumption, it was not possible to fit the experimental data. This point is illustrated in Fig. 2 where several attempted fits are shown. All calculated excitation functions were constrained to pass through the experimental point at the lowest bombarding energy. The combination of parameters ranged from $B_f = 1.1\, B_f^{LD}$, $a_f/a_n = 1.315$ for curve A, to $B_f = 0.6\, B_f^{LD}$, $a_f/a_n = 0.92$ for curve F. It is clear that none of the fits is adequate.

In an attempt to examine the effects of the $\sigma_{CN} = \sigma_R$ assumption, we have performed the following calculation. We have assumed that at our lowest E_L (110.4 MeV), σ_{CN} remains equal to σ_R. By fitting our calculated σ_f to this lowest energy point, we obtained a set of B_f and a_f/a_n values (identical to those given in Fig. 2). At each higher energy, we have assumed that the highest partial waves lead to incomplete fusion and that compound nucleus formation takes place only up to some value of angular momentum J_C. The value of J_C was obtained from our calculation as follows. For a particular combination of B_f and a_f/a_n and at a particular bombarding energy, the fission cross-section $\sigma_{f,J}$ was calculated for each partial wave; J_C was then obtained from $\sum_{J=0}^{J_C} \sigma_{f,J} = \sigma_f$, where σ_f is the measured fission cross-section at that bombarding energy.

This procedure is illustrated for a particular case in Fig. 3. Here the heavy solid line gives the calculated total reaction cross-section and the lighter solid curve, continued by a dashed curve, gives the calculated fission cross-section. The location of J_C was obtained by making the shaded area equal to the measured fission cross-section. The assumption is that the compound nucleus cross-section is given by the area of the triangle to the left of the vertical J_C line (i.e., $\sigma_{CN} = \sum_{J=0}^{J_C} \sigma_{R,J}$) and that for $J > J_C$ compound nucleus formation does not take place, and fission is thus not observed.

In this procedure, the calculated fission cross-section is forced to reproduce the experimental measurements, and the ratio σ_{CN}/σ_R is deduced from the calculation. A plot of this ratio for two sets of B_f and a_f/a_n values is shown in Fig. 4. As was pointed out, the ratio is arbitrarily set equal to 1 at 110.4 MeV. Curves of the type shown in Fig. 4 can also be obtained for other sets of B_f and a_f/a_n values. Also shown in Fig. 4 is the result from a track-detector complete-fusion measurement of Natowitz [5]. It can be seen that this experimental result is consistent with the curve for $B_f = B_f^{LD}$ and $a_f/a_n = 1.22$. Thus a consistent picture can be obtained if a liquid drop fission barrier is used in the calculation and if the ratio

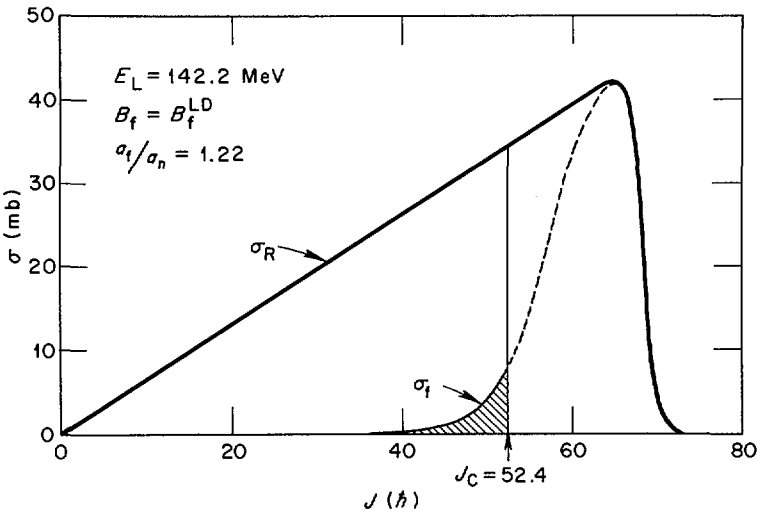

FIG. 3. Illustration of method of excitation function analysis. σ_R is the calculated total reaction cross-section (heavy solid line). σ_f is the calculated fission cross-section (light solid line, changing to dashed line). Location of angular momentum limit J_C is such that the shaded area is equal to the measured fission cross-section. Compound nucleus formation is expected to take place only for $J < J_C$.

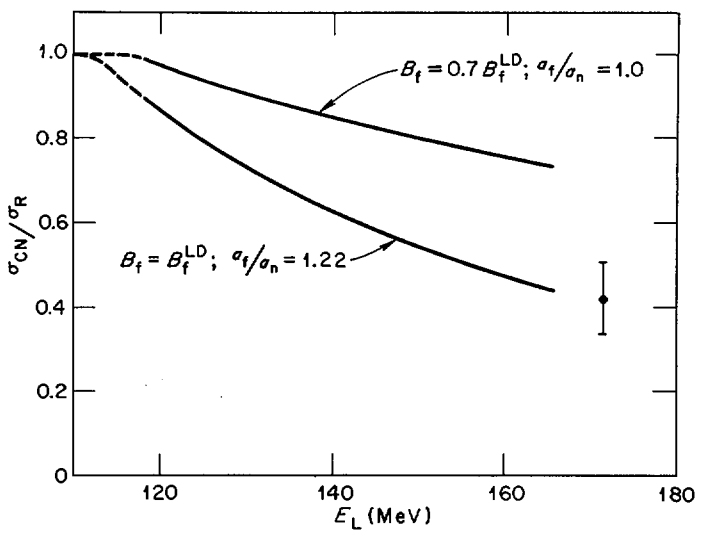

FIG. 4. Calculated ratio of compound nucleus cross-section to total reaction cross-section for two sets of B_f and a_f/a_n values as a function of bombarding energy. Both curves were arbitrarily required to pass through $\sigma_{CN}/\sigma_R = 1$ at E_L = 110.4 MeV. The dashed portions of the curves represent extrapolations. The filled circle is a complete-fusion measurement of Natowitz [5].

TABLE I. Parameters from Analysis of Excitation Function

B_f (units of B_f^{LD})	a_f/a_n	E_L (MeV)	σ_f (mb)	σ_{CN} (mb)	σ_R (mb)	σ_{CN}/σ_R	J_C ($\hbar$)
1.0	1.22	117.7	4.08	1107	1230	0.90	52
		129.0	13.2	1031	1390	0.74	52
		142.2	33.3	927	1541	0.60	52
		165.6	73.3	761	1739	0.44	51
0.7	1.0	117.7	4.08	1222	1230	0.99	55
		129.0	13.2	1275	1390	0.92	58
		142.2	33.3	1294	1540	0.84	62
		165.6	73.3	1271	1739	0.73	66

B_f is the fission barrier in units of the liquid drop barrier B_f^{LD}, a_f/a_n is the ratio of the level density parameters for fission and for particle (neutron, proton, alpha) emission, E_L is the laboratory bombarding energy, σ_f is the measured fission cross-section, σ_{CN} is the compound nucleus cross-section as obtained from the analysis described in section III B, σ_R is the calculated total reaction cross-section and J_C is the angular momentum limit discussed in the text.

a_f/a_n assumes a reasonable value, when compared with a_f/a_n values from the analysis of fission induced by light particles [18] (where σ_{CN} is expected to equal σ_R). Values of σ_f, σ_{CN}, σ_R and J_C at several bombarding energies, for the two cases shown in Fig. 4, are given in Table I. One interesting feature in the table is that while J_C, as a function of bombarding energy, varies from 55 $\hbar$ to 66 $\hbar$ for $B_f = 0.7\ B_f^{LD}$ and $a_f/a_n = 1.0$, it remains at a constant value of about 52 $\hbar$ for the B_f^{LD} and $a_f/a_n = 1.22$ case.

In conclusion, we wish to point out that we were not able to extract an unambiguous value for the fission barrier of our compound nucleus ^{127}La. This could presumably be done if a complete-fusion excitation function were available. We hope to undertake such measurements in the future. It is worthwhile to point out that all earlier extractions of B_f values from heavy-ion fission data did not consider the possibility of the σ_{CN}/σ_R ratio changing with bombarding energy. This may be the reason why Sikkeland et al. [2,11] were able to fit only the steep parts of their excitation functions. Our conclusion is that the assumption of a fixed σ_{CN}/σ_R ratio makes the barriers obtained in references 2 and 11 unreliable. While we believe that the σ_{CN}/σ_R effect is likely to be an important one in heavy-ion-induced fission, we do not rule out the possibility that other contributing effects, such as effective changes in the a_f/a_n ratio with increasing excitation energy [19], may also play an important role.

IV. MASS AND TOTAL KINETIC ENERGY DISTRIBUTIONS

To explore in greater detail the fission characteristics of the ^{127}La compound nucleus, we have measured the fragment mass and total kinetic distribution at a bombarding energy of 165.6 MeV. As was stated in the introduction, our primary motivation was to compare the widths of our distribution with those predicted by the liquid drop model [7]. Apart from this specific purpose, however, these distributions were of general interest, since the lightest system for which published results were available was ^{186}Os [10].

A. Experimental Details

A beam of $^{20}Ne^{6+}$ ions from ORIC was incident on a thin self-supported ^{107}Ag target, oriented at 90° to the beam, and located at the center of a scattering chamber. Detector 1 was collimated with a 0.4 cm aperture, and located at 7.64 cm from the target center and at an angle of 60° with respect to the beam axis. Detector 2 was collimated with a 1.8 cm diameter aperture. It was located at 6.4 cm from the target and at 62° to the beam axis. Thus detectors 1 and 2 subtended angles of 3° and 16° respectively, at the target center. From our angular correlation measurement we have concluded that, with this geometric arrangement, complementary fragments of more than 77% of all fission events incident on detector 1 were detected by detector 2. Both detectors were silicon surface-barrier detectors of the heavy-ion type (ORTEC). Permanent magnets, placed in front of the collimator of detector 2, prevented the detection of stray electrons. Beam levels were held to below 60 nA charge current to minimize pileup effects. The stability of the electronic system and pileup effects were monitored with a precision pulse generator. Pulser events were recorded together with fission events, and the data were later corrected on a computer for small electronic drift.

Correlated pulse heights related to fragment energies were recorded event-by-event on a magnetic tape and processed as described earlier [14]. The calculated fragment masses obtained from the data are very close to pre-neutron-emission masses [14,20]. The target thickness was measured with ^{252}Cf fragments and was found to be 115 $\mu g\ cm^{-2}$. A standard target thickness correction was applied to the data [14]. The detectors were calibrated with a ^{252}Cf source, and the calibration constants of Schmitt et al. [21] were

used. We have also used the recently developed calibration method of Kaufman et al. [22], and found that in the region of mass and energy in which we were working (mass $\approx$ 64 amu, energy $\approx$ 45 MeV), the two calibration methods give similar results. For example, the average fragment total kinetic energy was 86.9 MeV according to the calibration method of Schmitt et al. and 89.8 MeV according to the method of Kaufman et al. The results presented below were obtained by the calibration method of reference 21.

B. Results and Discussion

Approximately 6600 events were measured. The mass distribution was found to be peaked at symmetric mass divisions, and the overall average fragment total kinetic energy $\langle E_K \rangle$ was found to be 86.9 ± 2 MeV. This energy can be compared with predictions from the systematics of Viola [23]. Reference 23 gives two sets of predictions: an empirical relationship given by $E_K = 0.1071\ Z^2/A^{1/3} + 22.2$ and a semi-empirical relationship given by $E_K = 0.1240\ Z^2/A^{1/3}$. For our system, E_K values predicted by the two relationships are 91.4 MeV and 80.1 MeV respectively. Our measured average value, uncorrected for neutron emission, happens to fall between the two predictions. We have corrected our value of $\langle E_K \rangle$ for neutron emission as described in [24] to give $\langle E_K \rangle$ = 91.3 MeV. The agreement between this corrected value and Viola's empirical prediction is extraordinarily good, particularly when we consider that most of the data on which the Viola relationship is based are at E_K > 150 MeV.

In Fig. 5 the mass vs. total kinetic energy distribution is shown. The kinetic energies are not corrected for neutron emission from the fragments. The general features of the distribution are similar to those found in earlier heavy-ion-induced fission measurements [10]. The mass distribution is shown in Fig. 6, together with the average total kinetic energy (uncorrected for neutron emission) as a function of mass. While the contours in Fig. 5 have been smoothed and symmetrized, the mass distribution in Fig. 6 has not, and its symmetry is to some extent a measure of the quality of the data.

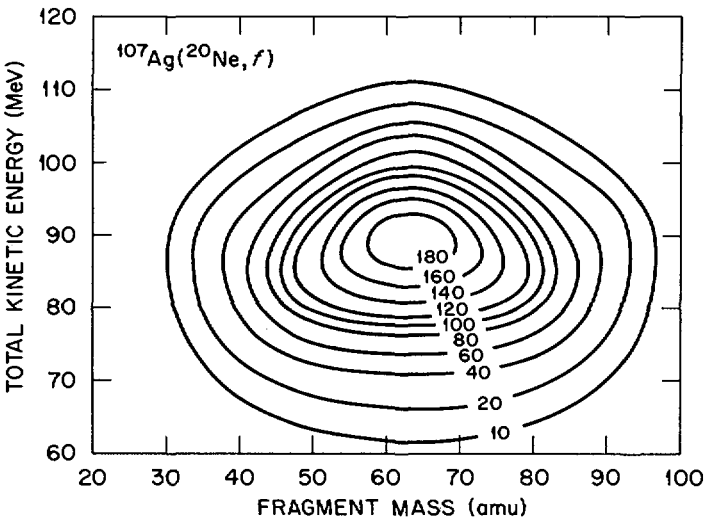

FIG. 5. Fragment mass versus total kinetic energy contour diagram. The labels on the contours refer to numbers of events in regions of 5 MeV by 5 amu. The data were symmetrized and smoothed. The total kinetic energies have not been corrected for neutron emission from the fragments.

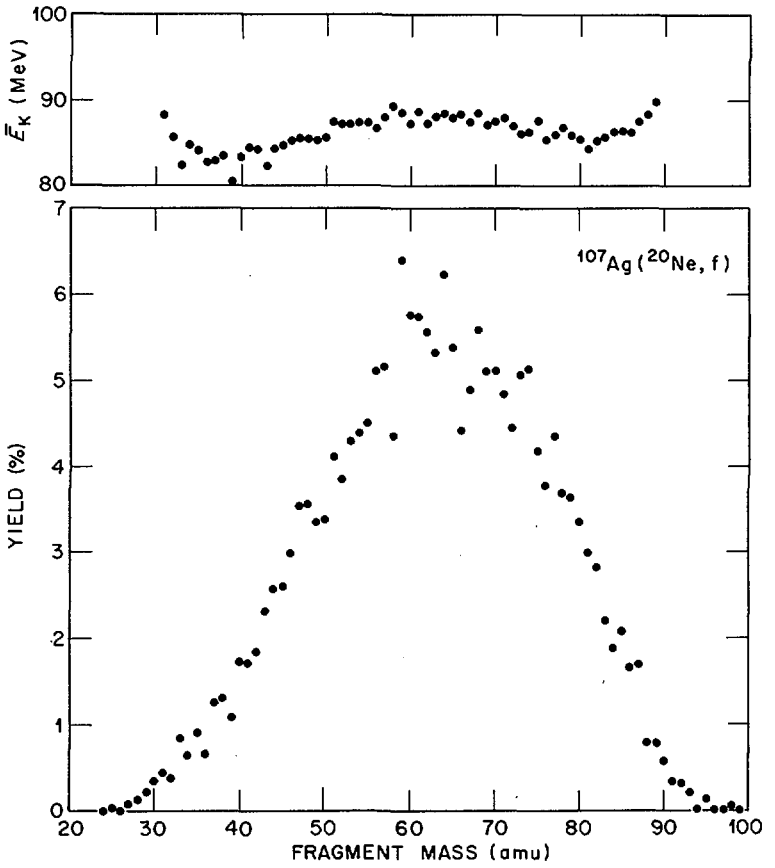

FIG. 6. Fragment mass distribution and fragment average total kinetic energy as a function of mass. The kinetic energies have not been corrected for neutron emission from the fragments.

To compare the widths of the mass and total kinetic energy distributions with Nix's [7] predictions, it was necessary to calculate the nuclear temperature θ at the saddle point. This was accomplished by means of the relationship $E_x^{SP} = a\,\theta^2 - \theta$, where E_x^{SP} is the excitation energy at the saddle and where a, the level density parameter, was taken to be 15.9 MeV^{-1}. It is probable that most observed fission events are due to the fission of compound nuclei with angular momenta approximately equal to 51 $\hbar$ (see Section III, Table I and Fig. 3). Thus, E_x^{SP}, which is a function of angular momentum J, was evaluated at J = 51 $\hbar$. The nuclear temperature obtained in this manner was 2.16 MeV. Using this value, we obtain from reference 7 the prediction that our mass distribution should have a FWHM of 38.2 amu, and that the total kinetic energy distribution should have a FWHM of 14.2 MeV. Our measured widths were found to be 36.4 amu FWHM (13.16 rms width) for the mass distribution and 22.5 MeV FWHM (9.60 rms width) for the total kinetic energy distribution. The agreement between experiment and theory is excellent in the case of the mass distribution, but not very good in the case of the total kinetic energy distribution.

V. CONCLUSION

From our measurements we conclude that the characteristics of ^{20}Ne-induced fission of ^{107}Ag are consistent with the expected fission properties of the compound nucleus ^{127}La. The measured fragment kinetic energy and mass distributions are in reasonable agreement with theoretical liquid-drop-model predictions, and the average total kinetic energy agrees with the value expected from fission systematics. Analysis of the fission excitation function indicates, in agreement with a complete-fusion measurement [5], that a large fraction of the total reaction cross-section does not involve compound nucleus formation, and does not contribute to the fission cross-section. It was not possible to extract a value for the fission barrier of ^{127}La, but the data are consistent with liquid-drop-model fission barriers. The liquid-drop-model value of B_f for ^{127}La at zero angular momentum is 40.3 MeV [25].

REFERENCES

[1] GILMORE, J., THOMPSON, S. G., PERLMAN, I., Phys. Rev. 128 (1962) 2276.

[2] SIKKELAND, T., Phys. Rev. 135 (1964) B669.

[3] COHEN, S., PLASIL, F., SWIATECKI, W. J., Lawrence Berkeley Laboratory Report LBL 1502 (1972), to be published in Annals of Physics.

[4] BLANN, M., PLASIL, F., Phys. Rev. Lett. 29 (1972) 303.

[5] NATOWITZ, J. B., Phys. Rev. C 1 (1970) 623.

[6] BUSINARO, U. L., GALLONE, S., Nuovo Cimento 5 (1957) 315.

[7] NIX, J. R., Nucl. Phys. A130 (1969) 241.

[8] OBUKHOV, A. I., PERFILOV, N. A., SHIGAEV, O. E., and TKACHENKO, E. G., Sov. Journal of Nucl. Phys. 11 (1970) 543, translated from Yad. Fiz. 11 (1970) 977.

[9] CABOT, C., Doctoral Thesis, Orsay, France (1972) unpublished.

[10] PLASIL, F., BURNETT, D. S., BRITT, H. C., THOMPSON, S. G., Phys. Rev. 142 (1966) 696.

[11] SIKKELAND, T., CLARKSON, J. E., STEIGER-SHAFRIR, N. H., VIOLA Jr., V. E., Phys. Rev. C 3 (1971) 329.

[12] SIKKELAND, T., HAINES, E. L., VIOLA Jr., V. E., Phys. Rev. 125 (1962) 1350.

[13] VIOLA Jr., V. E., MINOR, M. M., SALWIN, A. E., BONDELID, R. O., THEUS, R. B., Nucl. Phys. A174 (1971) 321.

[14] PLASIL, F., FERGUSON, R. L., PLEASONTON, F., SCHMITT, H. W., Phys. Rev. C 7 (1973) 1186.

[15] ZEBELMAN, A. M., MILLER, J. M., Phys. Rev. Lett. 30 (1973) 27.

[16] BLANN, M., PLASIL, F., to be published.

[17] THOMAS, T. D., Phys. Rev. 116 (1959) 703.

[18] BURNETT, D. S., GATTI, R. C., PLASIL, F., PRICE, B. P., SWIATECKI, W. J., THOMPSON, S. G., Phys. Rev. 134 (1964) B952.

[19] MORETTO, L. G., THOMPSON, S. G., ROUTTI, J., GATTI, R. C., Phys. Lett. 38B (1972) 471.

[20] SCHMITT, H. W., NEILER, J. H., WALTER, F. J., Phys. Rev. 141 (1966) 1146.

[21] SCHMITT, H. W., KIKER, W. E., WILLIAMS, C. W., Phys. Rev. 137 (1965) B837.

[22] KAUFMAN, S. B., STEINBERG, E. P., WILKINS, B. D., UNIK, J., GORSKI, A. J., FLUSS, M. J., (1973) Argonne preprint.

[23] VIOLA Jr., V. E., Nucl. Data 1 (1966) 391.

[24] FERGUSON, R. L., PLASIL, F., FREIESLEBEN, H., BEMIS Jr., C. E., SCHMITT, H. W., Phys. Rev. (in press).

[25] MYERS, W. D., SWIATECKI, W. J., Ark. Fys. 36 (1967) 343.

DISCUSSION

V.E. VIOLA: With regard to your observation concerning the inaccuracy of the earlier fission barriers measured in heavy-ion reactions, I believe we used a value of σ_{CN}/σ_R of 0.5 for neon-induced reactions, which is in good agreement with the Natowitz value. However, there were definite energy uncertainties at low bombarding energies in the measurement of our σ_f excitation functions and I would agree that an energy-dependent σ_{CN}/σ_R function should have been used. Hence there is need for re-analysis and/or re-measurement of these data.

F. PLASIL: I agree with your comment. Actually the value of σ_{CN}/σ_R used by Sikkeland and co-workers was 0.6 for ^{22}Ne, but the main problem was that this fraction was assumed to be independent of bombarding energy, which is almost certainly wrong.

B. TAMAIN: I should like to make a comment on your results for the widths of the kinetic energy and mass distributions. You mention that they are in good agreement with the Nix calculations and I mentioned in my paper that we are in disagreement with them. In fact, as I have also mentioned, this disagreement does not exist for low-mass compound nuclei. More precisely, for the system Ar + Mo we obtain the same results as you and it is only when fissility is high that there is a significant difference between theory and experiment.

I should also like to comment on the results you presented for critical angular momentum. In your first set of results, the critical angular momentum is independent of the beam energy, while in the second it is an increasing function of energy. The results we have obtained at Orsay in fission and transfer reaction experiments show clearly that the critical angular momentum is an increasing function of mass and projectile energy.

F. PLASIL: As I mentioned, the two sets of parameters used, and hence the two sets of critical angular momenta, are largely arbitrary. We favour slightly the constant value of critical angular momentum because in that case the ratio σ_{CF}/σ_R seems to agree with Natowitz's measurement, and also the fission σ_{CN} barrier is equal to the liquid drop fission barrier.

H.C. BRITT: I would only comment that the $1/\sin\theta$ angular distribution is the classical high angular momentum limit. Information on the moments of inertia comes mainly from deviations from the $1/\sin\theta$ behaviour and so far we have been unable to get to small enough angles to observe significant deviations.

THE ANGULAR MOMENTUM DEPENDENCE OF THE FISSION PROBABILITY OF ^{170}Yb COMPOUND NUCLEI AT AN EXCITATION OF 107 MeV*

A.M. ZEBELMAN, K. BEG, Y. EYAL, G. JAFFE, D. LOGAN, J. MILLER, A. KANDIL, L. KOWALSKI
Department of Chemistry,
Columbia University,
New York, N.Y.,
United States of America

Abstract

THE ANGULAR MOMENTUM DEPENDENCE OF THE FISSION PROBABILITY OF ^{170}Yb COMPOUND NUCLEI AT AN EXCITATION OF 107 MeV.

Fission and complete-fusion cross-sections are presented for four entrance channels leading to ^{170}Yb compound nuclei excited to 107 MeV: ^{11}B+ ^{159}Tb, ^{12}C+ ^{158}Gd, ^{16}O+ ^{154}Sm, and ^{20}Ne+ ^{150}Nd. The measured fission cross-sections are 5.9 ± 0.6 mb, 16.0 ± 2.0 mb, 40.0 ± 4.0 mb, and 89.0 ± 9.0 mb for the ^{11}B, ^{12}C, ^{16}O, and ^{20}Ne entrance channels, respectively. The complete-fusion cross-sections for these same entrance channels are 980.0 ± 150 mb, 1100 ± 160.0 mb, 1260.0 ± 190.0 mb, and 1450.0 ± 220.0 mb. The data are combined using a technique which yields the dependence of fission probability over three relatively narrow ranges of angular momentum.

The results of the analysis just described are compared to a theoretical calculation based on the Bohr-Wheeler formalism for fission widths and the Weisskopf formalism for neutron and charged particle widths. The calculations include the effects of multiple chance fission but assume that second and higher chance fission is non-negligible only if preceded by s-wave neutron emission rather than charged particle emission. Good agreement between the experimental results and the theoretical calculations is found for a ratio of level density parameters for the saddle point and the compound nucleus equal to 1.2 ± 0.1.

1. INTRODUCTION

Among the interesting questions that have evolved in the study of fission is that of the angular momentum dependence of the fission probability. The estimation of fission probabilities was first formulated by Bohr and Wheeler within the framework of the statistical model using liquid drop model fission barriers [1]. As energetic particle beams, especially of heavy ions, became available, the effects of angular momentum on the fission process had to be explicitly taken into account. Studies by Pik-Pichak [2,3], Hiskes [4], and Plasil [5] were concerned with the effect of angular momentum on the fission barrier. More recently, Gadioli and co-workers [6] have modified the angular-momentum-independent calculations of Burnett and co-workers [7] to include the effects of angular momentum in the calculations of fission probabilities.

The present work focuses on an experimental determination of the dependence of fission probability on angular momentum and a comparison of the results with current theoretical predictions. The compound nucleus

* Work supported by the US Atomic Energy Commission.

TABLE I. ENTRANCE CHANNEL SPECIFICATIONS

Entrance channel	Laboratory energy (MeV)	Excitation energy (MeV)	Fission targets		Complete-fusion targets	
			Thickness (mg/cm^2)	Abundance (%)	Thickness (mg/cm^2)	Abundance (%)
$^{11}B + ^{159}Tb$	115	107	1.58	0.99	0.162	0.99
$^{12}C + ^{158}Gd$	126	107	1.00	0.98	1.00	0.98
$^{16}O + ^{154}Sm$	137	107	0.87	0.99	0.87	0.99
$^{20}Ne + ^{150}Nd$	144	107	1.01	0.95	0.216	0.99

chosen for study was ^{170}Yb. A relatively light system was selected in order that the angular momentum dependence of the fission probability not be masked by a fission probability close to unity. The production of ^{170}Yb via a heavy-ion entrance channel is indicated in order to produce compound nuclei with significant amounts of angular momentum.

Bombardments with heavy ions produce compound nuclei with a broad distribution of angular momenta. The large range of this distribution makes the average angular momentum a quantity of uncertain value in data analysis. However, a method of analysis, to be outlined later, has been developed which allows the calculation of partial cross-sections for events arising from compound nuclei characterized by a relatively narrow range of angular momenta [8, 9]. Characterizing these relatively narrow angular momentum distributions by their average, now more sharply defined, in principle allows the more accurate determination of the angular momentum dependence of the phenomena (in this case fissionability) under study. The method of analysis requires data obtained from a number of different entrance channels forming the same compound nucleus at the same excitation energy, but which differ in their angular momentum distributions. The calculation of fission probability and its dependence on angular momentum from the experimental results requires the measurement of both the fission and complete-fusion cross-sections for the entrance channels concerned.

The reactions which formed the entrance channels of ^{170}Yb in this work are:

$$^{11}B + ^{159}Tb$$

$$^{12}C + ^{158}Gd$$

$$^{16}O + ^{154}Sm$$

$$^{20}Ne + ^{150}Nd$$

The beam energies, included in Table I, were chosen so as to produce the same excitation energy of 107 MeV in all of the channels.

2. EXPERIMENTAL METHOD

The heavy ion bombardments were carried out at the Yale University Heavy Ion Accelerator.

Self-supporting and isotopically enriched targets of ^{158}Gd, ^{154}Sm, and ^{150}Nd were obtained from Oak Ridge National Laboratory. The ^{159}Tb target, an isotope whose natural abundance is 100%, was prepared by evaporation of the metal on to a carbon film of about 40 $\mu g/cm^2$. In the same manner, targets for the complete-fusion measurement in the ^{11}B and ^{20}Ne entrance channels were prepared from the metals of naturally occurring isotopic abundance.

Both solid state detectors and mica detectors were used in the fission cross-section measurements. The solid state detectors consisted of a 9-μm detector upstream of a 3-mm detector. A very thin upstream detector was chosen because scattered beam and other particles whose masses are small compared to those of fission fragments deposit little energy in such a detector. Fission fragments, on the other hand, deposit all or most of their energy in a 9-μm detector.

Mica detectors were also used to measure fission cross-sections. Each piece of mica was etched in 48% hydrofluoric acid for 3 h prior to exposure. Following a bombardment, the mica detectors were again etched in 48% hydrofluoric acid for 30 min at room temperature and then scanned under a microscope. The fission cross-sections determined with the solid state detectors and the mica detectors were in excellent agreement.

Following the work of Kowalski and co-workers [10] and Natowitz [11], mica track-detectors were used in all of the complete-fusion cross-section measurements. The mica detectors were prepared as described in the previous paragraph, except that they were cleaved prior to their pre-bombardment etching so as to have a surface as free of defects as possible.

3. EXPERIMENTAL RESULTS

The centre-of-mass differential fission cross-sections are shown in Fig. 1. These cross-sections were calculated directly from the measured laboratory cross-sections in the manner described by Sikkeland and co-workers [12]. The fission cross-sections obtained by integrating the angular distributions of Fig. 1 are included in Table II.

The complete-fusion angular distributions are shown in Figs 2 - 5. The complete-fusion cross-sections are given in Table II along with the fission cross-sections.

There are a few features of the complete-fusion angular distributions that merit comment. The first feature is that of the angular spread of the distributions. The data from the ^{12}C and ^{16}O entrance channels exhibit much broader angular distributions than do the data from the ^{11}B and ^{20}Ne entrance channels. This is a direct consequence of the much thicker targets that were used in the collection of the data in the former entrance channels. Referring to Fig. 5, the second feature of interest is the anomalous "bump" at about 15° in the ^{20}Ne complete-fusion angular distribution. The data shown are the results of three separate experiments, two of which yielded data in the region of concern. An estimate of the upper limit of the cross-section for the reactions that give rise to the bump may be made by assuming that all of the differential cross-sections for angles greater than 15° contribute to that cross-section. Under this assumption, the cross-section for those reactions is about 90 mb.

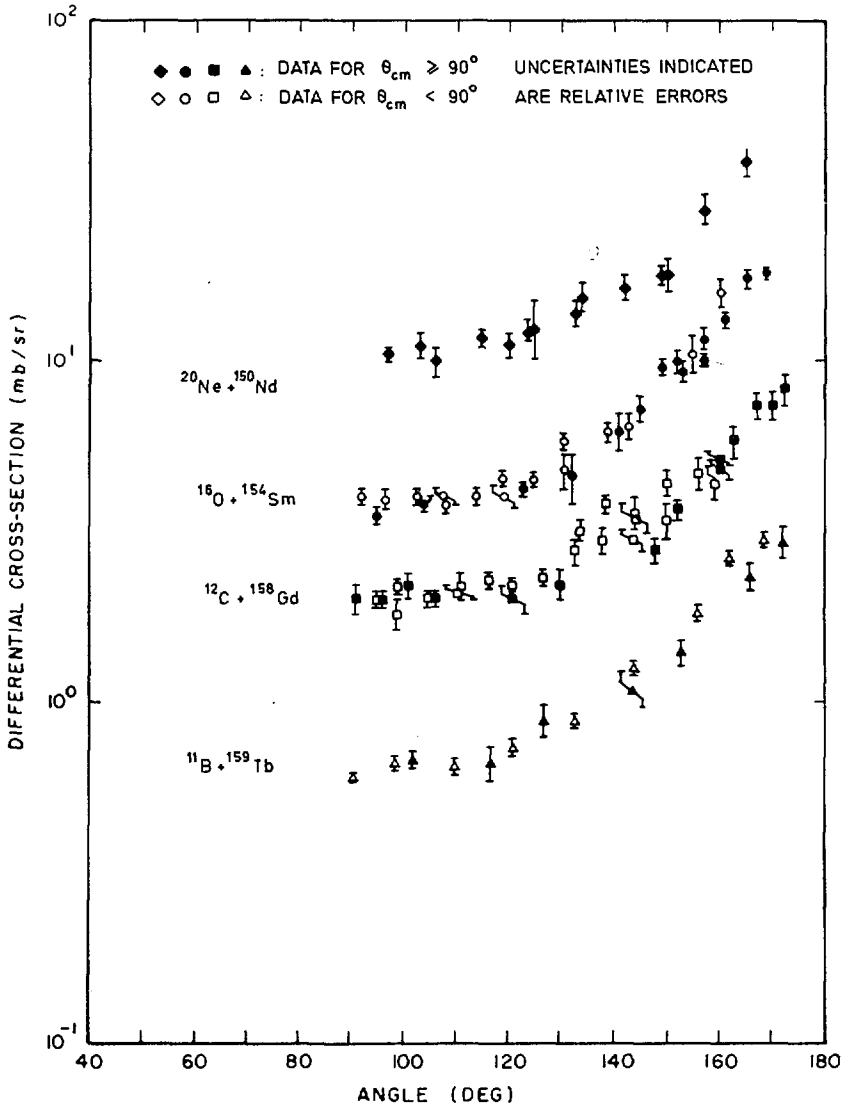

FIG. 1. Centre-of-mass fission fragment angular distributions for the four ^{170}Yb entrance channels studied in this work.

TABLE II. FISSION AND COMPLETE-FUSION CROSS-SECTIONS

Entrance channel	Excitation energy (MeV)	Fission cross-section (mb)	Complete-fusion cross-section (mb)
$^{11}B + ^{159}Tb$	107	5.9 ± 0.6	979 ± 147
$^{12}C + ^{158}Gd$	107	16.0 ± 1.6	1096 ± 164
$^{16}O + ^{154}Sm$	107	40.0 ± 4.0	1262 ± 189
$^{20}Ne + ^{150}Nd$	107	89.0 ± 9.0	1450 ± 220

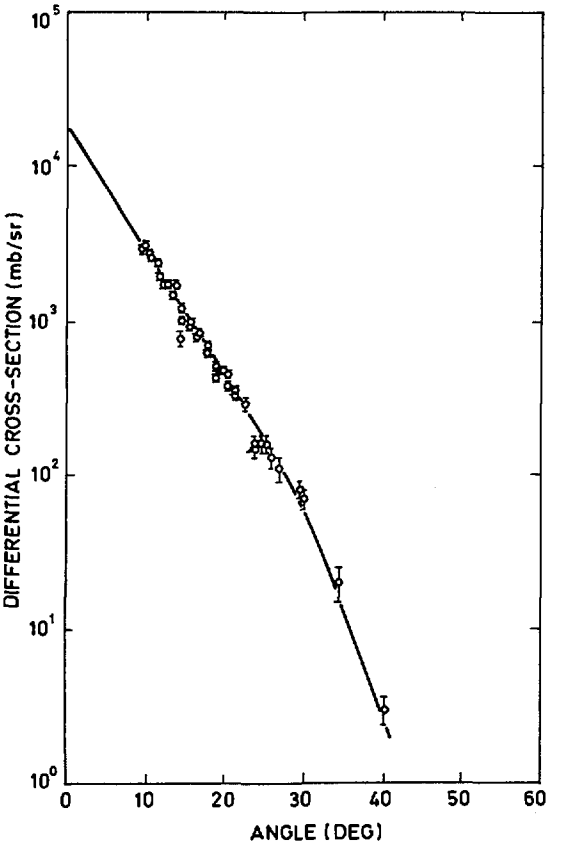

FIG. 2. Complete-fusion angular distribution for 115-MeV $^{11}B + ^{159}Tb$.

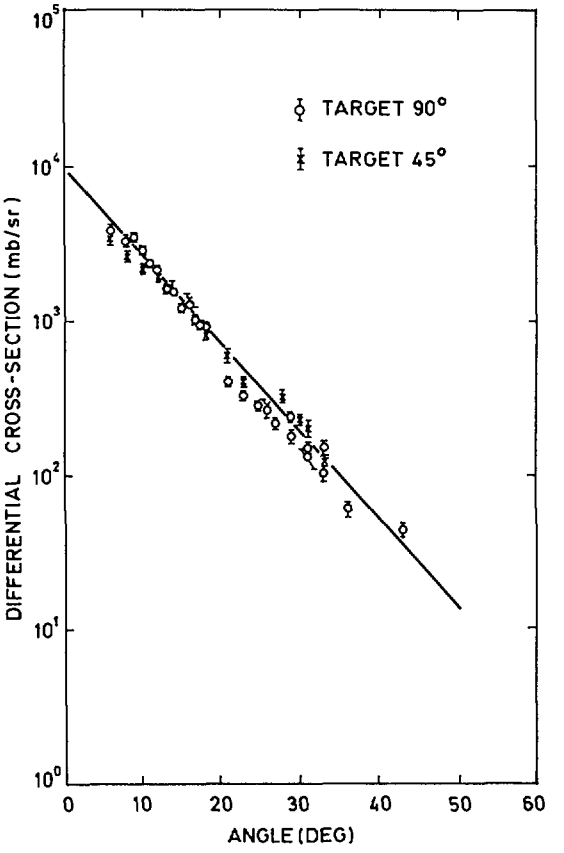

FIG. 3. Complete-fusion angular distribution for 126-MeV $^{12}C + ^{158}Gd$.

The registration of heavy recoil products arising from multinucleon transfer reactions may explain the "bump" in the angular distribution. Kinematic calculations in which it is assumed that the light residual products will have the same MeV/nucleon as the incident ^{20}Ne beam show that reactions which result in the transfer of 10 or more nucleons will give rise to heavy recoils all of which will register in mica. Only a fraction of the reactions corresponding to less than a 10-nucleon transfer will register. For example, the transfer of ^{8}Be to the target nucleus, which results in ^{12}C in the exit channel, will give rise to a heavy residual nucleus with enough energy to register in the mica only when the ^{12}C appears at laboratory angles greater than 30°. An estimate of cross-sections for such multinucleon transfer reactions was made by bombarding the ^{158}Gd target with 144-MeV ^{20}Ne. Unfortunately, at the time of this experiment a Nd target was not available. However, as noted by Croft and co-workers [13],

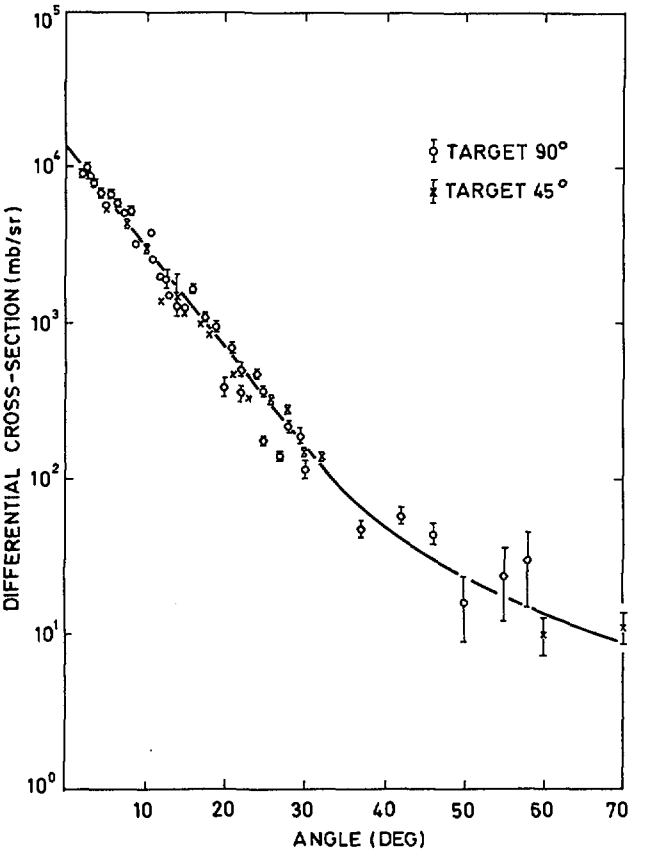

FIG. 4. Complete-fusion angular distribution for 137-MeV $^{16}O + ^{154}Sm$.

transfer cross-sections are not expected to be very sensitive to a small change in the atomic number of the target. The sum of the cross-sections for transfer reactions which result in the formation of Li, Be and B products was found to be 50 ± 10 mb. The cross-section for producing C in the exit channel at laboratory angles ≳ 30° is 42 ± 4 mb out of a total cross-section of 80 ± 8 mb. Thus it is expected that multinucleon transfer reactions will result in the ^{20}Ne complete-fusion cross-section being about 100 mb too large, in good agreement with the magnitude of the cross-section attributed to the "bump".

A question arises now as to the effects of multinucleon transfer reactions in the other entrance channels studied. Kinematic calculations show that as the mass of the incident projectile decreases from ^{20}Ne to ^{11}B there is a corresponding increase in the minimum angle at which a product registering in mica would appear. There is also a corresponding increase in the

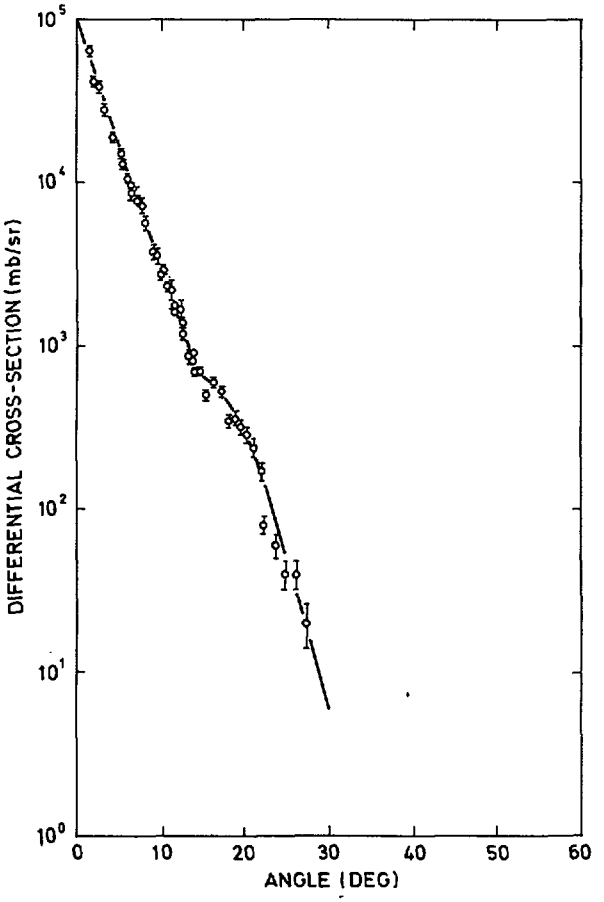

FIG. 5 Complete-fusion angulat distribution for 144-MeV $^{20}Ne+^{150}Nd$.

laboratory angle of its light partner. Differential cross-sections of the light products are well-known to decrease sharply with increasing angle. Thus it is expected that the registration of direct reaction events will make an ever decreasing contribution to the measured complete-fusion cross-section as one goes from ^{20}Ne to ^{11}B.

4. DISCUSSION

The treatment of the experimental data in a manner that yields the angular momentum dependence of fissionability is discussed in the following paragraphs. The results are then compared with conventional calculations of this quantity.

4.1. Data analysis

The probability that a compound nucleus formed via an entrance channel x with a given initial excitation energy will undergo fission at some point in its de-excitation is just

$$\sigma_f(x)/\sigma_{CF}(x) \tag{1}$$

where σ_f is the cross-section for compound nuclear fission and σ_{CF} is the complete-fusion cross-section. To extract the angular momentum dependence of the fission probability from the experimental cross-sections, one may exploit the Bohr independence hypothesis. According to the Bohr hypothesis, the compound nucleus fission cross-section for a particular entrance channel, x, may be written:

$$\sigma_f(x) = \sum_{J=0}^{\infty} \sigma_{CF}(x|J)\, W_f(J) \tag{2}$$

where $\sigma_{CF}(x|J)$ is the cross-section for the formation of the compound nucleus characterized by a given excitation energy and by a given angular momentum, J, in the entrance channel x; $W_f(J)$ is the probability that the compound nucleus with the given angular momentum and excitation energy will fission. The independence hypothesis demands that $W_f(J)$ be purely a property of the compound nucleus and thus is independent of its mode of formation.

The complete-fusion cross-section for total angular momentum J may be written as

$$\sigma_{CF}(x|J) = \pi \lambda\!\!\!^{-2}_x \frac{(2J+1)}{(2s+1)(2j+1)} \sum_{S=|j-s|}^{j+s} \sum_{\ell=|J-S|}^{J+S} T^1_\ell(x) \tag{3}$$

where s and j are the projectile and target spins, respectively; S is the channel spin; and $T^1_\ell(x)$ is the transmission coefficient for compound nucleus formation in entrance channel x. When s and j are zero or are small compared to the maximum value of ℓ, Eq.(3) reduces to

$$\sigma_{CF}(x|J) = \pi \lambda\!\!\!^{-2}_x (2J+1)\, T^1_J(x) \tag{4}$$

Substituting Eq.(4) in Eq.(2), we find

$$\sigma_f(x) = \pi \lambda\!\!\!^{-2}_x \sum_{J=0}^{\infty} (2J+1)\, T^1_J(x)\, W_f(J) \tag{5}$$

From Eq.(4), the complete-fusion cross-section is

$$\sigma_{CF}(x) = \pi \lambda\!\!\!^{-2}_x \sum_{J=0}^{\infty} (2J+1)\, T^1_J(x) \tag{6}$$

If the ratio of Eq.(5) to Eq.(6) is taken according to the prescription of Eq.(1), the expected result is obtained that the ratio of the fission to the complete-fusion cross-sections is just $W_f(J)$ averaged over the entire spin distribution of entrance channel x

$$\sigma_f(x)/\sigma_{CF}(x) = \sum_{J=0}^{\infty}(2J+1)\,T_J'(x)\,W_f(J)\Big/\sum_{J=0}^{\infty}(2J+1)\,T_J'(x)$$
$$\equiv \langle W_f(J)\rangle_x \qquad (7)$$

As shown in Refs [8,9], when data are available from a number of corresponding entrance channels that lead to compound nuclei of the same Z, A and excitation energy, further use of the Bohr independence hypothesis allows the isolation and study of the behaviour of compound nuclei having a range of angular momentum which is much narrower than the spin distribution in any one of the particular entrance channels. To see this, consider equations analogous to Eqs (5) and (6) for another corresponding entrance channel, y

$$\sigma_f(y) = \pi\lambda\!\!\!^{-2}_y \sum_{J=0}^{\infty}(2J+1)\,T_J'(y)\,W_f(J) \qquad (8)$$

and

$$\sigma_{CF}(y) = \pi\lambda\!\!\!^{-2}_y \sum_{J=0}^{\infty}(2J+1)\,T_J'(y) \qquad (9)$$

If Eqs (5), (6), (8), and (9) are divided by their respective values of $\pi\lambda\!\!\!^{-2}$ (from this point on, any cross-section, σ, divided by $\pi\lambda\!\!\!^{-2}$ for the corresponding entrance channel will be denoted by σ', i.e. $\sigma' \equiv \sigma/\pi\lambda\!\!\!^{-2}$) and differences taken between Eqs (5) and (8) as well as between Eqs (6) and (9), there results

$$\sigma_f(x)/\pi\lambda\!\!\!^{-2}_x - \sigma_f(y)/\pi\lambda\!\!\!^{-2}_y \equiv \sigma_f'(x-y) = \sum_{J=0}^{\infty}(2J+1)\,W_f(J)[T_J'(x) - T_J'(y)] \qquad (10)$$

$$\sigma_{CF}(x)/\pi\lambda\!\!\!^{-2}_x - \sigma_{CF}(y)/\pi\lambda\!\!\!^{-2}_y \equiv \sigma_{CF}'(x-y) = \sum_{J=0}^{\infty}(2J+1)[T_J'(x) - T_J'(y)] \qquad (11)$$

There are two central points that are to be noted:

(a) It is the independence hypothesis that allows the factoring of $W_f(J)$ in Eq.(10).
(b) The quantities $\sigma_f'(x-y)$ and $\sigma_{CF}'(x-y)$ represent cross-sections for compound nuclei within the relatively narrow range of J for which $[T_J'(x) - T_J'(y)] \neq 0$.

If now the ratio of Eq.(10) to Eq.(11) is taken,

$$\frac{\sigma_f'(x-y)}{\sigma_{CF}'(x-y)} = \frac{\sum_{J=0}^{\infty}(2J+1)\,W_f(J)[T_J'(x)-T_J'(y)]}{\sum_{J=0}^{\infty}(2J+1)[T_J'(x)-T_J'(y)]} \equiv \langle W_f(J)\rangle_{x-y} \qquad (12)$$

the result is the average fission probability over the region of J for which $[T_J'(x)-T_J'(y)] \neq 0$.

In the present experiment it is possible to identify three such regions: ^{12}C-^{11}B, ^{16}O-^{12}C, and ^{20}Ne-^{16}O, which we shall denote as regions I, II, and III, respectively. Thus, for example

$$\frac{\sigma_f'(II)}{\sigma_{CF}'(II)} = \frac{\sigma_f'(^{16}O)-\sigma_f'(^{12}C)}{\sigma_{CF}'(^{16}O)-\sigma_{CF}'(^{12}C)} \equiv \langle W_f(J)\rangle_{II} \qquad (13)$$

The values of $\langle W_f(J)\rangle_x$ for each of the entrance channels as well as the $\langle W_f(J)\rangle_{I\text{-}III}$ for each narrow region are presented in Table III. It should be emphasized that these values are obtained directly from the experimental data with no intervening theoretical approximations other than the assumption of the independence hypothesis. To know the regions of angular momentum (also given in Table III) over which they are the average, though, it is necessary to make theoretical estimates of the $T_J(x)$ and $T_J'(x)$.

TABLE III. COMPARISON OF EXPERIMENTAL AND THEORETICAL FISSION PROBABILITIES

Errors indicated on $\langle W_f(J)\rangle_{theoret.}$ are due to the uncertainty in J_{CRIT}

Region	J_{CRIT} (ħ)	J range (ħ)	$\langle W_f(J)\rangle_{exper.}$	$\langle W_f(J)\rangle_{theoret.}$
^{11}B	40 ± 3	0 - 40	0.006 ± 0.001	$0.006^{+0.001}_{-0.001}$
^{12}C	46 ± 4	0 - 46	0.015 ± 0.003	$0.011^{+0.003}_{-0.004}$
^{16}O	58 ± 4	0 - 58	0.032 ± 0.006	$0.038^{+0.012}_{-0.018}$
^{20}Ne	70 ± 6	0 - 70	0.060 ± 0.01	$0.14^{+0.16}_{-0.08}$
I		41 - 46	0.04 ± 0.03	$0.017^{+0.003}_{-0.001}$
II		47 - 58	0.06 ± 0.03	$0.066^{+0.001}_{-0.02}$
III		59 - 70	0.12 ± 0.07	$0.34^{+0.3}_{-0.07}$

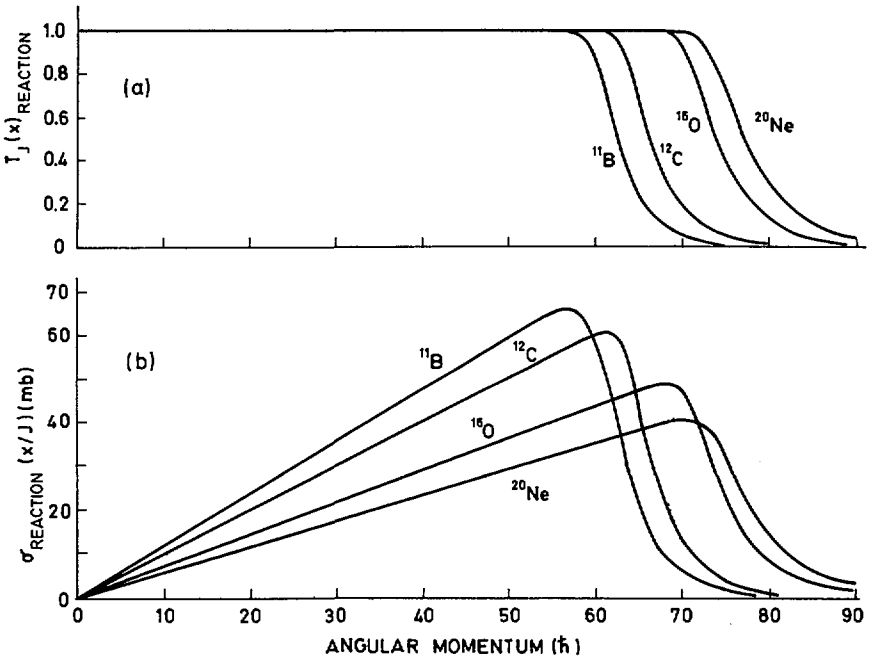

FIG. 6(a) Optical model transmission coefficients for 115-MeV $^{11}B + ^{159}Tb$, 126-MeV $^{12}C + ^{158}Gd$, 137-MeV $^{16}O + ^{154}Sm$, and 144-MeV $^{20}Ne + ^{150}Nd$; (b) optical model partial reactions for the above entrance channels.

4.2. Estimate of T_J and T_J'

The transmission coefficients, $T_J(x)$, as distinct from $T_J'(x)$, may be calculated within the framework of the optical model. This was done using the optical model code ABACUS-2 [14] with parameters from Auerbach and Porter [15]. The resulting transmission coefficients and partial cross-sections characterizing the total reaction cross-sections for the ^{11}B, ^{12}C, ^{16}O, and ^{20}Ne entrance channels are shown in Figs 6a and 6b, respectively. The fact that these are transmission coefficients and partial cross-sections for the total reaction cross-section means that $T_J'(x)$ and $\sigma_{CF}(x|J)$ are but a subset of them. Thus one must appeal to another model to separate the transmission coefficients and the partial cross-sections for complete fusion from the larger set characterizing the total reaction cross-sections. The model generally chosen to accomplish this is the sharp-cutoff model. According to this model, the set of partial cross-sections for complete fusion in a particular entrance channel may be found by summing from $J = 0$ the partial cross-sections calculated with the optical model until the sum of the partial cross-sections most closely equals the experimentally measured complete-fusion cross-section. The largest value of J which contributes to the complete-fusion cross-section is termed J_{CRIT}. All the transmission coefficients and partial cross-sections corresponding to J

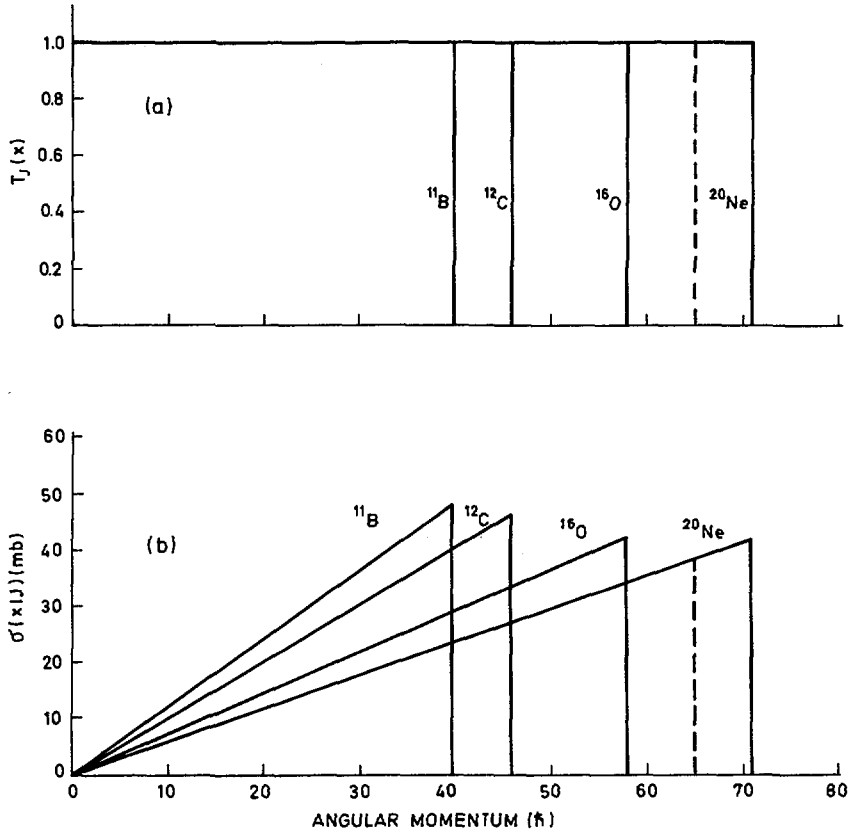

FIG. 7(a) Sharp-cutoff-model complete-fusion transmission coefficients; (b) sharp-cutoff-model complete-fusion partial cross-sections.

values in excess of J_{CRIT} are taken to refer to the incomplete fusion or direct reaction cross-section. In general, there is a different J_{CRIT} for each entrance channel. The values of J_{CRIT} for the entrance channels measured here are included in Table III. The $T_J'(x)$ and $\sigma_{CF}(x|J)$ distributions determined with the optical model but modified by the sharp-cutoff approximation are shown in Fig. 7.

Some justification for the sharp-cutoff model arises from studies of direct reactions which show that these reactions are evidently nuclear-surface reactions [16]. In other words, direct reactions are characterized by relatively large impact parameters and concomitantly large values of angular momentum. A sharp-cutoff is made at J_{CRIT} since the paucity of data concerning the angular momentum dependence of direct reactions does not at this time justify a more refined approximation.

4.3. Calculation of $W_f(J)$ from the statistical model

Having made an estimate of the regions of J over which the $\langle W_f(J) \rangle$ were measured, it is now of interest to compare these values with those that result from conventional statistical theory. In particular, it is of interest to see if the rather strong dependence of fission probability on J can be reproduced.

At high excitation energies fission may occur at any one of several points in the decay of the initial compound nucleus. In general, then, one must deal with the possibility of fission occurring from a spectrum of residual nuclei characterized by a spectrum of excitation energies and angular momenta. To make the fission probability calculations tractable, a number of assumptions are made: (1) Competition between fission and neutron, proton, or alpha-particle emission is allowed at each step. Competition with gamma-ray emission is ignored. (2) Residual nuclei which arise as a result of proton or alpha-particle emission are assumed to have a negligible chance of fissioning. (3) Evaporated neutrons are assumed to carry off no angular momentum; the angular momentum distribution which characterized the initial compound nuclei also characterizes the nuclei resulting from neutron evaporation.

In accordance with the above assumptions, the fission probability depends on the quantities $\Gamma_f(J)$, $\Gamma_n(j)$, $\Gamma_\alpha(J)$, and $\Gamma_p(J)$ which are the angular-momentum and excitation-energy dependent widths for fission, neutron, alpha, and proton emission, respectively, along the decay chain. For ease of later reference, let us define

$$\Gamma_T(J) = \Gamma_n(J) + \Gamma_p(J) + \Gamma_\alpha(J) \tag{14}$$

The calculation of $W_f(J)$ proceeds as follows: (1) $\Gamma_f(J)$ and $\Gamma_T(J)$ are calculated for the initial compound nucleus ^{169}Yb excited to 107 MeV. (2) The spectrum of residual excitation energies for ^{169}Yb is determined from an evaporation calculation, this spectrum of energies is then used in the calculation $\Gamma_f(J)$ and $\Gamma_T(J)$ for ^{169}Yb. As noted above, the spin distribution which characterized ^{170}Yb is assumed to characterize the residual nucleus also. (3) Steps analogous to (2) are repeated until further steps would have a negligible effect.

The quantity $\Gamma_T(J)$ was calculated using a conventional angular-momentum-dependent evaporation code called Evamco [17].

The calculation of the fission width is based on the formalism developed by Bohr and Wheeler [1]. As shown in Ref. [6] the fission width for a particular value of J, including the effects of barrier penetrability is

$$\Gamma_f(J) = \frac{1}{2\pi\,\rho(E,J)} \int_0^E d\epsilon \, \frac{\rho^*(\epsilon, J)}{1 + \exp[-2\pi(E - B_f - \epsilon)/\hbar\omega]} \tag{15}$$

where ϵ is the energy in the non-fission degrees of freedom. The energy ϵ is related to E, B_f (the fission barrier), and T (kinetic energy in the fission degree of freedom) by

$$\epsilon = E - B_f - T \tag{16}$$

The form of the spin-dependent level densities used in Eq.(15) was the same as that used in the $\Gamma_T(J)$ calculation. With the expressions for $\Gamma_f(J)$ and $\Gamma_T(J)$ in hand, one may now proceed to compute $\langle W_f(J)\rangle_x$ and $\langle W_f(J)\rangle_{I\text{-}III}$.

The theoretical expression for $\langle W_f(J)\rangle$ involves a large number of parameters. These include the fission barrier, B_f; the moments of inertia for the saddle shape and the compound nucleus; the pairing corrections to the excitation energy for the compound nucleus and the saddle configuration; the value of $\hbar\omega$; and the level density parameter, a, for the saddle point and the compound nucleus. Further, there are different values of these parameters for each residual nucleus in the decay chain of the original ^{170}Yb compound nucleus. As one could no doubt fit almost any data by freely varying the values of this large number of parameters, we chose to fix the values of all but one of the parameters to those that have been fairly well established in the literature. The only parameters that were varied to bring calculated values to within the uncertainties in the experimental data were the saddle point level density parameter and the compound nucleus level density parameter. The values of these as well as the other parameters will now be discussed.

The fission barriers used in the calculation of Γ_f are the semi-empirical barriers of Myers and Swiatecki [18,19]. The barriers are calculated from experimental ground state masses and saddle point masses obtained from a semi-empirical mass equation which includes corrections for shell and pairing effects. The fission barriers for the nuclei of concern in the study are given in Table IV.

The saddle point moments of inertia are taken from the work of Cohn and Swiatecki [20]. Spherical rigid body moments of inertia are used for the compound nuclei.

Odd-even effects in the level density are corrected for by using the values of Δ_p and Δ_n given by Gilbert and Cameron [21].

The value of 1 MeV is chosen for $\hbar\omega$ in the fission width calculations [7]. The calculations were found to be insensitive to reasonable variations of this parameter.

The level density parameter, a, appears in the level density expression for both the fission width and the particle widths. It was found, however, that the calculated fission width essentially depended only upon the ratio

TABLE IV. SEMI-EMPIRICAL FISSION BARRIERS OF MYERS AND SWIATECKI[a]

Nucleus	Barrier (MeV)
^{170}Yb	30.6
^{169}Yb	30.5
^{168}Yb	29.5
^{167}Yb	29.5

[a] Ground state masses taken from tabulated values of GARVEY, G.T., et al., Rev. Mod. Phys. 41 (1969) 51.

of the level density parameter for the saddle point configuration to that for the compound nucleus, a_s/a_{cn}, rather than on their absolute values. Thus this ratio was taken as the only free parameter in the calculation.

The results of the fissionability calculations are given in Table III along with the experimental values of $\langle W_f(J) \rangle$. The value of a_s/a_{cn} is found to be 1.22 when it is required that the calculated value of $\langle W_f(J) \rangle_{11_B}$ reproduce the experimentally determined value of 0.006. From Table III it may be seen that there is reasonable agreement between experiment and theory.

5. SUMMARY AND CONCLUSIONS

The experimental data, quite apart from any parameter-dependent theory, clearly demonstrate that fissionability is an increasing function of angular momentum for the ^{170}Yb compound nucleus with 107-MeV excitation energy. The fact that the excitation energies were matched in the four entrance channels studied avoided the complications introduced by the energy dependence of fissionability and allowed the isolation of the behaviour of compound nuclei characterized by a relatively narrow range of angular momenta.

The theoretical calculations of fission probability have reproduced rather well the qualitative and quantitative experimental results with a reasonable set of parameters.

REFERENCES

[1] BOHR, N., WHEELER, J.A., Phys. Rev. 56 (1939) 426.
[2] PIK-PICHAK, G.A., Sov. Phys. – JETP 7 (1958) 238.
[3] PIK-PICHAK, G.A., Sov. Phys. – JETP 16 (1963) 1201.
[4] HISKES, J., University of California Radiation Laboratory Rep. UCRL-9275 (1960).
[5] PLASIL, F., Private communication.
[6] GADIOLI, E., IORI, I., MOHLO, N., ZETTA, L., Nucl. Phys. A151 (1970) 16.
[7] BURNETT, D.S., GATTI, R.C., PLASIL, F., PRICE, P.B., SWIATECKI, W.J., THOMPSON, S.G., Phys. Rev. B134 (1964) 952.
[8] REEDY, R.C., FLUSS, M.J., HERZOG, G.F., KOWALSKI, L., MILLER, J.M., Phys. Rev. 188 (1969) 1771.
[9] KOWALSKI, L., ZEBELMAN, A.M., MILLER, J.M., HERZOG, G.F., REEDY, R.C., Phys. Rev. C1 (1969) 259.
[10] KOWALSKI, L., JODOGNE, J.C., MILLER, J.M., Phys. Rev. 169 (1969) 894.
[11] NATOWITZ, J.B., Phys. Rev. C1 (1970) 623.
[12] SIKKELAND, T., LANSK, A., GORDON, G.E., Phys. Rev. 123 (1961) 2112.
[13] CROFT, P., ALEXANDER, J., STREET, K., Phys. Rev. 165 (1967) 1380.
[14] AUERBACH, E.H., ABACUS-2, Brookhaven National Laboratory Rep. 6562 (962).
[15] AUERBACH, E.H., PORTER, E.C., in Proc. 3rd Conf. on Reactions Between Complex Nuclei, University of California Press, Berkeley (1963).
[16] KAUFMAN, R., WOLFGANG, R., Phys. Rev. 121 (1961) 192, 206.
[17] REEDY, R.C., Columbia University Rep. CU-1019-72 (1969).
[18] SWIATECKI, W.J., Proc. Int. Conf. on Nuclear Masses 2 (1963) 58.
[19] MYERS, W.D., SWIATECKI, W.J., Nucl. Phys. 81C (1966) 1.
[20] COHN, S., SWIATECKI, W.J., Ann. Phys. (N.Y.) 22 (1963) 406.
[21] GINDLER, J.E., HUIZENGA, J.R., "Nuclear Fission", in Nuclear Chemistry (YAFFE, L., Ed.), Academic Press, New York (1968).

STUDY OF A FISSION-LIKE ENVIRONMENT IN REACTIONS WITH VERY HEAVY IONS*

L.G. MORETTO, D. HEUNEMANN, R.C. JARED, R.C. GATTI, S.G. THOMPSON
Lawrence Berkeley Laboratory,
University of California,
Berkeley, Calif.,
United States of America

Abstract

STUDY OF A FISSION-LIKE ENVIRONMENT IN REACTIONS WITH VERY HEAVY IONS.

The dynamical aspects of the later stages of fission can be studied in the broader context of those reactions where the collective degrees of freedom play a dominant role. The interaction of large heavy ions with nuclei provides an ideal tool to sample the conditions prevailing in a scission-like environment. For this purpose a program has been started to study the reactions between ^{40}Ar and various targets. Energetic particles produced in these reactions are observed at various angles by means of a counter telescope. The analysis of the data provides the atomic number of the emitted particles, their angular distribution and their kinetic energy distribution. The reactions between ^{40}Ar and both a Cu and a Ag target at 288 MeV bombarding energy show an impressive emission of particles ranging in atomic number from 1 to 25 and above, matched in variety only by the fission process itself. The angular distributions are mostly peaked forward with the exception of the fragments with atomic number close to 18 in the case of the Cu target, for which a cross-section increasing with angle is observed. The Z distribution at various angles suggests that the system is relaxing along the mass asymmetry coordinate. In the case of the Cu target the charge distribution seems to drift toward lower Z while in the case of the Ag target the drift is in the direction of larger Z. This is consistent with the potential energy of two spherical liquid drops in contact and rigidly rotating. The kinetic energy distributions are Gaussian-like and peak at energies close to the Coulomb energies of two touching spheres. Both the charge distributions and the kinetic energy distributions suggest the picture of a very viscous dynamical evolution dominated by the potential energy. This evidence is consistent with the assumption of a *viscous dynamical* process in the latter stages of fission.

1. INTRODUCTION

Most of the progress which has occurred in understanding the fission process over the years is the result of improved knowledge of the potential energy of the system together with the applications of statistical mechanics in suitable critical stages of the reaction. The liquid drop model, corrected for shell effects by means of the Strutinsky procedure, has provided an adequate understanding of the behaviour of the nuclear potential energy as a function of deformation not only in the neighbourhood of the ground state but also at the saddle point deformations. The use of statistical mechanics in describing the random access to the saddle point has provided a quantitative understanding of the fission decay widths and of the fission fragment angular distributions. Finally the de-excitation of the excited fragments in flight is also well understood in terms of the standard statistical theory of evaporation. However, this series of flattering successes is interrupted at a crucial stage of the fission process where the present

* Work performed under the auspices of the US Atomic Energy Commission.

theoretical understanding is unsatisfactory notwithstanding the detailed experimental evidence available. This stage is the descent from saddle to scission. In this region the lack of stationary points in the potential energy makes it necessary to perform dynamical calculations. Two new quantities are required to specify the dynamical evolution of a system: the viscosity tensor and the inertia tensor. Both quantities are very difficult to calculate from the nucleon-nucleon interaction or even empirically and very little experimental information is available. However there is hope that one might be able to decide whether the system behaves more like a viscous or like a non-viscous fluid. In the former case the system is prevented from achieving large velocities and the potential energy dominates the outcome of the reaction. In the latter case the system can achieve large velocities and the inertias dominate the course of the reaction. At first sight one might hope that a simple check on the fission fragment kinetic energies could provide direct information about the viscosity of the saddle to scission descent. To be able to draw any conclusion one must have experimental information on how the total kinetic energy is divided into a pre-scission and a post-scission component. Unfortunately there is almost no experimental information on the subject. Calculations have been performed with various assumptions about the inertias and the viscosity [1 - 4]. However it appears that a definite answer about the viscosity of nuclear matter must depend on experimental data.

The fission kinetic energies provide ambiguous information regarding the viscosity associated with the collective degrees of freedom. However it is possible to visualize a suitable scission-like environment where the same collective degrees of freedom are called into play and where the initial kinetic energy injected into the system can be chosen at will. Such a scission-like environment can be easily obtained in the collision between nuclei and large heavy ions. The non-compound nucleus reactions occurring in these collisions are associated with the production of a large variety of particles and strongly suggest the involvement of collective degrees of freedom [5 - 7].

The two touching nuclei can evolve along many different collective coordinates, like the mass asymmetry, the charge asymmetry and various deformation parameters. This evolution may lead to the formation of the compound nucleus or to the direct re-emission of another fragment. The charges, masses, and the kinetic energies of these fragments emitted in a direct process contain information about the dynamical conditions prevailing in a scission-like environment. In particular one may gather information about the relaxation times associated with the various collective degrees of freedom and about macroscopic quantities such as friction coefficients and viscosity tensors.

In the present paper some preliminary results are presented about the charge distributions, kinetic energy distributions and angular distributions of the fragments emitted in the interaction between Cu and Ag targets with 288-MeV Ar ions.

2. DESCRIPTION OF THE EXPERIMENT

Two different targets, a 1.37-mg/cm^2 Cu target and a 0.9-mg/cm^2 Ag target, have been bombarded with a 288-MeV ^{40}Ar beam provided by the

Berkeley Super-HILAC. The beam is collimated into a 3-mm-diameter spot by means of a set of three carbon collimators. This beam, after passing through the target, is collected using a Faraday cup and integrated to provide the total charge to which the target has been exposed. The particles emitted in the reaction are detected by means of two solid state counter telescopes. The first telescope was composed of a 9.6-μm ΔE detector and of a 380-μm E detector; the second telescope was composed of a 28-μm ΔE detector and of a 380-μm E detector. The thicker ΔE telescope was used to detect lighter particles, the thinner ΔE telescope was used to detect heavier particles. The two telescopes were mounted on movable arms and could be placed at various angles with respect to the beam. A schematic diagram of the electronic equipment is shown in Fig. 1. The pulses coming from the two telescopes are fed to a standard linear and logic circuitry and are finally digitized by an analogue multiplexer and ADC system. The digitized information accompanied by identification markers is fed to the computer event by event, through a CAMAC system, packaged and recorded on magnetic tape. A "busy" signal fed back by the computer is used to turn off a scaler which counts the single events in one of the ΔE counters. At the same time another scaler counts the single events from the same ΔE counter without interruption. The counts from both scalers are used to correct for the dead time.

For monitoring purposes the signals from each telescope are fed to a Landis-Goulding particle identifier which produces a preliminary identification spectrum. The data recorded on magnetic tape are analysed on a 7600 CDC computer. A E-ΔE map is generated and simultaneously a particle identification function (PI) of a standard type is calculated. The adequacy of the particle identification function is checked by means of a PI, E_{Total} map. The kinetic energy distributions associated with each atomic

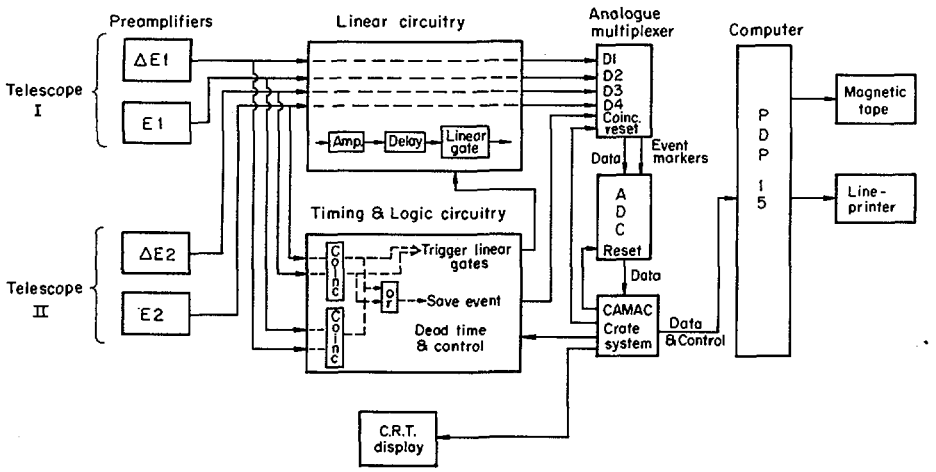

FIG. 1. Schematic diagram of the data collection system.

number are corrected for the target thickness and for the dead layers of the various counters. The integrated counting rate for each atomic number is transformed into cross-section using the known detection efficiency of the telescopes, the total charge collected in the Faraday cup, the mean charge of Ar when entering the Faraday cup and the target thickness.

The effects of possible contaminants (C, O) on the experimental results have been checked by bombarding a 50-$\mu g/cm^2$ C target and by collecting the fragments with the same equipment described above. The amount of C deposited on the targets during the various bombardments has been estimated by visually comparing the target beam spots with a series of targets on which different amounts of C were evaporated. In the case of the Cu targets the C contamination appeared to be $< 3\ \mu g/cm^2$, in the case of the Ag targets the C contamination appeared to be $< 2\ \mu g/cm^2$. Because of the rapid drop of the cross-section for the C target with increasing Z, the contamination effects are more serious at low Z. At $Z = 8$ the C contamination contributes to the cross-section less than 1% in the Cu bombardment and less than 10% in the Ag bombardment. At $Z = 10$ the contribution to the cross-section due to contamination is less than 0.1% in Cu and less than $\sim$ 1% in Ag. At larger Z the corrections are completely negligible.

3. EXPERIMENTAL RESULTS

A very large variety of fragments is produced in the reactions of both targets which have been studied here. Portions of the particle identification spectra for Cu and Ag targets are shown in Fig. 2. More detailed information about the actual range in atomic numbers which has been investigated experimentally can be obtained from the following figures. In the case of Cu the Z range is from $Z = 5$ to $Z = 19$ while in the case of Ag the Z range is from $Z = 5$ to $Z = 25$. The boundaries of these ranges are purely instrumental. It has been ascertained that particles with $Z < 5$ are also abundantly produced and can be easily identified. Particles with $Z > 19$ for Cu and with $Z > 25$ for Ag are also produced. However their identification becomes more difficult and the kinetic energy spectra are substantially cut off on the low-energy side because of the thickness of the ΔE counter.

The cross-sections for the production of fragments with various Z at each angle are shown in Fig. 3. In the case of the Cu target a peak in the cross-section is observed at $Z = 12$ for the 20° and 30° angles, while at the 50° angle the cross-sections increase with some alternation from $Z = 6$ to $Z = 18$.

In the case of the Ag target the cross-sections tend to increase with increasing atomic number both at 30° and at 40°. At the 50° angle the cross-section peaks around $Z = 21$. Even-odd fluctuations can be discerned in some of the distributions. The yield of $F(Z = 9)$ is quite remarkable and is systematically low in all the distributions for both targets.

The angular distributions in the experimental angular range associated with the various atomic numbers are shown in Fig. 4. For the Cu target the angular distributions are strongly peaked forward for the lower atomic numbers. The forward peaking decreases with increasing Z until, for $Z \simeq 15$, the cross-section is approximately equal at all angles. Above $Z = 15$ the cross-section appears to increase at larger angles. On the other hand, for the Ag target, the angular distributions are peaked forward

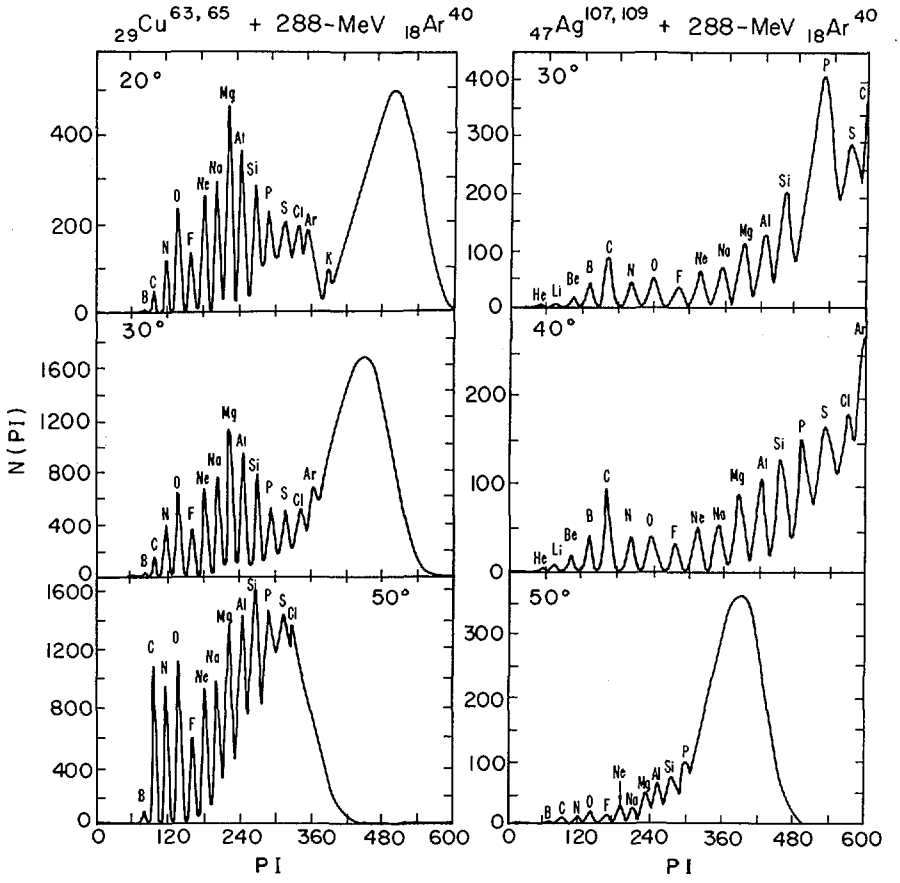

FIG. 2. Examples of particle identification spectra for both Cu and Ag targets at various angles. The ΔE counter thickness is 9.6 μm and the E counter thickness is 380 μm.

for all the atomic numbers. The kinetic energy distributions, corrected for target thickness and for the detector dead layers, appear as broad Gaussian distributions. Some examples of such distributions are shown in Fig. 5. The most probable kinetic energies are presented in Fig. 6. In both cases the most probable kinetic energies for each angle increase with atomic number. Such an increase becomes slower at the highest atomic numbers where in fact a slight decrease begins to appear. The widths of the kinetic energy spectra are very large. The FWHM ranges from ~ 20 MeV at Z = 5 to ~ 45 MeV for Z = 25 for the Ag target and from ~ 30 MeV to ~ 60 MeV for the Cu target.

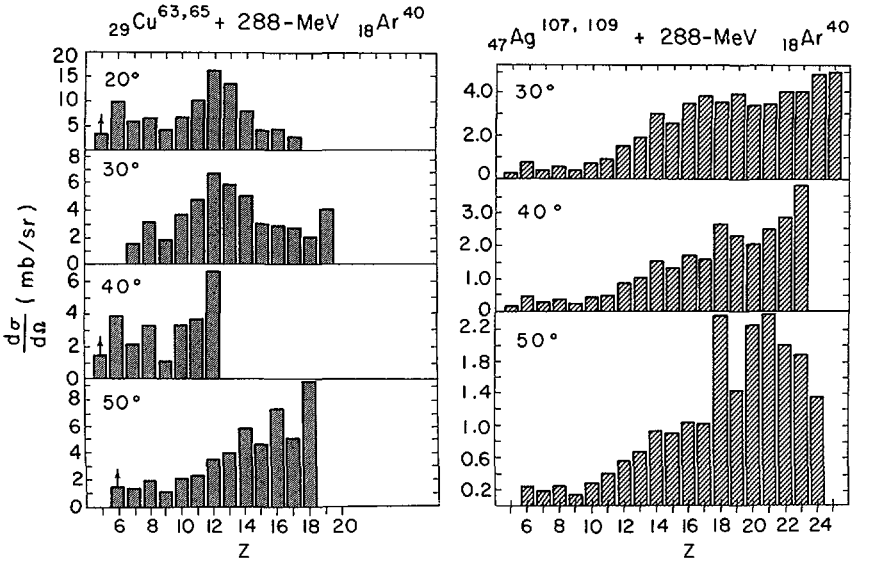

FIG. 3. Cross-sections for the production of the identified elements at various angles.

4. DISCUSSION

4.1. Evidence of a two-body kinematics

The results of the present experiment may be related to the conditions prevailing in the scission of a fissioning nucleus only if the observed reaction is mainly a two-body process. Only a coincidence experiment can give a definite answer to this question. However there are a few tests which may provide evidence for or against the binary nature of the process. Kinematic evidence can be obtained by transforming the observed laboratory kinetic energies to the centre-of-mass system. If the kinetic energies observed at various laboratory angles transform to essentially the same kinetic energy in the centre of mass it should be a good indication in favour of a binary disintegration. To perform such a transformation it is necessary to determine the masses of the fragments. In the present experiments only the charges and not the masses of the products are measured. Therefore one must make an assumption about the charge-to-mass ratio to obtain the necessary mass of the fragment. For lack of better knowledge, two extreme choices have been made: in one case it is assumed that the charge-to-mass ratio of the observed fragment is the same as in ^{40}Ar, in the second case it is assumed that the charge-to-mass ratio is the same as in the combined system. For the Cu + Ar system the two choices are practically identical, for the Ag + Ar system the two choices differ only slightly. The transformations of the most probable kinetic energies to the centre-of-mass systems

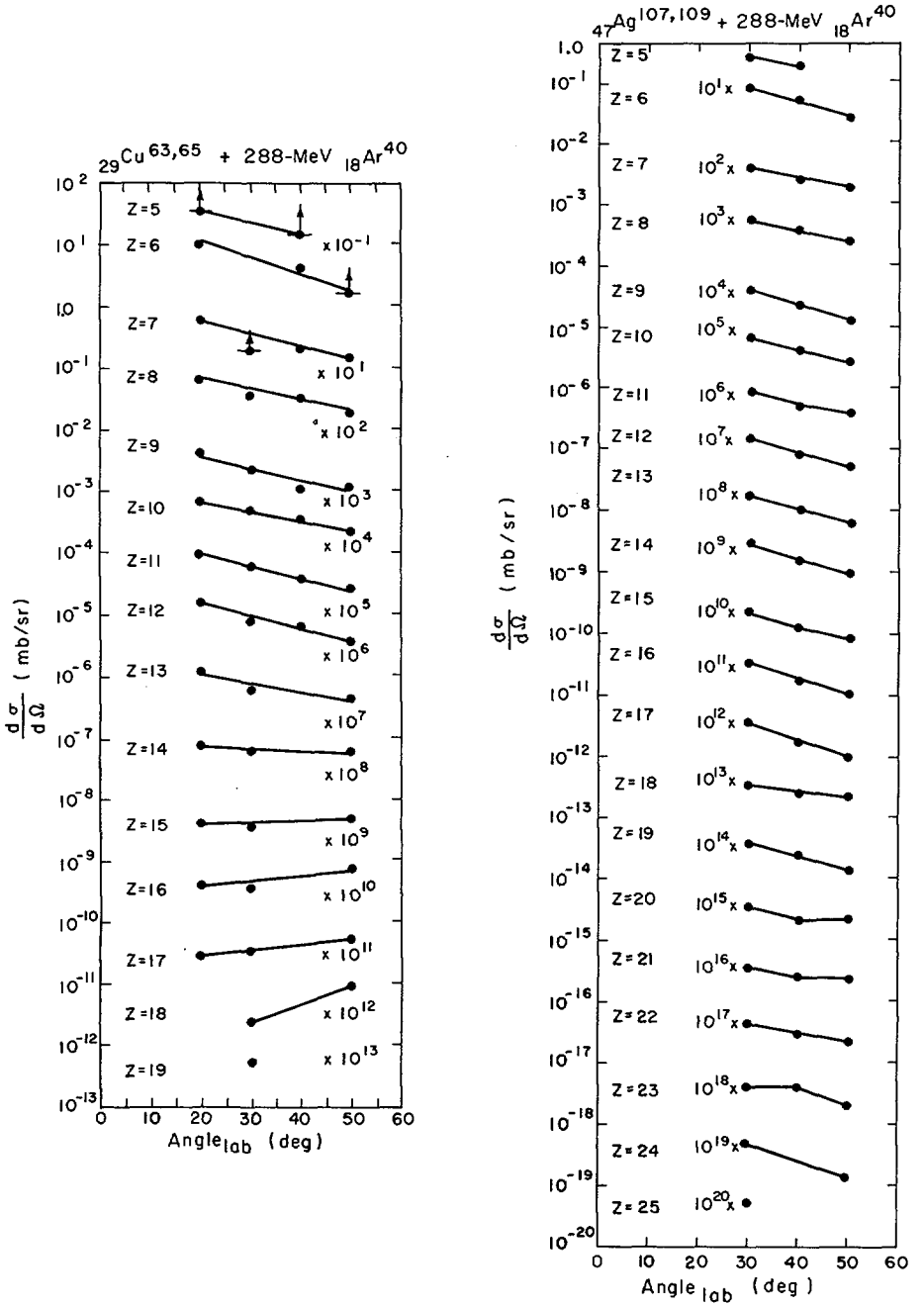

FIG. 4. Angular distributions for the various elements.

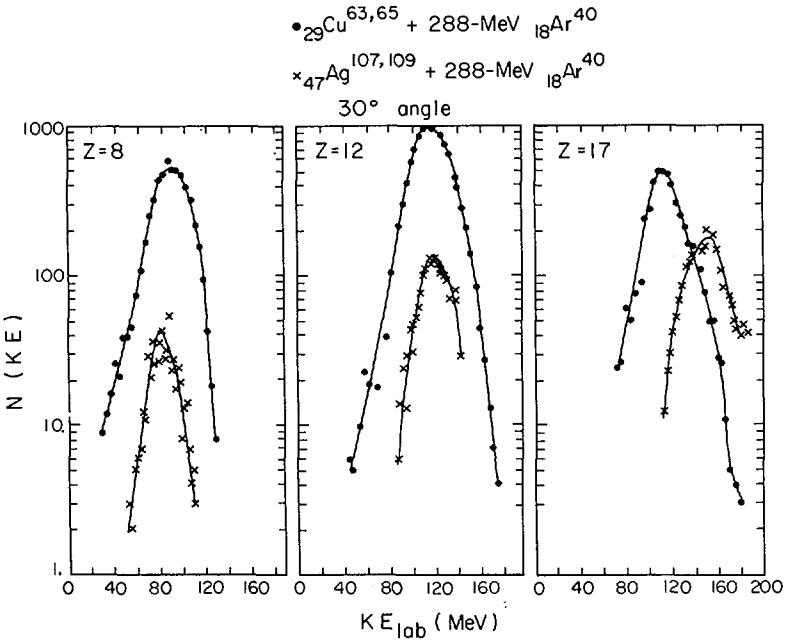

FIG. 5. Examples of kinetic energy distributions in the laboratory system.

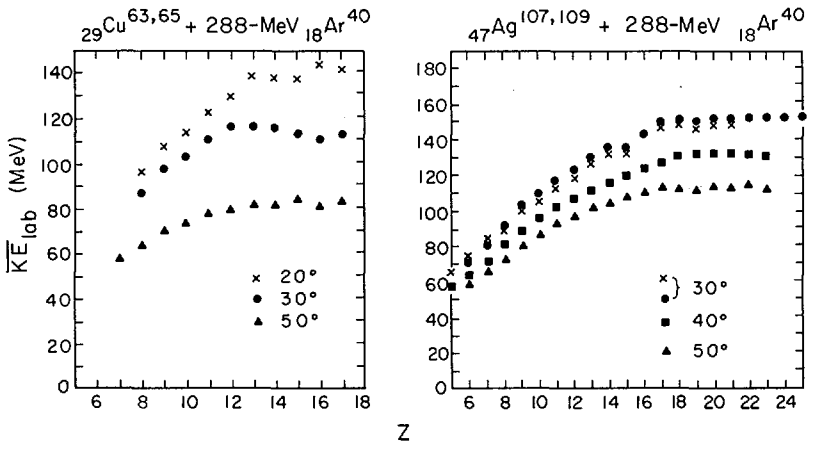

FIG. 6. Most probable kinetic energies as a function of atomic number of the fragments at various angles.

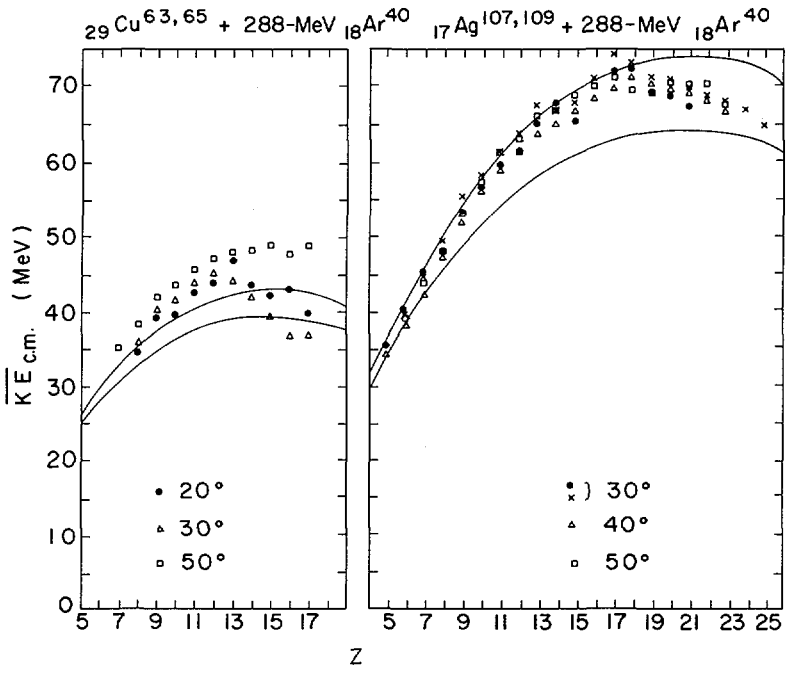

FIG.7. Most probable kinetic energies as a function of atomic number of the fragments in the centre-of-mass system. The upper lines correspond to the Coulomb energies of two touching spheres. The lower lines correspond to the Coulomb energies of two touching spheroids at equilibrium deformation.

have been carried out and the results are shown in Fig.7. It can be observed that the most probable kinetic energies for each given Z obtained at the various angles, once transformed to the centre-of-mass system, agree remarkably well with each other, better in the case of the Ag target than in the case of the Cu target. In the same figures the kinetic energies which the fragments would obtain if just repelled by the Coulomb interaction are also shown. Such theoretical kinetic energies are strikingly close to the experimental values. The flattening out and bending down of the kinetic energy curve as a function of Z, because of the energy taken off by the recoiling partner, is observed in the experimental data as well. This is further evidence of the validity of two-body kinematics. This evidence does not rule out that some of the particles arise from the break-up of an Ar-like excited particle obtained by the transfer of a limited number of nucleons [8]. However it seems that the great majority of the particles with $Z > 6$ are obtained by means of a large transfer of nucleons from the projectile. This is further supported by the identification of particles with Z as large as 25 and with unresolved Z larger than 25.

Thus the discussion will be continued under the assumption that the process is essentially binary.

4.2. The fragment kinetic energies

The values of the kinetic energies of the emitted particles represent a most revealing observation. As mentioned above, the most probable values of the kinetic energies essentially coincide with the kinetic energies that the fragments would have as a result of the Coulomb repulsion. The initial kinetic energy brought in by the projectile seems to be completely dissipated in the short time interval during which projectile and target interact with each other. This relaxation phenomenon can be attributed classically to a very large viscosity and friction associated with the relevant collective degrees of freedom of the system at the instant of collision. The behaviour of a dynamical system can be characterized in terms of the potential energy, the inertia tensor and the viscosity tensor. When the components of the viscosity tensor are small the system becomes controlled by the inertia and by the potential energy. On the other hand, if the viscosity tensor is large, the effect of the inertias is inhibited so that the system in its behaviour reflects mainly the potential energy and the viscosity tensor. In the present case the latter condition seems to apply since the effect of the Coulomb potential is observed so clearly.

The disappearance of such a large amount of kinetic energy suggests that a strong thermalization process takes place in which the kinetic energy becomes shared among the internal degrees of freedom of the system. There are indications that the overall system is characterized by a rather large temperature in the width of the kinetic energy distributions. Such widths are much larger than any expected temperature; however it is known that thermal fluctuations in the shape of the system can be strongly amplified by the Coulomb field producing very large fluctuations in the kinetic energy of the fragments at infinity [9].

Further evidence of a large temperature is related to the fact that the two-body kinematics are more apparent in the case of the Ag target than in the case of the Cu target. For the same emitted fragment the partner is heavier for a Ag target than for a Cu target. The heavier the partner, the more its share of excitation energy and the less the excitation energy of the primary light fragment. Therefore, for a Ag target, the small fragment may have less chance to decay and the main features of the two-body kinematics remain distinctly observable.

4.3. The charge and mass distribution

As a system removed from equilibrium evolves, the degrees of freedom with highest natural frequency are expected to achieve thermal equilibrium faster than the degrees of freedom with lower frequency. This rule should be obeyed if the viscous damping is the same for all the degrees of freedom. It seems that the experiment indicates a nearly complete relaxation of the single particle degrees of freedom whose phonon energy is approximately $\hbar\omega_0 = 41\ A^{-\frac{1}{3}}$. Similarly there is evidence for the relaxation of the charge asymmetry mode (dipole giant resonance) whose phonon energy is of the order of 10 to 15 MeV. On the other hand the mass asymmetry degree of freedom is expected to have a small phonon energy ($\sim$ 1 MeV) and does not seem to have achieved equilibrium. The experimental evidence of such a condition is visible in the experimental charge distribution which is expected

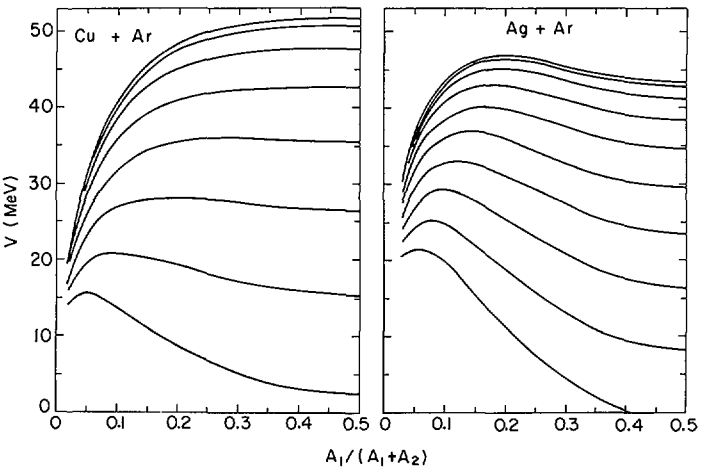

FIG. 8. Potential energies of two touching, rigidly rotating spheres as a function of the mass asymmetry parameter $A_1/(A_1 + A_2)$. The upper line corresponds to zero angular momentum. The spacing between the subsequent lines is 10 ħ.

to follow closely the mass distribution. To better appreciate the potential energy experienced by the system in its motion along the mass asymmetry coordinate, the potential energies of two touching liquid drop spheres, rigidly rotating with different amounts of angular momentum, are plotted in Fig. 8 as a function of the asymmetry parameter $A_1/(A_1 + A_2)$ for the composite systems Cu + Ar and Ag + Ar. In the case of Cu + Ar at zero angular momentum the potential energy has a maximum at symmetry and decreases as the system becomes more asymmetric. This reflects the instability in the mass asymmetry mode of the fission saddle point below the Businaro-Gallone point (x = 0.396). A system experiencing such a potential tends to slide down towards larger and larger asymmetries.

As the angular momentum increases, the maximum in potential energy becomes flatter until a depression is generated and a minimum appears in correspondence to the symmetric saddle point. In other words, the angular momentum tends to stabilize the mass asymmetry mode.

The Ag + Ar system exhibits a minimum in the potential energy at symmetry even without angular momentum. If the initial asymmetry is small, the system tends to become more symmetric. If the initial asymmetry is large, the system, as in the Cu + Ar case, tends to drift towards larger and larger asymmetries. As the angular momentum increases, the symmetric minimum becomes deeper and the maximum is displaced towards larger and larger asymmetries.

Many values of the angular momentum can be involved in the two reactions. The Cu + Ar system is characterized by a maximum classical angular momentum $I_{max} = 106$ ħ. The corresponding average angular momentum $\sqrt{\overline{I^2}}$ is 75 ħ. In the case of the Ag + Ar system, $I_{max} = 166$ ħ and $\sqrt{\overline{I^2}} = 118$ ħ. Without taking such calculations too quantitatively one may be led to conclude that in the case of Cu + Ar there should be a tendency in the system to move towards larger asymmetries while in the case of Ag + Ar the system should move towards lesser asymmetries.

An inspection of the Cu + Ar charge distributions shows that at the 50° angle the yields peak at Ar (it may be at higher Z but no data are available). At smaller angles the main yields move downward in Z, peaking at Z ~ 12 and showing a dramatic depletion in the Ar region.

The charge yields in the Ag + Ar system show a broad peak at an angle of 50°, between Z = 18 and Z = 22. At smaller angles the yield distribution becomes broader and flatter while the peak moves up to Z ~ 25. This behaviour can be interpreted qualitatively if one assumes that the distributions at the various angles correspond to a time sequence. Such an assumption can be justified in the following general discussion on the angular distributions.

4.4. The angular distributions

Under the condition of strong friction between target and projectile, the idea of a nearly unperturbed Coulomb trajectory associated with the extreme impact parameters becomes useless. Similarly the critical angle θ_c should not appear as a significant quantity in the angular distributions. If a large friction is experienced by a particle on a grazing trajectory, the particle will lose the greatest part of its tangential velocity, aside from the amount necessary for angular momentum conservation. If the particle is instantaneously re-emitted it is expected to move away radially at a well defined angle θ_R. If the target nucleus is assumed to have infinite mass and moment of inertia, such an angle is

$$\theta_R = \frac{\theta_c + \pi}{2}$$

which is in most cases much larger than θ_c. For a finite target nucleus mass, the angle θ_R is different but nevertheless large.

If the two particles remain attached to one another for a certain time, the system rotates rigidly with an angular velocity defined by the total angular momentum and by the moment of inertia. If the characteristic splitting time is very small as compared to the rotation period, then the emitted particle should peak at angles close to θ_R. For a splitting time comparable but smaller than the rotation period, the angular distribution should be peaked in the forward direction, while for a splitting time much larger than the rotation period the angular distribution should be symmetric about 90°. The experimental lack of symmetry about 90° suggests that the splitting time is smaller than the rotation period. Therefore the observation of the particles at various angles does indeed correspond approximately to different times, longer for the smaller angles.

In conclusion, the change in charge distribution observed in going from larger to smaller angles can indeed be interpreted as a time evolution of the system under the effect of the potential illustrated in the previous subsection.

5. CONCLUSION

The results discussed in the previous section seem to indicate that short relaxation times and consequently large viscosities are associated with the collective degrees of freedom involved in heavy-ion collisions.

These conclusions may be relevant to systems in the neighbourhood of the scission point. The inability of the collective degrees of freedom to have any substantial amount of kinetic energy suggests that the descent from saddle to scission should be very slow. Under these conditions one should not expect any relevant amount of pre-scission kinetic energy. Furthermore such an extreme viscous limit suggests that the dynamical evolution of the system is controlled by the slowest mode (perhaps the neck constriction mode) while all the other faster modes, collective and intrinsic, remain constantly in thermal equilibrium.

The tentative conclusions reached here should be valid in general. However there might be some exception associated with very low energy or spontaneous fission, where the system could retain its superfluidity from saddle to scission. The present results may be relevant also to the formation of superheavy nuclei in heavy-ion bombardments. The quick dissipation of kinetic energy along the collective coordinates may prevent the system from achieving the near-spherical configuration necessary for the shell effects to operate.

REFERENCES

[1] NIX, J.R., Nucl. Phys. 130 (1969) 241.
[2] HASSE, R.W., Nucl. Phys. A118 (1968) 577; A128 (1969) 609; Phys. Rev. C4 (1971) 572.
[3] SCHIMER, J., KHAAK, S., SÜSSMANN, G., Nucl. Phys. A199 (1973) 31.
[4] WIECZOREK, R., HASSE, R.W., SÜSSMANN, G., Paper IAEA-SM-174/02, these Proceedings, Vol.1.
[5] GALIN, J., GUERRAY, D., LEFORT, M., PÉTER, J., TARRAGO, X., RASILE, R., Nucl. Phys. A159 (1970) 461.
[6] ARTUKH, A.G., GRIDNEV, G.F., MIKHEEV, V.L., VOLKOV, V.V., WILCZYŃSKI, J., Dubna, JINR-E7-6970 (1973).
[7] LEFORT, M., NGÔ, C., PÉTER, J., TAMAIN, B., IPNO-RC-73-06, Orsay (1973).
[8] BONDORF, J.P., NÖRENBERG, W., Phys. Lett. 44B (1973) 487.
[9] MORETTO, L.G., Phys. Lett. 40B (1972) 185.

DISCUSSION

J.B. NATOWITZ: I would like to ask a question about the experiment. We have also seen the data of Gutbrod and co-workers for reactions of ^{40}Ar with Ag.[1] They looked at the heavy species ejected, observing products as low as Z = 18. In your experiment we see the lighter products emitted at large angles with substantial kinetic energies. If the process giving rise to such light products is a binary process, the heavy fragments should be observed in the laboratory with reasonably high energies. Such heavy partners were not apparent in the data shown by Gutbrod, unless they appear in the group described as "fission-like", for which the fission cross-section has been determined. Since their differential fission cross-sections must be derived by summation of the fission-like products and division by 2, a significant error could result if partners of lighter products were included. Could you, or perhaps Mr. Gutbrod, comment on this.

D. HEUNEMANN: As I have already mentioned, our system is not yet sensitive enough to detect the heavier partner. The data of Gutbrod

[1] GUTBROD, H.H., et al., Paper IAEA-SM-174/59, these Proceedings, Vol.2.

and co-workers do indeed show "fission-like" fragments in the Z-range corresponding to the heavier partner. However, the angular range of Gutbrod's experiment does not cover the whole region necessary to detect the heavier partner corresponding to the light particles which we detect.

H.H. GUTBROD: We also see light particles, but with very low cross-section, about 10 times less than the observed fission yield around Z = 30. We did not investigate whether they are produced in reactions involving light element contamination, as was done by Heunemann and co-workers. The light particle yield we observe is less than the error bars with which we quote our cross-sections for fission-like products.

H. NIFENECKER: We have measured the yields of the heavy products of the reactions (Ar + Cu), (Ar + In), (Ar + Tb), (Ar + Au) with 285-MeV argon ions. The yields were measured by detecting the X-rays emitted after electron capture in the decay of the products. The results for (Ar + In) and (Ar + Cu) show few-nucleon transfer reactions, compound nucleus reactions and events which seem to correspond to the heavy complementary fragments of the light particles referred to in Heunemann's paper (this agreement is based on range and angular distributions). For the Tb and Au targets an additional phenomenon appears, where products corresponding to the target stripped of up to 30 nucleons with a laboratory kinetic energy less than $\sim$ 10 MeV are found.

FUSION AND FISSION IN THE REACTIONS OF ^{12}C WITH ^{27}Al

E. T. CHULICK, M. N. NAMBOODIRI, J. B. NATOWITZ
Department of Chemistry and Cyclotron Institute,
Texas A & M University,
College Station, Tex.,
United States of America

Abstract

FUSION AND FISSION IN THE REACTIONS OF ^{12}C WITH ^{27}Al.

Detector telescopes which include a very thin (1.5 μm to 8.4 μm) front detector have been employed to measure elemental yields for nuclei produced in the interaction between ^{12}C projectiles and ^{27}Al target nuclei at energies of 100 MeV and 180 MeV. Fusion cross-sections, including the cross-section for fusion followed by fission, have been determined by use of the principle of conservation of charge. The fusion cross-section is 1.00 barns at 100 MeV and 1.02 barns at 180 MeV. The sharp cutoff limiting angular momentum for fusion at 100 MeV is 29 ħ. The limiting angular momentum for fusion at 180 MeV is 40 ħ, equal to the limit calculated with the liquid drop model. The measured yield distributions, energy spectra and angular distributions indicate that fission accounts for less than 7% of the fusion cross-section at 100 MeV and less than 18% of the fusion cross-section at 180 MeV.

INTRODUCTION

In several recent studies, the cross-section for fusion of a heavy ion projectile with a target nucleus has been determined by detection of the recoiling product nuclei.[1-3] At the high projectile energies employed in those experiments (10 to 15 MeV/amu) the measured fusion cross-sections are found to be well below the corresponding total reaction cross-sections. Complementary experiments[4]have indicated an increase in the probability of direct reactions in the same energy region where the fusion cross-sections decrease. However, only a few of the possible direct reaction products were observed, and a substantial portion of the total reaction cross-section remained unaccounted for.

It has recently been suggested[5]that there may be an appreciable cross-section for fission of the light elements when an excited nucleus is formed with very high angular momentum. In such a case the fission component might not be included in the fusion cross-section measurements as they are typically performed. The measured cross-section would then be interpreted as the cross section for the formation of a non-fissioning fused nucleus. This expectation of high probability of fission is based upon liquid drop model calculations [6] which indicate that the fission barrier decreases with increasing angular momentum. The angular momentum at which the fission barrier disappears is viewed as the maximum angular momentum at which fusion will occur. In view of the fact that the fission barrier is low for angular momenta near the limiting value, fission is predicted to be an important competing mode of de-excitation for nuclei produced with those angular momenta. The available data on fusion cross-sections are indeed reasonably well reproduced by evaporation calculations in which fission competition is included and the angular momentum dependence of the fission barrier is taken into account. [5]

To study the competition between various possible reaction mechanisms which might be important when heavy ion projectiles have orbital angular momenta

comparable to or greater than the limiting angular momentum calculated according to the liquid drop model, we have studied the reactions of 100-MeV and 180-MeV ^{12}C projectiles with ^{27}Al. If fusion were to occur at the maximum possible impact parameter for nuclear reactions, the ^{39}K compound nucleus would be produced with angular momenta as high as 40 $\hbar$ in the 100-MeV irradiation and as high as 52 $\hbar$ in the 180-MeV irradiation. The angular momentum at which the fission barrier of ^{39}K disappears has been calculated to be 40 $\hbar$. [6]

From our measurements of the energy spectra and angular distributions of the nuclei produced in these reactions, we have determined the fusion cross-sections, including the cross-section for fusion followed by fission. Limiting angular momenta for fusion have been calculated using a sharp-cutoff approximation and are compared with the theoretical limit.

EXPERIMENTAL PROCEDURES

Data Acquisition - Nuclei produced in the reactions of 100-MeV and 180-MeV ^{12}C projectiles with a 107-$\mu g/cm^2$ ^{27}Al target were detected with a counter-telescope. A three-detector telescope was used so that a wide range of reaction products could be observed simultaneously, e.g., with a <10μ thick first detector, a 500-1000 μ thick second detector and a $\leq$2000 μ thick third detector we could observe products from protons to potassium.

The telescope was mounted on a movable arm inside a 43 cm diameter scattering chamber. A monitor detector was also mounted inside the scattering chamber at a vertical angle of 13°. The beam stopped in a Faraday cup mounted at the rear of the scattering chamber.

The preamplified signals from the detector telescope were routed to standard linear and logic electronics. Figure 1 shows the arrangement of the electronics.

Energy calibrations were performed using a pulser which had been normalized at 5.48 MeV using a ^{241}Am alpha source. For detectors that were thinner than the range of the alpha particles, the residual energy of the alpha was measured by a thick detector behind the thin detector and the energy loss used to normalize the pulser. The energy calibration and identification procedures were also checked by moving the counter telescope directly into the cyclotron beam. With no ion source power the beam level was sufficiently low to allow this calibration check which was also used to check the "cleanliness" of heavy-ion beams.

An IBM 7094 computer was used on-line for data acquisition. Data were recorded event by event on magnetic tape for those signals which were above the energy threshold in either the ΔE_1 detector or in the ΔE_2 detector. Each time a valid event trigger was obtained, the data from all three ADC's were stored as a single 36 bit computer word. The resolving time of the system was of the order of 500 ns. This method of data acquisition, in addition to allowing us to identify nuclei over a broad span of atomic numbers and energies, also made it possible to obtain the energy spectrum of particles stopped in the first detector. The ADC channel conversion position in the computer word was determined by the ADC connection to a Lecroy interface. A DCB tag which came in coincidence with a computer read signal was used to signify a valid event to the computer. During the processing of a valid event the linear gates were blocked for approximately 70 μs to allow the interface and ADC's to clear and reset before accepting more data. Thus the acquisition dead time was fixed at approximately 70 μs.

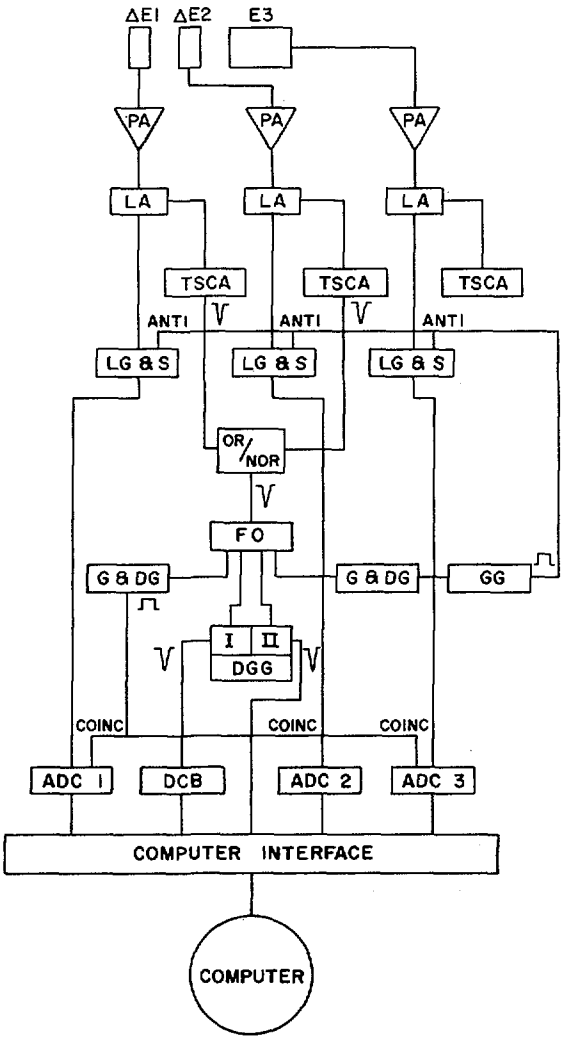

FIG. 1. A schematic diagram of the electronics associated with the three-detector telescope used for the experiments reported in this paper.

Five displays of the data were available during the data acquisition. In addition to the singles spectrum of each of the three detectors, a pair of two-dimensional arrays could be displayed (Figure 2). The first of these was a plot of the ΔE_1 signal versus the E_2 signal for coincident events in which the particle stopped in the second detector. The other two-dimensional array was a similar plot of the ΔE_2 signal versus the E_3 signal for particles which entered the third detector. The displays were refreshed by the computer each time the data buffer was filled with 1020 words. At the end of a run the live display arrays were printed off-line for a first hard copy of the raw data.

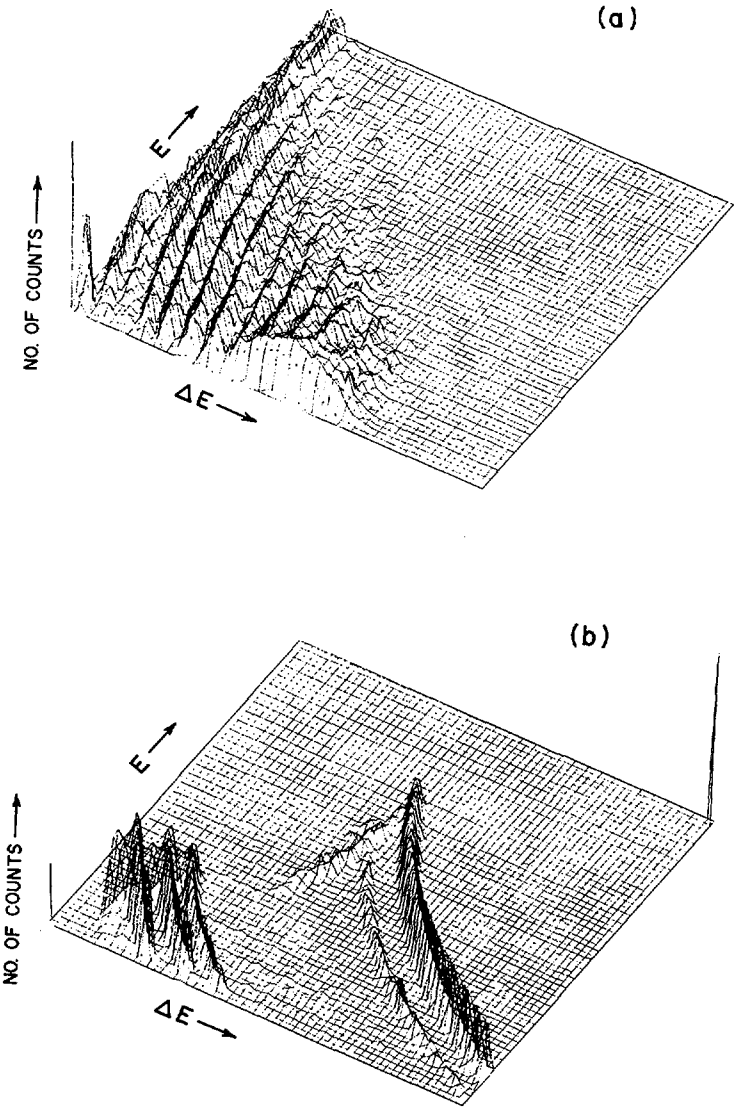

FIG. 2. Data obtained with a three-detector telescope for the reactions of 180-MeV ^{12}C projectiles with ^{27}Al. Fig. 2(a) is a plot of energy loss in the first detector, ΔE, versus the energy in the second detector, E, for nuclei which stop in the second detector. Fig. 2(b) is a plot of energy loss in the second detector, ΔE, versus the energy in the third detector, E, for nuclei which reach the third detector. Some He nuclei which have penetrated the third detector appear in a ridge at the centre of the figure.

Data Processing - All of the data processing was done off-line using an IBM 7094 computer and a data analysis program called BINIT.[7] BINIT was designed to construct the desired arrays by binning events according to total energy or according to the identity of the particle. For example, an identification spectrum could be constructed of events that either stopped in the second detector or the third detector and whose total energy ranged between an upper and lower energy limit. Particle identification values were calculated using the schemes outlined in references [8] and [9]. Energy spectra were constructed by building an energy array of events whose identification value ranged between an upper and lower identification value. The resultant energy spectra could contain contributions from nuclei which stopped in the second detector and those which were energetic enough to go through to the third detector. Figure 3 shows a yield plot of the raw data represented in Figure 2 after analysis with BINIT. Figure 3a is for the case where nuclei stopped in the second detector. The PIO value scale at the top corresponds closely to the Z of the product. The first detector was too thin to permit mass identification except for deuterons, tritons, and, because ^{8}Be is missing, of ^{7}Be and ^{9}Be. The gap between channels 150 and 210 is caused by a change in the function used to calculate the identification tags. Figure 3b is the same type of plot as Figure 3a except that the nuclei included have reached the third detector. The second detector was too thick to allow nuclei heavier than beryllium to register in the third detector. Figure 4 shows some typical energy spectra extracted with BINIT. The spectra shown are not all from the same run and only Figure 4c is from the same run shown in Figures 2 and 3. For Figure 4a and 4b, the He and B spectra, some of the particles stopped in the second detector and some stopped in the third detector so that there are two sets of PIO windows. For Figure 4c, the Mg spectrum, all the nuclei stopped in the second detector.

In order to obtain total differential cross-sections, it was necessary to extrapolate measured energy spectra to low energies. For the lighter products at forward laboratory angles, these corrections were small and easily made. The corrections become larger as the angle increases but because of the large center-of-mass motion, the angular distributions tend to be very forward peaked so that the data at large angles generally make a small contribution to the total elemental cross-section. At backward angles, the observed nuclei were primarily H and He nuclei and the spectra of particles stopped in the first detector were useful in determining the low-energy corrections to the spectra.

In Figure 5 the laboratory angular distributions for elements with atomic numbers from 1 to 8 produced in the 180-MeV irradiations are shown.

The summed energy spectrum for nuclei with $Z \geq 9$ could be obtained to low energies by use of the first-detector-only spectra since the maximum energy losses for lighter products in the thin front detectors were low. However identification of individual elements in the first-detector-only spectrum is not possible. Therefore, we have not attempted to extrapolate the energy spectra of individual elements with $Z \geq 9$. Rather, for each atomic number $Z \geq 9$ we have assumed that the angular distribution for nuclei stopped in the first detector is the same as for the nuclei of that element which stop in the second detector (and are therefore identified).

In this way, the fraction of unidentified heavy nuclei to be associated with each element was determined. In Figure 6 we present the angular distributions for products with atomic numbers ≥ 9 at a projectile energy of 180 MeV.

By integration of the laboratory differential cross-sections, we have determined elemental yields for the observed products.

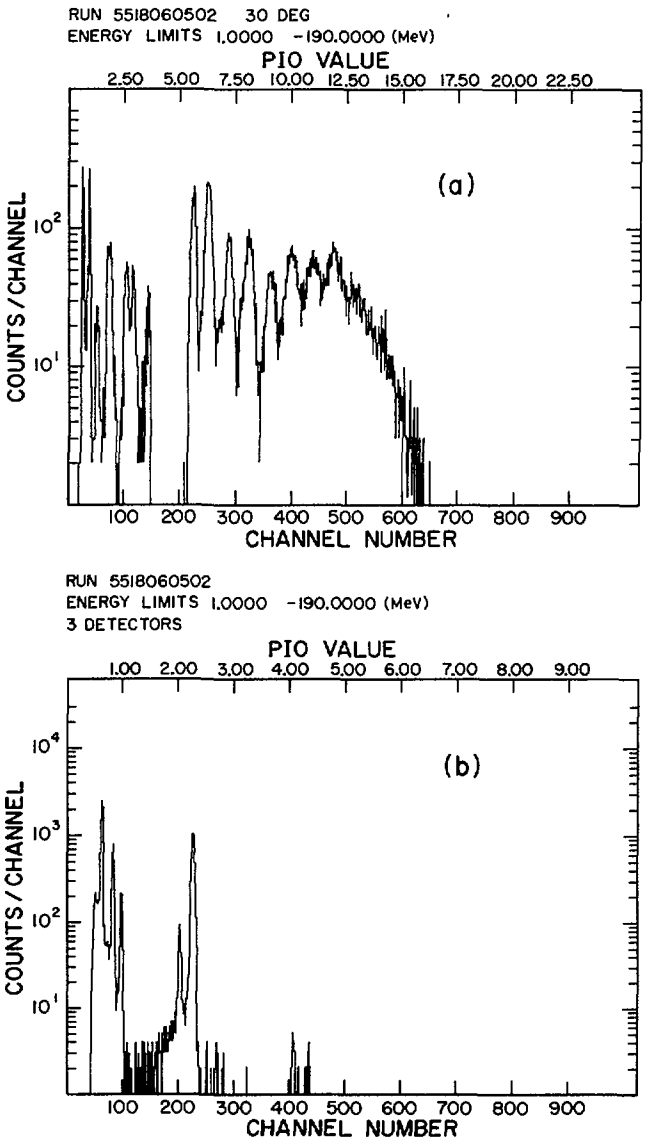

FIG. 3. Identification spectra obtained for the data shown in Fig. 2. The PIO values are approximately equal to the atomic numbers of the identified nuclei. The identified spectrum of all nuclei stopped in the second detector is shown in Fig. 3(a). The break in the spectrum near channel 200 results from a change in the identification algorithm being used. Identification is by atomic number only since the first detector was too thin to permit mass resolution. In Fig. 3(b) the identified spectrum of nuclei reaching the third detector is shown.

RESULTS

The yield distributions are presented in Figures 7 and 8. Also indicated in the figures are the laboratory angles within which one quarter, one half, and three quarters of the total elemental yield is observed. Thus, the smaller those angles, the more forward peaked is the angular distribution. The following features of the data in those figures may be noted:

1. Products with atomic numbers equal to or close to that of the projectile have angular distributions which are strongly forward-peaked. These angular distributions apparently represent the predominantly direct mechanisms for reactions leading to those products. The dominant yield in this region of atomic number is that for carbon isotopes. Although it is not indicated on the figures, the inelastic scattering of ^{12}C accounts for the bulk of the carbon yield. The remainder of the yield consists of ^{11}C and ^{13}C, the neutron transfer products.

2. Products of atomic number ≥ 9 have similar angular distributions which become more forward-peaked as the atomic number increases. Such a trend suggests that these nuclei are residual recoiling products of the stepwise de-excitation of a ^{39}K compound nucleus. The energy spectra of these products are consistent with such an interpretation. The yield pattern of these products also appears consistent with that expected for a statistical de-excitation of the compound nucleus.

3. The yield of H and He isotopes at each energy is greater than the total reaction cross-section, and must represent multiple emission of these species during the de-excitation of heavier nuclei. At 180 MeV, the angular distribution of the He isotopes shows a strong forward peaking which was found on further study to be associated only with the ^{4}He isotope and not with ^{3}He, which comprises about 10% of the total He yield. Based upon comparisons between the ^{3}He and ^{4}He angular distributions, we estimate that the additional forward-directed component of ^{4}He has a production cross-section of 1 barn. This is a much higher cross-section than could result from the break-up of ^{8}Be (for which we expect cross-sections similar to those for production of ^{7}Be and ^{9}Be) and presumably results primarily from projectile break-up. [10]

4a. At 100 MeV, the angular distributions of N and O nuclei are broader than those of C but slightly more forward peaked than those of higher Z elements. The energy spectra for those ions extend to high energies, indicating that the yield of these elements results primarily from a direct reaction process.

4b. At 180 MeV, the angular distributions of N and O nuclei fit very well within the trends established for the higher Z products. The energy spectra of both (except for a small high-energy component of the N spectrum which results from ^{13}N, the proton pick-up product of a direct reaction) are qualitatively very similar to those observed for the higher Z products. The yields of O and N (even when the ^{13}N direct reaction product is excluded) are slightly greater than the F yield. This larger yield of N and O could indicate some selective mode of decay in the last stages of the de-excitation of the fusion nucleus or alternatively might signal the presence of another reaction mechanism.

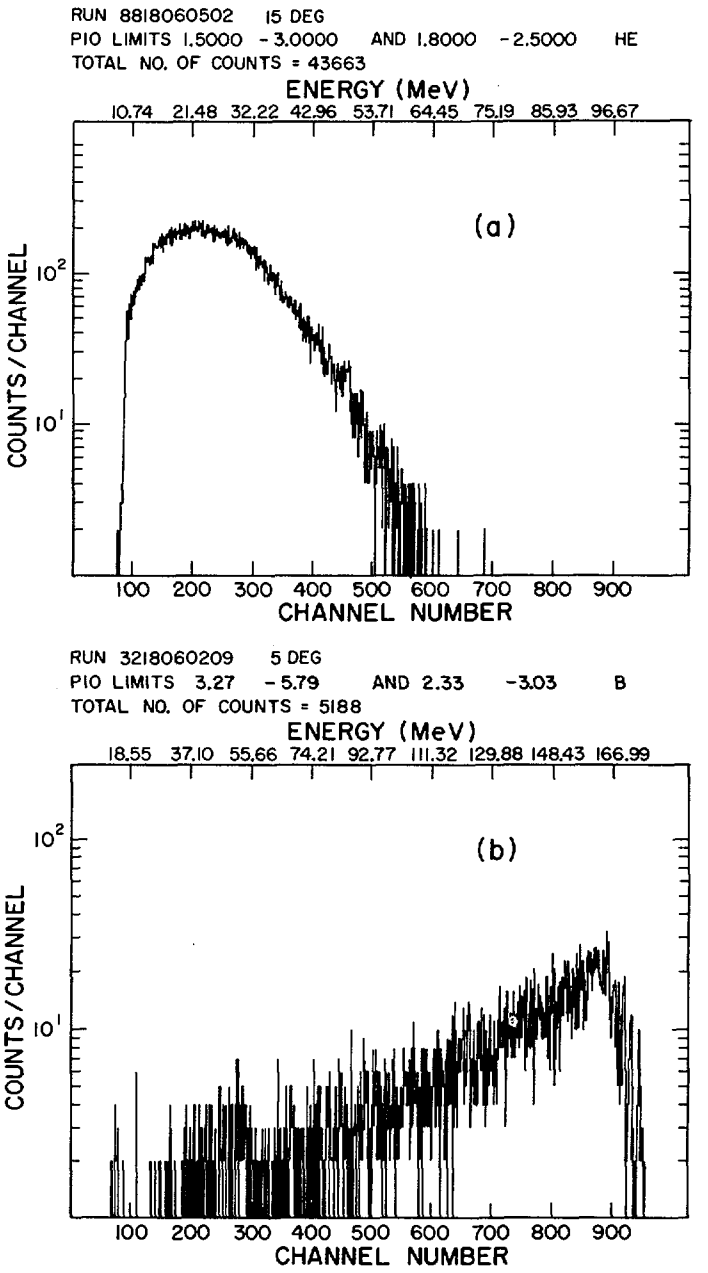
RUN 8818060502 15 DEG
PIO LIMITS 1.5000 -3.0000 AND 1.8000 -2.5000 HE
TOTAL NO. OF COUNTS = 43663
ENERGY (MeV)
10.74 21.48 32.22 42.96 53.71 64.45 75.19 85.93 96.67
(a)
COUNTS / CHANNEL
10^2
10^1
100 200 300 400 500 600 700 800 900
CHANNEL NUMBER
RUN 3218060209 5 DEG
PIO LIMITS 3.27 -5.79 AND 2.33 -3.03 B
TOTAL NO. OF COUNTS = 5188
ENERGY (MeV)
18.55 37.10 55.66 74.21 92.77 111.32 129.88 148.43 166.99
(b)
COUNTS / CHANNEL
10^2
10^1
100 200 300 400 500 600 700 800 900
CHANNEL NUMBER

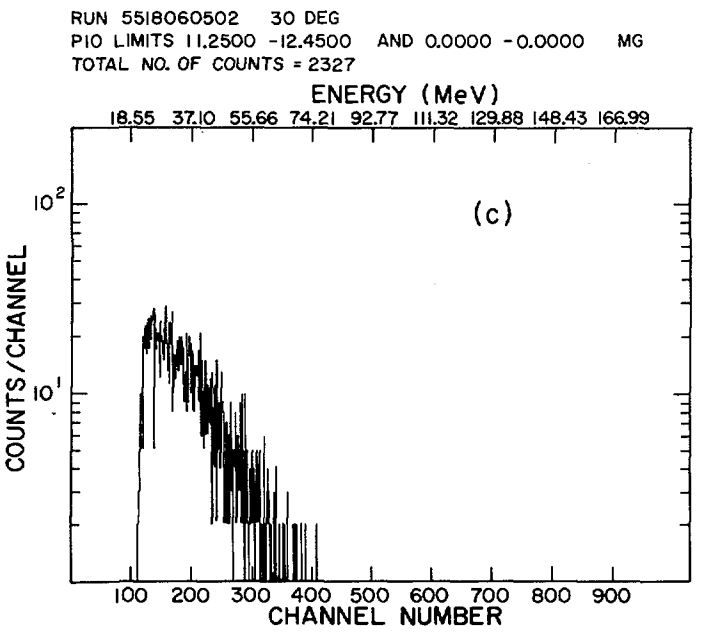

FIG. 4. Representative energy spectra for (a) He, (b) B, and (c) Mg nuclei produced in the reactions of 180-MeV ^{12}C projectiles with ^{27}Al. The spectra were obtained in three different irradiations. The spectra for He and B nuclei include contributions from all three detectors. The Mg nuclei all stopped in the second detector.

DISCUSSION

The recoiling heavy partners of inelastic scattering or few nucleon transfer reactions are not counted in our experiment. The only nuclear reactions for which more than one product nucleus will be counted are those which involve nuclear fission or ejection of charged fragments. If we sum the yields of the observed products, temporarily excluding the H and He isotopes which must primarily represent light particle emission from heavier species, we find that the total cross-section for production of isotopes with Z>3, with no correction for ^{8}Be emission, is 1608 mb at 100 MeV and 1637 mb at 180 MeV. These summed cross-sections for Z>3 products are very close to the expected total reaction cross-sections[11] of 1550 mb, and 1750 mb at 100 MeV and 180 MeV respectively. It appears therefore, that relatively little double counting is done for Z>3 products i.e., that nuclear fission cannot account for a very large fraction of the total reaction cross-section. This preliminary conclusion could be in error only if there were a high probability for production of excited nuclei which totally disintegrate into isotopes of H and He.

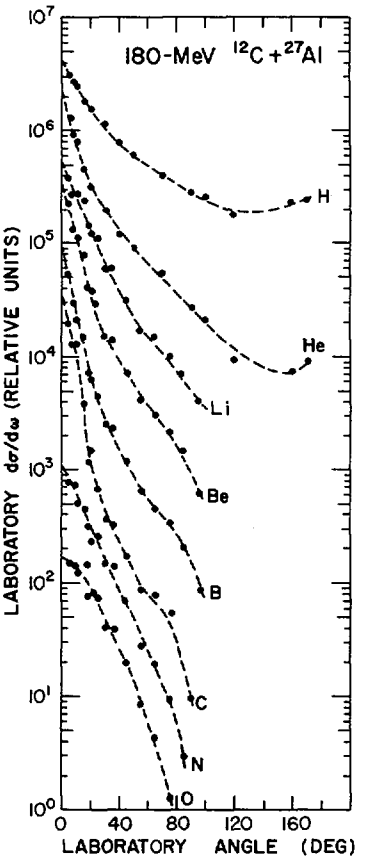

FIG. 5. Laboratory angular distributions of nuclei with $Z \leq 8$ produced in the reactions of 180-MeV ^{12}C projectiles with ^{27}Al. Relative differential cross-sections for the production of each element are represented by solid circles. The data for individual elements are not normalized relative to the data for the other elements included in the figure.

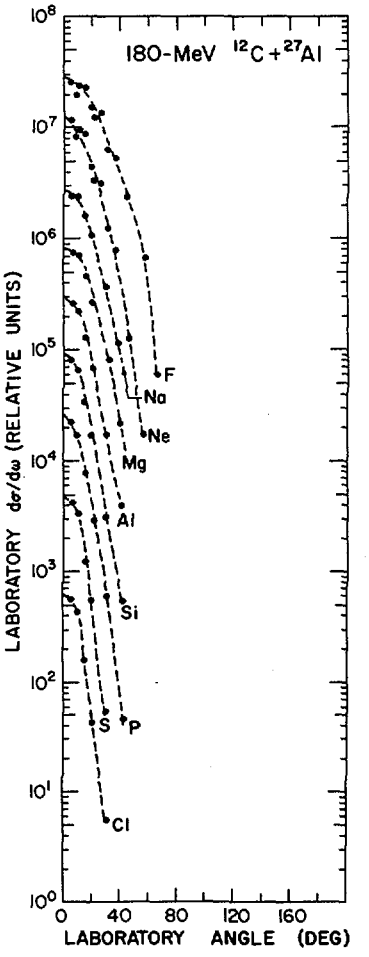

FIG. 6. Laboratory angular distributions of nuclei with $Z \geq 9$ produced in the reactions of 180-MeV ^{12}C projectiles with ^{27}Al. Relative differential cross-sections for the production of each element are represented by solid circles. The data for individual elements are not normalized relative to the data for the other elements included in the figure.

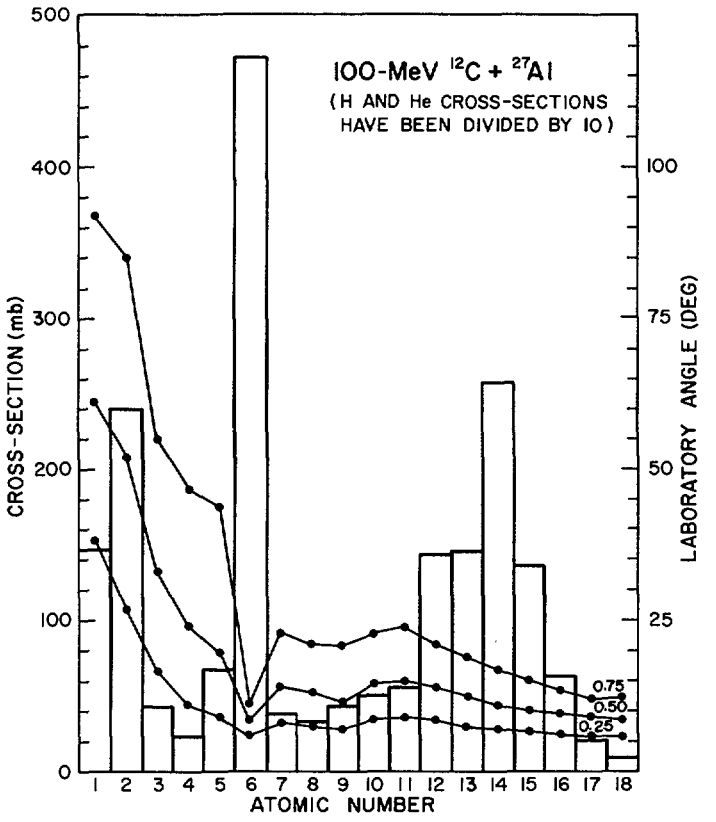

FIG. 7. Elemental yields for nuclei produced in the reactions of 100-MeV ^{12}C projectiles with ^{27}Al. Cross-sections are indicated by a bar graph (left-hand scale). Cross-sections for production of H and He have been divided by 10. Also shown, with solid circles, are the angles within which fractional yields of 0.25, 0.50, and 0.75 of the total are observed (right-hand scale).

Since products from H through K could be observed in our experiment, we may use conservation of atomic number to determine the cross-sections for fusion. We first write

$$\sigma_R = \sigma_{CF} + \sigma_D \tag{1}$$

Where σ_R is the total reaction cross-section, σ_{CF} the fusion cross-section and σ_D the cross-section for direct reactions (by which we mean all non-fusion processes). We define $\overline{Z}$ as the average observed atomic number per nuclear reaction. The experimental value of $\overline{Z}$ may be determined from the elemental yields as

$$\overline{Z} = \frac{\Sigma_Z(\sigma_Z)(Z)}{\sigma_R} \tag{2}$$

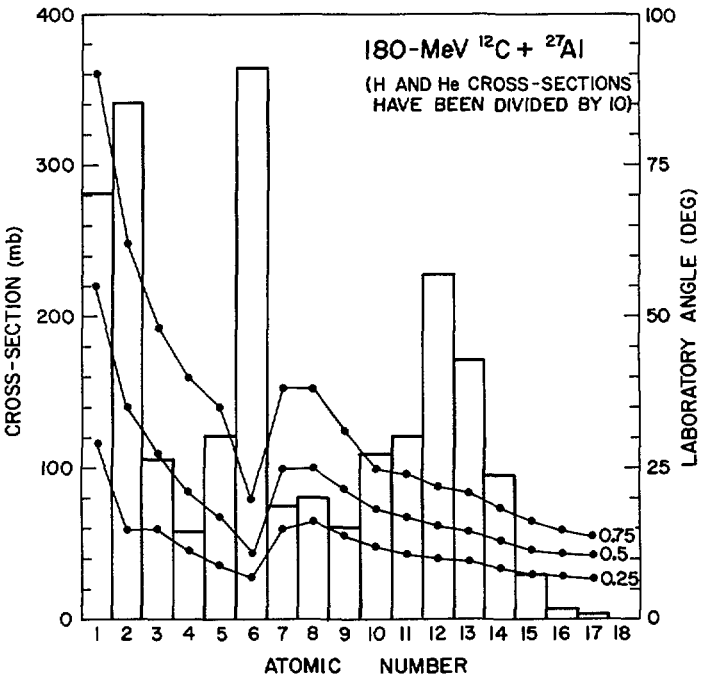

FIG. 8. Elemental yields for nuclei produced in the reactions of 180-MeV ^{12}C projectiles with ^{27}Al. Cross-sections are indicated by a bar graph (left-hand scale). Cross-sections for production of H and He have been divided by 10. Also shown, with solid circles, are the angles within which fractional yields of 0.25, 0.50, and 0.75 of the total are observed (right-hand scale).

where σ_Z is the cross-section for production of a nucleus of atomic number Z. If we designate the total observed charge for fusion and direct reactions as Z_{CF} and Z_D we may write

$$\overline{Z} = \frac{(\sigma_{CF})(Z_{CF}) + (\sigma_D)(Z_D)}{\sigma_R} = \frac{(\sigma_{CF})(Z_{CF}) + (\sigma_R - \sigma_{CF})Z_D}{\sigma_R} \qquad (3)$$

For the reactions studied here, Z_{CF} is 19. In view of the large yield of C isotopes at very forward angles, a value of 6 for Z_D cannot be much in error.

Using the elemental yield data in Figs. 7 and 8, we obtained 14.5 and 13.6 for the values of $\overline{Z}$ at 100 MeV and 180 MeV, respectively. Substituting the appropriate values into Eq. (3) we find σ_{CF} = 1.00 barns at 100 MeV and 1.02 barns at 180 MeV. A change of $\overline{Z}_D$ to 5 or 7 will change these calculated values by no more than 65 mb. We estimate uncertainties of ±10% on these fusion cross-sections.

Turning again to the data of Figure 7 we note that at 100 MeV, the summed yield of products with $Z \geq 9$ is 927 mb, which is in good agreement with the 1.00 barn cross-section calculated from charge conservation. This agreement, coupled with the fact that the energy spectra, angular

distributions and yield patterns of the $Z \geq 9$ products were entirely consistent with production in a stepwise de-excitation of ^{39}K lead us to the conclusion that fission does not occur in more than 7% of the ^{39}K nuclei produced in the fusion of ^{27}Al with 100-MeV ^{12}C projectiles.

At 180 MeV, the summed yields for $Z \geq 9$ is 834 mb. Thus, the yield data alone indicate a maximum fission cross-section of 181 mb. This value is obtained by taking the difference between the summed yield of $Z \geq 9$ products and the calculated fusion cross-section, where the products with $Z \geq 9$ are taken to be residual nuclei from de-excitation of ^{39}K by emission of small fragments and photons.

Since the energy spectra and angular distributions of the N and O nuclei appear to follow the trends established by the higher Z products, we could probably view the N and O as also being produced in the stepwise de-excitation of the fusion nucleus ^{39}K. The inclusion of the N and O nuclei yields would increase the apparent fusion cross-section to 989 mb, in excellent agreement with the fusion cross-section derived from charge conservation. However, the yields of N and O are slightly greater than the yield of F and we cannot rule out the possibility of some contribution to the N and O yields via a fission process.

If it is assumed that the fusion reactions occur preferentially at small impact parameters and that the transition between fusion and non-fusion processes may be characterized by a maximum impact parameter for fusion, the limiting angular momentum for fusion may be derived from the cross-section data. In the sharp-cutoff model, the relationship between the limiting angular momentum for fusion, usually called J_{crit} and the maximum possible angular momentum J_{max} (which would be realized if the fusion cross-section were identical with the total reaction cross-section) is

$$J_{crit} = \left(\frac{\sigma_{CF}}{\sigma_R}\right)^{1/2} J_{max} \qquad (4)$$

Using the values of the fusion cross-section derived from charge conservation, we find that J_{crit}=29 $\hbar$ at 100 MeV and 40 $\hbar$ at 180 MeV.

CONCLUSIONS

The limiting angular momentum for fusion of ^{27}Al with 100 MeV ^{12}C projectiles is 29 $\hbar$, well below the 40 $\hbar$ limit calculated using the liquid drop model. Since the measured limit is based upon fusion cross-sections which include the cross-section for fusion followed by fission, the limit would appear to result from limitations imposed by nuclear dynamics.

The limiting angular momentum for fusion of ^{27}Al with 180 MeV ^{12}C projectiles is 40 $\hbar$, equal to the theoretical limit. Such an agreement may be fortuitous and further experiments are required to determine whether or not the limit results from dynamic properties or from equilibrium properties of the compound nucleus. However, even though ^{39}K nuclei have apparently been produced with angular momenta as high as that for which the fission barrier is calculated to disappear, less than 18% of those nuclei fission.

ACKNOWLEDGEMENT

This research was supported by the United States Atomic Energy Commission and the Robert A. Welch Foundation.

REFERENCES

[1] KOWALSKI, L., JODOGNE, J. C., MILLER, J. M., Phys. Rev. 169 (1968) 894.
[2] NATOWITZ, J. B., Phys. Rev. C1 (1970) 623.
[3] NATOWITZ, J. B., CHULICK, E. T., NAMBOODIRI, M. N., Phys. Rev. C6 (1972) 2133.
[4] PUHLHOFER, F., DIAMOND, R. M., Nucl. Phys A191 (1972) 561.
[5] BLANN, M., PLASIL, F., Phys. Rev. Lett. 29 (1972) 303.
[6] COHEN, S., PLASIL, F., SWIATECKI, W. J., Rep. LBL 1502 (1973).
[7] CHULICK, E. T., NAMBOODIRI, M. N., SMITH, G., MUNDEN, S. SCHNATTERLY, C., NATOWITZ, J. B., to be published in Nucl. Instr. and Meth.
[8] BUTLER, G. W., POSKANZER, A. M., LANDIS, D. A., Nucl. Instr. and Meth., 89 (1970) 189.
[9] CHULICK, E. T., NATOWITZ, J. B. AND SCHNATTERLY, C., Nucl. Instr. and Meth., 109 (1973) 171.
[10] BRITT, H. C., QUINTON, A. R., Phys. Rev. 124 (1961) 877.
[11] WILKINS, B., IGO, G. Proceedings of the Third Conference on Reactions Between Complex Nuclei, Pacific Grove, California, University of California Press, Berkeley (1963) p. 241; T. D. THOMAS, Phys. Rev. 116 (1959) 703.

DISCUSSION

F. PLASIL: I should like to say first of all that one needs to be careful about applying the liquid drop model to such very light nuclei. Secondly, it seems to me that a fair portion of your reaction involves partial waves that are below the Businaro-Gallone line, where the fission mass distribution is expected to have a minimum at symmetric mass divisions, and maxima near the compound nucleus mass and also at very light particles (such as H and He). Thus it may be difficult conceptually to separate fission from particle evaporation in this region, and this may have an influence on your conclusions.

J.B. NATOWITZ: It is true that one may run into semantic difficulties in discussing the fission of light elements. But in answer to your comment regarding the Businaro-Gallone limit, we appear to have made nuclei with angular momenta as high as 40 ħ. In the ^{39}K nucleus, the Businaro-Gallone limit occurs at an angular momenum of 32 ħ. Assuming that any fission results overwhelmingly from the high angular momentum states, our upper limit of 180 mb for the fission cross-section implies that nuclei with angular momenta of 37-40 ħ are those which fission. These nuclei are above the Businaro-Gallone limit. Thus, while the mass distribution from fission may be broadened, the liquid drop model predicts symmetric fission. Extremely asymmetric fission would not be expected. If fission were so asymmetric as to be indistinguishable from small particle evaporation, then the heavy partner would appear to be an evaporation residue and the cross-section for evaporation residues would be the fusion cross-section.

J. R. HUIZENGA: The calculation of the fission cross-section by the Blann-Plasil program must be considered as only a very approximate calculation and one should not expect to be able to calculate absolute fission cross-sections from a given set of parameters. However, the general philosophy of the calculation must be correct and, hence, for some angular momentum fission must compete with particle evaporation.

J. B. NATOWITZ: There certainly are problems involved in such a calculation, but since the calculations have been interpreted as suggesting a very large difference between the fusion cross-section and the cross-section for nuclei surviving fission (the evaporation residues), we feel that detailed comparisons must be made.

M. BLANN: Plasil and I tried to specify what we could and could not calculate in the published letter describing these calculations, but the point seems to have been lost. The idea of the model is that, as the angular momentum increases, the fissionability increases. At low values of the angular momentum in light systems the de-excitation is likely to be by particle emission and not by fission. Consider a plot of partial reaction cross-section, as one might calculate from an optical model, versus angular momentum J. At some low value of J the calculation says the fission barrier is high and the system should de-excite by particle emission. When the angular momentum becomes sufficiently high, the system becomes more likely to de-excite by fission. Now, to simplify the argument, assume that the system, above some angular momentum, does de-excite by fission. Then, below that angular momentum is the cross-section you are likely to find as the evaporation residue, and thus we say we can predict the cross-section for making the evaporation residue. What we do not say is that we therefore predict the cross-section for fission. As Mr. Wilczyński has pointed out (and the Zebelman-Miller experiments have shown), the systems may not form a compound nucleus above this critical angular momentum, according to calculations based on the contact configuration of the two bodies. Hence, in our calculation we could add another thousand partial waves to the calculation and the amount that would come out in the evaporation residue simply would not change, because the calculation gives the amount which is likely to survive fission at low angular momentum. It does not really claim that everything above that did form a compound nucleus and did come into the fission cross-section.

J. B. NATOWITZ: I do not think that the argument about high partial waves has been misunderstood. My point is simply that we make nuclei with 40 $\hbar$, equal to the liquid-drop-calculated limit, and well above the 22 $\hbar$ limit calculated by Wilczyński. After throwing away all partial waves with $J > 40\,\hbar$ your model predicts that 50% of the fused nuclei will fission. Less than 18% do fission. The validity of the statistical model approach would seem to require a cross-section for real fission of 500 mb.

LIGHT-PARTICLE-ACCOMPANIED FISSION

(Session IX)

Chairman: L. Yaffe (Canada)

RECENT STUDIES ON POLAR EMISSION*

E. PIASECKI, M. DAKOWSKI, A. KORDYASZ
Institute of Nuclear Research,
Świerk near Warsaw,
Poland

Abstract

RECENT STUDIES ON POLAR EMISSION

The intensities and spectra of the polarly emitted protons, deuterons, tritons and ^{6}He-particles have been investigated in the slow neutron fission of ^{235}U. The intensities of these particles relative to the alpha-particle polar emission are 21.5 ± 1.5, 2.75 ± 0.5 and 7.3 ± 0.9% and the mean kinetic energies are equal to 10 ± 0.5, 11 ± 0.5 and 13 ± 0.5 MeV, respectively. Not one polar ^{6}He event was detected per 1600 polar alphas. These results are compared with the theoretical predictions based on the evaporation hypothesis of polar emission. The phenomenon can partly be explained using this hypothesis, but some puzzling disagreements with theory have been observed.

The angular and energy distributions of alpha particles emitted during fission suggest that the time and place of emission is somewhere in the vicinity of the scission point. However, recent measurements have proved [1-4] that a certain proportion of alpha particles fly along the fission axis, which is difficult to interpret assuming the usual tripartition mechanism. Calculations of the classical trajectories have shown that alpha particles emitted from the neck (or, more generally, from the inner part of the two-fragment system) would be deflected off the fission axis owing to the fragment Coulomb forces. This phenomenon is called "polar emission". For these particles, shadow cones would exist, centred along the fission axis, on the outer sides of the system.

The experimental facts regarding polar emission are briefly as follows: its intensity, determined on the basis of the angular distribution [2], is about 2% of the total tripartition rate, thus it occurs once per 25 000 fissions; emission along the light fragment trajectory is over three times as frequent as that in the opposite direction, the mean energy of the alpha particles being about 23 MeV; the mean masses of fragments in this process are similar to the ones observed in binary fission, but the mean kinetic energy of the fragments flying in the direction of the alphas is diminished by about 12 MeV (as measured for the light fragments). We performed extensive calculations [2,5] trying to verify the hypothesis that polar emission is the result of the in-flight evaporation from the excited fission fragments. We were able to explain quantitatively the mean masses of fission fragments in this process, the energy spectra of alphas emitted in both directions, as well as the intensity of emission in the heavy-fragment flight direction, without applying parameter fitting. The observed large anisotropy of polar alpha-particle emission (in the fragment reference system) and the intensity of emission from the light fragments are difficult to interpret. This intensity appeared to be about 12 times greater than that calculated.

* This work has been carried out under the International Atomic Energy Agency Contract No. 1126/RC.

It was possible to explain the latter fact by taking into account the deformation of light fragments. However, this explanation was uncertain because of the approximation used and because of the sensitivity of the results to the parameter uncertainties.

It was possible to predict [2, 5], on the basis of the evaporation hypothesis, the intensity and spectra of particles other than alphas. To verify these predictions we performed an experiment in which we searched for the polar protons, deuterons, tritons and ^{6}He.

The experimental setup was briefly as follows; the ^{235}U target was irradiated in the reactor neutron beam, the polar particles were identified and their intensities and spectra were measured using a solid state telescope and the two-parameter analyser in a E-ΔE configuration gated by fission fragments. The geometry of the experiment is shown in Fig. 1.

The preliminary results are reported here. Our calculations [2, 5] indicate that the ^{6}He particles would be practically absent in the shadow cones, the predicted intensity being of the order of 10^{-3} % of the polar alphas, and this can be compared with the 1% relative intensity in normal tripartition. During our measurements, we registered 1600 polar alphas and not a single polar ^{6}He event, which at least does not contradict our prediction. The calculated results for protons, deuterons and tritons are somewhat shifted towards higher energies as compared with the experimental spectra (Fig. 2). These differences cannot be accounted for by experimental errors only, and this fact had already been observed in alpha polar emission. In the latter case the agreement was improved when fragment deformation was taken

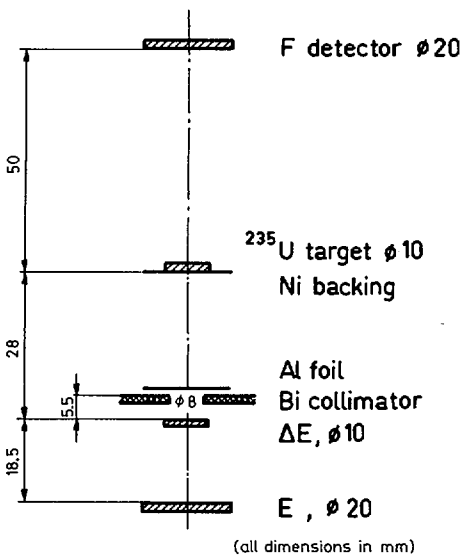

FIG. 1. Geometry of the experiment. ø denotes the diameter.

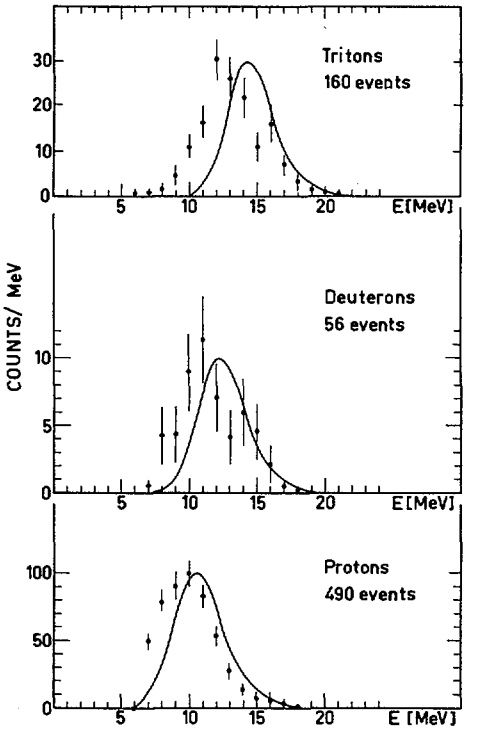

FIG. 2. Calculated and measured spectra of polar particles.

into account. Comparison of the predicted and measured intensities of polar particles in the fission of ^{236}U is shown in Fig. 3. It may be seen that the evaporation model accounts quite well, without any parameter fitting, for the relative intensities of polar emission of the particles examined, but all the theoretical results are too low by a factor of about four. The reason for this is not yet clear. In the case of alpha particles only a part of the discrepancy can be accounted for by the uncertainties of the model parameters. Most of it is connected with the emission from the light fragments, and we have linked it with their deformation. In the present experiment we did not differentiate between the fragments. However, according to our calculations, the inclusion of deformation in the evaporation model results in a substantial improvement in the agreement with experiment for the alpha particles but not for protons, deuterons or trirons.

The main conclusions of this work are:

(a) There exists not only alpha but also proton, deuteron and triton polar emission. In fact, the magnitude of the proton polar emission intensity is comparable to that of normal proton tripartition.

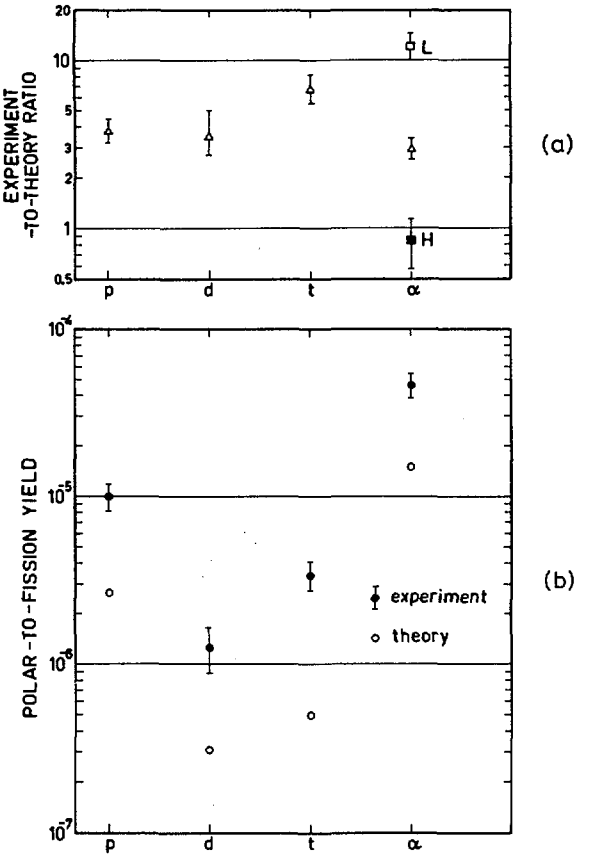

FIG. 3. Comparison of the measured and calculated ratios (a) and yields (b) of polar particles. Note that for alpha particles, disagreement is observed only for light (L) fragments.

(b) Some of the predictions based on the evaporation hypothesis agree remarkably well with the experimental results, and it is difficult to believe that this could be purely accidental. On the other hand, the results of this experiment can be considered as an indication that either the approximation used to account for the deformation is not applicable in this case or the nature of polar emission is more puzzling than we had expected.

REFERENCES

[1] PIASECKI, E., DAKOWSKI, M., KROGULSKI, T., TYS, J., CHWASZCZEWSKA, J., Phys. Lett. 33B (1970) 568.
[2] PIASECKI, E., BŁOCKI, J., Nucl. Phys. A128 (1973) 381.
[3] NADKARNI, D.M., KATARIA, S.K., KAPOOR, S.S., RAMA RAO, P.N., Nucl. Phys. A196 (1972) 209.
[4] RAJAGOPALAN, M., THOMAS, T.D., Phys. Rev. C5 (1972) 1402.
[5] PIASECKI, E., BŁOCKI, J., Acta Phys. Pol. (in press).

DISCUSSION

S.S. KAPOOR: Did your evaporation calculations take into account the distributions in the isotopic composition, excitation energy and fragment spin?

E. PIASECKI: The calculations were performed for over 500 different nuclei produced in fission and we took into account the excitation energy distribution, the dependence of this distribution on the fragment mass, and the primary fragment spin distribution. We did however assume that the spin distribution is independent of other variables, such as A, Z, and E_x.

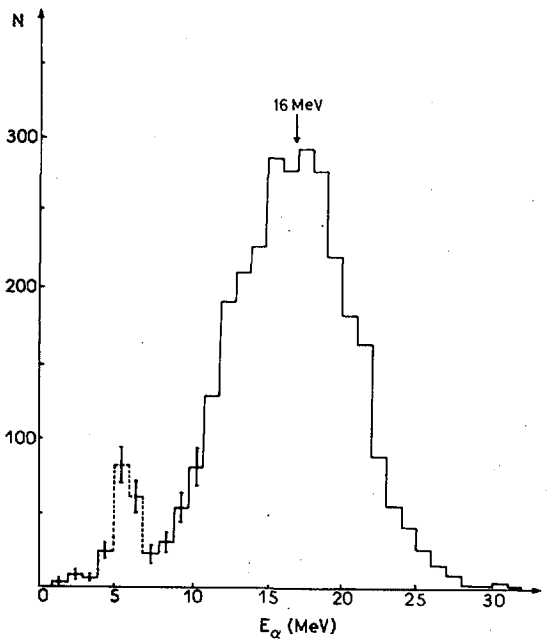

FIG. A. Kinetic energy distribution of alpha particles accompanying fission.

M. ASGHAR: It seems that three types of particles are emitted in light-particle-accompanied fission. We have just seen the data of M. Piasecki and his colleagues for "polar" light particles; our figure (Fig. A) now shows two other types, firstly, the normal long-range alpha particles with $\langle E \rangle \approx 16$ MeV and, secondly, the short-range alpha particles with $E_{max.} \leq \sim 7.5$ MeV. These short-range alpha particles seem to have the same form of angular distribution as the long-range ones[1]. I feel that any effort to consider the emission probability of these light particles should take into account these different types of particles.

D.G. VASS: Feather[2] has recently considered the origin of the short-range alpha particles in fission. He suggests that these alpha particles are

[1] ASGHAR, M., CARLES, C., DOAN, T.P., CHASTEL, R., (unpublished results), Bordeaux.

[2] FEATHER, N., Proc. R. Soc. Edinb. 71A (1973) Part 4.

emitted from certain fragments after neutron emission is complete. The residual fragment is left with excitation energy less than its neutron binding energy but greater than its alpha-particle binding energy, so that an alpha particle may be emitted in competition with gamma-ray de-excitation. The kinetic energy of the alpha particle is of course confined to a rather narrow energy range.

SIMULTANEOUS EMISSION OF TWO LIGHT-CHARGED PARTICLES IN SPONTANEOUS FISSION OF ^{252}Cf§

S.K. KATARIA, E. NARDI, S.G. THOMPSON
Lawrence Berkeley Laboratory,
University of California,
Berkeley, Calif.,
United States of America

Abstract

SIMULTANEOUS EMISSION OF TWO LIGHT-CHARGED PARTICLES IN SPONTANEOUS FISSION OF ^{252}Cf.

The emission of two light-charged particles in the spontaneous fission of ^{252}Cf has been observed and studied. Two particle telescopes were placed on opposite sides of a strong ^{252}Cf source covered on both sides by platinum foils. The coincidences between the two telescopes were mainly of the type ^{4}He-^{4}He although ^{4}He-^{3}H events were also observed. The energy spectra of the detected particles – alphas and tritons – are similar in shape to the spectra of normal long-range particles, but the mean energies are lower by about 2 MeV. The mean energy of one alpha particle in the ^{4}He-^{4}He coincidences does not change as a function of the energy of the other particle. The angular correlation between these particles has also been measured in another experiment (at five angles: 180°, 90°, 66°, 45°, 35°) without particle identification. The overall emission rate of the coincident particles is approximately two per million binary fission events. The hypothesis of independent emission of these two particles seems to be consistent with most of the observed data. Trajectory calculations are being performed to deduce the condition of the fissioning nucleus at scission configuration.

INTRODUCTION

The process of nuclear fission accompanied by a third light-charged particle (LCP) has been the subject of many investigations [1]. The prime reason for these studies is that the light-charged particles appear to be coming from the region between the larger fragments at a time close to scission. Therefore, the study of this process is expected to yield information on the fissioning nucleus at the scission point. Recently, Kapoor and co-workers [2] found evidence for the simultaneous emission of two LCP in coincidence with fission fragments in the thermal-neutron-induced fission of ^{235}U. In the present work we have observed the occurrence of the simultaneous emission of two LCP in the spontaneous fission of ^{252}Cf, we have identified the coincident LCP and obtained their energy distributions, and we have measured the angular correlation between the two particles. Various correlations between the two coincident LCP have also been studied.

The experiment has been performed in two parts. In the first part, two particle telescopes were used to identify the coincident LCP and to obtain the energy distribution of each type of particle observed. In the second part, two surface barrier detectors were used to obtain the yield of the coincident LCP events without any particle identifications for various angles between the two detectors.

§ Work performed under the auspices of the US Atomic Energy Commission.

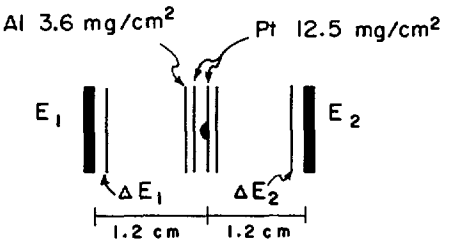

FIG. 1a. The schematic diagram of the detector-source configuration used in the Part 1 experiment. The first set of measurements were made using 50-μm ΔE_1 and 48-μm ΔE_2 counter telescopes. The second measurement used 37-μm ΔE_1 and 24-μm ΔE_2 counter telescopes.

EXPERIMENTAL PROCEDURE

Part 1. Identification of the LCP in quaternary fission

Two semiconductor particle telescopes were placed on opposite sides of a strong ^{252}Cf source as shown in Fig. 1a. Each telescope was at a distance of 1.2 cm from the source. The source strength was 0.6×10^7 fissions per minute. The source was covered on both sides by two absorber foils: 12.5 mg/cm^2 of platinum and 3.6 mg/cm^2 of aluminium. The thicknesses of the foils were selected in such a way as to prevent the fission fragments and the 6.18-MeV alpha particles from reaching the particle telescope. Two measurements were made using different thicknesses for the ΔE counters in the particle telescopes. The first measurement was performed with a 50-μm ΔE_1 and a 48-μm ΔE_2 counter. The second measurement was carried out using a 37-μm ΔE_1 and a 24-μm ΔE_2 counter to study the low-energy part of the alpha-particle distributions in quaternary fission.

A four-parameter data acquisition system was used to record the information from the coincidence events. The four-parameter system was triggered by the occurrence of a fast coincidence between the two ΔE counters. Therefore, all the two-fold events ($\Delta E_1 - \Delta E_2$), three-fold events (ΔE1-TEL2 and vice-versa), and four-fold events (TEL1-TEL2) were recorded. The fast coincidences were realized by using the zero cross-over technique with a time resolution of 40 nsec. The energy calibrations for all the detectors were done twice a week during the entire measurement which lasted for two months. The timing between the two ΔE counters was monitored using a ^{228}Th source (8.78-MeV alpha particles). Essentially, no timing or pulse-height shift was observed. The data analysis was done off-line. The particle identification was performed by using a power law approximation to the range-energy curves [3].

Part 2. Angular correlation between the two LCP

The angular correlation experiment was carried out with a ^{252}Cf source, stronger by an order of magnitude than the one used in the Part 1 experiment. With the new source, the true-to-chance rate decreased to a ratio of 2 to 1 within the two-telescope setup. Therefore, to have a reasonable true-to-chance ratio, both telescopes were replaced by semiconductor

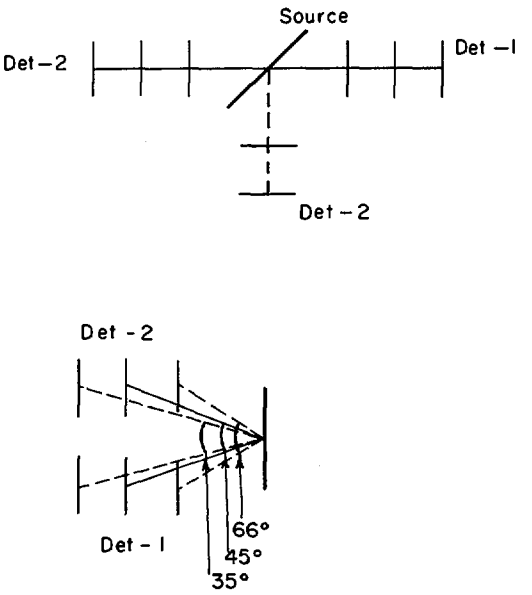

FIG. 1b. The schematic diagram of the eight measurements of the Part 2 experiment. Three different distances were used for 180° and two distances were used for 90° measurements. Three measurements were made for 66°, 45° and 35° angles between the two detectors.

detectors and the electronic configuration was also modified. The modified configuration was not possible with the two-telescope setup and the available four-parameter data acquisition system. Two time pickoff units were used to obtain the timing signals which were fed to a time-to-amplitude converter (TAC). The two linear energy signals from the two counters and the linear time signal from the TAC were recorded event by event on the multiparameter data recording system. The time distribution obtained showed a time resolution of 3 nsec. The window on the time signal was set at 6 nsec as compared to 40 nsec in the first part. The true-to-chance ratio varied from 20 to 1 for the 45° measurement to 8 to 1 for the 90° measurement.

Figure 1b shows the various configurations of the two detectors which were used to obtain the angular correlation between the two LCP. These measurements were divided into three sets. In the first set A (Table I), the distance between the detectors and the source was 2.0 cm for the 90° and 180° measurements and 2.2 cm for the 66° measurement. In the second set, these distances were 3.2 cm for the 90° and 180° measurements and 3.5 cm for the 45° measurement. The third set includes measurements for angles 180° and 35°; the corresponding distances were 4.5 cm and 4.75 cm. For the 90° and 180° measurements the effective thickness of the absorber foils was identical for both detectors (1.4 times thickness), whereas for 66°, 45° and 35° the effective thickness of the absorber foils varied (1.2 - 1.15 times thickness).

Table I. Summary of angular correlation experimental data. $\bar{E}_1$ and $\bar{E}_2$ are the mean energies of the distribution observed in detector 1 and 2 with E_{min} = 5 MeV. Quantity P is a measure of the angular correlation as defined in the text.

Set	Angle	Time (h)	Events	P	Quaternary		Ternary	
					$\bar{E}_1$	$\bar{E}_2$	$\bar{E}_1$	$\bar{E}_2$
A.	66°	495	581	2.8±0.3	10.1±0.2	9.85±0.2	12.61±0.2	12.72±0.2
	90	220	309	1.65±0.2	10.7±0.5	10.0±0.5	12.20±0.2	11.91±0.2
	180	187	335	2.2±0.2	9.2±0.6	10.2±0.4	11.77±0.4	11.71±0.2
B.	45°	520	410	10.2±0.6	10.1±0.2	9.8±0.2	11.30±0.2	12.20±0.2
	90	520	113	1.5±0.2	11.2±0.5	9.9±0.5	13.5±0.3	12.7±0.3
	180	384	109	2.3±0.2	10.2±0.5	10.2±0.5	12.2±0.3	12.7±0.3
C.	35°	362	79	8.5±1.0	9.5±0.7	9.4±0.7	11.91±0.2	12.3±0.2
	180	691	52	2.1±0.5	9.3±0.8	9.4±0.8	12.37±0.2	11.8±0.2

RESULTS

Part 1. Identification of LCP

The coincident events were predominantly of the type ^4He-^4He but ^4He-^3H and ^4He-^1H events were also observed. No coincident events involving particles heavier than Z = 2 particles were observed. A significant part of the events involving ^1H is due to the fast-neutron-induced (n, p) reaction in the detectors in coincidence with long-range alpha particles. However, the contribution of (n, p) reactions to the (^1H, ^4He) events where the energy of ^1H is larger than 5 MeV is insignificant [4]. Table II shows the observed number of various types of coincidence events using thick 50-μm ΔE counter telescopes. Table III contains the relative yields of protons, tritons, ^4He and ^6He normalized to unity for each telescope

Table II. The total number of events for various types of coincidences between the two light-charged particles (LCP) emitted in the spontaneous fission of ^{252}Cf observed in the experiment using 50-μm ΔE telescope systems. p: protons, t: tritons, α: alpha particles.

Telescope-1	-	Telescope-2	No. of events
p	-	p	10
p	-	t	0
p	-	α	16
t	-	p	5
t	-	t	1
t	-	α	66
α	-	p	12
α	-	t	82
α	-	α	551

Table III. The relative abundances of protons, tritons and alpha particles, normalized to unity, observed in each telescope for quaternary and ternary fission events with 50-μm ΔE telescopes in the experiment set 1.

Relative Prob.	Quaternary		Ternary	
	Tel-1	Tel-2	Tel-1	Tel-2
Protons	.035±.01	.03±.01	.03±.01	.015±.01
Tritons	.097±.01	.11±.01	.09±.01	.09±.01
Alphas	.87 ±.01	.85±0.01	.88±.01	.895±.01
^6He			.01±.005	.01±.005

in ternary and quaternary fission events. It can be seen that, within the statistical error, these relative yields in normal ternary fission events are equal to the corresponding relative yields in the fission events with two light-charged particles (quaternary fission).

Figures 2a to 2e show the energy distributions of alphas, tritons, and protons observed in quaternary fission. The smooth curves passing through the experimental points are calculated curves. They are obtained by fitting to the experimental spectrum a Gaussian distribution with $\hat{E}$, $\hat{\sigma}$ as the most probable energy and variance parameter, after making corrections for the energy loss in the absorber foils. These energy loss corrections were performed using a Monte Carlo technique to take into account the finite source-detector geometry. The fitted values of $\hat{E}$ and $\hat{\sigma}$ for various spectra are shown in Table IV. The dashed curves shown in Figs 2a to 2d are the corresponding energy distributions observed in normal ternary fission using the same telescopes. Figure 2a shows the energy spectrum of alpha particles in coincidence with alpha particles obtained with the 50-μm ΔE counter telescope in the first measurement. Figure 2b shows the same energy spectrum obtained in the second measurement with the 24-μm ΔE counter telescope. The second measurement was needed to obtain reliable values of $\hat{E}$ and $\hat{\sigma}$ for the alpha particles whereas the first measurement gives reliable information on tritons in coincidence with alpha particles. The energy distribution of alpha particles in coincidence with tritons is shown in Fig. 2c. From these figures it is concluded that the energy distributions of the alpha particles in quaternary fission is lower, compared to normal ternary fission, by about 2 MeV as given in Table IV. It can also be concluded that the alpha energy distribution in quaternary fission does

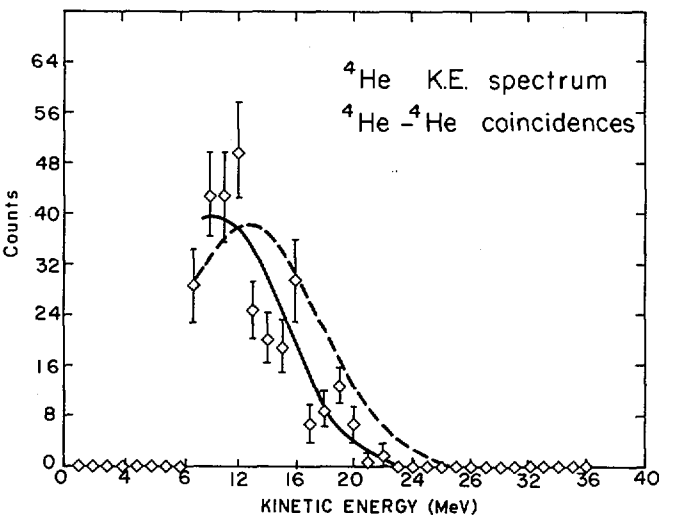

FIG. 2. The kinetic energy distribution of LCP in quaternary fission. The dashed curve is the kinetic energy distribution of LCP in normal ternary fission. The continuous curve is the fitted curve as explained in the text. (a) ^{4}He K.E. spectrum in ^{4}He-^{4}He events with 50-μm ΔE telescope.

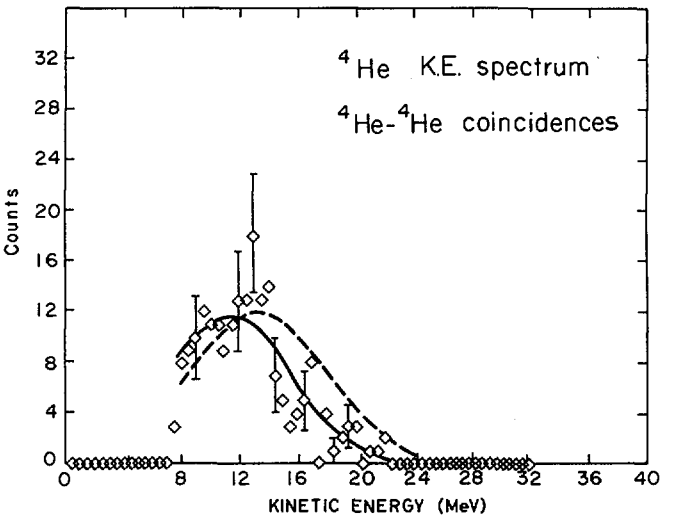

FIG. 2(b). ^{4}He K.E. spectrum in ^{4}He-^{4}He events with 24-μm ΔE telescope.

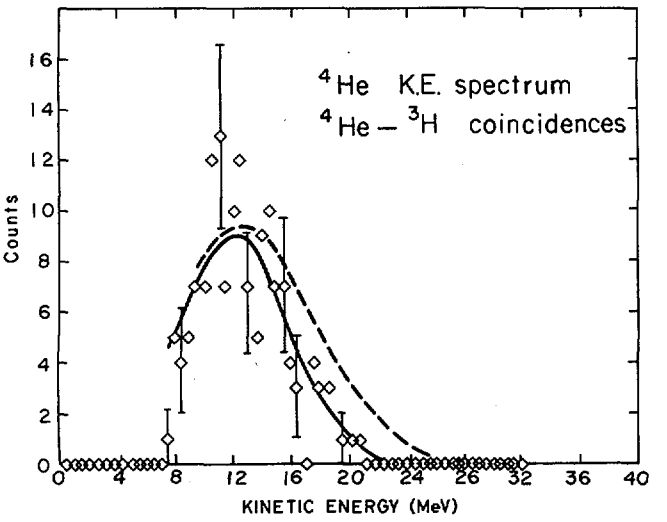

FIG. 2(c). ^{4}He K.E. spectrum in ^{4}He-^{3}H events with 50-μm ΔE telescope.

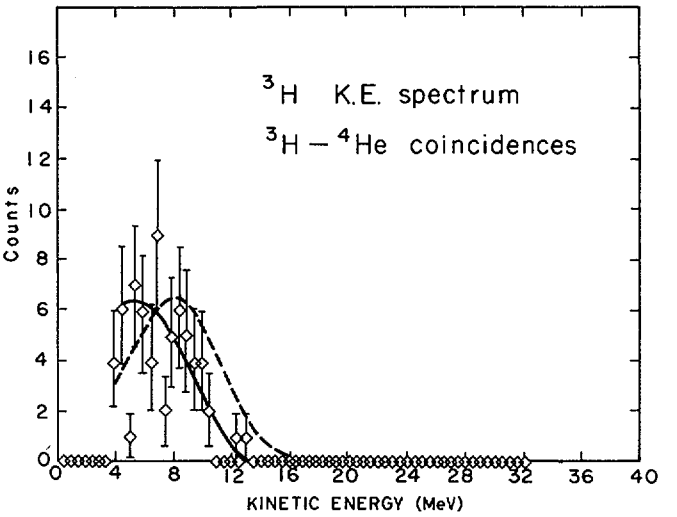

FIG. 2(d). ^{3}H K.E. spectrum in ^{4}He-^{3}H events with 50-μm ΔE telescope.

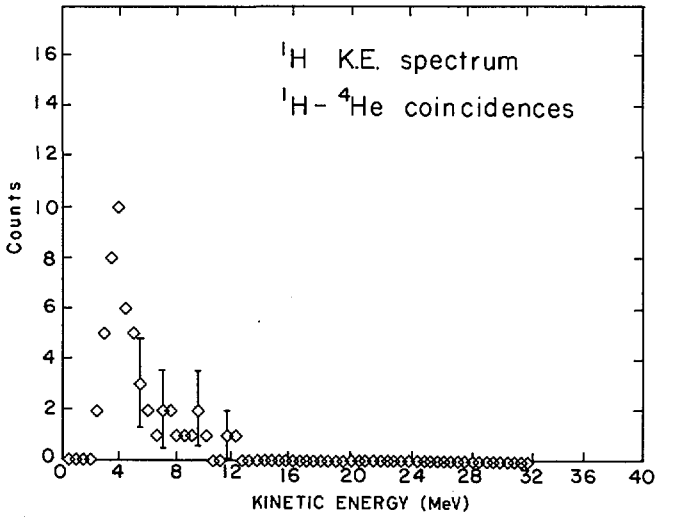

FIG. 2(e). ^{1}H K.E. spectrum in ^{4}He-^{1}H events with 50-μm ΔE telescope.

Table IV. Experimental and fitted parameters for energy distributions shown in Fig. 2a to 2e. $\hat{E}$ and $\hat{\sigma}$ are the most probable energy and the variance parameters of the Gaussian distribution. Fitted $\overline{E}$ and $\overline{\sigma}$ represent the mean energy and the variance of the energy distribution with (E_{min} = 8 MeV for α-particles and E_{min} = 4.0 MeV for tritons) computed after making corrections for the energy loss in the absorber cover foils to the Gaussian distribution. Experimental $\overline{E}$ and $\overline{\sigma}$ are the mean energy and the variance calculated from the experimentally observed energy distributions.

Identification	Fitted Parameters				Exp.	
	$\hat{E}$	$\hat{\sigma}$	$\overline{E}$	$\overline{\sigma}$	$\overline{E}$	$\overline{\sigma}$
Set-1. Alpha's in quaternary (α-α) events	13.5±0.5	4.0	12.9	2.8	12.9±0.5	2.9
Set-1. Alpha's in quaternary (α-t) events	14.00±0.8	4.0	13.06	3.2	12.75±0.5	2.9
Set-1. Alpha's in ternary events	16.1±0.2	4.4	14.5	3.6	14.2±0.2	3.7
Set-2. Alpha's in quaternary (α-α) events	14.0±0.6	4.2	12.9	3.4	12.7±0.6	3.6
Set-2. Alpha's in ternary fission	16.2±0.2	4.4	14.2	4.2	14.1±0.2	4.2
Set-1. Tritons in quaternary (t-α) events	6.6±0.8	2.6	7.2	1.9	7.3±0.5	2.1
Set-1. Tritons in ternary events	8.8±0.5	2.8	8.7	3.0	8.8±0.5	2.8

not depend on the charge of the coincident light particle. The mean energy of the alpha particles does not depend on the energy of the coincident alpha particle as shown in Fig. 3. Figure 2d shows the energy distribution of tritons in coincidence with alpha particles. The energy spectrum in quaternary fission is seen to be lower compared to the corresponding distribution in normal ternary fission. The difference in the most probable energy $\hat{E}$ for tritons in quaternary and ternary fission is about 2.0 MeV. The energy distribution of the protons in coincidence with alpha particles is shown in Fig. 2e. The low-energy peak at 4.0 MeV is due to the fast-neutron-induced reactions in the silicon detector. The statistical uncertainties were too large to obtain any information on the most probable energy.

Part 2. Angular correlation of LCP

The experimental results of the eight measurements are given in Table I. The lower energy cutoff used in the off-line analysis of the data was 5.0 MeV in the two counters, to reduce the contribution of the fast-neutron-induced reactions in the detector material which are in coincidence with the normal ternary fission events. The coincidence rate varied from 3 events per hour to 0.1 events per hour. The measurements were carried

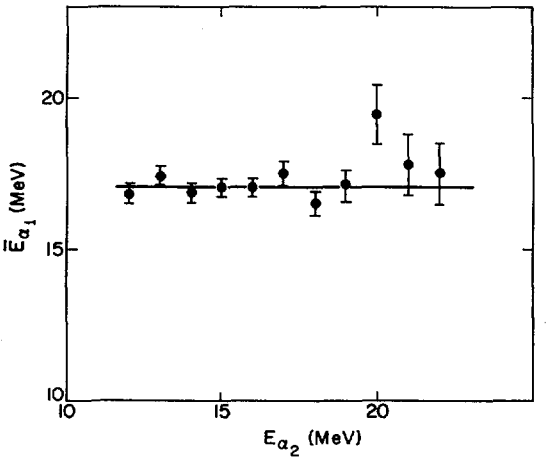

FIG.3. The mean kinetic energy distribution of alpha particles detected in telescope 1 plotted as a function of the kinetic energy of the coincident alpha particles detected in telescope 2.

out for a period of about six months to obtain good statistics. During the entire measurement no deterioration in the detector performance was observed. Table V summarizes the experimental information on the energy spectra of the coincident LCP and various other quantities of interest. The yields are given in terms of the constant P defined as follows:

$$N_1(\theta) = N P_3 \Omega_1(\theta) \epsilon_1$$

$$N_2(\theta) = N P_3 \Omega_2(\theta) \epsilon_2$$

$$N_{12}(\theta) = N P_4(\theta) \Omega_1(\theta) \Omega_2(\theta) \epsilon_1' \epsilon_2'$$

where

N is the source strength in fissions/h
P_3 and P_4 are the probabilities of ternary and quaternary fission per binary fission
Ω_1 and Ω_2 are the solid angles for the two detectors at angle θ
ϵ_1, ϵ_2, ϵ_1', ϵ_2' are the correction factors due to the absorber foils and the lower energy cutoffs
$N_1(\theta)$ and $N_2(\theta)$ are the number of ternary events in one measurement detected by detectors 1 and 2 respectively
$N_{12}(\theta)$ is the number of quaternary events in one measurement of duration H hours

$$P = \frac{N_{12}(\theta)\, H}{N_1(\theta)\, N_2(\theta)}$$

$$= \frac{N P_4(\theta) \Omega_1(\theta) \Omega_2(\theta) \epsilon_1' \epsilon_2'}{N^2 P_3^2 \Omega_1(\theta) \Omega_2(\theta) \epsilon_1 \epsilon_2} = \frac{P_4(\theta) \epsilon_1' \epsilon_2'}{N P_3^2 \epsilon_1 \epsilon_2} \qquad (1)$$

Table V. Fitted parameters $\hat{E}$ and $\hat{\sigma}$ are the most probable energy and the variance parameters of the Gaussian distributions for alpha particles fitted to the experimental spectra observed in angular correlation experiment. The energy loss corrections used were based on assumed values of triton/alpha probability and the assumed parameters for triton energy distribution as observed in Part 1 experiment. The fits were made only to four measurements.

Set	Detector	$\hat{E}$	σ	$\hat{E}$	σ
		Quaternary		Ternary	
A 66°	1	13.15±0.8	4.20	15.3±0.5	4.72
	2	12.70±0.8	3.65	16.30±0.5	4.90
90°	1	14.08±0.8	4.0	15.6±0.5	4.6
	2	15.0±0.8	4.8	16.05±0.5	4.21
180°	1	14.22±0.8	3.63	15.0±0.5	4.70
	2	13.5±0.8	4.3	15.5±0.5	4.45
B 45°	1	11.81±0.8	4.20	14.4±0.	4.24
	2	12.88±0.8	3.65	15.2±0.5	4.20

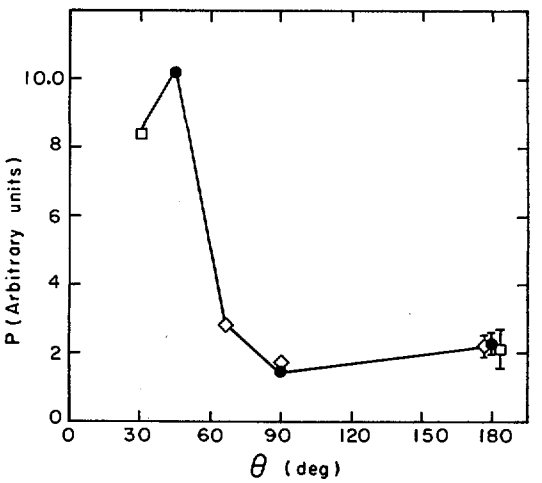

FIG.4. Plot of the quantity P which is a measure of the angular correlation as defined in the text for the eight measurements of the Part 2 experiment. The abscissa gives the angles between the two lines joining the centres of the detectors to the source. No corrections were made in this plot.

The probability of quaternary fission P_4 can be obtained from P, using the above relation. In Fig. 4, the measured value P for eight measurements is plotted against the angle θ between the two detectors. Figure 5 shows the plot of P_4 versus θ. These values were calculated using Eq. (1) and taking into account explicitly the finite source and finite detector geometry of the various measurements. The correction factors ϵ_1, ϵ_2, ϵ_1', ϵ_2' were calculated assuming that the energy spectrum of the light particles

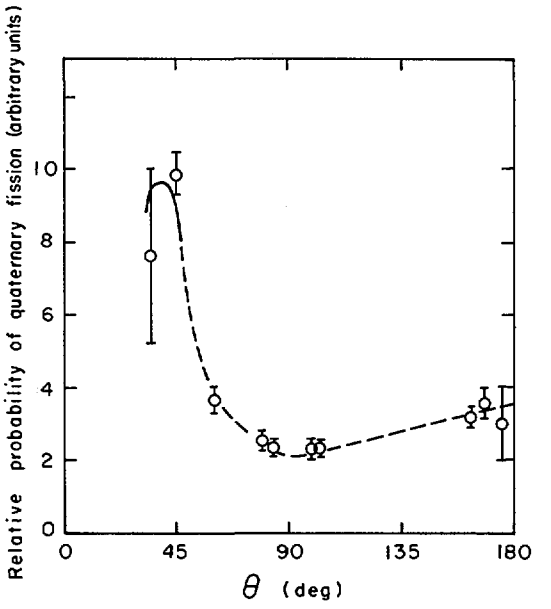

FIG. 5. Plot of the angular correlation between the two light-charged particles corrected for the energy loss in the absorber foils and the finite geometry of the detector-source geometry.

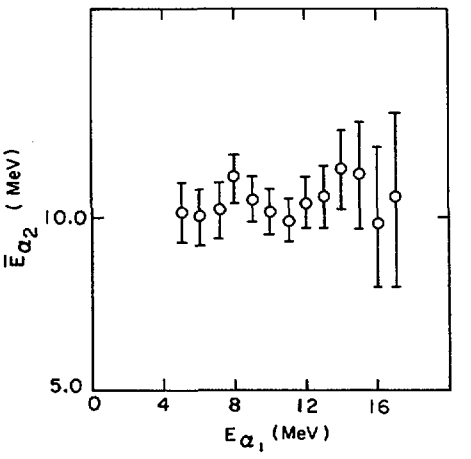

FIG. 6. The mean energies of light-charged particles in detector 1 in quaternary fission as a function of the energy of the second light-charged particle for set A-3.

does not depend on the angle θ. The parameters for the energy distribution involved were taken from the previous parameters measured with the two telescopes.

The mean energy of particles detected in one counter does not depend on the energy of the particle detected in the other counter, as shown in Fig. 6 for one measurement. This conclusion holds for all the measurements. Moreover, it is observed that the most probable energy $\hat{E}$ of the particles in quaternary fission does not depend on the angle between the two counters as shown in Table V for four measurements. The total probability obtained by integrating $P_4(\theta)$ is $(1.5 \pm 0.5 \times 10^{-6})$ per binary fission.

DISCUSSION

The experimental results on the energy distributions, angular correlation and the relative abundances of various particles in quaternary and ternary fission indicate that the two processes have very much in common. The relative abundances of tritons and alpha particles are identical within statistical error in the two types of fission events. The energy distribution of alpha particles in quaternary fission does not seem to depend on the nature of the coincident particle (tritons or alphas).

The energy distributions of tritons and of alpha particles in quaternary fission are very similar to the corresponding energy distributions in the normal ternary fission except for the fact that mean energies for these particles in quaternary fission are lower than in ternary fission. The angular correlation experiment shows that the yield at 90° is smaller than at 30° or 180°, although the yield at 30° is higher than the yield at 180°. It seems that the emission mechanism of light particles in quaternary fission is similar to the emission mechanism of light particles in ternary fission. If one assumes that the light particles in ternary fission are produced at scission from one of the two fragments when the interaction between the two fragments has vanished, then the quaternary fission events represent the cases where each fragment has contributed one LCP. Under the assumption that each fragment can emit only one LCP with probability P_i, which does not depend on the other fragment, the total probability of quaternary fission is $P_4 = P_1 P_2$. The probability of ternary fission will be equal to $P_1 + P_2$. Taking the experimental value of $P_1 + P_2 = 1/300$ and assuming $P_1 = P_2$, P_4 is equal to 2.6×10^{-6} per fission, which is in good agreement with the experimental value of P_4. This hypothesis is also consistent with the constancy of relative abundances of tritons and ^{4}He in two types of fission events.

Under the assumption that each LCP in the quaternary fission has a sharply peaked angular distribution with respect to the motion of the fission fragment, as in normal ternary fission, and assuming that the two LCP are emitted statistically independent of each other, there is an angular correlation between the two LCP as shown in Fig. 7. The calculated curve is symmetrical around 90°. The magnitude of the quantity $W(180°)/W(90°)$ is of the order observed in the experiment. However, the experimental correlation is not symmetrical around 90° as calculated under the hypothesis.

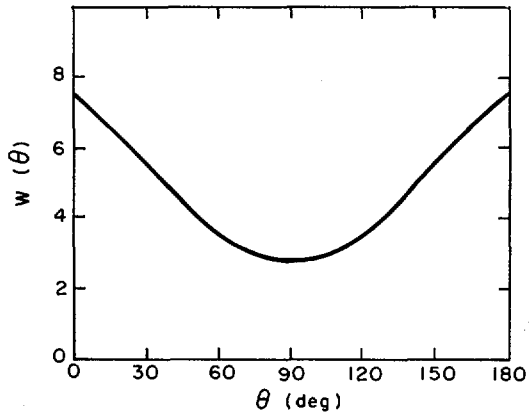

FIG.7. The angular correlation expected for quaternary fission based on the angular distribution of light-charged particles in ternary fission.

Trajectory calculations are being performed in an attempt to explain the lower mean energies of particles in quaternary fission compared to normal ternary fission and the observed asymmetry in the angular correlation data.

REFERENCES

[1] HALPERN, I., Ann. Rev. Nucl. Sci. 21 (1971) 245.
[2] KAPOOR, S.S., CHAUDHARY, R.K., KATARIA, S.K., MURTHY, S.R.S., RAMAMURTHY, V.S., Paper presented at the Nuclear Physics and Solid State Physics Symposium, Chandigarh, India, December 28-31, 1972 (Proceedings to be published).
[3] GOULDING, F.S., LANDIS, D.A., CERNY, J., PEHL, R.H., IEEE Trans. Nucl. Sci. NS-13 (1966) 514.
[4] CASPER, S.W., CERNY, J., GATTI, R.C., Phys. Rev. 154 (1967) 1193.

DISCUSSION

M. J. FLUSS: I would like to point out that the probabilities P_1 and P_2 for the emission of ternary particles may be calculated under either an independent or dependent probability assumption.

For the independent case: $P_1(1-P_2)+P_2(1-P_1) = 1/300$ and $P_1 P_2 = 1.5\times 10^{-6}$, giving $P_1 = 2.7\times 10^{-3}$, $P_2 = 0.55\times 10^{-3}$.

Similarly for the dependent case, assumed in your paper: $P_1(1-P_2) = 1/300$ and $P_1P_2 = 1.5\times 10^{-6}$, giving $P_1 \sim 3.33\times 10^{-3}$, $P_2 \sim 0.45\times 10^{-3}$.

The two assumptions give such similar probabilities, however, that they are not capable in themselves of elucidating the mechanism.

S. BJØRNHOLM: Is it possible that some of the quaternary events are due to the break-up of ^{8}Be?

S.K. KATARIA: The angle between the two alpha particles coming from the decay of ^{8}Be in the ground state is about 10° and they will

therefore not be detected in our experimental setup. The decay of ^{8}Be from the first excited state may be detected and therefore can be responsible for the higher yield at 35°.

D.G. VASS: I agree with Bjørnholm that ^{8}Be may be emitted in fission, and disintegrate in flight into two ^{4}He particles. If ^{8}Be nuclei are emitted in ternary fission, then we can estimate from the data given by Halpern[1] for other Be isotopes that the emission rate of ^{8}Be is approximately 0.3 per 10^{6} binary fission events. This rate is comparable with that of quaternary fission of 2 per 10^{6} binary fission events.

The calculation of the angular correlation of the ^{4}He particles is difficult, depending on the energy release in the break-up of ^{8}Be into ^{4}He particles and the lifetime of ^{8}Be. A simpler yet similar situation has been considered by Feather and myself[2] for the break-up of ^{5}He emitted in fission, as observed by Cheifetz and co-workers[3].

---

[1] HALPERN, I., Ann. Rev. Nucl. Sci. 21 (1971) 245.

[2] FEATHER, N., VASS, D.G., Proc. R. Soc. Edinb., 71A (1973) 233;
FEATHER, N., VASS, D.G., Proc. R. Soc. Edinb., 71A (1973) Part 4.

[3] CHEIFETZ, E., EYLON, B., FRAENKEL, Z., GAVRON, A., Phys. Rev. Lett. 29 (1972) 805.

ENERGY AND ANGULAR DISTRIBUTIONS OF ALPHA PARTICLES IN THE FISSION OF ^{252}Cf

K. TSUJI, A. KATASE, Y. YOSHIDA, T. KATAYAMA,
F. TOYOFUKU, H. YAMAMOTO
Department of Nuclear Engineering,
Faculty of Engineering,
Kyushu University,
Fukuoka, Japan

Abstract

ENERGY AND ANGULAR DISTRIBUTIONS OF ALPHA PARTICLES IN THE FISSION OF ^{252}Cf.

The energy distributions of the alpha particles emitted in the fission of ^{252}Cf have been measured with a good angular resolution to investigate the dependence on the angle between the alpha particle and the light fragment. The energies of one of the fission fragments and the alpha particle and the time difference between the signals for the two particles were measured and recorded event by event. The time resolution was about 2 nsec and the accidental events could be eliminated sufficiently. The light and heavy fragments were sorted by their kinetic energy.

The energy spectra were obtained at 9 angles from 65° to 105° and were well fitted by the Gaussian distribution for energies above about 13 MeV for each angle. The values of the most probable energy were found to have a minimum value of 14.0 MeV at 84° and increase rapidly with angle on both sides of 84°. The widths of the energy distributions were nearly independent of the angle and the FWHM value was about 8.6 MeV. The most probable angle of alpha particles with energy above 12.5 MeV with respect to the light fragment was found to be 84.3° and the FWHM value of the angular distribution was about 18°.

The alpha-particle energy distributions were calculated by the Monte Carlo method in the three-point-charge approximation. In this calculation, the distributions of the mass ratio and the total kinetic energy were taken into consideration, together with the distributions of the initial emission position, initial kinetic energy and emission angle of the alpha particle. The energy spectra, which were very similar to one measured at 90°, were obtained for some values from 21.5 fm to 26 fm of the distance D_f between two fission fragments at the emission of the alpha particle. From the comparison of the calculated distributions with the experimental ones for other angles, the value of about 22 fm for D_f was seen to be most consistent with the present experimental results.

1. INTRODUCTION

One of the characteristic features of the long-range alpha-particle-accompanied fission (LRA fission) is the angular distribution sharply peaked at about 90° with respect to fission fragments. This experimental fact has been interpreted to be the evidence showing that the alpha particle is emitted from a point between fragments at or shortly after scission. Because of this localization of position and time of the alpha-particle emission, the alpha particle has been considered to be a useful probe to investigate the dynamics of the scission stage.

As suggested by Halpern [1], there are two aspects of the study on the emission of the alpha particle. One is related to the mechanism of the particle emission, and the other to the motion of the particle in the Coulomb field after the emission. The chief aim of the latter is to determine the initial dynamical variables of the scission stage from the experimentally observed distributions. In connection with this problem a number

of experiments [2-6] have been done. These experimental results have usually been analysed in the framework of the three-point-charge model. The initial dynamical variables such as the distance between fission fragments and the kinetic energies of fission fragments and alpha particles at the instant of emission have been investigated [3-5, 7-11].

The results of the above investigations do not seem to agree with each other. For instance the values obtained for the distance between fission fragments are scattered in the range from 21.5 fm to 26 fm as summarized in the recent work by Rajagopalan and Thomas [5]. In the close scission configuration the fission fragments move rather slowly at the instant of scission, while in the stretched scission configuration the initial kinetic energy of the fragments amounts to 30-40 MeV. This dispersion in the values obtained for the initial conditions is considered to be due to the ambiguities of the experimental results which have been used in the analyses. The experimental values of the FWHM in the angular distribution range from 32° to 18.5° in the LRA fission of ^{252}Cf [2, 3, 5, 6]. These large differences result in quite different conclusions about the initial values of the dynamical variables. On the other hand, as discussed by Krogulski [10], there may be a possibility to reproduce the angular distribution and the energy spectrum of the alpha particles by using some other sets of the initial dynamical variables. So, one can expect to obtain more reliable conclusions by investigating the angle-energy correlation of alpha particles. The experimental results reported by Fraenkel [2] showed the qualitative behaviour of this correlation, but they are not sufficient for quantitative comparison with the results of trajectory calculations.

In the present work the angular distribution and the energy spectra of alpha particles in the fission of ^{252}Cf were measured with a good angular resolution (FWHM of 12°) from θ_L = 65° to 120° with respect to the light fragment. The results were analysed using the three-point-charge model. Monte Carlo calculations were performed by assuming rather reliable distributions for the initial conditions in a rather broad range of the distance D_f between fission fragments (D_f = 21.5-26 fm). The calculated energy spectra were compared with the experimental spectra at each angle θ_L to obtain the most probable values of the initial dynamical variables.

2. EXPERIMENTAL PROCEDURE

The experimental arrangement is shown schematically in Fig. 1. The intensity of a ^{252}Cf source was 6.0×10^4 fissions/sec. The alpha particle and one of the fission fragments were detected with surface barrier detectors of thickness 380 μm and 100 μm, respectively. The sentitive area of both detectors was confined by a rectangular aluminium slit of 5 mm $\times$ 17 mm to provide good angular resolution. The distance of the slit from the source was 30 mm for each detector. The alpha detector was fixed at 45° to the plane of the source. The fission detector was mounted on a rotating table. The angular dispersion provided by this geometrical arrangement was 12° (FWHM). The alpha detector was covered with an aluminium foil of 8.75 mg/cm^2 to stop the 6.11-MeV alpha particles and the fission fragments from the ^{252}Cf source. The aluminium foil stopped alpha particles up to the energy of 7.0 MeV.

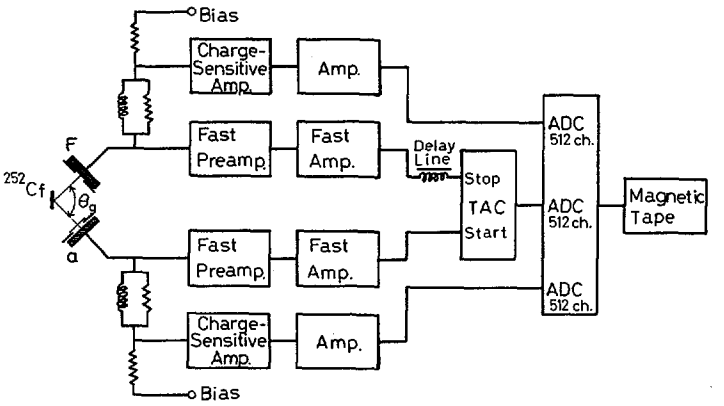

FIG. 1. Schematic diagram of the experimental setup.

As shown in Fig. 1, the energy signals and fast timing signals were provided from each detector. The fast timing signals were sent to a time-to-amplitude convertor (TAC). The energy signals of alpha particles and fission fragments and TAC output signals were fed to a multidimensional pulse-height analyser and stored event by event on a magnetic tape. Singles counting rates of the alpha-particle detector and fission detector were 91.2 counts/sec and 638 counts/sec, respectively. The TAC output was 2.2 counts/sec at an angle at 90°.

The measurements were done at the geometrical angles 70°, 75°, 80°, 85°, 90° and 100° with rather good statistics (110-210 h at each angle). Other short runs were performed to check the angular distribution at angles from 65° to 105° in steps of 5° (21-40 h at each angle). The total number of accumulated coincident events was about 70 000 for alpha particles above 10 MeV.

For the energy calibration of the alpha-particle detector, alpha particles of 6.058 and 8.780 MeV from ThC and ThC' were measured every 24 h. For the calibration of the fission detector, the energy spectra of the binary fission of ^{252}Cf were measured about every 12 h. The adopted peak energies of the light and heavy fragments were 103.8 MeV and 79.4 MeV, respectively. The fission detector was replaced after a few days' use, because further use caused deterioration in the fragment spectrum by the damage due to fission fragments.

Particle identification was not done in the present work. Therefore it was possible for light particles other than alpha particles to contaminate the spectrum. However, the contamination was negligible in the energy spectrum of the alpha particles above 13 MeV for the following reason. The triton is the most prominent contamination. The maximum energy of the triton expended in the alpha detector of 380 μm thickness can be considered to be less than about 10 MeV. This maximum energy of the triton corresponds to 13 MeV after the correction (t considered as an alpha particle) for the energy loss in the aluminium foil.

3. EXPERIMENTAL ANALYSIS AND RESULTS

The data stored on a magnetic tape were analysed after the measurements. For every event the channel number of the energy signal was converted to the energy value by using the results of the calibration measurements for each run and by correcting the energy loss of alpha particles in the aluminium foil. The timing spectrum is shown in Fig. 2a. The overall time resolution (FWHM) was 2.5 nsec. The width of the timing gate in the data analysis was chosen to be 12 nsec as shown in Fig. 2a. The accidental events were less than 1% of the true events at any angle. The energy distribution of the LRA fission fragments at $\theta_g = 90°$ is shown in Fig. 2b. (θ_g is the geometrical angle as shown in Fig. 1.) The most probable energies of the light and heavy fragments were 97.5 MeV and 74.5 MeV respectively, which agree with the previously reported values [2]. In the present work the light or heavy fragments were sorted by their kinetic energy. The discrimination energy was chosen to be the energy of the valley in the kinetic energy distributions at each geometrical angle This method did not completely discriminate light fragments from heavy fragments. The contribution from fragments of the other type was estimated to be less than 10% at any angle.

The energy spectra of the alpha particles were obtained for each angle θ_L or θ_H. The angle θ_H with respect to the heavy fragment was converted to the angle θ_L with respect to the light one according to the relation $\theta_L = 180° - \theta_H + \theta_R$, where θ_R is the recoil angle and was taken to be 4.5°. By summing the alpha particles above 12.5 MeV in the energy distribution at each angle, the angular distribution of the alpha particles with respect to the light fragment was obtained. It is shown in Fig. 3. The solid points show the number of alpha particles coincident with the light fragment, and the open circles show the alpha particles coincident with the heavy fragment. These two angular distributions were in agreement. The measured angular distribution of alpha particles with energy above 12.5 MeV has a FWHM of 22°.

The angular dispersion due to the finite size of the detectors and the source was calculated at each measured angle with the Monte Carlo method. The source was confirmed to have nearly uniform density within a 7-mm diameter by counting the fission fragment tracks in a polycarbonate sheet put on the source. The FWHM of the angular dispersion was 12.0°. The most probable angle and the width of the intrinsic angular distribution (assumed to be Gaussian) were obtained from a χ^2-fit. In this procedure the convolutions of the intrinsic distribution and the geometrical angular dispersions were calculated at all angles in order to obtain a fit to the experimentally observed angular distribution. The most probable angle and the FWHM of the intrinsic angular distribution were found to be 84.3° and 18.3°, respectively. The result of the fitting is shown in Fig. 3, where the dashed line gives the convoluted angular distribution and the solid line gives the obtained intrinsic one.

The present value of the FWHM is in good agreement with the recently reported value of 18.5° by Fluss and co-workers [6], but considerably smaller than the values of Fraenkel (32°) [2] and of Rajagopalan and co-workers (23.5°) [5]. As for the most probable angle, the present result is in very good agreement with the value by Fluss and co-workers (84.3°) [6], whose measurement was done with a good angular resolution.

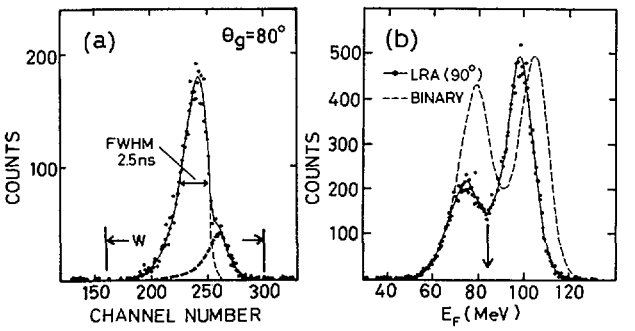

FIG. 2. (a) Timing spectrum at the angle θ_g = 80°. The dashed lines show the alpha particles coincident with the light (larger peak) and heavy (smaller peak) fragments. The region W was used in the data analysis. (b) The kinetic energy distribution of fission fragments for LRA fission at θ_g = 90° and for binary fission. The value of 85 MeV was used for the discrimination of the light and heavy fragments at this angle.

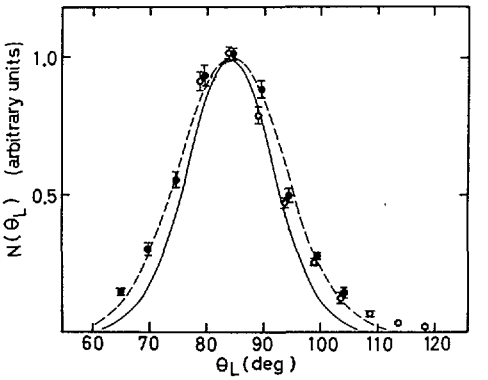

FIG. 3. Angular distribution of alpha particles with energy above 12.5 MeV. The solid circles show the alpha particles coincident with the light fragments. The open circles show the alpha particles coincident with the heavy fragmentss. The open circles are plotted at θ_L converted from θ_H with the relation $\theta_L = 180° - \theta_H + \theta_R$. ($\theta_R$ is taken to be 4.5°.) The dashed line gives the result of the fitting, and the solid line gives the intrinsic distribution obtained after correction for the finite size of the detectors and the source. $N(\theta_L)$ is the number of alpha particles.

The energy spectra of alpha particles were obtained at 70°, 75°, 80°, 90° and 100° for θ_L and θ_H with rather good statistics, and at θ_L = 65°, 95° and θ_H = 95°, 105° with rather poor statistics. Typical energy spectra at θ_L = 90°, 70° and θ_H = 70° are shown in Fig. 4. The energy spectrum at θ_L = 90° is in better agreement with the result by Raisbeck and Thomas [3] than with the one by Fraenkel [2]. Fraenkel's alpha-particle spectrum at θ_2 = 90° is broader than ours because his angular resolution is poor.

In the present work the most probable energy of the alpha particle was observed to depend strongly on the angle θ_L. The variation of the mean energy with the angle θ_L is shown in Fig. 5 for the alpha particles above

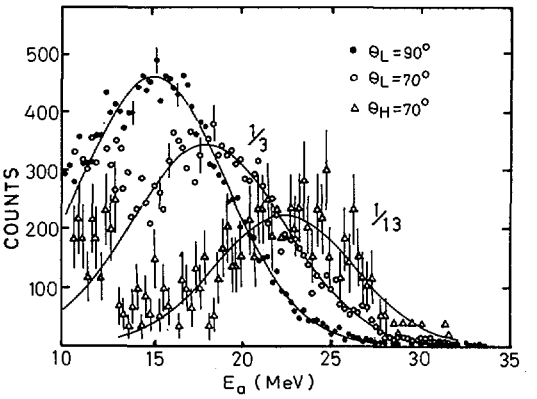

FIG. 4. Energy spectra of alpha particles at θ_L = 90°, 70° and θ_H = 70°. The solid lines are the results of the fit to the Gaussian curve at each angle for energies above 13 MeV.

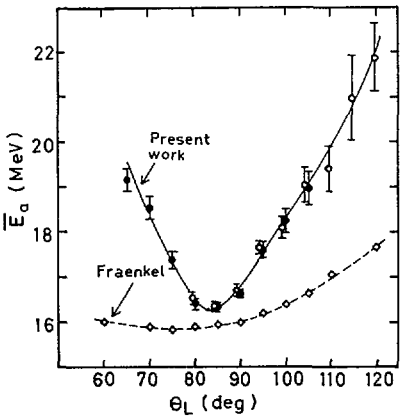

FIG. 5. Mean energy of alpha particles averaged above 12.5 MeV as a function of θ_L. The solid and open circles denote the same as in Fig. 3.

12.5 MeV. The similar result by Fraenkel is also shown in which the energy of the alpha particles above 11 MeV was averaged. The good angular resolution in the present work gives a strong dependence on the angle. The disagreement with respect to the angle where the average energy takes the minimum value is considered to be caused by the difference of the experimental method. In Fraenkel's work, both fission fragments were detected by two back-to-back fission detectors, and the non-collinearity of the fission fragments makes the effective angle larger than the geometrical one, as pointed out by Gazit and co-workers [4].

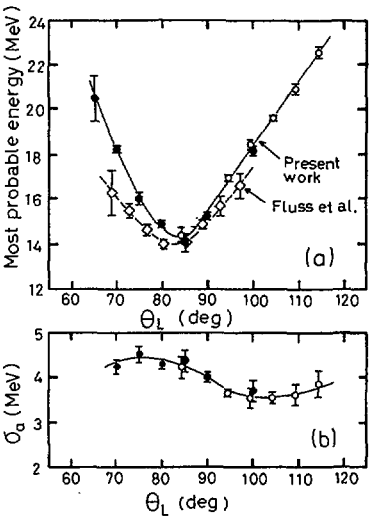

FIG. 6. (a) The most probable energy of alpha particles and (b) the standard deviation, both as a function of θ_L, obtained by fitting the energy spectrum above 13 MeV to a Gaussian curve. The error in the figure is due to the fit. The solid and open circles denote the same as in Fig. 3.

At angles far from the most probable angle, some increase in the number of alpha particles was observed below 13 MeV (see Fig. 4, θ_L = 70° or θ_H = 70°). It is not clear whether this is due to the contamination by tritons or due to some enhanced distribution of alpha particles at lower energy. In the energy spectrum according to the particle identification by Raisbeck and Thomas [3], some increase below 12 MeV was also observed at 60°.

To obtain reliable values of the most probable energy and the width of the distribution, the measured energy spectra were fitted to a Gaussian curve for energies greater than 13 MeV, where the distributions were considered to be free from triton contamination. The fit was rather good. The values obtained for the most probable energy and the standard deviation σ_a of a distribution are shown in Figs 6a and 6b, respectively, as a function of the angle θ_L and compared with the result by Fluss and co-workers. Both results show fairly good agreement. The most probable energy was found to have a minimum value of 14.0 MeV at about 84° and to increase rapidly with angle on both sides of 84°. On the other hand, the widths of the energy distributions were nearly constant and the value of the standard deviation was about 3.8 MeV.

4. THREE-POINT-CHARGE MODEL CALCULATION

The three-point-charge model calculations were performed to investigate to what extent the assumed sets of initial conditions could explain the present experimental results. Details of the trajectory calculation

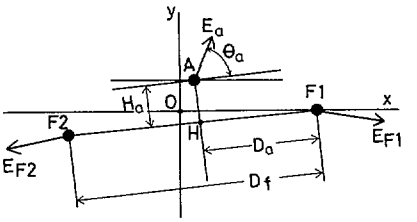

FIG. 7. Schematic diagram of the initial parameters of the calculation.

were described in a previous paper [9]. For a given mass ratio R and total kinetic energy E_T of three particles, the initial conditions were described with the following five quantities (see Fig. 7): (1) the distance D_f between two fission fragments, (2) the distance D_a between the light fragment F_1 and the foot H of the vertical line from the alpha particle A perpendicular to the fission axis, (3) the distance H_a of the alpha particle from the fission axis, (4) the initial kinetic energy E_a of the alpha particle and (5) the initial emission angle θ_a of the alpha particle with the fission axis.

To obtain the final distributions to be compared with the experimental results, Monte Carlo calculations were done by assuming distributions for the initial conditions, which are tabulated in Table I. In the previous calculations [9] the values R, E_T, and H_a were fixed, but in the present calculation the distributions of these values were taken into consideration. The distributions of R and E_T were estimated from the work by Fraenkel [2]. The ratios of the partial variance caused by the distribution of the value of each parameter to the total variance of the angular or energy distribution are given in Table I for D_f = 21.5 fm and 26 fm. The distribution of the mass ratio is a considerable contribution to the angular distribution, especially in the case of the smaller value of D_f. The distribution of H_a plays no important role in the final distribution, and the value of the standard deviation was taken rather arbitrarily. In the case of the larger value of D_f, the final energy distributions are determined principally by the distributions of E_a and θ_a, and the final angular distribution by the distribution of D_a. However, in the case of the smaller value of D_f, the contributions of each initial parameter are more complex. A change of the initial conditions causes a larger change of the motion in the Coulomb field in this case.

The calculations were made for D_f = 21.5, 22, 24, and 26 fm. The free parameters E_a and σ_{D_a} were adjusted to reproduce the most probable energy and the width of the angular distribution of alpha particles at θ_L = 90° for each value of D_f. The sets of the values obtained are shown in Table II. Using these values Monte Carlo calculations were done 7500 times and the energy distribution of alpha particles was calculated in steps of 1° of θ_L. The angular distribution was obtained by summing the number of alpha particles with energy greater than 12.5 MeV.

To compare with the measured energy spectra, the energy distributions were obtained by the convolution of the energy distributions calculated above

and the geometrical angular dispersion of the present experimental arrangement. The results of the calculations and comparisons with experimental results are:

(a) The width of the angular distribution and the most probable energy of alpha particles at θ_L = 90° were well reproduced by every set of values tabulated in Table II.
(b) The most probable angle of the calculated angular distribution shifted from 84° to 87° with an increase in the value of D_f. The experimental value of the most probable angle, 84.3°, is consistent with the smaller value of D_f.
(c) The FWHM of the energy distribution at θ_L = 90° increased slowly from about 7.5 MeV to 9 MeV with an increase in the value of D_f. This situation can be understood as follows. If D_f is small, the mean value of E_a must be small to reproduce the observed most probable energy. As E_a is assumed to have a Raisbeck-Thomas distribution, the small value of $\overline{E}_a$ causes a small width in the distribution of E_a, and the width of the final energy distribution has a tendency to be narrow. The energy spectra were rather well reproduced except for D_f = 21.5 fm, for which the width of distribution was somewhat narrower than the experimental one.
(d) For D_f = 21.5 fm rather good agreement was obtained between the calculated energy distributions and those measured at θ_L = 65° and 70°, but at the angles larger than 75° the FWHM of the distribution was narrower than the experimental one by 1-1.5 MeV. For D_f = 22 fm, good agreement was obtained with almost all the energy spectra from θ_L = 65° to 109.5°. It was observed in the results of the calculations that the distribution had a rather narrow width at the larger values of θ_L. This tendency agrees with the experimental one (see Fig. 6).

For D_f = 24 and 26 fm, a remarkable increase in the number of alpha particles was observed at the lower energy of the calculated energy distribution at angles far from the most probable angle, especially at θ_L = 65° and 70°. This increase is explained as follows. The alpha particles, which are emitted at the angle θ_L far from the most probable angle, will have two different origins in the present model: (1) alpha particles emitted at a point near one of the fission fragments; this case results in the higher final energy. (2) alpha particles emitted at an initial angle far from 90° and reflected by the Coulomb field of the fragment in the direction of the alpha particle; this case results in the lower final energy. Trajectory calculations were done for the conditions corresponding to the latter case, and the results showed that the effect of the scattering was quite strong for the larger value of D_f, because the focusing action by the Coulomb field of the two fragments after scattering was rather weak compared with the case of the smaller value of D_f. The observed enhancement of the calculated distribution of alpha particles at lower energy is considered to be due to (2) given above. Although there was some increase in the experimental distribution in the lower energy region (which may involve the contamination by tritons), it was not so remarkable as that calculated for D_f = 24 or 26 fm.

From the results mentioned above, it is concluded that the set of parameters for D_f = 22 fm is the one most consistent with the present experimental results. In Fig. 8, comparisons of the calculated with the

TABLE I. THE DISTRIBUTION OF EACH INITIAL PARAMETER USED IN MONTE CARLO CALCULATIONS AND THE RATIO OF THE PARTIAL VARIANCE TO THE TOTAL VARIANCE [a]

Parameter [b]	Distribution	Mean value	Standard deviation	Ratio of the partial variance to the total variance [e]			
				D_f = 21.5 fm		D_f = 26.0 fm	
				Angular distribution	Energy distribution	Angular distribution	Energy distribution
R [c]	Gaussian in the range of R = 1.0 - 2.0	1.33	0.14	0.148	0.020	0.092	0.002
E_T	Gaussian	180 MeV	10 MeV	0.010	0.110	0.006	0.023
D_f	Fixed	21.5 - 26 fm	-	-	-	-	-
D_a	Gaussian	Potential minimum	Adjustable	0.712	0.169	0.745	0.003
H_a	Gaussian	0 fm	0.85 fm	0.006	0.030	0.005	0.004
E_a	Raisbeck-Thomas [3] [d]	Adjustable	Determined by the mean value	0.017	0.439	0.053	0.790
θ_a	Isotropic	-	-	0.106	0.235	0.099	0.180

[a] The ratio of the partial variance caused by the distribution of each parameter to the total variance of the angular or energy distribution.
[b] The meanings of these parameters are explained in the text (see Fig. 7).
[c] The charge ratio of the fission fragment is assumed to be the same as the mass ratio.
[d] Gaussian distribution is assumed for each component of the momentum. $P(E_a) = \sqrt{E_a}\exp(-3E_a/2\bar{E}_a)$.
[e] The values of the adjustable parameters are taken to be $\bar{E}_a$ = 0.5 MeV, σ_{D_a} = 2.1 fm for D_f = 21.5 fm and $\bar{E}_a$ = 3.0 MeV, σ_{D_a} = 1.3 fm for D_f = 26.0 fm.

TABLE II. SETS OF THE INITIAL PARAMETERS[a]

No.	D_f (fm)	E_a (MeV)	σ_{D_a} (fm)	Most probable kinetic energy of fission fragments (MeV)
1	21.5	0.6	2.1	4
2	22.0	1.0	1.8	10
3	24.0	2.0	1.7	21
4	26.0	3.3	1.5	32

[a] The initial parameters were adopted to reproduce the experimental values of the width of the angular distribution and the most probable energy of alpha particles at $\theta_L = 90°$.

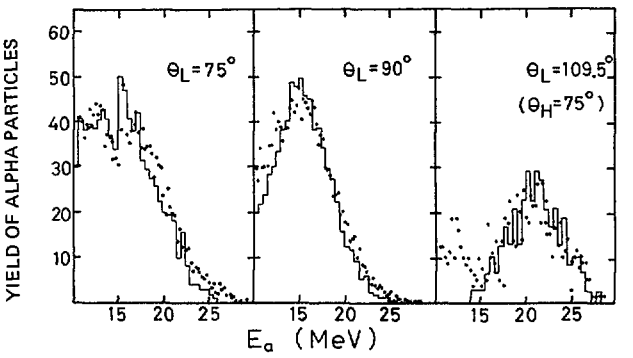

FIG. 8. Comparisons of the calculated and measured energy spectra at the angles θ_L = 75°, 90° and 109.5°. Histograms show the calculated and points show the measured spectra.

experimental energy spectra are shown. The value of D_f = 22 fm means that the total kinetic energy of the fragments is about 10 MeV at scission. These values of the initial parameters are similar to those obtained by Rajagopalan and co-workers [5], except for the initial kinetic energy of the alpha particles. Their value of E_a = 2.0 MeV seems to be too large to reproduce the energy spectrum. We believe that the two fission fragments at the initial stage in the LRA fission of ^{252}Cf are not so far apart as reported by Boneh and co-workers [7], and not so close as predicted by the statistical theory of Fong [12].

5. SUMMARY

The energy spectra of alpha-particle-accompanied fission of ^{252}Cf were measured at 9 angles from 65° to 105° with a good angular resolution. By identifying the light or heavy fragment from its kinetic energy, the

energy distributions of the alpha particles were obtained for the angle θ_L from 65° to 114.5°. These energy spectra show a strong dependence on the angle θ_L. The most probable energy of the distribution has the minimum value of 14 MeV at 84° and increases rapidly with angle on both sides of 84° The width of the energy distribution at each angle is nearly constant and the value of FWHM is about 8.6 MeV.

The most probable angle and the FWHM in the angular distribution of alpha particles above 12.5 MeV are 84.3° and 18.3°, respectively. These values are in good agreement with the values reported recently by Fluss and co-workers [6].

These experimental results were compared with the results of Monte Carlo calculations using the three-point-charge model. The distributions of initial parameters were assumed to be independent of each other as shown in Table I. In these calculations various sets of initial conditions were examined. The set D_f = 22 fm, $\bar{E}_a$ = 1.0 MeV and σ_{D_a} = 1.8 fm is the one most consistent with the angular distribution and the energy spectrum of alpha particles at each angle. Using the distributions of the initial dynamical variables adopted in the present work, it was difficult to reproduce the energy spectrum at each angle with the more stretched configuration as reported by Boneh, Fraenkel and Nebenzahl [7] or with the closer configuration as predicted by the statistical theory [12].

There may be some correlations in the initial conditions, for instance, the emission point of the alpha particle may correlate with the mass ratio associated with the fragment deformability at scission, as discussed by Fraenkel [2]. To clarify the possible correlation, more detailed experimental studies are desirable.

ACKNOWLEDGEMENTS

The authors greatly appreciate many fruitful discussions with members of the Department of Nuclear Engineering of Kyushu University. Thanks are also due to K. Marubayashi for his help in the programming and maintenance of the computer and to Y. Matsumoto for preparing the electronic circuits for the experiment.

REFERENCES

[1] HALPERN, I., in Physics and Chemistry of Fission (Proc. Symp. Salzburg, 1965) 2, IAEA, Vienna (1965) 369.
[2] FRAENKEL, Z., Phys. Rev. 156 (1967) 1283.
[3] RAISBECK, G.M., THOMAS, T.D., Phys. Rev. 172 (1968) 1272.
[4] GAZIT, Y., KATASE, A., BEN-DAVID, G., MOREH, R., Phys. Rev. C4 (1971) 223.
[5] RAJAGOPALAN, M., THOMAS, T.D., Phys. Rev. C5 (1972) 2064.
[6] FLUSS, M.J., KAUFMAN, S.B., STEINBERG, E.P., WILKINS, B.D., Phys. Rev. C7 (1973) 353.
[7] BONEH, Y., FRAENKEL, Z., NEBENZAHAL, I., Phys. Rev. 156 (1967) 1305.
[8] NARDI, E., BONEH, Y., FRAENKEL, Z., in Physics and Chemistry of Fission (Proc. Symp. Vienna, 1969), IAEA, Vienna (1969) 143.
[9] KATASE, A., J. Phys. Soc. Japan 25 (1968) 933.
[10] KROGULSKI, T., BLOCKI, J., Nucl. Phys. A144 (1970) 617.
[11] VITTA, P.B., Nucl. Phys. A170 (1971) 417.
[12] FONG, P., Phys. Rev. 102 (1956) 434; 122 (1961) 1543; B135 (1964) 1338.

CONNECTION BETWEEN LRA TO BINARY FISSION CROSS-SECTION RATIO FOR RESONANCE AND THERMAL-NEUTRON-INDUCED FISSION IN ^{239}Pu AND RESONANCE SPINS

A.J. DERUYTTER, W. BECKER
CBNM, Euratom, Geel

C. WAGEMANS*
SCK-CEN, Mol,
Belgium

Abstract

CONNECTION BETWEEN LRA TO BINARY FISSION CROSS-SECTION RATIO FOR RESONANCE AND THERMAL-NEUTRON-INDUCED FISSION IN ^{239}Pu AND RESONANCE SPINS.

The LRA to binary fission cross-section ratio was measured at an 8-m flight-path station of the CBNM LINAC. The heavy fission fragments in binary fission and the energetic light particles (E_α > 15 MeV) in LRA fission were subsequently counted with banks of solid state detectors on both sides of a double-faced ^{239}Pu sample, as a function of the incident neutron energy. Two measurements were performed, one to cover the neutron energy range up to 50 eV and the other to obtain accurate information through the 0.3-eV resonance. The T/B values were obtained by a division of the resonance areas in the first measurement. In the low-energy run the TOF spectra were divided in energy intervals from 0.02 to 1 eV and the ratios of the areas in the corresponding TOF spectra were calculated. The data analysis yielded for the 15.5-eV resonance a T/B value which was about 10% higher. In the low-energy region no inconsistency was found with a unique value for the ratio.

On the other hand, a careful analysis was performed of the accurate low-energy fission cross-section of ^{239}Pu obtained at CBNM, Geel, below 20 eV with the use of an interference formula. It was possible to show that this low-energy fission cross-section can only be adequately described when the 15.5-eV resonance has a spin and parity 0^+ and the other positive energy resonances below 20 eV are 1^+. These measurements suggest that a high T/B value is correlated with a 0^+ resonance.

1. INTRODUCTION

A preceding paper dealt with the ratio of ternary (two heavy fragments and a light fragment) to binary fission for the resonance neutron-induced fission of ^{235}U[1]. In this paper similar experiments are described for ^{239}Pu(n, f). We covered the low resonance region from 1 to 50 eV, and also the thermal range and through the first large resonance, i.e. from 0.020 eV to 1 eV. We furthermore performed a precise fission cross-section measurement in the low resonance and thermal region by comparison of the ^{239}Pu(n, f) rate and the rate of a ^{10}B foil. We tried to describe this cross-section with an interference formula and showed that the cross-section can only be adequately fitted with a spin 0^+ for the broad 15.5 eV resonance, which also showed a larger T/B value in the previous experiments.

By s-wave neutron (l = 0, s = 1/2) bombardment of ^{239}Pu nuclei (spin-parity $1/2^+$) compound states 0^+ and 1^+ are formed. According to the Bohr[2] and Wheeler[3] model, the 0^+ channels correspond

* NFWO, University of Ghent, Belgium.

either to the ground state or to the quadrupole vibration β of the nucleus at the saddle point, which are both essentially symmetric. The 1^+ channel is considered to be formed by a coupling of the two octupole vibrations $K = 0^-$ and $K = 1^-$, both asymmetric in nature. Based on the different characteristics of the 0^+ and the 1^+ fission channels, many attempts have been made to find a classification of the neutron resonances into two groups corresponding to both spin-states by measuring the mass-asymmetry[4], the total kinetic energy of the heavy fission fragments[5] and the average number of neutrons $\bar{\nu}$ emitted in fission[6][7][8].

The simple picture of transition states on the top of an inverted oscillator potential, and even the existence of this channel structure has been questioned recently in view of the description of the fission process with a double-humped barrier with discrete levels in the second well. However, the measurements reported here tend to confirm the channel theory of fission, although the subsequent interactions taking place between saddle point and scission point may produce an overall attenuation of the magnitude of the effects.

In the measurements described here we tried to classify the resonances according to their T/B ratio. In the region 1eV to 50 eV we calculated the T/B values for the resolved resonances. In the region from 20 meV to 1eV we calculated T/B throughout the whole spectrum. We also controlled the ternary α -PH spectrum, as recorded in the TOF experiment, by a subsequent measurement with a high-intensity neutron beam.

2. EXPERIMENTAL APPARATUS

The measurements were performed at an 8.1-m flight path of the CBNM linac (see Fig. 1). By bombarding a mercury-cooled uranium target with the 70 MeV electron beam of the linac, fast neutrons were produced which were then slowed down in a polyethylene slab mounted on top of the linac target. The target is surrounded by lead rings which suppress the γ - flash produced in the target by the impact of the electron beam of the linac. The neutrons travel down a well-collimated flight-path to the detection chamber.

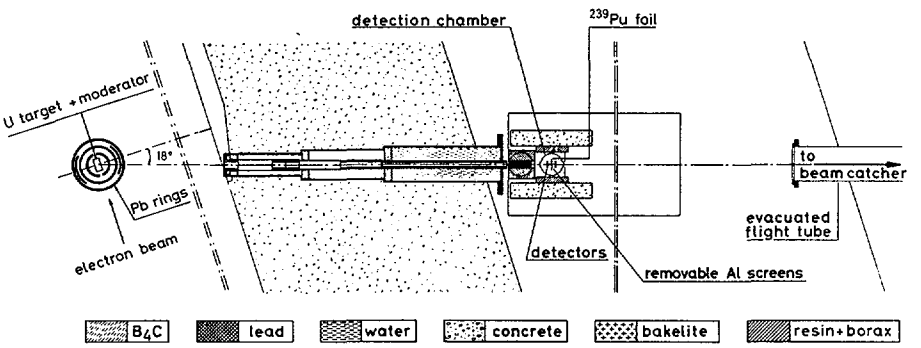

FIG.1. Experimental arrangement and collimation of flight path 17 at the CBNM-LINAC.

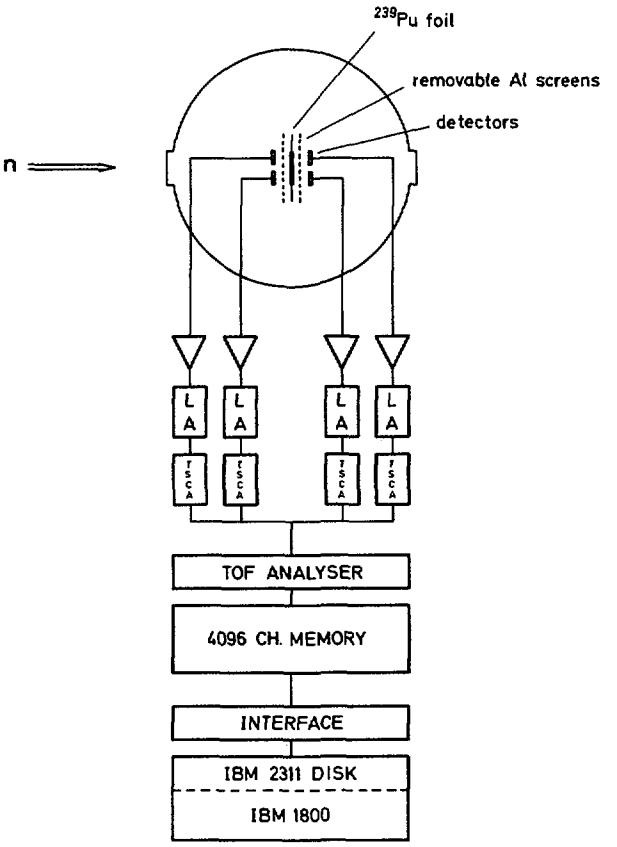

FIG.2. Layout of the detection and data collection system.

Figure 2 gives the lay-out of the detection and data-collection system. The detection chamber is an evacuated cylindrical chamber with thin aluminium entrance and exit windows; its inner diameter is 50 cm. In the center of this chamber a double faced ^{239}Pu layer (99.956 at.%; 1 mg/cm^2 thick) is mounted, viewed on each side by a bank of four large Si(Au) surface barrier detectors. These detectors were calibrated daily based on the pulse-height of the natural plutonium α - particles. Moreover, aluminium screens of different thicknesses can be inserted (ternary fission) or withdrawn (binary fission) from between the layers and the detectors. This detection technique allows rather good resolution of the time-of-flight spectra in the low-energy region, since only one back-to-back deposit of ^{239}Pu is used. Moreover, in this way less scattering material is introduced into the neutron beam than with a multi-plate ionization chamber.

Pairs of detectors are connected in parallel and the signals from each pair are amplified by a charge-sensitive preamplifier and a DDL main amplifier. The amplified signals are sent into a fast-timing

TABLE I. Experimental conditions for the different measurements

Measurement number	Energy region	Linac parameters	Overlap filter
I	0.1 - 50 eV	24 ns, 600 Hz E_{el} = 65 MeV, i_{av} = 45 μA P = 3 kW 70 ns, 400 Hz E_{el} = 65 MeV, i_{av} = 50 μA P = 3.25 kW	Cd
II	0.1 - 50 eV	33 ns, 400 Hz E_{el} = 67 MeV, i_{av} = 44 μA P = 3 kW	Cd
III	0.01 - 15 eV	1.2 μs, 100 Hz E_{el} = 53 MeV, i_{av} = 45 μA P = 2.4 kW	none

single channel analyser (TSCA). After mixing, all the fast-timing signals are fed into a 4096-channel time-of-flight analyser with an "accordéon" system. From the analyser memory the data are transferred via an interface unit to an IBM 2311 disk for storage. The data handling is performed afterwards with an IBM 1800 system.

3. MEASUREMENTS

Three measurements of the binary-to-ternary fission cross-section ratio were performed. Table I gives some details of the different experimental conditions. The first and the second measurement cover the energy region from 0.1 eV to 50 eV; the third covers the region from 10 meV to 15 eV. The total discrimination level (Al absorbers plus electronic bias) for the ternary α-particles was fixed at about 15 MeV α-energy for all three measurements.

Each measurement consists of binary, ternary and background runs. In the binary runs the heavy fission fragments are registered as a function of time-of-flight; there are no aluminium screens between the Pu-layers and detectors. The discriminators were set to register only the heavy fission fragments and to cut out the intense natural α-particles and their pile-up pulses. In the ternary time-of-flight runs only the light ternary fission particles are registered in the memory. These light particles are separated from the heavy fission fragments and the natural α-particles emitted by the Pu-isotopes by inserting a 20-μm-thick aluminium screen between detectors and targets. By appropriate discriminator-settings the detection levels were adjusted to 15 MeV α-energy. Typical TOF spectra for binary and ternary fission are shown in Fig. 3 for the two first runs, and for the low-energy run in Fig. 4. The background runs for binary and ternary fission were performed by putting the appropriate neutron filters into the beam. Moreover, for measurement III, runs were also performed with a cadmium filter in the beam to evaluate background due to untimed epicadmium neutrons in the beam and room neutron background (in the energy region below 0.1 eV). In all the measurements a thorough search for the various possible background sources has been done. A detailed description of this background study is given in [1]. As a result of all these background measurements, we found that the different background contributions were extremely small, especially in measurement III where the repetition frequency was only 100 Hz.

The same detection system as described before was moved to the BR2 high flux reactor of S.C.K./C.E.N., Mol, where it was installed at a beam tube and connected to a pulse-height analyser. With this apparatus, several pulse-height spectra of binary fission fragments and of ternary α-particles were registered to control the quality of these spectra and to verify the exact position of the detection levels. Fig. 5 shows a typical ternary α pulse-height spectrum with a detection level of 15 MeV.

4. TREATMENT OF DATA, RESULTS AND COMPARISON WITH OTHER T/B MEASUREMENTS

In the energy region above 1 eV we applied a rather straightforward analysis. After correction for background and underlying cross-section, the areas under the isolated resonances in ternary and binary fission

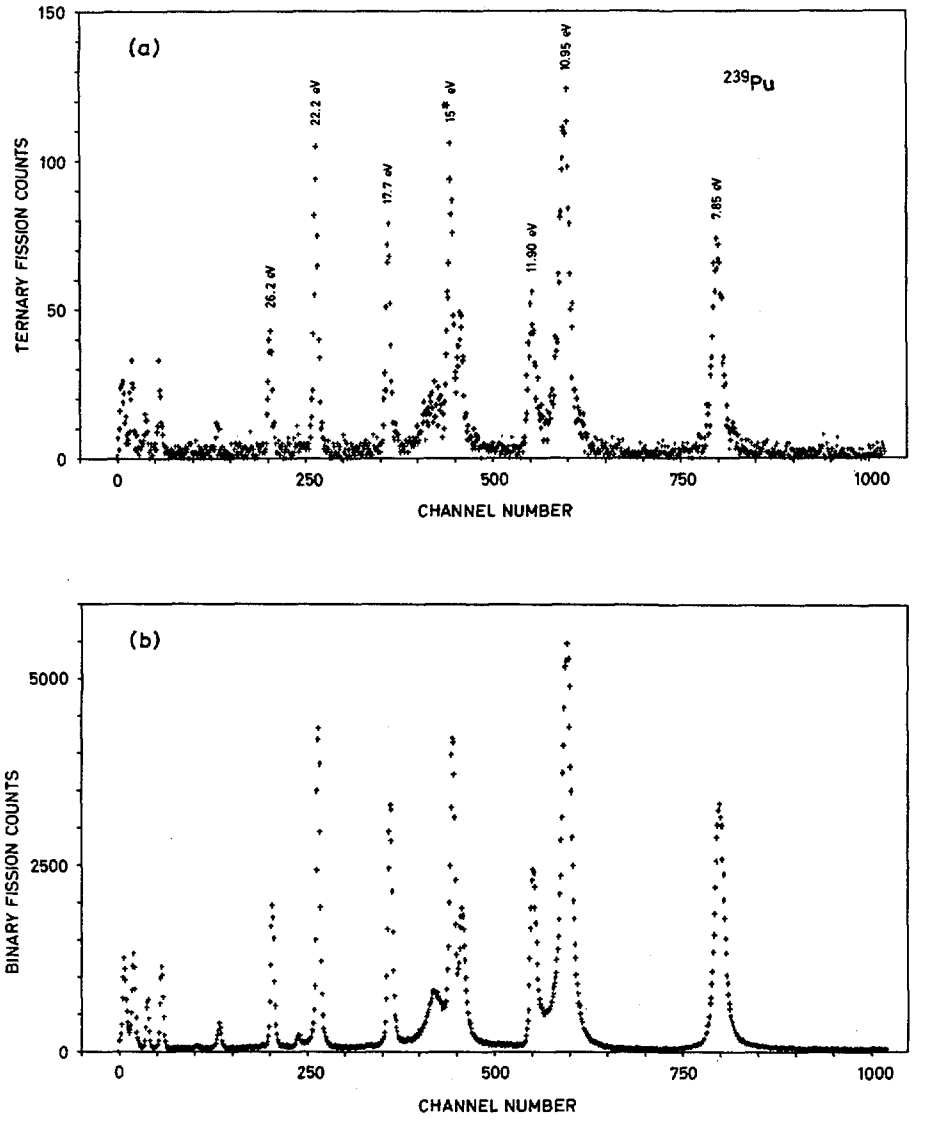

FIG. 3. (a) ^{239}Pu ternary alpha time-of-flight spectrum (Run I); (b) corresponding binary fission time-of-flight spectrum.

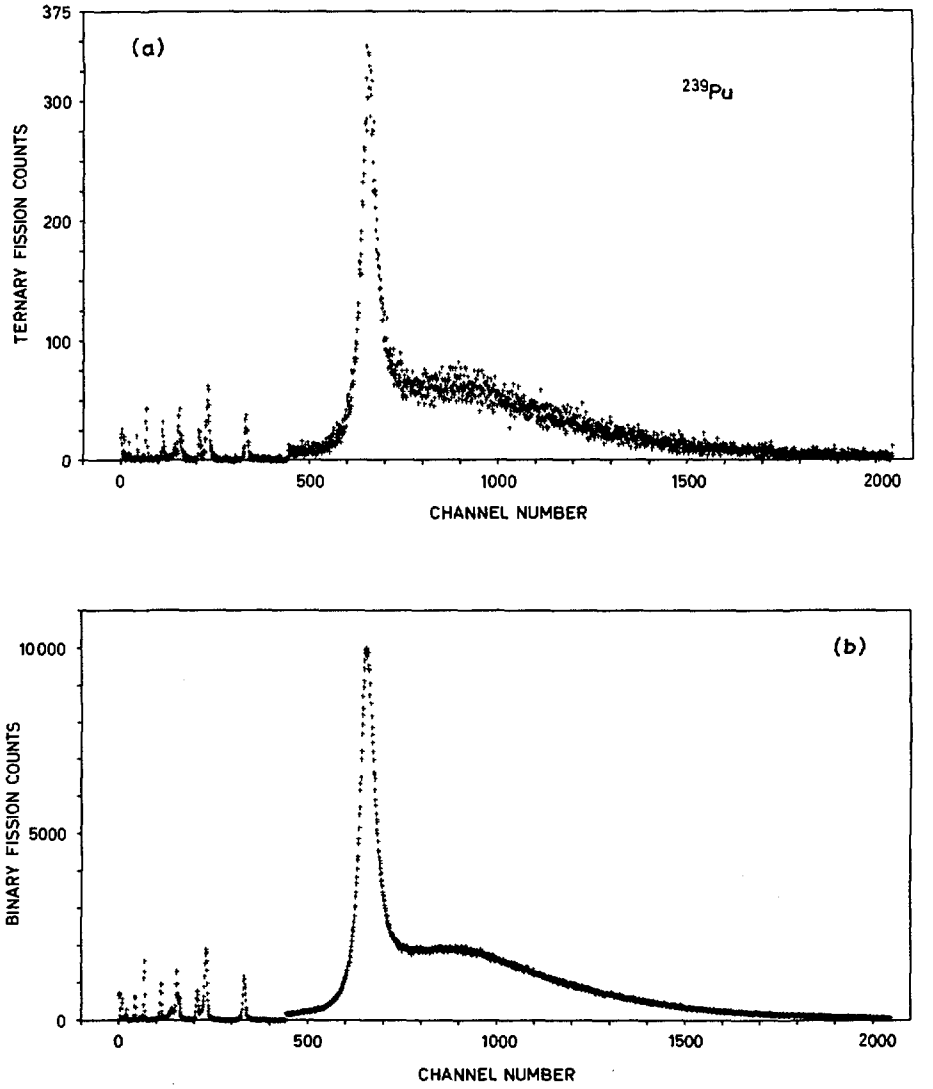

FIG.4. (a) ^{239}Pu ternary alpha time-of-flight spectrum (Run III); (b) corresponding binary fission time-of-flight spectrum.

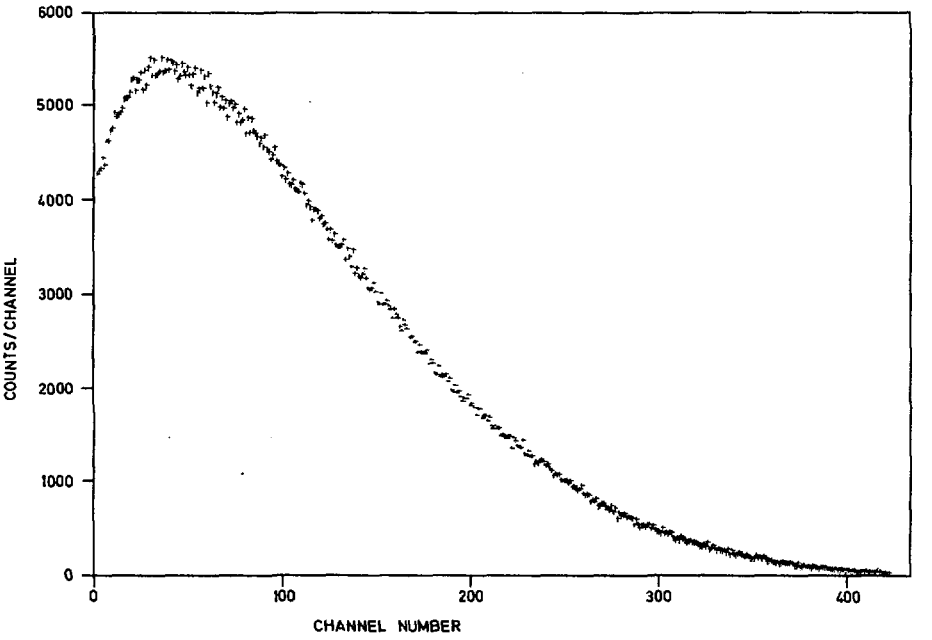

FIG. 5. Pulse-height spectrum of ternary α-particles (discrimination level: 15 MeV).

were computed and divided. These ratios are shown in Table II for the two measurements as well as the weighted mean of the two different runs. They are normalized to T/B = 100 for the 10.95 eV resonance (the largest resonance in this region). We tried a classification of these values with the following criteria "high T/B" H for T/B $\geq$ 106; uncertain U for a value of T/B fulfilling 106 > T/B > 103; a low value L for T/B $\leq$ 103. Brackets are used when the statistical error is such that one standard deviation extends from the high to the low group or vice versa. We find a significant difference between the value for the 15.5 eV resonance (H) and most other strong resonances at 7.85 eV, 10.95 eV and 11.90 eV which have a low value of T/B. This higher α-counting-rate cannot be caused by α-particles from the $^{239}Pu(n,\alpha)^{236}U$ reaction since the highest energy α-line generated in this reaction is 11.46 MeV which is well below the detection bias in the experiment.

Some statistical tests were performed on these data. We calculated the weighted average values $\overline{X}_w$ for the different measurements, taking into account all the data, namely L + (L) and H + (H). These results are summarized in Table III where we also calculated the hx-values of Birge [9]:

$$hx = \frac{X_1 - X_2}{\sqrt{2(\sigma_1^2 + \sigma_2^2)}}$$

Here X_1 and X_2 represent the weighted mean of the low group and the high group (essentially the 15.5 eV resonance) and σ_1 and σ_2 are the corresponding statistical errors. Taking into account that the probability that X_1 and X_2 are compatible with a unique value is smaller than 0.01 for $hx > 1.83$ we may conclude from this table that there is an indication for a significant difference.

The only other measurements of T/B for ^{239}Pu + n in this region was performed by Melkonian et al.[5]. They are, however, difficult to compare as they did not publish numerical values for individual resonances because of the rather poor statistics. Nevertheless they found that T/B was significantly larger for two resonances with J = 0, in qualitative agreement with our results.

As we did observe an effect in the 15.5 eV resonance we decided to look for a fit to our highly precise fission cross-section measurement obtained in another experiment at the linac [10] and tried to fit the cross-section curve below 20 eV. We only optimized the positions of the fission vectors in the space of the two outgoing fission channels (interference contribution) and the parameters of the negative resonances step by step, in such a way that the interference formula describes the experimental points between the resonances and in the thermal region at best. The interference has the largest percentage effect between the resonances. Especially the energy regions between the resonances 11 and 11.9 eV and between 11.9 and 14.3 eV are critical regions for such an optimalization. It follows from these considerations that a good description of the fission curve is only possible with the assumption of J = 0 for the 15.5 eV resonance. It is possible, however, to obtain a good fit with J = 1 for the 0.3 eV resonance.

In the neutron energy region below 1 eV (third measurement) the T/B data were analyzed in a somewhat different way. By putting cadmium filters in the beam we checked the background in the energy region below 0.2 eV and found it negligible compared to the counting rate in that region. Then we divided the ternary and binary fission TOF spectra in several intervals in the energy region from 20 meV to 1 eV (thus including the strong 0.3 eV resonance) and calculated the ratios of the areas of the corresponding intervals. These results, which are normalized to the first two measurements, are represented graphically in fig. 6 and given numerically in Table IV. We find that there is no significant difference between these T/B values.

Moreover, if we consider the weighted averages given in the fourth column of this table, we deduce that the 0.296 eV resonance is very probably a "low" one and that also the thermal T/B value is predominantly low. Within the experimental errors, our results agree with those of Panov et al. [11] (10 % exp. error) and Schröder [12] (2 % exp. error).

Finally we examined whether our low-energy data are compatible with a unique value or not. Therefore we calculated χ^2, and the corresponding probability $P(\chi^2 > \chi^2_p) \simeq 70$ %. Furthermore we obtained for the Birge ratio [9][13] $R \equiv \sigma_E / \sigma_I$ a value of 0.869 and a probable deviation of R from unity of 0.076.

TABLE II. Results normalized to T/B = 100 for the 10.95 eV resonance

Resonance energy (eV)	Measurement I		Measurement II		Weighted mean (Meas.I and II)		Class.
	T/B	Stat.err.	T/B	Stat.err.	T/B	Stat.err.	
7.85	98.7	2.8	99.3	3.1	99	2.1	L
10.95	100	2.1	100	2.4	100	1.6	L
11.90	101.5	3.9	98.1	4.5	100	3	L[a]
14.30)	107.5	4.5	106.2	5	106.9	3.4	H
14.68)	103.7	3.4	96.9	3.8	100.7	2.6	L
15.50)	112.4	4.3	108.1	5	110.6	3.3	H
15[b]	106.9	2.3	102.2	2.6	104.9	1.8	
17.7	104.8	4	99.5	4.6	102.5	3	L
22.2	105.6	3.7	101.4	4.2	103.8	2.8	U
26.2	106.4	5.6	106.8	6.7	106.6	4.3	(H)
47.8	99.5	7.8	96.6	9	98.3	5.9	(L)
50.1	104.4	7.5	97.2	8.4	101.2	5.6	(L)

Classification: H: $T/B \geq 106$
U: $106 > T/B > 103$
L: $103 \geq T/B$

Brackets indicate that the statistical error is too large to be conclusive.

[a] An unambiguous classification is impossible due to the influence of the underlying tail of the 15.5 eV resonance.

[b] This stands for the group of resonances at 14.30, 14.68 and 15.50 eV.

TABLE III. Weighted average values and hx-values of Birge

Measurement number	Data used	$\bar{X}_w$ (weighted average)	hx
I	all data	102.81 ± 1.11	
	L + (L)	101.03 ± 1.29)	1.92
	H + (H)	109.20 ± 2.72))	
II	all data	100.51 ± 1.26	
	L + (L)	98.96 ± 1.46)	1.66
	H + (H)	107.08 ± 3.13))	
weighted mean of I and II	all data	101.82 ± 0.84	
	L + (L)	100.14 ± 0.98)	2.49
	H + (H)	108.29 ± 2.1))	
III	all data	102.32 ± 0.40	

TABLE IV. Results from Measurement III normalized to the weighted mean of the 7.85, 10.95 and 11.90 eV resonances, as obtained from Measurements I and II (T/B = 99.7 ± 1.2)

E(eV)	T/B	Stat. err.	Weighted mean
0.296	102.2	0.65	
7.85	97	4.6)	
10.95	102.2	3.7)	99.7 ± 2.7
11.90	97	6.7)	
0.886[a)]	102.4	2.9	
0.465	102.0	2.2	
0.374	103.9	2.9	
0.345	99.9	2.2	
0.319	100.9	1.8)	
0.296	102.2	1.6)	101.4 ± 1
0.275	101	1.7)	
0.257	102.7	2.0	
0.240	102.3	2.3	
0.225	105.5	2.6	
0.205	101.8	2.1	
0.182	106.2	2.5	
0.163	105.9	2.6	
0.146	104.0	2.6	
0.132	101.1	2.6	
0.120	103.8	2.6	
0.110	102.5	2.6	
0.101	98.7	2.6	
0.0925	101.4	2.6	
0.0853	105.4	2.6	
0.0790	103.4	2.6	
0.0733	102.9	2.6	
0.0683	104.0	2.6	
0.0637	103.7	2.6	
0.0596	102.8	2.7	
0.0558	102.0	2.7	
0.0524	98.7	2.9	
0.0493	100.3	2.9	
0.0465	97.6	3.0	
0.0439	103.1	3.1	
0.0404	98.9	2.3	
0.0364	102.7	2.4	
0.0329	104.3	2.6	
0.0299	99.1	2.7)	
0.0273	106.1	3.0)	
0.0250	100.3	3.0)	102.3 ± 1.3
0.0230	104.2	3.3)	
0.0212	100.5	3.5)	
0.0197	105.0	3.8)	

[a)] The energies indicated below correspond to the middle of the energy interval considered.

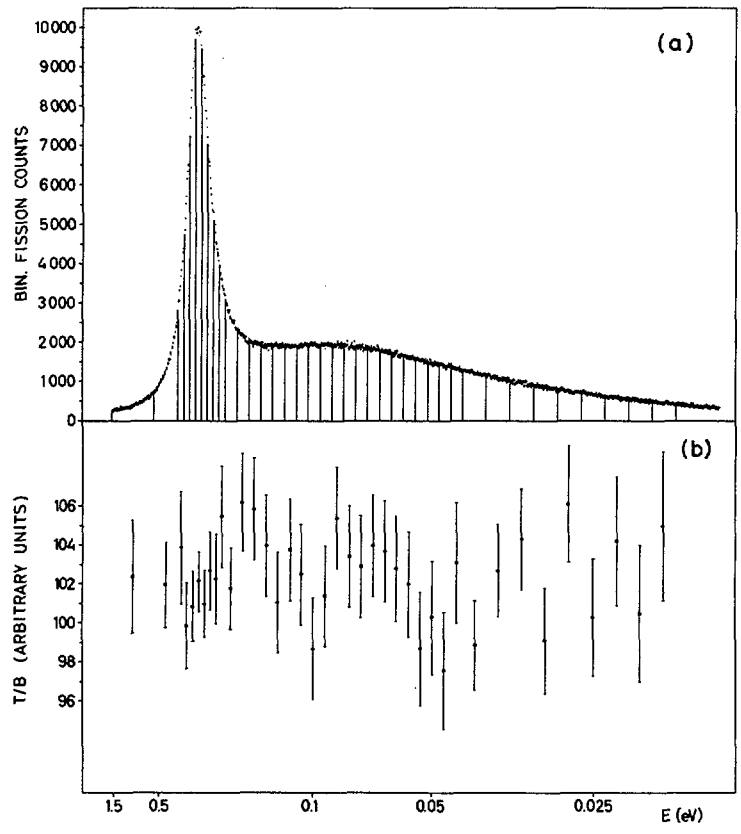

FIG.6. (a) Binary fission counts for the energy region 0.02 - 1 eV; (b) T/B ratios in the same energy region (Run III).

From these tests we deduce that the data considered are compatible with a unique value, although the scattering of the data is rather large. No interference effects of the magnitude found by Mostovaya[14] for ^{235}U in the neighbourhood of the 2 eV resonance were detected.

5. DISCUSSION

In Tables Va and Vb we compare our proposed classification of the resonances based on their T/B value with the direct determination of the resonance spin J and with some other fission characteristics. These tables clearly demonstrate that there is a complete agreement between our unambiguously classified resonances and the direct spin-determinations of Sauter and Bowman[15], Ashgar[16], Trochon et al.[17] and Simpson et al.[18]. Compared with the spin values of Fraser and Schwartz[9], one of the five common resonances disagrees. However, it must be stressed that none of them determined the spin

TABLE V a . Comparison of our classification of the resonances via their T/B values with other classification methods

E(eV)	Spin determinations (J^{π})								Our classification via T/B values
	via neutron scattering					via γ-ray detection	via interference method		
	ref. [19]	ref. [15]	ref. [16]	ref. [17]	ref. [18]	ref. [20]	ref. [21]	ref. [22]	
0.296						1^+		1^+	L(1^+)
7.85	1^+	1^+			1^+			1^+	L
10.95	1^+	1^+			1^+			1^+	L
11.90	1^+	1^+			1^+			1^+	L
14.30		1^+			1^+		1^+	1^+	H[c]
14.68	0^+	1^+	1^+	1^+	1^+		1^+	1^+	L
15.50							0^+	0^+	H(0^+)
17.7	1^+	1^+	1^+	1^+	1^+		1^+	1^+	L
22.2	0^+	1^+	1^+	1^+	1^+		1^+		U
26.2			1^+		1^+		1^+		(H)
47.8		0^+	0^+	0^+	(1^+)		0^+		L
50.1			1^+	1^+	1^+				(L)

c) Influenced by other resonances

TABLE V b. Comparison of our classification of the resonances via their T/B values with other classification methods.

E(eV)	Kinetic energy of the fission fragments[a] ref. [5]	Fission symmetry meas.[b] ref. [4][23]	Fission neutron ($\bar{\nu}$) measurements[d] ref. [6]	ref. [7]	Our classification via T/B values
0.296		$A(1^+)$	$L(1^+)$		$L(1^+)$
7.85	$H(1^+)$		L	$H(1^+)$	L
10.95	H		L	H	L
11.90	H		L	H	L
14.30	H		L	H	H[c]
14.68	H		L	H	L
15.50	H	A[c]	$H(0^+)$	$L(0^+)$	$H(0^+)$
17.7	H	A	L	H	L
22.2	H	A	L	H	U
26.2	(H)	A	L	L	(H)
47.8	H	A	H	U	L
50.1	(L)		L	H	(L)

[a] The notation L means lower average kinetic energy of the fission fragments and H higher average kinetic energy.
[b] The notation A means predominant asymmetric fission.
[c] Influenced by other resonances.
[d] The notation L means here lower $\bar{\nu}$ value and H higher $\bar{\nu}$ value.

of the important 0.296 eV and 15.5 eV resonances. This has been done for the 0.296 eV resonance by Chrien et al.[20] via the detection of high-energy capture γ-rays. They assigned $J^\pi = 1^+$ for this resonance, which agrees with our result. Moreover Farrell[21] and Becker[22] assigned both $J^\pi = 0^+$ for the 15.5 eV resonance based on the "interference method" (indirect determination).

When comparing our results with the average kinetic energy of the fission fragments measured by Melkonian and Mehta[5] we find a difference for the important 15.5 eV resonance. The same may be said for the fission symmetry measurements of Cowan et al.[4] in the 15.5 eV resonance. However our $J^\pi = 1^+$ result for the 0.296 eV resonance agrees with Cowan's proposal for this resonance, which is based on the results of Regier et al.[23]

A rather difficult criterium for comparison is the fission neutron multiplicity $\bar{\nu}$. If we examine the various measurements we observe a rather clear bias due to the detection method.

(a) Weston et al.[8] and Trochon et al.[24] find no variation in $\bar{\nu}$. They both detected the fission neutrons directly.

(b) Weinstein et al.[6], Ryabov et al.[7] and Shackleton et al.[25] find a variation of $\bar{\nu}$ from resonance to resonance. They detected the fission neutrons after moderation.

If we compare the data of Weinstein and Ryabov shown in Table Vb, we see that they are generally anticorrelated. Nevertheless this is not so for their spin assignments, which are almost in agreement. This is especially the case for the 0.296 eV and 15.5 eV resonances, which are also in agreement with our results.

6. CONCLUSIONS

In the energy region from 20 meV to 50 eV we observe only one resonance with a significantly higher T/B value : i.e. the 15.5 eV resonance. We assign $J^\pi = 0^+$ for resonances with a high T/B value and $J^\pi = 1^+$ for resonances with a low T/B value. This higher value for 0^+ resonances cannot be due to an eventual loss of binary fission counts for one spin state — thus a B-value which would be too small — since the difference between the kinetic energies of the 0^+ and the 1^+ states is only about 0.7% according to Melkonian and Mehta[5]. Furthermore the spin assignment 0^+ to the 15.5 eV is substantiated by the careful study of the low-energy fission cross-section . This higher α-yield for 0^+ resonances is in the sense expected according to Bohr[2] and Wheeler[3], since the 0^+ states are more symmetric than the 1^+ states. More symmetric fission corresponds in general to a lower total kinetic energy of the fission fragments, a higher excitation energy of the fragments and a higher probability for ternary α-emission.

We can reach the same conclusions based on energetic considerations. From several analyses of experimental data we know that the average fission width for 0^+ states is much larger than that for 1^+ states : $\langle\Gamma_f\rangle_{0^+} \gg \langle\Gamma_f\rangle_{1^+}$. This implies that the number of open fission channels for 0^+ states $N(0^+)$ is larger than $N(1^+)$, thus that the 0^+ channel lies below the 1^+ channel in the transition channel spectrum. From this we deduce that the remaining excitation energy via a

0^+ channel is larger than for fission via a 1^+ channel, implying a higher probability for ternary fission via a 0^+ channel than via a 1^+ channel.

ACKNOWLEDGEMENTS

The authors wish to thank Dr. Nève de Mévergnies for fruitful discussions. They are indebted to many colleagues from CBNM, Geel for the preparation of the samples and the operation of the linac. They especially acknowledge the skilful assistance of R. Barthelemy, G. Le Dez and J. Van Gils during these experiments.

REFERENCES

[1] WAGEMANS, C., DERUYTTER, A.J., Nucl. Phys. A194 (1972) 657.
[2] BOHR, A., in Int. Conf. Peaceful Uses of Atomic Energy (Proc. Conf. Geneva, 1955) 2, UN, New York (1956) 151.
[3] WHEELER, J.A., in Int. Conf. on Nuclear Reactions (Proc. Conf. Amsterdam, 1956), Physica 12 (1956) 1103.
[4] COWAN, G., BAYHURST, B., PRESTWOOD, R., GILMORE, J., KNOBELOCH, G., Phys. Rev. 144 (1966) 979.
[5] MELKONIAN, E., MEHTA, G., in Physics and Chemistry of Fission (Proc. Symp. Salzburg, 1965) 2, IAEA, Vienna (1965) 355.
[6] WEINSTEIN, S., REED, R., BLOCK, R., in Physics and Chemistry of Fission (Proc. Symp. Vienna, 1969), IAEA, Vienna (1969) 477.
[7] RYABOV, Y., SO DON SIK, CHIKOV, N., YANEVA, N., Sov. J. Nucl. Phys. 14 5 (1972) 519.
[8] WESTON, L., TODD, J., in Neutron Cross-Sections and Technology (Proc. Conf. Knoxville, 1971), USAEC Rep. CONF. 710301 (1971) 861.
[9] BIRGE, R.T., Phys. Rev. 40 (1932) 207.
[10] DERUYTTER, A.J., WAGEMANS, C., J. Nucl. Energy 26 (1972) 293.
[11] PANOV, A., Sov. Phys. JETP 16 5 (1963) 1408.
[12] SCHRÖDER, I.G., Nucl. Phys. A195 (1972) 257.
[13] TAYLOR, B., PARKER, W., LANGENBERG, D., The Fundamental Constants and Quantum Electrodynamics, Academic Press, New York (1969).
[14] MOSTOVAYA, T.A., JAKOVIEV, G., Rep. IAE-1439 (1967).
[15] SAUTER, G. BOWMAN, D., Phys. Rev. Lett. 15 19 (1965) 761.
[16] ASGHAR, M., in Nucl. Data for Reactors (Proc. Conf. Paris, 1966) 2, IAEA, Vienna (1966) 185.
[17] TROCHON, J., DERRIEN, H., LUCAS, B., MICHAUDON, A., in Nucl. Data for Reactors (Proc. Conf. Helsinki, 1970) 1, IAEA, Vienna (1970) 495.
[18] SIMPSON, F., MILLER, L., MOORE, M., HOCKENBURY, R., KING, T., Nucl. Phys. A164 (1971) 34.
[19] FRASER, J., SCHWARTZ, R., Nucl. Phys. 30 (1962) 269.
[20] CHRIEN, R., WASSON, O., DRITSA, S., BOKHAREE, S., GARG, J., in Nucl. Data for Reactors (Proc. Conf. Helsinki, 1970) 1, IAEA, Vienna (1970) 377.
[21] FARRELL, J., Phys. Rev. 165 4 (1968) 1371.
[22] BECKER, W., Doctorate thesis, Philipps-Univ., Marburg/Lahn (1973).
[23] REGIER, R., BURGUS, W., TROMP, R., SORENSEN, B., Phys. Rev. 119 6 (1960) 2017.
[24] TROCHON, J., LUCAS, B., MICHAUDON, A., in Conf. European Nuclear Physics (Proc. Conf. Aix-en-Provence, 1972) 2, European Physical Society and Société française de Physique, Paris (1972) 23.
[25] SHACKLETON, D., TROCHON, J., FREHAUT, J., LE BARS, M. Phys. Lett. 42B 3 (1972) 344.

DISCUSSION

J. P. FELVINCI: Previous measurements have shown that the negative level in ^{239}Pu is of opposite spin to that of the 0.3-eV level and is usually assigned 0^+, so it is interesting to see that your low-energy data do not show any increase in the T/B yield.

My second comment is a warning. It is very risky to associate spin with certain measurements, like $\bar{\nu}$, T/B or mass asymmetry. These measurements may depend more on the deformation of the fissioning nucleus and thus on the K quantum number than on the spin. In cases where there is no one-to-one correspondence between the spin and the K-bond (^{235}U, ^{233}U, ^{241}Pu) this procedure may give erroneous results. This problem is much less critical in ^{239}Pu, where the 0^+ and 1^+ spins also belong to two distinct deformation bonds.

A. J. DERUYTTER: I certainly agree that one has to be cautious in relating T/B to J and I think this was sufficiently stressed in our paper. Moreover, the excellent paper presented by Keyworth, and co-workers[1] also sounds a very clear warning in this respect.

The low-energy ratios presented here for ^{239}Pu do not show any significant variation, although the value at thermal energy is slightly higher than that for the 0.296-eV level, as may be seen from Table IV of the paper.

I. G. SCHRODER: In our measurements on the binary to ternary fission ratio in ^{239}Pu performed in the subthermal and resonance region (0.3 eV), we made a detailed study of the energy distribution of the α-particles and found no difference in the distributions in the three regions considered or in the binary to ternary ratio. One should remember that in these regions there is a large variation in the ratio of symmetric to asymmetric binary mass division. Thus, as Felvinci has just mentioned, one should be extremely careful about comparing these two different phenomena from resonance to resonance.

A. J. DERUYTTER: I agree. However, the T/B ratio does not have to be related to the symmetry of the fission process for both spin states. Other factors may be involved, such as the amounts of excitation energy available for fission at the saddle point through 0^+ or 1^+ states.

M. J. FLUSS: I should just like to remind you that a very strong effect appears in the excitation function for triton/fission yields in ^{236}U between thermal and 170-keV neutrons.[2]

A. J. DERUYTTER: In the type of experiments described here we can register only the total spectrum of light particles because of intensity limitations. It is impossible to use an E - ΔE system, for instance. The variations observed may be due to any of the light particles, although the most probable cause is the ^4He particle.

---

[1] KEYWORTH, G. A., et al., Paper IAEA-SM-174/65, these Proceedings, Vol. 1.

[2] FLUSS, M. J., et al., Phys. Rev. C6 (1972) 2252.

CHARGE DISTRIBUTION OF THE FRAGMENTS EMITTED IN TERNARY FISSION*

H. NIFENECKER
Lawrence Berkeley Laboratory,
University of California,
Berkeley, Calif.,
United States of America

Abstract

CHARGE DISTRIBUTION OF THE FRAGMENTS EMITTED IN TERNARY FISSION.

It is possible, in principle, to derive the charge distribution of the fragments produced in LRA fission of ^{252}Cf by comparing the K X-ray spectra observed in binary and LRA fission respectively. However, it has been shown by Watson that such a procedure is inaccurate because the K X-ray emission probability depends on the isotopic distributions which should be somewhat different in binary and LRA fission. It was found that the total number of prompt neutrons emitted by the fragments measured in coincidence with the K X-rays gives a good indication of the extent of this dependence of the K X-ray emission probabilities on the isotopic distributions. This dependence is not strong for most of the light fragment isotopes and for the higher Z region of the heavy group. On this basis, it was possible to derive the elemental yields for LRA fission in the applicable regions. The K X-ray emission probabilities are higher in ternary fission for the lower Z region of the heavy fragments. This difference indicates that, in this region, the ternary fragments are more neutron-rich than the binary fragments. These experimental results are compared with predictions based on different hypotheses regarding the alpha formation mechanism.

1. INTRODUCTION

While our knowledge of the angular and energy distributions of the light charged particles sometimes emitted in fission has acquired a high degree of sophistication [1-3] we still do not know the mechanism which is responsible for this emission. Both the angular and energy distributions show that the light particle is created a short time after scission or in the act of scission itself at a position which lies somewhere between the two nascent fragments. Whether the light particle is created at the expense of one of the already separated fragments or at the expense of the collapsing "neck region" at the time of scission remains an open question. Very recent experimental evidence [4], based on the study of the very rare event when two light charged particles are emitted in the course of fission, appears to favor the hypothesis of an emission by the fragments. On the other hand, the striking similarities in the properties of the two heavy fragments in both binary and ternary fission has been interpreted [5] as an indication of an emission of the α particle at the expense of the neck region, with an almost constant probability.

Halpern [6] has pointed out that the comparison of the mass yields of the heavy products in binary and ternary fission could not provide an unambiguous answer to the question of the origin of the light particle.

Watson [7] used a comparison between the X-ray production by the fragments in binary and ternary fission in an effort to obtain additional

* Work performed under the auspices of the US Atomic Energy Commission.

information on the light particle origin. However, the selective nature of the X-ray emission process made it difficult for him to draw a firm conclusion from his measurement.

We have used the same approach as Watson, but, in addition to X-ray production by the heavy fragments we have measured the total number of neutrons emitted in ternary fission as a function of the charges of the heavy fragments. This additional measurement has proven itself very useful in evaluating the effects of the selectivity in the X-ray process on the ternary to binary charge yields comparison. Furthermore, it allowed us to take advantage of this selectivity to obtain a qualitative understanding of the changes in mass-to-charge ratios of binary and ternary fragments, respectively.

2. EXPERIMENTAL

A 5×10^4 fissions/min ^{252}Cf source, deposited on a beryllium backing, was placed at the center of a diametrical hole managed into a large gadolinium-loaded liquid scintillator. On top of the Cf source, a 35-μm aluminium foil stopped the fission fragments but allowed the long-range particle to reach a solid state detector. Immediately behind the beryllium backing of the fission source a lithium drifted silicon detector was used as an X-ray detector.

A data acquisition sequence was started whenever the long-range particle and X-ray detectors were activated in coincidence. The coincidence gate was 200-ns wide. In the acquisition sequence the following quantities were digitally coded and stored on an event-by-event basis on an incremental magnetic tape:

(a) Pulse height delivered by the long-range particle detector.
(b) Pulse height delivered by the X-ray detector.
(c) Time difference between those two detectors.
(d) Number of neutrons counted in the liquid scintillator between 1 μs and 36 μs after the beginning of the sequence.

Except for the detection of the charged particles, the experimental arrangement was essentially similar to that used in the study of even-odd effects in binary fission as described in another paper at this Symposium [8]. Special care was taken to ensure that the coincidence gates were the same in binary and ternary fission experiments. Such a condition is necessary to make valid comparisons between ternary and binary fission as can be seen in Appendix I, where the time dependence of the X-ray production as a function of the charge of the fragments in the binary fission of ^{252}Cf is studied.

3. TOTAL NUMBER OF NEUTRONS RESULTS

The total number of neutrons $\bar{\nu}_T(Z)$ was obtained as a function of one of the two large fragment charges using the data analysis technique described in Ref. [8]. The results are shown on Fig. 1 where the total number of neutrons $\bar{\nu}_T(m)$ obtained by Mehta and co-workers [5] as a function of the fragment masses is also shown for comparison. The charge and mass scales

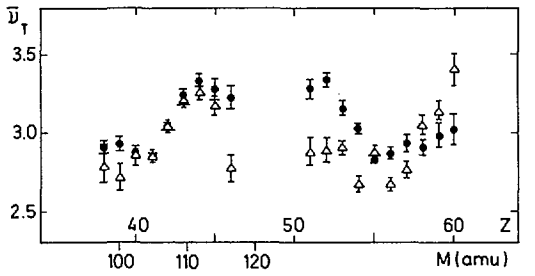

FIG. 1. Measured average total number of neutrons emitted in the ternary fission of ^{252}Cf, △: as a function of the fragments' charges, ●: as a function of the fragments' masses. The charge and mass scales reflect the charge-to-mass ratios of the binary fission fragments.

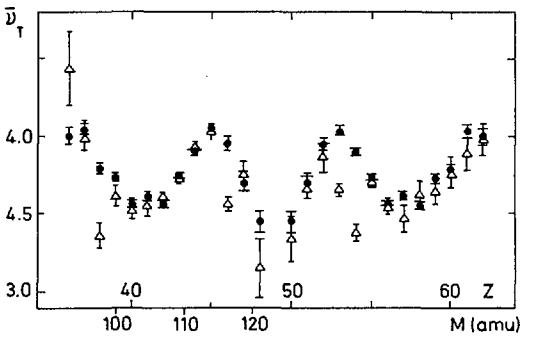

FIG. 2. Same as Fig. 1 for binary fission.

on Fig. 1 reflect the variations of the average masses of the fragments as a function of their charges. We have assumed in Fig. 1 that the difference between the most probable mass and the charge obtained with the unchanged charge density hypothesis was the same in binary and ternary fission. Figure 2 shows the similar results obtained in the study of binary fission. We have indicated in Ref. [8] that the differences observed in the values of $\bar{\nu}_X(Z)$ and $\bar{\nu}_T(m)$ for corresponding values of Z and m were an effect of the selectivity of the X-ray process. This point is developed in more detail in Appendix II, where it is shown that, to a good approximation, the relation

$$\bar{\nu}_T(Z) = \bar{\nu}_T(\bar{m}(Z)) \qquad (1)$$

is fulfilled. In Eq. (1), $\bar{\nu}_T(Z)$ is the true total number of neutrons emitted when one of the fragments has a charge equal to Z; $\bar{\nu}_T(\bar{m}(Z))$ is the total number of neutrons obtained from an interpolation of the variations of $\bar{\nu}_T(m)$ for the average mass $\bar{m}(Z)$ corresponding to fragments of charge Z.

If $Y(Z, m^*)$ are the yields of fragments with charge Z and post-neutron mass m^*, $C(Z, m^*)$ the probability that such fragments emit an X-ray, the measured values of the total number of neutrons is then equal to

$$\bar{\nu}_X(Z) = \frac{\sum_{m^*} \nu_T(Z,m^*)\ C(Z,m^*)\ Y(Z,m^*)}{\sum_{m^*} C(Z,m^*)\ Y(Z,m^*)} \tag{2}$$

and

$$\bar{\nu}_T(Z) = \frac{\sum_{m^*} \nu_T(Z,m^*)\ Y(Z,m^*)}{\sum_{m^*} Y(Z,m^*)} \tag{3}$$

From Eqs (2) and (3) we show in Appendix II that, in general, $\bar{\nu}_X(Z)$ and $\bar{\nu}_T(Z)$ can only be equal if $C(Z, m^*)$ is independent of m^*. This condition is also required for a valid comparison of binary and ternary charge yields. In this case, the charge yields obtained from the X-ray yields can be written

$$Y_B^X(Z) = \sum C(Z,m^*)\ Y_B(Z,m^*)$$

$$Y_T^X(Z) = \sum C(Z,m^*)\ Y_T(Z,m^*)$$

and if the quantities $C(Z, m^*)$ do not depend on m^*

$$\frac{Y_B^X(Z)}{Y_T^X(Z)} = \frac{\sum_{m^*} Y_B(Z,m^*)}{\sum_{m^*} Y_T(Z,m^*)} = \frac{Y_B(Z)}{Y_T(Z)} \tag{4}$$

4. CHARGE DISTRIBUTION IN THE TERNARY FISSION OF ^{252}Cf

From the preceding discussion, it appears on Figs 1 and 2 that the selectivity effects are weak for most of the light fragments both in binary and ternary fission. The only noticeable exception occurs for charge 46. For this charge, in both types of fission, the measured value $\bar{\nu}_X(Z)$ was approximately 0.5 neutrons below the corresponding value of $\nu_T(m)$. This suggests that the selectivity effects affect equally the yields of the element 46 in ternary and binary fission and that Eq. (4) could hold in that case as well as for the other light fragments. We have thus applied Eq. (4) to the light fragment charge yields reported by Reisdorf and co-workers [9] for the binary fission case, to obtain the ternary fission charge yields. The yields of the heavy fragment charges are obtained by symmetry with regard to the charges 49 and 48 in the binary and ternary cases, respectively. Figure 3 compares the charge yields obtained in ternary fission to those obtained by Reisdorf and co-workers [9] in binary fission. Knowing the ternary fission charge yields it is possible to obtain the X-ray yields for

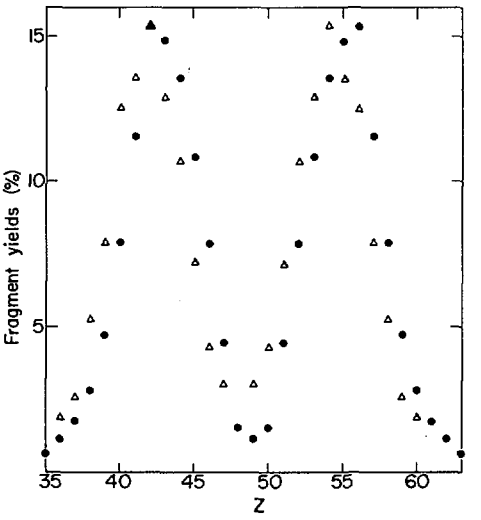

FIG.3. Comparison of the binary and ternary fission charge yields. △: ternary fission charge yields, ●: binary fission charge yields.

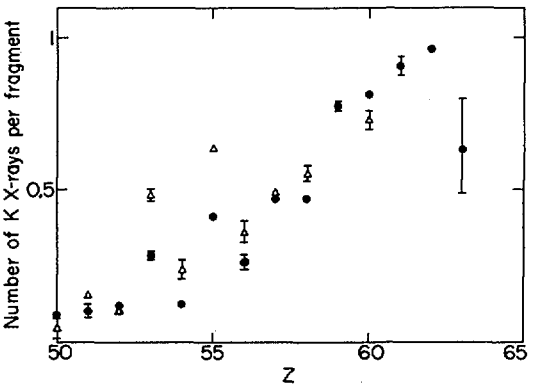

FIG.4. Comparison of the K X-ray yield per fragment in binary and ternary fission. △: K X-ray yields in ternary fission, ●: K X-ray yields in binary fission.

fragments in the heavy region. Figure 4 compares the X-ray yields per fragment in binary and ternary fission. The light fragment region is not shown in Fig. 4 since our treatment assumes that the X-ray yields are the same in the two types of fission under study. It can be seen on the figure that the X-ray yields are higher in the "light-heavy" fragment region for the ternary fission case; the well-known even-odd effects on the yields are also

TABLE I. SUMMARY OF THE RESULTS. Y_B^Z: binary charge yields (in %), Y_T^Z: ternary charge yields (in %), N_X^B: number of X-rays per fragment in binary fission, N_X^T: number of X-rays per fragment in ternary fission, I_T/I_B: ratio of X-ray yields in ternary and binary fission.

Z	Y_B^Z	Y_T^Z	N_X^B	N_X^T	$\frac{I_T}{I_B}$
36	1.13	1.93	0.065	0.065	1.706
37	1.77	2.59	0.078	0.052	0.98
38	2.89	5.29	0.075	0.075	1.83
39	4.73	7.90	0.108	0.108	1.67
40	7.93	12.53	0.197	0.197	1.58
41	11.59	13.56	0.204	0.204	1.17
42	15.35	15.35	0.225	0.225	1.00
43	14.88	12.94	0.437	0.437	0.87
44	13.58	10.72	0.272	0.272	0.79
45	10.82	7.25	0.170	0.170	0.67
46	7.84	4.31	0.166	0.166	0.55
47	4.49	3.05	0.177	0.177	0.68
48	1.57		0.086		
49	2.3	3.05	0.09[a]	0.052	0.77
50	1.57	4.31	0.09	0.048	1.43
51	4.49	7.25	0.106	0.154	2.36
52	7.84	10.72	0.119	0.122	1.40
53	10.82	12.94	0.287	0.481	2.00
54	13.58	15.35	0.123	0.238	2.18
55	14.88	13.56	0.419	0.648	1.40
56	15.35	12.53	0.267	0.362	1.11
57	11.59	7.90	0.475	0.494	0.71
58	7.93	5.29	0.454	0.557	0.82
59	4.73	2.59	0.781	0.781	0.55
60	2.89	1.93	0.815	0.732	0.60
61	1.77		0.911		
62	1.13		0.966		

[a] Assumed value.

more pronounced in this case and start in the neighbourhood of charge 51 rather than 53. This is in agreement with the neutron measurements which show selectivity effects for the charges 51 and 52 in ternary fission but none in binary fission. The selectivity effects observed for the charges 51 to 54 in ternary fission and 53 and 54 in binary fission are probably related to the closure of the 82-neutron-shell which is known to occur in the binary final fragments for the charge 52. Before the shell closure, the lower neutron states belong to the $2d_{3/2}$ configurations while they belong to the $2f_{7/2}$ or possibly $1h_{9/2}$ configurations after shell closure. In odd-odd isotopes the unpaired neutron has to be coupled to an unpaired proton in the $1g_{7/2}$ subshell. Thus, the range of possible spin values for low excitation levels increases sharply after the 82-neutron-shell closure. Since low-energy transitions between levels having very different spins are highly converted, one expects a strong enhancement of the X-ray emission by odd-odd fragments, in agreement with the observed odd-even effects. The experiment, therefore, suggests that the 82-neutron-shell closure occurs for a smaller fragment charge in ternary than in binary fission. A hypothesis made on the origin of the light particle should, therefore, predict more neutron-rich "light-heavy" fragments in ternary than in binary fission.

The experimental results are summarized in Table I. The binary charge yields have been taken from the work of Reisdorf and co-workers [9] except for charge 49. For this charge we used a value of the number of X-rays per fragment of 0.09 derived from consideration of the neighbouring values and of the values obtained for the same charge in ternary fission. From this value we derive a yield of 2.3% for fragments of charge 49. Since there are two such fragments at the same time, only half this value is to be compared to the other charge yields. The peak-to-valley ratio in binary fission is then found to be approximately 13, significantly lower than the suggested [10] value of 750, but comparable with the peak-to-valley ratio of 18 found from the mass yields. As explained above, the ternary charge yields were obtained from the light fragment X-ray yields with the exception of charge 37 where the heavy fragment X-ray yields were used.

As is well known [6], the comparison of the mass yields in binary and ternary fission can only provide ambiguous information with regard to the formation process of the light particle. In principle, the simultaneous consideration of the charge yields could remove part of this ambiguity. If we make a specific hypothesis on the formation of the α-particle, for example that it comes solely from the heavy fragment, then the probability that a specific heavy fragment emits the α-particle is given by

$$P_\alpha(m) = \frac{Y_T(m-4)}{Y_T(m)}$$

and

$$P_\alpha(Z) = \frac{Y_T(Z-2)}{Y_T(Z)}$$

It is clear that the values of $P_\alpha(Z)$ and $P_\alpha(m)$ should be almost equal when the mass corresponds to the most probable mass of the fragments with

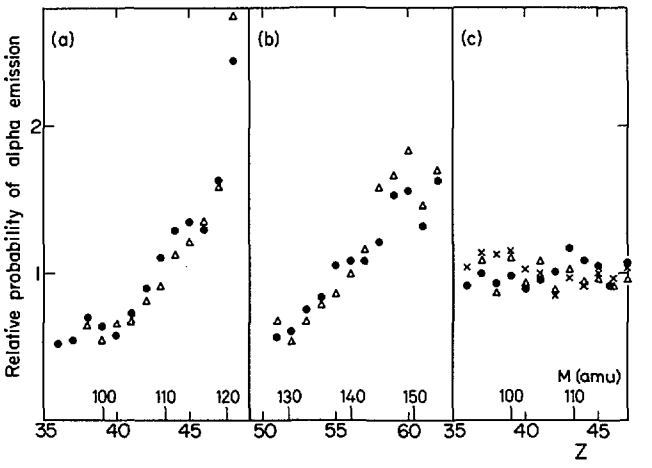

FIG. 5. Comparison of the relative α-emission probabilities as a function of fragment masses (●), and of fragment charges (Δ) assuming three different hypotheses: (a) α-particle emitted by the light fragment, (b) α-particle emitt by the heavy fragment, (c) each fragment contributes 1 proton and 1 neutron to α-particle. The mass and charge scales reflect the mass-to-charge ratio of the binary fission fragments. x: values of the ratio $\frac{Y_B(Z-1)+Y_B(Z+1)}{2\,Y_B(Z)}$.

charge Z. Figure 5 shows how the values of $P_\alpha(Z)$ and $P_\alpha(m)$ compared for three different hypotheses, namely:

(a) The α-particle comes solely from the heavy fragment
(b) The α-particle comes solely from the light fragment
(c) Each fragment contributes one proton and one neutron to the α-particle.

In all three hypotheses, we assume that all light particles are α-particles. From Fig. 5 it can be seen that a choice between the three hypotheses cannot be made on the basis of the mass and charge yields measurements. The question of the origin of the α-particle would therefore require additional information such as, for example, a comparison of the isotopic distributions of fragments of given charges in binary and ternary fission. This comparison could be made with the help of the γ-rays emitted by the fragments. However, the total number of neutron measurements already indicates that the light-heavy fragments, and possibly all of the heavy fragments, are more neutron-rich in the ternary fission. This could be an indication that, as suggested by Feather [11], the α-particles are formed mostly at the expense of the heavy fragments. Figure 5(c) presents a clear even-odd effect. It is interesting to determine the origin of this effect. This figure was obtained by plotting the values of

$$P_\alpha^1(Z) = \frac{Y_T(Z-1)}{Y_B(Z)}$$

corresponding to hypothesis (c).

With the relation used to obtain the ternary yields, we have

$$P_{\alpha}^{1}(Z) = \frac{Y_B(Z-1)}{Y_B(Z)} \quad \frac{I_T(Z-1)}{I_B(Z-1)}$$

We have shown in Fig. 5(c) the values of

$$\frac{Y_B(Z-1) + Y_B(Z+1)}{2Y_B(Z)}$$

It appears that these values, obtained from the binary yields of Reisdorf and co-workers [9], do show an even-odd effect in the same direction as $P_{\alpha}^{1}(Z)$. However, except for the symmetric charges, the effect observed in $P_{\alpha}^{1}(Z)$ is much more important than that observed in the above ratios. Most of the effect is thus a consequence of either a residual selectivity of the X-ray emission process or an enhancement of α-emission when the two fission fragments have an odd charge.

APPENDIX I

From our binary fission experiment we have obtained an array $N(X_i, T_i)$ of the number of events giving rise to an X-ray pulse height X_i and a time difference T_i between the liquid scintillator prompt pulse and the X-ray pulse.

A suitable grouping of the time channels was made, providing 35 different X-ray spectra, each corresponding to a specified time interval. The X-ray spectra were analysed in terms of their charge components. Thus, a time spectrum was obtained for each charge. The 21 time spectra corresponding to charges ranging from 39 to 59 were in turn analysed in terms of two or if necessary three time components, one prompt and the other(s) delayed, so that the shapes of the time spectra were assumed to be the convolution product

$$N_Z(t) = R_Z(t) * \left(a_0 + \frac{a_1}{\lambda_1} \exp - \frac{t}{\lambda_1} + \frac{a_2}{\lambda_2} \exp - \frac{t}{\lambda_2}\right)$$

The quantities a_0, a_1, λ_1 and when necessary a_2, and λ_2 were determined by a non-linear least squares fit.

The prompt responses $R_Z(t)$ were determined in two auxiliary experiments: the contribution $r_1(t)$ of the liquid scintillator to the response $R_Z(t)$ was obtained by the measurement of the time differences between the pulses provided by a fission fragment detector on which a small amount of ^{252}Cf had been deposited and those delivered by the scintillator in response to the prompt fission gamma rays. The contributions $r_2(E_X, t)$ of the X-ray detector were determined by measuring the time differences between the X-ray detector and a fast plastic scintillator fired in coincidence by the γ-rays of a ^{60}Co source. For each charge the contribution $r_2(Z, t)$ was obtained when the γ-ray energy deposited in the X-ray detector was equal to the K X-ray energy of this charge. The overall prompt response was then obtained by the convolution

$$R_Z(t) = r_1(t) * r_2(Z,t)$$

It was found that these prompt response functions could be adequately represented analytically by

$$R_Z(t) = \frac{1}{\sigma_Z\sqrt{2\pi}} e^{-t^2/2\sigma_Z^2} * \left[\frac{b_{1Z}}{\tau_{1Z}} H(+t) \exp - \frac{t}{\tau_{1Z}} + \frac{b_{2Z}}{\tau_{2Z}} H(-t)\ e^{t/\tau_{2Z}}\right]$$

where $b_1 + b_2 = 1$ and H(t) is a step-function.

The values of σ_Z, b_{1Z}, b_{2Z}, τ_{1Z}, τ_{2Z} have been presented as a function of Z on Fig. 6. The values of τ_{1Z} which fall around 5 - 6 ns approximately set the lower limit of the lifetimes which could be measured in this experiment.

Figure 7 shows both the time spectra and the fits resulting from the least squares analysis. The values of the parameters a_0, a_1, a_2, λ_1 and λ_2 are shown as a function of Z on Fig. 8. The intensities a_0, a_1 and a_2 have been estimated in terms of the number of corresponding X-rays per fission and normalized so that the total yield $a_0 + a_1 + a_2$ for charge 56 is equal to the value found by Watson and co-workers [12]. For almost all charges the time spectra show a delayed component with a lifetime greater than about 40 ns.

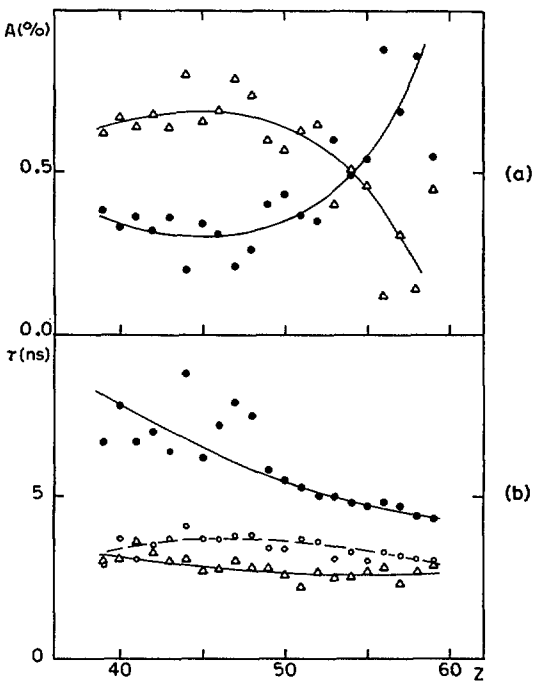

FIG. 6. Parameters of the prompt response curve. (a) ●: relative intensity of time component 1 (b_{1Z}). △: relative intensity of time component 2 (b_{2Z}); (b) ●: time constant of component 1 (τ_{1Z}), △: time constant of component 2 (τ_{2Z}), ○: root mean square of the Gaussian function σ_Z.

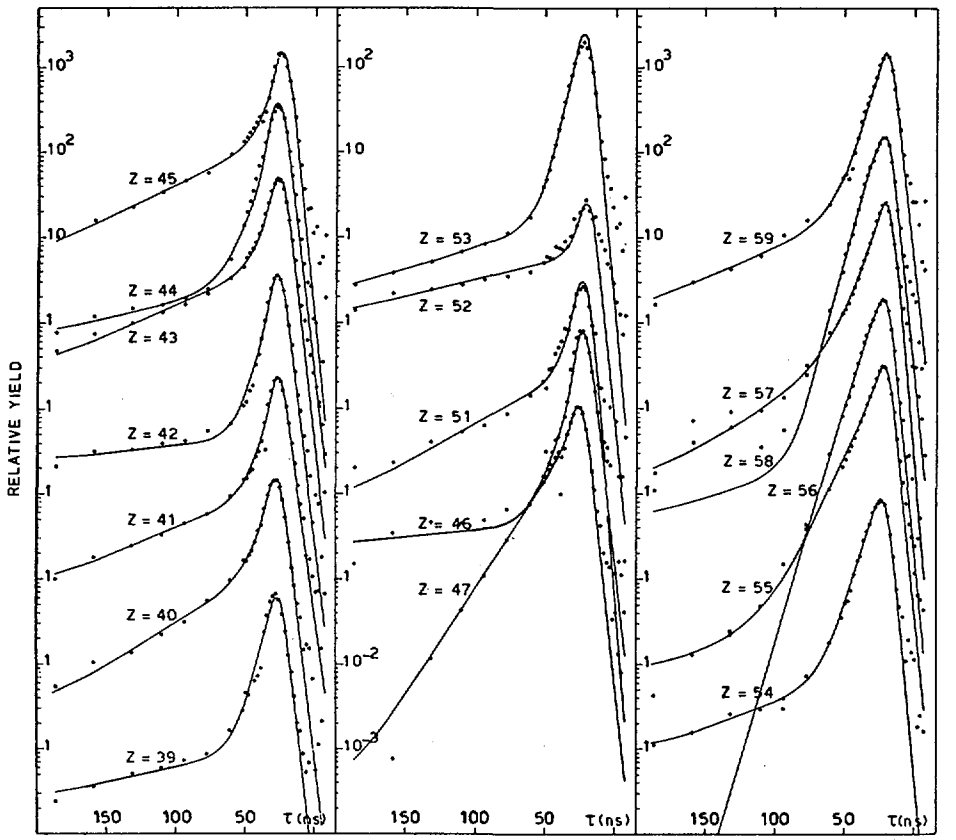

FIG.7. Experimental X-ray decay curves. The full curves show the result of the least squares fits.

The intensity of this delayed component drops markedly after the closure of the 82-neutron shell but shows no even-odd effect. An intermediate (5 - 15 ns) component appears around the 82-neutron-shell closure, whose intensity likewise shows no even-odd effect. The prompt component, on the contrary, is responsible for most of the even-odd effect on the total X-ray yields.

APPENDIX II

In this appendix we want to show that, to a good approximation,

$$\bar{\nu}_T(Z) = \bar{\nu}_T(\bar{m}(Z))$$

where $\bar{m}(Z)$ is the most probable mass of fragments with charge Z, and that any selectivity in the X-ray emission process will be reflected in the measured values $\bar{\nu}_X(Z)$.

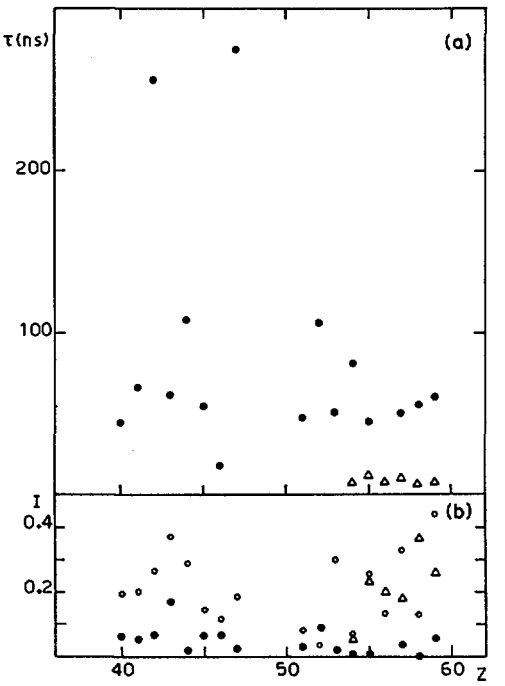

FIG.8. Results of the fits. (a) time constants τ, △: intermediate component (5 ns $\leq \tau \leq$ 15 ns), ●: delayed component ($\tau \geq$ 15 ns); (b) intensity I (number of decays per fragment) of the time components, ○: prompt component ($\leq$ 5 ns), △: intermediate component (5 ns $\leq \tau \leq$ 15 ns), ●: delayed component ($\tau \geq$ 15 ns).

Let $\bar{\nu}_T(Z, m)$ be the average total number of neutrons emitted when one of the fragments has charge Z and pre-neutron emission mass m, and Y(Z, m) is the yield of this particular fragment. Then

$$\bar{\nu}_T(Z) = \frac{\sum_m \bar{\nu}_T(Z,m)\ Y(Z,m)}{\sum_m Y(Z,m)}$$

To first order we have

$$\bar{\nu}_T(Z,m) = \bar{\nu}_T(Z,\bar{m}) + a(m-\bar{m})$$

and

$$\bar{\nu}_T(Z) = \bar{\nu}_T(Z,\bar{m})$$

Similarly, with obvious definitions,

$$\bar{\nu}_T(m) = \bar{\nu}_T(\bar{Z},m)$$

A good representation of the yields Y(Z, m) has the form

$$Y(Z,m) = \frac{Y(m)}{\sigma_m\sqrt{2\pi}}\, e^{-\frac{(m-\alpha Z-\beta)^2}{2\sigma_m^2}}$$

For a fixed value of m the average value of Z is thus

$$\bar{Z} = \frac{m+\beta}{\alpha}$$

and, provided the variations of Y(m) are not too rapid, the average value of m for fixed Z is

$$\bar{m} = \alpha Z + \beta$$

Thus

$$\bar{Z}\,(\bar{m}(Z)) = Z$$

and

$$\bar{\nu}_T(\bar{m}) = \bar{\nu}_T(Z,\bar{m}) = \bar{\nu}_T(Z)$$

The above treatment requires that the average total number of neutrons can be represented by a continuous function, which does not have even-odd fluctuations. This has been shown to be the case in Ref. [8].

The probability of observing a pre-neutron mass m for a fragment of charge Z can be written

$$P(m:Z) = \frac{1}{\sigma_m\sqrt{2\pi}}\, e^{-\frac{(m-\bar{m})^2}{2\sigma_m^2}}$$

after emission of ν neutrons the mass of a fragment becomes

$$m^* = m - \nu$$

and, if we assume a Gaussian distribution for the number of neutrons we obtain the joint probability distribution for pre-neutron and post-neutron masses

$$P(m,m^*:Z) = \frac{1}{\sigma_m\,\sigma_\nu\,2\pi}\, e^{-\frac{(m-\bar{m})^2}{2\sigma_m^2} - \frac{(m-m^*-\bar{\nu})^2}{2\sigma_\nu^2}}$$

where we assume that $\bar{\nu}$ is independent of m.

The average value of the pre-neutron mass for fixed post-neutron mass is then

$$\langle m:m^* \rangle = \frac{\bar{m}\,\sigma_\nu^2 + (m^*+\bar{\nu})\,\sigma_m^2}{\sigma_\nu^2 + \sigma_m^2}$$

and the average number of neutrons

$$\langle \nu : m^* \rangle = \langle m : m^* \rangle - m^* = \frac{\bar{m}\,\sigma_\nu^2 + \bar{\nu}\,\sigma_m^2 - m^*\,\sigma_\nu^2}{\sigma_\nu^2 + \sigma_m^2}$$

or

$$\langle \nu : m^* \rangle = (\bar{m} - m^*)\,\frac{\sigma_\nu^2}{\sigma_\nu^2 + \sigma_m^2} + \bar{\nu}\,\frac{\sigma_m^2}{\sigma_\nu^2 + \sigma_m^2}$$

The measured value of the average number of neutrons as obtained from the X-ray experiments is given by

$$\bar{\nu}_X(Z) = \frac{\int \langle \nu : m^* Z \rangle \;\; C(Z,m^*) \;\; P(Z,m^* : Z)\, dm^*}{\int C(Z,m^*)\; P(m^* : Z)\, dm^*}$$

and from the first part of the appendix we have

$$\bar{\nu}_X(Z) = \langle \nu : \bar{m}^* Z \rangle$$

where $\bar{m}^*$ is the average value of m^* for the squewed distributions

$$C(Z,m^*)\; P(Z,m^* : Z)$$

If $C(Z, m^*)$ is independent of m^*, it can easily be shown that

$$\bar{m}^* = \bar{m} - \bar{\nu}$$

while, if $C(Z, m^*)$ has a positive slope with respect to m^*,

$$\bar{m}^* = \bar{m} - \bar{\nu} + \Delta > \bar{m} - \bar{\nu}$$

with Δ positive, and

$$\bar{\nu}_X(Z) = \bar{\nu} - \Delta\,\frac{\sigma_\nu^2}{\sigma_\nu^2 + \sigma_m^2}$$

In the heavy fragment region the slope of $C(Z, m^*)$ as a function of m^* is very probably positive so that $\bar{\nu}_X(Z)$ should be less than $\bar{\nu}(m)$, as found experimentally.

It should also be noted that, if the probability of X-ray emission is higher for nuclei with an odd neutron number, the apparent average binding energy of the last neutron emitted will increase and, for a given excitation energy, the number of emitted neutrons will decrease.

REFERENCES

[1] BONEH, Y., FRAENKEL, Z., NEBENZAHL, I., Phys. Rev. 156 (1962) 1305.
[2] RAJAGOPALAN, M., THOMAS, T.D., Phys. Rev. C5 (1972) 2064.
[3] FLUSS, M.J., KAUFMAN, S.B., STEINBERG, E.P., WILKINS, B.D., Phys. Rev. C7 (1973) 353.
[4] KATARIA, S.K., NARDI, E., THOMPSON, S.G., Paper IAEA-SM-174/63, these Proceedings, Vol. 2.
[5] MEHTA, G., POITOU, J., RIBAG, M., SIGNARBIEUX, C., Phys. Rev. C7 (1973) 373.
[6] HALPERN, I., Annu. Rev. Nucl. Sci. 11 (1971) 577.
[7] WATSON, R.L., Phys. Rev. 179 (1969) 1109.
[8] NIFENECKER, H., SIGNARBIEUX, C., BABINET, R., POITOU, J., Paper IAEA-SM-174/207, these Proceedings, Vol. 2.
[9] REISDORF, W., UNIK, J.P., GRIFFIN, H.C., GLENDENNING, N.K., Nucl. Phys. A177 (1971) 337.
[10] TSANG, C.F., WILHELMY, J.B., Nucl. Phys. A184 (1972) 417.
[11] FEATHER, N., in Physics and Chemistry of Fission, (Proc. Symp. Salzburg, 1965) 2, IAEA, Vienna (1965) 397.
[12] WATSON, R.L., BOWMAN, H.R., THOMPSON, S.G., Phys. Rev. 162 (1967) 1169.

APPLICATIONS OF THIN FILM SCINTILLATOR DETECTORS TO FISSION INVESTIGATIONS*

L. MUGA, A. CLEM, G. GRIFFITH
The University of Florida,
Gainesville, Fla.,
United States of America

Abstract

APPLICATIONS OF THIN FILM SCINTILLATOR DETECTORS TO FISSION INVESTIGATIONS.

The invention and development of the thin film detector (TFD) for the detection and identification of energetic heavy ions is traced. The manner in which the elementary parameters, nuclear charge Z and velocity V, of the heavy ion affect the TFD pulse-height response is described. Although in the velocity range normally encountered for fission fragments the resolution of a thin film scintillator detector is not adequate for a precise determination of individual fission fragment charge, it can be used to describe the mean nuclear charge of a group of ions previously selected as to mass. For example, mass determinations may be made by measuring the velocity (through time-of-flight techniques) and residual energy of individual fission fragments. Alternately, the kinetic energies of complementary fission fragment pairs may be determined. In addition to these dual parameter sets, the TFD response is simultaneously recorded event-by-event. For selected mass groups, plots of TFD response versus fragment velocity may be used to derive the mean fragment charge as a function of pertinent parameters such as total kinetic energy release. This method constitutes a new experimental approach for the determination of this quantity. Errors and limitations associated with this method and possible alternate interpretations of the thin film detector response to fission fragments are discussed.

1. INTRODUCTION

The thin film scintillator detector (TFD) was developed in response to the need for a simple transmission detector of energetic heavy ions [1,2]. It consists of a thin film (0.1 mg/cm^2) of plastic scintillator, suitably supported, and placed perpendicular to two opposing photomultiplier tubes [3]. In addition to transiting ion detection, the TFD pulse height response (proportional to the specific luminescence ($\Delta L/\Delta x$) has been found to depend on nuclear charge Z and velocity V of the transiting energetic ion. The nature of this dependence is shown in Figs. 1-3. Figure 1 gives the TFD pulse height as a function of incident ion velocity for some transmitted light ions (Z=1, A=1,2; Z=2, A=3,4) [4]. It demonstrates the mass non-dependence and the charge dependence of the TFD. The curves of Figs. 2 and 3, respectively, establish the trends expected in $\Delta L/\Delta x$ for selected heavy ions of known mass when plotted as a function of energy and velocity [5]. The crossing-over of TFD response curves plotted vs. energy (Fig. 2) is removed and simplified when plotted as a function of velocity (Fig. 3).

Although, in the velocity range normally encountered for fission fragments, the resolution of the pulse height response (at its current stage of development) is not adequate for a precise determination of individual fission fragment charge, it

* Supported in part by the US Atomic Energy Commission.

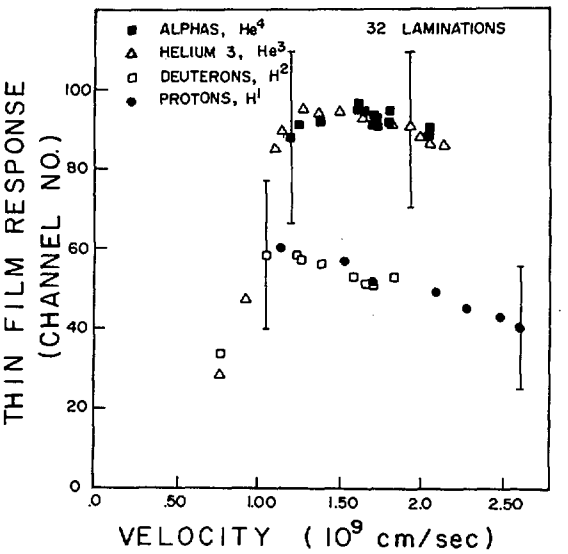

FIG. 1. Thin film detector (TFD) response as a function of velocity of ions incident on a film of 32 laminations (approx. 0.7 mg/cm^2). Designated limits on the ordinate axis represent the full-width at half-maximum (FWHM) distribution of individual TFD pulse-height responses. Reproducibility of peak positions is indicated by the spread of data points representing transiting monoenergetic alpha particles.

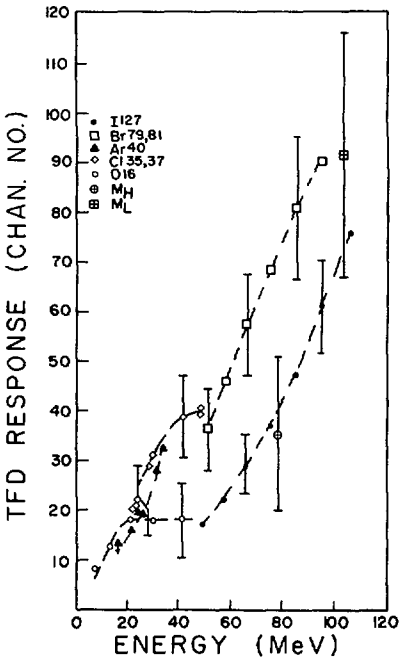

FIG. 2. TFD response plotted as a function of the kinetic energy of ions incident on a film of 4 laminations (approx. 0.1 mg/cm^2). Limit bars indicate the FWHM of the TFD pulse height distributions. M_H and M_L refer respectively to the mean heavy- and light-mass fragments from ^{252}Cf spontaneous fission. The dashed curves are drawn as a visual aid.

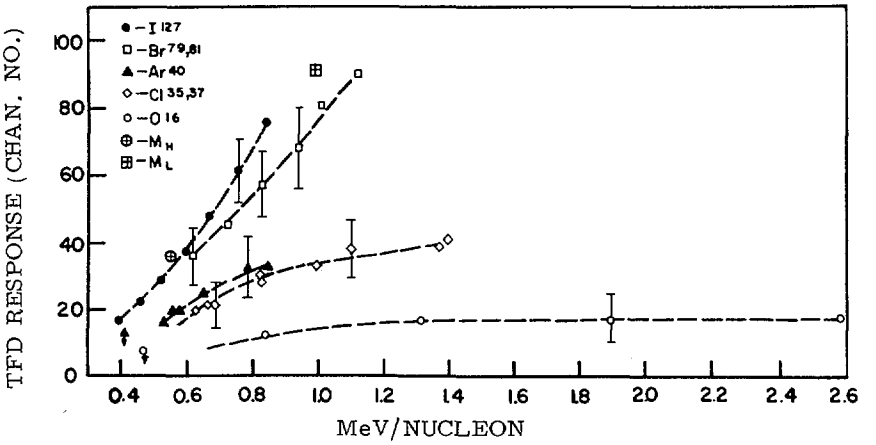

FIG. 3. TFD response versus energy per nucleon (proportional to velocity squared) of incident ions for the same data as Fig. 2. Limit bars and M_L and M_H are also as described in Fig. 2.

can be used to describe the mean nuclear charge of a group of ions previously selected as to mass. On the basis of this approach, we have explored the TFD response to selected mass groups of fission fragments from spontaneous fission decay of ^{252}Cf and the thermal-neutron-induced fission of ^{235}U.

2. EXPERIMENTAL

Masses of fission fragments were determined by the energy-velocity (time-of-flight) method. The arrangement used is shown in Fig. 4. Basically, it consisted of a) an evacuated system with the ^{252}Cf or ^{235}U fission source, b) a TFD of four laminations (0.1 mg/cm^2) to mark the beginning of a one-meter flight path and for measurement of characteristic luminescence of the transmitted fission fragment, c) a silicon surface-barrier detector (SSD) to measure residual fragment energies and mark the end of flight.

For these experiments, a thin 0.01 mg/cm^2 uranium (99.7% ^{235}U) oxide target was irradiated in the University of Florida Training Reactor at a power level of 100 kW. The flux of fission fragments was collimated and emerged from three meters within the reactor structure to begin the measured 1.000-meter flight path. The identical system was shared with ^{252}Cf, except that this spontaneous fission source was inserted only a few centimeters in front of the TFD. Pulse heights of the TFD and SSD and the pulse height of the inverse flight time between the TFD and SSD were simultaneously collected (event-by-event) with a 6-parameter analyzer and recorded digitally on magnetic tape for computer processing. Energy calibration was made by removing the TFD and exposing the SSD directly to the ^{236}U* fission fragments; the Schmitt [6] mass-dependent prescription was applied. Timing calibrations were made by a) successively shortening the flight path and extrapolating to obtain the time zero channel at zero flight distance and by b) using an ORTEC precision time calibrator to determine the time per channel slope. The TFD response was used directly as pulse height channel number.

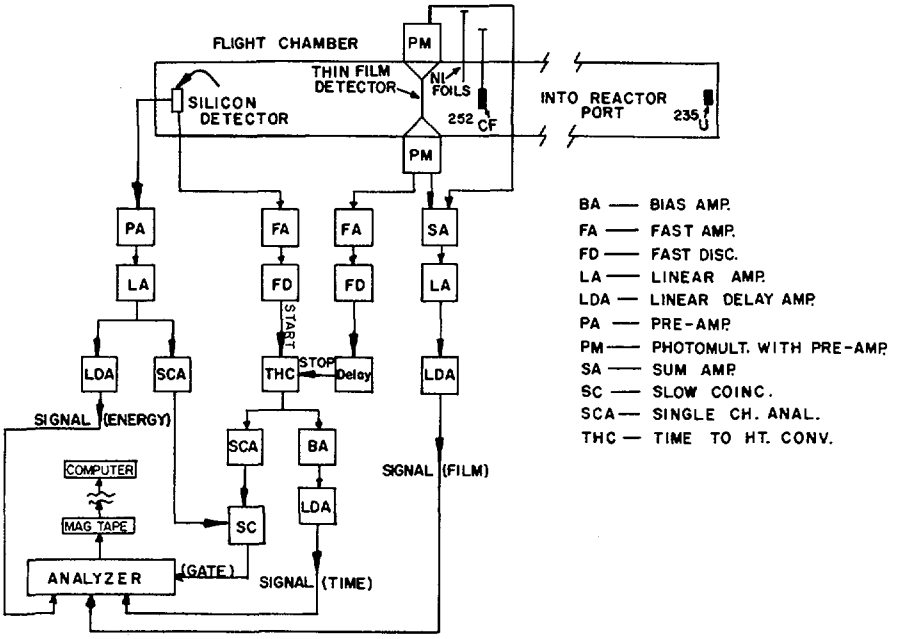

FIG. 4. Block diagram of the energy, time-of-flight experimental arrangement and electronic system. Plungers containing the degrader foils and ^{252}Cf may be inserted into the flight path as desired.

In order to investigate TFD behavior at slightly lower fragment energies, a 0.3 mg/cm^2 nickel degrader foil was inserted between source and detectors. The effect of this foil was to reduce the average fission fragment energy by about 10 MeV. Approximately one-half million events of each of the four kinds (Cf and U, degraded and undegraded) were analyzed. Additional data (about two million events of each type) were collected for future reference and possible delineation of any less frequent or unusual occurences. Mass resolution (FWHM) was 2-3%.

In still another approach, an independent method of fragment mass selection from spontaneous fission decay of ^{252}Cf was based on the measurement of complementary fragment energies. An experimental chamber was used in which a thin film detector-solid state detector (TFD-SSD) system and a lone second SSD were placed on opposite sides of a thin backed (5×10^{-6}-in.-thick nickel foil) ^{252}Cf fission source. The first solid state detector (SSD) was calibrated by placing it in front of the TFD and exposing it to the bare ^{252}Cf source. A second ^{252}Cf fission fragment spectrum taken with the SSD placed in position behind the TFD served to measure the average energy loss suffered by typical light- and heavy-mass fission fragments.

For each recorded fission event a three-parameter measurement for the TFD response and residual energy of each of the complementary fragments was made. An initial straight-line calibration (using the two fission fragment peak positions)

was applied to determine the residual energy and to this value (for the first SSD) was added a constant energy loss (as previously determined) to give incident (on TFD) fragment energies. These temporary energies were used to form a temporary mass determination using the relations derived from momentum conservation requirements and constant mass summation ($M_L + M_H = 252$). Reiteration of the procedure, but now using a mass-dependent calibration scheme, produced a final set of fragment masses and incident energies. The TFD signal was retained as a relative response in pulse height channel number. After reduction of the recorded data to mass, energy values, events were gathered in selected mass groups each containing three atomic mass units. The full-width at half-maximum resolution in determining mass by this method was approximately 5-6 amu and a total of 440K events were registered.

3. RESULTS AND DISCUSSION

As a check on the performance of the calibration procedure, a ^{252}Cf fission post-neutron mass distribution was first obtained and is shown in Fig. 5. The measured peak-to-valley ratio of about 100/1 is comparable with that obtained by others using TOF techniques. The one percent fewer counts under the heavy mass peak (with respect to the light fragment peak) is attributed to preferential scattering out of the one-meter flight path by the TFD.

An overall view of the TFD response vs. residual energy for selected mass fragments from ^{252}Cf decay is shown in Fig. 6 with an overlay contour response (all fragments) for comparison. Fig. 7 represents a similar plot for ^{252}Cf fission fragment masses selected from back-to-back complementary fragment energy measurements. Equivalent results from two different experimental approaches lend confidence to the accumulated data. The following general characteristics are evident from Figs. 6 and 7. The heavy and light mass regions are clearly separated. In the energy region displayed, the heavier fragments produce the lower TFD response. Convergence of the light mass fragment response curves at higher energies is suggested.

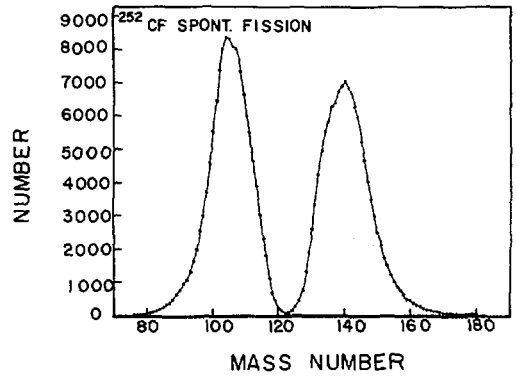

FIG. 5. ^{252}Cf spontaneous fission post-neutron mass distribution (uncorrected for experimental resolution) via the single fragment energy, time-of-flight correlation method of this work.

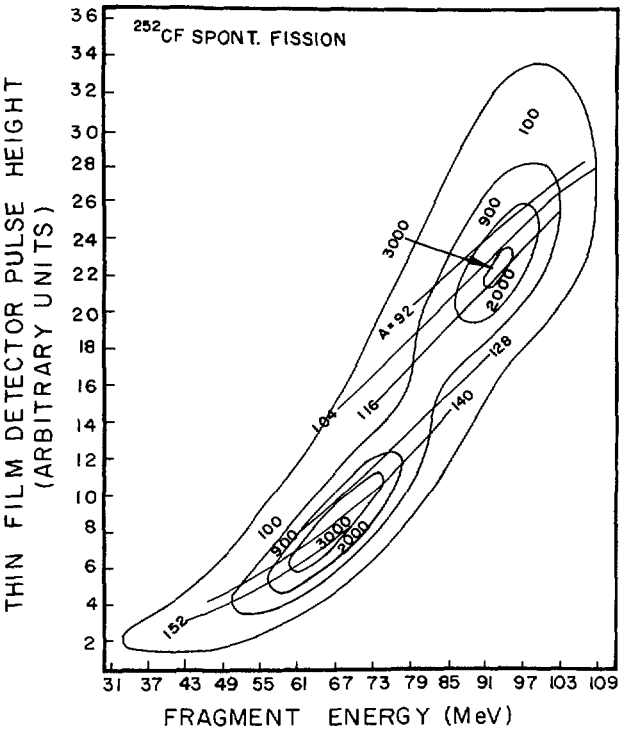

FIG. 6. TFD response versus residual energy for several selected masses obtained by the energy, time-of-flight technique for ^{252}Cf spontaneous fission. The two-dimensional "overlay contour" (all masses) is included for reference.

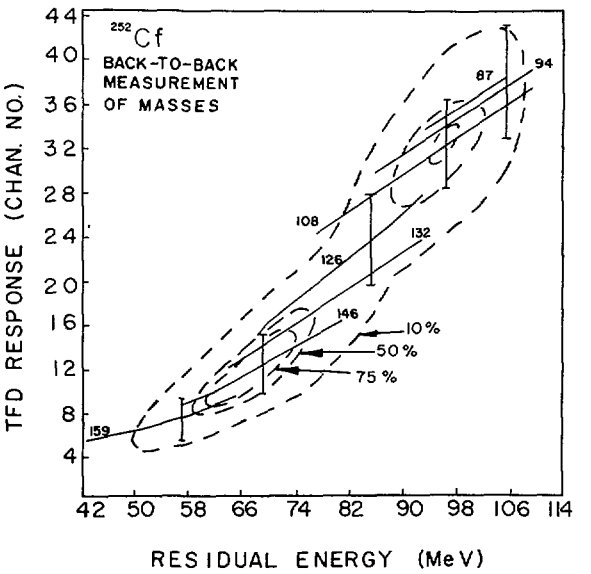

FIG. 7. Comparable to Fig. 6, these data were obtained in an independent experiment in which ^{252}Cf fission fragment masses were determined by back-to-back complementary fragment energy measurements.

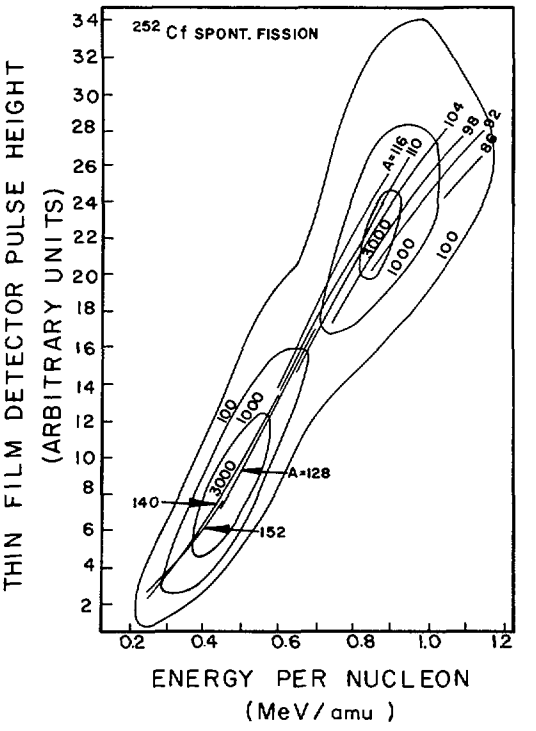

FIG. 8. TFD response versus residual energy per nucleon (proportional to velocity squared) for several ^{252}Cf fragment masses selected by the energy, time-of-flight experiment. An overlay of the two-parameter contour (all masses) is shown for comparison.

When plotted against energy/nucleon (proportional to velocity squared) the TFD response curves appear as in Fig. 8 for ^{252}Cf fission fragments. An overlay of the two-parameter contour is shown for comparison. A similar series of curves was obtained from "back-to-back" energy data. Separation of the light fragment response curves is enhanced at higher velocities but the curves appear to converge at lower velocities. In the lower velocity region, no clear distinction in the heavy mass response curves is apparent. The overall view of the TFD response as it appears in Figs. 6-8 is consistent with previous results as reviewed in Figs. 1-3.

For the $^{235}U + n_{th}$ system, the TFD response to transiting fission fragments as a function of energy and energy per nucleon is shown in Figs. 9 and 10, respectively. In Fig. 9, the convergence of the light fragment curves is again clearly shown with a crossing of the lighter mass response curves by the 104 amu mass line. Although, on the basis of Fig. 2, we should expect a crossing of the response curves as their respective maxima are approached, an apparently slower convergence of the light fragment response curves for the ^{252}Cf system (Fig. 6) is evident by comparison with similar curves for the $^{235}U^*$ system (Fig. 9). The velocity

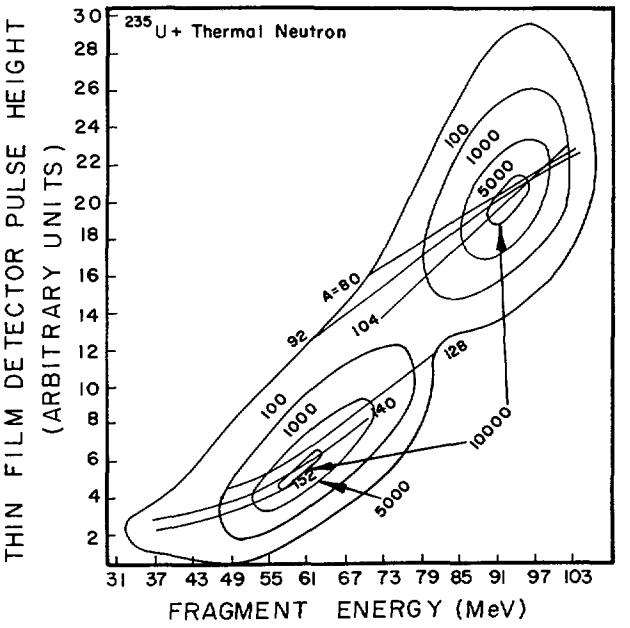

FIG. 9. TFD response versus residual energy for selected masses (via energy, time-of-flight) from ^{235}U thermal neutron fission. Compares with Fig. 6.

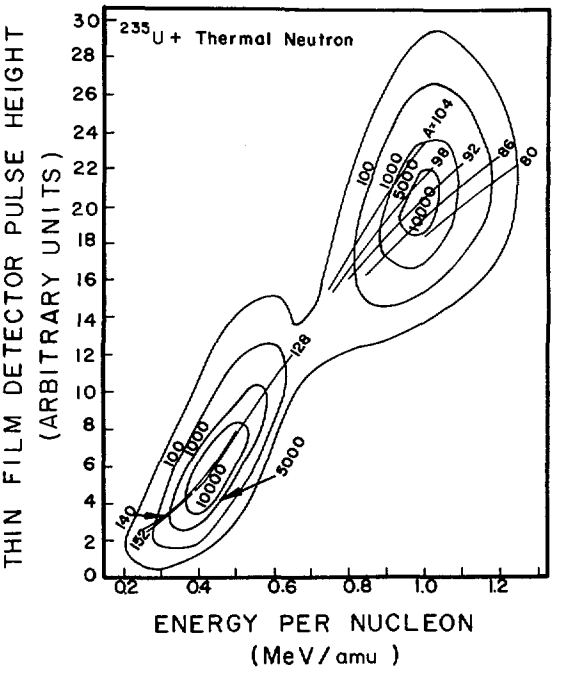

FIG. 10. TFD response versus residual energy per nucleon for selected masses (energy, time-of-flight) from ^{235}U thermal neutron fission. Compares with Fig. 8.

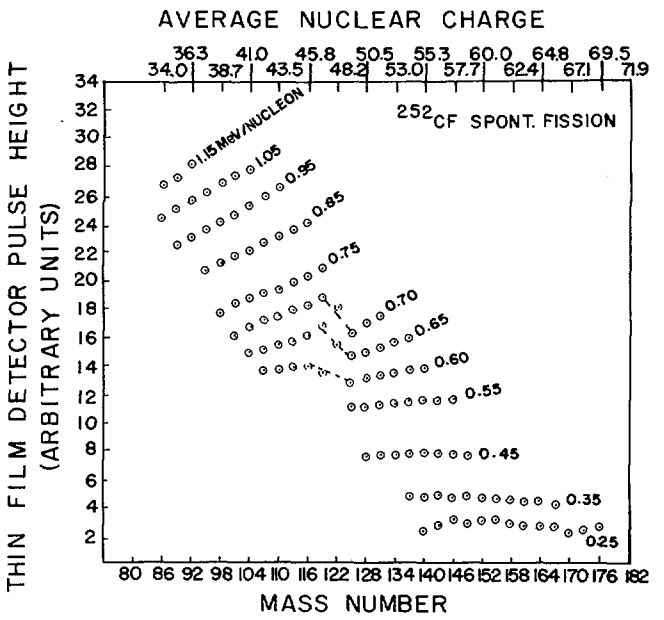

FIG. 11. TFD response as a function of mass (via energy, time-of-flight) at constant velocity for ^{252}Cf spontaneous fission fragments. A measure of the mean fragment nuclear charge shown along the upper horizontal axis was obtained simply by assuming a uniform charge density for all fragments and is given by the fraction 98/248 multiplied by the fragment mass.

dependence (Fig. 10) is entirely consistent with previous results (Fig. 3) found for accelerated heavy ions. The better distinction between heavy and light mass groupings (as compared to the ^{252}Cf system, Fig. 8) is explained in terms of the wider mass separation between typical light and heavy mass fragments.

A measure of the mean fragment charge may be obtained by viewing the TFD response as a function of the experimental mass groupings at constant velocity as shown in Fig. 11 for ^{252}Cf. Taking the mean charge Z as proportional to the fission fragment mass, it appears that the charge sensitivity of the TFD response increases at higher velocities, as previously reported for accelerated heavy ions. The discontinuous feature between velocity sets common to heavy and light mass groups may be partially explained in terms of the familiar "saw tooth" neutron evaporation function for which the heaviest of the light mass fragments evaporate a larger share of neutrons, thereby attaining a higher Z/A ratio than otherwise expected. This effect would lead to a horizontal translation but not to the observed vertical dislocation. In addition to possible nuclear effects (brought about by unusual nuclear charge distribution) this effect may be engendered by atomic phenomena (e.g. atomic shell effects or non-equilibration of ion charge at the time of TFD passage). It must be noted that the discontinuous feature is associated with a small proportion of the total number of events. Notwithstanding this unexplained feature, it is clear that the TFD may be used to indicate the average nuclear charge of selected fission fragment mass groups and constitutes a novel experimental approach for this purpose.

REFERENCES

[1] MUGA, M. L., BURNSED, D. J., STEEGER, W. E., TAYLOR, H. E., Nucl. Instr. and Meth. 83 (1970)135.

[2] MUGA, M. L., Nucl. Instr. and Meth., 95 (1971)349.

[3] MUGA, M. L., BURNSED, D. J., STEEGER, W. E., Nucl. Instr. and Meth., 104 (1972)605.

[4] MUGA, M. L., GRIFFITH, G., Nucl. Instr. and Meth., 109 (1973)289.

[5] MUGA, M. L., GRIFFITH, G. L., SCHMITT, H. W., TAYLOR, H. E., Nucl. Instr. and Meth., in press, 1973.

[6] SCHMITT, H. W., KIKER, W. E., WILLIAMS, C. W., Phys. Rev., B137 (1965) 837.

DISCUSSION

Z. FRAENKEL: What is the time resolution of this detector?

L. MUGA: Our best results are 0.7 nsec FWHM when timing between a TFD-SSD combination.

SUMMARY OF THE SYMPOSIUM

K. DIETRICH
Physik Department der Technischen Universität München,
Garching bei München, Federal Republic of Germany

I have the honour of giving this summary in place of Professor Strutinsky to whom we owe an essential part of the recent spectacular development in the field of nuclear fission.

In the first part I shall try to summarize the progress which has been made in recent years in the understanding of nuclear fission, and which we have witnessed in this Symposium. In the second part, I wish to summarize the most striking unresolved questions, which appeared and reappeared during this meeting. Here let us recall the words of Professor Wheeler, namely that it is the paradoxes of today which lead to the progress of tomorrow.

Where did we stand at the time of the Symposium in Vienna, 1969?

Experimentally, the central point had been the discovery of an increasing number of fission isomers with a vast range of lifetimes (10^{-16} sec to 10^{-6} sec) and the display of a fine structure of these subthreshold resonances with a spacing in the eV range typical for compound states in the same range of the excitation energy.

Theoretically the central point of discussion had been the "shell-correction method" proposed by Strutinsky. It offered an explanation of the fission isomers in terms of quasistable states which have a deformation different from that of the ground state and which decayed essentially by tunnelling through the outer barrier of a double-hump potential.

At the same time, it had been emphasized by Strutinsky, Griffin and a number of other authors that shell effects would also produce a strong dependence of the collective inertia on the shape variables. The hope had been that a dynamical treatment based on the liquid drop (LD) plus shell energy as a potential and a kinetic energy with variable inertia would — at least for spontaneous and very low-energy fission — explain the preponderance of asymmetric fission for most heavy actinides.

In spite of these optimistic prospects, there had been no direct experimental proof that "fission isomers" were indeed "shape isomers". On the theoretical side, it had been unclear whether the Strutinsky method was a skilfully designed phenomenological recipe of introducing shell effects into the LD picture or whether it could be derived from a fundamental microscopic theory.

What has been achieved since the Symposium in Vienna? Let me first turn to the most prominent experimental work. If the observed fission isomers are to be interpreted as metastable states of a deformation larger than that of the ground state, then there must be rotational bands with a moment of inertia which corresponds to this large deformation. Thus the crucial experiment for Strutinsky's interpretation was to find rotational bands built on the vibrational states of the second valley. This has been achieved by the beautiful experiment of Specht, Weber, Konecny, and Heunemann [1]. The agreement between the measured and the calculated moment of inertia is surprisingly good.

TABLE I. SELECTION OF EXPERIMENTAL RESULTS

Subjects	Results
Fission isomers	
	Discovery of rotational bands built on states of second valley [1].
	Discovery of γ-decay back to first valley [2].
	Identification of excited intrinsic states with a deformation of second valley [3].
	Determination of spins for fine structure peaks of class II states [4].
	Systematics of parametets of the double-hump barrier [5].
Fragment distributions	
Angular distribution and mass distribution	Measurement of cross-section for fission of Ra and Ac isotopes close to threshold: probably different threshold energies for symmetric and asymmetric fission; rapid decrease of peak-to-valley ratio as a function of energy [8]. Odd-even effects in mass yield and average kinetic energy as a function of neutron and proton number of fragment [13,14].
Distribution of kinetic energies	More experiments concerning dependence of average kinetic energy $\langle E_K \rangle$ from excitation energy [9].
	^{255}Fm(n,f): $\langle E_K \rangle$ larger for symmetric fission than for asymmetric fission [11].
De-excitation of fragments	Average number of emitted photons and average energy released by γ-decay as a function of mass number of fragments. Occasionally, lifetimes and multipolarities of individual transitions. Odd-even effects in these quantities [13]. Conclusions from these experiments. Distribution of spins at scission.
Variances of distribution of excitation energy	Result: energy of scission configuration (E_B - 13 MeV).
Heavy-ion reactions and fission	Difference between fusion and fission barrier [27].

There were a number of other significant experimental achievements which I have put together in Table I.

If there is a second valley in the deformation landscape with quasi-stationary states localized in this valley, these states must not only decay through fission but also through γ-decay back into the first valley (see Fig. 1). This decay was shown to exist in a beautiful experiment by Russo, Pedersen and Vandenbosch [2]. One can only encourage the authors to continue these studies to nuclei lighter than Th where shape isomers can probably no longer be discovered through fission decay.

If the second valley is sufficiently deep, one expects intrinsic excitations with a deformation corresponding to the second valley. Such states have been identified in a number of cases, as reported in this Symposium in the review paper of Vandenbosch [3].

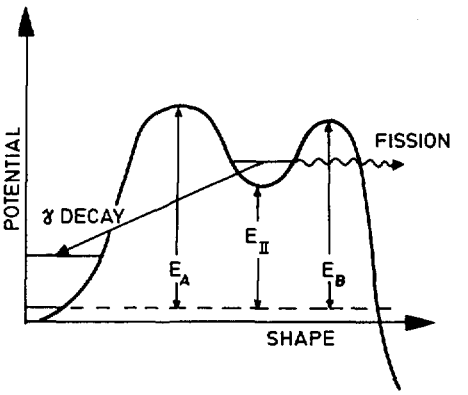

FIG. 1. Deformation energy as a function of the nuclear shape variables. E_A, E_B, E_{II} are the energies of the first barrier, second barrier and second valley, respectively.

If the observed fine structure is produced by the coupling of class II states to many compound states of class I, the fine structure peaks which belong to the same intermediate resonance must have the same spin I. This has indeed been shown in an (n,f) experiment using polarized neutrons as well as polarized target nuclei [4].

The careful and comprehensive analysis by Britt and co-workers [5] of existing data on the production and decay of fission isomers in terms of the parameters of the double-hump barrier must be considered as a big step forward. Note that, in this analysis, no distinction was made between the "dynamical barrier" [6] and the potential barrier. A discussion remark of Bowman [7] on having measured photofission far below the barrier at extremely low yield deserves to be noticed because such experiments, as well as the γ-decay back to the first valley, may serve to pin down the parameters of the first barrier.

As a whole, one can say that experimentalists have furnished the proof that the picture of the double-hump barrier with its manifold implications holds true and that the calculated values of barrier heights and deformations of class II states are essentially correct.

I now turn to experiments related to the distribution of final fragments.

Here again there is a very informative experiment by Konecny, Specht and Weber [8] who measured the cross-section for fission of Ra- and Ac-isotopes in the region of the threshold energy. Their result probably implies that the threshold energy for symmetric fission is larger than the one for asymmetric fission by about 2 MeV. Furthermore, once the threshold for symmetric fission is reached, the yield for symmetric fission increases far more rapidly than the one for asymmetric fission. If the rapid increase of the "peak-to-valley ratio" is to be explained in terms of level densities in the uniform model, a ratio of level density parameters

$$\frac{a_{symm}}{a_{asymm}} = 1.3$$

is required. This is uncomfortably large to explain.

The existence of two thresholds is indicated in the calculations by Pauli and co-workers and by Nix and co-workers. In any case, one is probably here at the limit of accuracy to be expected from the Strutinsky method. The experiment is relevant since it demonstrates that the decision on the final mass split begins already at the saddle point.

Concerning the distribution of kinetic energies, new experiments by Unik and co-workers complement earlier experiments by Specht and co-workers, Holubarsch and co-workers, and by other authors [9]. The situation is complicated: In most cases, the average kinetic energy decreases slightly (a couple of MeV) as the excitation energy is raised from some 5 to 10 MeV (e.g. ^{239}Pu(d,p)), the increase always being due to the asymmetric component. The cases reported by Unik and co-workers show the opposite trend. Experiments of this kind are of great value for the understanding of viscosity on the descent from saddle to scission. A decrease of the average kinetic energy as the excitation energy rises implies an increase of viscosity, i.e. an increase of the probability of populating intrinsic excitations. One of the mechanisms resulting in such an increase is provided by Nörenberg's theory [10].

Furthermore, I should like to remind you of the measurement of kinetic energy distributions for ^{255}Fm(n_{th},f) and ^{251}Cf(n_{th},f) by Ragaini and co-workers [11] which shows that for fission of Fm the kinetic energy of the fragments is larger for symmetric than for asymmetric fission, i.e. the opposite of the trend close to U. This is probably related to shell effects making the fragments for symmetric fission more rigid, contrary to the case for lighter actinides.

I should now like to mention the work concerning the de-excitation of fragments [12]. Emission of γ-rays by the fragments has been studied by Pleasonton and co-workers, Jared and co-workers, Wilhelmy and co-workers and other authors continuing and refining earlier work by Armbruster and co-workers. The results give: average number of γ-rays, average energy emitted through γ-emission, in some cases multipolarities and lifetimes of individual transitions as well as odd-even effects.

These results are very valuable for the determination of the spin distribution of nascent fragments. In turn, this distribution is apt to test our ideas on the descent from saddle to scission. More detailed experiments of this kind, which would furnish the probability distribution of the individual transitions together with the multipolarities, would be of great value.

New results on the emission of prompt neutrons were reported in the review paper by Nifenecker [13]. By studying the variance of the excitation energy of a given fragment for a given total excitation energy of both fragments, Nifenecker and co-workers [13] were able to determine the energy of the scission configuration (about 13 MeV below the second saddle). I think that this is one of the most significant contributions to this Symposium.

Last but not least, I wish to emphasize the importance of the measured odd-even fine structure of the mass yield as a function of the proton- and (more difficult) neutron-number of the fragments [13,14]. These effects show up as differences as large as 30% in yields for fragments of neighbouring mass numbers. They are correlated with corresponding odd-even effects in the distribution of kinetic energies, indicating that most of the energy necessary for breaking pairs is missing in the kinetic energy of fragments. These odd-even effects provide, in my opinion, the most direct evidence that a complete statistical equilibrium cannot be assumed to exist

at scission. At the same time, we should recognize that Fong's early theory contains a lot of truth and was a very ingenious suggestion made at a very early stage of our understanding of nuclear fission. The recent discovery of odd-even effects may justify Nörenberg's hypothesis of a partial equilibrium at scission. Experiments measuring the odd-even effect as a function of the excitation energy would be of great value. In particular, Nörenberg's theory would imply that odd-even effects should decrease at energies $E > E_B + 2\Delta$ (for even-even nuclei). In "modern" language we may say that odd-even effects are a sensitive function of nuclear viscosity on the way from saddle to scission.

I shall now turn to the progress in theory in recent years (see Table II).

Here, from the work of Strutinsky and co-workers, Balian and Bloch, Bohr and Mottelson and other authors [15], it has become clear that the shell correction term represents a fundamental piece in the description of a many-body system with the following properties:

(a) The intrinsic energy of the system can be represented as a functional of the density ρ: $E = E[\rho]$.

(b) The density ρ can be decomposed into a smooth part $\bar{\rho}$ and a fluctuation $\delta\rho$ so that the Taylor expansion

$$E[\rho] = E[\bar{\rho}] + \left(\frac{\delta E}{\delta \rho}\right)_{\bar{\rho}} \delta\rho + \ldots$$

converges rapidly. Evaluation of the term $\left(\frac{\delta E}{\delta \rho}\right)_{\bar{\rho}} \delta\rho$ within the Hartree-Fock approximation and definition of $\bar{\rho}$ by smearing the occupation pattern close to the Fermi surface yields Strutinsky's shell correction term.

TABLE II. SELECTION OF THEORETICAL RESULTS

Subjects	Results
Potential energy	Better theoretical understanding of the shell-correction method [15, 16].
	Extensive and rewarding application of Strutinsky method in the actinide region [6, 17, 21].
	First Hartree-Fock calculations with density-dependent interactions [18].
Kinetic energy and dynamics	Extensive calculation of variable inertia within the cranking approach, calculation of maximal penetrability of the multidimensional barrier (see Ref. [6], and references therein).
Statistical theories	Improved level density formulae [19], connection between level density and symmetries [20].
Coupling of external to internal degrees of freedom	Estimates of viscosity constants [26], microscopic models for calculating population of internal degrees of freedom [24, 25].

The rapid convergence of the series was displayed by Brack and Quentin [16] within the Hartree-Fock approach. Bloch and Balian [15] have studied the average level density in terms of the semi-classical approximation of quantum mechanics. Bohr and Mottelson [15] investigated the relation between the density of single particle levels and the breaking of symmetries.

A study of the term $\left(\frac{\delta E}{\delta \rho}\right)_{\bar{\rho}} \delta\rho$ in theories going beyond the HF or HB approximation is contained in a paper by Strutinsky and co-workers [15]. My personal opinion is that the last-mentioned studies could provide us with an understanding of why the shell correction turns out to be systematically too large for magic configurations. As a whole, we have achieved a much better understanding of the shell correction term, and of its implications as well as its generality.

Careful, laborious, and valuable application of the Strutinsky method by several groups [6,17,21] has provided a detailed insight into the potential landscapes of the fissile actinides.

The WKB calculation of spontaneous and isomer lifetimes by Pauli and Ledergerber [6] reproduced quite nicely the dependence of the most probable mass split on the number of neutrons and protons. This work also demonstrated the implications of the variable inertia, whereby the system at the energies of spontaneous and isomeric fission prefers not to pass below the saddle points ("dynamical barrier"). We should be prepared for the fact that these calculations might be modified, if the theory of inertia is improved on the lines indicated by Wilets.

A very significant step towards a more microscopic theory was taken by Flocard and co-workers [18] in their calculation of potential landscapes using the constrained Hartree-Fock method with density-dependent forces. Th· theoreticians must unfortunately admit that the great successes resulting from the use of density-dependent interactions are a bit ahead of their understanding.

Turning to fission at higher excitation energies, the very useful work done by Moretto [19] on improved level density formulae should be mentioned. In this connection, I should also like to point out the work by Bjørnholm, Bohr and Mottelson [20] who treat the influence of symmetry-breaking on level densities.

In the second part of my talk, I want to review open problems which were discussed during this Symposium. Let me first note a number of discrepancies between our present theory and experiment:

(a) The Strutinsky shell correction is systematically too large at magic numbers of neutrons or protons [3,21] and this is particularly striking in the case of ^{208}Pb.
(b) The observed systematic and pronounced odd-even effect in the isomer- and spontaneous half-lives is not fully accounted for by the theory [3] although possible origins of this effect (specialization energy or odd-even effects in the mass parameters or both) can be given.
(c) There is a discrepancy between empirical and theoretical E_{II} values as a function of the neutron number [3], especially for the Am isotopes. This may be related to difficulty (a).
(d) The calculated height of the first barrier is too low for Th and too high for Cm ("Cm-Th anomaly"). Larsson and Leander [17] showed that the barrier for Cm is decreased if the γ-deformation is included. Pauli

and Ledergerber note that this lowering of E_A due to γ-deformation does not improve the lifetimes for spontaneous fission. Nix discussed the possible existence of a third barrier [17].

(e) For fission of ^{232}Th, Dowdy [22] reported the surprising result that the average number of emitted prompt neutrons remains constant for excitation energies between 7 and 10 MeV. This result is in contradiction to our usual experience that an increase of excitation energy of the fissioning nucleus shows up in the form of an increase of the average excitation energy of fragments, i.e. also of $\bar{\nu}$. In this connection Gozani [23] reported the observation that photofission experiments showed an increase of the ratio Y_n / Y_f of the prompt neutron and fission yields below the threshold energy for ^{232}Th and ^{238}U.

(f) I note again the observation by Konecny, Specht and Weber [8] of the very rapid increase of the cross-section near threshold for symmetric fission for Ra and Ac isotopes which is at present hardly understood. As Armbruster remarked to me, the anomalies (d) may be related to the rapid change from asymmetric to symmetric mass-division as a function of energy.

Besides these difficulties there is the basic open problem of the coupling between the collective degrees and the intrinsic degrees of freedom of the system, i.e. the problem of nuclear viscosity. We have seen a number of first orientating steps in this Symposium. I should like to mention the interesting contribution by Schütte and Wilets [24], the model calculation by Boneh and co-workers [25], and the estimates of the viscosity constant by Wieczorek, Hasse and Süssmann [26]. In nuclear fission, the point which is mainly debated is the descent from saddle to scission. The character of this descent is determined by the average velocity $\langle \dot{r} \rangle$ of descent and the average coupling $\langle H' \rangle$ between appropriately chosen unperturbed states (e.g. shell model states). Qualitatively speaking, one may say:

(a) If $\langle \dot{r} \rangle$ is sufficiently small and $\langle H' \rangle$ sufficiently large, a complete thermal equilibrium is produced at scission (the theory of Fong).

(b) If $\langle \dot{r} \rangle$ is relatively small, and $\langle H' \rangle$ is only large between states of the same hierarchy, one arrives at a partial thermal equilibrium at scission (e.g., the theory of Nörenberg).

(c) If $\langle \dot{r} \rangle$ is large and $\langle H' \rangle$ sufficiently small, one arrives at excitations through slippage (the theory of Griffin).

(d) If $\langle \dot{r} \rangle$ is large and $\langle H' \rangle$ only large and non-negligible for a restricted number of collective degrees, one obtains the dynamical theory of Nix and Swiatecki. It is our homework for the time until the next Symposium to decide which of these alternatives is closest to the truth, a problem which is intimately connected with the understanding of heavy ion reactions. Very remarkable results on the difference between the thresholds for fusion and fission as reported by Tamain and co-workers [27] as well as the theoretical work by Nix and Sierk [28] should be noted in this context.

I should like to conclude with a few comments on the problem of viscosity which might serve as a link between the present work of Schütte and Wilets [24] and considerations by Swiatecki and Bjørnholm [29]:

Consider a reaction between two even-even nuclei at an energy comparable or larger than the Coulomb barrier. If the de Broglie wavelength

of the relative motion is small compared to the nuclear radii we may treat the relative motion of the two mass centres classically. The distance of these mass centres is called r(t) and is treated as a classical function of time. Let us assume, as in the work of Schütte and Wilets, that the quasiparticle states at each given value r(t) provide an appropriate basis of unperturbed states:

$$H = E_{BCS}(r) + \sum_n E_n(r)\, \xi_n^\dagger \xi_n + H'$$

$$E_n = \sqrt{(\epsilon_n - \lambda)^2 + \Delta^2}$$

All quantities are functions of r, where

E_n	=	quasiparticle energy
E_{BCS}	=	BCS-ground state energy
H'	=	interaction between quasiparticles
ϵ_n	=	single particle energy
λ	=	chemical potential
Δ	=	gap parameter
$\xi_n^\dagger$	=	creation operator for a quasiparticle.

Assume that, at large distances, the energy of the system is E_{BCS}, i.e. the two nuclei are described by the respective BCS wave functions. The lowest intrinsic excitations, i.e. the two quasiparticle (2qp) excitations, are separated from the ground state by twice the gap 2Δ. As the nuclei approach each other, the 2qp states and the higher intrinsic states will be populated through the combined effect of H' and the finite velocity $\dot{r}$. The probability of these intrinsic excitations is, however, reduced by the finite gap. This just means that a nearly superfluid system shows little viscosity. Wilets has shown (using, instead of the distance r(t), a deformation $\alpha(t)$ as adiabatic variable) that there may be a significant depletion of the lowest state in spite of this gap. The depletion of the lowest state is, however, expected to be still larger because of the coupling to excitations which lie within the gap. This is so for rotations and for vibrations. We assume, for the sake of simplicity, that there are only vibrations. To study their effect, let us decompose the Hamiltonian into the Hamiltonian H_{RPA} which describes unperturbed bosons and an interaction H'' between phonons

$$H = H_{RPA}(r) + H''(r)$$

$$= \mathscr{E}_0^{RPA}(r) + \sum_n \mathscr{E}_n(r)\, B_n^\dagger B_n + H''(r)$$

where

$\mathscr{E}_0^{RPA}(r) (\cong E_{BCS}(r))$	=	RPA – ground state energy
$\mathscr{E}_n(r)$	=	boson energy
$B_n^\dagger$	=	creation operator of a boson
$H''(r)$	=	interaction between bosons

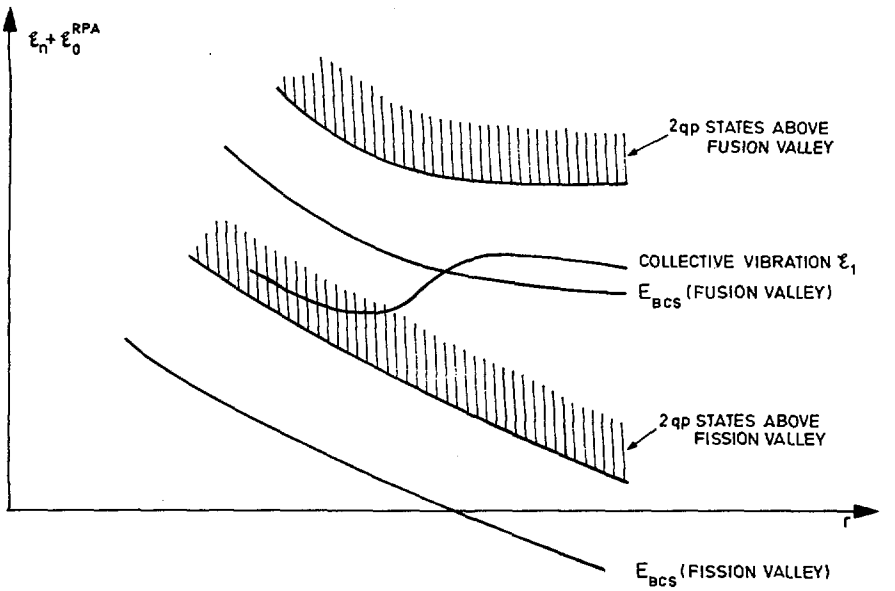

FIG. 2. "Adiabatic states" as a function of r.

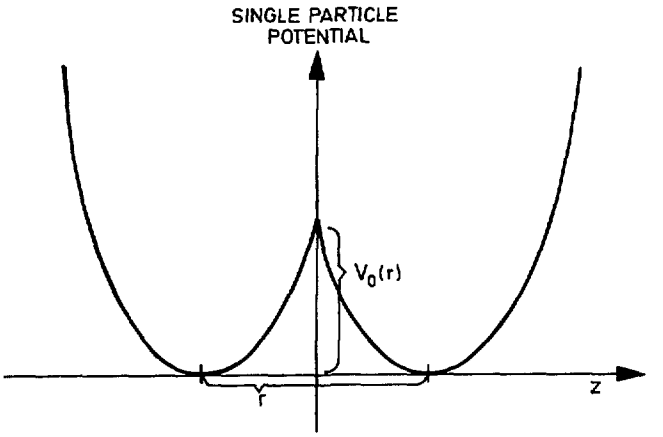

FIG. 3. Two-centre potential.

The RPA ground state energy $\mathcal{E}_0^{RPA}$ is about equal to E_{BCS} and the non-collective phonon energies are about equal to sums of quasiparticle energies. H_{RPA} describes independent phonons and H'' the interaction between them.

It is known that, for critical values of an external parameter such as r(t), the lowest collective RPA vibration may become zero, i.e. unstable. At this point the energy $\mathcal{E}_1$ crosses E_{BCS}(fu-va) and may be transformed into a vibration around the ground state E_{BCS}(fi-va) of a possibly existing

fission valley which lies, for given values of r, at a lower energy [29] (see Fig. 2). The calculation of the occupation probabilities as a function of r(t) will be more complicated as in the Zener problem because there are several collective vibrations and because these states are fed even without the occurrence of crossings. If the downgoing vibrational state ends up being more than 2Δ above the fission valley (see Fig. 2), it will be strongly damped into the multitude of 2qp and higher excitations built on the fission valley. If it ends up below $E_{BCS}(\text{fi-va}) + 2\Delta$, this will be much less so.

Thus one concludes that the degree of viscosity which is encountered on the ascent to the barrier depends on details of the microscopic structure.

The unstable collective modes may thus play an important role in the population of intrinsic excitations. Their role might be comparable to the one of "doorway states".

From Swiatecki [29] we learned that it is a vibration of the neck which is expected to become unstable at certain critical distances.

I think that there is also a microscopic reason for this: consider the case of two nuclei of equal size at a distance r(t). Let us describe the two nuclei by a two-centre potential (Fig. 3).

If the spin-orbit coupling is neglected, one can classify the single particle states into "gerade" and "ungerade" states. As r(t) is decreased, the barrier $V_0(r)$ decreases. As a result, the single particle energies which move most drastically downward are the "gerade" states with a small number of modes in z-direction (z-axis in the direction of $\vec{r}(t)$) because they profit from a lowering of the barrier $V_0(r)$. States of this character, if they are to lie close to the Fermi energy λ, must have a large number of nodes in directions perpendicular to the z-axis. That is, the single particle levels which move most strongly as a function of r describe nucleons which move in orbitals parallel to the (xy)-plane. A coherent linear combination of such states produces vibrations of the neck!

The importance of the reflection symmetry and its breaking for the understanding of the fission process was emphasized in the historical paper by Hill and Wheeler [30].

I am convinced that this symmetry is indeed also the reason why all calculations of fission landscapes beyond the second saddle show valleys which closely follow the neck coordinate. An analysis of these results under this viewpoint would be interesting. The remarks above imply that this symmetry may also have a bearing on the detailed behaviour of the viscosity encountered between saddle and scission.

I want to conclude with my warmest thanks to all my colleagues and friends who have patiently explained their work to me during this Symposium.

REFERENCES

[1] SPECHT, H.J., WEBER, J., KONECNY, E., HEUNEMANN, D., Phys. Lett. 41B (1972) 43.
[2] RUSSO, P.S., PEDERSEN, J., VANDENBOSCH, R., Paper IAEA-SM-174/96, these Proceedings, Vol. 1.
[3] VANDENBOSCH, R., Paper IAEA-SM-174/203, these Proceedings, Vol. 1.
[4] KEYWORTH, G.A., LEMLEY, J.R., OLSON, C.E., SEIBEL, F.T., DABBS, J.W.T., HILL, N.W., Paper IAEA-SM-174/65, these Proceedings, Vol. 1.
[5] BACK, B.B., BRITT, H.C., GARRETT, J.D., HANSEN, O., LEROUX, B., Paper IAEA-SM-174/201, these Proceedings, Vol. 1.

[6] PAULI, H.C., LEDERGERBER, T., Paper IAEA-SM-174/206, these Proceedings, Vol. 1, and reference to earlier work.
[7] BOWMAN, C., discussion remark on Paper IAEA-SM-174/201, these Proceedings, Vol. 1.
[8] KONECNY, E., SPECHT, H.J., WEBER, J., Paper IAEA-SM-174/20, these Proceedings, Vol. 2.
[9] UNIK, J.P., GINDLER, J.E., GLENDENIN, L.E., FLYNN, K.F., GORSKI, A., SJOBLOM, R.K., Paper IAEA-SM-174/209, these Proceedings, Vol. 2;
HOLUBARSCH, W., PFEIFFER, E., GOENNENWEIN, F., Nucl. Phys. A171 (1971) 631;
SPECHT, H.J., FRASER, J.S., MILTON, J.C.D., DAVIES, W.G., in Physics and Chemistry of Fission (Proc. Symp. Vienna, 1969), IAEA, Vienna (1969) 363.
[10] NÖRENBERG, W., in Physics and Chemistry of Fission (Proc. Symp. Vienna, 1969), IAEA, Vienna (1969) 51.
[11] RAGAINI, R.C., HULET, E.K., LOUGHED, R.W., Paper IAEA-SM-174/72, these Proceedings, Vol. 2.
[12] JARED, R.C., NIFENECKER, H., THOMPSON, S.G., Paper IAEA-SM-174/62, these Proceedings, Vol. 2;
PLEASONTON, F., FERGUSON, R.L., SCHMITT, H.W., Phys. Rev. C6 (1972) 1023;
ARMBRUSTER, P., HOSSFELD, F., LABUS, H., REICHELT, K., in Physics and Chemistry of Fission (Proc. Symp. Vienna, 1969), IAEA, Vienna (1969) 545;
BROOKS, J.W., REINES, F., Phys. Rev. C7 (1973) 1579;
WILHELMY, J.B., THOMPSON, S.G., JARED, R.C., CHEIFETZ, E., Phys. Rev. Lett. 25 (1970) 1122.
[13] NIFENECKER, H., SIGNARBIEUX, C., BABINET, R., POITOU, J., Paper IAEA-SM-174/207, these Proceedings, Vol. 2.
[14] AMIEL, S., FELDSTEIN, H., Paper IAEA-SM-174/25, these Proceedings, Vol. 2.
[15] BUNATIAN, G.G., KOLOMIETZ, V.M., STRUTINSKY, V.M., Nucl. Phys. A188 (1972) 225;
BALIAN, R., BLOCH, C., Ann. Phys. (New York) 60 (1970) 401; Ann. Phys. (New York) 63 (1971) 592;
BOHR, A., MOTTELSON, B.R., Nuclear Structure, Vol. II, W.A. Benjamin, New York, to be published (1974);
TYAPIN, A.S., Yad. Fiz. 13 (1971) 32;
BASICHIS, W.H., KERMAN, A.K., TSANG, C.F., TUERPE, D.R., WILETS, L., in Magic without Magic: John Archibald Wheeler, Freeman, San Francisco (1972);
DIETRICH, K., Structure of Nuclei – Lectures of an International Course on Nuclear Theory, Trieste, 1971, IAEA, Vienna (1972) 373.
[16] BRACK, M., QUENTIN, P., Paper IAEA-SM-174/98 these Proceedings, Vol. 1.
[17] NIX, J.R., MÖLLER, P., Paper IAEA-SM-174/202, these Proceedings, Vol. 1, and reference to earlier work;
LARSSON, S.E., LEANDER, G., Paper IAEA-SM-174/06, these Proceedings, Vol. 1, and reference to earlier work of Lund group;
MOSEL, U., Phys. Rev. C6 (1972) 971 and reference to earlier work of H.W. SCHMITT and U. MOSEL.
[18] FLOCARD, H., QUENTIN, P., VAUTHERIN, D., KERMAN, A.K., IAEA-SM-174/38, these Proceedings, Vol. 1.
[19] MORETTO, L.G., Paper IAEA-SM-174/204, these Proceedings, Vol. 1.
[20] BJØRNHOLM, S., BOHR, A., MOTTELSON, B.R., Paper IAEA-SM-174/205, these Proceedings, Vol. 1.
[21] BRACK, M., DAMGAARD, J., PAULI, H.C., JENSEN, A.S., STRUTINSKY, V.M., WONG, C.Y., Rev. Mod. Phys. 44 (1972) 320.
[22] CALDWELL, J.T., DOWDY, E.J., WORTH, G.M., Paper IAEA-SM-174/100, these Proceedings, Vol. 1.
[23] GOZANI, T., Abstract IAEA-SM-174/90, these Proceedings, Vol. 2, and preprint. Intelcom Rad. Tech., P.O.B. 81608, San Diego, Cal.
[24] SCHÜTTE, G., WILETS, L., Paper IAEA-SM-174/210, these Proceedings, Vol. 1.
[25] BONEH, Y., FRAENKEL, Z., PALTIEL, Z., Paper IAEA-SM-174/22, these Proceedings, Vol. 1.
[26] WIECZOREK, R., HASSE, R.W., SÜSSMANN, G., Paper IAEA-SM-174/2, these Proceedings, Vol. 1.
[27] HANAPPE, F., NGÔ, C., PÉTER, J., TAMAIN, B., Paper IAEA-SM-174/42, these Proceedings, Vol. 2.
[28] SIERK, A.J., NIX, J.R., Paper IAEA-SM-174/74, these Proceedings, Vol. 2.
[29] SWIATECKI, W.J., BJØRNHOLM, S., Phys. Lett. 4C (1972) 325.
[30] HILL, D.H., WHEELER, J.A., Phys. Rev. 89 (1953) 1102.

ADDITIONAL ABSTRACTS

The following abstracts, many of them revised since their original submission to the Symposium, are included since, although there was not sufficient time for oral presentation of these papers nor sufficient space for their publication in full, they do provide important supplementary information to the Proceedings.

A TWO-NUCLEUS SINGLE PARTICLE MODEL WITH PAIRING AND ITS APPLICATION TO THE SCISSION REGION (IAEA-SM-174/01).

R. W. Hasse,
Universität München,
Garching, Federal Republic of Germany

The Hamiltonian of a system of two interacting nuclei close to each other is rewritten by using the dual (biorthogonal) basis of single particle states of the non-interacting fragments. Equations similar to the usual BCS and gap equations resulting from a variational principle then provide an alternative to the two-centre shell model in the scission region. As applications, these equations are solved approximately, in order to study the change of the Fermi energies and pairing gaps with the distance between the fragments, and numerically, in order to obtain the interaction potential of the fragments from fission of ^{236}U. As a result, the short-range nuclear interaction energy of the fragments at scission, which can be interpreted as a modified surface energy, amounts to approximately -10 MeV. It lowers the long-range Coulomb interaction energy and gives rise to a very flat total interaction potential which may even exhibit a minimum in the separation degree of freedom. Thus the existence of a scission minimum is supported.

INDEPENDENT YIELDS OF ^{150}Pm IN THE THERMAL NEUTRON FISSION OF ^{233}U, ^{235}U AND ^{239}Pu (IAEA-SM-174/04).

H. Gäggeler, H. R. von Gunten*,
Anorg. chemisches Institut,
Universität Bern, Switzerland

The recent availability of fast separation procedures for rare earth elements makes these elements accessible for determinations of independent fission yields. The rare earth region is of special interest in the investigation of charge distribution because it is complementary to the region of light fragments which are influenced by the 50-neutron shell. Furthermore, the rare earth fission products furnish results for charge distribution in very asymmetric fission.

The shielded nuclide ^{150}Pm is very suitable for such measurements owing to its half-life and well-known gamma-ray spectrum. It has already been determined indirectly in the thermal neutron fission of ^{235}U through a measurement of stable ^{150}Sm (unpublished work done by Chu in 1959) and in the spontaneous fission of ^{252}Cf by radiometric techniques done by von Gunten in 1969. The distribution of charge for ^{233}U and ^{239}Pu is very poorly known in the region of the 50-neutron shell.

Promethium was separated from irradiated targets by a carrier-free ion-exchange procedure followed by two reversed phase chromatographic separations with di-(2-ethylhexyl) orthophosphoric acid (HDEHP) on a diatomaceous silica column. The promethium fraction was counted on a calibrated Ge(Li) gamma spectrometer. Three photopeaks of 1165 keV, 1324 keV and 1736 keV, respectively, were used to compute the absolute activity of the

* and Eidg. Institut für Reaktorforschung, Würenlingen, Switzerland.

^{150}Pm formed. The decay of these photopeaks was followed for radiochemical purity. The activity of the peaks of ^{150}Pm was compared to the activity of the 340-keV photopeak of ^{151}Pm in the same sample.

The independent fission yields for ^{150}Pm in the thermal neutron fission of ^{233}U, ^{235}U and ^{239}Pu were found to be $(6.0 \pm 0.3) \times 10^{-4}$%, $(5.4 \pm 0.3) \times 10^{-4}$%, and $(1.7 \pm 0.08) \times 10^{-3}$%, respectively. The corresponding fractional chain yields lead to empirical Z_p (most probable charge) values of 58.67 ± 0.18, 58.62 ± 0.18 and 58.75 ± 0.17 for ^{233}U, ^{235}U and ^{239}Pu, respectively, if a Gaussian charge dispersion function with a σ of 0.59 ± 0.06 is used. The Z_p value for ^{235}U is in agreement with the Z_p function proposed by Wahl. However, for ^{233}U and ^{239}Pu, the Z_p values calculated for ^{150}Pm, using ν_A values of 1.7 neutrons, deviate significantly from the Z_p function constructed with the light fragments available in this region.

FISSION FRAGMENT GAMMA-RAY ANISOTROPY (IAEA-SM-174/08).

A.T. Kandil, L.S. El-Mekkawi,
Atomic Energy Authority,
Cairo, Arab Republic of Egypt

R. Holub,
Florida State University,
Tallahassee, Florida,
United States of America

The anisotropy of fission fragment gamma rays in the reaction ^{239}Pu (n_{th}, f) and ^{235}U (n_{th}, f) has been measured. In this work, two gamma energy bands were used to confirm the energy independence of the anisotropy. For the gamma energy band 0.83 - 0.92 MeV, the anisotropies were found to be 0.18 ± 0.03, 0.13 ± 0.03 and 0.19 ± 0.03, 0.11 ± 0.03 for the ^{239}Pu and ^{233}U targets respectively. The data have been corrected for the Doppler effect, and the time of flight was large enough to eliminate the counting of neutrons. Comparisons with the Nix, Swiatecki and Strutinsky theories have been made, as well as corrections for the fragment rotation along the fission axis.

TEMPERATURE SMEARING METHOD OF DETERMINING SHELL CORRECTION ENERGIES – EXTENSION TO REALISTIC SINGLE PARTICLE LEVELS AND CALCULATION OF FISSION BARRIERS (IAEA-SM-174/09).

V.S. Ramamurthy, S.S. Kapoor,
Bhabha Atomic Research Centre,
Trombay, Bombay, India

In an earlier work a method was proposed to determine the ground state shell correction energies of nuclei from the high-temperature behaviour of the thermodynamic properties of excited nuclei and the results of these calculations for modified harmonic oscillator level schemes were reported. These calculations have been extended to the single particle level schemes of realistic potentials having a continuum. An outline of this method is as follows: at sufficiently high temperatures, the entropy S and the total energy E of the nucleus become independent of the local fluctuation $\delta g(\epsilon)$ of the single particle

level density $G(\epsilon)$ and depend only on the smoothly varying part $g(\epsilon)$ of $G(\epsilon)$. It can be shown that this asymptotic behaviour of S and E is given by the relations $S = \sum_i a_i T^i$, and $E = \overline{E}_g + \int TdS = \overline{E}_g + \sum_i a_i T^{i+1} i/(i+1)$ where the a_i are related to $g(\epsilon)$, and $\overline{E}_g$ is the ground state energy corresponding to the smoothly varying part $g(\epsilon)$ of the level scheme. Since one also has $E = E_g + E_x$, where E_g is the actual ground state energy, the shell correction energy can be obtained from the relation $E_g - \overline{E}_g = \sum_i i a_i T^{i+1}/(i+1) - E_x$. Therefore from a numerical evaluation of the entropy S and excitation energy E_x as a function of temperature T, the shell correction can be obtained by fitting the asymptotic temperature dependence of the entropy S, thereby obtaining the coefficients a_i. These calculations have been carried out for a variety of nucleon numbers and deformations with the single particle level schemes obtained for the folded Yukawa potential by Nix and co-workers. These results are discussed and compared with the results of the usual Strutinsky smearing procedure. The shell correction energies obtained here have also been used to calculate the fission barriers of a number of heavy nuclei using the Pauli-Ledergerber liquid drop model parameters.

The possibility of extending the present method to systems with only a restricted number of single particle levels around the Fermi level is also being examined to remove any uncertainties associated with the continuum, and the results of these investigations will also be presented.

HIGH-RESOLUTION MEASUREMENTS OF PROMPT GAMMA RAYS IN THE FISSION OF ^{252}Cf ACCOMPANIED BY LIGHT CHARGED PARTICLES (IAEA-SM-174/11).

N. N. Ajitanand, R. K. Choudhury, S. S. Kapoor,
Bhabha Atomic Research Centre,
Trombay, Bombay, India

The present work investigates the mechanism of light charged particle (LCP) emission in fission through a comparative measurement of the yields of specific primary fission products formed in binary fission and in fission accompanied by LCP. Since the assignment of several well-resolved gamma-ray lines to specific primary fission product nuclei is well established for ^{252}Cf fission, in this work high-resolution measurements of the prompt gamma rays emitted from fission fragments accompanied by LCP and those emitted from normal binary fission fragments in ^{252}Cf fission were simultaneously carried out using a 30-cm^3 Ge(Li) detector. A "sandwich" type arrangement in the source-particle detector assembly was used to eliminate Doppler effects on the gamma-ray lines in both the cases. Most of the well-resolved gamma-ray lines were assigned to specific isotopes by comparison with published results for binary fission, and the ratio of the yields of these gamma-ray lines in LCP fission and binary fission were determined. A striking feature noted in results was that some low-energy gamma lines (e. g. corresponding to the isotopes ^{144}Ce, ^{146}Ce, ^{138}Cs, ^{140}Cs, ^{142}Ba and ^{116}Pd) were almost absent in LCP fission, although they appeared intensely in binary fission. Assuming that 2^+ to 0^+ transition intensities of even-even isotopes are a measure of their yields, the yields of several such isotopes in LCP fission relative to binary fission were obtained. A quantitative analysis of these results is being attempted to evaluate the most probable mass and width of the mass distribution for

some specified fission products with constant charge in the case of LCP fission, with a view to examining the different proposed mechanisms of LCP emission in fission.

ELECTRON-INDUCED FISSION OF ^{232}Th (IAEA-SM-174/13).

P. Rasch, G. Fiedler,
II. Physikalisches Institut der Universität Giessen,
E. Konecny,
Physik-Department, Technische Universität München,
Federal Republic of Germany

Excitation functions, fission fragment angular distributions and kinetic energy spectra have been observed for electron-induced fission of ^{232}Th for electron energies $8.7 \leq E_e \leq 63$ MeV. For low energies (although above the fission threshold) the angular distributions have a large (90°/0°)-anisotropy ratio and show a considerable $\sin^2(2\theta)$ component. The anisotropy decreases rapidly for higher electron energies but reveals smaller (90°/0°)-peaks after the onset of second-, third- and fourth-chance fission. Anisotropies have been calculated under the assumption of different K-values combining all possible M and I values with their correct statistical weights. These calculations show that the observed anisotropies peaking at 90° can only be understood if the effective fission barriers for both odd-neutron nuclei ^{231}Th and ^{229}Th are characterized by $K = 1/2$.

The kinetic energy spectra were detected with a resolution almost comparable to that of electronic surface barrier detectors by observation of fission track etch pit areas in glass detectors. The dominant asymmetric character of Th fission is not completely washed out even for electron energies up to 60 MeV.

GAMMA-DECAY PROBABILITY OF FISSIONING ISOMERIC STATES (IAEA-SM-174/17).

E. Takekoshi,
Japan Atomic Energy Research Institute,
Tokai Research Establishment,
Tokai-mura, Ibaraki-ken
T. Takemasa, M. Sano,
Osaka University, Toyonaka,
and
Japan Atomic Energy Research Institute
M. Wakai,
Osaka University,
Toyonaka, Japan

To estimate the magnitude of the gamma transition probability between the fissioning isomeric state and a state in the ground state rotational band,

the B(E2) value in the even-even actinide nuclei was calculated. The wave function with a given spin IMK describing the ground state and isomeric state rotational bands is given as

$$\Psi_{IMK} = a^I \Phi_{IMK}(\delta_1) + b^I \Phi_{IMK}(\delta_2)$$

where the components $\Phi_{IMK}(\delta_1)$ and $\Phi_{IMK}(\delta_2)$ are situated in the regions of the first and second minimums with the deformations δ_1 and δ_2, respectively, and a^I and b^I are the mixing coefficients which could be determined by diagonalizing the Hamiltonian in the oblique coordinate system. The component wave function $\Phi_{IMK}(\delta)$ is obtained by the projecting state of good angular momentum from Nilsson+BCS intrinsic states. The deformation parameters δ_1 and δ_2 are taken from the work of Nilsson and co-workers. The calculated interband B(E2) values in the even-even actinide nuclei are hindered by a factor of 10^{-30} - 10^{-50} relative to the intraband B(E2) values in the ground state rotational band, if it is assumed that these states describing the ground state and isomeric state rotational bands are of pure configurations corresponding to each equilibrium deformation. These calculated intraband B(E2) values may correspond to the values of the lower limit. If the admixture of the component $\Phi(\delta_2)$ contained in the ground state wave function Ψ_{IMK} is 1% of Ψ_{IMK}, the interband B(E2) values increase up to the value of about 10^{-3} relative to the intraband B(E2) values in the ground state rotational band. These results are almost the same for all of the actinide nuclei.

QUADRUPOLE PAIRING EFFECTS AT THE FISSION SADDLE POINT (IAEA-SM-174/18).

M. Sano, T. Takemasa,
Osaka University, Toyonaka,
and
Japan Atomic Energy Research Institute

M. Wakai,
Osaka University, Toyonaka,

E. Takekoshi,
Japan Atomic Energy Research Institute,
Tokai Research Establishment,
Tokai-mura, Ibaraki-ken, Japan

Most experimental data for values of the energy gap $2\Delta_f$ at the fission saddle point show that the Δ_f values are about two times the Δ_0 values at the ground state. No satisfactory explanation has been made for the large pairing effect observed at the saddle point by using the usual monopole pairing force. In the present work, the quadrupole pairing interaction has been introduced, in addition to the monopole pairing interaction. The quadrupole pairing energy increases with increasing nuclear deformation.

In the numerical calculations, the parameters defining the single particle level spectrum employed by Gustafson and co-workers were used and took into account the (Z-40) or (N-70) levels above and below the proton and neutron

Fermi surfaces. The values of G_0 and G_2 for the monopole and quadrupole pairing interactions were taken to be $G_0 = 22.1\ A^{-1}$ MeV for protons, $G_0 = 15.7\ A^{-1}$ MeV for neutrons, and $G_2 = 3.8\ A^{-5/3}$ MeV for both protons and neutrons. With these interaction strengths it is possible to reproduce both the experimental energy gap parameters at the ground state and those at the saddle point.

By introducing the quadrupole pairing interaction, the potential energy surface based on the Strutinsky prescription was calculated and compared with the case when the value of G_0 is proportional to the surface area and the value of G_2 is equal to zero. In conclusion it can be said that the quadrupole pairing interaction makes the energy of the second barrier lower by about 2 MeV than the result for the case when G_0 is proportional to the surface area. For ^{240}Pu, the moment of inertia was calculated using the cranking model formula. The calculated values are $\mathcal{I}_g = 64.6\ \text{MeV}^{-1}$ at the ground state and $\mathcal{I}_f = 134\ \text{MeV}^{-1}$ at the fissioning isomeric state, and are found to be in fairly good agreement with the experimental values of $\mathcal{I}_g = 69.5\ \text{MeV}^{-1}$ and $\mathcal{I}_f = 150.1\ \text{MeV}^{-1}$.

NEW STUDIES ON THE THERMODYNAMIC MOLECULAR MODEL (IAEA-SM-174/23).

W. Nörenberg,
Universität Heidelberg,
Federal Republic of Germany

It has been known since 1963, from the scission point model introduced by Vandenbosch, that several fission phenomena (kinetic energies and excitation energies of the fragments) are determined most likely at the later stages of fission. Considerable efforts are now being made to take friction into account during the descent from the saddle to the scission point. The thermodynamic molecular model (TMM) has been introduced to incorporate into the scission point model this damping from the fission degree into other degrees of freedom. The TMM is obtained by taking into account the large coupling between the collective degrees of freedom and assuming a statistical equilibrium between all collective states at the scission point.

The TMM has been applied to new experimental data on mass distributions: data on the symmetric-to-asymmetric mass yields as a function of the compound excitation energies well above the threshold have been analysed. The relation between the mass distributions for ^{239}Pu (n_{th}, f) and the spontaneous fission of ^{240}Pu and ^{240m}Pu has been established and compared with experimental results. The abrupt increase of symmetric mass yields in ^{257}Fm (n_{th}, f) as compared to the spontaneous fission of ^{257}Fm has been explained by assuming $K \leq 3/2$ for the second saddle point state. Recent experiments on the threshold behaviour for symmetric and asymmetric mass yields in ^{226}Ra (^{3}He, df) and ^{226}Ra (^{3}He, pf) support a two-mode mechanism in the TMM.

Additional studies are concerned with the dependence of kinetic energies on the compound excitation energy, with total spin distribution and with the width of the isobaric charge distribution.

A SEMI-EMPIRICAL APPROACH TO FISSION INERTIAS AND FISSION HALF-LIVES (IAEA-SM-174/29).

J. Randrup,
Lawrence Berkeley Laboratory,
University of California,
Berkeley, Calif.,
United States of America
and
Institute of Physics, University of Aarhus,
Aarhus, Denmark

The problem of determining the inertia associated with the nuclear spontaneous fission process and calculating the corresponding half-lives is approached by a semi-empirical method. For the purpose of determining an effective fission inertia, a test group of (32) known even nuclei, ranging from U to Rf/Ku, is selected. For this group, appropriate fission paths, together with the fission barrier potentials along these paths, are established on the basis of potential energy surfaces which have been obtained by the macroscopic-microscopic method. The macroscopic part of the energy is provided by the liquid drop model of Myers and Swiatecki, modified however to reproduce well the experimentally known second barriers in the actinide region. The microscopic correction-energy contribution to the potential energy surfaces is based on the modified-oscillator single particle model in which allowance has been made for mass-asymmetric (P_3 and P_5) as well as axial-asymmetric (γ) distortions. Indications from existing hydrodynamical and microscopic calculations of the nuclear inertia as well as from the known isomeric half-lives are used to construct a simple one-parameter smooth trial inertia which is then fitted to the half-lives for the test group. The equivalent centre-of-mass separation r (corresponding to ellipsoidal shapes and equal-mass fragments) proves to be a preferable fission-path coordinate. The inertia obtained in this way reproduces those half-lives to within a factor of 25 on the average. Furthermore, the general trend of the calculated half-lives supports the extrapolation of the established inertial function to so far unobserved nuclei. A part of the deviations from the experimental results can be understood in terms of certain deficiencies in the underlying potential energy surfaces, and refinements of the approach (such as taking into consideration the multi-dimensionality of the fission path, or allowing for more freedom in the trial inertia) give no significant improvement of the fit. Application has been made to several problems of current interest, as, for example, the predictions of fission half-lives for isotopes of the element 106 (and heavier elements), the calculation of the hindrance factors associated with fission of odd isotopes, and the possibility of a neutron-capture path to the superheavy region.

AN ANALYTICAL EXPRESSION FOR THE DECAY CURVES OF PHOTONS COMING OUT OF THE ^{235}U FISSION PRODUCTS (IAEA-SM-174/30).

T. Yarman,
Massachusetts Institute of Technology,
Cambridge, Mass.,
United States of America

A correlation between the data relevant to the delayed photons from ^{235}U fission products and the data relevant to the delayed photoneutrons generated by those photons in D_2O has been sought. To this end the fission of one atom of ^{235}U in an infinite medium of D_2O was considered. An attempt was then made to calculate the number N of delayed photoneutrons generated by the delayed photons from ^{235}U fission products through the data relevant to the generation of delayed photons from ^{235}U fission products and the attenuation and photoneutron reaction cross-sections of photons in D_2O. This number is composed of an infinity of terms, namely the number of photoneutrons generated by the uncollided photons, the number of photoneutrons generated by those photons having had one and only one collision on their way to the photoneutron reaction, etc. The study of the first and second terms (of the expansion of N) and the comparison of the number N (composed of its first and second terms only) with the data relevant to the delayed photoneutrons from ^{235}U fission-product gamma rays on D_2O have shown that the higher order terms (in the expansion of N) can be fairly neglected. Thus the data relevant to the generation of delayed photons from ^{235}U fission products are found to be consistent with the attenuation and photoneutron reaction cross-sections of photons in D_2O and the correlation that was sought has been established. Next, an empirical (time-independent) energy dependence of the ^{235}U fission-product gamma rays was found. This, together with the correlation in question, led to an analytical representation of the decay curves of the ^{235}U fission-product gamma rays with an energy – greater than 2.23 MeV – sufficient to cause photoneutron reactions in D_2O, in terms of the nine exponentials relevant to the decay data of the nine (time-wise) groups of delayed photoneutrons from ^{235}U fission-product gamma rays on D_2O. (In a further study this analytical representation has been found very useful in computing the number of photoneutrons generated in the D_2O reflector of a light-water-cooled research reactor – MITR II – in the course of the transient analysis of this reactor.)

MEASUREMENT OF GAMMA-RAY SPECTRA FROM THE SPONTANEOUSLY FISSIONING ISOMER OF ^{236}U (IAEA-SM-174/31).

A. Lajtai, L. Jéki, Gy. Kluge, I. Vinnay, F. Engard,
Central Research Institute for Physics,
Budapest, Hungary

Yu. P. Gangrsky, B.N. Markov,
Joint Institute for Nuclear Research,
Dubna, USSR

The direct confirmation of Strutinsky's model of a double-humped potential in fission isomerism, i.e. the observation of gamma transitions preceding the spontaneous fission of isomeric states, was found to be inconclusive in the case of the 70-130 nsec ^{236m}U state. Browne and Bowman, who bombarded a ^{235}U target with neutrons, could estimate from the time distribution of gamma rays with energies above 0.5 MeV only an upper limit of $\leq 6 \times 10^{-5}$ for the ratio of delayed fission events, subsequent to the emission of gamma rays, to prompt fission events. A similar result was obtained by Konecny and coworkers for conversion electrons preceding the isomeric fission of ^{236m}U.

The aim of the reported experiments is the observation of single lines corresponding to pre-fission gamma decay in the energy spectrum from 150 keV to 1.5 MeV of the gamma rays from the ^{235}U(n_{th}, γf) reactions. Using a fast-slow coincidence setup, the gamma rays are detected with a 10-cm^3 Ge(Li) detector, and the fission fragments are counted with a gas scintillation counter. The energy distribution of the pre-fission gamma rays is evaluated from counts taken simultaneously in four 100-nsec-wide intervals before the fission event.

In this way both the cross-section for isomeric fission and the lifetime of the fissioning isomeric state can be evaluated.

It seems from the analysis of the measured gamma spectra that five peaks can be attributed to pre-fission gamma transitions. They appear at 450, 475, 687, 808 and 882 keV. The ratio of the rate of isomeric fission events with pre-fission gamma rays to the rate for prompt fission events, σ_i/σ_f, is lower than 10^{-5} for each of these lines. The time behaviour of the gamma peak intensities was found to be consistent with a ^{236m}U lifetime of about 100 nsec. It can be assumed that these peaks correspond to radiation transitions in the second potential well.

KINETIC ENERGY AND NEUTRON EMISSION OF FISSION FRAGMENTS FROM ^{252}Cf SPONTANEOUS FISSION (IAEA-SM-174/33).

H. Hipp, H. Henschel, F. Gönnenwein,
Universität Tübingen,
Federal Republic of Germany

In a three-parameter experiment the kinetic energies of both and the velocity of one of the correlated fragments in ^{252}Cf spontaneous fission have been measured with two surface barrier detectors facing each other. For the time calibration of the system, delay cables were inserted in the fast-timing signal path and calibrated under the conditions of the experiment.

With detectors of 4.5-cm^2 area, the time resolution achieved was 300 psec (FWHM). The flight path was 60 cm. From the raw data, the fragment mass A_f (both before and after prompt neutron emission), the total fragment kinetic energy $E_K(A_f)$, the number of neutrons emitted $\nu(A_f)$ and correlations between the above quantities were calculated. The result obtained for the mean primary fragment energy is $\langle E_K \rangle = 181.2 \pm 1.2$ MeV. This value is significantly lower than some values given in the literature. When the detector calibration constants are arranged to yield the mean kinetic energy given above (essentially by subtracting a constant amount of energy for each fragment as compared with existing detector calibration constants) the resulting dependence of prompt neutron number on mass number $\nu(A_f)$ is in excellent agreement with direct measurements of this quantity. A ratio of the mean neutron number from the light and heavy fragments, $\nu_L / \nu_H = 1.08 \pm 0.03$, was found. The variation of ν with the kinetic energy E_K is characterized by a mean slope $dE_K/d\nu = 7.4$ MeV.

ELECTROFISSION OF ^{238}U FOR ELECTRON ENERGIES BETWEEN 20 AND 80 MeV (IAEA-SM-174/37).

A.C. Shotter, M.F. McCann,
Department of Natural Philosophy,
University of Edinburgh,

J.M. Reid, J.M. Hendry,
Department of Natural Philosophy,
University of Glasgow,
United Kingdom

Electrofission of ^{238}U has been studied for electron bombarding energies between 20 and 80 MeV. This work was done using the electron linear accelerator of the University of Glasgow. For each electron energy within the above range, the mass and energy distributions for the emitted fission fragments were determined. Surface barrier silicon detectors, calibrated with ^{252}Cf, were used to measure the kinetic energy of coincident fission fragments, from which the distributions were determined.

The ratio of the peak mass of the light fragment to the peak mass of the heavy fragment is 0.74 ± 0.1. This ratio remains constant over the entire electron energy range, and is to be compared with the ratio 0.70 for fission induced by bremsstrahlung at 48 and 100 MeV maximum gamma-ray energy. The average kinetic energy released from the electrofission of ^{238}U increases from 167.5 MeV at 20 MeV incident electron energy, to 172 MeV at 80 MeV electron energy. At each electron energy a study has been made of the variation of kinetic energy released with fragment mass ratio. It has been found that the energy is a maximum at a mass ratio of 0.82. The difference between this maximum energy and the energy corresponding to symmetric mass division varies from 7 MeV to 12 MeV over the electron energy range.

The ratio of the yield for asymmetric to symmetric fission also varies with electron energy. This ratio for an electron energy of 20 MeV is 10.5 and

falls to 7.0 for an electron energy of 80 MeV. The trend over the higher electron energy is similar to photofission experiments on ^{238}U, but there seems to be a deviation from the photofission experiments for lower electron bombarding energies.

Work is now proceeding on the interpretation of these results in the framework of inelastic electron scattering and current fission theories.

THE (n,γf) REACTION IN THE RESONANCE NEUTRON INDUCED FISSION (IAEA-SM-174/39).

D. Shackleton, J. Trochon,
CEA, Centre d'études nucléaires de Saclay,
Gif-sur-Yvette, France

To look for the (n,γf) reaction in the neutron resonances of ^{239}Pu, a fission gamma-ray multiplicity experiment has been carried out at Saclay [1]. Up to (14 ± 3)% variations have been observed, strongly correlated with the fission widths Γ_f of the resonances. These results are typical of a competition between the (n,f) process and the (n,γf) process in which a gamma ray is emitted before fission. Such a process also permits the understanding of the variations observed in the total energy $\overline{E}_\gamma$ of gamma rays and in the average number $\overline{\nu}$ of prompt neutrons emitted per fission [2, 3]. The width $\Gamma_{\gamma f}$ and the average pre-fission gamma-ray energy $\langle E_\gamma \rangle$ are expected to be constant from resonance to resonance because the (n,γf) reaction has a great number of exit channels. Therefore its contribution is relatively large in the resonances with small fission widths. For these resonances, the gamma-ray multiplicity and $\overline{E}_\gamma$ are large and $\overline{\nu}$ is small. Defining ΔE as the energy represented by the variation of $\overline{E}_\gamma$ and $\overline{\nu}$, with respect to the extrapolated value for infinite fission width, one may write $\Delta E = (\Gamma_{\gamma f}/\Gamma_f)\langle E_\gamma \rangle$. Hence, the product $\Delta E \cdot \Gamma_f$ must be constant from one resonance to another. This is experimentally verified. From the experimental value [3] the width $\Gamma_{\gamma f}$ and the 1^- fission barrier height are obtained in the framework of Bohr's theory with a single-humped barrier ($\hbar\omega$ = 500 keV) and assuming that a single gamma ray of E1 character is emitted before the compound nucleus undergoes fission. The $\Gamma_{\gamma f}$ value obtained (5.4 ± 1.2 meV) is in good agreement with Lynn's calculations [4], but the 1^- fission barrier is located 1.2 MeV below the neutron binding energy. This low barrier results from the too approximate assumption of the single-humped barrier. A more complete calculation with a double-humped fission barrier is in progress.

REFERENCES

[1] RYABOV, Y., TROCHON, J., et al., submitted to Nucl. Phys.
[2] SHACKLETON, D., TROCHON, J., FREHAUT, J., Phys. Lett. 42B 3 (1972) 344.
[3] FREHAUT, J., SHACKLETON, D., Paper IAEA-SM-174/47, these Proceedings, Vol. 2.
[4] LYNN, J.E., Phys. Lett. 18 (1965) 31.

ETUDE DETAILLEE DE LA STRUCTURE INTERMEDIAIRE DANS LA SECTION EFFICACE DE FISSION DE ^{237}Np (IAEA-SM-174/43).

S. Plattard*, D. Paya,
CEA, Centre d'études nucléaires de Saclay,
Gif-sur-Yvette, France

Une nouvelle mesure à haute résolution de la section efficace de fission de ^{237}Np, pour des neutrons d'énergie comprise entre 3 eV et 35 keV, a permi une étude détaillée des états situés dans le deuxième puits de la barrière de fission.

L'existence de deux familles d'états apparaissant avec des amplitudes très différentes est confirmée; il est suggéré que ces familles sont caractérisées par des valeurs différentes du spin. Plus de cent niveaux appartenant à une même famille sont observés en dessous de 6 keV, il est donc possible d'en faire une étude statistique et de déterminer, avec l'aide des paramètres tirés de l'analyse des résonances individuelles, les principaux paramètres de la barrière de fission.

L'étude détaillée du comportement des résonances autour d'un état intermédiaire est faite au voisinage de 40 eV où on bénéficie d'une excellente résolution (échantillon refroidi à 77°K) et d'une absence quasi totale de bruit de fond. Autour de l'énergie de l'état intermédiaire, la largeur moyenne de fission des grandes résonances, supposées de même spin, varie suivant une fonction de Lorentz, l'écart par rapport à la moyenne étant bien représenté par une loi de Porter et Thomas. Dans l'hypothèse d'un couplage faible entre les états des deux puits, l'état intermédiaire doit apparaître sous la forme d'une résonance large servant de piédestal aux résonances étroites observées habituellement : une telle résonance n'est pas observée; si elle existe, sa largeur neutronique est inférieure à 56 μeV.

Les paramètres obtenus pour la barrière de fission de ^{238}Np sont les suivants : $E_A \simeq 6,08$ MeV; $E_B \simeq 5,45$ MeV; $\hbar\omega_A \simeq 0,77$ MeV; $\hbar\omega_B \simeq 0,45$ MeV; $E_{II} \simeq 1,84 \pm 0,20$ MeV.

English translation of the preceding Abstract (IAEA-SM-174/43)

A DETAILED STUDY OF INTERMEDIATE STRUCTURE IN THE ^{237}Np FISSION CROSS-SECTION.

On the basis of a new high-resolution measurement of the ^{237}Np fission cross-section for neutrons with energies between 3 eV and 35 keV, it has been possible to carry out a detailed study of states in the second well of the fission barrier.

The existence of two families of states with widely differing amplitudes is confirmed and it is suggested that these families have different spin values. More than a hundred levels belonging to the same family are observed below 6 keV; it is therefore possible to study them statistically and to determine the main parameters of the fission barrier with the help of parameters obtained by analysing individual resonances.

---

* Adresse actuelle : Centre d'études de Bruyères-le-Châtel, Montrouge, France.

The behaviour of the resonances around an intermediate state is examined in detail in the neighbourhood of 40 eV, where the resolution is very good (sample cooled to 77°K) and where there is practically no background. Around the energy of the intermediate state the mean fission width of broad resonances, which are assumed to have the same spin, varies as a Lorentz function, the spread from the mean being well-described by a Porter-Thomas law. On the assumption that there is weak coupling between the states of the two wells, the intermediate state should have the form of a broad resonance serving as a pedestal for the narrow resonances normally observed. No such resonance is observed; if one exists, its neutron width is less than 56 μeV.

The parameters found for the fission barrier of ^{238}Np are: $E_A \cong 6.08$ MeV; $E_B \cong 5.45$ MeV; $\hbar\omega_A \cong 0.77$ MeV; $\hbar\omega_B \cong 0.45$ MeV; $E_{II} \cong 1.84 \pm 0.20$ MeV.

FISSION DES ELEMENTS DE MASSE MOYENNE INDUITE PAR DES IONS ^{14}N DE 126 MeV (IAEA-SM-174/44).

C. Cabot, C. Ngô, J. Péter, B. Tamain*,
Institut de physique nucléaire,
Orsay, France

Les auteurs ont mesuré les sections efficaces de fission induite sur des cibles de Ni, Se, Mo, Ag, Ho et Au par des ions ^{14}N de 126 MeV. Le moment angulaire important apporté par le projectile entraîne des probabilités de fission très supérieures à celles obtenues par les mêmes noyaux fissionnants formés par bombardement avec des particules alpha de 167 MeV, comme l'ont fait Lecerf, Pate et Péter qui utilisaient des détecteurs de traces étalonnés.

Les auteurs du mémoire ont utilisé des détecteurs à barrière de surface; la mesure des énergies des deux fragments et de la différence de temps de vol a permis de sélectionner aisément les événements de fission.

Comme dans le cas de la fission induite par particules alpha de 167 MeV, la fissilité décroît exponentiellement avec le rapport Z^2/A du noyau fissionnant jusqu' à une valeur de Z^2/A voisine de 19 (molybdène), et augmente ensuite à nouveau. Les auteurs ont calculé l'évolution de la fissilité en tenant compte de la compétition évaporation-fission de long des chaînes de désexcitation. Ils ont inclus l'effet du moment angulaire et pris les valeurs des barrières de fission calculées par Myers et Swiatecki à partir du modèle de la goutte liquide. Ce calcul donne bien la position observée pour le minimum de fissilité; le maximum de la barrière semble donc bien au voisinage du molybdène, mais la valeur absolue expérimentale est beaucoup plus grande, aussi les barrières peuvent-elles être moins élevées que prévu. Les énergies cinétiques totales mesurées sont un peu supérieures aux prévisions de Nix utilisant le modèle de la goutte liquide. La forme des distributions de masse indique que la valeur de x_{BG} (point de Businaro-Gallone) est très inférieure à 0,4.

---

* Détaché du Laboratoire de physique corpusculaire de Clermont, France.

English translation of the preceding Abstract (IAEA-SM-174/44)

FISSION INDUCED BY 126-MeV IONS OF ^{14}N IN ELEMENTS OF MEDIUM MASS.

Fission cross-sections were measured in targets of Ni, Se, Mo, Ag, Ho and Au bombarded by 126-MeV ions of ^{14}N. The strong angular momentum supplied by the projectile implies much greater fission probabilities than are obtainable when the same nuclei are bombarded with 167-MeV α-particles — as was done by Lecerf, Pate and Péter, using calibrated trace-detectors.

Surface barrier detectors were used; measuring the energies of the two fragments and the difference in time-of-flight made it possible to select the fission events without difficulty.

As in the case of fission induced by 167-MeV α-particles, fissility decreases exponentially with the ratio Z^2/A of the fissioning nucleus until $Z^2/A \approx 19$ (molybdenum), and then increases again. The variation in fissility was determined, taking into account evaporation-fission competition along the deexcitation chains. The effect of angular momentum was included and the fission barrier values calculated by Myers and Swiatecki from the liquid drop model were used. This calculation gives the position observed for minimum fissility and the barrier maximum therefore does appear to be in the neighbourhood of molybdenum, but the experimental absolute value is much greater. The barriers may thus be lower than has been imagined. The total kinetic energies measured are somewhat higher than the predictions of Nix based on the liquid drop model. The shape of the mass distributions indicates that the value of x_{BG} (Businaro-Gallone point) is much lower than 0.4.

ETUDE DES RESONANCES DE FISSION SOUS LE SEUIL DE LA REACTION ^{239}Pu (d, pf): VARIATION DE LA PROBABILITE DE FISSION AVEC LE RAPPORT DES MASSES (IAEA-SM-174/45).

J. Lachkar, Y. Patin, J. Sigaud,
CEA, Centre d'études de Bruyères-le-Châtel,
Montrouge, France

La réaction ^{239}Pu (d, pf) a été étudiée à l'énergie de deutérons de 12,5 MeV Ceux-ci sont accélérés par le Van de Graaff Tandem du Centre d'études de Bruyères-le-Châtel. Les protons de la réaction sont détectés à 90° par rapport au faisceau incident et les fragments de fission par deux paires de diodes à barrière de surface disposées respectivement dans la direction de recul du noyau et dans la direction perpendiculaire. Les informations délivrées par ces détecteurs permettent de déterminer les masses des fragments de fission et leurs énergies cinétiques. Un total de 325 000 événements de fission en coïncidence avec les protons a été enregistré.

Les auteurs ont analysé, pour différents groupes de masses des fragments et pour chaque paire de détecteurs, les spectres d'amplitude des signaux protons et fission en coïncidence; ils en ont déduit, pour une énergie d'excitation donnée, la distribution en masse des fragments et le rapport de leur probabilité d'émission à 0° et 90°.

Il apparaît que les structures résonnantes sous le seuil de fission présentent des variations significatives de leurs intensités relatives et de leurs anisotropies avec le rapport des masses des fragments. Ces variations

portent sur la valeur du rapport pic-vallée dans la distribution des masses des fragments, les valeurs moyennes des masses légères et lourdes restant par ailleurs constantes.

Ces résultats peuvent être interprétés en admettant que l'énergie potentielle du noyau fissionnant en fonction de la déformation dépend de l'état du noyau et de la voie de sortie considérée.

English translation of the preceding Abstract (IAEA-SM-174/45)

A STUDY OF FISSION RESONANCES BELOW THE THRESHOLD OF THE ^{239}Pu (d, pf) REACTION: VARIATION OF FISSION PROBABILITY WITH MASS RATIO.

The ^{239}Pu (d, pf) reaction was studied at a deuteron energy of 12.5 MeV. The deuterons were accelerated by the Van de Graaff Tandem at the Centre d'études de Bruyères-le-Châtel. The protons from the reaction were detected at 90° to the incident beam and the fission fragments by two pairs of surface barrier diodes arranged, respectively, in the direction of recoil of the nucleus and in the perpendicular direction. The information provided by these detectors makes it possible to determine the masses and kinetic energies of the fission fragments. A total of 325 000 fission events was recorded in coincidence with protons.

For different fragments mass groups and for each pair of detectors the amplitude spectra of the proton and fission coincidence signals were analysed; from this analysis the mass distribution of the fragments and the ratio of their emission probabilities at 0° and 90° for a given excitation energy were derived.

The resonant structures below the fission threshold were found to vary considerably in intensity and anisotropy depending on the mass of the fragments. These variations were observed in the peak-to-valley ratio in the fragment mass distribution; the mean values of the light and heavy masses remained constant.

These results can be interpreted by the assumption that the potential energy of the fissioning nucleus, as a function of the deformation, depends on the state of the nucleus and on the exit channel.

FISSION BARRIERS FOR Pa AND Np ISOTOPES (IAEA-SM-174/46).

B. B. Back, Ole Hansen,
Los Alamos Scientific Laboratory,
Los Alamos, N. Mex., USA

H. C. Britt,
Los Alamos Scientific Laboratory, and
Nuclear Structure Research Laboratory,
University of Rochester, USA

J. D. Garrett,
Los Alamos Scientific Laboratory, and
Brookhaven National Laboratory,
Upton, N. Y., USA

B. Leroux,
Los Alamos Scientific Laboratory, USA, and
Centre d'études nucléaires de Bordeaux-Gradignan,
Université de Bordeaux, France

The variation of the fission probability with the excitation energy has been measured for the isotopes $^{231, 232, 233}$Pa and $^{234, 235, 236, 237, 238, 239}$Np, using (d, p), (t, p) and (^{3}He, d) reactions on the available Th, U and Np targets. No resonance structure has been observed in these fission probabilities, except in the case of ^{232}Pa. The fission probabilities are analysed with a statistical model which assumes complete damping of the resonance structure in the second well, and takes into account the competition between the different exit channels. The fission, neutron and gamma decay widths are calculated using continuous level densities obtained from single particle spectra calculated at the first minimum and two maxima of the fission barrier (rotational bands built on single particle discrete levels are added at low energy when odd-A nuclei are concerned, to get a more realistic level density). This analysis provides estimates of the height and curvature of the two barriers; the different sets of parameters which are able to fit the experimental data are discussed and compared with the theoretical predictions.

MISE EN EVIDENCE DE LA CORRELATION ENTRE L'EMISSION D'UNE PARTICULE LEGERE ET DE DEUX FRAGMENTS LOURDS DANS LES INTERACTIONS DE PROTONS D'ENERGIE SUPERIEURE A 0,6 GeV ET DES NOYAUX U ET Pb (IAEA-SM-174/48).

G. Rémy, M. Debeauvais,
CNRS, Centre de recherches nucléaires de Strasbourg-Cronenbourg, France

La fission des noyaux U et Pb induite par des protons de haute énergie est étudiée à l'aide d'un détecteur visuel à seuil qui permet d'observer les trajectoires des fragments de masse supérieure à environ 25 uma.

L'analyse porte sur trois types d'événements: a) événements binaires sans moment transverse, b) événements binaires avec moment transverse, c) événements ternaires.

Les désintégrations ternaires mettent en jeu préférentiellement deux fragments lourds et un fragment léger. L'analyse des événements du type b) montre que le moment transverse mis en évidence ne résulte ni d'un transfert par interaction directe, ni d'un processus d'évaporation, mais de l'émission d'une troisième particule, légère, non enregistrable dans le détecteur, corrélée directionnellement avec les trajectoires des deux fragments les plus lourds.

Les sections efficaces du type a) décroissent à partir de 0,6 GeV de manière analogue aux fonctions d'excitation des fragments excédentaires en neutrons déterminées en radiochimie.

Par contre, les sections efficaces des événements des types b) et c), caractérisées par un seuil près de 0,6 GeV, croissent fortement jusqu' à une énergie comprise entre 3 et 11 GeV, comme les rendements en fragments légers, d'une part, et lourds déficients, d'autre part.

Ces résultats montrent la coexistence de deux classes de réactions à haute énergie parmi les désintégrations des noyaux fissiles en plusieurs fragments: 1° la rupture en deux fragments, analogue à la fission induite aux énergies basses et intermédiaires, dont la probabilité décroît à partir de quelques centaines de MeV; 2° la rupture en 3 (ou plus de 3 fragments éventuellement) dont la fréquence croît à partir de 0,6 GeV et qui, contrairement au cas 1°, est favorisée par les dépôts élevés d'énergie d'excitation.

English translation of the preceding Abstract (IAEA-SM-174/48)

CORRELATION BETWEEN THE EMISSION OF A LIGHT PARTICLE AND TWO HEAVY FRAGMENTS IN INTERACTIONS BETWEEN PROTONS WITH ENERGIES ABOVE 0.6 GeV AND U AND Pb NUCLEI.

Fission of U and Pb nuclei induced by high-energy protons is studied by means of a visual threshold detector with which it is possible to observe the trajectories of fragments of mass greater than 25 amu.

Three types of event are analysed: (a) binary events without transverse momentum; (b) binary events with transverse momentum; (c) ternary events.

Ternary disintegrations usually involve two heavy fragments and one light fragment. An examination of type (b) shows that the transverse momentum observed results neither from transfer by direct interaction nor from an evaporation process but from the emission of a third (light) particle which is not recorded by the detector and which is correlated directionally with the trajectories of the two heavier fragments.

The cross-sections for type (a) events decrease above 0.6 GeV in a manner similar to the excitation functions for fragments with excess neutrons as determined in radiochemistry.

The cross-sections for types (b) and (c) on the other hand — with a threshold near 0.6 GeV — increase steeply up to an energy between 3 and 11 GeV, as yields of light fragments and of heavy neutron-deficient fragments.

The results indicate the co-existence of two classes of high-energy reactions among the disintegrations of nuclei which fission into several fragments: (1) Breaking into two fragments, similar to the case of fission induced at low and intermediate energies, the probability of which decreases above a few hundred MeV; (2) Breaking into three (or more) fragments, which occurs with increasing frequency above 0.6 GeV and (unlike case (1) above) is favoured by high excitation-energy deposits.

ISOMER RATIOS IN ANTIMONY NUCLEI FORMED BY THE REACTIONS Bi(C, f), Au(Ne, f) AND Sn(α, pn) (IAEA-SM-174/49).

A. K. A. R. Ahmed, J. E. Freeman, G. W. A. Newton,
V. J. Robinson, I. S. Grant, M. Rathle,
University of Manchester,
United Kingdom

Isomer ratios of Sb isotopes have been studied to obtain information about the angular momentum distributions of fission fragments produced in heavy-ion reactions. The average angular momentum of the fragments cannot be derived directly from their isomer ratios because the later stages of the decay are dominated by specific properties of the low-lying states. To overcome this difficulty the same Sb nuclei were made by (α, pn) reactions, where the angular momentum distribution before gamma emission can be derived from statistical calculations.

In the case of ^{126}Sb the 0.667-MeV gamma in the daughter nucleus ^{126}Te is fed by β-decay from both the ground state and the isomer. One can make a direct comparison of the relative yields of this gamma ray from (α, pn) and fission reactions, and there is no need for a detailed knowledge of decay schemes and counter efficiencies.

The average angular momentum of Sb nuclei, produced by (α, pn) reactions, varies from 8 $\hbar$ to 15 $\hbar$ and the isomer ratios cover the range observed in proton induced fission. However, for heavy-ion reactions, the high-spin to low-spin isomer ratios are much larger, with neon giving higher values than carbon. This shows a clear relation between the fragment spin and the total angular momentum of the compound nucleus. The results are discussed in terms of the saddle point configuration as calculated by Nix.

MASS DISTRIBUTION OF NEUTRON INDUCED FISSION FOR ^{239}Pu AT THE 0.297-eV RESONANCE (IAEA-SM-174/51).

P. H. M. van Assche,
SCK/CEN, Mol

G. Vandenput, L. Jacobs, J. M. van den Cruyce, R. Silverans,
University of Louvain, Belgium

The mass distribution of fission products for neutron induced fission of ^{239}Pu has been studied in an epi-Sm spectrum, with more than 90% of the fissions being due to the 0.297-eV resonance. The experimental method consists of a detailed comparison of gamma spectra from ^{239}Pu targets, irradiated in thermal and in epi-Sm spectra. Fission product identification is made without chemical separation; only gamma energies and lifetimes are used for this purpose.

Significant variations of the mass distribution for epi-Sm induced fission are observed in the mass regions $A < 89$ and $105 < A < 129$ for more than seven mass numbers. The decrease in symmetric fission, as observed previously,

is confirmed, e.g. a decrease of (35 ± 4)% for the A = 115 fission yield. In addition to this, evidence for a narrowing of the mass distribution is also found. This could be related to the increase of (0.73 ± 0.04) MeV in the total kinetic energy of the fission products of the epi-Sm fission of ^{239}Pu, as compared to thermal neutron fission, observed by J. Toraskan and E. Melkonian (Phys. Rev. C4 (1971) 267).

ON THE POSSIBILITY OF INCREASING NUCLEAR REACTION RATES (IAEA-SM-174/52).

A. Kallio, M. Karras, K.E. Lassila,
Oulun Yliopisto,
Oulu, Finland

Several energy-producing reactions having positive Q values are considered which are initiated by ^{3}He (and ^{3}H) projectiles incident on various targets to produce one to three alpha particles in the final state. The three-alpha states typically proceed through a ^{8}Be + α intermediate state from which ^{8}Be fissions into two alphas, e.g.

$$^{3}\mathrm{He} + {}^{10}\mathrm{B} \rightarrow \mathrm{p} + 3\alpha \quad \text{or} \quad {}^{3}\mathrm{He} + {}^{9}\mathrm{Be} \rightarrow \alpha$$

In view of this, a procedure is suggested and detailed investigations made which lead to the prediction that considerable enhancement of the nuclear matrix element due to the Bose nature of ^{4}He particles will result. The relation of this increased reaction rate to possible energy production is discussed.

INVESTIGATION OF THE γ-DECAY OF SUBTHRESHOLD FISSION RESONANCES OF ^{242}Pu TO A FISSION ISOMERIC STATE (IAEA-SM-174/54).

J.C. Browne,
Lawrence Livermore Laboratory,
University of California,
Livermore, Calif.

C.D. Bowman,
National Bureau of Standards,
Washington, D.C.,
United States of America

A pure class-II state can be defined in terms of a double-humped fission barrier as a state in the second well which has two modes of decay: fission through the outer barrier (Γ_{fII}) and γ-decay ($\Gamma_{\gamma II}$) to the ground state in the second well (fission isomer). The purpose of this experiment was to measure the branching ratio ($\Gamma_{\gamma II}/\Gamma_{fII}$) for an almost-pure class-II state in the ^{242}Pu + n system, thereby establishing for the first time a direct connection between fission intermediate structure and shape isomerism. Analysis of the available data on ^{243}Pu has shown that the coupling between levels in the two wells is very weak. One resonance in each subthreshold fission group has the characteristics of a nearly pure class-II state. For the measurement, a 10-g sample

of ^{242}Pu was bombarded by neutrons from the Livermore 100-MeV LINAC. Both the energy of a neutron inducing an event and the time relationship between gamma rays detected in a pair of C_6D_6 scintillators were stored in a two-dimensional matrix consisting of 7.7×10^5 channels. If a resonance in the ^{242}Pu + n system has a gamma-decay branch to the fission isomer, the time relationship between gamma rays detected in the two scintillators will exhibit the 33-ns half-life of the ^{243}Pu isomer. Analysis of subthreshold fission groups at neutron energies of 763 eV and 1839 eV showed no evidence of a gamma-decay branch to the 33-ns fission isomer. From the limit on the branching ratio ($\Gamma_{\gamma II}/\Gamma_{fII}$) obtained from these data, an upper limit of $\Gamma_{\gamma II} < 1$ meV was derived. Since theoretical calculations predict $\Gamma_{\gamma II} \cong 8$-10 MeV for ^{243}Pu, it can be seen that this experiment had a sensitivity which is a factor of ten lower than should have been necessary to observe the gamma decay to the fission isomer. From the present results and from previous measurements on ^{243}Pu, it was concluded that there may exist an additional longer-lived isomer in ^{243}Pu ($\sim 160\,\mu$s) similar to the other odd-Pu isotopes. In this case the 33-ns isomer may be a two-quasiparticle state or may be associated with a different deformation shape which cannot be reached with low-energy neutrons.

PROMPT GAMMA RAYS EMITTED IN THE THERMAL-NEUTRON-INDUCED FISSION OF ^{233}U, ^{235}U, AND ^{239}Pu AND THE SPONTANEOUS FISSION OF ^{252}Cf (IAEA-SM-174/55).

Frances Pleasonton, Robert L. Ferguson, H.W. Schmitt,
Oak Ridge National Laboratory,
Oak Ridge, Tenn.,
United States of America

A series of four experiments, corresponding to four different fission reactions, were performed to determine the average energy $\bar{E}_\gamma$ and average number $\bar{N}_\gamma$ of gamma rays emitted within ~ 5 nsec after fission as functions of two variables, fragment mass m and fragment total kinetic anergy E_K. The experimental apparatus and instrumentation were identical for all four experiments, and conditions were maintained to be as nearly identical as possible. Energies of coincident fragment pairs were measured with heavy-ion surface barrier detectors (ORTEC), and gamma-ray energies were measured with a large NaI(Tl) detector which was located 89 cm from the target and positioned coaxially with the fragment detectors. The time difference between a fission-fragment and a gamma-ray pulse was also measured, to allow time-of-flight discrimination against fission neutrons. The correlated 4-parameter data were recorded and analysed event-by-event.

The gamma-ray data were analysed with a "weighting method" proposed by Maier-Leibnitz to deduce average numbers and energies of gamma rays from measured pulse heights. The Doppler shift in the laboratory angular distribution of gamma emission was utilized to obtain the number and energy of gamma rays as functions of single-fragment mass.

For all four nuclei, the results for both average number $\bar{N}_\gamma$ and average energy $\bar{E}_\gamma$ exhibit a saw-tooth behaviour as functions of fragment mass. Further, the $\bar{E}_\gamma$(m) results for all four cases are nearly congruent, as are

the $\bar{N}_\gamma(m)$ results, for fragment masses less than ~105 amu and heavier than ~135 amu. There is a strong similarity of both the $\bar{E}_\gamma(m)$ and $\bar{N}_\gamma(m)$ functions to the functions describing neutron emission, $\nu(m)$, in these same fission reactions. The average photon energy $\bar{\epsilon} = \bar{E}_\gamma / \bar{N}_\gamma$ has also been obtained as a function of m; $\epsilon(m)$ increases in mass regions near closed-shell nuclei. The average total gamma-ray energy (for both fragments) $\bar{E}_{\gamma T}(m)$ and average total number $\bar{N}_{\gamma T}(m)$ vary less than 30% for each case; a marked minimum occurs in $\bar{N}_{\gamma T}(m)$ in the region of the double magic fragment mass 132. Taken as functions of total fragment kinetic energy E_K, both $\bar{E}_{\gamma T}$ and $\bar{N}_{\gamma T}$ decrease as E_K increases. Trends in all of these results may be qualitatively understood in terms of fragment nuclear structures.

A MEASUREMENT OF PROMPT FISSION NEUTRONS FROM ^{235}U USING A NEW TECHNIQUE (IAEA-SM-174/61).

R.E. Howe, T.W. Phillips,
Lawrence Livermore Laboratory,
University of California,
Livermore, Calif.

C. D. Bowman,
National Bureau of Standards,
Washington, D.C.,
United States of America

Recent discussion of the dependence of fission neutron multiplicity, $\bar{\nu}$, on the spin of the fissioning nuclear resonance indicates that no agreement on the existence of a correlation with spin or a mechanism for such a correlation has been reached. A new technique for measuring $\bar{\nu}$ was developed to provide further experimental information about the fission process and its spin dependence. Using neutrons from the Livermore 100-MeV LINAC, a measurement of $\bar{\nu}$ for neutron induced fission of ^{235}U was performed. The sample consisted of 100 mg of ^{235}U in a multiplate ionization chamber which served as the fission detector. Fast, spectrally independent detection of the prompt fission neutrons was achieved by situating the sample within a 2.9-cm-thick spherical shell of ^{235}U which was in turn surrounded by two concentric shells of ^{6}Li and Pb, respectively. The full width at half maximum of the time distribution of neutrons from this system is approximately 50 nsec. Prompt fission neutrons emitted by the sample interact with the ^{235}U- ^{6}Li-Pb system, causing multiple fissions in the uranium shell. Eventually neutrons from these subsequent fissions are detected in a pair of liquid benzene scintillators which use pulse shape discrimination to separate neutrons and gamma-rays. In this way, the nearly flat neutron fission cross-section of ^{235}U over the energy range of the fission neutron spectrum provides a decoupling of the prompt fission neutron spectrum originating from the sample and the energy-dependent efficiency of neutron-detecting scintillators. Measurements were performed with incident neutrons between 0.5 and 100 eV. The data for $\bar{\nu}$ were obtained with an accuracy of 0.2% for strong resonances. No apparent spin dependence larger than 0.2% was found, although some evidence is presented for a nonstatistical spread of resonance $\bar{\nu}$ values. A comparison of these data with previous $\bar{\nu}$ measurements is also included.

AN EVALUATION OF CALIBRATION PROCEDURES FOR THE RESPONSE OF SURFACE BARRIER DETECTORS TO FISSION FRAGMENTS AND HEAVY IONS (IAEA-SM-174/64).

S.B. Kaufman, E.P. Steinberg, B.D. Wilkins, J.P. Unik, A.J. Gorski, M.J. Fluss,
Argonne National Laboratory,
Argonne, Ill.,
United States of America

Surface barrier detectors have been extensively used for the detection and energy measurement of fission fragments and other heavy ions. The calibration of such detectors is complicated by the presence of the pulse-height defect (PHD), which makes the response of the detector dependent on the mass, atomic number and energy of the ion. Based on the results of measurements of the PHD of heavy ions with detectors of different resistivities, a new calibration technique for such detectors is proposed. Unlike the widely used technique proposed by Schmitt and co-workers, which assumes the PHD to be linear in both mass and energy, the present procedure reproduces the observed non-linearities. It is based on separating the energy of the ion into two terms, one of which is strictly proportional to the pulse height and is, in fact, the energy which a light ion, such as an alpha particle, of that pulse height would have. The second term is the energy defect of the ion, and is a function of ion energy, mass and atomic number.

An assessment of the present status of the use of surface barrier detectors in fission studies and the applicability and limitations of calibration techniques is presented. Applications to the analysis of data from various experiments are presented. Included are double-energy measurements of the fissioning systems $^{235}U + n$ and $^{252}Cf(sf)$, energy and time-of-flight measurements of the masses of fragments from the high-energy (11 GeV) proton induced fission of ^{238}U, and energy and time-of-flight mass measurements for energy-degraded fission fragments.

A SEMI-EMPIRICAL INTERPRETATION OF NUCLEAR FISSION BASED ON DEFORMED SHELL EFFECTS (IAEA-SM-174/78).

B.D. Wilkins, E.P. Steinberg, R.R. Chasman,
Argonne National Laboratory,
Argonne, Ill.,
United States of America

Using a simple static model of a fissioning system, a strong correlation was found between the potential energy and the fission yield of a given mass split. This model treats the fissioning system as two nearly tangent spheroids. The fragment shell corrections are obtained from the Strutinsky prescription with single particle levels calculated using a momentum-dependent Woods-Saxon potential. β_H^{Min} and β_L^{Min} denote the quadrupole deformations of the heavy and light fragments calculated to give an absolute minimum in the total potential energy. This absolute minimum is associated with a unique mass split. The total potential energy for all other mass splits is then calculated using these same deformations β_H^{Min} and β_L^{Min}. Nucleons are presumed

free to exchange between the two nascent fragments until the system has extended and "necked-in" sufficiently to prevent further nucleon transfer. At this point the shell structure in the nascent fragments (at β_L^{Min} and β_H^{Min}) is sufficiently strong so as to be the controlling factor in the mass determination. For fissioning systems such as U, Pu, and Cf, the deepest minimum in the potential energy versus deformation surface occurs for an asymmetric mass split, whereas in the mass regions around Ra and Fm competitive minima appear at different β_L and β_H which favour symmetric mass splits.

Comparisons are given with empirical mass and charge distributions for all the fissioning systems studied (Po to Fm). Total kinetic energy distributions are also obtained in this model from calculations similar to those previously published by others.

A SHELF IN THE "SUBTHRESHOLD" PHOTOFISSION CROSS-SECTION (IAEA-SM-174/80).

C. D. Bowman, I. G. Schroder, C. E. Dick,
National Bureau of Standards,
Washington, D. C.,
United States of America

In this paper attention is drawn to the existence of a shelf in the "subthreshold" photofission cross-section and to its implications for study of the properties of the double-humped fission barrier. From consideration of competition between fission and gamma decay in the second minimum, it is shown that at low excitation energies isomeric fission becomes more probable than prompt fission. This occurs because, as the excitation energy in the second minimum decreases, the penetrability of the outer barrier decreases much more rapidly than the probability for gamma decay. When the gamma decay becomes predominant, which occurs at about 4 MeV, the nucleus nearly always decays to the isomeric state where it rests until it decays by fission no matter how long it has to wait (neglecting tunnelling to the ground state deformation). In effect, when gamma decay predominates, the fission cross-section depends primarily on the inner barrier and is independent of the outer barrier transmission. Thus when $\Gamma_{fII} \gg \Gamma_{\gamma II}$, both barriers are penetrated whereas when $\Gamma_{\gamma II} \gg \Gamma_{fII}$, the net effect is as if only the inner barrier is penetrated. Other things being equal, the cross-section falls off only half as fast in the latter case as it does in the former — hence the appearance of a shelf in the cross-section.

The cross-section on the shelf can be several orders of magnitude larger than otherwise expected. The position in energy of the shelf, its width, as well as slope and the slope above and below the shelf all provide information on the deep-well properties of both inner and outer fission barriers. For isotopes of U and Pu where the two barriers are thought to be of about equal height, the prompt and delayed fission are equal at about 10^{-8} to 10^{-7} b where the energy $E_\gamma = 4$ MeV. With the NBS 4-MeV electron Van de Graaff accelerator operating at a current of 1 mA, it is believed that experiments can be done with a sensitivity better than 10^{-12} b. Already a fission cross-section of 10^{-9} b in ^{238}U at 3.8 MeV has been measured. It is intended to map out the shelf for this and a number of other nuclei to compile information on deep-barrier parameters as a basis for extending the theory of fission.

CUMULATIVE FISSION YIELDS OF KRYPTON AND XENON ISOTOPES PRODUCED BY IRRADIATION OF URANIUM AND PLUTONIUM ISOTOPES WITH THERMAL-FISSION-SPECTRUM AND 15-MeV NEUTRONS (IAEA-SM-174/82).

J.H. Kaye, N.E. Ballou,
Battelle Pacific Northwest Laboratories,
Richland, Wash.,
United States of America

Variations of cumulative fission yields with energy of fission-inducing neutrons have been determined for nuclides in the regions of the neutron closed shells of N = 50 and N = 82. The cumulative yields of ^{85m}Kr, ^{87}Kr, ^{88}Kr, ^{89}Kr, ^{137}Xe and ^{138}Xe were measured for the cases of fission of ^{239}Pu with thermal neutrons, and for fission of ^{235}U, ^{238}U and ^{239}Pu with fission-spectrum and 15-MeV neutrons. The rare gas activities resulting from irradiation of stearate samples of each nuclide were collected in a lucite counting cell, and the gamma radiation from each sample was measured with a Ge(Li) diode coupled to a PDP 8-E computer/analyser. The relative production rate of each nuclide with respect to that of a reference nuclide, either ^{88}Kr or ^{138}Xe, was determined. The cumulative yield values were then obtained by comparison of relative production rates in a given fission system with similar measurements for thermal neutron irradiation of ^{235}U and by estimation of the cumulative yields of the reference nuclides.

INDEPENDENT FISSION YIELDS OF ISOTOPES OF Br, Rb, I, AND Cs BY ON-LINE MASS SPECTROMETRY (IAEA-SM-174/83).

P.L. Reeder, R.A. Anderl, N.E. Ballou, J.J. Stoffels,
Battelle Pacific Northwest Laboratories,
Richland, Wash.,
United States of America

Independent fission yields for $^{84-91}Br$, $^{88-97}Rb$, $^{133-140}I$, and $^{137-145}Cs$ in thermal neutron fission of ^{235}U have been determined by on-line mass spectrometry. Uncertainties on the relative independent yields are 1-5%.

Measurements were made on a mass spectrometer which is set up on-line to a ^{235}U target/ion-source located deep in the thermal column of a 1-MW TRIGA reactor. The target consists of UC microspheres mixed with graphite powder and is located within a Ta oven heated to over 1500°C. Fission products recoil out of the UC, diffuse out of the graphite, and are ionized on the hot oven surface. Positive ions of Rb and Cs or negative ions of Br and I are accelerated through a 3-m-long evacuated tube to bring the ions to the mass spectrometer located outside the thermal column shield. The ions are mass analysed by a 60° deflection magnetic sector and are detected by an electron multiplier operating in the pulse-counting mode.

To obtain independent fission yields, mass spectra of fission products are recorded for short time intervals (~1 sec) for both beam-on and beam-off conditions. Pulsed neutron fluxes at the ^{235}U target are obtained by means

of a Cd shutter which surrounds the target/ion-source. Diffusion and radioactive decay corrections to the relative intensities of the mass peaks are obtained in separate experiments which measure the diffusion times of the fission products. The relative yields are normalized to independent yields of the longer-lived isotopes which have been measured radiochemically.

BRANCHING RATIOS FOR DELAYED FISSION (IAEA-SM-174/87).

J.K. Archer, J.B. Natowitz,
Texas A&M University,
College Station, Texas,
United States of America

A recoil collection technique has been employed to determine excitation functions for the production of α-emitting and delayed fission activities ($t_{1/2} \geq 2$ sec) in the reactions $^{237}Np + ^{4}He$ (≤ 110 MeV), $^{237}Np + ^{3}He$ (≤ 100 MeV) and $^{230}Th + ^{10}B$ (≤ 100 MeV). Based on these measurements and the systematics of nuclear reactions in this mass region, branching ratios for delayed fission are estimated.

ON THE CORRELATION BETWEEN THE MULTIPLICITY AND SPECTRUM OF PROMPT FISSION GAMMA RAYS (IAEA-SM-174/88).

T. Gozani,
Intelcom Radiation Technology,
San Diego, Calif.,
United States of America

The existence and extent of the correlation between energy spectra and the number of prompt neutrons (ν_n) and gamma rays (ν_γ) emitted from fission is important to the understanding of some aspects of the fission process. This correlation may also appreciably influence the determination of the detection efficiency of coincidence detectors, such as the fission multiplicity detector (FMD), which are being used in increasing numbers in the nuclear industry.

In the case of prompt neutron emission from the spontaneous fission of ^{252}Cf, there is a strong indication that no correlation exists between the multiplicity of the emitted neutrons and their energy distribution. There have been no similar measurements on the gamma multiplicity and its correlation to the energy distribution; this work describes such a measurement.

The FMD consists of four large plastic scintillators which determine various degrees of the multiplicity by measuring coincidences between any two detectors out of the four, any three detectors, and between all four detectors. The detection efficiency of the FMD is highly dependent on the ν_γ. For example, for a change of ν_γ from 3 to 8 the detection efficiency (for a certain energy bias condition) for any three detectors in coincidence changes from about 0.003 to 0.09. Thus the FMD with its four detectors scans all gamma-ray multiplicities.

The experimental setup contained a surface barrier fission detector in contact with a small (0.005 μg) ^{252}Cf source placed at the centre of the FMD. This 2π geometry ensures almost complete elimination of the effects of any angular correlation between fission fragments and the prompt gamma rays, which are detected by the surrounding FMD. When events with the required multiplicity are signalled, a linear gate is opened which lets a linear signal from a large 5 in. x 5 in. NaI(Tl) be processed in a multichannel analyser. The NaI(Tl) thus measures, within its resolution limits, the prompt fission gamma spectra of a limited range of ν_γ. This range is altered by changing the coincidence requirements, say, from 1 out of 4, 2 out of 4 through 4 out of 4. In addition to these measurements, which were made at low bias (~100 keV), a few measurements were done at higher bias (~750 keV). In this case only high-energy gamma rays can fulfil the coincidence requirements.

All spectra obtained with the NaI(Tl) were compared to the basic fission spectra, where only the fission detector gated the NaI(Tl).

The resulting spectra were rather similar — roughly decreasing exponentially with energy — thus indicating that the multiplicity of the prompt fission gamma rays is, to a large extent, uncorrelated with their energy spectra. A closer examination reveals that spectra taken with high energy bias on the FMD are slightly softer than the fission spectrum. They show less photons of energy higher than 1.2 MeV by about 10%, while the low-energy region is higher by a few per cent. Similar differences, but to a smaller extent, can be observed in the low bias cases.

PHOTON- AND NEUTRON-INDUCED FISSION ASSAY SYSTEMS (IAEA-SM-174/89).

T. Gozani,
Intelcom Radiation Technology,
San Diego, Calif.,
United States of America

Since the 1969 Symposium on Physics and Chemistry of Fission in Vienna, nuclear material active assay systems which are based on photon (bremsstrahlung)- and neutron-induced fission have made big strides. More than a score of systems have been installed around the world in nuclear fuel facilities as a part of quality as well as production and process controls. The systems which are already operational, as well as those being made now, use mainly ^{252}Cf as a neutron source with intensities of as high as 10^{10} to as low as 10^7 neutrons/sec. Other neutron sources such as PuLi, AmLi, and PuBe are also used. The observed fission signatures are in many cases the numerous prompt gamma rays and/or neutrons emitted within 20 - 100 nsec after the fission events. In other applications, the delayed gammas and sometimes the delayed neutrons are observed in the time ranges of tenths of a second to several minutes following the fission.

The paper describes the principles of the operational systems, their successes and limitations, future trends and some possible related areas of fission physics research.

INTEGRAL PHOTOFISSION EXPERIMENTS NEAR THRESHOLD OF ^{238}U AND ^{232}Th (IAEA-SM-174/90).

T. Gozani,
Intelcom Radiation Technology,
San Diego, Calif.,
United States of America

Low-energy photons are a very powerful tool for studying the fission process in general and channel theory in particular, because of the small number of possible channels they can excite. The only practical intense sources of low-energy photons ($E_\gamma \leq 6$ MeV) are bremsstrahlung from low-energy LINACS or Microtrons. With such devices, directly measured quantities are integral ones, namely, yields. Previous measurements concentrated on fission fragment angular distribution and on the fission yields (Y_f) from which the photofission cross-section can be derived. The new results reported here concentrate on prompt (Y_n) and delayed (Y_d) neutron yields defined as the number of prompt and delayed neutrons, respectively, emitted per unit gamma-ray dose. The former quantity divided by the fission yield, namely Y_n/Y_f, below the (γ, n) threshold energy, is closely related to the number of prompt neutrons emitted per photofission (ν_n). Y_d/Y_f is closely related to the number of delayed neutrons per fission ($\nu\beta$). Y_n, Y_d and Y_f were measured simultaneously using the Rad Tech high current single section low-energy LINAC. Y_f was measured using fission foils sandwiched between solid state track detectors. Y_n and Y_d were measured using a thermalized neutron detector with a suppressed gamma sensitivity.

Targets such as ^{232}Th and ^{238}U are very amenable to the study reported here because of their relatively high (γ, n) thresholds (6.4 MeV and 6.1 MeV, respectively), allowing investigation of the photofission process with no competition from opening neutron channels. Some measurements with ^{235}U and ^{239}Pu targets were made for comparison.

The measured delayed and prompt neutron yields as well as the previously measured fission yield in the subthreshold region of ^{232}Th show clearly the existence of structure in the photofission cross-section around 5.7 - 5.8 MeV. Measurements on the other isotopes, namely ^{235}U, ^{238}U, and ^{239}Pu, made under exactly the same conditions, did not indicate such a structure.

The ratio Y_n/Y_f (which is related to the ν_n and to a much lesser extent to their energy spectrum) was determined as a function of the bremsstrahlung end-point energy (E_e) from these experiments. It did not show, as expected, significant dependence on E_e around the threshold energy. It did show, however, an unexpected increase below the threshold energy for both ^{232}Th and ^{238}U. In the case of ^{232}Th the increase is rather dramatic.

Significant increase in the effective delayed neutron fraction in the subthreshold regions was also observed. The paper presents the techniques used and the complete results obtained.

ANGULAR DISTRIBUTION OF FRAGMENTS FROM FISSION OF ^{238}U WITH 150-MeV ^{4}He IONS (IAEA-SM-174/91).

N. K. Aras, G. E. Gordon, V. E. Viola, Jr.,
University of Maryland,
College Park, Md.,
United States of America

The angular distributions of fragments from fission of ^{238}U have been measured with 150-MeV ^{4}He ions. A target of 480-μg/cm^2 ^{238}U on thin nickel backing foil was bombarded for 8 h in a scattering chamber with a ^{4}He beam of about 200-nA intensity from the University of Maryland Cyclotron. Fission fragments were collected on 10-mg/cm^2 Mylar catchers of 1.6-cm radius. Catchers were placed at 18-cm distance from the target at 11°, 71°, 90° and 169° laboratory angles. Gamma rays emitted by the fission products in each catcher foil were observed with a 65-cm^3 Ge(Li) detector coupled with a 4096-channel analyser. Spectra were taken at several times after irradiation and fission products were identified from their gamma-ray energies, relative intensities and half-lives. From the areas under photopeaks produced by gamma rays from specific products, the angular distributions of the following fission products were measured: ^{91}Sr, ^{95}Zr, ^{97}Zr, ^{97}Nb, ^{99m}Tc, ^{103}Ru, ^{105}Rh, ^{111m}Pd, ^{112}Ag, ^{113}Ag, ^{115m}In, ^{117}In, ^{127}Te, ^{131}I, ^{132}I, ^{133}Xe, ^{140}La, ^{141}Ce, ^{144}Ce.

The angular distributions were transformed into the centre-of-mass system under the assumption that only binary fission contributes to the total fission cross-section at this energy; hence, the angular distributions must be symmetric about the centre-of-mass angle of 90°. The results of this analysis yield a value for the average momentum transfer from the projectile to the struck nucleus that is 0.65 ± 0.08 the value expected for compound-nucleus formation. The centre-of-mass anisotropies for symmetric and asymmetric fission fragments are compared to distinguish any possible differences in the fission mechanism responsible for the production of each type of mass distribution.

RESONANCE AND THERMAL $\bar{\nu}$ MEASUREMENTS ON ^{239}Pu (IAEA-SM-174/93).

R. W. Hockenbury, R. L. Reed, R. C. Block,
Rensselaer Polytechnic Institute,
Troy, N. Y.,
United States of America

The prompt fission neutron average multiplicity $\bar{\nu}$ of ^{239}Pu has been measured at the RPI LINAC from 0.01 to 100 eV using a fission chamber and a 0.75-m-diameter Gd-loaded liquid scintillator. Values of $\bar{\nu}$ have been determined for 22 resonances with standard deviations ranging from 0.2 to 0.5%. The $\bar{\nu}$ values fluctuate significantly from resonance to resonance, and statistical tests of the values indicate their distribution is consistent with two or more populations. There is a tendency for higher $\bar{\nu}$ values to be associated with resonances with spin $J = 0^+$ while almost all the lower values correspond to resonances of spin $J = 1^+$. In the 0.3 to 0.01 eV range,

$\overline{\nu}$ increases with decreasing energy, with $\overline{\nu}$ for the 0.3-eV resonance significantly lower than the value at 0.0253 eV. From 0.10 to 0.011 eV, $\overline{\nu}$ increases with a slope of approximately 0.6%. These new data follow the same trend with resonance energy as the earlier results of Weinstein and co-workers if their data in the 40 to 100 eV region are re-normalized downwards slightly. Comparisons have also been made to recent measurements at Oak Ridge and Saclay. In the resonance region, the results of the work reported here also show the same trend with resonance energy as the results reported by Oak Ridge, but the Oak Ridge $\overline{\nu}$ values do not show the tendency to divide into groupings as do the RPI and Saclay data. On the other hand, the present results do not show the same trend with energy as the Saclay results, and in particular there is a strong reversal in the two sets of data for the $\overline{\nu}$ values of the 41.4-eV and 44.6-eV resonances.

NEUTRON MULTIPLICITY MEASUREMENTS ON ^{233}U AND ^{235}U (IAEA-SM-174/94).

R. L. Reed, R. W. Hockenbury, R. C. Block,
Rensselaer Polytechnic Institute,
Troy, N.Y.,
United States of America

Measurements of prompt neutron emission as a function of incident neutron energy for fission of ^{233}U and ^{235}U have been made using multiplate fission chambers and a Gd-loaded liquid scintillator tank. The neutron source was the RPI LINAC and incident neutron energies were determined by the time-of-flight method. Values of $\overline{\nu}$ were determined for ^{235}U in the thermal to 30-eV energy range and for ^{233}U in the thermal to 100-eV energy range. $\overline{\nu}$ was measured to be constant to 0.1% in the thermal region from 0.10 to 0.011 eV for both ^{235}U and ^{233}U. In the epithermal energy region, relative $\overline{\nu}$ values were determined for each resolvable resonance and the data were normalized to the well-established thermal values. For ^{235}U, the distribution of the resonance $\overline{\nu}$ values cannot be fit by a single population. If one assumes two populations, then $\overline{\nu}$ falls into two groups separated by about 0.5% with mean values of 2.406 ± 0.002 and 2.417 ± 0.002. Statistical errors (standard deviations) for the ^{235}U resonance $\overline{\nu}$ values range from 0.1% to 0.3%. The maximum deviation from the average of all the resonance $\overline{\nu}$ values is 0.7% while the maximum difference between any two resonance $\overline{\nu}$ values is 1%. Resonance spin assignments for ^{235}U are made based on the assumed $\overline{\nu}$ grouping. The ^{233}U resonance $\overline{\nu}$ values also exhibit variations not consistent with a single population. However, no definitive groupings as for ^{235}U are observed. The errors on the ^{233}U resonance $\overline{\nu}$ values range from 0.1% to 0.5% with maximum deviations from the average of 1% and maximum resonance-to-resonance differences of 2%.

NUCLEON AND CHARGE REDISTRIBUTION AND THE ASYMMETRY IN FISSION (IAEA-SM-174/95).

R. K. Nair, W. H. Ellis,
University of Florida,
Gainesville, Fla.,
United States of America

The treatment of Myers and Swiatecki for incorporation of inhomogeneity and nucleon and charge redistribution in computing the energy of spherical nuclei has been extended to include nuclei with deformed shapes. To accommodate computation of the deformation energy, and asymmetry, the deformed nucleus was represented by two spheres connected by a conicoid (spheroid → hyperboloid → hyperboloid of two sheets at the point of scission). The configuration, uniquely characterized by four shape parameters, allowed the computation of the energy of the deformed nucleus, and the development of multiparameter search routines for determining the extremum in energy.

The energy surface, nuclear shape parameters, and nucleon and charge densities, as a function of deformation, were computed for the compound nucleus ^{236}U with three asymmetry ratios, $R_2 = 1.0$, 1.1, and 1.2. Energy barriers computed for the ratios were 11.78, 9.57, and 8.76 MeV, respectively. Saddle point configurations became more elongated and necked-down as the asymmetry ratio was increased. Nucleon ratios between the two halves of the deformed nucleus at saddle point for $R_2 = 1.2$ corresponded closely with those of most probable fission fragment pairs for thermal-neutron-induced fission of ^{235}U, i.e. (^{139}Ba-^{95}Kr); $A_2/A_1(A_H/A_L) = 1.36\,(1.46)$, $Z_2/Z_1\,(Z_H/Z_L) = 1.57\,(1.55)$, $N_2/N_1(N_H/N_L) = 1.27\,(1.41)$. Asymmetric configurations had lower energies than symmetric, and energy barriers were observed to decrease with increasing asymmetry, contrary to previous predictions based on the liquid drop model. The symmetric energy barrier of 11.78 MeV, agreeing with the 11.8 MeV previously reported, was much higher than the 5.8-MeV fission threshold of ^{235}U. However, the asymmetric cases with barrier energies of 9.57 and 8.76 MeV show a favourable trend toward the experimental value, suggesting that heavy nuclei in the neighbourhood of ^{235}U favour an asymmetric saddle shape en route to fission. Similarities between the computed nucleon and charge ratios of the asymmetric saddle point shapes, and those observed for most probable fission fragment pairs, suggest that the nucleon configuration of fragments are determined as early as the saddle point.

The results obtained suggest that effects of inhomogeneity and redistribution of nucleons and charge may offer a classical explanation for the lowered fission barrier and asymmetry observed in the fission of heavy nuclei.

NEUTRON FISSION CROSS-SECTION OF ^{249}Cf (IAEA-SM-174/99).

J.W.T. Dabbs, C.E. Bemis, N.W. Hill,
Oak Ridge National Laboratory,
Oak Ridge, Tenn.,
United States of America

G.D. James,
Oak Ridge National Laboratory, and
UKAEA, Atomic Energy Research Establishment,
Harwell, Berks, United Kingdom

M.S. Moore, A.N. Ellis,
Los Alamos Scientific Laboratory, Los Alamos, N.Mex.,
United States of America

It has been known for some time that ^{249}Cf has a very large fission resonance integral. Previous work, primarily that of Silbert at LASL, has failed to account for this large integral above 20 eV.

Time-of-flight measurements of the neutron induced fission cross-section of ^{249}Cf have been performed at ORELA, using an ultra-pure 128-μg sample of ^{249}Cf and compared with that of a 458-μg sample of ^{235}U measured simultaneously on the same flight path. Identical diffused junction fission fragment detectors were used. An α-particle count rate of 10^7/sec caused substantial deterioration of the ^{249}Cf detector during each overnight run. A total of $\sim 7 \times 10^5$ Cf fission events were recorded. The present results are comparable in resolution to those obtained by Silbert at LASL above 20 eV, in which an underground nuclear explosion served as the pulsed neutron source.

Eleven new resonances were found between 0.3 eV and 20 eV, including a very large resonance at 0.71 eV of total width ~ 0.15 eV and $\sigma_0 \sim 4000$ b. This resonance accounted for $\sim 75\%$ of the total fissions recorded, and is believed to account for the large resonance integral.

ENERGY LOSS IN ARGON OF ^{252}Cf SPONTANEOUS FISSION FRAGMENTS OF DIFFERENT MASSES (IAEA-SM-174/101).

A. Bertin, M. Bruno, G. Vannini, A. Vitale,
Istituto di Fisica dell' Università Bologna, and
Istituto Nazionale di Fisica Nucleare, Sezione di Bologna

M. Forte,
Physics Division,
Euratom CCR-ISPRA,
Italy

The energy loss of fission fragments along their range in argon has been measured with a method which also allowed the determination of the initial energy and the mass of the fragments in each observed binary fission event. The two fragments, emitted in opposite directions from a thin ^{252}Cf source, were slowed down while traversing a given distance in argon, where the

ionization produced was measured by a two-section gridded ionization chamber which was operated at different gas pressures. The residual energy was measured by two solid state detectors which stopped the fragments.

By an extensive analysis, which allowed reconstruction of the energies and masses of the fragments with an uncertainty of about 0.5 MeV and 3 amu, respectively, the following data have been derived: Range-energy curves for 20 mass intervals of 3 amu (from 93 to 155 amu), selecting (a) fragments with an initial energy equal to the most probable one, and (b) fragments where the initial energy was chosen as $E_0 = 104.1$ MeV for the light group, and $E_0 = 79.3$ for the heavy group; (c) range-energy curves for 10 different values of the initial energy for the mass intervals 105 - 107 amu and 141 - 143 amu (most probable fragments).

The first part of the range-energy curves, where the fragment loses energy mainly by ionization and electronic excitations, has been compared with the relations obtained from the theory of Lindhard, Scharff and Schiøtt (LSS). These relations appear to be inadequate for representing the experimental data, unless one modifies the dependence of the relations on the fragment nuclear charge.

More precisely, data (a) and (b) have been fitted by a relation $x = h(E^{\frac{1}{2}} - E_0^{\frac{1}{2}})$, leaving h free. For the light group, the fitting gave distinct values of h, depending on the fragment mass. For the fragments in the heavy group, a constant value of h was found.

A nearly constant h is also predicted by the LSS theory (though the agreement is not a quantitative one), and this fact suggests that the hypothesis leading to this theory may be correct in the limit of very heavy ions ($M > 130$ amu). On the basis of the present results, the possibility of determining, from ionization measurements, the probable nuclear charge of fragments of known mass is being considered.

TERNARY FISSION IN THE LIQUID DROP MODEL (IAEA-SM-174/103).

H. Diehl, W. Greiner,
Universität Frankfurt,
Federal Republic of Germany

The fissioning of a nucleus into three equal fragments is investigated in the framework of a three-parameter liquid drop model. Potential energy surfaces are calculated for direct oblate and prolate ternary fission. Barrier heights are given for both modes. Comparisons of the potential energy curves of binary and ternary fission lead to a qualitative explanation of the dependence of the ternary fission yield on charge and energy of the fissioning nucleus.

CHAIRMEN OF SESSIONS

Session VI	S. S. Kapoor	India
Session VII	P. Ribon	France
Session VIII	Tasneem A. Khan	Pakistan
Session IX	L. Yaffe	Canada

SECRETARIAT

Scientific Secretary	S. L. WHETSTONE	Division of Research and Laboratories, IAEA
Administrative Secretary	C. DE MOL VAN OTTERLOO	Division of External Relations, IAEA
Editor	F. MAUTNER MARKHOF	Division of Publications, IAEA
Records Officer	P. B. SMITH	Division of Languages, IAEA

LIST OF PARTICIPANTS

AUSTRALIA

Pearce, J.W.	Australian Atomic Energy Commission, 45 Beach Street, Coogee, NSW

BELGIUM

Hanappe, F.	Université Libre de Bruxelles, 50 av. F.D. Roosevelt, 1050 Brussels
Marmol, P., del	Centre d'étude de l'énergie nucléaire CEN/SCK, 200 Boeretang, 2400-MDL

BRAZIL

Nair, R.K.	Instituto Militar de Engenharia, Pça Gal. Tibúrcio, Praia Vermelha, Rio de Janeiro

CANADA

Knowles, J.W.	Chalk River Nuclear Laboratories, Chalk River, Ont.
Milton, J.C.D.	Chalk River Nuclear Laboratories, Chalk River, Ont.
Yaffe, L.	Department of Chemistry, McGill University, P.O. Box 6070, Montreal 101, P.Q.

DENMARK

Back, B.B.	Niels Bohr Institute, Blegdamsvej 17, 2100 Copenhagen
Bjørmholm, S.	Niels Bohr Institute, Blegdamsvej 17, 2100 Copenhagen
Christensen, C.J.	Danish AEC Research Establishment, Risø, 4000 Roskilde

Jensen, A.S. — Nordita, Blegdamsvej 17, 2100 Copenhagen

Metag, V. — Niels Bohr Institute, Tandem Accelerator Laboratoriet, Risø, 4000 Roskilde

Randrup, J. — Institute of Physics, University of Aarhus, Aarhus

Wilczyński, J. — Niels Bohr Institute, Tandem Accelerator Laboratoriet, Risø, 4000 Roskilde

FRANCE

Asghar, M. — Institut Laue-Langevin, Cédex 156, 38 Grenoble-Gare

Babinet, R. — Département de physique nucléaire, CEA, Centre d'études nucléaires de Saclay, B.P. n° 2, 91190 Gif-sur-Yvette

Blachot, J. — CEA, Centre d'études nucléaires de Grenoble, B.P. n°85, Centre de Tri, 38041 Grenoble-Cédex

Bions, J. — CEA, Centre d'études nucléaires de Saclay, B.P. n°2, 91190 Gif-sur-Yvette

Carraz, L.-C. — CEA, Centre d'études nucléaires de Grenoble, B.P. 85, Centre de Tri, 38041 Grenoble-Cédex

Cauvin, B. — CEA, Centre d'études nucléaires de Saclay, B.P. n°2, 91190 Gif-sur-Yvette

Communeau, Françoise — Commissariat à l'énergie atomique, B.P. n°27, 94190 Villeneuve-St. Georges

Debeauvais, Monique — Centre de recherches nucléaires, Lab. Phys. Corpusculaire, Rue du Lœss, 67000 Strasbourg-Cronenbourg

Fréhaut, J. — Commissariat à l'énergie atomique, 29 rue de la fédération, 75 Paris 15

Lachkar, J.C. — CEA, Centre d'études de Bruyères-le-Châtel, B.P. n°61, 92120 Montrouge

Laubuge, R. — CEA, Centre d'études de Bruyères-le-Châtel, B.P. n°61, 92120 Montrouge

Leroux, B. — Université de Bordeaux, CENBG, Domaine du Haut-Vigneau, 33170 Gradignan

Ngô, C.	Faculté d'Orsay, B.P. n°1, 91406 Orsay
Ouvry, Françoise	Commissariat à l'énergie atomique, 29 rue de la fédération, 75 Paris 15
Poitou, J.	CEA, Centre d'études nucléaires de Saclay, B.P. n°2, 91190 Gif-sur-Yvette
Quentin, P.	Division de physique théorique, IPN, B.P. n°1, 91406 Orsay
Ribon, P.	CEA, Centre d'études nucléaires de Saclay, B.P. n°2, 91190 Gif-sur-Yvette
Sicre, A.	Université de Bordeaux, CENBG, Domaine du Haut-Vigneau, 33170 Gradignan
Signarbieux, C.	CEA, Centre d'études nucléaires de Saclay, B.P. n°2, 91190 Gif-sur-Yvette
Soleilhac, M.	CEA, Centre d'études de Bruyères-le-Châtel, B.P. n°61, 92120 Montrouge
Tamain, B.	Institut de physique nucléaire, B.P. n°1, 91406 Orsay
Trochon, J.	CEA, Centre d'études de Bruyères-le-Châtel, B.P. n°61, 92120 Montrouge

GERMANY, FEDERAL REPUBLIC OF

Armbruster, P.J.	Gesellschaft für Schwerionenforschung, Postfach 541, 61 Darmstadt
Denschlag, H.O.	Institut für Kernchemie, Universität Mainz, Friedrich v. Pfeiffer-Weg 14, 6500 Mainz
Diehl, H.	Institut für Theoretische Physik der Universität, Robert-Mayer-Str. 8-10, 6 Frankfurt/Main
Dietrich, K.	Technische Universität München, Reaktorgelände, 8046 Garching
Gönnenwein, F.	Universität Tübingen, Physikalisches Institut, 74 Tübingen
Hasse, R.W.	Sektion Physik der Universität München, Am Coulombwall 1, 8046 Garching
Konecny, E.	Physik-Department, Universität München, 8046 Garching
Krappe, H.J.	Hahn-Meitner-Institut, Berlin

Kratz, J.-V.	Institut für Kernchemie, Universität Mainz, Friedrich v. Pfeiffer-Weg 14, 6500 Mainz
Maruhn, J.	Institut für Theoretische Physik der Universität, Robert-Mayer-Str. 8-10, 6 Frankfurt/Main
Mosel, U.	Institut für Theoretische Physik, Universität Giessen, 63 Giessen
Nörenberg, W.	Institut für Theoretische Physik, Universität Heidelberg, Philosophenweg 16, Heidelberg
Sistemich, K.	Kernforschungsanlage Jülich, Artillerie-Str. 44, 517 Jülich
Specht, H.J.	Sektion Physik der Universität München, Am Coulombwall 1, 8046 Garching
Wurm, J.	Max-Planck Institut für Kernphysik, Postfach 1248, 69 Heidelberg 1

HUNGARY

Kluge, Gy.	Central Research Institute for Physics, P.O. Box 49, H-1525 Budapest 114

INDIA

Kapoor, S.S.	Nuclear Physics Division, Bhabha Atomic Research Centre, Trombay, Bombay 400085
Ramamurthy, V.S.	Nuclear Physics Division, Bhabha Atomic Research Centre, Trombay, Bombay 400085

ISRAEL

Amiel, S.	Soreq Nuclear Research Centre, Yavne
Boneh, Y.	Nuclear Research Centre, P.O. Box 9001, Beer-Sheva
Cheifetz, E.	Weizmann Institute of Science, Rehovot
Fraenkel, Z.	Weizmann Institute of Science, Rehovot

JAPAN

Katase, A.	Department of Nuclear Engineering, Kyushu University, Fukuoka 812
Takekoshi, E. (Mrs.)	Japan Atomic Energy Research Institute, Tokai Research Establishment, Tokai-mura, Ibaraki-ken 319-11

NIGER

Foulani, P.	Centre d'enseignement supérieur, Département de physique, B.P. n°237, Niamey

PAKISTAN

Khan, Tasneem A.	Pakistan Institute of Nuclear Science, Nilore, Rawalpindi

POLAND

Piasecki, E.	Institute of Nuclear Research, Dept. IA, Świerk
Sowinski, M.	Institute of Nuclear Research, Warsaw

ROMANIA

Vîlcov, N.	Institute for Atomic Physics, P.O. Box 35, Bucharest-Magurele

SWEDEN

Alm, A.	Lund Institute of Technology, Nuclear Physics Department, Sölvegatan 14, S-223 62 Lund
Bengtsson, R.	Lund Institute of Technology, Sölvegatan 14, S-223 62 Lund
Larsson, S.E.	Lund University, Department of Mathematical Physics, P.O. Box 725, S-220 07 Lund

SWITZERLAND

Gunten, H.R. von	Eidg. Institut für Reaktorforschung, Würenlingen

Ledergerber, T.	Institut für Theoretische Physik der Universität Basel, Klingelbergstr. 82, CH-4000 Basel
Pauli, H.C.	Present address: Max-Planck-Institut für Kernphysik, Saupfercheckweg 1, D-69 Heidelberg 1, Federal Republic of Germany

UNITED KINGDOM

Grant, I.S.	Physics Department, Manchester University, Manchester M13, 9PL
James, D.G.	Oak Ridge National Laboratory, P.O. Box X, Oak Ridge, Tenn. 37830, United States of America
Scobie, J.	Scottish Universities Research and Reactor Centre, East Kilbride, Glasgow
Scott, R.D.	Scottish Universities Research and Reactor Centre, East Kilbride, Glasgow
Shotter, A.C.	Edinburgh University, Physics Department, James Clerk Maxwell Bldg., Mayfield Rd., Edinburgh
Vass, D.G.	Edinburgh University, Physics Department, James Clerk Maxwell Bldg., Mayfield Rd., Edinburgh

UNITED STATES OF AMERICA

Albrecht, K.	Nuclear Structure Research Laboratory, University of Rochester, Rochester, N.Y. 14627
Alpen, E.L.	Battelle-Northwest Laboratory, P.O. Box 999, Richland, Wash. 99352
Aras, N.K.	University of Maryland, Department of Chemistry, College Park, Md. 20742
Auchampaugh, G.F.	Los Alamos Scientific Laboratory, P.O. Box 1663, Los Alamos, N. Mex. 87544
Ballou, N.E.	Battelle-Northwest Laboratory, P.O. Box 999, Richland, Wash. 99352
Behkami, A.N.	University of Rochester, Rochester, N.Y. 14627

Bhandari, B.S.	Ohio University, Department of Physics, Athens, Ohio 45701
Bigeleisen, J.	University of Rochester, Rochester, N.Y. 14627
Blann, M.	University of Rochester, Rochester, N.Y. 14627
Block, R.C.	Rensselaer Polytechnic Institute, Nuclear Engineering, Troy, N.Y. 12181
Bowman, C.D.	National Bureau of Standards, Washington, D.C.
Boyno, J.S.	Cyclotron Laboratory, Michigan State University, East Lansing, Mich. 48824
Brack, M.	State University of New York at Stony Brook, Department of Physics, Stony Brook, N.Y. 11790
Britt, H.C.	Nuclear Structure Research Laboratory, University of Rochester, Rochester, N.Y. 14627
Browne, J.C.	Lawrence Livermore Laboratory, P.O. Box 808, Livermore, Calif. 94550
Clark, D.D.	Cornell University, Ward Laboratory of Nuclear Engineering, Ithaca, N.Y. 14850
Clark, R.G.	University of Maryland, College Park, Md. 20742
Cowan, G.A.	Los Alamos Scientific Laboratory, P.O. Box 1663, Los Alamos, N. Mex. 87544
Dabbs, J.W.T.	Oak Ridge National Laboratory, P.O. Box X, Oak Ridge, Tenn. 37830
De Saussure, G.	Oak Ridge National Laboratory, P.O. Box X, Oak Ridge, Tenn. 37830
Doron, J.E.	Chemical Abstracts Service, Columbus, Ohio 43210
Dowdy, E.J.	Los Alamos Scientific Laboratory, P.O. Box 1663, Los Alamos, N. Mex. 87544

Felvinci, J.P.	Columbia University, New York, N.Y. 10027
Ferguson, Robert L.	Oak Ridge National Laboratory, P.O. Box X, Oak Ridge, Tenn. 37830
Fluss, M.J.	Argonne National Laboratory, 9700 South Cass Ave., Argonne, Ill. 60439
Fong, P.	Emory University, Department of Physics, Atlanta, Ga. 30322
Ford, G.P.	Los Alamos Scientific Laboratory, CHC-11, P.O. Box 1663, Los Alamos, N. Mex. 87544
Francis, N.C.	KAPL, Knolls Atomic Power Laboratory, River Rd., Schenectady, N.Y. 12309
Freiesleben, H.	Nuclear Structure Research Laboratory, University of Rochester, Rochester, N.Y. 14627
Gardner, D.G.	Lawrence Livermore Laboratory, P.O. Box 808, Livermore, Calif. 94550
Garrett, J.D.	Brookhaven National Laboratory, Upton, N.Y. 11973
Gatti, R.C.	Lawrence Berkeley Laboratory, Berkeley, Calif. 94720
Gindler, J.E.	Argonne National Laboratory, 9700 South Cass Ave., Argonne, Ill. 60439
Glendenin, L.E.	Argonne National Laboratory, 9700 South Cass Ave., Argonne, Ill. 60439
Goldstone, P.D.	State University of New York at Stony Brook, Department of Physics, Stony Brook, N.Y. 11790
Gozani, T.	Intelcom Rad Tech, 7650 Convoy Ct., San Diego, Calif. 92118
Greenwood, R.C.	Aerojet Nuclear Co., 550 Second St., Idaho Falls, Idaho 83401
Griffin, H.C.	University of Michigan, Department of Chemistry, Ann Arbor, Mich. 48104

Griffin, J.J.	University of Maryland, Department of Physics, College Park, Md. 20742 and Lawrence Berkeley Laboratory, Nuclear Chemistry Division, Berkeley, Calif. 94720
Gutbrod, H.H.	Gesellschaft für Schwerionenphysik, Postfach 541, 61 Darmstadt, Federal Republic of Germany and Lawrence Berkeley Laboratory, Building 71, Berkeley, Calif. 94720
Harker, Y.D.	Aerojet Nuclear Co., 550 Second St., Idaho Falls, Idaho 83401
Heffner, R.H.	University of Washington, Nuclear Physics Laboratory, Seattle, Wash. 98195
Helmer, R.G.	Aerojet Nuclear Co., 550 Second St., Idaho Falls, Idaho 83401
Heunemann, D.	Lawrence Berkeley Laboratory, Building 70, Berkeley, Calif. 94720
Hoffman, Darleane C.	Los Alamos Scientific Laboratory, CNC-11, P.O. Box 1663, Los Alamos, N. Mex. 87544
Howard, W.M.	Los Alamos Scientific Laboratory, P.O. Box 1663, Los Alamos, N. Mex. 87544
Howe, R.E.	Lawrence Livermore Laboratory, P.O. Box 808, Livermore, Calif. 94550
Huizenga, J.R.	University of Rochester, Rochester, N.Y. 14627
Hulet, E.K.	Lawrence Livermore Laboratory, P.O. Box 808, Livermore, Calif. 94550
Ihochi, H.	Chemical Abstracts Service, The Ohio State University, Columbus, Ohio 43210
Jared, R.C.	Lawrence Berkeley Laboratory, Berkeley, Calif. 94720
Kan, K.-K.	University of Maryland, College Park, Md. 20742

Kane, J. H.	US Atomic Energy Commission, Washington, D. C. 20545
Kataria, S. K.	Lawrence Berkeley Laboratory, Berkeley, Calif. 94720
Keyworth, G. A., II	Los Alamos Scientific Laboratory, P. O. Box 1663, Los Alamos, N. Mex. 87544
Knoll, G. F.	University of Michigan, Department of Nuclear Energy, Ann Arbor, Mich. 48104
Leachman, R. B.	Defense Nuclear Agency, Washington, D. C. 20305
Lee, L. L., Jr.	State University of New York at Stony Brook, Stony Brook, N. Y. 11790
Loveland, W.	Radiation Center, Oregon State University, Corvallis, Oreg. 97331
Matthews, S. M.	Lawrence Livermore Laboratory, P. O. Box 808, Livermore, Calif. 94550
Matuszek, J. M.	Radiological Sciences Laboratory, 30 Russell Road, Albany, N. Y. 12206
Meadows, J. W.	Argonne National Laboratory, 9700 South Cass Ave., Argonne, Ill. 60439
Melkonian, E.	Columbia University, Morningside Heights, New York, N. Y. 10027
Miller, J.	Columbia University, Department of Chemistry, New York, N. Y. 10027
Möller, P.	Los Alamos Scientific Laboratory, P. O. Box 1663, Los Alamos, N. Mex. 87544
Moore, M. S.	Los Alamos Scientific Laboratory, P. O. Box 1663, Los Alamos, N. Mex. 87544
Moretto, L. G.	Lawrence Berkeley Laboratory, Berkeley, Calif. 94720
Muga, L.	University of Florida, 406 Nuclear Science Bldg., Gainesville, Fla. 32601

Mustafa, M. G.	Oak Ridge National Laboratory, P.O. Box X, Oak Ridge, Tenn. 37830
Myers, W.D.	Lawrence Berkeley Laboratory, Berkeley, Calif. 94720
Nalcioglu, O.	University of Rochester, Department of Physics, Rochester, N.Y. 14627
Namboodiri, M.N.	Cyclotron Institute, Texas A & M University, College Station, Tex. 77843
Natowitz, J.B.	Cyclotron Institute, Texas A & M University, College Station, Tex. 77843
Nethaway, D.R.	Lawrence Livermore Laboratory, P.O. Box 808, Livermore, Calif. 94550
Nifenecker, H.	Lawrence Berkeley Laboratory, Berkeley, Calif. 94720
Nix, J.R.	Los Alamos Scientific Laboratory, P.O. Box 1663, Los Alamos, N. Mex. 87544
Paperiello, C.J.	New York State Department of Health, 84 Holland Ave., Albany, N.Y.
Perry, D.G.	Los Alamos Scientific Laboratory, P.O. Box. 1663, Los Alamos, N. Mex. 87544
Philipps, G.W.	US Naval Research Laboratory, Washington, D.C. 20375
Plasil, F.	Oak Ridge National Laboratory, P.O. Box X, Oak Ridge, Tenn. 37830
Prince, A.	Brookhaven National Laboratory, Upton, N.Y. 11973
Reeder, P.L.	Battelle-Northwest Laboratory, P.O. Box 999, Richland, Wash. 99352
Rengan, K.	Eastern Michigan University, Department of Chemistry, Ypsilanti, Mich. 48197
Roche, C.T.	University of Maryland, Department of Chemistry, College Park, Md. 20742

Russo, Phyllis	University of Washington, Nuclear Physics Laboratory, Seattle, Wash. 98195
Schmitt, H.W.	Oak Ridge National Laboratory, P.O. Box X, Oak Ridge, Tenn. 37830
Schroder, I.G.	National Bureau of Standards, Washington, D.C. 20234
Schütte, G.	University of Washington, Seattle, Wash. 98195
Seglie, E.	Rensselaer Polytechnic Institute, Troy, N.Y. 12181
Sierk, A.J.	Los Alamos Scientific Laboratory, P.O. Box 1663, Los Alamos, N. Mex. 87544
Sletten, G.	University of Washington, Seattle, Wash. 98195
Sperber, D.	Rensselaer Polytechnic Institute, Troy, N.Y. 12181
Steinberg, E.P.	Argonne National Laboratory, 9700 South Cass Ave., Argonne, Ill. 60439
Stevenson, P.C.	Lawrence Livermore Laboratory, P.O. Box 808, Livermore, Calif. 94550
Stubbins, W.F.	University of Cincinnati, Department of Physics, Cincinnati, Ohio 45221
Sutcliffe, W.G.	Lawrence Livermore Laboratory, P.O. Box 808, Livermore, Calif. 94550
Takahashi, H.	Brookhaven National Laboratory, Upton, N.Y. 11973
Tsang, C.F.	Lawrence Berkeley Laboratory, Berkeley, Calif. 94720
Unik, J.P.	Argonne National Laboratory, 9700 South Cass Ave., Argonne, Ill. 60439
Vandenbosch, R.	Nuclear Physics Laboratory, University of Washington, Seattle, Wash. 98195
Van Dyken, A.R.	US Atomic Energy Commission, Washington, D.C. 20545

Vaz, L.C.	State University of New York at Stony Brook, Department of Chemistry, Stony Brook, N.Y. 11790
Viola, V.E., Jr.	University of Maryland, Department of Chemistry, College Park, Md. 20742
Wahl, A.C.	Washington University, Department of Chemistry, St. Louis, Mo. 63130
Wehring, B.W.	University of Illinois, Urbana, Ill. 61801
Wheeler, J.A.	Princeton University, Department of Physics, Princeton, N.J. 08540
Wilets, L.	University of Washington, Department of Physics, Seattle, Wash. 98195
Wilhelmy, J.B.	Los Alamos Scientific Laboratory, P.O. Box 1663, Los Alamos, N. Mex. 87544
Wilkins, B.D.	Argonne National Laboratory, 9700 South Cass Ave., Argonne, Ill. 60439
Winkler, P.	State University of New York at Stony Brook, Stony Brook, N.Y. 11790
Wolfsberg, K.	Los Alamos Scientific Laboratory, CNC-11, P.O. Box. 1663, Los Alamos, N. Mex. 87544
Wong, C.Y.	Oak Ridge National Laboratory, P.O. Box X, Oak Ridge, Tenn. 37830
Zirkind, P.	Picatinny Arsenal, Building 65, Dover, N.J. 07801

VENEZUELA

Groening, H.	Venezuelan Institute of Scientific Investigations, Caracas

CEC (Commission of the European Communities)

Deruytter, A.J.	Central Bureau for Nuclear Measurements, EURATOM, Steenweg naar Retie, 2440 Geel, Belgium

Forte, M. EURATOM CCR,
21020 Ispra,
Varese, Italy

NEA (Nuclear Energy Agency)

Schett, A. OECD/Centre NEA de compilation de données neutroniques,
B.P. n°9, 91190 Gif-sur-Yvette, France

AUTHOR INDEX

Numbers underlined refer to the first page of a paper.
Other page numbers refer to discussion comments.

HOW TO ORDER IAEA PUBLICATIONS

Exclusive sales agents for IAEA publications, to whom all orders and inquiries should be addressed, have been appointed in the following countries:

UNITED KINGDOM	Her Majesty's Stationery Office, P.O. Box 569, London SE 1 9NH
UNITED STATES OF AMERICA	UNIPUB, Inc., P.O. Box 433, Murray Hill Station, New York, N.Y. 10016

In the following countries IAEA publications may be purchased from the sales agents or booksellers listed or through your major local booksellers. Payment can be made in local currency or with UNESCO coupons.

ARGENTINA	Comisión Nacional de Energía Atómica, Avenida del Libertador 8250, Buenos Aires
AUSTRALIA	Hunter Publications, 58 A Gipps Street, Collingwood, Victoria 3066
BELGIUM	Office International de Librairie, 30, avenue Marnix, B-1050 Brussels
CANADA	Information Canada, 171 Slater Street, Ottawa, Ont. K 1 A OS 9
C.S.S.R.	S.N.T.L., Spálená 51, CS-11000 Prague Alfa, Publishers, Hurbanovo námestie 6, CS-80000 Bratislava
FRANCE	Office International de Documentation et Librairie, 48, rue Gay-Lussac, F-75005 Paris
HUNGARY	Kultura, Hungarian Trading Company for Books and Newspapers, P.O. Box 149, H-1011 Budapest 62
INDIA	Oxford Book and Stationery Comp., 17, Park Street, Calcutta 16
ISRAEL	Heiliger and Co., 3, Nathan Strauss Str., Jerusalem
ITALY	Libreria Scientifica, Dott. de Biasio Lucio "aeiou", Via Meravigli 16, I-20123 Milan
JAPAN	Maruzen Company, Ltd., P.O.Box 5050, 100-31 Tokyo International
NETHERLANDS	Marinus Nijhoff N.V., Lange Voorhout 9-11, P.O. Box 269, The Hague
PAKISTAN	Mirza Book Agency, 65, The Mall, P.O.Box 729, Lahore-3
POLAND	Ars Polona, Centrala Handlu Zagranicznego, Krakowskie Przedmiescie 7, Warsaw
ROMANIA	Cartimex, 3-5 13 Decembrie Street, P.O.Box 134-135, Bucarest
SOUTH AFRICA	Van Schaik's Bookstore, P.O.Box 724, Pretoria Universitas Books (Pty) Ltd., P.O.Box 1557, Pretoria
SPAIN	Nautrónica, S.A., Pérez Ayuso 16, Madrid-2
SWEDEN	C.E. Kritzes Kungl. Hovbokhandel, Fredsgatan 2, S-10307 Stockholm
U.S.S.R.	Mezhdunarodnaya Kniga, Smolenskaya-Sennaya 32-34, Moscow G-200
YUGOSLAVIA	Jugoslovenska Knjiga, Terazije 27, YU-11000 Belgrade

Orders from countries where sales agents have not yet been appointed and requests for information should be addressed directly to:

Publishing Section,
International Atomic Energy Agency,
Kärntner Ring 11, P.O.Box 590, A-1011 Vienna, Austria

INTERNATIONAL
ATOMIC ENERGY AGENCY
VIENNA, 1974

PRICE: US $24.00
Austrian Schillings 470,-
(£10.70; F.Fr.120,-; DM 64,-)

SUBJECT GROUP: III
Physics/
Nuclear Physics, Reactor Physics, Fission